Geologic Studies in the Basin and Range–Colorado Plateau Transition in Southeastern Nevada, Southwestern Utah, and Northwestern Arizona, 1992

U.S. GEOLOGICAL SURVEY BULLETIN 2056

Cover. False color composite TM image of the western half of the BARCO area. This mosaic was prepared by Kevin F. Mullins, U.S. Geological Survey, at Flagstaff, AZ. TM Bands 1, 4, and 7 are blue, green, and red, respectively. A polar orbit at 500 to 800 km elevation was used by the satellite that collected this image. These data were radiometrically corrected for instrument and atmospheric effects by Pat Chavez (1989, Radiometric calibration of landsat thematic mapper multispectral images: Photogrammetric Engineering and Remote Sensing, v. 55, no. 9, p. 1285–1294). The area shown extends from about lat 38° N., long 115° W. in the northwest corner to about 36°30′N., 113°30′W. in the southeast corner, about 165 km in a north-south direction and about 135 km in an east-west direction. The Escalante Desert in the northeastern area contains circular irrigation patterns; the city of St. George, Utah, is about 80 km to the south. The southern area is dominated by the domal Mormon Mountains flanked by the Virgin River to the southeast and Meadow Valley Wash to the west, all in Nevada. The northwestern area covers the North Pahroc Range, and east of that, Dry Lake Valley. Clouds cover much of the Bull Valley Mountains and the eastern end of the Caliente caldera complex about at the Nevada-Utah border.

Geologic Studies in the Basin and Range–Colorado Plateau Transition in Southeastern Nevada, Southwestern Utah, and Northwestern Arizona, 1992

By Robert B. Scott *and* W C Swadley, *Editors*

U.S. GEOLOGICAL SURVEY BULLETIN 2056

Chapter titles are listed on volume contents page

UNITED STATES GOVERNMENT PRINTING OFFICE, WASHINGTON : 1995

U.S. DEPARTMENT OF THE INTERIOR
BRUCE BABBITT, Secretary

U.S. GEOLOGICAL SURVEY
Gordon P. Eaton, Director

For sale by U.S. Geological Survey, Information Services
Box 25286, Federal Center
Denver, CO 80225

Library of Congress Cataloging-in-Publication Data

Geologic studies in the Basin and Range–Colorado Plateau transition in southeastern Nevada, southwestern Utah, and northwestern Arizona, 1992 / by Robert B. Scott and W C Swadley, editors.
p. cm. — (U.S. Geological Survey bulletin ; 2056)
Includes bibliographical references.
Supt. of Docs. no.: I 19.3:2056
1. Geology—Nevada. 2. Geology—Utah. 3. Geology—Arizona. I. Scott, Robert B. II. Swadley, W C III. Series.
QE75.B9 no. 2056
[QE137]
557.3 s—dc20 94–16278
[557.93] CIP

CONTENTS

[Letters designate chapters]

Introduction

By Robert B. Scott *and* W C Swadley

The scientific purpose of the Basin and Range to Colorado Plateau Transition (BARCO) Study Unit is to use the results of detailed geologic mapping and related research to investigate the tectonic and magmatic evolution of the eastern part of the Basin and Range province to the stable Colorado Plateaus province; the area includes the transition zone between the two provinces (figs. 1 and 2). BARCO is a U.S. Geological Survey multidisciplinary mapping Study Unit within the National Geologic Mapping Program, authorized by the National Geologic Mapping Act of 1992. This new National Geologic Mapping Program superseded the preexisting mapping program by the same name, under which the BARCO Study Unit operated from 1988 to 1992. The highest priority of the new program is the synthesis of 1:100,000-scale, 30×60-minute quadrangles compiled from more detailed general-purpose geologic maps, in areas where improved knowledge of the geologic framework is needed by the private sector, government agencies, and academic institutions for environmental purposes, geologic hazard reduction, land-use planning, and basic research. More detailed maps are being produced where they are needed to portray geologic relations too complex to be displayed at 1:100,000 scale.

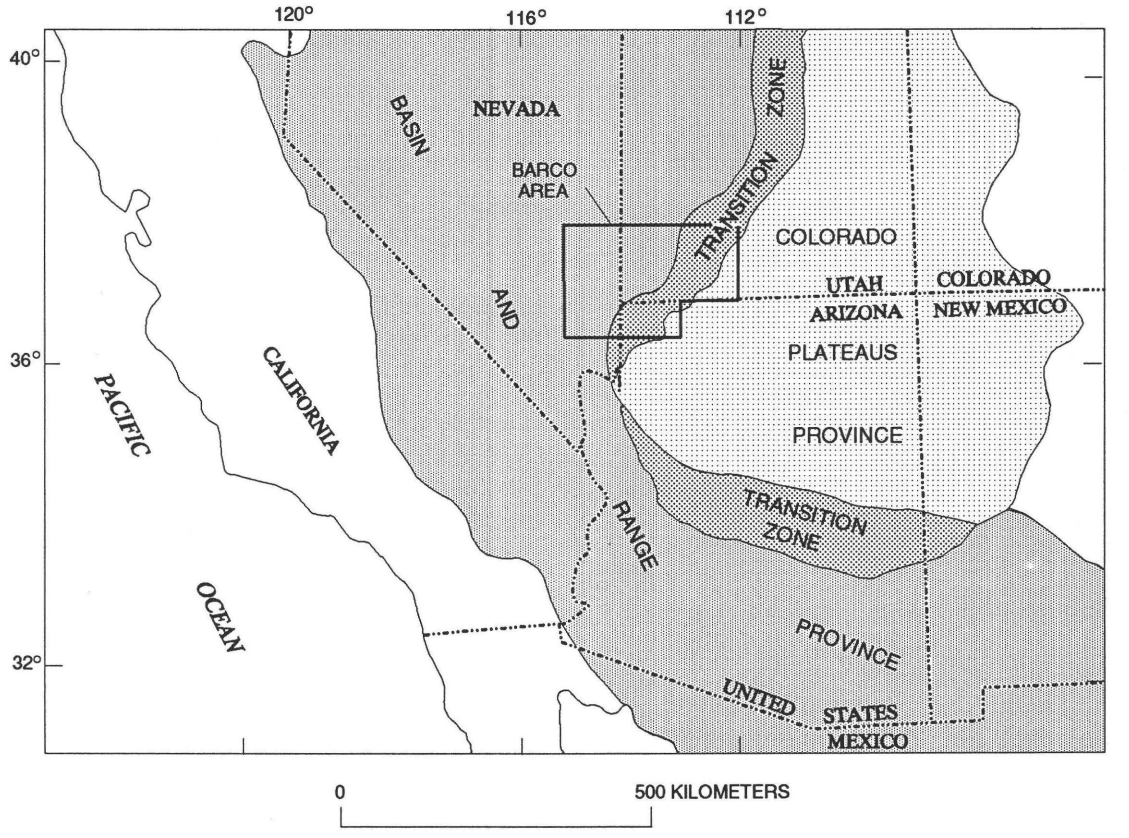

Figure 1. Regional map showing the BARCO Study Unit area, boundaries of the Basin and Range and Colorado Plateaus provinces, and transition zone between the provinces.

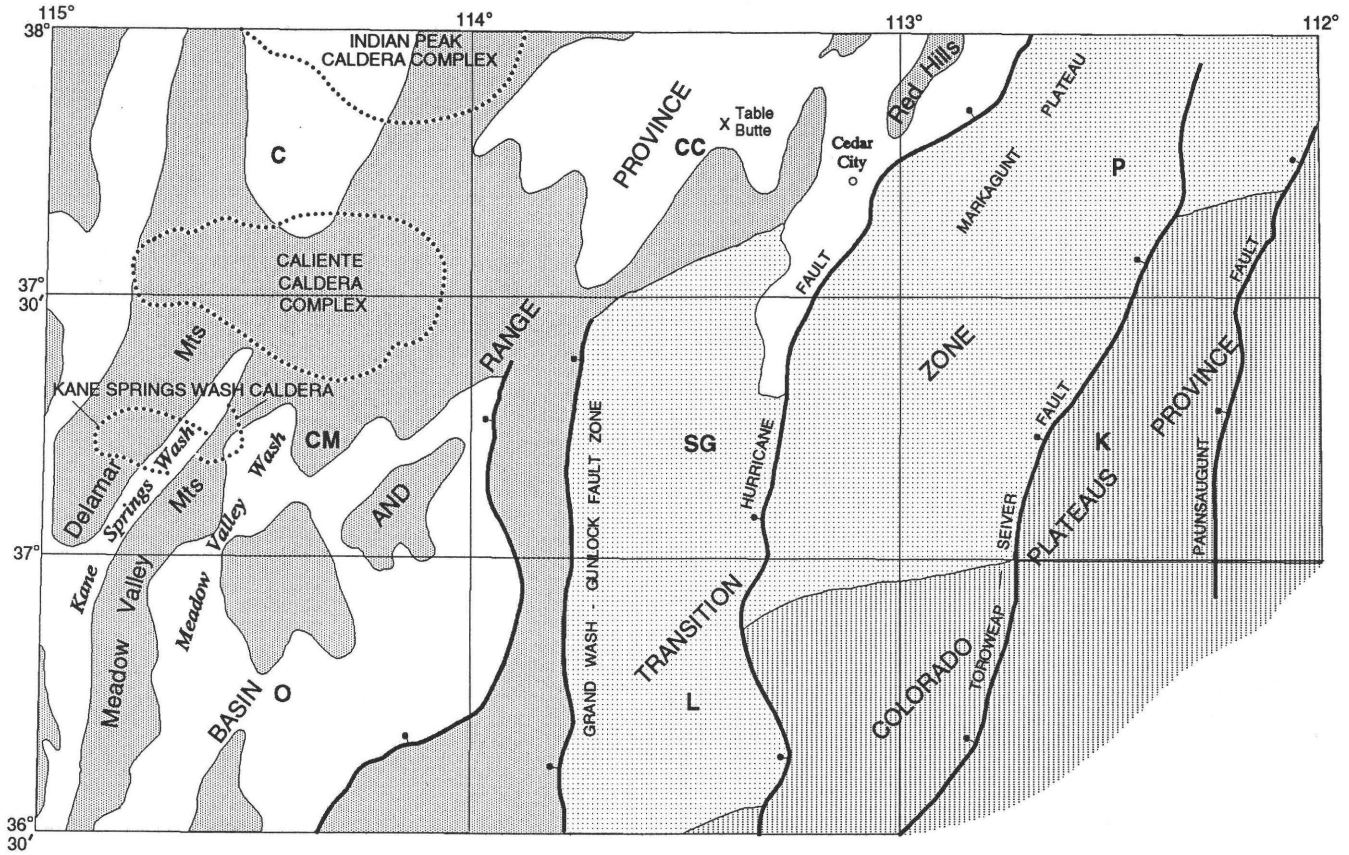

Figure 2. Map of BARCO Study Unit area including locations of the eight 30×60-minute quadrangles: C, Caliente; CM, Clover Mts.; O, Overton; CC, Cedar City; SG, St. George; L, Littlefield; P, Panguitch; K, Kanab. The Basin and Range province is shown by shaded ranges and unshaded basins, the transition zone is shown by a stipple pattern, and the Colorado Plateaus province is shown by a vertical line pattern. Heavy line fault; bar and ball on downthrown side.

The Basin and Range province has been extensionally deformed during the Neogene in an east-west direction. It is topographically expressed in eastern Nevada and western Utah by a series of north- to north-northeast-trending, roughly 10- to 20-km-wide bedrock ranges separated by 10- to 25-km-wide alluvial basins, and it is magmatically expressed by the most voluminous terrestrial record of silicic ash-flow tuff volcanism. In contrast, the Colorado Plateaus province remained an essentially undeformed stable highland, subjected only to minor peripheral basalt volcanism during the Cenozoic. We refer readers to several summaries of the geology of these two intermontane provinces that describe the contrasting generalized tectonic and magmatic histories and the crustal geophysical character of the regions; these summaries include those in Geological Society of America Memoir 172 (Anderson, 1989; Pakiser, 1989; Smith and others, 1989; Hamilton, 1989) and those by Gordon Eaton (Eaton, 1979; 1982). Although most of the modern topographic expression in the Basin and Range is the result of high-angle late Cenozoic Basin-Range-style normal faulting formed mostly since about 10 Ma, widespread evidence supports the existence of older, middle- Tertiary low-angle normal faults and detachment faults at depth (for example, Wernicke and others, 1988); this pattern of extensional faulting is further complicated by strike-slip faults related to the process of extension. Although in broad perspective, Cenozoic extension in the Basin and Range province is associated with silicic volcanism, in detail, volcanism and extension appear to be somewhat decoupled (Best and Christiansen, 1991).

The transition zone between stable Colorado Plateau and extensionally deformed Basin and Range is characterized by faults that are similar to those in the Basin and Range but generally show a decrease in abundance and amount of offset toward the plateau. A distinction based on degree of deformation alone, however, cannot be applied universally because the transition zone includes areas that have been more extensively deformed than some relatively undeformed areas within the Basin and Range. In general, we consider the transition zone to be bounded on the west by the Grand Wash–Gunlock fault zone and bounded on the east by an east-stepping margin marked by the Hurricane fault in the southeastern part, by the Toroweap-Sevier fault systems in the eastern part, and by the Paunsaugunt fault in the northeastern part of the BARCO area (fig. 2).

The status of mapping within the BARCO Study Unit area at the end of 1992 is shown in figure 3. Geologic maps published in conjunction with this Study Unit represent an area equivalent to about ninety 7.5-minute quadrangles.

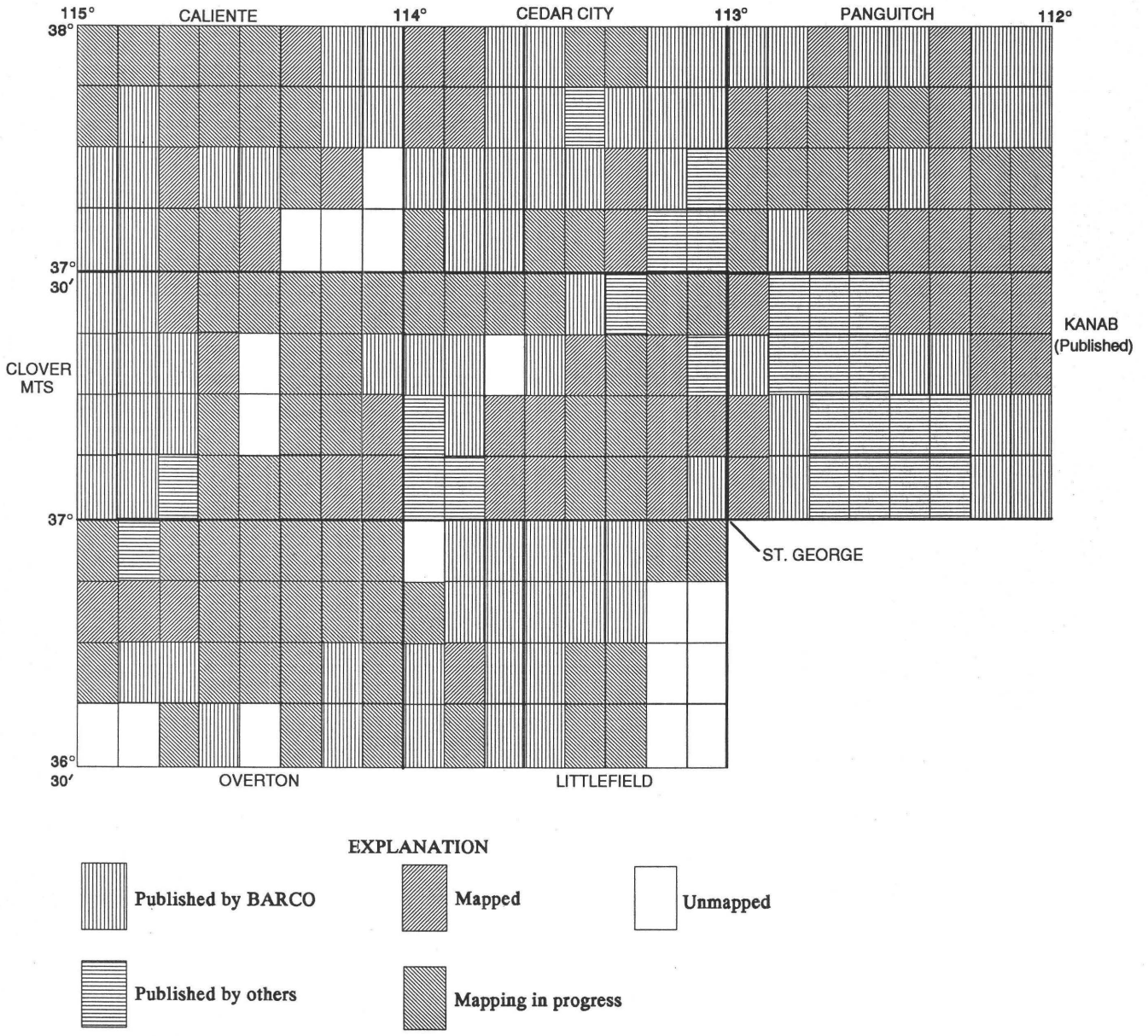

Figure 3. Map of the status of mapping in the BARCO Study Unit area at the end of 1992 by display of 7.5-minute quadrangles without regard to scale of mapping. The eight 30×60-minute quadrangles of the Study Unit are named on the margin.

Most of these maps are at scales of 1:24,000, but they also include smaller scales, for example, the 1:100,000-scale map of the Kanab 30×60-minute quadrangle. In addition, published maps covering an area equivalent to about twenty-five 7.5-minute quadrangles have been produced by geologists who have no association with this Study Unit. Unpublished mapping by geologists supported by the Study Unit covered an area equivalent to approximately fifty 7.5-minute quadrangles at the end of 1992. Finally, areas covering about seventy 7.5-minute quadrangles have been partially mapped, mostly by geologists associated with this Study Unit. Mapping scales range from 1:12,000 to 1:100,000 and are chosen to solve the geologic problems locally encountered. Many maps of the BARCO area are published as U.S. Geological Survey Open-File Reports to make them available for the public at the earliest possible date. Most maps are also being published as U.S. Geological Survey Geologic Quadrangle Maps (GQ maps), Miscellaneous Geologic Investigations Maps (I maps), or Miscellaneous Field Studies Maps (MF maps). Some mapped areas will remain unpublished at larger scales but will be directly incorporated into 1:100,000-scale syntheses of 30×60-minute quadrangle I maps. Still other maps are published cooperatively by the Utah Geological Survey.

The first part of this volume addresses stratigraphic, magmatic, and tectonic topics in the Basin and Range part of the BARCO area (fig. 2). Stratigraphic nomenclature is established for Oligocene and Miocene ash-flow tuffs that cover much of the Basin and Range in the BARCO area by correlation of cooling units, using petrographic, geochemical, paleomagnetic, and isotopic age data, in addition to knowledge gained by establishing relative stratigraphic position during detailed mapping. The locations and boundaries of the sources for several of these ash-flow tuffs are established or confirmed to be in the Indian Peak, Caliente, and Kane Springs Wash caldera complexes. Initial petrological investigations of several ash-flow tuffs are provided by preliminary isotopic and trace-element studies. Insight into the geometry, timing, and evolution of compressional and extensional tectonism that affected the BARCO area is also derived from relationships recognized from detailed mapping and paleomagnetic investigations. Stratigraphic studies also include correlations between some Quaternary and Tertiary alluvial units from separate basins within the BARCO area.

The second part of the volume concerns the transition zone west of the stable Colorado Plateau. Early Miocene deformation in the transition zone includes chaotic deformation of Oligocene and younger volcanic strata that overlie undeformed older sedimentary strata; the degree and areal extent of this shallow crustal deformation are considerably greater than that previously recognized or reported, and they present a contrast with deeper crustal detachment found in the Basin and Range. Deformation adjacent to the Hurricane fault includes an impressive 60-m offset of a middle Pleistocene geomorphic surface.

Acknowledgment.—We acknowledge the editing by L.M.H. Carter and the computer graphics efforts of Ramon E. Sabala, both of which improved the report and facilitated its completion.

REFERENCES CITED

Anderson, R.E., 1989, Tectonic evolution of the Intermontane System; Basin and Range, Colorado Plateau, and High Lava Plains, *in* Pakiser, L.C., and Mooney, W.D., eds., Geophysical framework of the Continental United States: Geological Society of America Memoir 172, p. 163–176.

Best, M.G., and Christiansen, E.H., 1991, Limited extension during peak Tertiary volcanism, Great Basin of Nevada and Utah: Journal of Geophysical Research, v. 96, p. 13509–13528.

Eaton, G.P., 1979, Regional geophysics, Cenozoic tectonics, and geologic resources of the Basin and Range province and adjoining regions, *in* Newman, G.W., and Goode, H.D., eds., Basin and Range Symposium and Great Basin Field Conference: Rocky Mountain Association of Geologists, Denver, Colo., and Utah Geological Association, Salt Lake City, p. 11–39.

———1982, Basin and Range province; Origin and tectonic significance: Annual Review of Earth and Planetary Sciences, v. 10, p. 409–440.

Hamilton, W.B., 1989, Crustal geologic processes of the United States, *in* Pakiser, L.C., and Mooney, W.D., eds., Geophysical framework of the Continental United States: Geological Society of America Memoir 172, p. 743–781.

Pakiser, L.C., 1989, Geophysics of the intermontane system, *in* Pakiser, L.C., and Mooney, W.D., eds., Geophysical framework of the Continental United States: Geological Society of America Memoir 172, p. 235–247.

Smith, R.B., Nagy, W.C., (Smith) Julander, K.A., Viveiros, J.J., Barker, C.A., and Gants, D.G., 1989, Geophysical and tectonic framework of the eastern Basin and Range–Colorado Plateau–Rocky Mountain transition, *in* Pakiser, L.C., and Mooney, W.D., eds., Geophysical framework of the Continental United States: Geological Society of America Memoir 172, p. 205–233.

Wernicke, Brian, Axen, G.J., and Snow, J.K., 1988, Basin and Range extensional tectonics at the latitude of Las Vegas, Nevada: Geological Society of America Bulletin, v. 100, p. 1738–1757.

Stratigraphic Relationships of Tertiary Volcanic Rocks in Central Lincoln County, Southeastern Nevada

By Robert B. Scott, C. Sherman Grommé, Myron G. Best, Joseph G. Rosenbaum, *and* Mark R. Hudson

GEOLOGIC STUDIES IN THE BASIN AND RANGE–COLORADO PLATEAU TRANSITION IN SOUTHEASTERN NEVADA, SOUTHWESTERN UTAH, AND NORTHWESTERN ARIZONA, 1992

U.S. GEOLOGICAL SURVEY BULLETIN 2056–A

UNITED STATES GOVERNMENT PRINTING OFFICE, WASHINGTON : 1995

CONTENTS

FIGURES

TABLE

Stratigraphic Relationships of Tertiary Volcanic Rocks in Central Lincoln County, Southeastern Nevada

By Robert B. Scott, C. Sherman Grommé, Myron G. Best,[1]
Joseph G. Rosenbaum, *and* Mark R. Hudson

ABSTRACT

Regional ash-flow sheets in central Lincoln County, Nevada, were deposited by major ash flows erupted initially from three major caldera complexes and finally from one small caldera complex in central and eastern Nevada active between about 30 and 13 Ma. The oldest of the outflow sheets (30–27 Ma) are large-volume, crystal-rich dacites; one sequence of ash flows, which formed the Needles Range Group, issued from the major Indian Peak caldera complex in northeastern Lincoln County and adjacent Utah, and a second sequence of ash flows ejected from the major Central Nevada caldera complex to form the Monotony Tuff. In contrast, younger pyroclastic rocks (27–22 Ma) are rhyolites that include the Leach Canyon Formation, probably derived from the major Caliente caldera complex in central Lincoln County, the Condor Canyon Formation, definitely derived from the Caliente caldera complex, and the Shingle Pass Tuff and Pahranagat Formation, certainly derived from the Central Nevada caldera complex. Intercalated between the Needles Range and Leach Canyon sheets are tuffs of the trachytic Isom Formation as well as other pre-Isom, Isom-compositional-type ash-flow tuffs, the sources for which are uncertain. The trachyandesitic to andesitic Harmony Hills Tuff (about 22 Ma), whose source close to the eastern end of the Caliente caldera complex remains uncertain, broke this chemical pattern. The last widespread calc-alkalic outflow sheet in the southeastern Great Basin, the rhyolitic Hiko Tuff (18.6 Ma), erupted from the western end of the Caliente caldera complex, although minor calc-alkalic activity persisted within that complex for several more million years. Subsequently, erupted magmas became more alkalic, even mildly peralkaline, forming a high-silica rhyolite-basalt association (16–14.5 Ma); ash flows and lavas erupted from the relatively small Kane Springs Wash caldera complex to form the Kane Wash Tuff, several older, chemically related ash-flow sheets, and overlying basalts in central and southern Lincoln County. This southward shift of volcanism and associated shift to more alkalic compositions are generally mirrored in time by similar shifts in space and composition by eruptive products of the Southwest Nevada volcanic field.

Several ash-flow tuffs with similar petrography, age, chemical composition, and distribution are here combined with the previously named Pahranagat Lakes Tuff to form the newly defined Pahranagat Formation. Recent changes in stratigraphic terminology restrict the Kane Wash Tuff that was derived from the youngest feature of the Kane Springs Wash caldera complex, the Kane Springs Wash caldera, to three ash-flow tuff cooling units. The lower cooling unit is the Grapevine Spring Member, the middle cooling unit is the lower part of the Gregerson Basin Member, and the upper cooling unit is the upper part of the Gregerson Basin Member; their new sanidine $^{40}Ar/^{39}Ar$ dates are 14.67±0.22 Ma, 14.55±0.14 Ma, and 14.39±0.28 Ma, respectively. Two older units, whose rocks were formerly included in the Kane Wash Tuff, now have new formation-status names, in ascending order the Delamar Lake Tuff and Sunflower Mountain Tuff, proposed because the magmas that supplied these tuffs were erupted from undefined sources, probably northwest and southwest of the Kane Springs Wash caldera, respectively. Wall segments of a precursor to the Kane Springs Wash caldera, the Narrow Canyon caldera that also erupted peralkaline magmas, are found just north of the Kane Springs Wash caldera. The youngest ash-flow tuff between the Caliente caldera complex and the Kane Springs Wash caldera is the rhyolitic tuff of Etna (about 14 Ma); it is distinctly older than the youngest ash-flow tuff in the Bull Valley Mountains area of Utah, the petrographically similar rhyolitic Ox Valley Tuff (about 12.5 Ma).

Detailed mapping in central Lincoln County indicates that drainage north of the Timpahute lineament was disrupted, probably by prevolcanic, top-to-the-east extension, forming a structural basin into which an intercalated sequence consisting of the Needles Range Group, lacustrine limestone, and fluvial clastic rocks accumulated, none of which are found south of the lineament. Progressive tilting and extension occurred between about 23 and 12 Ma in the South Pahroc Range and the Meadow Valley Mountains but not in the intervening Delamar Mountains. Although extension continued after 14.5 Ma, major tilting ceased after about 12 Ma, followed by basin-range faulting to the present.

[1]Myron G. Best, Brigham Young University, Provo, UT 84602.

INTRODUCTION

PURPOSE AND SCOPE

The purpose of this report is to describe the progress of stratigraphic investigations of widespread Oligocene and Miocene volcanic units in the central part of Lincoln County, southeastern Nevada. These investigations are part of the Basin and Range to Colorado Plateau Transition (BARCO) Study Unit of the U.S. Geological Survey National Geologic Mapping Program (figs. 1, 2). (Also see figures 1, 2, and 3 in Introduction to volume.) Because most of the volcanic rocks are regional ash-flow tuffs, covering much of southeastern Nevada and southwestern Utah, correlation between tuffs is the key to recognition of stratigraphic relationships in this area. In addition to detailed mapping (fig. 2, and also fig. 3 of Introduction to volume), we correlated these ash-flow sheets by using geochronologic, paleomagnetic, petrographic, and to some degree geochemical data. These stratigraphic studies allowed us to identify nested caldera complexes (fig. 1), but we do not discuss here post-collapse intracaldera volcanic units. Also these multidisciplinary

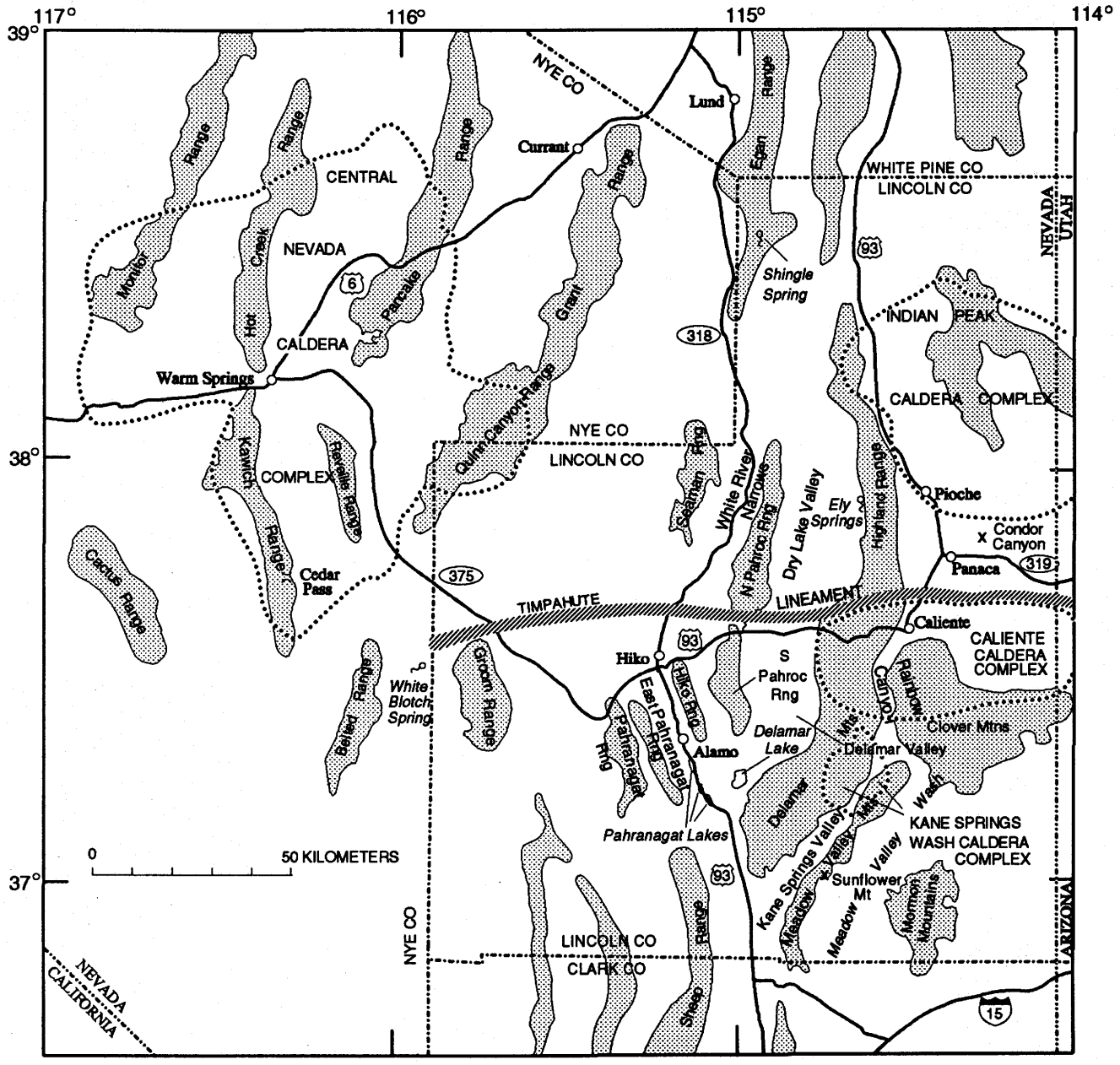

Figure 1. Geographic and geologic features in southeastern and central Nevada. Light lines and pattern delineate ranges. Dotted lines delineate approximate margins of caldera complexes. Timpahute lineament from Ekren and others (1976).

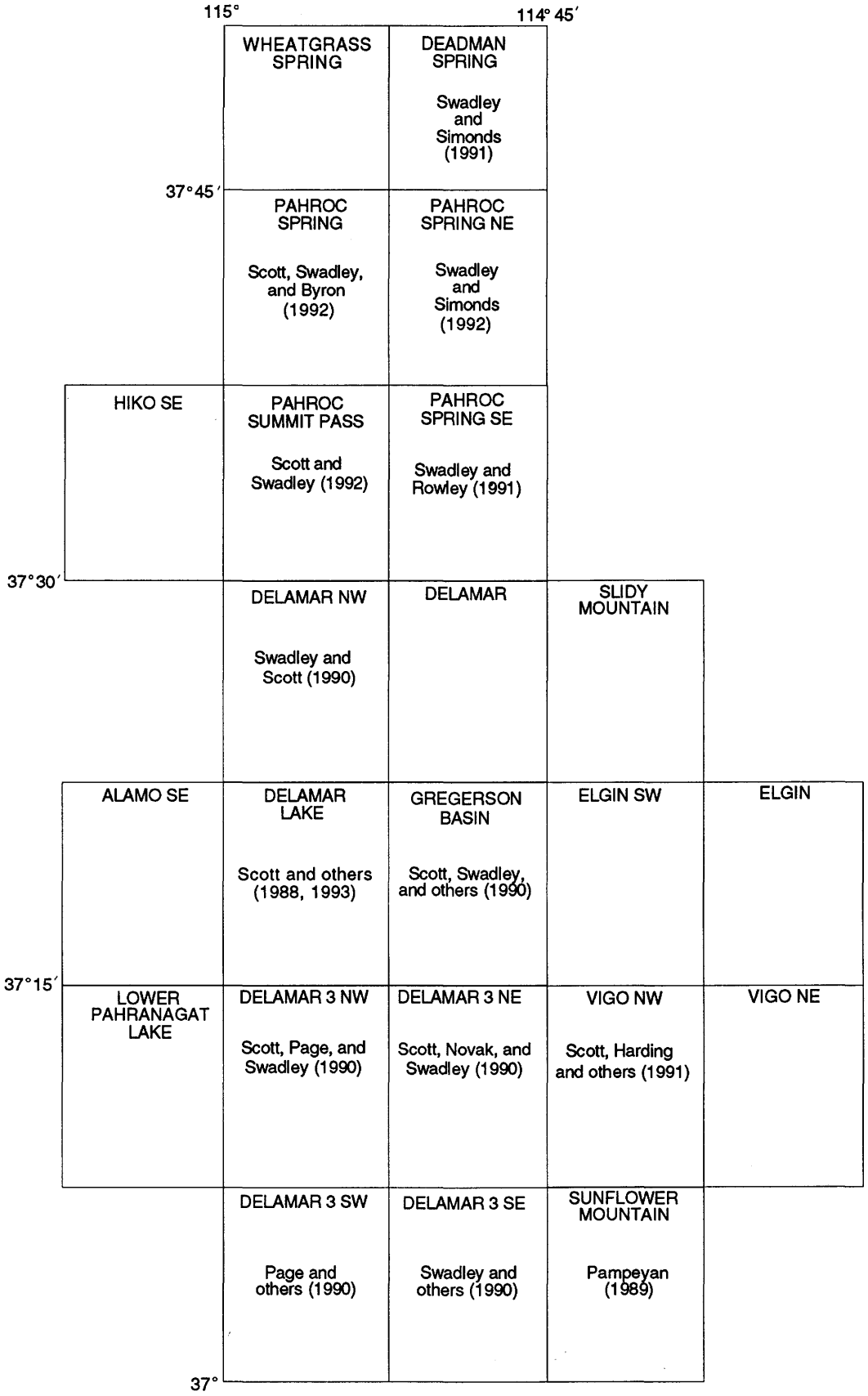

Figure 2. Location of 7.5-minute quadrangles in central Lincoln County, Nevada, discussed in this report. Reference to published maps indicated.

stratigraphic studies have provided us with the means to recognize new ash-flow tuffs intercalated within the framework of previously recognized and named tuffs. Although we briefly discuss Tertiary sedimentary units because of their importance to tectonic interpretations, we do not attempt correlations of units between sedimentary basins. This report is supplemented by two accompanying stratigraphic studies in this volume, one by Harding and others on volcanic units associated with the eastern part of the Kane Springs Wash caldera, and the other by Rowley and others on volcanic units associated with the Caliente caldera complex.

ACKNOWLEDGMENTS

The authors of this manuscript received support through the U.S. Geological Survey National Geologic Mapping Program. We enjoyed the luxury of new K-Ar and $^{40}Ar/^{39}Ar$ data from Harald H. Mehnert and Lawrence W. Snee that provided us with important time constraints. The background of knowledge in the area provided by R. Ernest Anderson and Peter D. Rowley was a critical resource and an inspiration to us. W C (Dub) Swadley, W. Ric Page, and Steve W. Novak contributed significantly to the mapping effort; Novak provided us with a copy of his dissertation and maps (Novak, 1985). Two student volunteers to the U.S. Geological Survey, Anne E. Harding (University of Colorado) and Barbara Byron (Fort Lewis College) helped in the mapping. Myron G. Best's research in the Great Basin was also supported by Brigham Young University and the National Science Foundation through grants EAR-8604195, 8618323, and 8904245. We thank Ren A. Thompson and Peter D. Rowley for constructive review of the manuscript.

GEOLOGIC SETTING AND PREVIOUS WORK

Mackin (1960), followed by his students Cook (1965) and Williams (1967), pioneered work on the volcanic stratigraphy of southwestern Utah and southeastern Nevada, recognizing that individual cooling units of ash-flow tuffs could be correlated by comparison of phenocryst abundance ratios. Noble (1968), Novak (1984), and Novak and Mahood (1986) studied ash-flow tuffs in the area of Kane Springs Wash caldera. Ekren and others (1977) mapped the distribution of major chronologic groups of Tertiary volcanic rocks in Lincoln County, Nev., at a scale of 1:250,000. Pampeyan (1989) mapped the Meadow Valley Mountains at a 1:50,000 scale. A review of previous isotopic dates for each stratigraphic unit is in table 1.

By far, most Tertiary volcanic rocks in southeastern Nevada and southwestern Utah are ash-flow tuff. These regionally extensive ash-flow sheets are commonly tens, and in some places hundreds, of meters thick, extend more than 100 km from their source, and total thousands of cubic kilometers of eruptive material (Best, Christiansen, and others, 1989). Magma systems that fed these voluminous pyroclastic eruptions are marked by large caldera complexes tens of kilometers across, consisting of nested and partially overlapping calderas commonly identified on the basis of thick (commonly 2 km) prisms of intracaldera tuffs that are correlated to outflow deposits by their similar petrologic character, paleomagnetic direction, and precise $^{40}Ar/^{39}Ar$ dates. Intracaldera tuffs are commonly intercalated with coarse caldera collapse breccias and landslide blocks during and following explosive eruption. Numerous calderas occur in Lincoln County (fig. 1): the Oligocene Indian Peak caldera complex (Best, Christiansen, and Blank, 1989) lies along the Nevada-Utah border in northeastern Lincoln County; the Miocene Caliente caldera complex (Rowley and others, this volume) extends from central Lincoln County, Nev., eastward to western Utah; and the smaller middle Miocene Kane Springs Wash caldera is exposed in southern Lincoln County in both the Delamar Mountains (Novak, 1984) and the Meadow Valley Mountains in southern Lincoln County (Harding and others, this volume). Most ash-flow sheets in Lincoln County were derived from these three sources or from the Central Nevada caldera complex 70 to 170 km to the west (fig. 1) (Best and others, 1992). Reconnaissance mapping by us indicates that additional sources of thin, densely welded, trachytic ash-flow tuffs (Isom Formation and chemically and lithologically similar units) probably exist in the vicinity of the Indian Peak and Caliente caldera complexes and west of the North Pahroc Range (fig. 1). The area between the three major caldera complexes was repeatedly flooded by large-volume ash flows erupted from the magma systems between late Oligocene and middle Miocene, forming a remarkable "outflow alley" of as many as 20 outflow sheets. Stacks of tuff sheets exposed in tilted and uplifted ranges include few intervening lava flows and sedimentary deposits (Best and Christiansen, 1991).

Although rhyolite tuffs occur throughout the Tertiary of the Great Basin, petrographic and bulk chemical analyses reveal that ash-flow tuffs of particular compositions were deposited at particular times in the Great Basin (Scott and others, 1971; Best, Christiansen, and others, 1989). Northwest of central Lincoln County, early Oligocene tuffs are for the most part quartz-rich, biotite-bearing rhyolite. The most voluminous late Oligocene (about 31–27 Ma) tuffs between central Nevada and southwestern Utah are crystal-rich dacite of a chemical compositional type characterized by the Monotony Tuff. These dacitic tuffs were overlain in the latest Oligocene and earliest Miocene (about 27–23 Ma) by widespread rhyolitic ash-flow tuffs, intercalated with widespread crystal-poor ash-flow tuffs of a distinct calc-alkalic trachytic composition characterized by the Isom Formation (Christiansen and Best, 1989; Christiansen and others, 1989). These younger, mostly rhyolitic ash-flow tuffs

are again dominantly calc-alkalic. Still younger ash-flow tuffs (<about 17 Ma) are alkalic to peralkaline; peralkaline tuffs include the sanidine-quartz-hedenbergite-fayalitic olivine-bearing rhyolite outflow sheets (14.5 Ma) derived from the Kane Springs Wash caldera complex that includes those chemically related products from the precursor Narrow Canyon caldera (Scott, Blank, and Page, 1991).

The timing and nature of Tertiary extensional tectonism were heterogeneous within the Basin and Range province, and tectonism appears not to be directly related in time or space to Tertiary volcanism (Best and Christiansen, 1991; Taylor and Bartley, 1992; Scott, 1990). In northern Lincoln County and surrounding areas to the east in southwestern Utah and the west in Nye County, Nev., three major tectonic periods are recognized (Bartley and others, 1988; Taylor and others, 1989). The earliest period is characterized by prevolcanic (pre-30.6 Ma) Paleogene faults, principally the top-to-the east, low-angle Stampede detachment fault and related high-angle normal faults (Axen and others, 1988; Rowley and others, 1992) that our mapping restricts to latitudes north of the east-striking Timpahute lineament of Ekren and others (1976). Taylor and Bartley (1992) suggested that the Stampede detachment may be part of a larger system of prevolcanic faults above their proposed detachment of the east-directed Seaman breakaway fault.

The main episode of extension occurred between at least 19 Ma and about 12 Ma; the faults of this episode form complex patterns of high-angle strike-slip, oblique-slip, and normal faults and low-angle normal faults (Rowley and others, 1992; Axen and others, 1988; Anderson and Hintze, 1993). Unlike the prevolcanic episode and the youngest episode, the main episode of extension generally overlaps with the period of volcanic activity in the Caliente caldera complex (Rowley and others, 1992; Angelier and others, 1987; Bowman, 1985). Of the strike-slip faults, those with north to northeast strikes are sinistral, and those with east or northwest strikes are dextral (Rowley and others, 1992; Anderson and Hintze, 1993). The major low-angle fault of this episode is the top-to-the-west Highland detachment that was active about 15 Ma in the Highland Range (Axen and others, 1988) and has been mapped north of the Caliente caldera complex (Rowley and others, 1992; Rowley and others, 1991). Although many strike-slip faults have offsets of at least 1 km as far south as the northern margin of the Kane Springs Wash caldera, they are not present south of that caldera (Scott, Swadley, and others, 1990). Progressive tilting restricted to the northern and central Meadow Valley Mountains and to the South Pahroc Range records this episode of extension south and northwest of the Kane Springs Wash caldera in Lincoln County (Scott, Harding, and others, 1991). This main episode of extension overlaps partly with the slightly younger principal phase of extension that occurred between 15 and 10 Ma near the latitude of Las Vegas, Nev., largely south of Lincoln County (Wernicke and others, 1988).

Basin-range faults have controlled the major north- to north-northeast-trending topographic grain of this part of the Basin and Range province since at least 10 Ma into the Quaternary (Anderson and others, 1983; Tschanz and Pampeyan, 1970; Ekren and others, 1977). These faults postdate basalts that have ages of 12.7 to 11.5 Ma (Snee and others, 1990). The direction of the minimum horizontal stress for these normal fault systems is west-northwest, a change of about 60° from the previous west-southwest minimum stress direction (Anderson, 1989; Zoback and others, 1981).

Since 1988, a team of geologists in the U.S. Geological Survey, academic institutions, State geological surveys, and volunteers have been mapping in southwestern Utah, southeastern Nevada, and northwestern Arizona across the transition from the Colorado Plateau to the Basin and Range. As part of this team effort, a block of quadrangles in central Lincoln County, Nev., have been mapped at a scale of 1:24,000 (fig. 2, and also see fig. 3 of the Introduction to volume); this work forms the basis for many conclusions reached in this report. The maps shown in figure 2 are exclusive of other mapping by the team in Lincoln County by Rowley and others (this volume), Keith and others (1992), Best and others (1991), Anderson and Hintze (1993), and Pampeyan (1989).

CORRELATION METHODS

In our study, careful attention to stratigraphic position, field characteristics, chemical composition, and phenocryst mineralogy enabled successful correlation of many ash-flow tuffs, but most remaining stratigraphic ambiguities were resolved by the added constraints provided by paleomagnetic data and isotopic dating.

One of the most powerful correlation tools is modal analyses of phenocrysts, particularly the comparison of ratios of phenocryst abundances, as introduced by Mackin (1960) and his students, Cook (1965) and Williams (1967); compaction in ash-flow tuffs changes abundances of phenocrysts by as much as a factor of two but not ratios of phenocryst abundance. Phenocryst volume percent was determined in this study by point counting 200–1,000 counts of phenocrysts per thin section stained for potassium feldspar.

Where differences in age between stratigraphic units were greater than about 1 m.y., stratigraphic correlation ambiguities could be resolved by conventional K-Ar dating. H.H. Mehnert (U.S. Geological Survey) considerably aided our correlations by conventional K-Ar dating, using the methods of Dalrymple and Lanphere (1969) and the constants of Steiger and Jäger (1977). Where more precise isotopic dating was required to resolve differences less than 1 m.y., L.W. Snee (U.S. Geological Survey) used the $^{40}Ar/^{39}Ar$ dating method to obtain dates with a 2-sigma error less than 0.3 m.y. using the methods of Shubat and Snee (1992).

Another powerful correlation technique used in our study has been the comparison of paleomagnetic directions of ash-flow cooling units. Ash-flow tuffs acquire stable thermoremanent magnetization parallel to the ambient geomagnetic field during initial cooling. In nearly all instances, plastic deformation (compaction or rheomorphism) ceases at a higher temperature than the Curie point (630° C or less), so that the magnetization direction remains undistorted; however, a notable exception to this rule is the Swett Tuff Member of the Condor Canyon Formation in eastern Condor Canyon (Gose, 1970). Typical intensities of natural thermoremanent magnetization range from 0.01 to 0.5 A/m (amperes/meter).

The geomagnetic field exhibits two sorts of time variations in direction that enable correlation or lack of correlation of tuff sheets by means of their natural remanent magnetization directions. (1) *Secular variation* follows a randomly directed but continuous looping path with a characteristic time constant of one to a few centuries and an amplitude of 10° to 20° of arc. The time-averaged center of secular variation, the center of its probability distribution, is the direction corresponding to a geocentric axial dipole. (2) *Reversal of polarity* exhibits a characteristic frequency of a few thousand centuries but a random likelihood of occurrence. Thus, the geomagnetic field has two maximally stable states, normal and reversed. Clearly, if two ash-flow sheets have paleomagnetic directions that are opposite in polarity or differ greatly from one another, they cannot have been erupted at the same time. Conversely, if two otherwise similar ash-flow occurrences also have paleomagnetic directions that are not significantly different from one another, the probability that they could have resulted from the same eruption depends on how far their common direction is from the nearest stable axial dipole field direction (Cox, 1971; Bogue and Coe, 1981). The more unusual the magnetization direction is relative to the normal or reversed axial dipole direction, the greater is the strength of the correlation. For the purpose of this report, the stable normal axial dipole field direction is taken to be that at Caliente, Nev., having inclination 55.9° downward and declination 351.6° E., as calculated from the Oligocene reference paleomagnetic pole position for North America given by Diehl and others (1983).

Where ash-flow sheets have been tilted, the measured paleomagnetic directions require corrections to directions one would observe in equivalent horizontal sheets. Where possible, structural attitudes are measured in the field on the planar tops of ash-flow tuff sheets. Because of exposure limitations, however, one must generally measure the attitude of the eutaxitic compaction foliation within the tuff sheet. Where tuffs have been draped over appreciable pre-eruption topographic relief, the distortion of foliation attitudes cannot be evaluated (Hagstrum and Gans, 1989); hence pre-eruption topography may result in errors in paleomagnetic directions if structural corrections have to be made. This effect would be expected to diminish upward in a single thick tuff sheet or in a sequence of several sheets (Cook, 1965, p. 44). For these reasons, we have always attempted to sample continuous stratigraphic sequences rather than isolated exposures of ash-flow tuffs. Nearly all samples were collected from outflow sheets, although some were obtained from intracaldera tuffs at the source.

Eight or more oriented cores were collected from each site using a portable gasoline-powered diamond drill. Azimuthal orientation was both by magnetic and by sun compass. Remanent magnetizations were measured with a commercial superconducting magnetometer or a commercial spinner magnetometer, and all demagnetizations were done with commercial 400-Hz alternating-field (af) tumbling apparatus. For most sites, pilot demagnetizations of one specimen from each of two cores was done over 10 steps to 100 mT. From these results, four appropriate steps were chosen to demagnetize one specimen from each remaining core. For the remaining sites, all samples were subjected to stepwise af demagnetization over eight steps to 80 mT. Demagnetization directions for each specimen were calculated using principal component analysis (Kirschvink, 1980). Mean directions and statistics and, in most cases, mean poles to bedding attitudes for each site were calculated by the method of Fisher (1953).

STRATIGRAPHIC RELATIONSHIPS

PREVOLCANIC SEDIMENTARY ROCKS

In central Lincoln County, most of the oldest Tertiary volcanic strata rest directly on the angular unconformity above Paleozoic rocks deformed along the Sevier orogenic belt (Armstrong, 1968), but in some places prevolcanic Tertiary sedimentary deposits intervene. The character of these sedimentary rocks is summarized here because interpretation of their depositional environment constrains interpretation of prevolcanic tectonism in this part of the Basin and Range province. We have not attempted to correlate them with established older prevolcanic Tertiary stratigraphic units such as the Claron Formation of latest Cretaceous(?) or Paleocene(?) into Oligocene age (Anderson and Rowley, 1975; Taylor, 1993) because we have no reliable age control.

The oldest prevolcanic unit noted here may be a well-cemented, poorly sorted, grayish-pink to light-gray, boulder to pebble conglomerate consisting of well-rounded Paleozoic carbonate and quartzite clasts. About 100 to 150 m of this conglomerate occurs roughly conformably between the 23-Ma Bauers Tuff Member of the Condor Canyon Formation and the Cambrian Highland Peak Formation 7 km north-northwest of the Kane Springs Wash caldera on the western side of the Delamar Mountains (Ekren and others, 1977; Scott, Swadley, and others, 1990) (fig. 1). Tschanz and Pampeyan (1970) suggested that the conglomerate may be

Cretaceous to Tertiary in age, but they had no age control. The highly cemented character of the conglomerate may have resulted not from greater age but from contact metamorphism by an adjacent Miocene stock that also recrystallized the limestone and dolomite of the Highland Peak Formation to marble. Boulders 0.5 m across occur at the base, but higher in the sequence the conglomerate consists of 70 percent pebbles in a sand matrix.

At the southern end of the Delamar Mountains and on the western side of the Meadow Valley Mountains, prevolcanic Tertiary conglomerate and subordinate sandstone, shale, and limestone locally overlie an angular unconformity above Cambrian through Pennsylvanian strata. On the eastern side of the Delamar Mountains about 6 km south of the Kane Springs Wash caldera, 60 m of pale-red conglomerate with a ferruginous, calcareous cement are interbedded with sandstone, shale, and limestone (Swadley and others, 1990). The sandstone and shale are thin to medium bedded and are crossbedded in part. As much as 75 m of a lithologically similar unit is locally present along the western side of the southern end of the Delamar Mountains (Page and others, 1990). This unit thins to 7 m of pale-red conglomerate overlain by 3–7 m of very light gray, medium-grained, recrystallized lacustrine limestone 10 km to the north on the western side of the Delamar Mountains (Scott, Page, and Swadley, 1990). A very light gray to pinkish-gray, lacustrine limestone containing recrystallized disrupted algal plates is locally present at the base of the volcanic sequence in the Meadow Valley Mountains and is as much as 55 m thick (Scott, Harding, and others, 1991).

All these prevolcanic sedimentary units that occur south of the Timpahute lineament (fig. 1) are relatively thin and discontinuous. In the absence of evidence of erosion or angular unconformities above these deposits, we consider their depositional basins to have been isolated from one another. We also conclude that the small thicknesses of conglomerates and lacustrine limestones are evidence that only relatively minor tectonic disruption of drainage occurred in the Tertiary before initiation of voluminous volcanism south of the Timpahute lineament. However, the angular unconformity above prevolcanic conglomerate in the North Pahroc Range suggests that pre-30.6-Ma extension (Taylor, 1989) probably affected the area north of the Timpahute lineament to a greater degree than areas south of the lineament.

CALC-ALKALIC VOLCANIC ROCKS

NEEDLES RANGE GROUP

The Needles Range Formation was originally defined by Mackin (1960); this definition was elaborated by Best and others (1973). Subsequently, S.K. Grant (Best and Grant, 1987) recognized that, in addition to the crystal-rich dacite tuffs that make up the greatest volume erupted from the Indian Peak caldera complex, rhyolite tuffs, which are chiefly found within the caldera complex, were also erupted from the same long-lived magma system. Thus, Best and Grant (1987) raised the Needles Range unit to group rank to include all dacitic and rhyolitic intracaldera and outflow deposits associated with the Indian Peak caldera complex (Best, Christiansen, and Blank, 1989) (fig. 1).

The three large-volume, crystal-rich, dacite ash-flow sheets of the Needles Range Group are (from oldest to youngest) the Cottonwood Wash Tuff, the Wah Wah Springs Formation, and the Lund Formation and are restricted to the northern part of Lincoln County, north of the Timpahute lineament. All three units are compositionally similar to the dacite tuff of the Monotony Tuff (fig. 3) and therefore are included as part of the so-called Monotony compositional type. (See Best, Christiansen, and others, 1989, fig. 6.) The dacite tuffs of the Needles Range Group and the Monotony Tuff are crystal rich, and contain dominant plagioclase and lesser amounts of quartz, biotite, hornblende, and pyroxene, but are petrographically distinguishable (fig. 4). The Cottonwood Wash is distinguished by the presence of uncommonly large books of biotite (as much as 8 mm in diameter), large embayed quartz, and lesser amounts of hornblende, the Wah Wah Springs by the absence of sanidine but relative abundance of hornblende, and the Lund by the relative abundance of quartz and accessory sphene (fig. 4). In addition to these dacitic units, a relatively small volume rhyolite tuff unit, the Mackleprang Tuff Member of the Ryan Spring Formation, characterized by phenocrysts of plagioclase and biotite, occurs locally near the southern and western margin of the Indian Peak caldera complex between the Wah Wah Springs and Lund units.

The Cottonwood Wash Tuff, Wah Wah Springs Formation, and Lund Formation have been mapped in the North Pahroc Range (Taylor, 1989; Scott, Swadley, and Byron, 1992). In the field, the Cottonwood Wash Tuff is distinguished by the largest biotite books and a distinctive pale-greenish-yellow to pale-olive color, and the Lund Formation has the smallest biotite books, which are not aligned as well to the plane of compaction as those of the other two units. All three units are separated from one another by tens of meters of interbedded boulder conglomerate and lacustrine limestone. The clasts in the conglomerate consist of Paleozoic dolomite, limestone, and quartzite boulders as much as 2 m across. The southernmost exposures of all these volcanic and sedimentary units lie just north of the Timpahute lineament (fig. 1) (Ekren and others, 1976), suggesting that the lineament may have presented a topographic barrier to the southward spread of ash-flow tuffs about 30–28 Ma (Best, Christiansen, and Blank, 1989). Locally, the Lund Formation is overlain by interbedded lacustrine limestones and conglomerate (0–60 m thick), similar to those between formations of the Needles Range Group except that the clast size is smaller and the conglomerate is less abundant.

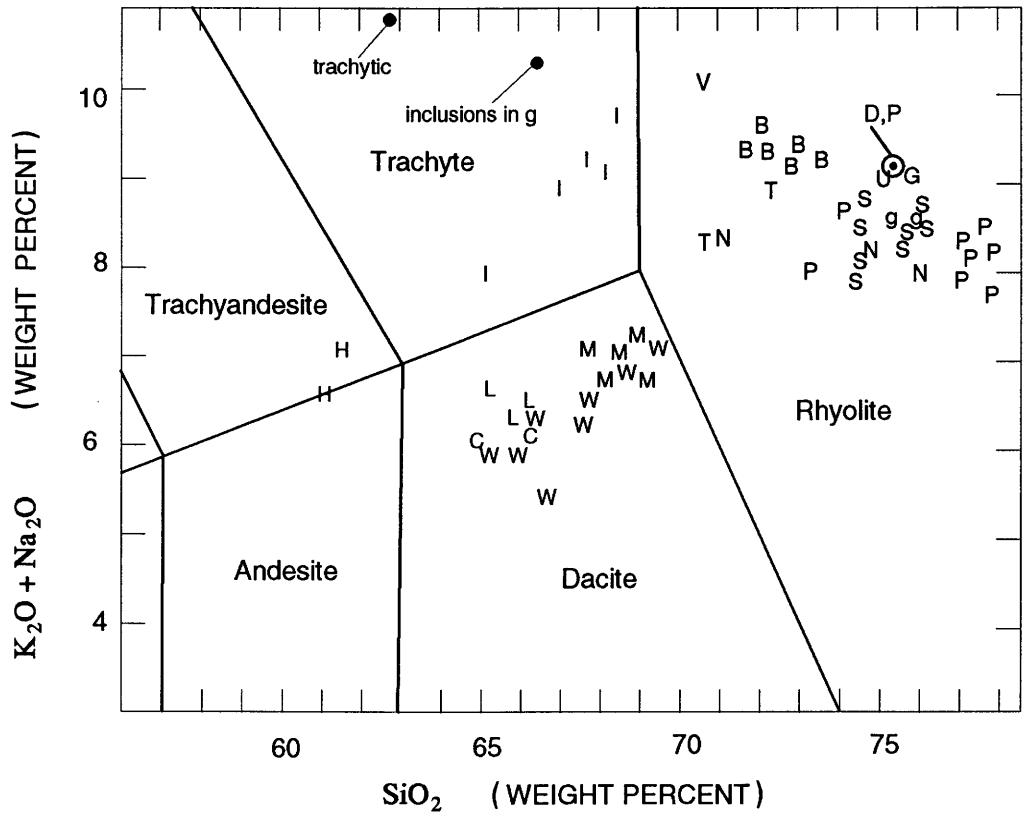

Figure 3. IUGS classification (Le Maitre, 1989) of ash-flow tuff units. Data from Best, Christiansen, and Blank (1989), Williams (1967), Phillips (1989), Novak (1984), Harding and others (this volume), and unpublished data of M.G. Best and R.B. Scott. G, upper cooling unit of Gregerson Basin Member of Kane Wash Tuff; g, lower cooling unit of Gregerson Basin Member of Kane Wash Tuff; V, Grapevine Spring Member of Kane Wash Tuff; U, Sunflower Mountain Tuff; D, Delamar Lake Tuff; H, Harmony Hills Tuff; P, Pahranagat Formation; B, Bauers Tuff Member of Condor Canyon Formation; T, Swett Tuff Member of Condor Canyon Formation; N, Leach Canyon Formation; S, Shingle Pass Tuff; I, Isom Formation; M, Monotony Tuff; L, Lund Formation; W, Wah Wah Springs Formation; C, Cottonwood Wash Tuff. For chemical data on the tuff of Etna and the Hiko Tuff, see Rowley and others (this volume).

These four formations of the Needles Range Group were sampled for paleomagnetic character east of Ely Springs, Nev. Our results for the dacite units do not differ significantly from those of Shuey and others (1976) and Nairn and others (1975). We have also obtained supplementary paleomagnetic data for the Wah Wah Springs and Lund Formations at White River Narrows and Condor Canyon. The Cottonwood Wash Tuff has normal magnetic polarity with large between-site dispersion of paleomagnetic directions that generally are within 30° of the Oligocene axial dipole field direction. The Wah Wah Springs is reversely magnetized with low between-site dispersion of directions and a magnetic inclination that is systematically about 25° shallower than the Oligocene axial dipole field direction. The Mackleprang Tuff Member is also reversely magnetized, but with a steep magnetic inclination; its direction is about 40° different from that of the Wah Wah Springs. The Lund has normal magnetic polarity with a large between-site dispersion of directions, and its direction is similar to that of the Cottonwood Wash Tuff, though a pair of geomagnetic reversals intervened between them. At Ely Springs and at White River Narrows, the Lund Formation underlies the reversely magnetized trachytic Petroglyph Cliff Ignimbrite; at Ely Springs another reversely magnetized trachytic tuff of unknown provenance occurs between them.

Ages of the dacitic formations of the Needles Range Group are not precisely known, in spite of numerous K-Ar dates of the units (table 1). For example, although the average age of 16 dates for the Wah Wah Springs Formation is 29.5 Ma (Best and Grant, 1987), subsequent $^{40}Ar/^{39}Ar$ dating of volcanic units older and younger than the Wah Wah Springs indicates that this date is too young, possibly by as much as 1 million years (Best and others, 1993, table 1).

PETROGLYPH CLIFF IGNIMBRITE OF COOK (1965)

The type section of the Petroglyph Cliff Ignimbrite of Cook (1965) is at White Rock Spring, a few kilometers north

of White River Narrows on the eastern flank of the Seaman Range (fig. 1). Martin (1957) referred to these same rocks as the White Rock Spring ignimbrite unit. The Petroglyph Cliff Ignimbrite is a trachytic(?) ash-flow tuff that contains 10–15 percent phenocrysts consisting of about 80 percent plagioclase and 20 percent clinopyroxene and orthopyroxene. This unit has the phenocryst mineralogy and thin, highly welded ash-flow tuff morphology typical of the Isom Formation (described in a following section), but is unusual among Isom compositional-type ash-flow tuffs in containing a high concentration of apparently cognate lapilli and blocks (Best, Christiansen, and others, 1989). Commonly, lapilli have been welded to large fiamme flattened parallel to the plane of foliation; where chilled they are black vitrophyres, and where devitrified they range from moderate orange pink to moderate red in a lighter colored matrix.

At White Rock Spring, the Petroglyph Cliff Ignimbrite underlies the Monotony Tuff. We should point out, moreover, that at the Petroglyph Cliff itself, the Petroglyph Cliff Ignimbrite is present only below ground level; the petroglyphs were carved in the Monotony Tuff. The Petroglyph Cliff Ignimbrite is reversely magnetized both at White Rock Spring and Ely Springs (fig. 1), the only localities where we have identified it paleomagnetically.

In the North Pahroc Range, three and probably four Isom compositional-type cooling units occur at the general stratigraphic position occupied by the Petroglyph Cliff Ignimbrite of Cook (1965), that is, above the Lund Formation and below the Monotony Tuff. In ascending order these are (1) a lowest cooling unit, (2) the cooling unit that is lithologically correlative with the Petroglyph Cliff Ignimbrite at White Rock Spring, (3) a vitrophyric cooling unit, and (4) a devitrified cooling unit. The lowest, the vitrophyric, and the devitrified cooling units have been recognized only locally in the North Pahroc Range. The lowest cooling unit (1) resembles the Petroglyph Cliff Ignimbrite (2) except for a greater abundance of large fiamme; the lowest cooling unit (1) is present only in the central part of the Wheatgrass Spring quadrangle, where it is separated from the overlying Petroglyph Cliff (2) by a bedded tuff. The largely vitrophyric cooling unit (3) differs from the Petroglyph Cliff (2) by containing distinctly smaller pumice fiamme and by having no cognate blocks. The vitrophyric cooling unit is locally present in both the Pahroc Spring and the Wheatgrass Spring quadrangles. The devitrified cooling unit (4) is lithologically indistinguishable from the Petroglyph Cliff Ignimbrite (2) but is separated from the Petroglyph Cliff (2) by a local andesite flow in the northern part of the Wheatgrass Spring quadrangle. The abundance of cooling units in the North Pahroc Range that closely resemble the Petroglyph Cliff Ignimbrite suggests that the source of these ash-flow tuffs is probably close by. Possible petrological associations with the Petroglyph Cliff Ignimbrite remain to be investigated.

In both the Wheatgrass Spring and Pahroc Spring quadrangles a very light gray to medium-light-gray nonwelded tuff containing abundant unflattened pumice fragments commonly overlies the Petroglyph Cliff Ignimbrite. This nonwelded tuff definitely is not petrologically associated with the Petroglyph Cliff Ignimbrite because the nonwelded tuff has significantly lower rare earth element, zirconium, iron, and strontium abundances than the Isom compositional-type tuffs. The pore spaces in the nonwelded tuff commonly have been partly filled by calcite, probably derived from the depositional environment of thin lacustrine limestones, which occur above and below the nonwelded tuff (Scott, Swadley, and Byron, 1992).

As previously mentioned, at Ely Springs (fig. 1), below the Petroglyph Cliff and an underlying lava, another unnamed trachytic tuff occurs above the Lund Formation; whether this oldest trachytic tuff is associated petrologically with the Petroglyph Cliff Ignimbrite or Isom compositional-type tuffs also remains to be studied. If future investigations confirm that all these units are indeed related petrologically, the eruptive events related to the emplacement of the Petroglyph Cliff Ignimbrite may be considerably more complex than previously suspected.

MONOTONY TUFF

This crystal-rich dacite ash-flow tuff (figs. 3, 4) was referred to as the tuff of Monotony Valley by Cornwall (1972) and was defined as the Monotony Tuff by Ekren and others (1971), who noted its widespread and thick occurrence in central Nye and northwestern Lincoln Counties. They suggested that the unit has a volume of more than 2,900 km^3 and a source in the southern Pancake Range. Subsequent geologic mapping in that area, summarized in Ekren and others (1974; see especially p. 607), disclosed segments of a northern caldera wall, labeled the Pancake Range caldron by Ekren and others (1972). Sargent and Roggensack (1984) referred to the Pancake Range caldera, but did not associate it with the Monotony Tuff. Best and others (1992; see also Best, Christiansen, and others, 1989, p. 114) subsequently accepted the Pancake Range caldera in the Central Nevada caldera complex as the source area for the Monotony, somewhat modified its boundary and relation to other calderas, and assigned an age of 27.3 Ma to the Monotony Tuff (table 1).

The Monotony compositional type is, of course, named after the Monotony Tuff and is represented by the compositional variation of the Monotony Tuff and the dacite tuffs of the Needles Range Group in figure 3. (Also see Best, Christiansen, and others, 1989, fig. 6.) The Monotony contains 20–60 percent phenocrysts that consist of 2–15 percent quartz, 5–25 percent sanidine, 45–65 percent plagioclase, 5–20 percent biotite, 0–10 percent hornblende, 0–10 percent clinopyroxene, and Fe-Ti oxides (fig. 4). Ekren and others (1971) noted the lithologic similarity of the Monotony Tuff to the Needles Range Group, but distinctions

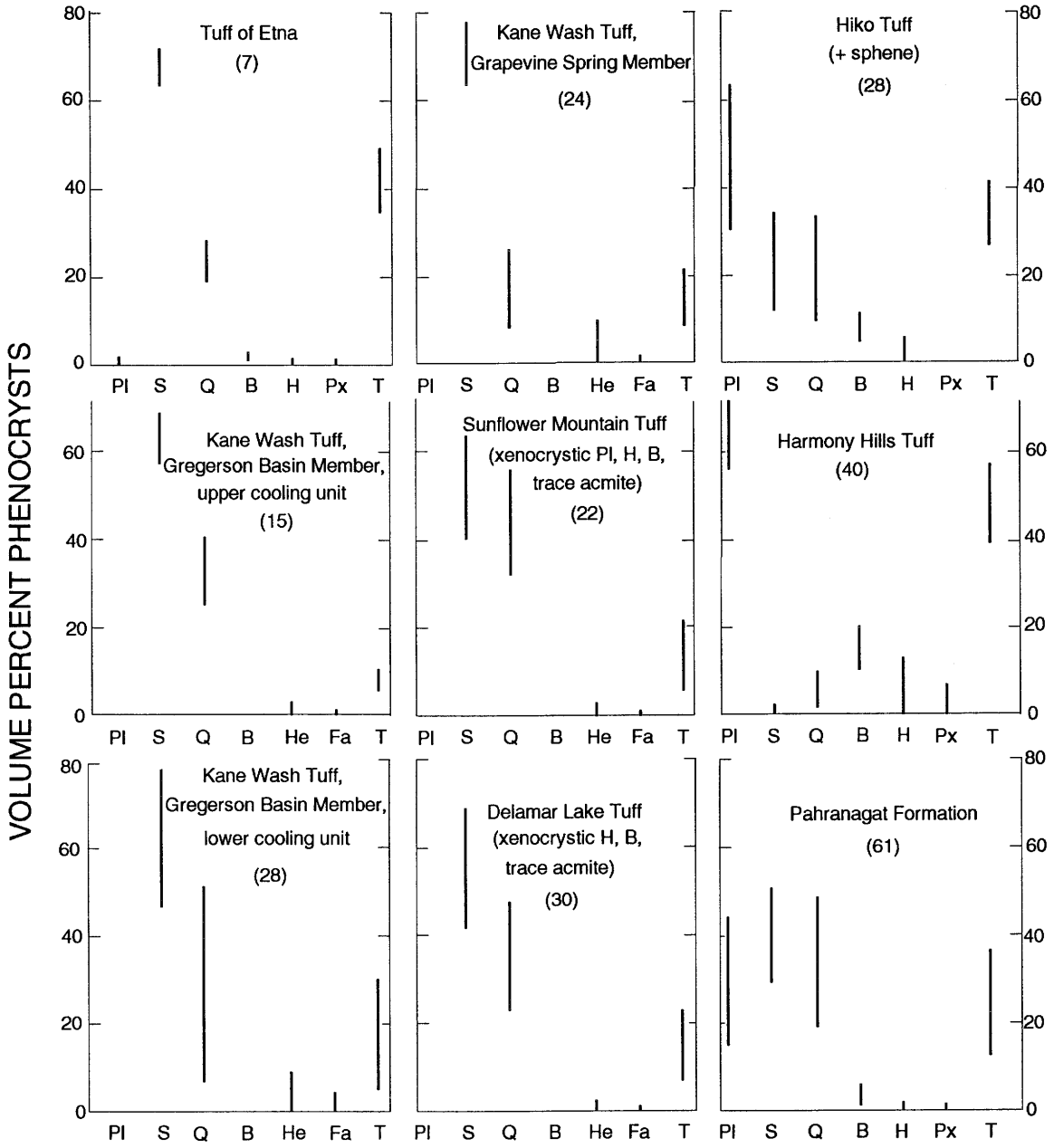

Figure 4 (above and facing page). Modal composition (volume percent) of Oligocene and early Miocene ash-flow units. Number of samples encompassed in line-bar ranges is in parentheses after unit name. Data from Anderson and Rowley (1975), Siders and Shubat (1986), Williams (1967), and unpublished data of M.G. Best, R.B. Scott, A.E. Harding, and R.E. Anderson. Phenocrysts include Pl, plagioclase; S, sanidine; Q, quartz; B, biotite; H, hornblende; He, hedenbergite; Px, pyroxene; and Fa, fayalite. T, total phenocrysts relative to whole rock; tr, trace.

between phenocrysts of the Monotony Tuff and the phenocrysts of the three dacite formations of the Needles Range Group have been made. In ascending order in the group, the lesser abundance of quartz and sanidine in the Cottonwood Wash Tuff, generally more hornblende than biotite and absence of sanidine in the Wah Wah Springs Formation, and the presence of trace amounts of sphene in the Lund Formation are distinctive from the phenocrysts of the Monotony Tuff (fig. 4).

Although as many as three cooling units of the Monotony Tuff are known just northwest of the North Pahroc Range on the eastern and western side of the Grant Range, only one simple cooling unit occurs in central Lincoln County. In the southern Delamar Mountains (Swadley and others, 1990; Page and others, 1990; Scott, Page, and Swadley, 1990), the lowest ash-flow tuff in the section is the Monotony Tuff. This unit has a very distinctive magnetization direction, southeast and downward, about 80° away

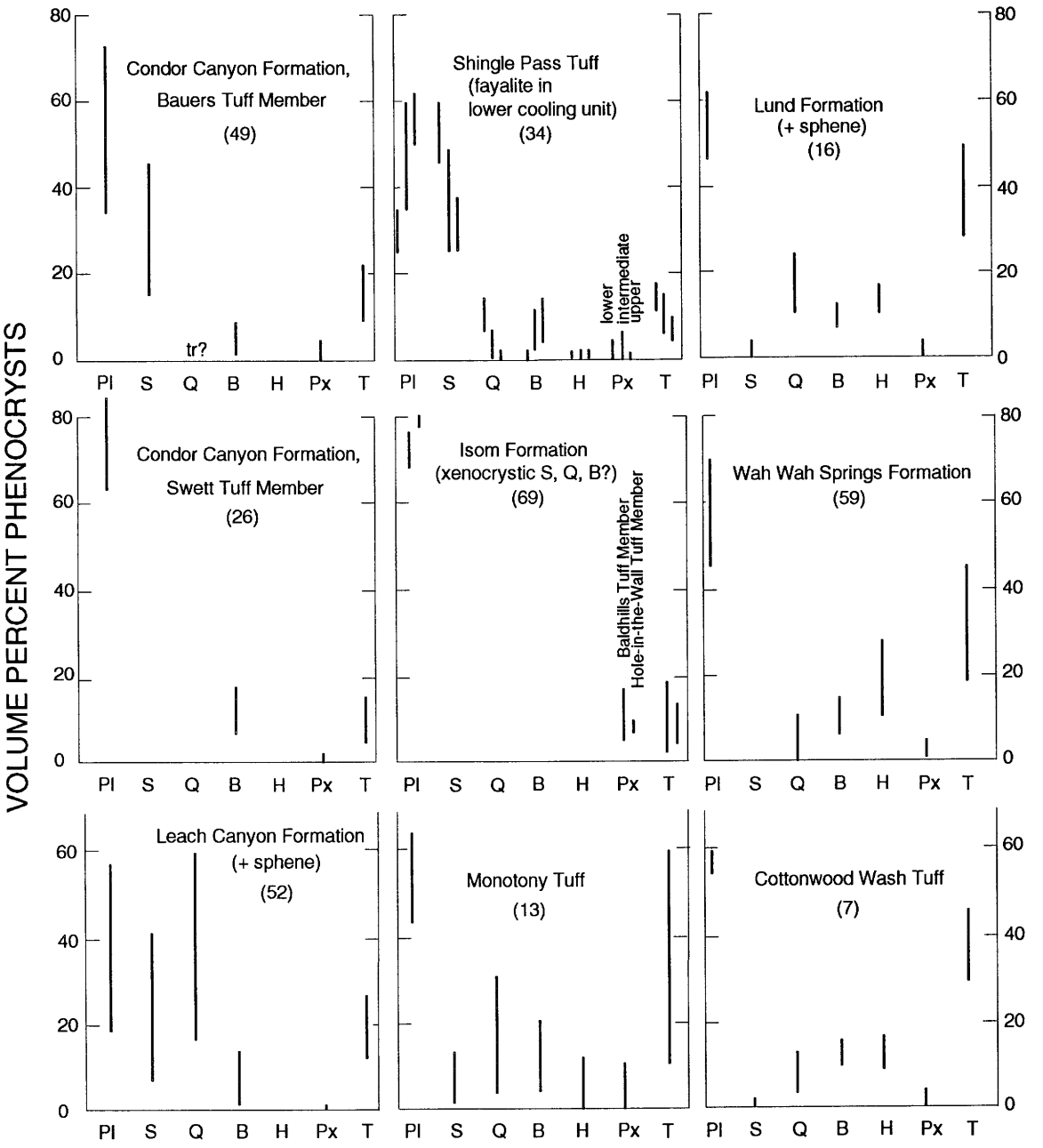

from the reversed Oligocene dipole field direction. This same direction is present in the single Monotony cooling unit at White River Narrows (the tuff at the northernmost petroglyph site), and is also found in the Monotony Tuff at localities to the south and west of White River Narrows. At the Narrows, the Monotony Tuff underlies an Isom compositional-type tuff and overlies the type Petroglyph Cliff Ignimbrite as defined by Cook (1965). One Monotony cooling unit has been mapped above the Petroglyph Cliff Ignimbrite at the south end of the North Pahroc Range (Scott, Swadley, and Byron, 1992), and preliminary paleomagnetic data indicate that it is the same cooling unit.

A new K-Ar date for biotite separated from the Monotony Tuff from the southern Delamar Mountains is 28.5±1.0 Ma (H.H. Mehnert, written commun., 1990). This date falls within the error range of other dates for the Monotony Tuff given in table 1.

ISOM FORMATION AND RELATIONSHIPS WITH OTHER ISOM COMPOSITIONAL-TYPE UNITS

Generally densely welded, locally rheomorphic, trachytic ash-flow tuffs are the namesake of the so-called Isom compositional type, which is shown by the distribution of compositions of the Isom Formation in figure 3. (Also see Best, Christiansen, and others, 1989, fig. 6.) The tuffs are characterized by 4–20 percent phenocrysts that consist of

Table 1. Published isotopic dates for ash-flow units, recalculated as necessary to new constants.

[*, mineral pair from one sample. New or revised stratigraphic names are underlined. Errors are expressed as 2 sigma and dates have been recalculated as necessary to new constants. We conclude that an addition of 0.4 m.y. should be applied to dates reported by Novak (1984) because Novak's dates are consistently about 0.4 m.y. younger than dates for the same rocks reported by L.W. Snee and H.H. Mehnert, in this report]

Unit	Material dated	Method	Date (Ma)	Reference
Kane Wash Tuff, Gregerson Basin Mbr. upper cooling unit	sanidine	K-Ar	14.4 ± 0.6	Noble (1968).
Gregerson Basin Mbr.	sanidine	K-Ar	14.1 ± 0.4	Novak (1984).
Grapevine Spring Mbr.	sanidine	K-Ar	14.0 ± 0.4	Novak (1984).
	sanidine	K-Ar	14.2 ± 0.4	Novak (1984).
Sunflower Mountain Tuff	sanidine	K-Ar	14.7 ± 0.4	Novak (1984).
Delamar Lake Tuff	sanidine	K-Ar	15.5 ± 0.4	Novak (1984).
	sanidine	K-Ar	15.8 ± 0.4	Novak (1984).
Hiko Tuff	*biotite/ hornblende mixture	K-Ar	18.1 ± 0.6	Armstrong (1970).
	*plagioclase	K-Ar	18.2 ± 1.0	Armstrong (1970).
	biotite	K-Ar	18.4 ± 0.4	Armstrong (1970).
	sanidine	K-Ar	20.1 ± 0.5	Noble and others 1968); Noble and McKee (1972).
	biotite	$^{40}Ar/^{39}Ar$	18.5 ± 0.4	Taylor and others (1989).
Harmony Hills Tuff	biotite	K-Ar	20.4 ± 0.5	Noble and McKee (1972).
	biotite	K-Ar	20.3 ± 0.4	Armstrong (1970).
	biotite	K-Ar	21.9 ± 0.4	Armstrong (1970).
	biotite	K-Ar	20.9 ± 0.4	Armstrong (1970).
	plagioclase	K-Ar	21.5 ± 1.0	Armstrong (1970).
Pahranagat Formation	biotite	K-Ar	23.6 ± 1.0	Snyder and others (1972).
	sanidine	K-Ar	22.1 ± 1.0	Snyder and others (1972).
	sanidine	K-Ar	23.4 ± 0.7	Ekren and others (1971).
	sanidine	K-Ar	22.9 ± 0.7	Ekren and others (1971).
	sanidine	K-Ar	21.8 ± 0.7	Ekren and others (1971).
	biotite	K-Ar	23.8 ± 0.7	Ekren and others (1971).
	biotite	K-Ar	21.5 ± 0.5	Ekren and others (1971).
	biotite	K-Ar	20.0 ± 0.6	McKee and John (1987).
	biotite	K-Ar	21.6 ± 0.6	Kleinhampl and Ziony (1985).
	sanidine	$^{40}Ar/^{39}Ar$	22.64 ± 0.02	Deino and Best (1988).
	sanidine	$^{40}Ar/^{39}Ar$	22.62 ± 0.03	Deino and Best (1988).
	sanidine	$^{40}Ar/^{39}Ar$	22.66 ± 0.02	Deino and Best (1988).
	sanidine	$^{40}Ar/^{39}Ar$	22.65 ± 0.02	Deino and Best (1988).

Table 1. Published isotopic dates for ash-flow units, recalculated as necessary to new constants—Continued.

Unit	Material dated	Method	Date (Ma)	Reference
Condor Canyon Formation,	plagioclase	K-Ar	25.0 ± 0.8	Fleck and others (1975).
Bauers Tuff Member	plagioclase	K-Ar	22.7 ± 0.6	Fleck and others (1975).
	whole rock	K-Ar	21.2 ± 0.5	Fleck and others (1975).
	whole rock	K-Ar	23.5 ± 0.4	Fleck and others (1975).
	sanidine	K-Ar	22.2 ± 0.4	Armstrong (1970).
	biotite	K-Ar	21.9 ± 0.5	Armstrong (1970).
	biotite	K-Ar	22.5 ± 0.9	Noble and McKee (1972).
	sanidine	$^{40}Ar/^{39}Ar$	22.78 ± 0.03	Best, Christiansen, and others (1989).
Swett Tuff Member	*biotite	K-Ar	24.1 ± 0.5	Armstrong (1970).
	*plagioclase	K-Ar	23.2 ± 1.7	Armstrong (1970).
	glass	K-Ar	21.9 ± 0.4	Armstrong (1970).
	biotite	K-Ar	23.9 ± 0.5	Armstrong (1970).
	*biotite	K-Ar	23.9 ± 0.5	Armstrong (1970).
	*plagioclase	K-Ar	25.4 ± 0.7	Armstrong (1970).
Leach Canyon Formation	*biotite	K-Ar	24.6 ± 0.5	Armstrong (1970).
	*sanidine	K-Ar	22.9 ± 0.5	Armstrong (1970).
	plagioclase		26.7 ± 1.0	Armstrong (1970).
	zircon	fission track	24.2 ± 2.0	Kowallis and Best (1990).
	sanidine	$^{40}Ar/^{39}Ar$	23.8 ± 0.05	Best and others (1993).
Shingle Pass Tuff	*biotite	K-Ar	26.1 ± 0.6	Marvin and others (1973).
	*sanidine	K-Ar	24.4 ± 0.6	Marvin and others (1973).
	biotite	K-Ar	26.0 ± 0.7	Marvin and others (1973).
	*biotite	K-Ar	28.1 ± 0.9	Marvin and others (1973).
	*split of same	K-Ar	26.2 ± 1.0	Marvin and others (1973).
	*sanidine	K-Ar	22.4 ± 0.7	Marvin and others (1973).
	*split of same	K-Ar	23.1 ± 0.6	Marvin and others (1973).
Upper member	sanidine	K-Ar	25.1 ± 1.0	Sargent and McKee (1969).
	sanidine	$^{40}Ar/^{39}Ar$	26.00 ± 0.03	Best, Christiansen, and others (1989).
intracaldera unit	*sanidine	$^{40}Ar/^{39}Ar$	26.2 ± 0.5	Taylor and others (1989).
	*biotite	$^{40}Ar/^{39}Ar$	26.2 ± 0.5	Taylor and others (1989).
	sanidine	K-Ar	25.8 ± 1.0	Sargent and McKee (1969).
lower cooling unit	sanidine	$^{40}Ar/^{39}Ar$	26.68 ± 0.03	Best, Christiansen, and others (1989).
Isom Formation,	whole rock	K-Ar	25.7 ± 0.5	Armstrong (1970).
Baldhills Tuff Member	plagioclase	K-Ar	25.7 ± 0.4	Fleck and others (1975).
Blue Meadows Tuff Member	plagioclase	K-Ar	25.9 ± 0.4	Fleck and others (1975).

Table 1. Published isotopic dates for ash-flow units, recalculated as necessary to new constants—Continued.

Unit	Material dated	Method	Date (Ma)	Reference
Monotony Tuff	biotite	K-Ar	28.1 ± 0.8	Marvin and others (1973).
	biotite	K-Ar	28.5 ± 0.8	Marvin and others (1973).
	biotite	K-Ar	27.7 ± 0.8	Marvin and others (1973).
	biotite	K-Ar	26.8 ± 0.7	Marvin and others (1973).
	biotite	K-Ar	29.2 ± 1.3	Marvin and others (1973).
	biotite	K-Ar	27.1 ± 1.0	Marvin and others (1973).
	biotite	K-Ar	29.1 ± 0.8	Marvin and others (1973).
	*biotite	$^{40}Ar/^{39}Ar$	27.1 ± 0.6	Taylor and others (1989).
	*hornblende	$^{40}Ar/^{39}Ar$	26.7 ± 0.3	Taylor and others (1989).
	sanidine	$^{40}Ar/^{39}Ar$	27.31 ± 0.03	Best, Christiansen, and others (1989).
Needles Range Group, Lund Formation	unspecified, average of four analyses		27.9	Best and Grant (1987).
Wah Wah Springs Formation	unspecified, average of sixteen analyses		29.5	Best and Grant (1987).
Cottonwood Wash Tuff	unspecified, average of four analyses		30.6	Best and Grant (1987).

70–80 percent plagioclase, 10 percent clinopyroxene and orthopyroxene, and minor magnetite (fig. 4); biotite, quartz, sanidine, and hornblende occur only in inconsistent trace amounts and may be xenocrystic. Considering its silica content (67–68 percent), the Isom (and the Isom compositional type) has relatively high TiO_2 (0.8 percent), K_2O (5.7 percent), Zr (500 ppm), Ba (1,500 ppm), and Rb (220 ppm) but is calc-alkaline (Best, Christiansen, and Blank, 1989), and therefore it is unlike much younger peralkaline trachyte magmas erupted from the Kane Springs Wash caldera and related younger centers.

As originally defined by Mackin (1960) from sites west of Cedar City, Utah, and redefined by Anderson and Rowley (1975), the Isom Formation consists of three members, in ascending order, the Blue Meadows, Baldhills, and Hole-in-the-Wall Tuff Members. The oldest and youngest members are apparently simple tuff cooling units, whereas the Baldhills Tuff Member consists of several tuff cooling units and local lava flows. The Blue Meadows Tuff Member is confined solely to the Markagunt Plateau in south-central Utah. (See fig. 2 of Introduction to volume.) The younger two members, however, are widespread in the Great Basin and appear to have been erupted from an undetermined source just southeast of the Indian Peak caldera complex either from what is now the Escalante Desert (Anderson and Rowley, 1975) or from the mountains just to the west (Best, Christiansen, and others, 1989; Best, Christiansen, and Blank, 1989). But no caldera is exposed in these areas of widespread, thick, younger tuffs and lava flows.

Published K-Ar dates for the Isom Formation range from 25.7 to 25.9 Ma (table 1). However, more precise $^{40}Ar/^{39}Ar$ dates for the underlying Monotony Tuff and overlying Shingle Pass Tuff indicate that the age of the Baldhills Tuff Member of the Isom is between 27.3 and 26.7 Ma. A new K-Ar date for plagioclase from the Baldhills Tuff Member collected from the southern Delamar Mountains is 25.9±0.8 Ma, compatible with these age constraints (H.H. Mehnert, written commun., 1990). The age of the Hole-in-the-Wall Tuff Member of the Isom is between 26.0 Ma, the age of the upper unit of the Shingle Pass Tuff, and 23.8 Ma, the age of the Leach Canyon Formation (table 1 and p. 24).

Paleomagnetic data collected from stratigraphic sequences that demonstrate the relationships of the members of the Isom Formation with the members of the Shingle Pass Tuff and the Petroglyph Cliff Ignimbrite are shown in figure 5. We sampled rocks from the type locality of the Isom Formation in the Bald Hills of southwestern Utah, at the canyon named Hole-in-the-Wall 3 km north of Mackin's (1960) designated type locality for the Isom. Here, the formation consists of four densely welded cooling units; the upper is Mackin's (1960) Hole-in-the-Wall Tuff Member, and the lower three are assigned to his Baldhills Tuff Member. The

Hole-in-the-Wall Tuff Member has reversed magnetic polarity and a southeast declination about 17° from the reversed axial dipole field direction. The lowest cooling unit of the Baldhills Tuff Member has normal polarity, but slightly shallow inclination and north-northeast declination, about 35° from the normal axial dipole direction. The middle cooling unit of this member was too fractured to sample, and the uppermost cooling unit of this member has a magnetic direction similar to, but a shallower normal inclination than, the lowest cooling unit. These results are similar but not identical to those reported by Nairn and others (1975).

In Condor Canyon, Cook (1965) originally showed in his columnar section a series of five tuffs underlying the Leach Canyon Formation and overlying a sequence of lava flows that in turn rest on the Needles Range Group. Later investigations (M.G. Best, unpub. data, 1981; G.J. Axen, unpub. mapping, 1989) demonstrated that in the western part of the canyon (west of the Hamlight fault) at least seven Isom compositional-type welded tuffs are intercalated with the upper cooling unit of the Shingle Pass Tuff (fig. 5); all seven tuffs are contained within a thick sequence of mafic lava flows, rhyolitic tuffs, and minor sedimentary rocks (not shown in fig. 5). In the eastern part of the canyon (east of the Hamlight fault) in a repeated part of the section, at least four or five Isom compositional-type tuffs are present (fig. 5) beneath a thick mafic lava sequence. Axen showed "a probable upper member" of the Shingle Pass Tuff above the mafic lavas and below probable Blawn Formation in eastern Condor Canyon as shown in figure 5, but this unit was not sampled for paleomagnetic study.

In both the eastern and western parts of Condor Canyon, the uppermost of the Isom compositional-type tuffs is reversely magnetized. This direction is nearly identical to that reported just previously in the type locality of the Hole-in-the-Wall Tuff Member. Moreover, to the west at White River Narrows, the upper unit of the Shingle Pass Tuff is directly overlain by a reversely magnetized Isom compositional-type tuff; this reversed direction is nearly identical to those in Condor Canyon and at Hole-in-the-Wall. From this evidence, it seems likely that the Hole-in-the-Wall Tuff Member extends from its type locality in southwestern Utah as far west as White River Narrows (fig. 5). Preliminary paleomagnetic data suggest that the Hole-in-the-Wall Tuff Member also occurs beneath the Leach Canyon Formation in the North Pahroc Range, as it does in Condor Canyon and at White River Narrows. We have not, however, found the Hole-in-the-Wall elsewhere, for example, in the south Delamar Mountains or in the area of Ely Springs.

The paleomagnetic stratigraphy in normally magnetized Isom compositional-type tuffs in Condor Canyon is more complex than that described for other localities (fig. 5). Both east and west of the Hamlight fault, beneath the thick section of mafic lavas, the uppermost cooling unit has a shallow magnetic inclination; this direction, however, is both shallower and closer to due north than that at the top of the type locality of the Baldhills Tuff Member. Moving down section from this tuff, the paleomagnetic directions in the Isom compositional-type tuffs become progressively steeper, much more so than in units of the type Baldhills Tuff Member. West of the Hamlight fault, three Isom compositional-type tuffs occur beneath both the mafic lavas and the upper cooling unit of the Shingle Pass Tuff, whereas east of the Hamlight fault there are at least three and perhaps four. In each of these two nearby sections, the lowest Isom compositional-type cooling unit directly overlies the Lund Formation, but the two Isom compositional-type cooling units have quite different magnetization directions although both are normal and steeply inclined.

Near Swiss Bob Well, about 8 km north-northeast of Ely Springs, two Isom compositional-type tuffs crop out; in this area they form the uppermost part of the Tertiary ash-flow tuff section. The pattern of normal magnetization directions in these two tuffs is similar to that described for the lower tuffs at Hole-in-the-Wall in the Bald Hills, suggesting that these are also part of the Baldhills Tuff Member.

In the southern Delamar Mountains, the Monotony Tuff at the base of the Tertiary volcanic section is overlain by an Isom compositional-type unit (Swadley and others, 1990; Page and others, 1990; Scott, Page, and Swadley, 1990). Its magnetization direction has normal polarity and shallow inclination, and although this direction is slightly shallower than that in the uppermost cooling unit of the type Baldhills Tuff Member, the two do not differ significantly.

In summary, the time-progressions of magnetization directions in these lowest Isom compositional-type tuffs are similar at eastern and western Condor Canyon, Swiss Bob Well, and the Bald Hills, but Isom compositional-type tuffs in Condor Canyon are older than at the other two localities. On the paleomagnetic evidence illustrated in figure 5, however, it seems reasonable to designate them all as the Baldhills Tuff Member of the Isom Formation, including the single trachytic tuff in the southern Delamar Mountains.

Further complicating the stratigraphy of the Isom compositional-type tuffs in Condor Canyon is the occurrence west of the Hamlight fault of three more Isom compositional-type tuffs overlying mafic lavas and the upper member of the Shingle Pass Tuff and underlying the reversely magnetized Hole-in-the-Wall Tuff Member (fig. 5). These three tuffs are normally magnetized, with directions that are near the Oligocene axial dipole field direction. The same tuff sequence has been mapped east of the Hamlight fault, but there the exposure is insufficient for paleomagnetic sampling, and only one of these three Isom compositional-type tuffs may be present there. Because these tuffs are stratigraphically within the Isom Formation as we have identified it, and have the same trachytic composition, we consider them to form a new member of the Isom and here informally name them the tuff member of Hamlight Canyon after the nearby northern tributary to Condor Canyon.

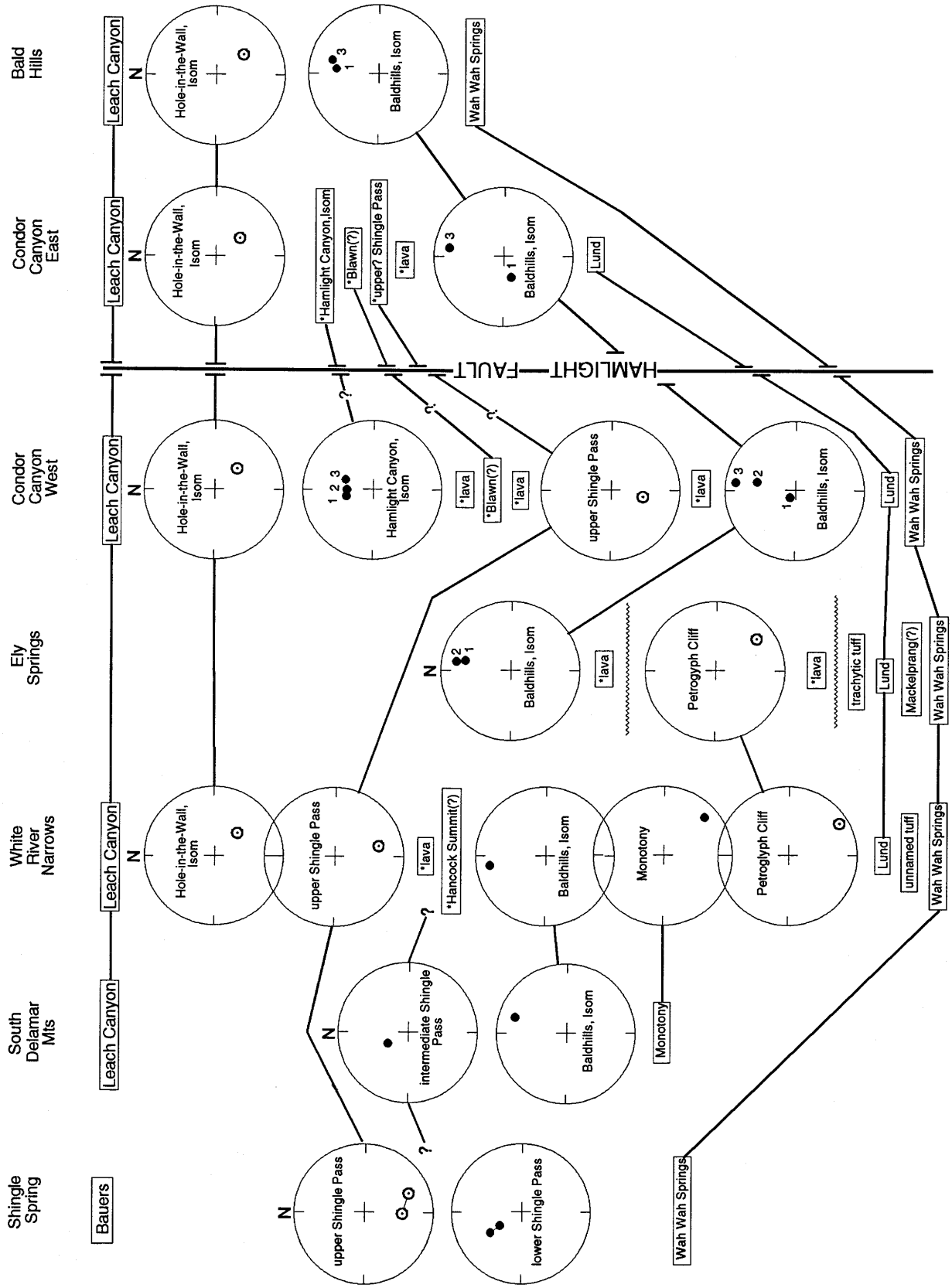
Shingle Spring
South Delamar Mts
White River Narrows
Ely Springs
Condor Canyon West
Condor Canyon East
Bald Hills
Bauers
Leach Canyon
N
upper Shingle Pass
lower Shingle Pass
intermediate Shingle Pass
Baldhills, Isom
Monotony
Hole-in-the-Wall, Isom
*Hancock Summit(?)
*lava
?
Petroglyph Cliff
Petrogyph Cliff
trachytic tuff
Hamlight Canyon, Isom
*Blawn(?)
upper Shingle Pass
Lund
unnamed tuff
Mackelprang(?)
Wah Wah Springs
HAMLIGHT—FAULT
*Hamlight Canyon,Isom
*upper? Shingle Pass

These stratigraphic relationships are supported by detailed mapping and preliminary paleomagnetic data in the North Pahroc Range, where the Hole-in-the-Wall Tuff Member overlies two or three Isom compositional-type cooling units that may be correlative with the tuffs of Hamlight Canyon; these Isom compositional-type cooling units in turn overlie several mafic lavas, a tuff lithologically similar to the Blawn Formation, and two members of the Shingle Pass Tuff. In many localities, the cooling units proposed to be correlative with the tuffs of Hamlight Canyon are not present below the Hole-in-the-Wall Tuff Member. Below the Shingle Pass Tuff, the Baldhills Tuff Member overlies the Monotony Tuff (Scott, Swadley, and Byron, 1992).

The stratigraphically highest Isom compositional-type ash-flow tuff in central Lincoln County occurs between the Swett and Bauers Tuff Members of the Condor Canyon Formation in the North Pahroc Range (Scott, Swadley, and Byron, 1992) and between the Leach Canyon Formation and overlying Bauers Tuff Member in the northeastern part of the South Pahroc Range (Scott and Swadley, 1992). At least two cooling units are present locally. Where the Swett Tuff Member and Harmony Hills Tuff are absent along the northern part of the east-facing cliffs of the South Pahroc Range, this Isom compositional-type cooling unit is nearly 100 m thick; this abnormal thickness for Isom compositional-type tuffs may be related to a nearby source, but no caldera has been recognized. Where this Isom compositional-type cooling unit occurs in the well-exposed section northwest of Pahroc Spring, preliminary paleomagnetic data indicate that it has normal polarity; we are here giving it the informal name "tuff of Pahroc Valley."

It is evident from the foregoing discussion that the Isom Formation and the upper member of the Shingle Pass Tuff are roughly coeval, although several geomagnetic reversals occurred between their eruptions. Preliminary paleomagnetic data from the North Pahroc Range together with the correlations suggested here imply that both the upper and lower members of the Shingle Pass Tuff were erupted after the Baldhills Tuff Member and before the tuff member of Hamlight Canyon, both members of the Isom Formation. The time during which all Isom compositional-type magmas were erupted covers a much greater period, between about 27.9 Ma (age of the Lund Formation) and 22.8 Ma (age of the Bauers Tuff Member of the Condor Canyon Formation), or roughly 5 m.y.

Figure 5 (facing page). Tilt-corrected site-mean paleomagnetic directions for ash-flow tuffs of the Isom Formation, Shingle Pass Tuff, Petroglyph Cliff Ignimbrite, and Monotony Tuff. Locations of stratigraphic sections are shown in figure 1; the Bald Hills are in southwestern Utah, 20 km northwest of Cedar City. (See fig. 2 of Introduction to volume.) Solid circles are directions of normally polarized rocks on lower hemispheres of equal-area projections; open circles are directions of reversely polarized rocks on upper hemispheres. Confidence intervals are not shown. For the Shingle Spring section, lines connect directions at each of two sites in both cooling units. For the Baldhills Tuff Member and tuff member of Hamlight Canyon of the Isom Formation, numbers indicate the sequence of directions in multiple cooling units in ascending order, where present at a site. Stratigraphic positions of ash-flow sheets that enclose the Petroglyph Cliff Ignimbrite and the Isom Formation are indicated by names in boxes, as are intervening volcanic units; those units that have no paleomagnetic data are marked by asterisks. For the Ely Springs section, wavy line, angular unconformity. **Bauers**, Bauers Tuff Member of the Condor Canyon Formation; **Leach Canyon**, Leach Canyon Formation, undivided; **upper, intermediate, and lower Shingle Pass**, corresponding cooling units of the Shingle Pass Tuff; **Hole-in-the-Wall, Hamlight Canyon, and Baldhills**, Hole-in-the-Wall Tuff Member, tuff member of Hamlight Canyon, and Baldhills Tuff Member of the Isom Formation; **Monotony**, one cooling unit of the Monotony Tuff; **Hancock Summit(?)**, informally named ash-flow tuff of Hancock Summit in White River Valley; **Blawn(?)**, unnamed tuff unit tentatively correlated with the Blawn Formation; **Petroglyph Cliff**, densely welded cooling unit of the Petroglyph Cliff Ignimbrite; **Lund**, tuff member of the Lund Formation; **Mackleprang(?)**, tentatively identified as the Mackleprang Tuff Member of the Ryan Spring Formation; **Wah Wah Springs**, outflow tuff member of the Wah Wah Springs Formation. Lines between columns indicate stratigraphic correlations; queried where probable.

SHINGLE PASS TUFF

At Shingle Spring in the Egan Range, Cook (1965) assigned the name "Shingle Pass Ignimbrite" to a rhyolitic tuff (fig. 3) overlying a dacite tuff that we now recognize as the outflow tuff member of the Wah Wah Springs Formation. Cook (1965) found the Shingle Pass over a wide area of southeastern Nevada, but subsequent work showed it to be distributed over an even larger area of 40,000 km^2 (Best, Christiansen, and others, 1989, fig. R19) around a probable source area in the Quinn Canyon Range (Sargent and Roggensack, 1984; Best and others, 1992). Three additional rhyolitic ash-flow tuffs overlying the Shingle Pass at Shingle Spring were indicated but unnamed by Cook (1965, figs. 5, 7). The rocks of the upper two rhyolite units we now recognize (Best, Christiansen, and others, 1989) as the Bauers Tuff Member of the Condor Canyon Formation and the outflow tuff member of the Pahranagat Formation (discussed later). Work by several U.S. Geological Survey geologists in and around the Central Nevada caldera complex has disclosed as many as three rhyolite cooling units that they have designated as the Shingle Pass Tuff (for example, Ekren and others, 1971); two of these cooling units are petrographically and paleomagnetically correlative with the two rhyolitic tuffs between the Wah Wah Springs Formation and Bauers Tuff Member at Shingle Spring (Best, Christiansen, and others, 1989) and are widespread over much the same part of southeastern Nevada around the apparent Quinn Canyon Range source area in the Central Nevada caldera complex.

The lower of the two cooling units at the type section of the Shingle Pass Tuff contains sanidine and lesser plagioclase, but is petrographically unique among Basin and Range tuffs because of its mafic phenocryst assemblage of two pyroxenes, fayalite-rich olivine, amphibole, magnetite, ilmenite, allanite, and xenocrystic(?) biotite as well as its corroded and Christmas-tree-like quartz phenocrysts (fig. 4). The upper cooling unit, in contrast, has more plagioclase than sanidine, little or no quartz, no olivine or ilmenite, and biotite as the dominant mafic phenocryst; the upper cooling unit also has amphibole and xenocrystic pyroxenes. At Shingle Spring, the lower cooling unit is normally magnetized and the upper cooling unit is reversely magnetized; the directions are from 15° to 30° away from the respective axial dipole field directions, and hence they are not particularly diagnostic.

Intercalated within the Isom Formation at White River Narrows and in western Condor Canyon is a single cooling unit of the Shingle Pass that is reversely magnetized, with approximately the same direction as the upper cooling unit at Shingle Spring. Preliminary paleomagnetic data from the North Pahroc Range indicate that both of the Shingle Pass cooling units found at Shingle Spring may be present there, having the same stratigraphic relationship to Isom compositional-type tuffs. These stratigraphic relationships have been confirmed during mapping in the North Pahroc Range (Scott, Swadley, and Byron, 1992). We have not, however, found the Shingle Pass Tuff in the area of Ely Springs. In the southern Delamar Mountains, a single Shingle Pass cooling unit overlies the Isom compositional-type tuff and underlies the Leach Canyon Formation (Swadley and others, 1990). This tuff is normally magnetized, having the same direction as the lower cooling unit at the type section, but petrographically it more closely resembles the upper cooling unit at the type section, so that we refer to it as a so-called intermediate Shingle Pass cooling unit.

Sandwiched between the upper and lower cooling units of the Shingle Pass Tuff in the North Pahroc Range, a rhyolitic ash-flow tuff is tentatively correlated with the tuff of Hancock Summit, which is exposed at the White River Narrows section (fig. 5). This tuff is relatively phenocryst- and quartz-rich compared to the adjacent Shingle Pass cooling units; preliminary petrographic data indicate that the cooling unit contains about 25 percent phenocrysts that consist of about 40 percent quartz, 25 percent sanidine, 25 percent plagioclase, 10 percent biotite, minor Fe-Ti oxides, and common accessory zircon (Scott, Swadley, and Byron, 1992).

Between the upper cooling unit of the Shingle Pass Tuff and the Hole-in-the-Wall Tuff Member of the Isom Formation in the North Pahroc Range, a nonwelded, nearly white, rhyolitic ash-flow tuff underlies a series of basalt flows (Scott, Swadley, and Byron, 1992). Preliminary petrographic data suggest that this nonwelded tuff is distinctive by having relatively high abundances of subequal biotite and hornblende and by abundances of quartz greater than those of plagioclase, which in turn are greater than those of sanidine. This nonwelded tuff is tentatively correlated with tuffs of the Blawn Formation noted in Condor Canyon (fig. 5).

LEACH CANYON FORMATION

The Leach Canyon Formation was originally named by Mackin (1960; see also Cook, 1965). Anderson and Rowley (1975) have adopted the Narrows Tuff Member and the overlying Table Butte Tuff Member as subdivisions of the Leach Canyon Formation and described the formation as the oldest in the Quichapa Group, following the terminology used by Williams (1967). The two members have similar phenocryst abundances (fig. 4). Total phenocrysts range from about 25 to 30 percent of the rock, and phenocrysts consist of 20–50 percent quartz, 10–30 percent sanidine, 20–60 percent plagioclase, as much as 15 percent biotite, and trace amounts of hornblende, pyroxene, and, most characteristic of the formation, accessory sphene. Abundant concentrations of pumice lapilli and small dark volcanic lithic fragments characterize the Table Butte Tuff Member.

The Leach Canyon Formation occurs in the same stratigraphic position as older units of the petrographically similar but sphene-free tuffs of the Blawn Formation, which we have not sampled for paleomagnetic study. Blawn eruptions were of small volume and did not produce known calderas; numerous vents are marked by rhyolite lava flows and lava domes in an east-northeast-trending zone extending from Pioche, Nev., to Milford, Utah (70 km north of Cedar City, Utah) (Best and others, 1987). Although some of the tuff shown by Williams as the Leach Canyon Formation (1967, fig. 9; compare Best, Christiansen, and others, 1989, fig. R40) near Milford is probably the Blawn Formation instead, Williams' isopach map nonetheless indicates a source for the Leach Canyon in the Caliente caldera complex. However, mapping has not yet disclosed any surface manifestation of an appropriate fault-bounded caldera and, like that of the Isom Formation, the source of the Leach Canyon Formation appears to be concealed beneath younger deposits.

The average K-Ar age of the Leach Canyon Formation is 24.6 Ma, but the determinations range widely (table 1); an average age of 23.8 Ma, determined on a coexisting sanidine and biotite pair (Armstrong, 1970), provides a better estimate of the age. This has recently been confirmed emphatically by the $^{40}Ar/^{39}Ar$ date of 23.8 Ma reported by Best and others (1993).

Paleomagnetic sampling has been done in both members of the Leach Canyon Formation at seven localities: White River Narrows (Narrows Tuff Member), the North Pahroc Range (Narrows Tuff Member, preliminary results only), western and eastern Condor Canyon (both members), the southern Delamar Mountains (one undefined member), and at Table Butte in the Escalante Desert of

southwestern Utah (Table Butte Tuff Member). At all these localities, the Leach Canyon overlies either the Hole-in-the-Wall Tuff Member of the Isom Formation or, if this unit is absent, one or another of the cooling units of the Shingle Pass Tuff. All these sampling sites are reversely magnetized and have roughly the same paleomagnetic direction: east to east-southeast declination, and inclination between –35° and –60°. Neither the between-member nor the between-locality differences show any consistent pattern. Nairn and others (1975) had difficulty obtaining consistent paleomagnetic directions from the Leach Canyon Formation, and we conclude that the rock is a less than optimal magnetic recorder, perhaps because of the abundance of lithic fragments in it.

The Leach Canyon Formation is widespread in central Lincoln County (Best, Christiansen, and others, 1989, fig. R40). It is present in all the quadrangles shown in figure 2 except along the western side of the Delamar Mountains (Gregerson Basin quadrangle north to Pahroc Spring SE quadrangle).

CONDOR CANYON FORMATION

The Condor Canyon Formation was named by Cook (1965) to include two ash-flow tuff members, whose rocks were originally named the Swett Tuff and the overlying Bauers Tuff by Mackin (1960). Anderson and Rowley (1975) included the formation in the Quichapa Group, following the nomenclature used by Williams in his dissertation (1967). Anderson and Rowley also slightly revised Mackin's unit names when they adopted the Swett Tuff Member and the Bauers Tuff Member of the Condor Canyon Formation. Williams (1967) postulated that the source of the ash-flow tuffs of the Condor Canyon Formation lay in the Caliente area. Both members are largely densely welded biotite rhyolite, and are distinctive because neither contains phenocrysts of quartz (figs. 3, 4). The two members contrast petrographically: in addition to biotite and plagioclase common to both, the Bauers contains sanidine and a trace of clinopyroxene, whereas the Swett does not contain either. Average K-Ar ages of the two members differ by 1 million years (table 1); a more precise $^{40}Ar/^{39}Ar$ date of 22.78 Ma on the Bauers is in good agreement with its average K-Ar age of 22.7 Ma.

Paleomagnetic sampling has been done in the Swett Tuff Member at four localities: (1) White River Narrows, where the unit is little more than a thin vitrophyre; (2) North Pahroc Range; (3) western Condor Canyon, where the unit is a relatively thick compound cooling unit; and (4) Eightmile Hills, 10 km northeast of Mackin's (1960) type locality at the western end of the Swett Hills in southwestern Utah. At White River Narrows and in western Condor Canyon, the Swett Tuff Member is reversely magnetized, but directions at the two sites differ by about 18° and are 20° or less from the reversed Oligocene axial dipole field direction. Examination of preliminary data from the North Pahroc Range confirms the reversed polarity. Gose (1970) obtained anomalous directions from the Swett Tuff Member exposed on the north wall of eastern Condor Canyon; our new data are a good match to those that he obtained from the southern wall in the same area. The direction reported by Nairn and others (1975) for the Swett Tuff Member at Table Butte in southwestern Utah corresponds well to our data. (See fig. 2 in the Introduction of volume for location.) However, in the Eightmile Hills 27 km to the southeast of Table Butte, we find that the Swett Tuff Member is almost completely overprinted magnetically by the overlying Bauers Tuff Member, but af demagnetization of one of eight specimens resulted in a trajectory of directions that intersects the reversed direction found in western Condor Canyon. The Swett is not found in the South Pahroc Range, southern Delamar Mountains, the Meadow Valley Mountains, or the Ely Springs area. The assumed source of the Swett is the Caliente caldera complex.

The outflow sheet of the Bauers Tuff Member is almost everywhere a simple cooling unit. Pumice lumps increase in size closer to the source in the Caliente caldera complex. The source of the Bauers is the Clover Creek caldera in the Caliente caldera complex (Rowley and Siders, 1988; Rowley and others, this volume). The upper part of the unit in many places, as well as distal parts of the sheet, is more crystal poor relative to the lower part of the tuff and contains no large pumice fragments and smaller and less abundant phenocrysts than the lower part.

The Bauers Tuff Member has exceptionally closely grouped paleomagnetic directions. We have sampled it at six localities: White River Narrows (top and base), North Pahroc Range (preliminary data only), southern Delamar Mountains (the main part and the thin vitric upper unit), eastern Condor Canyon, Shingle Spring in the Egan Range, and in Leach Canyon in southwestern Utah, 10 km southwest of Mackin's (1960) type locality at Bauers Knoll. It has been mapped throughout central Lincoln County (figs. 1, 2) except along the western side of the Delamar Mountains in the Gregerson Basin quadrangle. The Bauers Tuff Member is absent near Ely Springs; at our other sampling sites it overlies either the Swett Tuff Member at White River Narrows and Condor Canyon, an Isom compositional-type ash-flow tuff in the North Pahroc Range, the Leach Canyon Formation in the southern Delamar Mountains and Leach Canyon, or the Shingle Pass Tuff at Shingle Spring. The Bauers Tuff Member is normally magnetized; its paleomagnetic direction is within 10° of the Oligocene axial dipole field direction, and hence is quite ordinary. Our data from the Bauers Tuff Member match well the results of Nairn and others (1975) from other localities in southwestern Utah, including at Bauers Knoll and Table Butte, but our data do not match the direction for eastern Condor Canyon reported by Gose (1970) and quoted by Nairn and others (1975); the reason for the difference is not known.

PAHRANAGAT FORMATION

Although Deino and Best (1988) and Best, Christiansen, and others (1989) provided the first published account of the age, correlation, and description of the Pahranagat Lakes Tuff, more than 20 years earlier Williams (1967) first recognized these rocks as a simple cooling unit of rhyolite ash-flow tuff lying between the Bauers Tuff Member of the Condor Canyon Formation and the Harmony Hills Formation in exposures west of the Pahranagat Lakes in the Pahranagat Range in southeastern Nevada (figs. 1, 3). Williams (1967) placed this rhyolite ash-flow tuff within the Quichapa Group, but it is not included in the Quichapa Group as defined by Anderson and Rowley (1975) or by Rowley and others (1991). Williams described the occurrence of this rhyolite ash-flow tuff in White River Narrows and indicated that the unit extended as far northeast as Condor Canyon (however, at this locality we believe that the thin tuff lying between the Bauers and the Harmony Hills is a local tuff belonging to the Blawn Formation and not to the Pahranagat Lakes Tuff). Williams proposed that the source for the unit might lie just west of Pahranagat Lakes, but conceded that data were inconclusive.

Based on precise single-crystal $^{40}Ar/^{39}Ar$ dates (Deino and Best, 1988; A.L. Deino, unpub. data, 1992) and paleomagnetic and petrographic data, our study reveals a widespread distribution of the simple cooling unit of this rhyolite ash-flow tuff to the west and north of Pahranagat Lakes where it had been originally recognized. However, in the northern and western parts of its distribution, this petrographically, paleomagnetically, and chronologically similar cooling unit has been referred to locally as (1) the tuff of White Blotch Spring, (2) the granite-weathering tuff, (3) the tuff of Kawich Range and the tuff of Kawich caldera, and (4) the tuff of Saulsbury Wash.

1. The tuff of White Blotch Spring (Ekren and others, 1971) consists of two outflow cooling units at White Blotch Spring between the Groom and Belted Ranges; correlative tuffs were mapped in the Cactus, Kawich, northern Belted, and southern Reveille Ranges (fig. 1). Our paleomagnetic and chronologic data show that only the upper of the two cooling units at White Blotch Spring is equivalent to the Pahranagat Lakes Tuff; the lower unit, although petrographically similar, is about 3 m.y. older and has a distinctly different remanent magnetization.

2. The granite-weathering tuff consists of an outflow cooling unit in the southern Hot Creek and Pancake Ranges (Quinlivan and Rogers, 1974; Ekren, Hinrichs, and Dixon, 1972; and Ekren, Rogers, and Dixon, 1973; Snyder and others, 1972) (fig. 1). We conclude that this outflow cooling unit is also equivalent to the Pahranagat Lakes Tuff.

3. Originally Rogers and others (1967) tentatively designated two petrographically similar cooling units in the Kawich and southern Reveille Ranges as the tuff of Kawich Range (fig. 1). Ekren and others (1971) then superseded the name "tuff of Kawich Range" with the tuff of White Blotch Spring. In a reconnaissance map of the northern Kawich Range, within the Kawich caldera, Gardner and others (1980) designated the intracaldera tuff facies as the tuff of Kawich caldera (which they included in the tuff of White Blotch Spring) and the overlying intracaldera tuff facies as the tuffs of Kawich Peak; Sargent and Roggensack (1984) adopted the terminology of Gardner and others (1980). We now believe this sequence of cooling units associated with the Kawich caldera in the Kawich and southern Reveille Ranges to be the intracaldera tuff facies equivalent of the outflow tuff facies of Pahranagat Lakes Tuff.

4. Kleinhampl and Ziony (1985, p. 122; see also Whitebread, 1989) designated the outflow tuff facies sheet in the southernmost Monitor Range as the tuff of Saulsbury Wash and noted its petrographic similarity to the tuff of White Blotch Spring (fig. 1). We conclude that the tuff of Saulsbury Wash is also equivalent to the Pahranagat Lakes Tuff.

The Pahranagat Formation is defined here to consist of two facies: (1) an intracaldera tuff facies restricted to within the Kawich caldera (consisting of rocks previously assigned to the tuff of Kawich Range, the tuff of Kawich caldera, the tuffs of Kawich Peak, and part of the tuff of White Blotch Spring) and (2) a widespread outflow tuff facies that is also called the outflow sheet (consisting of rocks previously assigned to the Pahranagat Lakes Tuff, the upper cooling unit of the tuff of White Blotch Spring at White Blotch Spring, the granite-weathering tuff, and the tuff of Saulsbury Wash). We follow Anderson and Rowley (1975) and Rowley and others (1991) by not including the Pahranagat Formation in the Quichapa Group as used by Williams (1967) because its rocks did not originate from the same long-lived magma system marked by the Caliente caldera complex, which was the source of at least the Bauers Tuff Member of the Condor Canyon Formation of the Quichapa (Rowley and others, this volume).

The Pahranagat Formation takes its name from the Pahranagat Lakes and the East Pahranagat and Pahranagat Ranges south and west of Alamo, Nev., where good exposures of the outflow tuff facies (or outflow sheet) are abundant. The type section of the Pahranagat Formation is designated in its outflow sheet in the East Pahranagat Range just north of Medsger Pass at lat 37°15'18" N., long 115°13'22" W., in the Alamo 7.5-minute quadrangle. Here, the outflow sheet is about 45 m thick, overlies the Bauers Tuff Member of the Condor Canyon Formation, and is overlain by the Harmony Hills Tuff. The Pahranagat Formation is a pumice-rich, generally pale purple to pinkish-gray tuff that contains approximately equal amounts of phenocrysts of embayed quartz (commonly as much as 5 mm in diameter), sanidine, and commonly intensely corroded plagioclase (fig. 4); small phenocrysts of biotite increase in abundance upwards and are joined by sparse hornblende and a trace of clinopyroxene near the top of the unit. As much as one-third

of the rock consists of white, light-gray to grayish-orange-pink pumice fragments. In the lowest 4 m of the partially welded basal part of the unit, pumice chunks are as much as 25 cm in diameter; in the overlying 40 m of moderately welded tuff, the pumice is lapilli- and small block-size; and in the top meter or so of partially welded tuff, pumice is as large as in the basal part. A reference section for the outflow sheet is located at the southern end of White River Narrows (see Williams, 1967, p. 81) on the west side of Nevada State Highway 318 in the White River Narrows 7.5-minute quadrangle at lat 37°50'17" N., long 115°02'20" W. Here, the unit is about 12 m thick and lies between the Bauers and the Harmony Hills. Above about a meter of bedded tuff, the ash-flow deposit in its lower half is nonwelded to partially welded and contains pumice lumps as much as 30 cm in diameter. The overlying partially to moderately welded tuff has crude joint columns and white pumice lapilli in a grayish-pink matrix that has about the same modal composition as at the type section in the East Pahranagat Range. A second reference section, a partial section of the outflow sheet whose rocks were previously designated as the granite-weathering tuff, is located in the southern Pancake Range on the western side of Black Beauty Mesa on the Lunar Crater 15-minute quadrangle (Snyder and others, 1972) at lat 38°16'40" N., long 116°06'25" W. Here 110 m of the unit are exposed above a densely welded plagioclase-pyroxene-phyric Isom compositional-type tuff. The lower part of the unit is a white, pumice-bearing ash that grades upwards into a moderately welded lapilli tuff lithologically resembling the Pahranagat Formation in the White River Narrows. A third reference section in the outflow sheet in an area where its rocks have been previously referred to as the tuff of Saulsbury Wash is located in the southern Monitor Range at the southeast end of Woodchopper Canyon on the Mud Spring 7.5-minute quadrangle at lat 38°09'53" N., long 116°50'52" W. Here, the outflow sheet overlies a local white, poorly exposed tuff and is overlain by a black lava flow containing small phenocrysts of olivine and pyroxene. At this reference section, the outflow sheet of the Pahranagat is about 144 m thick and grades upwards from a densely welded, devitrified pumice-poor tuff in its lowermost few tens of meters to more pumice rich, moderately welded tuff in its uppermost part that lithologically resembles the rocks in the White River Narrows. The section at White Blotch Spring on the Bombing and Gunnery Range has restricted access.

We have paleomagnetic data for the outflow sheet of the Pahranagat Formation from the southern Delamar Mountains, the North Pahroc Range (preliminary only), White River Narrows, and Shingle Spring in the Egan Range (where it forms the topmost unit of the Tertiary tuff section), as well as many localities to the west and north. The outflow sheet of the Pahranagat Formation is not found in the Ely Springs area. The unit is reversely magnetized; a preliminary mean direction from 11 sites has a declination about 10° west of south and an inclination about 5° steeper than the reversed Oligocene axial dipole field direction, and thus is not particularly distinctive. Probably as a consequence of only weak to moderate welding, some sites have paleomagnetic directions that are as much as 18° of arc away from this preliminary mean. The formation has been mapped in the southern Delamar Mountains and the South and North Pahroc Ranges, but does not reach the Meadow Valley Mountains (fig. 1).

Sanidine from the Pahranagat Formation has been precisely dated using the $^{40}Ar/^{39}Ar$ method by Deino and Best (1988), and its average age is about 22.6 Ma (early Miocene) based on four dates that only range from 22.62±0.03 to 22.66±0.02 Ma (table 1).

RHYOLITIC LAVA FLOWS OF DELAMAR VALLEY

A complex sequence of lava flows, lava domes, and subordinate encapsulating ash-fall and ash-flow tuffs that are distributed throughout the northern part of Delamar Valley (fig. 1) forms an important silicic volcanic center. Most of these rocks are phenocryst poor and contain about 10 percent sanidine and quartz; some are aphyric; and others contain 20 percent phenocrysts of sanidine, quartz, plagioclase, and biotite. Commonly vitrophyric and frothy margins enclose devitrified flow interiors. At several localities, many glasses have been partly or totally hydrated to perlite; nonhydrated remnants (Apache tears) are common along the base of the east-facing cliffs of the northern South Pahroc Range; an active perlite mine is located about 7.5 km south of U.S. Highway 93 in that area.

Along the cliffs on the east side of the northern South Pahroc Range, nonwelded ash-fall and ash-flow tuffs at the base of this sequence rest on the Pahranagat Formation, and the sequence of rhyolitic flows is covered by the Hiko Tuff. The absence of the Harmony Hills Tuff in the units exposed along the cliff was originally attributed to the presence of the rhyolitic domes and flows. However, samples of nonhydrated obsidian from the active perlite mine and adjacent devitrified aphyric rhyolite have been dated recently by whole rock K-Ar methods at 18.6±0.7 and 18.2±0.7 Ma, respectively (H.H. Mehnert, written commun., 1992). Thus, at least some of the rhyolitic sequence appears to be nearly as young as the overlying Hiko Tuff, too young to have created a barrier to ash flows from the source of the Harmony Hills Tuff. Although problems related to the absence of the Harmony Hills Tuff and the young dates of the rhyolite flows require further investigation, we assume that older rhyolites under those dated provided a barrier to emplacement of the Harmony Hills.

Within Delamar Valley, the Hiko Tuff and the members of the younger Delamar Lake Tuff are plastered against hills formed by the lava domes; probably these domes were positive topographic features that were not completely covered by subsequent ash-flow tuffs (Scott and Swadley, 1992). The cooling units of the Gregerson Basin Member of the Kane

Wash Tuff, the youngest cooling units in the area, occur in a few down-dropped blocks in the valley, and there is no evidence to suggest that they ever entirely covered the rhyolitic lava domes of Delamar Valley. If the domes remained uncovered by subsequent ash-flow tuffs, then the rhyolite domes may have had a local initial relief in excess of 500 m. Despite the thickness of the silicic rocks and their widespread distribution surrounding this volcanic center, evidence of associated hydrothermal activity is absent.

HARMONY HILLS TUFF

The Harmony Hills Tuff was originally defined as the youngest member of the Quichapa Formation by Mackin (1960); these units were subsequently raised in rank by Cook (1965) to the Harmony Hills Tuff (formation rank) and the Quichapa Group; Williams also used this nomenclature in his dissertation (1967). Isopach data of Williams (1967) suggest that the source of the ash flows of the Harmony Hills lies in the Bull Valley Mountains of Utah, east of the Caliente caldera complex. Blank (1959) cited the occurrence of two cooling units in the Bull Valley area as evidence for a source in the Bull Valley area of westernmost Utah, but P.D. Rowley (written commun., 1992) has made similar observations in the Caliente area. Rowley and others (1979) and Ekren and others (1977) observed similar or greater thickness in the Clover Mountains of Nevada and have suggested that the Harmony Hills may have had its source in the southern part of the Caliente caldera complex. Because the tuff of the Harmony Hills is the least silicic volcanic rock of the ash-flow tuffs in this area and its composition plots in the trachyandesite and andesite IUGS fields (fig. 3), we consider that the Harmony Hills probably was not erupted from the Caliente caldera complex, which erupted rhyolitic ash flows. The Harmony Hills Tuff is also among the most crystal-rich ash-flow tuffs in the Great Basin and contains about 50 percent phenocrysts, mostly plagioclase, and lesser (in diminishing amounts) biotite, clinopyroxene, hornblende, quartz, Fe-Ti oxides, and sanidine (fig. 4).

The average K-Ar age of the Harmony Hills Tuff is 21.0 Ma (table 1), but more recent dating of overlying rocks in Utah (Rowley and others, 1989) in addition to the age of the underlying Pahranagat Formation in eastern Nevada constrains the age of the Harmony Hills to between about 21.7 and 22.6 Ma.

The Harmony Hills Tuff was sampled for paleomagnetic study at three sites: the southern Delamar Mountains, eastern Condor Canyon, and the eastern end of Leach Canyon. At all three sites the Harmony Hills Tuff overlies the Bauers Tuff Member of the Condor Canyon Formation, and at the Nevada sites it underlies the Hiko Tuff. The Leach Canyon site is 4.5 km north of Mackin's (1960) type locality in the Harmony Mountains in southwestern Utah (Harmony Hills was dropped from official geographic names and replaced with Harmony Mountains). The Harmony Hills Tuff is normally magnetized, and our three sites show a relatively large dispersion in direction; the directions range from 5° to 27° of arc distant from the normal Oligocene axial dipole field direction. The paleomagnetic direction reported by Nairn and others (1975) for the Harmony Hills Tuff at Bauers Knoll in southwestern Utah is similar to our results. Gose (1970) reported results from the same site in eastern Condor Canyon as ours, and the two determinations are virtually the same. (See also Nairn and others, 1975.)

The Harmony Hills Tuff has been mapped throughout the areas mapped in central Lincoln County (figs. 1, 2), except in the northern part of Delamar Valley where the thick complex of rhyolitic lava domes and lava flows occurs at the stratigraphic level of the Harmony Hills in parts of the Delamar NW and Pahroc Summit Pass quadrangles. Local sequences of olivine-, clinopyroxene-, and plagioclase-bearing mafic flows as thick as 25 m are present between the Harmony Hills Tuff and the Hiko Tuff at two localities in the North Pahroc Range. Also, in the Meadow Valley Mountains southeast of the Kane Springs Wash caldera, a local sequence of tuffaceous sedimentary rocks and nonwelded to partially welded ash-flow tuffs forms wedges as much as 65 m thick between the Harmony Hills and Hiko Tuffs on the hanging-wall side of south-dipping small-offset normal faults. Neither the sedimentary rocks nor the tuffs are as biotite rich as the rocks of the Harmony Hills or Hiko Tuffs.

HIKO TUFF

The most ubiquitous and distinctive ash-flow tuff unit throughout central Lincoln County is the rhyolitic Hiko Tuff. The tuff was named by Dolgoff (1963) after exposures in the Hiko Range where bold cliffs and knobby, joint-controlled landforms are characteristic of the outflow facies. In most areas the Hiko consists of one cooling unit; it is a devitrified, nonwelded to densely welded tuff; a eutaxitic texture formed by pumice fragments and shards deformed around phenocrysts occurs in the partly vitric, more welded zone close to local vitrophyres. Phenocrysts form about 30–40 percent of the tuff and consist of about 10–35 percent very pale purple quartz, 15–35 percent sanidine, 30–65 percent plagioclase, 5–15 percent biotite, trace to 5 percent hornblende, traces of pyroxene and sphene, and several percent Fe-Ti oxides (fig. 4). Scott and others (1988) suggested that the magma from which the Hiko Tuff was erupted may have been compositionally zoned (Lipman and others, 1966) because they found a greater abundance of mafic minerals higher in the sequence of rocks of the Hiko Tuff. R.E. Anderson (written commun., 1992) also observed a distinct modal increase in plagioclase and ferromagnesian phases relative to quartz and sanidine in the upper part of the Hiko in southwestern Utah.

The Racer Canyon Tuff of Utah has a petrographic variability nearly identical to that of the Hiko Tuff of Nevada and, to add to stratigraphic complications, occurs at a stratigraphic level indistinguishable from that of the Hiko Tuff. After Cook (1965) correlated these two tuffs, attempts to distinguish between them have been numerous (Noble and McKee, 1972; Ekren and others, 1977; Rowley and others, 1979; and Siders and Shubat, 1986). Rowley and Shroba (1991) considered that the two tuffs may be related genetically, building on the conclusions of Noble and others (1968) and Noble and McKee (1972), who proposed that both units were erupted from the Caliente caldera complex. Ekren and others (1977) first recognized that the Hiko Tuff formed thick intracaldera facies in the westernmost lobe of the Caliente caldera complex; Rowley and Siders (1988) named that part of the caldera complex the Delamar caldera and confirmed it as the source of the Hiko Tuff.

Four K-Ar dates on mineral separates from the Hiko Tuff range from 18.1±0.6 to 20.1±0.5 Ma (Armstrong, 1970; Noble and others, 1968; Noble and McKee, 1972). However, $^{40}Ar/^{39}Ar$ dates provide a more precise measure of its age; Taylor and others (1989) obtained a 18.5±0.4 Ma-biotite plateau date, but concluded on the basis of additional unpublished dates that the best estimate of the age of the Hiko Tuff is 18.6 Ma.

Paleomagnetic investigations of the Hiko Tuff, which were designed to test degrees of vertical-axis rotation and to provide constraints for tectonic models (Hudson and others, this volume), also provide some insight into the emplacement history of the Hiko Tuff. Although the Hiko Tuff generally consists of one cooling unit, at a thick section of the Hiko in the southern South Pahroc Range, it includes two cooling units. Five sites in the Hiko from the Delamar and Meadow Valley Mountains, thought to be unaffected by vertical-axis rotation, yield an apparently well-defined mean paleomagnetic direction of reversed polarity (D=166°, I=–45°, and $alpha_{95}$=6.2°). However, in the southern South Pahroc Range section, two vitrophyres are present. Samples obtained from below the upper vitrophyre yield a mean paleomagnetic direction that differs significantly from the direction derived from samples from the upper part of the ash-flow sheet. (See Hudson and others, this volume.) A period of at least a few hundred years is required between emplacement and cooling of these two cooling units if the difference in paleomagnetic directions is due to average rates of secular variation. We are uncertain whether the upper or lower cooling unit is the single cooling unit so widespread elsewhere.

Paleomagnetic data for the Racer Canyon Tuff vary in direction and polarity from site to site (C.S. Grommé, unpub. data, 1991). These seeming ambiguities may be related to the presence of several cooling units within the tuffs of the Racer Canyon.

The thickest part of the Hiko Tuff occurs along the east-facing cliffs of the South Pahroc Range where more than 200 m of a single cooling unit are exposed. Probably the Hiko was deposited in this locality in a valley trending westward away from the source (P.D. Rowley, written commun., 1992), for the Hiko thins south toward the southern Delamar Mountains and the Meadow Valley Mountains to 25–75 m and north toward the southern North Pahroc Range to at least 130 m.

Local olivine-bearing mafic flows overlie the Hiko Tuff southwest of Delamar Lake in the Pahranagat shear system. Although these flows are as much as 250 m thick here, they pinch out 6 km to the north and 7 km to the northeast and the southeast. Novak (1984) obtained a K-Ar whole-rock date of 15.6±0.8 Ma for these flows, but a better estimate of the age of the basalt may be as much as 0.4 Ma older, about 16 Ma (see explanation in table 1).

PERALKALINE RHYOLITIC ASH-FLOW TUFFS AND MAFIC LAVA FLOWS

A significant change in the chemical composition of volcanic rock occurred between eruption of the Hiko Tuff (18.6 Ma) and the Delamar Lake Tuff (15.6 Ma). The Hiko Tuff is the youngest voluminous calc-alkalic ash-flow tuff in the central part of Lincoln County. Subsequent regional volcanism is characterized by a bimodal sequence of metaluminous to mildly peralkaline rhyolitic ash-flow tuffs commonly capped by alkalic olivine basalts.

Rocks younger than the Hiko Tuff in the southern Delamar Mountains and Meadow Valley Mountains were originally defined as the Kane Wash Formation by Cook (1965) based on his pioneering study of measured sections and his correlation of ash-flow tuffs by phenocryst modes. Cook proposed a type section for the formation at the western end of the Delamar Mountains that consists primarily of sanidine- and quartz-bearing ash-flow tuffs as well as sedimentary rocks and the basalt (reported in the previous section) that overlies the Hiko Tuff (fig. 6). Noble (1968) revised and renamed the unit the Kane Wash Tuff to exclude sedimentary rocks and basalts from Cook's definition (fig. 6); Noble also recognized the peralkaline chemical composition of the ash-flow tuff.

Initial K-Ar dating of the Kane Wash Tuff by Noble (1968) and Armstrong (1970) and of associated basaltic andesite by Best and others (1980) placed the age of the tuff at about 14 Ma. Subsequently Novak (1984) dated two of the three youngest cooling units of the Kane Wash Tuff that he established to have been erupted from the Kane Springs Wash caldera. He determined the K-Ar sanidine dates for the lower two cooling units, his members V1 and V2, to range from 14.0±0.4 to 14.2±0.4 Ma (2 sigma errors); the youngest cooling unit, his member V3, was not dated. However, a better estimate of the age of these ash-flow tuffs may be as much as 0.4 Ma older, about 14.6 Ma (see explanation in table 1). Novak and Mahood (1986) established the petrologic evolution of outflow sheets and intracaldera units from the Kane

Springs Wash caldera. Novak also recognized not only that two lower ash-flow tuffs included in Noble's Kane Wash Tuff predated the Kane Springs Wash caldera (15.5±0.4 and 15.8±0.4 Ma for Novak's member O and 14.7±0.4 Ma for Novak's member W; better estimates of the ages of these units may be closer to 16 and 15.1 Ma, respectively, as explained in table 1), but also that these units had a distribution incompatible with a source from the Kane Springs Wash caldera and a chemical composition distinct from that of units derived from the Kane Springs Wash caldera.

For the reasons outlined by Novak, Scott and others (1993) revised the stratigraphic nomenclature (fig. 6) previously applied to those units to exclude the two older units from the Kane Wash Tuff. Thus the redefined Kane Wash Tuff consists of only the three outflow cooling units derived from the Kane Springs Wash caldera; the lowest cooling unit (Novak's member V1) is called the Grapevine Spring Member and the upper two cooling units (Novak's members V2 and V3) are called the Gregerson Basin Member. The two cooling units of the Gregerson Basin Member are commonly indistinguishable both in the field and petrographically, particularly where complexly faulted or incompletely exposed. Rocks that make up Novak's (1984) members O and W have been raised to formation rank as the Delamar Lake Tuff and the overlying Sunflower Mountain Tuff, respectively (Scott and others, 1993).

DELAMAR LAKE TUFF

The rocks that now form the Delamar Lake Tuff were originally included as the lowest part of the Kane Wash Tuff (Noble, 1968; Novak, 1984, member O). The Delamar Lake Tuff is a crystal-poor metaluminous rhyolitic sequence of quartz-, sanidine-, fayalitic olivine-, and hedenbergite-bearing ash-flow tuffs (figs. 3, 4). The thickest accumulation is where four informal members (cooling units) are recognized on the western side of Delamar Valley about 10 km north of Delamar Lake, the namesake of the tuff. Because these four members are not exposed in a single section, Scott

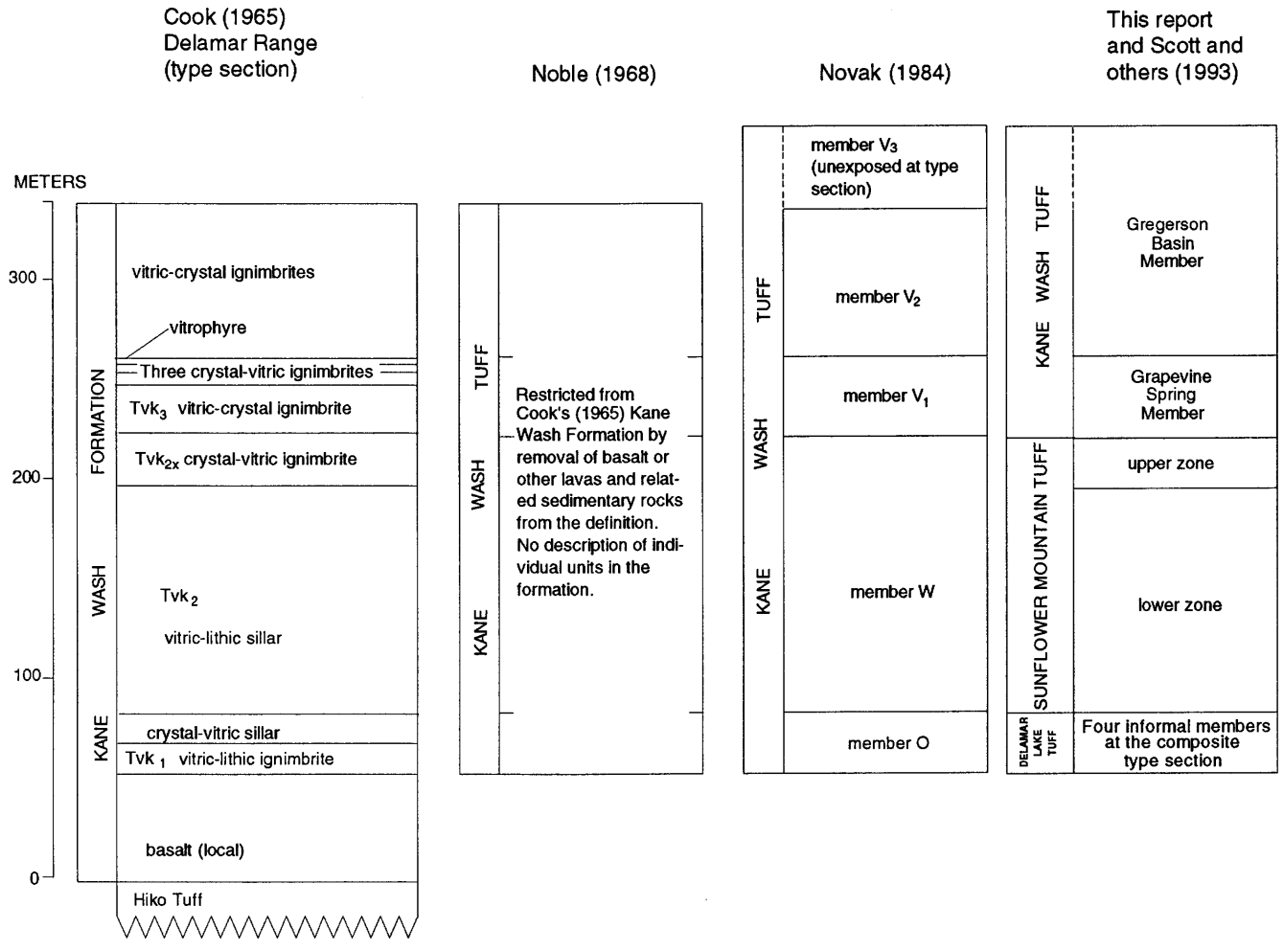

Figure 6. Evolution of stratigraphic nomenclature used for the Kane Wash Tuff. Hiko Tuff continues below jagged line. From Scott and others (1993).

and others (1993) proposed a composite type section for the Delamar Lake Tuff consisting of four individual sections. From oldest to youngest, the cooling units are the (1) lower cooling unit consisting of less than 50 m of nonwelded to moderately welded rhyolitic ash-flow tuff, (2) crystal-rich cooling unit consisting of as much as 120 m of relatively phenocryst-rich (20–25 percent) moderately to densely welded tuff, (3) pumice-rich cooling unit consisting locally of less than 35 m of noncompacted, but sintered, pumice similar to pumice-flow tuffs recognized in Japan and New Zealand, and (4) orange cooling unit consisting of as much as 65 m of moderately welded to densely welded tuff characterized by a moderate-red to dusky-red vitrophyre below a light-red to moderate-orange-pink devitrified zone. The lowest two cooling units are extensively exposed in the southern Delamar Mountains and Meadow Valley Mountains, where they underlie the Sunflower Mountain Tuff. The pumice-rich cooling unit is present only in Delamar Valley near the composite type section. The orange cooling unit and the crystal-rich cooling units occur between the Hiko Tuff and the overlying Kane Wash Tuff in the northern end of Delamar Valley. None of the cooling units of the Delamar Lake Tuff or the Kane Wash Tuff are present north of the Timpahute lineament (fig. 1). Although the source of the Delamar Lake Tuff is undetermined, it may be located northwest of the Kane Springs Wash caldera where the thickness of the cooling units is greater.

Paleomagnetic characterization of the Delamar Lake Tuff is based upon a single site from the unit located on the western side of the central Meadow Valley Mountains, where the rock is normally magnetized. At this locality, only one cooling unit of the Delamar Lake Tuff is present; it is uncertain whether this cooling unit correlates with the lower cooling unit or the crystal-rich cooling unit of the Delamar Lake in Delamar Valley.

SUNFLOWER MOUNTAIN TUFF

The Sunflower Mountain Tuff is a newly defined formation (Scott and others, 1993) that derives its name from Sunflower Mountain in the central Meadow Valley Mountains (fig. 1). The rocks of this formation were originally designated as member W of the Kane Wash Tuff by Novak (1984). The Sunflower Mountain Tuff is a metaluminous rhyolitic tuff that consists of a thick compound ash-flow tuff cooling unit above thinner indistinctly bedded tuffs. The Sunflower Mountain Tuff contains two mappable zones, whose rocks Cook (1965) designated as his unit Tvk_2 and its upper part, unit Tvk_{2x} (fig. 6). The rocks of both these mappable zones have been defined as informal members in the new nomenclature. The lower member consists of all the nonwelded to partially welded lower part of the Sunflower Mountain Tuff, including indistinct bedded ash-flow tuffs near its base. The massive, upper part of the lower member consists of a pale-orange, devitrified, nonwelded to partially welded, lithic- and pumice-fragment-rich (20 percent of each), crystal-poor (about 10 percent), ash-flow tuff that contains subequal amounts of quartz and sanidine phenocrysts and a trace of altered ferromagnesian minerals (fig. 4). Locally, near its middle part the lower member contains a thin interval of black fiamme. The lithologic distinction between the lower and upper members is based on an increase in degree of welding; no cooling break occurs between the members. The upper member is pinkish gray to pale red, devitrified, and partially to moderately welded to moderately to densely welded; it has few lithic fragments (1 percent) but has a phenocryst mineralogy indistinguishable from that of the lower member except for a greater total abundance (about 20 percent). The upper member contains about 20 percent flattened pumice fragments and has distinctive moderate-orange to pale-red mottled blotches. The type section of the Sunflower Mountain Tuff is 7.3 km north of Sunflower Mountain (Scott and others, 1993). Although the source of the Sunflower Mountain is unknown, its distribution suggests a source southwest of the Kane Springs Wash caldera.

The Sunflower Mountain Tuff is present throughout the southern Delamar Mountains and the Meadow Valley Mountains; it is more than 150 m thick 12 km west of the Kane Springs Wash caldera (fig. 1). Novak's (1984) reconnaissance mapping west of our mapping indicates that the thickest accumulation of the formation occurs about 25 km west of the Kane Springs Wash caldera; the tuff thins significantly to the north, east, and south. The tuff abruptly pinches out northeast of a line beginning about 4 km west of the Kane Springs Wash caldera and continuing to about 18 km northwest of that caldera. The Sunflower Mountain Tuff is notably absent northwest and north of the Kane Springs Wash caldera.

The upper member, the more welded part of the Sunflower Mountain Tuff, was sampled for paleomagnetic characterization on the western side of the central Meadow Valley Mountains. At this site, the Sunflower Mountain Tuff is reversely magnetized. Because the lower part of the tuff contains bedded tuff interbedded with nonwelded ash-flow tuffs, significant secular variations, if not reversals, could have been recorded in the lower part of the unit.

PERALKALINE PRECURSOR TO THE KANE WASH TUFF

Several thick, undated ash-flow tuffs of peralkaline compositions similar to the comendites of the Kane Wash Tuff (Scott, Blank, and Page, 1991) are present stratigraphically beneath the Kane Wash Tuff and a precaldera trachyte of Novak (1984) along the northern wall of the Kane Springs Wash caldera (Scott, Swadley, and others, in press). Mapping in the area between 9 and 14 km north of the Kane Springs Wash caldera has identified structurally shredded

fragments of a caldera wall in the vicinity of Narrow Canyon. Scott, Blank, and Page (1991) have considered these to be fragments of a precursor to the Kane Springs Wash caldera, which they called the Narrow Canyon caldera. East of Narrow Canyon, probable caldera-filling rhyolitic ash-flow tuffs, rhyolitic lava flows, and a shallow trachytic intrusion(?) related to caldera resurgence are exposed near the intersection of the Delamar, Slidy Mountain, Elgin SW, and Gregerson Basin quadrangles (fig. 2).

The extent of outflow sheets derived from the Narrow Canyon caldera remains relatively uncertain because mapping in the Elgin quadrangle and petrographic and geochemical investigations of potential outflow sheets are still in progress. Neither the Delamar Lake nor the Sunflower Mountain Tuffs are likely candidates for outflow sheets for this caldera because their distributions do not fit the Narrow Canyon source and because they are metaluminous, not peralkaline. The best candidates for outflow sheets are (1) a series of unnamed rhyolitic ash-flow tuffs found on the northeastern side of the Delamar Mountains between either the Kane Wash Tuff or the tuff of Etna and the Hiko Tuff, (2) a series of unnamed, post-Hiko Tuff/pre-Kane Wash Tuff ash-flow tuffs exposed near the Narrow Canyon caldera on the western side of the Delamar Mountains, (3) an undated peralkaline ash-flow tuff found in the northern topographic wall of the Kane Springs Wash caldera close to the northwestern edge of the Meadow Valley Mountains, and (4) a similar unnamed ash-flow tuff between the Kane Wash Tuff and the Hiko Tuff in the northern Meadow Valley Mountains. In all these cases, the ash-flow tuffs that are suspected to have been derived from the Narrow Canyon caldera have phenocryst assemblages similar to those of the Kane Wash Tuff. A thick sequence of peralkaline ash-flow tuffs exposed below the Kane Wash Tuff in the northern topographic wall of the Kane Springs Wash caldera in the central part of the Delamar Mountains is a good candidate for the intracaldera facies equivalent to the outflow sheets related to the Narrow Canyon caldera (Scott, Blank, and Page, 1991). But distinction between outflow units, intracaldera units, and post-collapse caldera-filling units is challenging in older, structurally disrupted, and largely buried calderas; more study of the Narrow Canyon caldera and related volcanic rocks is required.

KANE WASH TUFF

The Kane Wash Tuff caps the Tertiary volcanic succession throughout most of the Delamar Mountains and much of the Meadow Valley Mountains. Younger mafic lava flows and the tuff of Etna overlie the Kane Wash Tuff only in a few isolated exposures.

The Grapevine Spring Member of the Kane Wash Tuff was named for the west-facing cliff exposures of its type section above Grapevine Spring in the central Meadow Valley Mountains in the Vigo NW 7.5-minute quadrangle (Scott and others, 1993; Scott, Harding, and others, 1991). The Grapevine Spring Member is a slightly metaluminous rhyolite compound cooling unit (fig. 3); its peralkalinity index (PI=molar [Na+K]/Al) is slightly less than 1.0 (R.B. Scott, unpub. chemical data, 1990). The tuff includes a 3-m-thick, nonwelded, vitric basal zone, overlain by a 80-m-thick, densely welded, devitrified, moderate-brown, rough-weathering middle zone. The middle zone contains about 35 percent phenocrysts consisting of about 10–25 percent quartz, 65–75 percent sanidine, as much as 10 percent hedenbergite, less than 5 percent fayalitic olivine, and traces of ilmenite (fig. 4). The middle zone is overlain by a 20-m-thick, moderately to densely welded, devitrified, light-brownish-gray, smooth-weathering upper zone. The upper zone is relatively crystal poor, containing about 10 percent phenocrysts consisting of about 25 percent quartz, 60 percent sanidine, and a total of about 15 percent hedenbergite, fayalitic olivine, and ilmenite (fig. 4). In one locality about 3 km southwest of the Kane Springs Wash caldera in the southern Delamar Mountains, minor trachytic cognate scoriaceous inclusions occur in the upper part of the Grapevine Spring Member.

The Grapevine Spring Member is not uniformly distributed outside the Kane Springs Wash caldera. The member has a more or less uniform distribution northwest, west, and southwest of the caldera margin where the member thins to 0–10 m about 10–15 km from the caldera. South of the margin, the Grapevine Spring Member does not thin nearly so much and is 50 m thick 22 km from the caldera, but north of the margin it pinches out in only 8 km. Both the Grapevine Spring and Gregerson Basin Members of the Kane Wash Tuff pinch out against the resurgent structure in the Narrow Canyon caldera about 10 km north of the Kane Springs Wash caldera (Scott, Swadley, and others, in press).

The Gregerson Basin Member consists of two separate cooling units (members V_2 and V_3 of the Kane Wash Tuff of Novak, 1984), which are defined as a single member because the cooling units cannot be reliably mapped separately in complexly deformed terrane. The type section of the member (Scott and others, 1993) is about 5 km north- northwest of the Kane Springs Wash caldera; there, each of the two cooling units consists of a lower peralkaline rhyolite (PI>1) interval overlain by an upper trachytic interval (fig. 3). The lower intervals are also comenditic according to the classification of peralkaline, quartz-normative extrusive rocks (Macdonald, 1974). At the type section, comenditic intervals are devitrified, moderately to densely welded, and yellowish gray to light bluish gray. The rock has about 20 percent phenocrysts consisting of about 25 percent quartz, 60 percent sanidine, and a total of about 15 percent hedenbergite, fayalite and ilmenite (fig. 4). In the basal parts of the comenditic intervals, 1–2 m of welded pale-blue ash-flow tuff overlie 1–2 m of pale-yellowish-orange, nonwelded to partially welded ash-fall tuff. The bluish colors in the comenditic intervals appear to be related to vapor phase and deuteric(?) minerals, riebeckite and (or) arfvedsonite. The

upper cooling unit of the Gregerson Basin Member locally has striking bluish-gray colors and large altered riebeckite(?) crystals in lithophysal cavities and gas-expanded pumice fragments. The overlying trachytic intervals are devitrified, partially welded to moderately welded, and pale yellowish brown. The trachytic matrix is less mafic than common cognate inclusions of scoriaceous trachyte that contain about 50 percent phenocrysts consisting of alkali feldspar, abundant opaque phases, and remnant pyroxene. At the type section of the Gregerson Basin Member, the lower cooling unit contains about 260 m of comendite below 30 m of trachyte and the upper cooling unit contains about 170 m of comendite below 30 m of trachyte.

At the southern end of the Delamar Mountains, only the lower cooling unit is present and the Gregerson Basin Member has thinned to about 35 m thick, and it is only about 20 m thick in the southern part of the Meadow Valley Mountains. About 40 m of these cooling units of the member are present in the northwestern part of Delamar Valley, but the cooling units are absent farther north and west.

The new $^{40}Ar/^{39}Ar$ plateau sanidine dates from the Kane Wash Tuff are 14.67±0.22 Ma from the Grapevine Spring Member, 14.55±0.14 Ma from the lower cooling unit of the Gregerson Basin Member, and 14.39±0.28 Ma from the upper cooling unit of the Gregerson Basin Member (L.W. Snee, written commun., 1991). Although the 2-sigma errors overlap, the dates fall into the proper stratigraphic sequence supporting the probability that the time between eruptions of the cooling units is about 0.1–0.2 million years. As noted previously, these dates are about 0.4 Ma older than the K-Ar dates reported by Novak (1984).

Paleomagnetic samples were collected from the Kane Wash Tuff in the Delamar and Meadow Valley Mountains. Three sites in the Grapevine Spring Member yield tightly grouped site-mean directions of normal polarity and northwesterly declination (fig. 7). This tight grouping of directions is good evidence for the absence of vertical-axis rotation between these sites. Paleomagnetic results from five sites in the lower cooling unit and from three sites in the upper cooling unit of the Gregerson Basin Member all indicate a reversed polarity and a southerly declination. The difference in magnetic polarity requires an interval of at least a few thousand years between emplacement of the two members, whereas $^{40}Ar/^{39}Ar$ data allow an interval as long as almost 600,000 years, but more probably nearer to 120,000 years. The small but consistent difference between the mean directions of the lower and upper cooling units of the Gregerson Basin Member is great enough to require a minimum interval of a few hundred years between their emplacements.

Correlation between members of the Kane Wash Tuff and a series of thin welded ash-flow sheets interbedded with nonwelded tuff in Rainbow Canyon requires both paleomagnetic and petrographic data. In thesis work by Bowman (1985), sheets of welded tuffs in Rainbow Canyon were informally referred to as numbered "C" units. The paleomagnetic directions for Bowman's units C2–C4 are shown in figure 7. Although the Grapevine Spring Member is not exposed in Rainbow Canyon, the lower and upper cooling units of the Gregerson Basin Member appear to be correlative with units C2 and C3, respectively, based on mineralogical evidence (Rowley and others, this volume). However, units C2 and C3 have a distinct counterclockwise paleomagnetic declination relative to the declinations of the lower and upper cooling units of the Gregerson Basin Member sampled close to the Kane Springs Wash caldera. We propose that a small but measurable vertical-axis rotation has affected the strata in Rainbow Canyon relative to the Gregerson Basin Member where it is exposed to the south near Kane Springs Wash caldera.

We conclude that the Kane Springs Wash caldera is clearly nested into the southern part of the older Narrow Canyon, that the undetermined sources of the chemically and mineralogically similar Delamar Lake and Sunflower Mountains Tuffs are probably precursors to these two calderas, and therefore, that the four combined sources constitute a highly metaluminous to mildly peralkaline caldera complex, the Kane Springs Wash caldera complex.

TUFF OF ETNA

As much as 60 m of partially to moderately welded rhyolitic ash-flow tuff has been preserved in a few localities in the northern and northeastern Delamar Mountains, particularly in down-dropped blocks between blocks of the Kane Wash Tuff and on east-facing dip slopes beneath capping mafic lavas. We correlate this tuff, using petrographic and paleomagnetic data, with the informally named tuff of Etna, proposed by Rowley, Shroba, and others (1991) for thick accumulations in Rainbow Canyon (unit C4 of Bowman, 1985). Paleomagnetic studies of the tuff of Etna in Rainbow Canyon and in the northern Delamar Mountains identify a counterclockwise declination of the Rainbow Canyon rocks relative to those in the Delamar Mountains, similar to the differences in declinations found in the Gregerson Basin Member from those areas (fig. 7).

The tuff of Etna contains about 30–50 percent phenocrysts consisting of about 20–30 percent quartz, 60–75 percent sanidine, 1 percent plagioclase, and 2–3 percent altered biotite, and traces of hornblende, clinopyroxene, and opaque phases (fig. 4). Ekren and others (1977) reported a petrographically similar tuff, the Ox Valley Tuff, in the extreme eastern part of Lincoln County. Snee and others (1990) obtained a K-Ar date of 13.8±0.9 Ma for sanidine from a water-laid tuff above the tuff of Etna in Rainbow Canyon; that date and the 14.39±0.28 Ma date of the underlying upper cooling unit of the Gregerson Basin Member suggest that the age of the tuff of Etna is probably close to 14 Ma. The Ox Valley Tuff is apparently significantly younger (about 12.5 Ma) as noted by Rowley,

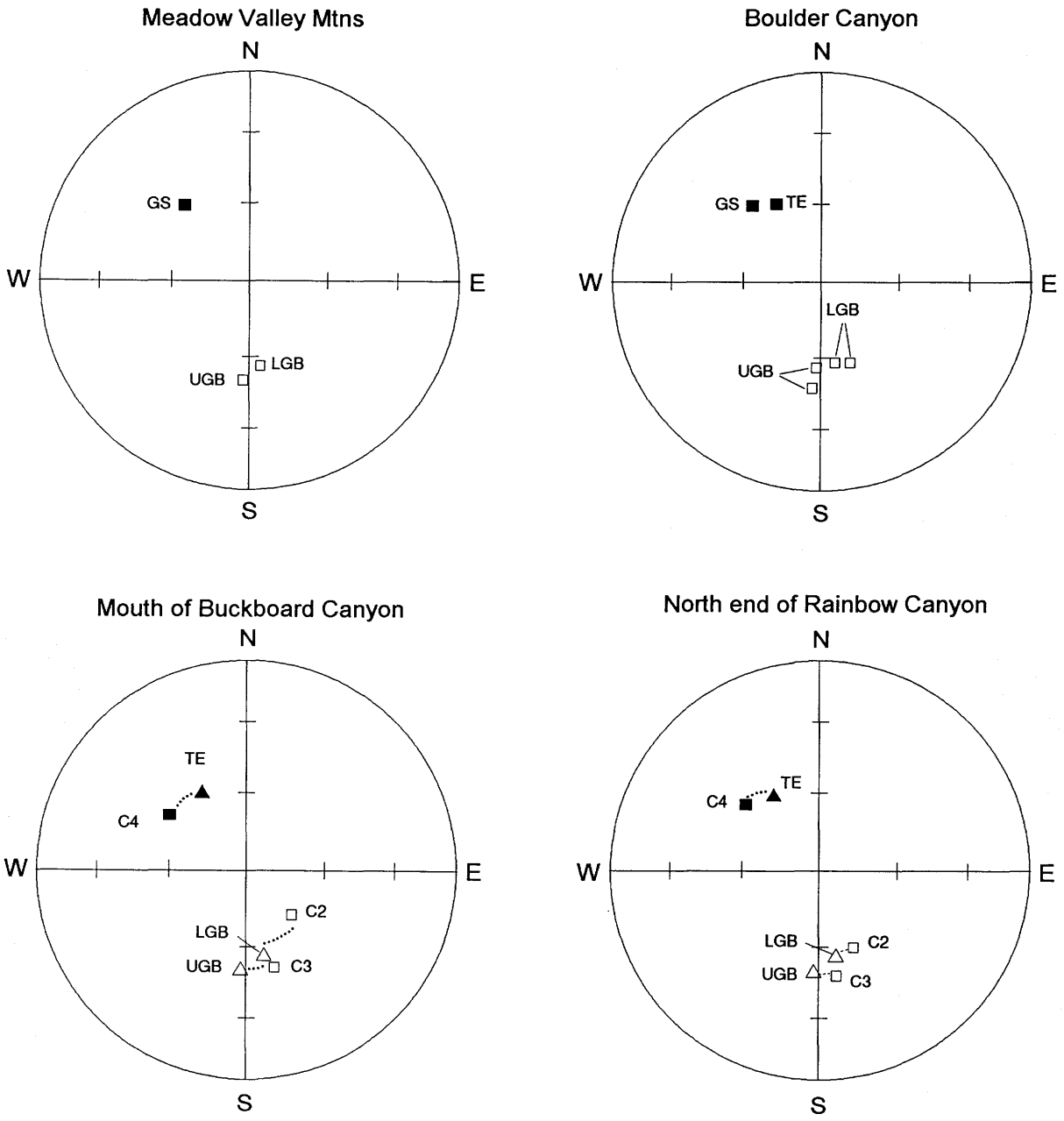

Figure 7. Tilt-corrected site-mean paleomagnetic directions for ash-flow tuffs collected from four sections. Alpha$_{95}$ confidence circles are not shown because they are all less than 4°. Meadow Valley Mountains site is from central part of western side of the mountains. Boulder Canyon section is located about 7 km north of intersection of the canyon mouth and northern margin of the Kane Springs Wash caldera. Mouth of Buckboard Canyon is about 4.5 km south of Caliente on western side of Rainbow Canyon. Northern end of Rainbow Canyon is about 0.5 km south of Caliente. GS, Grapevine Spring Member of the Kane Wash Tuff; LGB and UGB, lower and upper cooling units of the Gregerson Basin Member of the Kane Wash Tuff; TE, tuff of Etna; C2, C3, and C4 are informally named units of Bowman (1985) in Rainbow Canyon, referred to in text. Dotted lines connect stratigraphic correlatives and emphasize the basis for postulating slight counterclockwise vertical-axis rotation of Rainbow Canyon relative to surrounding areas to the south.

Shroba, and others (1991); thus, the Ox Valley Tuff probably is not present in the Delamar Mountain–Rainbow Canyon area. For a more thorough discussion of possible correlation of the tuff of Etna and the Ox Valley Tuff, see Rowley and others (this volume).

In one locality in the east-dipping dip slopes of the Delamar Mountains in the northeastern part of the Elgin SW 7.5-minute quadrangle (fig. 2), an undated mafic lava flow underlies the tuff of Etna. Based on stratigraphic constraints, the age of this flow should be about 14 Ma.

MAFIC LAVA FLOWS

Over much of central Lincoln County, the youngest volcanic rocks are mafic lava flows that appear to be conformable with underlying volcanic units in several areas. Where conformable relationships prevail, ages of these mafic lava flows generally provide maximum ages of Tertiary extension. Many of these mafic rocks cap the intracaldera-filling sequence in the Kane Springs Wash caldera and, therefore, are assumed to be related to the last phase of caldera-forming volcanism (Novak, 1984; Scott, Novak, and Swadley, 1990; Scott, Swadley, and others, 1990; Scott, Harding, and others, 1991; Scott, Swadley, and others, in press). However, other mafic lava flows farther removed from the caldera may have independent origins, even though they have petrographic characteristics similar to those flows associated with the caldera.

A series of extracaldera lava flows containing olivine phenocrysts and plagioclase megacrysts (classified as tholeiitic basalt and dated at 12.7±0.6 Ma by the whole-rock K-Ar method by Novak, 1984) occurs above the Kane Wash Tuff 2 km southwest of the Kane Springs Wash caldera. (A better estimate of the age of this lava flow may be closer to 13.1 Ma, as explained in table 1.) A large feeder dike cuts the older flows of this series, indicating a local extracaldera vent for at least some of these flows (Scott, Novak, and Swadley, 1990).

A second series of mafic lava flows (classified as alkali basalt, trachybasalt, and trachyandesite according to Novak and Mahood (1986), but classified as basalt, trachybasalt, and basaltic trachyandesite, respectively, according to Le Maitre (1989)) conformably caps the rocks that fill the Kane Springs Wash caldera in the Delamar Mountains. In some cases, these intracaldera mafic flows have a phenocryst mineralogy similar to that of the extracaldera basalt flows. Although Best and others (1980) reported a younger whole-rock K-Ar date of 12.1±0.5 Ma for a basaltic andesite from the intracaldera sequence, the dating error is large enough to leave the possibility that the intracaldera and extracaldera mafic flows are essentially coeval and were derived from the same magmatic system. The overlap in timing and location of eruption, petrographic character, and chemical composition of these two series permits several relationships: (1) These mafic lava flows were the result of the generation of mafic magmas regionally beneath this part of Lincoln County about 12.5 Ma, and they erupted both outside and coincidentally within the Kane Springs Wash caldera, independent of caldera magmatic evolution. (2) Both intracaldera and extracaldera mafic lava flows represent the final phase of caldera magmatism, some of which erupted outside the caldera. (3) Although these roughly coeval mafic lava flows may have been related to a regional mafic magma genesis within the mantle, those erupted from the caldera have been secondarily and independently involved with continued caldera magmatic evolution. (4) These mafic magmatic systems operated completely independently; their apparent coeval genesis is merely coincidental. The variation in reported chemical compositions is large, from tholeiitic basalt outside the caldera to trachyandesite and basaltic andesite inside the caldera, suggesting significant differences in magma genesis in space in spite of similar ages (Novak and Mahood, 1986). Obviously, more work on petrogenesis of these mafic lava flows is needed.

In the dip slopes on the eastern side of the northern Delamar Mountains, a mafic lava flow series conformable with the underlying tuff of Etna has been dated at 13.4±1.0 Ma by whole-rock K-Ar methods (H.H. Mehnert, written commun., 1993). In the northeastern part of the Meadow Valley Mountains adjacent to Meadow Valley Wash, R.E. Anderson collected from two mafic lava flows for dating at a similar stratigraphic position; dates of 13.3±0.6 and 13.24±0.6 Ma were obtained for these flows by H.H. Mehnert using whole-rock K-Ar methods (R.E. Anderson, written commun., 1992). Mafic flows at both these localities underlie a thick sequence of alluvial fill. A third mafic lava flow occurs within the thick sequence of alluvial fill between the northern end of the Meadow Valley Mountains and the Delamar Mountains; this mafic flow and the adjacent alluvial fill have been deformed by the left-lateral, oblique-slip Kane Springs Wash fault, which forms the northwestern boundary of the Meadow Valley Mountains. This flow has been dated by whole-rock K-Ar methods at 8.1±0.5 Ma by H.H. Mehnert (R.E. Anderson, written commun., 1992). The deformation of this flow and alluvium records movement younger than about 8 Ma, but faulting in middle Pleistocene fans records the most recent movement on the Kane Springs Wash fault.

One series of olivine-bearing mafic lava flows, some of which contain megacrysts of plagioclase, conformably caps the Kane Wash Tuff at the southwestern end of the Delamar Mountains, about 11 km from the Kane Springs Wash caldera. Similar flows are exposed a few kilometers southwest of the southwestern end of the Delamar Mountains in an area inhomogeneously deformed by the left-lateral Pahranagat shear system. At one locality, flows were deposited conformably on the underlying Kane Wash Tuff and were dated by whole-rock K-Ar methods at 14.5±1.0 Ma; but at another nearby locality, flows angularly overlie small breached domes of the Kane Wash Tuff and were dated by whole-rock K-Ar methods at 15.1±1.3 Ma (H.H. Mehnert, written commun., 1993). These relationships suggest that some deformation spatially related to the Pahranagat shear zone occurred shortly after emplacement of the 14.5-Ma Kane Wash Tuff, between about 14.5 and 13.8 Ma, given the large errors in dating of the mafic flows.

In contrast to these conformable relationships, angular unconformities exist beneath mafic lava flows in two places in central Lincoln County; dating of these flows provides minimum ages of deformation of underlying volcanic strata. One example provides a minimum age for most of the progressive tilting that affected the eastern part of the Kane

Springs Wash caldera in the Meadow Valley Mountains. A thick sequence of flows (classified as basalt by Novak, 1984) and associated scoriaceous material overlaps the southeastern wall of the Kane Springs Wash caldera and rests on both caldera filling units and outflow sheets of the Kane Wash Tuff (Harding and others, this volume; Scott, Harding, and others, 1991). Harding and others interpreted this sequence to have erupted from conduits that followed the caldera structural margin, ring-dike structures lying inboard of the caldera topographic wall. Novak (1984) determined whole-rock K-Ar dates for a basalt in this sequence to be 11.4±0.4 and 11.6±0.4 Ma. (A better estimate of the age of this lava flow may be closer to about 11.8–12.0 Ma, as explained in table 1.) Although these lava flows dip at only 5°–8° to the east and southeast, underlying silicic strata both within and outside the caldera dip more steeply at 20°–30°; and the oldest strata outside the caldera (Leach Canyon Formation and the Bauers Tuff Member of the Condor Canyon Formation) dip at 30°–40°, suggesting periods of progressive tilting and assumed extension in the Meadow Valley Mountains between about 24 and 12 Ma.

The second example of angular relationships occurs in the northern part of the Pahroc Summit Pass and southern part of the Pahroc Spring 7.5-minute quadrangles just south of the Timpahute lineament (figs. 1, 2). Here, on the downthrown side of the east-striking Pahroc Valley fault—a segment of the Timpahute lineament—nearly horizontal flows overlie tilted strata of the Hiko and Harmony Hills Tuffs (Scott, Swadley, and Byron, 1992). These flows also overlie an extremely coarse (clasts as great as 10 m in diameter) Tertiary boulder alluvial fan(?) deposit that rests on the angular unconformity. The mafic flows, recently dated by whole-rock K-Ar methods at 18.1±0.9 Ma (H.H. Mehnert, written commun., 1993), provide the minimum age of tilting and coarse fan growth associated with the Timpahute lineament.

TUFF AND BEDDED VOLCANIC ASH IN ALLUVIUM

About 1 km west of the Kane Springs Wash caldera, a tuff dipping 25° underlies an untilted ash in a complex sequence of alluvial deposits in a north-trending graben (Scott, Novak, and Swadley, 1990). The tilted tuff appears to be a deposit resulting from either a massive rhyolitic ash fall or a nonwelded ash flow and contains sanidine, quartz, minor biotite, and abundant pumice. A sanidine K-Ar date from the tilted tuff is 12.1±0.4 Ma, yet a hornblende K-Ar date from the untilted volcanic ash is 12.6±0.6 Ma (H.H. Mehnert, written commun., 1990). These dates are apparently out of stratigraphic order even though they are within the 2-sigma analytical error. Although the upper part of the volcanic ash was somewhat reworked by fluvial processes and contains evidence of bioturbation, it is unlikely that older hornblende was mixed with the ash because hornblende is sparse as a phenocryst phase in other volcanic units in the area. Probably the hornblende retained excess magmatic argon, providing an anomalously old date for the untilted ash; the hornblende is currently being redated by $^{40}Ar/^{39}Ar$ methods to avoid the excess-argon problem (L.W. Snee, written commun., 1991). These dates are conformable with other evidence that suggests that the last major tilting event in the area ended about 12 Ma (Snee and others, 1990).

Tertiary alluvial deposits in the southeastern side of Kane Wash Valley in the Delamar 3 SE quadrangle (Swadley and others, 1990) contain a bedded, biotite-bearing, silicic ash that is tilted at 24° above an angular unconformity above the Hiko Tuff. Although the ash has not been dated using isotopic methods, the shard color, morphology, and major-element chemistry are similar to those of tephra erupted from the Yellowstone–Snake River Plain sequence of eruptive sources; the most likely age based upon preliminary correlation with those sources is between about 4.3 and 5.4 Ma (A.M. Sarna-Wojcicki, written commun., 1992). If this age range is corroborated by samples submitted for $^{40}Ar/^{39}Ar$ dating, this is evidence for the youngest tilting in the area.

TIMING OF VOLCANISM AND EXTENSION

Although this report primarily concerns the stratigraphic framework of Tertiary volcanic rocks in central Lincoln County, the stratigraphic framework also records evidence of the nature and timing of tectonic events. We briefly summarize and comment on that evidence here. Some of this timing and nature of tectonic events has already been discussed in the previous sections, "Prevolcanic Sedimentary Rocks," "Mafic Lava Flows," and "Tuff and Bedded Volcanic Ash in Alluvium."

Evidence for a prevolcanic basin exists north of the Timpahute lineament (fig. 1); evidence in the North Pahroc Range consists primarily of thick prevolcanic limestones and clastic rocks including coarse boulder conglomerates (Scott, Swadley, and Byron, 1992; Taylor and Bartley, 1992). Axen and others (1993) and Taylor and Bartley (1992) attributed the sedimentary basin to prevolcanic (pre-32 Ma) extension related to the top-to-the-east Stampede detachment and postulated Seaman breakaway. Evidence for the Stampede detachment can be found no farther south than the northern boundary of the Caliente caldera complex, which coincides with the Timpahute lineament (Ekren and others, 1976; Rowley and others, 1992). In addition, the oldest volcanic units in that area, the formations of the Needles Range Group, are not present south of the Timpahute lineament, suggesting that the structural basin north of the lineament was still being filled by sediments and volcanic strata until at least about 28 Ma.

South of the Timpahute lineament, however, there is a conspicuous absence of evidence of significant sediment accumulation that would be expected if substantial prevolcanic extension had occurred. Axen and others (1993) referred to an example of pre-24 Ma extension in the southern Delamar Mountains where the Devonian rocks are attenuated along west-directed low-angle normal faults (Page and Scott, 1991); Axen and others suggested that this may be an example of prevolcanic extension south of the Caliente caldera complex. However, Page (this volume) provides evidence and logic suggesting that the low-angle faults in the southern Delamar Mountains probably formed considerably earlier than the Stampede detachment and probably were associated with gravitational collapse of overthickened crust during or shortly after Sevier compression.

Recent reevaluation of mapping by Swadley and others (1990) in the Delamar 3 SE quadrangle (fig. 2) in the Meadow Valley Mountains has identified at least one widespread attenuating low-angle normal fault, which is confined to Paleozoic rocks, between the Ordovician Pogonip Group and Ordovician Ely Springs Dolomite. Only highly deformed podlike remnants of the Eureka Quartzite exist along the fault zone. Overlying Tertiary volcanic rocks do not appear to be involved in typical upper plate extensional deformation, and therefore, the low-angle faults are probably prevolcanic. Evidence does not exist to determine whether this extension is related to Sevier compression or to a southern extension of a Stampede-age detachment. Only minor prevolcanic conglomerates exist on the angular unconformity above Paleozoic rocks.

Essentially conformable stacks of late Oligocene and early Miocene tuff sheets exposed in tilted and uplifted ranges in central Lincoln County include few intervening lava flows and sedimentary deposits. These relations indicate relatively limited concurrent crustal extension during the major episode of explosive volcanism in southeastern Nevada about 32–22 Ma (Best and Christiansen, 1991).

Beginning about 22 Ma and continuing to about 12 Ma, however, the stratigraphic record in central Lincoln County preserves local evidence of progressive tilting of Miocene ash-flow tuff sheets, requiring roughly coeval extensional tectonism and volcanism.

In the east-facing cliffs of the South Pahroc Range, the Leach Canyon–Bauers–Pahranagat sequence dips between 25° and 40° northwestward and is unconformably overlain by local rhyolitic tuffs and lavas. These rocks are overlain in turn by the Hiko Tuff that dips about 15° westward. All these rocks in turn are overlain by the Delamar Lake Tuff that dips about 5° westward. Between 22.6 and 18.6 Ma, 10°–25° of tilting clearly occurred, similar to the timing found by Best and others (1987) in the southern Wah Wah Mountains of southwestern Utah. Then, between 18.6 and about 16 Ma, another 10° of tilting occurred; and after the Delamar Lake Tuff was deposited, a final 5° of tilting occurred. Numerous normal faults cut the oldest strata, fewer cut the Hiko Tuff, and the least number cut the Delamar Lake Tuff; the amount of offset decreases on faults where they cut younger strata (Scott and Swadley, 1992). The downthrown sides of faults are generally filled with nonwelded tuffs. These "growth fault" relationships are similar to those observed by Bowman (1985) and Angelier and others (1987) in Rainbow Canyon.

Another example of progressive tilting is exposed on the eastern side of Delamar Valley, about 7.5 km northwest of the Kane Springs Wash caldera, where the Hiko Tuff and older volcanic strata dip between about 85° and 45° eastward and are overlain by only slightly dipping younger strata (Scott, Swadley, and others, 1990).

As described in the section, "Mafic Lava Flows," progressive tilting is also evident in the Meadow Valley Mountains, both within the intracaldera fill (Harding and others, this volume) and in outflow sheets south of the Kane Springs Wash caldera, where about 10°–15° southeastward tilting occurred between emplacement of the Leach Canyon Formation and the Kane Wash Tuff, followed by another 20° before emplacement of capping basalt flows (11.5 Ma), and by a final tilting of 5°–10° (Scott, Harding, and others, 1991).

Northeast of the Kane Springs Wash caldera in the northern Meadow Valley Mountains, the Harmony Hills Tuff dips about 60° northeastward, the Hiko Tuff dips about 50° northeastward, ash-flow tuff from the Narrow Canyon caldera dips about 25° northeastward, Kane Wash Tuff dips about 15°, and the tuff of Etna dips about 5° eastward. Thus, about 55° of progressive tilting occurred over about 7 m.y., during which about five major ash flows erupted from local sources.

We conclude that the distribution of progressive deformation in time was episodic. Also the degree and direction of extensional deformation were heterogeneous in space. Present-day extension on basin-range faults in the Basin and Range province is also inhomogeneous in time and space, perhaps analogous to the past record. The scale of past episodic fault movement and tilting cannot be easily measured in geologic time, but the geographic heterogeneity of extension is obvious. In Lincoln County, extensional processes were clearly not uniformly distributed; for example, the block of relatively undeformed strata in the southern Delamar Mountains is isolated within a "matrix" of more extended terrane (Scott, 1990). This stable pancake-like block is generally tilted less than 10° and is bounded by young basin-range faults. But even this block is intensely deformed locally by relatively small extensional structures, for example, the graben south and southwest of the Kane Springs Wash caldera (Scott, Novak, and Swadley, 1990) that splits the block in two.

In summary, inhomogeneity in time and space is the primary relationship between extension and volcanism during the Miocene in central Lincoln County, a pattern generally true for the Great Basin as a whole (Best and Christiansen, 1991).

REFERENCES CITED

Anderson, J.J., and Rowley, P.D., 1975, Cenozoic stratigraphy of southwestern high plateaus of Utah, *in* Anderson, J.J., Rowley, P.D., Fleck, R.J., and Nairn, A.E.M., 1975, Cenozoic geology of southwestern high plateaus of Utah: Geological Society of America Special Paper 160, p. 1–51.

Anderson, R.E., 1989, Tectonic evolution of the Intermontane System; Basin and Range, Colorado Plateau, and High Lava Plains, *in* Pakiser, L.C., and Mooney, W.D., eds., Geophysical framework of the continental United States: Geological Society of America Memoir 172, p. 163–176.

Anderson, R.E., and Hintze, L.F., 1993, Geologic map of the Dodge Spring quadrangle, Lincoln County, Nevada and Washington County, Utah: U.S. Geological Survey Geologic Quadrangle Map GQ-1721, scale 1:24,000.

Anderson, R.E., Zoback, M.L., and Thompson, G.A., 1983, Implications of selected subsurface data on the structural form and evolution of some basins in the northern Basin and Range province, Nevada and Utah: Geological Society of America Bulletin, v. 94, p. 1055–1072.

Angelier, Jacques, Faugère, Émeric, Michel-Noël, Gérard, and Anderson, R.E., 1987, Bassins en extension et tectonique synsedimentaire—Examples dans les "Basin and Range" (U.S.A.), *in* Genese et évolution des bassins sédimentaires: Notes et Mémoirs 21, Total Compagnie Francaise des Pétroles, p. 51–72.

Armstrong, R.L., 1968, Sevier orogenic belt in Nevada and Utah: Geological Society of America Bulletin, v. 79, p. 429–458.

_____1970, Geochronology of Tertiary igneous rocks, eastern Basin and Range province, western Utah, eastern Nevada, and vicinity, U.S.A.: Geochimica et Cosmochimica Acta, v. 34, p. 203–232.

Axen, G.J., Lewis, P.R., Burke, K.J., Sleeper, K.G., and Fletcher, J.M., 1988, Tertiary extension in the Pioche area, Nevada, *in* Bartley, J.M., Axen, G.J., Taylor, W.J., and Fryxell, J.E., Cenozoic tectonics of a transect through eastern Nevada near 38° N. latitude, *in* Weide, D.L., and Faber, M.L., eds., This extended land—Geological journeys in the southern Basin and Range: Geological Society of America, Cordilleran Section, Field Trip Guidebook, p. 3–5.

Axen, G.J., Taylor, W.J., and Bartley, J.M., 1993, Space-time patterns and tectonic controls of Tertiary extension and magmatism in the Great Basin of the western United States: Geological Society of America Bulletin, v. 105, p. 56–76.

Bartley, J.M., Axen, G.J., Taylor, W.J., and Fryxell, J.E., 1988, Cenozoic tectonics of a transect through eastern Nevada near 38° N. latitude, *in* Weide, D.L., and Faber, M.L., eds., This extended land—Geological journeys in the southern Basin and Range: Geological Society of America, Cordilleran Section, Field Trip Guidebook, p. 1–20.

Best, M.G., and Christiansen, E.H., 1991, Limited extension during peak Tertiary volcanism, Great Basin of Nevada and Utah: Journal of Geophysical Research, v. 96, p. 13509–13528.

Best, M.G., Christiansen, E.H., and Blank, H.R., Jr., 1989, Oligocene caldera complex and calc-alkaline tuffs and lavas of the Indian Peak volcanic field, Nevada and Utah: Geological Society of America Bulletin, v. 101, p. 1076–1090.

Best, M.G., Christiansen, E.H., Deino, A.L., Grommé, C.S., McKee, E.H., and Noble, D.C., 1989, Excursion 3A—Eocene through Miocene volcanism in the Great Basin of the western United States: New Mexico Bureau of Mines and Mineral Resources Memoir 47, p. 91–133.

Best, M.G., and Grant, S.K., 1987, Oligocene and Miocene volcanic rocks in the central Pioche-Marysvale igneous belt, western Utah and eastern Nevada: U.S. Geological Survey Professional Paper 1433–A, 28 p.

Best, M.G., Grommé, C.S., and Deino, A.L., 1992, Central Nevada caldera complex, northern Basin and Range province (Great Basin), U.S.A.: 29th International Geologic Congress, v. 2, p. 482.

Best, M.G., McKee, E.H., and Damon, P.E., 1980, Space-time-composition pattern of late Cenozoic mafic volcanism, southwestern Utah and adjoining areas: American Journal of Science, v. 280, p. 1035–1050.

Best, M.G., Mehnert, H.H., Keith, J.D., and Naeser, C.W., 1987, Miocene magmatism and tectonism in and near the southern Wah Wah Mountains, southwestern Utah: U.S. Geological Survey Professional Paper 1433–B, p. 29–47.

Best, M.G., Miller, D.S., Radke, L.E., and Kowallis, B.J., 1991, Geologic map of the Panaca Summit and Prohibition Flat quadrangles, Lincoln County, Nevada and Iron County, Utah: U.S. Geological Survey Open-File Report 91–124, scale 1:24,000.

Best, M.G., Scott, R.B., Rowley, P.D., Swadley, W C, Anderson, R.E., Grommé, C.S., Harding, A.E., Deino, A.L., Christiansen, E.H., Tingey, D.G., and Sullivan, K.R., 1993, Oligocene-Miocene caldera complexes, ash-flow sheets, and tectonism in the central and southeastern Great Basin, *in* Lahren, M.M., Trexler, J.H., Jr., and Spinosa, C., eds., 1993, Crustal evolution of the Great Basin and Sierra Nevada: Cordilleran/Rocky Mountain Section, Geological Society of America Guidebook, Department of Geological Sciences, University of Nevada, Reno, p. 285–311.

Best, M.G., Shuey, R.T., Caskey, C.F., and Grant, S.K., 1973, Stratigraphic relations of members of the Needles Range Formation at type localities in southwestern Utah: Geological Society of America Bulletin, v. 84, p. 3269–3278.

Blank, H.R., Jr., 1959, Geology of the Bull Valley district, Washington County, Utah: Seattle, Wash., University of Washington Ph. D. dissertation, 177 p.

Bogue, S.W., and Coe, R.S., 1981, Paleomagnetic correlation of Columbia River Basalt flows using secular variation: Journal of Geophysical Research, v. 86, p. 11883–11897.

Bowman, S.A., 1985, Miocene extension and volcanism in the Caliente caldera complex, Lincoln County, Nevada: Golden, Colo., Colorado School of Mines M.S. thesis, 143 p.

Christiansen, E.H., and Best, M.G., 1989, Compositional contrasts among middle Cenozoic ash-flow tuffs of the Great Basin, western United States: New Mexico Bureau of Mines and Mineral Resources Bulletin 131, p. 51.

Christiansen, E.H., Best, M.G., and Hoover, J.D., 1989, Petrology of a trachytic tuff from a calc-alkaline volcanic center—The Oligocene Isom Tuff, Indian Peak volcanic field, Utah and Nevada: Eos, v. 69, no. 44, p. 1494.

Cook, E.F., 1965, Stratigraphy of Tertiary volcanic rocks in eastern Nevada: Nevada Bureau of Mines Report 11, 61 p.

Cornwall, H.R., 1972, Geology and mineral deposits of southern Nye County, Nevada: Nevada Bureau of Mines and Geology Bulletin 77, 49 p.

Cox, Allan, 1971, Remanent magnetization and susceptibility of late Cenozoic rocks from New Zealand: New Zealand Journal of Geology and Geophysics, v. 14, p. 192–207.

Dalrymple, G.B., and Lanphere, M.A., 1969, Potassium-argon dating: San Francisco, Calif, W.H. Freeman, 258 p.

Deino, A.L., and Best, M.G., 1988, Use of high-precision single-crystal $^{40}Ar/^{39}Ar$ ages and TRM data in correlation of an ash-flow deposit in the Great Basin: Geological Society of America Abstracts with Programs, v. 20, no. 7, p. A397.

Diehl, J.F., Beck, M.E., Jr., Beske-Diehl, S., Jacobson, D., and Hearn, B.C., Jr., 1983, Paleomagnetism of the late Cretaceous–early Tertiary north-central Montana alkalic province: Journal of Geophysical Research, v. 88, p. 10593–10609.

Dolgoff, Abraham, 1963, Volcanic stratigraphy of the Pahranagat area, Lincoln County, southeastern Nevada: Geological Society of America Bulletin, v. 74, p. 875–900.

Ekren, E.B., Anderson, R.E., Rogers, C.L., and Noble, D.C., 1971, Geology of northern Nellis Air Force Base Bombing and Gunnery Range, Nye County, Nevada: U.S. Geological Survey Professional Paper 651, 91 p.

Ekren, E.B., Bucknam, R.C., Carr, W.J., Dixon, G.L., and Quinlivan, W.D., 1976, East-trending structural lineaments in central Nevada: U.S. Geological Survey Professional Paper 986, 16 p.

Ekren, E.B., Hinrichs, E.N., and Dixon, G.L., 1972, Geologic map of The Wall quadrangle, Nye County, Nevada: U.S. Geological Survey Miscellaneous Geologic Investigations Map I–719, scale 1:48,000.

Ekren, E.B., Orkild, P.P., Sargent, K.A., and Dixon, G.L., 1977, Geologic map of Tertiary rocks, Lincoln County, Nevada: U.S. Geological Survey Miscellaneous Investigations Series Map I–1041, scale 1:250,000.

Ekren, E.B., Quinlivan, W.D., Snyder, R.P., and Kleinhampl, F.J., 1974, Stratigraphy, structure, and geologic history of the Lunar Lake caldera of northern Nye County, Nevada: U.S. Geological Survey Journal of Research, v. 2, no. 5, p. 599–608.

Ekren, E.B., Rogers, C.L., and Dixon, G.L., 1973, Geologic and Bouguer gravity map of the Reveille quadrangle, Nye County, Nevada: U.S. Geological Survey Miscellaneous Geologic Investigations Map I–806, scale 1:48,000.

Fisher, R.A., 1953, Dispersion on a sphere: Royal Society [London] Proceedings, Series A, v. 217, p. 295–305.

Fleck, R.J., Anderson, J.J., and Rowley, P.D., 1975, Chronology of mid-Tertiary volcanism in high plateaus region of Utah, *in* Anderson, J.J., Rowley, P.D., Fleck, R.J., and Nairn, A.E.M., 1975, Cenozoic geology of southwestern high plateaus of Utah: Geological Society of America Special Paper 160, p. 53–61.

Gardner, J.N., Eddy, A.C., Goff, F.E., and Grafft, K.S., 1980, Reconnaissance geologic map of the northern Kawich and southern Reveille Ranges, Nye County, Nevada: Los Alamos Scientific Laboratory LA-8390-MAP, UC–51.

Gose, W.A., 1970, Palaeomagnetic studies of Miocene ignimbrites from Nevada: Geophysical Journal of the Royal Astronomical Society, v. 20, p. 241–252.

Hagstrum, J.T., and Gans, P.B., 1989, Paleomagnetism of the Oligocene Kalamazoo Tuff—Implications for middle Tertiary extension in east central Nevada: Journal of Geophysical Research, v. 94, p. 1827–1842.

Keith, J.D., Best, M.G., and Williams, V.S., 1992, Geologic map of the Ursine and Deer Lodge Canyon quadrangles, Lincoln County, Nevada and Iron County, Utah: U.S. Geological Survey Open-File Report 92–341, scale 1:24,000.

Kirschvink, J.L., 1980, The least-squares line and plane and the analysis of palaeomagnetic data: Geophysical Journal of the Royal Astronomical Society, v. 62, p. 699–718.

Kleinhampl, F.J., and Ziony, J.I., 1985, Geology of northern Nye County, Nevada: Nevada Bureau of Mines and Geology Bulletin 99A, 172 p.

Kowallis, B.J., and Best, M.G., 1990, Fission track ages from volcanic rocks in southwestern Utah and southeastern Nevada: Isochron/West, no. 55, p. 24–27.

Le Maitre, R.W., 1989, A classification of igneous rocks and glossary of terms: Boston, Mass., Blackwell, 193 p.

Lipman, P.W., Christiansen, R.L., and O'Connor, J.T., 1966, A compositionally zoned ash-flow sheet in southern Nevada: U.S. Geological Survey Professional Paper 524–F, p. F1–F47.

Macdonald, R., 1974, Nomenclature and petrochemistry of the peralkaline oversaturated extrusive rocks: Bulletin Volcanologique, v. 38, no. 3, p. 498–516.

Mackin, J.H., 1960, Structural significance of Tertiary volcanic rocks in southwestern Utah: American Journal of Science, v. 258, p. 81–131.

Martin, R.C., 1957, Vertical variations within some eastern Nevada ignimbrites: Moscow, Idaho, University of Idaho M.S. thesis, 85 p.

Marvin, R.T., Mehnert, H.H., and McKee, E.H., 1973, A summary of radiometric ages of Tertiary volcanic rocks in Nevada and eastern California, Part III, Southeastern Nevada: Isochron/West, no. 6, p. 1–30.

McKee, E.H., and John, D.A., 1987, Sample locality map and potassium-argon ages and data for Cenozoic igneous rocks in the Tonopah 1°×2° quadrangle, central Nevada: U.S. Geological Survey Miscellaneous Field Studies Map MF–1877–I.

Nairn, A.E.M., Rowley, P.D., and Anderson, J.J., 1975, Paleomagnetism of selected Tertiary volcanic units, southwestern Utah, *in* Anderson, J.J., Rowley, P.D., Fleck, R.J., and Nairn, A.E.M., 1975, Cenozoic geology of southwestern high plateaus of Utah: Geological Society of America Special Paper 160, p. 63–88.

Noble, D.C., 1968, Kane Springs Wash volcanic center, Lincoln County, Nevada, *in* Eckel, E.B., ed., Nevada Test Site: Geological Society of America Memoir 110, p. 109–116.

Noble, D.C., and McKee, E.H., 1972, Description and K-Ar ages of volcanic units of the Caliente volcanic field, Lincoln County, Nevada and Iron County, Utah: Isochron/West, no. 5, p. 17–24.

Noble, D.C., McKee, E.H., Hedge, C.E., and Blank, H.R., Jr., 1968, Reconnaissance of the Caliente depression, Lincoln County, Nevada: Geological Society of America Special Paper 115, p. 435–436.

Novak, S.W., 1984, Eruptive history of the rhyolitic Kane Springs Wash volcanic center, Nevada: Journal of Geophysical Research, v. 89, p. 8603–8615.

———1985, Geology and geochemical evolution of the Kane Springs Wash volcanic center, Lincoln County, Nevada: Stanford, Calif., Stanford University Ph. D. dissertation, 173 p.

Novak, S.W., and Mahood, G.A., 1986, Rise and fall of a basalt-trachyte-rhyolite magma system at the Kane Springs Wash caldera, Nevada: Contributions to Mineralogy and Petrology, v. 94, p. 352–373.

Page, W.R., and Scott, R.B., 1991, Ramping extensional faults in the Devonian Guilmette Formation, southern Nevada: Geological Society of America Abstracts with Programs, v. 23, no. 4, p. 55.

Page, W.R., Swadley, W C, and Scott, R.B., 1990, Preliminary geologic map of the Delamar 3 SW quadrangle, Lincoln County, Nevada: U.S. Geological Survey Open-File Report 90–336, scale 1:24,000, 17 p.

Pampeyan, E.H., 1989, Preliminary geologic map of the Meadow Valley Mountains, Lincoln and Clark Counties, Nevada: U.S. Geological Survey Open-File Report 89–182, scale 1:50,000.

Phillips, L.V., 1989, The petrology and magmatic evolution of the large volume ash-flow tuffs of the central Nevada caldera complex, Nye County, Nevada: Athens, Ga., University of Georgia Ph. D. dissertation, 285 p.

Quinlivan, W.D., and Rogers, C.L., 1974, Geologic map of the Tybo quadrangle, Nye County, Nevada: U.S. Geological Survey Miscellaneous Investigations Series Map I–821, scale 1:48,000.

Rogers, C.L., Anderson, R.E., Ekren, E.B., and O'Connor, J.T., 1967, Geologic map of the Quartzite Mountain quadrangle, Nye County, Nevada: U.S. Geological Survey Geologic Quadrangle Map GQ–672, scale 1:62,500.

Rowley, P.D., McKee, E.H., and Blank, H.R., Jr., 1989, Miocene gravity slides resulting from emplacement of the Iron Mountain pluton, southern Iron Springs mining district, Iron County, Utah: Eos, v. 70, no. 43, p. 1309.

Rowley, P.D., and Shroba, R.R., 1991, Geologic map of the Indian Cove quadrangle, Lincoln County, Nevada: U.S. Geological Survey Geologic Quadrangle Map GQ–1701, scale 1:24,000.

Rowley, P.D., Shroba, R.R., Simonds, F.W., Burke, K.J., Axen, G.J., and Olmore, S.D., 1991, Geologic map of the Chief Mountain quadrangle, Lincoln County, Nevada: U.S. Geological Survey Open-File Report 91–135, scale 1:24,000.

Rowley, P.D., and Siders, M.A., 1988, Miocene calderas of the Caliente caldera complex, Nevada-Utah: Eos, v. 69, no. 44, p. 1508.

Rowley, P.D., Snee, L.W., Mehnert, H.H., Anderson, R.E., Axen, G.J., Burke, K.J., Simonds, F.W., Shroba, R.R., and Olmore, S.D., 1992, Structural setting of the Chief Mining District, Eastern Chief Range, Lincoln County, Nevada, *in* Thorman, C.H., ed., Application of structural geology to mineral and energy resources of the central and western United States: U.S. Geological Survey Bulletin 2012, p. H1–H17.

Rowley, P.D., Steven, T.A., Anderson, J.J., and Cunningham, C.G., 1979, Cenozoic stratigraphy and structural framework of southwestern Utah: U.S. Geological Survey Professional Paper 1149, 22 p.

Sargent, K.A., and McKee, E.H., 1969, The Bates Mountain Tuff in northern Nye County, Nevada: U.S. Geological Survey Bulletin 1294–E, p. E1–E12.

Sargent, K.A., and Roggensack, K., 1984, Map showing outcrops of pre-Quaternary ash-flow tuffs and volcaniclastic rocks, Basin and Range province, Nevada: U.S. Geological Survey Water Resources Investigations Report WRIR 83-4119-E.

Scott, R.B., 1990, Significance of mild extension of a relatively stable area within highly extended terrane, southeastern Nevada: Geological Society of America Abstracts with Programs, v. 22, no. 3, p. 81.

Scott, R.B., Blank, H.R., Jr., and Page, W.R., 1991, Evidence for a precursor to the Kane Springs Wash caldera: Geological Society of America Abstracts with Programs, v. 23, no. 4, p. 91.

Scott, R.B., Harding, A.E., Swadley, W C, Novak, S.W., and Pampeyan, E.H., 1991, Preliminary geologic map of the Vigo NW quadrangle, Lincoln County, Nevada: U.S. Geological Survey Open-File Report 91–389, scale 1:24,000.

Scott, R.B., Nesbitt, R.W., Armstrong, R.L., and Dash, E.J., 1971, A strontium isotope evolution model for Cenozoic magma genesis, eastern Great Basin, USA: Bulletin Volcanologique, v. 35, p. 1–26.

Scott, R.B., Novak, S.W., and Swadley, W C, 1990, Preliminary geologic map of the Delamar 3 NE quadrangle, Lincoln County, Nevada: U.S. Geological Survey Open-File Report 90–33, scale 1:24,000.

Scott, R.B., Page, W.R., and Swadley, W C, 1990, Preliminary geologic map of the Delamar 3 NW quadrangle, Lincoln County, Nevada: U.S. Geological Survey Open-File Report 90–405, scale 1:24,000.

Scott, R.B., and Swadley, W C, 1992, Preliminary geologic map of the Pahroc Summit Pass and Hiko SE quadrangles, Lincoln County, Nevada: U.S. Geological Survey Open-File Report 92–423, scale 1:24,000.

Scott, R.B., Swadley, W C, and Byron, Barbara, 1992, Preliminary geologic map of the Pahroc Spring quadrangle, Lincoln County, Nevada: U.S. Geological Survey Open-File Report 92–613, scale 1:24,000.

Scott, R.B., Swadley, W C, and Novak, S.W., 1988, Preliminary geologic map of the Delamar Lake quadrangle, Lincoln County, Nevada: U.S. Geological Survey Open-File Report 88–576.

Scott, R.B., Swadley, W C, and Novak, S.W., 1993, Geologic map of the Delamar Lake quadrangle, Lincoln County, Nevada: U.S. Geological Survey Geologic Quadrangle Map GQ–1730, scale 1:24,000.

Scott, R.B., Swadley, W C, Novak, S.W., and Page, W.R., in press, Preliminary geologic map of the Elgin SW quadrangle, Lincoln County, Nevada: U.S. Geological Survey Open-File Report, scale 1:24,000.

Scott, R.B., Swadley, W C, Page, W.R., and Novak, S.W., 1990, Preliminary geologic map of the Gregerson Basin quadrangle, Lincoln County, Nevada: U.S. Geological Survey Open-File Report 90–646, scale 1:24,000.

Shubat, M.A., and Snee, L.W., 1992, High precision $^{40}Ar/^{39}Ar$ geochronology, volcanic stratigraphy, and general deposits of Keg Mountain, west-central Utah, *in* Thorman, C.H., ed., Application of structural geology to mineral and energy resources of the central and western United States: U.S. Geological Survey Bulletin 2012, p. G1–G16.

Shuey, R.T., Caskey, C.F., and Best, M.G., 1976, Distribution and paleomagnetism of the Needles Range Formation, Utah and Nevada: American Journal of Science, v. 276, p. 954–968.

Siders, M.A., and Shubat, M.A., 1986, Stratigraphy and structure of the northern Bull Valley Mountains and Antelope Range, Iron County, Utah, *in* Griffen, D.T., and Phillips, W.R., eds., Thrusting and extensional structures and mineralization in the

Beaver Dam Mountains, southwestern Utah: Utah Geological Association Publication 15, p. 87–102.

Snee, L.W., Mehnert, H.H., Rowley, P.D., Anderson, R.E., and Scott, R.B., 1990, New isotopic ages demonstrate extensional faulting of 19–12 Ma in the western Caliente caldera complex and vicinity, Lincoln County, Nevada: Eos, v. 71, p. 1612.

Snyder, R.P., Ekren, E.B., and Dixon, G.L., 1972, Geologic map of the Lunar Crater quadrangle, Nye County, Nevada: U.S. Geological Survey Miscellaneous Geologic Investigations Map I–700, scale 1:48,000.

Steiger, R.H., and Jäger, Emile, 1977, Subcommission on geochronology—Convention on the use of decay constants in geo- and cosmochronology: Earth and Planetary Science Letters, v. 36, p. 359–362.

Swadley, W C, Page, W.R., Scott, R.B., and Pampeyan, E.H., 1990, Preliminary geologic map of the Delamar 3 SE quadrangle, Lincoln County, Nevada: U.S. Geological Survey Open-File Report 90–221, scale 1:24,000.

Swadley, W C, and Rowley, P.D., 1991, Preliminary geologic map of the Pahroc Spring SE quadrangle: U.S. Geological Survey Open-File Report 92–7, scale 1:24,000.

Swadley, W C, and Scott, R.B., 1990, Preliminary geologic map of the Delamar NW quadrangle, Lincoln County, Nevada: U.S. Geological Survey Open-File Report 90–622, scale 1:24,000.

Swadley, W C, and Simonds, F.W., 1991, Preliminary geologic map of the Deadman Spring SE quadrangle: U.S. Geological Survey Open-File Report 91–627, scale 1:24,000.

———1992, Preliminary geologic map of the Pahroc Spring NE quadrangle: U.S. Geological Survey Open-File Report 92–16, scale 1:24,000.

Taylor, W.J., 1989, Geometry of faulting, timing of extension and their relationship to volcanism, near 38° N latitude, eastern Nevada: Salt Lake City, Utah, University of Utah Ph. D. dissertation, 204 p.

———1993, Stratigraphic and lithologic analysis of the Claron Formation in southwestern Utah: Utah Geological Survey Miscellaneous Publication 93–1, 52 p.

Taylor, W.J., and Bartley, J.M., 1992, Prevolcanic extensional Seaman breakaway fault and its geologic implications for eastern Nevada and western Utah: Geological Society of America Bulletin, v. 104, p. 255–266.

Taylor, W.J., Bartley, J.M., Lux, D.R., and Axen, G.J., 1989, Timing of Tertiary extension in the Railroad Valley–Pioche transect, Nevada—Constraints from $^{40}Ar/^{39}Ar$ ages of volcanic rocks: Journal of Geophysical Research, v. 94, p. 7757–7774.

Tschanz, C.M., and Pampeyan, E.H., 1970, Geology and mineral deposits of Lincoln County, Nevada: Nevada Bureau of Mines and Geology Bulletin 73, scale 1:250,000, 188 p.

Wernicke, Brian, Axen, G.J., and Snow, J.K., 1988, Basin and Range extensional tectonics at the latitude of Las Vegas, Nevada: Geological Society of America Bulletin, v. 100, p. 1738–1757.

Whitebread, D.H., 1989, Geologic map of the Tonopah 1°×2° quadrangle, central Nevada: U.S. Geological Survey Miscellaneous Field Studies Map MF–1877–A, scale 1:250,000.

Williams, P.L., 1967, Stratigraphy and petrography of the Quichapa Group, southwestern Utah and southeastern Nevada: Seattle, Wash., University of Washington Ph. D. dissertation, 139 p.

Zoback, M.L., Anderson, R.E., and Thompson, G.A., 1981, Cainozoic evolution of the state of stress and style of tectonism of the Basin and Range province of the western United States: Philosophical Transactions of Royal Society of London, v. A300, p. 407–434.

Stratigraphy of Miocene Ash-Flow Tuffs in and near the Caliente Caldera Complex, Southeastern Nevada and Southwestern Utah

By Peter D. Rowley, L. David Nealey, Daniel M. Unruh, Lawrence W. Snee, Harald H. Mehnert, R. Ernest Anderson, *and* C. Sherman Grommé

GEOLOGIC STUDIES IN THE BASIN AND RANGE–COLORADO PLATEAU TRANSITION IN SOUTHEASTERN NEVADA, SOUTHWESTERN UTAH, AND NORTHWESTERN ARIZONA, 1992

U.S. GEOLOGICAL SURVEY BULLETIN 2056–B

UNITED STATES GOVERNMENT PRINTING OFFICE, WASHINGTON : 1995

CONTENTS

FIGURES

CONTENTS

Stratigraphy of Miocene Ash-Flow Tuffs in and near the Caliente Caldera Complex, Southeastern Nevada and Southwestern Utah

By Peter D. Rowley, L. David Nealey, Daniel M. Unruh, Lawrence W. Snee, Harald H. Mehnert, R. Ernest Anderson, *and* C. Sherman Grommé

ABSTRACT

The Tertiary volcanic section of southeastern Nevada and southwestern Utah contains numerous regional and local ash-flow tuff sheets. Many of the tuffs in the upper (Miocene) part of this volcanic section were derived from the Caliente caldera complex of Nevada-Utah, centered southeast of Caliente, Nevada. The caldera complex is at least 80 kilometers east-west by 35 kilometers north-south and contains nested calderas that formed between at least 23 and 13 Ma. The volcanism that formed this complex coincided with the main episode of extension in this part of the Basin and Range province, and thus, caldera margins consist of a complex array of faults and subsided areas. Many of the tuffs in the upper part of the section are lithologically similar (nearly all are rhyolites) yet were erupted at different times from different sources, including the Caliente caldera complex. This report summarizes the Miocene stratigraphy and attempts to utilize petrographic, chemical, and paleomagnetic data in concert with geologic mapping to correlate the tuffs. This report also sets the stage for preliminary conclusions in this volume about the magmatic evolution of the caldera complex.

The oldest tuff for which we present data is the Leach Canyon Formation (23.8 Ma), which was thought to have been derived from the northern part of the Caliente caldera complex but whose source has not yet been found. The Bauers Tuff Member (22.8 Ma) and perhaps the underlying Swett Tuff Member (23.7? Ma), both of the Condor Canyon Formation, were derived from the Clover Creek caldera in the northwestern part of the Caliente complex. The Harmony Hills Tuff (22.5–22.0 Ma), although suggested to be from the Caliente complex, most likely was derived from well east of the complex. The source of the Racer Canyon Tuff (19.2?–18.7 Ma) is probably the east end of the Caliente caldera complex. The Hiko Tuff (18.6–18.2 Ma) was derived mostly from the Delamar caldera in the west end of the Caliente caldera complex. The Hiko cannot yet be distinguished from the Racer Canyon, so many questions remain about the relationship of each to the other; currently we suspect that they represent different eruptions from the same magma chamber. The tuff of Tepee Rocks (17.8 Ma) resembles the Racer Canyon and Hiko Tuffs but is a minor unit derived probably from directly east of the Delamar caldera. The change from calc-alkalic rocks to basalt and high-silica rhyolite then took place, and the Delamar Lake Tuff (15.8–15.5 Ma) was derived from a source suspected to be southwest of the Caliente caldera complex; outflow of this unit extended north from its source to just west of the complex. The tuff of Rainbow Canyon erupted at 15.6–15.2 Ma from the Buckboard Canyon caldera, which is inset into the Delamar caldera. The tuff of Kershaw Canyon (15.3?–14.0 Ma) probably came from a caldera just east of the Buckboard Canyon caldera. The tuff of Sawmill Canyon is a minor cooling unit intertongued with the lower part of the tuff of Kershaw Canyon south of Caliente and presumably derived in or near this area. The two outflow sheets (14.6–14.4 Ma) of the peralkaline Gregerson Basin Member of the Kane Wash Tuff are intertongued with the tuff of Kershaw Canyon, but the source is the Kane Springs Wash caldera 20 kilometers south of the Caliente caldera complex. The tuff of Etna (14.0 Ma) overlies the tuff of Kershaw Canyon; its source has not been found. The Ox Valley Tuff (12.6–11.4? Ma) of Utah may be derived from the same magma chamber as the tuff of Etna, but its source is farther east, probably in the southeast part of the complex.

INTRODUCTION

The Caliente caldera complex of southeastern Nevada and southwestern Utah is a large Miocene eruptive center that was the source of several of the most extensive regional ash-flow sheets in the southern Great Basin. The complex, centered southeast of the town of Caliente, Nev., is within one of two connected major igneous belts, the Pioche-Marysvale

and Delamar–Iron Springs, that extend east-northeastward into Utah and are well delineated by aeromagnetic anomalies (fig. 1). The belts also contain the major Indian Peak caldera complex (Best, Christiansen, and Blank, 1989), the source of the Oligocene Needles Range Group and Isom Formation, and at its east end the Marysvale volcanic field, a mineralized Oligocene and Miocene stratovolcano and caldera complex (Rowley and others, 1979; Steven and others, 1984, 1990; Rowley, Cunningham, and others, in press). The Caliente complex is dominated by silicic ash-flow tuffs and lava flows, but it also contains minor amounts of intermediate and mafic volcanic rocks. Volcanism in the complex began at least by 23 Ma and continued apparently to about 13 Ma (Rowley and others, 1990). Intracaldera deposits and outflow sheets from the complex are intercalated with outflow sheets from the nearby Kane Springs Wash caldera to the south. Outflow ash-flow tuffs from the Caliente complex also intertongue with outflow sheets from calderas to the west and northwest.

This report is a product of the Basin and Range to Colorado Plateau transition (BARCO) Study Unit of the National Geologic Mapping program of the U.S. Geological Survey. This project includes detailed quadrangle mapping of the Caliente caldera complex and nearby areas in order to better understand its igneous and tectonic evolutionary history and the setting of epithermal gold deposits. In conjunction, we are also studying the area's igneous petrology and geochemistry, structural geology, isotopic ages, isotopic

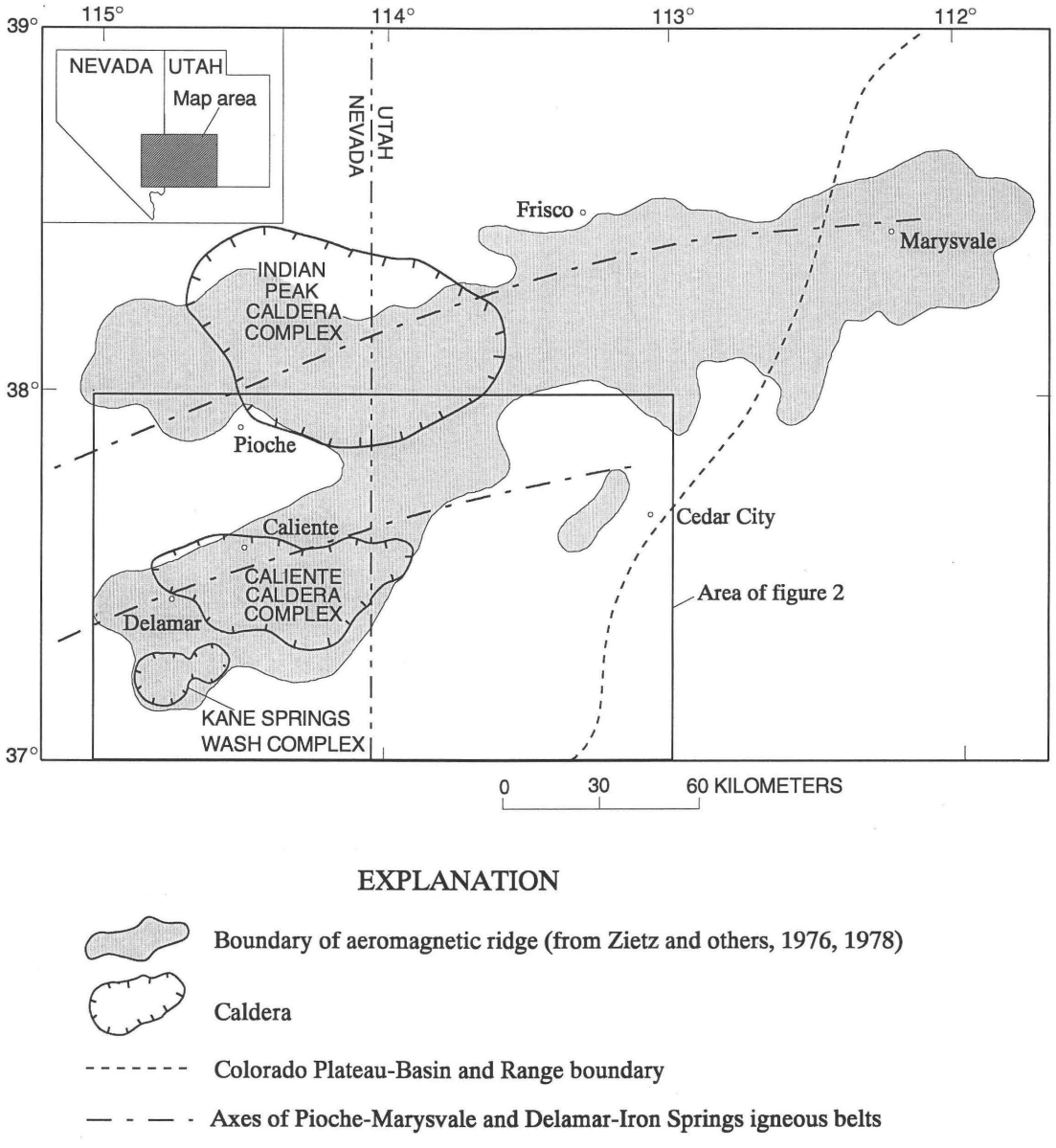

Figure 1. Map showing aeromagnetic ridge and tectonic setting of Caliente caldera complex, Nevada-Utah.

geochemistry, and paleomagnetism. Before the project began, the area of the complex had been mapped only at 1:250,000 scale (Ekren and others, 1977). Noble and others (1968) and Noble and McKee (1972) were the first to discover the caldera complex, which they called the Caliente depression. Ekren and others (1977) refined the shape of the complex, which they called the Caliente caldron complex. Numerous regional ash-flow tuffs had been predicted to be derived from the Caliente caldera complex: Leach Canyon and Condor Canyon Formations by Williams (1967) and Harmony Hills, Racer Canyon, Hiko, and Ox Valley Tuffs by Noble and others (1968) and Noble and McKee (1972). Yet before the current project began, only the Hiko Tuff had been confirmed to have erupted from the Caliente complex (Ekren and others, 1977), specifically from the west end of the complex.

This report summarizes the stratigraphy of ash-flow tuffs in and around the Caliente caldera complex that span the interval from about 24 to about 13 Ma, the probable interval of Caliente volcanism. These tuffs make up the upper part of the volcanic section in this part of Nevada and Utah and include all tuffs known or suggested to have been derived from the caldera complex. Some tuffs of this interval, however, erupted from sources other than the Caliente complex, and data for them are included for comparison and for completeness of this part of the stratigraphic section. Presently the study at Caliente is in its early stages and entails considerable confusion about many field relations and about the identification of and sources for numerous ash-flow tuffs that commonly look alike. As a first step in distinguishing the various tuffs, we here give data on lithology and on modal and chemical analyses and preliminary information on isotopic ages and paleomagnetism. Scott and others (this volume) present similar data on the stratigraphic section south and west of the Caliente complex; they also include information on the lower part of the section that we do not cover here. In work in progress we deal also with intercalated lava flows, including mafic sequences whose source plutons may represent the driving force for caldera magmatism (for example, Wiebe, 1993). Another purpose of the present report is to provide introductory information for two reports that follow, on preliminary geochemistry (Nealey and others, this volume) and isotopes (Unruh and others, this volume) of these tuffs. Together, the three studies provide our first impressions about the magmatic setting of the Caliente complex as well as of other calderas in the area that were active between about 24 and 13 Ma.

Several new $^{40}Ar/^{39}Ar$ mineral dates help constrain temporal relationships of tuffs in the area of the Caliente caldera complex. The $^{40}Ar/^{39}Ar$ isotopic dating method is a variant of the conventional K/Ar method; for $^{40}Ar/^{39}Ar$ analysis, samples are irradiated in a nuclear reactor to produce ^{39}Ar from ^{39}K. In this study, 50–100 mg of sanidine and biotite were irradiated in the USGS Denver TRIGA reactor for 30 hours at 1 MW (megawatt). Each sample was irradiated adjacent to an aliquant of standard MMhb-1 hornblende for which K=1.555 percent, $^{40}Ar_K=1.624\times10^{-9}$ mol/g, and K/Ar date=520.4 Ma (Samson and Alexander, 1987). Samples were experimentally degassed in a double-vacuum resistance furnace via step-heating in 12–15 steps under ultra-high vacuum for about 20 minutes at each temperature step. The mass 40, 39, 38, 37, and 36 isotopes of argon were analyzed using a Mass Analyser Products series 215 rare-gas mass spectrometer. Raw isotopic data were corrected for volume, mass discrimination, trap current, radioactive decay of ^{37}Ar and ^{39}Ar, and interfering isotopes of argon. Decay constants of Steiger and Jäger (1977) were used to recalculate dates of any cited samples that were analyzed before 1977.

ACKNOWLEDGMENTS

This study could not have been possible without the help of numerous persons, to whom we are indeed grateful. It is an outgrowth of dissertation studies by the senior author many years ago, supervised by the late J.H. Mackin. Since then, many forms of data, advice, and conclusions from J.J. Anderson, M.G. Best, P.L. Williams, D.S. Barker, R.B. Scott, E.B. Ekren, T.A. Steven, C.G. Cunningham, R.F. Hardyman, A.E. Harding, A.L. Deino, and M.A. Siders have been invaluable to our work. We thank M.R. Hudson and J.G. Rosenbaum for use of their unpublished paleomagnetic data. E.A. du Bray convinced us that trace-element chemical data obtained by energy-dispersive X-ray fluorescence spectrometry (using a Kevex 700 spectrometer) are useful to correlate tuffs, taught us the technique, and shared his own data with us. H.R. Blank helped with information on tuffs from the Bull Valley Mountains and geophysics of the Caliente area. D.R. Lux shared isotopic dates on tuffs in the Caliente area that he has analyzed. We thank D.M. Cheney and P.L. FitzMaurice for mineral separations from most of the rocks we dated. M.A. Siders, F.W. Simonds, and F.M. Haggett did some modal analyses. Technical reviews by Florian Maldonado, R.B. Scott, and W C Swadley, and a non-technical review by L.M. Carter that was beyond the call of duty greatly improved the manuscript. We are grateful for the many forms of assistance from each and every Young of Young's R.V. Park, Caliente, Nev.

GEOLOGIC SETTING OF THE CALIENTE CALDERA COMPLEX

The Caliente caldera complex occupies an area of at least 80 km east-west by 35 km north-south, mostly in Nevada but partly in Utah. Its generalized shape is shown by reconnaissance mapping (Ekren and others, 1977) and gravity data (Blank and Kuchs, 1989) (fig. 2), but detailed

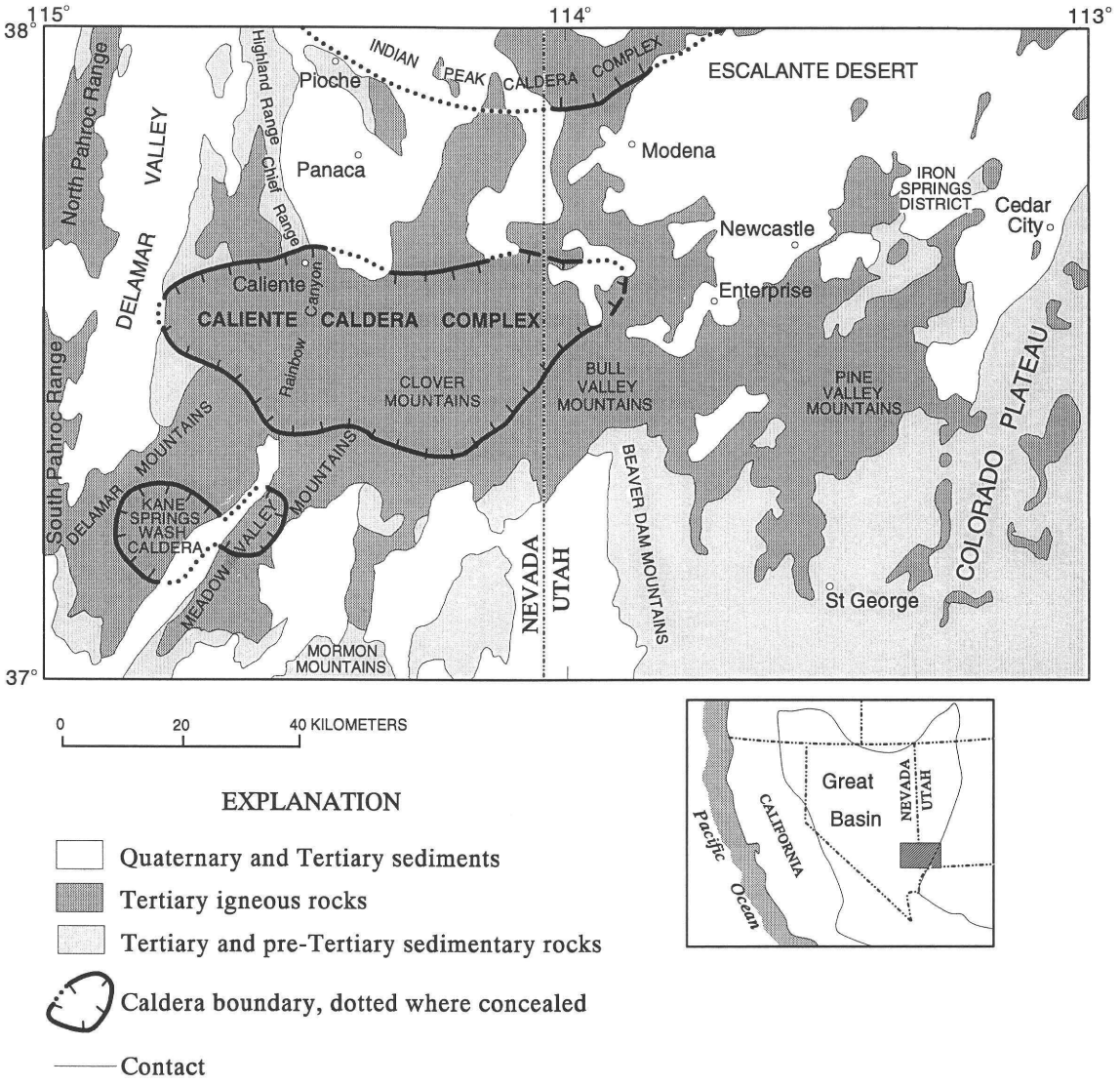

Figure 2. Map showing generalized geology and geographic features of Caliente caldera complex and vicinity.

mapping of the western part of the complex shows the margin to be complicated and to be largely defined by synchronous tectonic faults (fig. 3). The caldera complex includes numerous nested calderas, only four of which so far have been named (Rowley and Siders, 1988). The oldest named is the Clover Creek caldera (22.8 Ma), which formed in the northern part of the complex (fig. 3) as the result of the eruption of the Bauers Tuff Member of the Condor Canyon Formation (fig. 4). About 4 million years after this, at 18.6–18.2 Ma, the Hiko Tuff erupted from the western part of the complex, as Ekren and others (1977) determined; we call this the Delamar caldera (fig. 3). Later, at about 16 Ma, the Pine Park caldera (Rowley and Siders, 1988; Siders, 1991) formed in the eastern part of the complex; we have not yet studied in detail the deposits of this caldera, nor have we mapped it. Then, at about 15.6–15.2 Ma, eruption of the tuff of Rainbow Canyon led to subsidence of the Buckboard Canyon caldera in the western part of the Caliente complex; it is inset into the Delamar caldera (fig. 3).

In addition to the four named calderas, other vents or calderas formed in the Caliente complex, but their locations are uncertain or poorly defined. For example, the Racer Canyon Tuff (fig. 4) probably was derived from the east part of the complex (Siders and others, 1990; Siders, 1991), but we have not yet mapped that area. The tuff of Tepee Rocks (fig. 4) also probably came from the complex east of the Delamar caldera; but we are not certain of its source. The tuff of Kershaw Canyon is exposed south of Caliente and north of the caldera complex, and it probably was derived from east of the Delamar caldera; but we have not determined whether this tuff represents outflow or intracaldera deposits, let alone where its source walls are located. Outflow of the tuff of Etna has been mapped in the caldera complex and in nearby areas outside the complex. Earlier mapping suggested that its

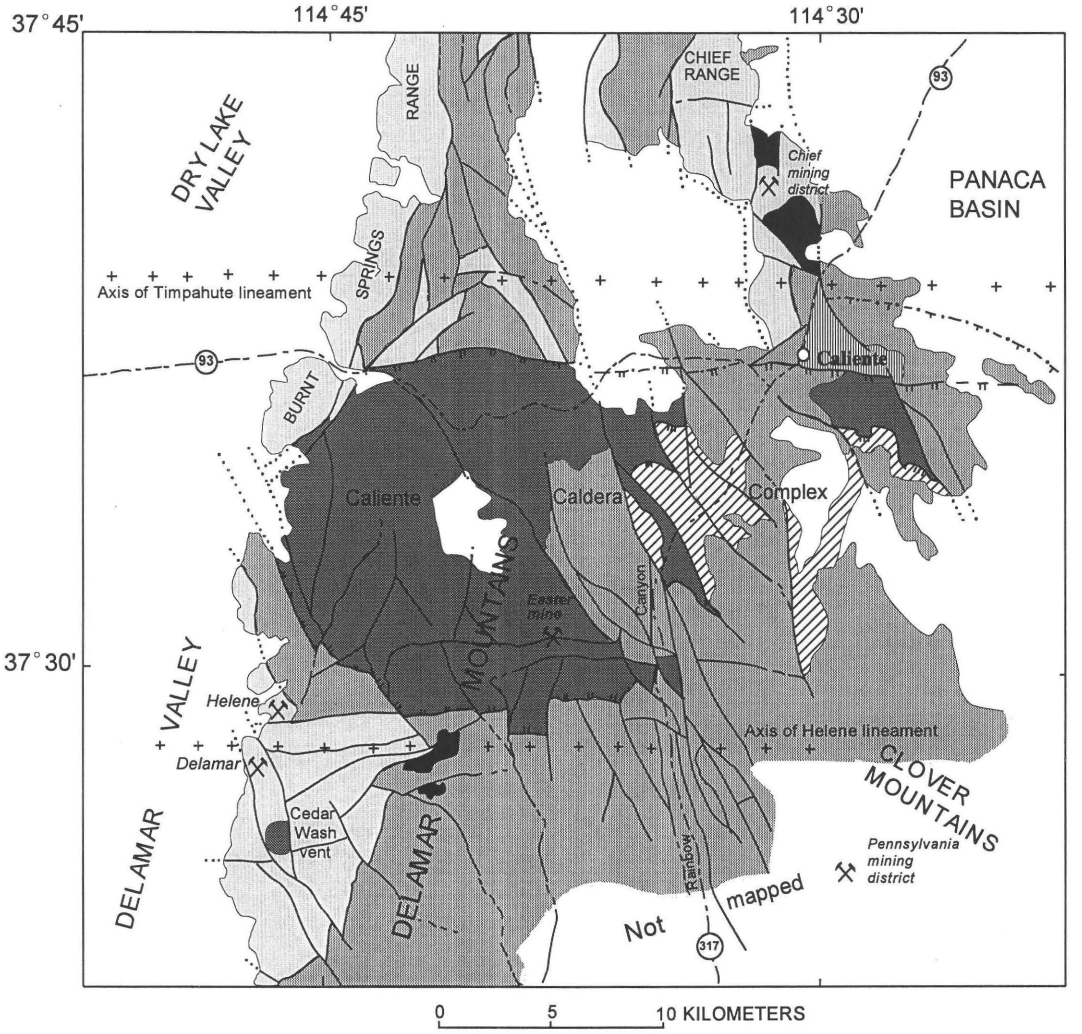

Figure 3. Generalized geologic map of western Caliente caldera complex and vicinity, based on 1:24,000-scale mapping in progress.

source was a fissure vent at the south edge of the Delamar caldera (Best and others, 1993), but recent mapping and petrologic studies now indicate otherwise; we do not know the exact location of the source of the tuff of Etna. The Ox Valley Tuff may have been derived from the southeastern part of the complex (Anderson and Hintze, 1993), but its specific source has not been located.

Other regional outflow tuff sheets have a less certain connection to the Caliente caldera complex, or they are unlikely to have come from the complex. Thus, the Leach Canyon Formation may have been derived from the northern Caliente complex, as Williams (1967) suggested, but our mapping and reconnaissance investigations in the area have not disclosed evidence of its caldera. The Harmony Hills

AGE	UNIT	SOURCE
Miocene	Ox Valley Tuff (12.6?-11.4? Ma)	Caliente
	tuff of Etna (14.0 Ma)	Caliente
	Kane Wash Tuff: Gregerson Basin Member: upper unit (14.4 Ma) / lower unit (14.6 Ma) — tuff of Kershaw Canyon (15.3?-14.2 Ma)	Kane Springs Wash
	tuff of Sawmill Canyon	Caliente
	tuff of Rainbow Canyon (15.6-15.2 Ma)	Buckboard Canyon
	Delamar Lake Tuff (15.8-15.5 Ma)	?
	tuff of Tepee Rocks (17.8 Ma)	Caliente
	lava flows of Buckboard Spring (18.0 Ma)	Delamar
	volcanic dome of Crows Nest Tank (18.2 Ma) / * *porphyry of Meadow Valley Wash (19.4-<18.2 Ma)*	Delamar
	Hiko Tuff (18.6-18.2 Ma)	Delamar
	Racer Canyon Tuff (19.2?-18.7 Ma)	Caliente
	lava flows of Indian Cove (21.9 Ma)	Clover Creek
	Quichapa Group: Harmony Hills Tuff (22.5-22.0 Ma)	?
	Quichapa Group: Condor Canyon Formation: Bauers Tuff Member (22.8 Ma) / *intrusive rocks of Clover Creek caldera (22.8 Ma)*	Clover Creek
	Quichapa Group: Condor Canyon Formation: Swett Tuff Member (23.7? Ma)	Caliente
	Quichapa Group: *Leach Canyon Formation (23.8 Ma)*	?
Oligocene	*Cobalt Canyon stock (24.8 Ma)*	

* dikes

Figure 4. Stratigraphic chart of igneous rocks in upper part of the Tertiary volcanic section in and near Caliente caldera complex. Ash-flow tuffs, which are discussed in this report, are shown in regular roman type; whereas lava flows and intrusive units discussed by Nealey and others (this volume) and Unruh and others (this volume) are shown in italic type. Numbers give isotopic or inferred ages, in Ma, of units; details are given in the text. "Source" refers to name of caldera source, where known. Use of "Caliente" for source indicates that the source is considered to be within the Caliente caldera complex but that the specific caldera has not been named or in some cases not found. Query, caldera has not been found; blank, not applicable.

Tuff, suggested by Noble and McKee (1972) to have been derived from the complex, more likely was derived from the Bull Valley Mountains of Utah (Blank, 1959; Williams, 1967), although the caldera has not been identified.

In addition to tuffs, plutons and lava flows were emplaced in and near the Caliente caldera complex at various times in the evolution of the complex. The Cobalt Canyon stock, which formed epithermal gold deposits in the Chief mining district 8 km north of Caliente (fig. 3) and whose exposed south edge is 3 km north of the caldera complex, may be related to caldera magmatism. However, the isotopic age of this quartz monzonite porphyry pluton, based on recently determined plateau $^{40}Ar/^{39}Ar$ dates, is 24.8 Ma (Snee and others, 1990; Rowley and others, 1992), and thus older than presently known ages of caldera magmatism. Isotopic data on this stock are given by Unruh and others (this volume). A faulted dioritic stock exposed as close as 3 km from the southwest edge of the caldera complex (fig. 3) and younger dikes and small plutons of rhyolite that extend west from the edge of the Delamar caldera may also be related to magmatism in the caldera complex. These intrusive rocks, which are synchronous with caldera magmatism, formed epithermal gold deposits in the major Delamar (Ferguson) mining district (Emmons, 1901; Callaghan, 1937; Ferris, 1991; P.D. Rowley, R.B. Scott, and W C Swadley, mapping in progress) just southwest of the caldera complex (fig. 3). Epithermal gold deposits also are known along east-striking faults at the Easter (Taylor) mine (fig. 3) and also occur in the Pennsylvania mining district (fig. 3) south of the Caliente caldera complex (Rowley and others, 1992; Best and others, 1993) and in the Goldstrike mining district just southeast of the caldera complex (Adair, 1986; Willden and Adair, 1986).

Intracaldera plutons probably formed during development of most calderas and other vents, but few have been found in the Caliente caldera complex. So far, only a small part of the intracaldera pluton of the Clover Creek caldera has been mapped. It occurs as a narrow piece of a pluton roof exposed about 1 km north of Caliente. This rhyolite porphyry resembles the Bauers Tuff Member except that phenocrysts are larger than in Bauers and generally unbroken. The rock has a preliminary plateau $^{40}Ar/^{39}Ar$ date on sanidine of 22.8±0.1 Ma (L.W. Snee, unpub. data, 1991). Isotopic data on this intrusion are given by Unruh and others (this volume).

Andesitic lava flows and volcanic mudflow breccia erupted from stratovolcanoes on the rims or within calderas of the Caliente complex. One such mafic volcanic dome, the lava flows of Indian Cove, rests on the apparent edge of the Clover Creek caldera several kilometers north of Caliente. Its eruption indicates consolidation of the magma chamber of the Clover Creek caldera. The dome consists of a thick sequence of lava flows and volcanic mudflow breccia of alkalic andesite, dacite, trachyandesite, and trachydacite. A sample received a plateau $^{40}Ar/^{39}Ar$ date on sanidine of 21.9±0.1 Ma (Snee and others, 1991; Rowley and others, 1992). Isotope data on this dome are given by Unruh and others (this volume).

Rim and intracaldera rhyolite domes also formed throughout the caldera history as magma chambers leaked magma to the surface. One such rhyolite lava-flow sequence is the volcanic dome of Crows Nest Tank, which occurs on

the north edge of the Delamar caldera about 9 km west of Caliente. It much resembles in lithology and chemistry the Hiko Tuff, as is to be expected for a magma from the same source chamber as Hiko. It has two preliminary plateau $^{40}Ar/^{39}Ar$ dates on sanidine and hornblende that average 18.2±0.1 Ma (L.W. Snee, unpub. data, 1991). Isotope data on this dome are given by Unruh and others (this volume). This dome is identical in age and lithology to another small rhyolite dome, the volcanic dome of Barnes Canyon, also on the north edge of the Delamar caldera but 6 km east of Caliente, that has two preliminary plateau $^{40}Ar/^{39}Ar$ dates on sanidine and biotite that average 18.2±0.2 Ma (L.W. Snee, unpub. data, 1991). Other rhyolite domes are common in the Caliente caldera complex, notably along the east-trending south edge of the Delamar caldera; none of them have been isotopically dated but they appear to be generally of Hiko age (P.D. Rowley, unpub. mapping, 1992–1993).

An unusual lava flow was analyzed by Unruh and others (this volume) and dated by L.W. Snee. It is a dark-gray and black, basaltic trachyandesite (fig. 5) containing a disequilibrium (commonly altered) assemblage of sanidine and plagioclase phenocrysts as long as 1.5 cm and of scattered quartz and hornblende phenocrysts. These crystals occur in a fresh rock with sparse small phenocrysts of olivine, orthopyroxene, and plagioclase in a flow groundmass of the same minerals as well as of Fe-Ti oxides. The flows overlie the uppermost intracaldera ash-flow tuffs of the Hiko Tuff in the Delamar caldera and thus mark the cessation of Hiko volcanism and consolidation of the magma chamber of the Delamar caldera. L.W. Snee determined a plateau $^{40}Ar/^{39}Ar$ date on sanidine of 18.0±0.2 Ma on a flow from this sequence, which we here call the lava flows of Buckboard Spring for exposures near this spring in upper Buckboard Canyon about 11 km west of Caliente.

The Caliente caldera complex formed during the main episode of regional extension in the area, the second of three episodes that affected the Caliente area (Rowley and others, 1992). Deformation during this episode occurred on complex mixtures of high-angle strike-slip, normal-slip, and oblique-slip faults, as well as low-angle detachment faults (Bowman, 1985; Michel-Noël and others, 1990; Rowley and others, 1992; Best and others, 1993). As such, the style of deformation in the Caliente area, and its synchroneity with volcanism, are similar to relationships described and origins interpreted in the Utah-Nevada-Arizona tricorner area by Anderson (1984, 1986, 1987, 1989, 1990), Anderson and Bohannon (1993), and Anderson and Barnhard (1993a, b). Distinctive porphyritic dacitic dikes and small plutons, characterized by similar modal ratios of minerals and by feldspar phenocrysts as long as 2 cm, were emplaced along some of the high-angle faults in widely scattered areas in and near the caldera complex as well as in the Panaca Summit area about 30 km northeast of Caliente (Best and others, 1991). One dike of this unit, the porphyry of Meadow Valley Wash, has $^{40}Ar/^{39}Ar$ dates averaging 19.4 Ma (Snee and others, 1990; Rowley and others, 1992); isotopic data on the unit are given by Unruh and others (this volume). The dates demonstrate that the main episode of major extension began before 19 Ma; it may have begun as early as 25 Ma, and thus controlled emplacement of the Cobalt Canyon stock. The start of this episode of tectonism may correlate with a major reorganization of continental plates in western North America at about 25 Ma (Mammerickx and Klitgord, 1982; Ward, 1991). Movement on related nearby high-angle faults of the same trend offset rocks as young as 12 Ma.

Because of the synchroneity of major extension and caldera volcanism, most if not all tuff sources of the Caliente caldera complex are calderas that contain walls that are in part recurrent high-angle faults, that are trapdoor (half-graben) type calderas, or that are fissure vents now occupied by dikes and plugs. These tuff sources are largely controlled by synchronous faults, notably zones of east-striking faults that define the north and south sides of the caldera complex. Similar faults partly define numerous broad, east-trending structural zones ("lineaments") that are abundant in the Great Basin (Ekren and others, 1976; Rowley and others, 1978; Rowley, Cunningham, and others, in press) and appear to represent strike-slip accommodation zones. The lineaments that bound the Caliente caldera complex are the Timpahute lineament (Ekren and others, 1976) on the north and the Helene lineament (Best and others, 1993) on the south (fig. 3). The resultant east-elongated caldera complex can be thought of as a volcanotectonic trough in the sense described by Burke and McKee (1979). The Caliente caldera complex differs from most described calderas in that Caliente caldera margins are commonly faults, the complex is unusually long lived (about 10 million years), many tuff eruptions are relatively small and do not form recognizable outflow sheets, intracaldera plutons are either sparse or deeper than the current surface of erosion, floors of older rocks may be exposed beneath the intracaldera fill, and venting of similar tuff batches can occur from widely separated sources presumably during chronologically different but similar episodes.

Most post-caldera (after 13–12 Ma) volcanism was basaltic and basaltic andesitic, and their deposits predate and locally intertongue with basin-fill sedimentary rocks, including the upper Miocene and Pliocene Panaca Formation of the Panaca basin several kilometers north of Caliente. The basaltic volcanism (12 Ma; Mehnert and others, 1989) took place near the end of the main episode of extension, and after that the third episode of extensional deformation, basin-range faulting, became the dominant form of tectonism.

DESCRIPTIONS OF LITHOLOGIC UNITS

Many of the regional ash-flow sheets in and near the Caliente caldera complex have been described by Anderson

and Rowley (1975), Rowley and others (1979), Siders and Shubat (1986), Best, Christiansen, and others (1989), Rowley, Mehnert, and others (1994), and Scott and others (this volume). A brief discussion of those units specific to the Caliente area is given by Rowley and others (1992). More detailed descriptions of regional and local units are provided by geologic maps by Siders and others (1990), Rowley and Shroba (1991), Rowley, Shroba, and others (1994), and Swadley and Rowley (1994).

The oldest rocks near the Caliente caldera complex consist of a thick sequence of orthoquartzite of Late Proterozoic and Early Cambrian age, overlain by thick limestone, dolomite, and shale sequences of Early through Late Cambrian age (Merriam, 1964; Tschanz and Pampeyan, 1970; Axen and others, 1988). These rocks are overlain by Oligocene and Miocene volcanic rocks, and in turn by upper Miocene, Pliocene, and Quaternary basin-fill sedimentary rocks (Rowley and others, 1992). Oligocene volcanic rocks consist mostly of ash-flow tuffs of the Needles Range Group from the Indian Peak caldera complex (Best, Christiansen, and Blank, 1989), but tuffs from calderas to the west and northwest are also represented (Best, Christiansen, and others, 1989). These rocks are overlain by ash-flow tuffs of the Oligocene Isom Formation, probably also derived from the Indian Peak complex, and by local, mostly thin intertongued lava flows, mudflow breccia, and sedimentary units of Miocene age (Rowley and others, 1992; Rowley and Shroba, 1991; Rowley, Shroba, and others, 1994; Swadley and Rowley, 1994). The Miocene Quichapa Group (Anderson and Rowley, 1975), which overlies the Isom Formation, is the oldest unit that will be discussed in this report: most ash-flow tuffs in the group are known or suspected to be derived from the Caliente complex.

We discuss the tuffs from oldest to youngest. Rock names are based on the classification of Le Bas and others (1986), shown in figure 5. Modal analyses are given in Appendix 1. Following a method of correlating ash-flow tuffs based on energy-dispersive X-ray fluorescence chemical analysis (EDXRF by Kevex instrumentation) suggested to us by E.A. du Bray (oral commun., 1990) and discussed by du Bray (1995), we give chemical data in Appendix 2 of elements that he considered most useful for correlation. As the reader will see herein, these methods are not always sufficient to distinguish rock units.

QUICHAPA GROUP

The name Quichapa Group was proposed by Cook (1957) for a sequence of informally named regional ash-flow tuffs in southwestern Utah and southeastern Nevada. Mackin (1960) reduced the unit in rank to the Quichapa Formation and divided it from base to top into the Leach Canyon, Swett, Bauers, and Harmony Hills Tuff Members. Anderson and

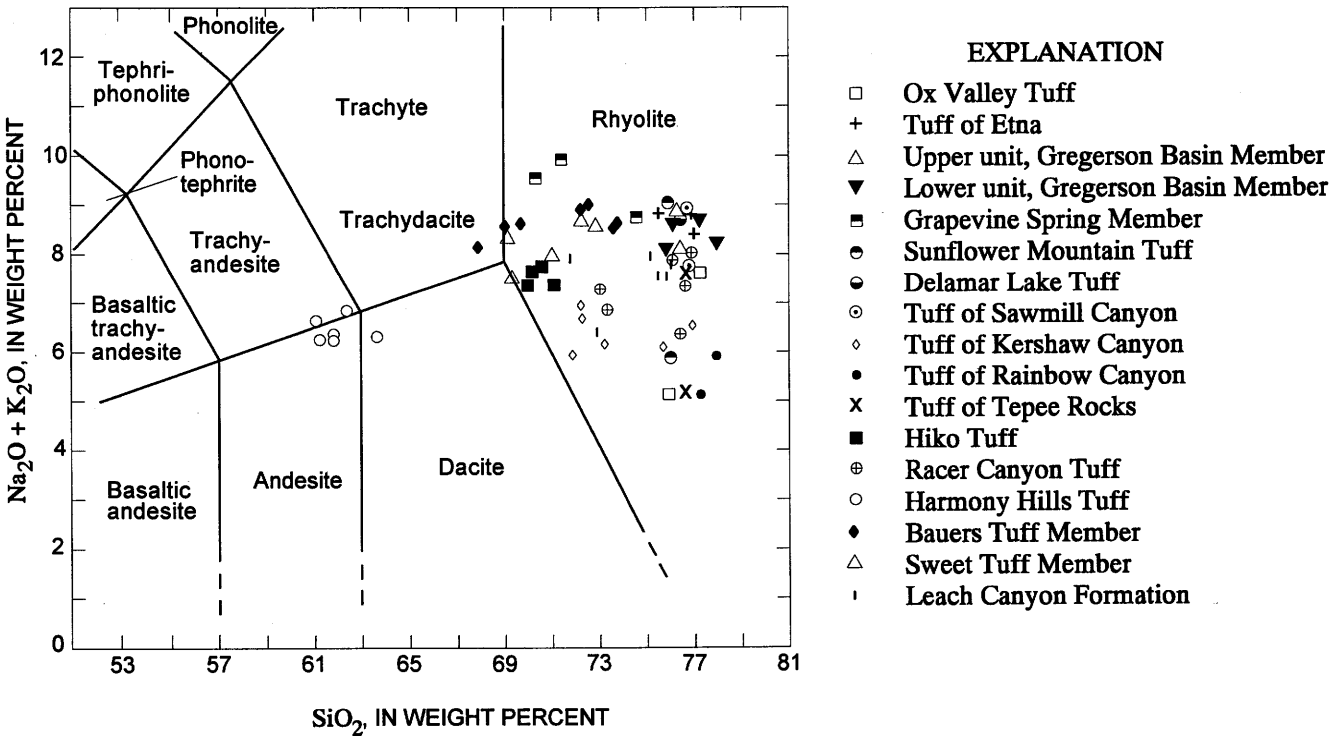

Figure 5. Chemical classification of ash-flow tuffs in and near Caliente caldera complex, using total alkali-silica diagram of Le Bas and others (1986). Includes data of Blank (1959, table 1), Williams (1967, table 5), Hausel and Nash (1977, table 6), Novak (1984, table 2), Novak and Mahood (1986, table 10), Harding (1991, Appendix IIA), and Harding and others (this volume, Appendix 2A).

Rowley (1975) followed Williams (1967) in revising the Miocene Quichapa Group to consist of the Leach Canyon Formation, the Swett and Bauers Tuff Members of the Condor Canyon Formation, and the Harmony Hills Tuff.

LEACH CANYON FORMATION

The Leach Canyon Formation consists of numerous outflow cooling units of tan and gray, crystal-poor, poorly welded, rhyolite ash-flow tuff. Total thickness of the cooling units of the formation is generally less than 100 m but locally is more than 300 m. These outflow tuffs are thickest on the north side of the Caliente complex, and overall tuff distribution is centered here as well, leading Williams (1967) to suggest that the source caldera was in the Panaca-Caliente area. Most of the area at the center of tuff distribution is the Panaca basin, which is covered by much younger basin-fill sedimentary rocks; thus we have at present confirmed no such caldera.

The formation comprises two members. The lower is the Narrows Tuff Member, which covered at least 15,000 km^2 (Best, Christiansen, and others, 1989, fig. R40) after the effects of east-west extension (50 percent assumed) are removed from its present distribution of at least 22,000 km^2 (Williams, 1967). The overlying Table Butte Tuff Member covered 4,000 km^2 if the same formula is applied to its current distribution of 6,000 km^2 (Williams, 1967). Because the members are difficult to separate without detailed petrography, we generally do not separate them in our mapping. Distinguishing features of tuffs of the Leach Canyon Formation are their abundance of mostly red, angular volcanic rock fragments and their abundant, partly collapsed pumice fragments; volume of pumice fragments increases upward in the formation.

We plot modal data to show phenocryst minerals relative to total phenocrysts (fig. 6) and to show quartz, sanidine, and plagioclase (QSP) relative to each other (fig. 7) from Appendix 1 and published sources. Modal amounts of minerals show considerable variation in the Leach Canyon Formation, but overall the unit consists of 10–30 percent phenocrysts of quartz (10–50 percent of total phenocrysts), sanidine (5–45 percent), and plagioclase (25–65 percent), biotite (<15 percent of total phenocrysts), hornblende (<6 percent), clinopyroxene (<1 percent in some thin sections), Fe-Ti oxides (<7 percent), and accessory sphene. Generally plagioclase exceeds quartz, which in turn exceeds sanidine. Differences in amounts of minerals through a vertical stratigraphic sequence of the Leach Canyon are characterized generally by an upward increase in percent of plagioclase and a decrease in quartz and sanidine, as would be expected if the eruption were tapping increasingly lower parts of a compositionally zoned magma chamber (Lipman and others, 1966). This trend in plagioclase versus quartz and sanidine is evident in samples collected in stratigraphic sections within members and in the overall petrographic difference between

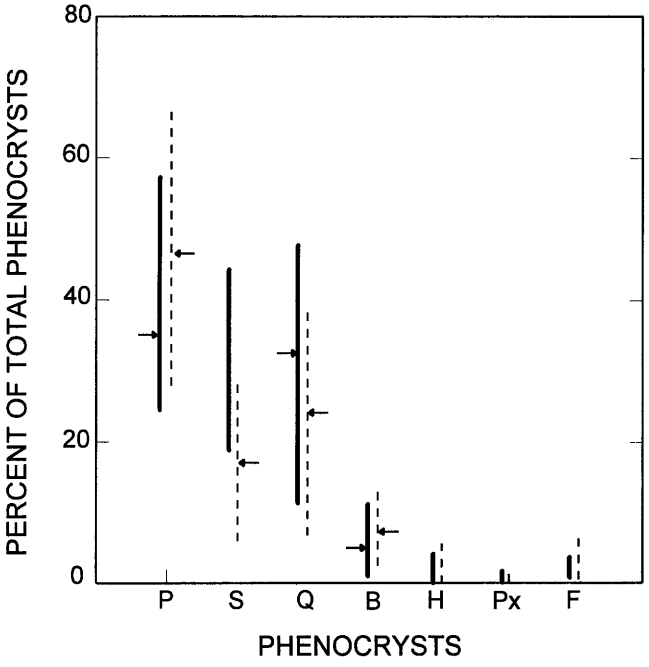

Figure 6. Plot of percentages of major phenocrysts in the Narrows (solid lines) and Table Butte (dashed lines) Tuff Members of the Leach Canyon Formation. From data in Appendix 1 and from Williams (1967). Averages of most abundant minerals shown by arrows. P, plagioclase; S, sanidine; Q, quartz; B, biotite; H, hornblende; Px, pyroxene; F, Fe-Ti oxides.

the members (fig. 6); in addition, in the QSP diagram, samples higher in the stratigraphic section plot closer to the plagioclase corner (fig. 7). Kevex EDXRF data (Appendix 2; fig. 8) are characterized by relatively low total iron and zirconium and variable strontium and neodymium compared with other tuffs we have examined; barium increases upward in the formation. Although these data are few, the values are similar for Leach Canyon samples analyzed by du Bray (1995) during his mapping of the Seaman Range (du Bray and Hurtubise, 1994; Hurtubise and du Bray, 1992), which is 55 km northwest of Caliente.

The average K-Ar age of the Leach Canyon Formation is 24.0 Ma based on three K-Ar dates by Armstrong (1970) and two fission-track dates by Kowallis and Best (1990), but considerable range (26.7–21.6 Ma) exists in published dates, causing doubt as to the actual age of the formation. Based on dating in progress by A.L. Deino and M.G. Best (Institute of Human Origins in Berkeley, Calif., and Brigham Young University, respectively, oral commun., 1991), the best estimate for the age of the Leach Canyon Formation is 23.8 Ma (Best and others, 1993).

CONDOR CANYON FORMATION

The Condor Canyon Formation, a name originally applied by Cook (1965), consists of mostly brown and purple,

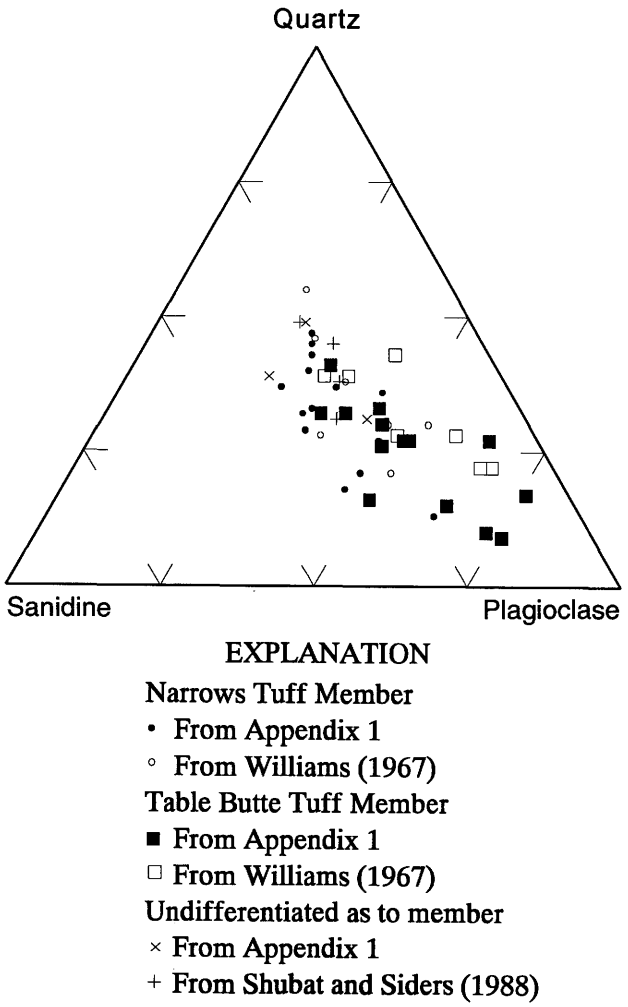

Figure 7. Ternary quartz-sanidine-plagioclase diagram of the Narrows and Table Butte Tuff Members and of samples undifferentiated as to member, Leach Canyon Formation.

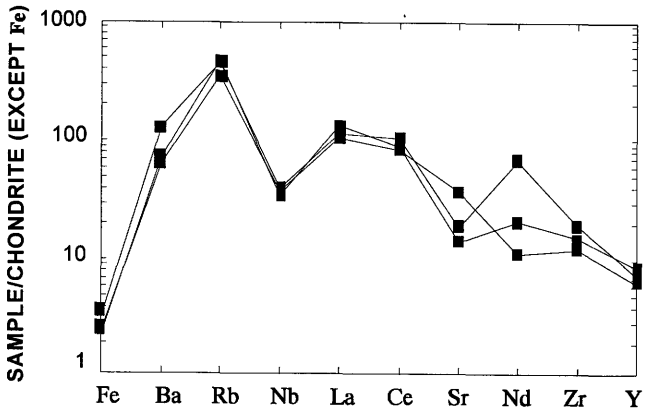

Figure 8. Plot of selected elements determined by energy-dispersive X-ray fluorescence (Kevex) of samples of the Leach Canyon Formation. Member name and data given in Appendix 2. Iron (in weight percent) values result from dividing the raw data by 0.5; other elements (in parts per million) normalized by dividing by chondrite abundances according to values given by Thompson (1984).

crystal-poor, low-silica rhyolite ash-flow tuff made up of two members, the Swett Tuff Member and Bauers Tuff Member. Outflow cooling units are densely welded and commonly contain a black basal vitrophyre zone overlain by a lenticulite zone; in some outcrops of the Bauers, the lenticulite zone is overlain by a gray vapor-phase zone. Where the Bauers is thick, its upper lenticulite or vapor-phase part is in places flow foliated probably due to movement during the latest stages of emplacement. Williams (1967) predicted that the source of the Bauers was the Caliente caldera complex, and this was confirmed by Rowley and Siders (1988), who named the source the Clover Creek caldera (fig. 3). Only faulted fragments of the caldera remain exposed at and north of Caliente (Rowley and Shroba, 1991; Rowley and others, 1992). Because of its petrologic similarity with the Bauers, the Swett may also be derived from the Clover Creek caldera or, more likely, a predecessor caldera in about the same place that was either largely destroyed by Clover Creek caldera subsidence or covered by younger basin-fill sedimentary rocks so that no trace remains exposed.

The Swett Tuff Member consists of one and rarely several thin (generally less than 15 m) ash-flow cooling units that formerly covered an area of at least 6,000 km^2 (Williams, 1967) after the effects of east-west extension are removed. The Swett Member (figs. 9, 10) contains 5–15 percent phenocrysts of mainly plagioclase (70–90 percent) with small amounts of biotite (10–20 percent) and Fe-Ti oxides (<7 percent). Kevex data (fig. 11) show that the Swett contains variable strontium, high barium, and relatively high cerium. The average of six K-Ar dates of the Swett is 23.7 Ma (Armstrong, 1970), but its true age is probably closer to the age of the Bauers.

The Bauers Tuff Member consists of one or as many as three cooling units totalling generally about 50 m but locally as much as 120 m, that spread over an area of at least 23,000 km^2 (Best, Christiansen, and others, 1989, fig. R40). The Bauers is similar in appearance to the Swett except that it is thicker and better zoned; it is easily distinguished from the Swett by the presence of sanidine and pyroxene in the Bauers. The member (figs. 9, 10) contains 10–20 percent phenocrysts of sanidine (25–50 percent), plagioclase (40–70 percent), biotite (2–10 percent), clinopyroxene (<3 percent), and Fe-Ti oxides (1–8 percent). The relative amount of plagioclase to sanidine appears to generally increase upward in the member. The member (fig. 12) has similar Kevex values to the Swett. The preferred age of the Bauers is 22.8 Ma (Best, Christiansen, and others, 1989) based on the average of two $^{40}Ar/^{39}Ar$ dates by A.L. Deino.

HARMONY HILLS TUFF

The Harmony Hills Tuff consists of a pink, tan, and gray, crystal-rich, moderately welded, andesitic ash-flow tuff that generally is exposed as a simple or multiple cooling

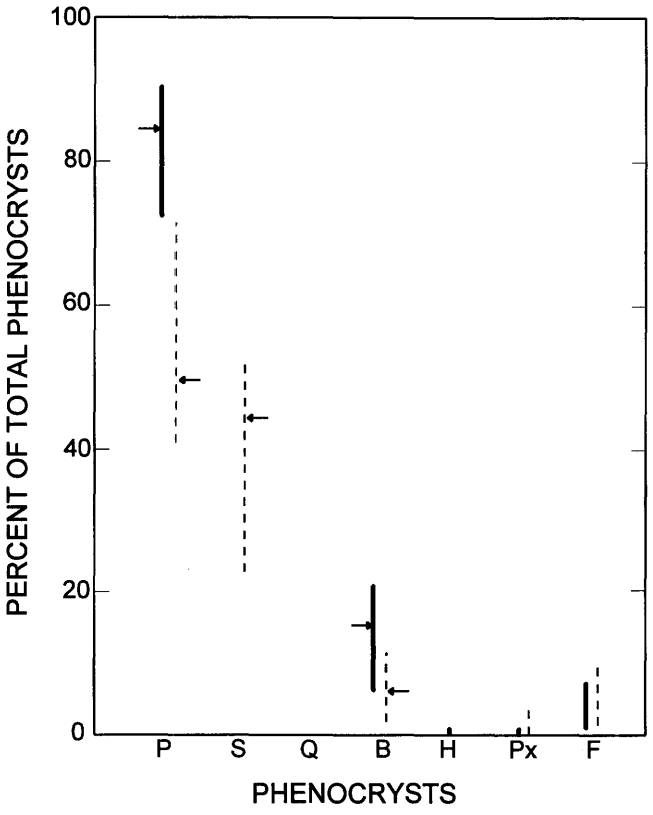

Figure 9. Plot of percentages of major phenocrysts in the Swett (solid lines) and Bauers (dashed lines) Tuff Members of the Condor Canyon Formation. From data in Appendix 1, Williams (1967), and Shubat and Siders (1988). Averages of most abundant minerals shown by arrows. P, plagioclase; S, sanidine; Q, quartz; B, biotite; H, hornblende; Px, pyroxene; F, Fe-Ti oxides.

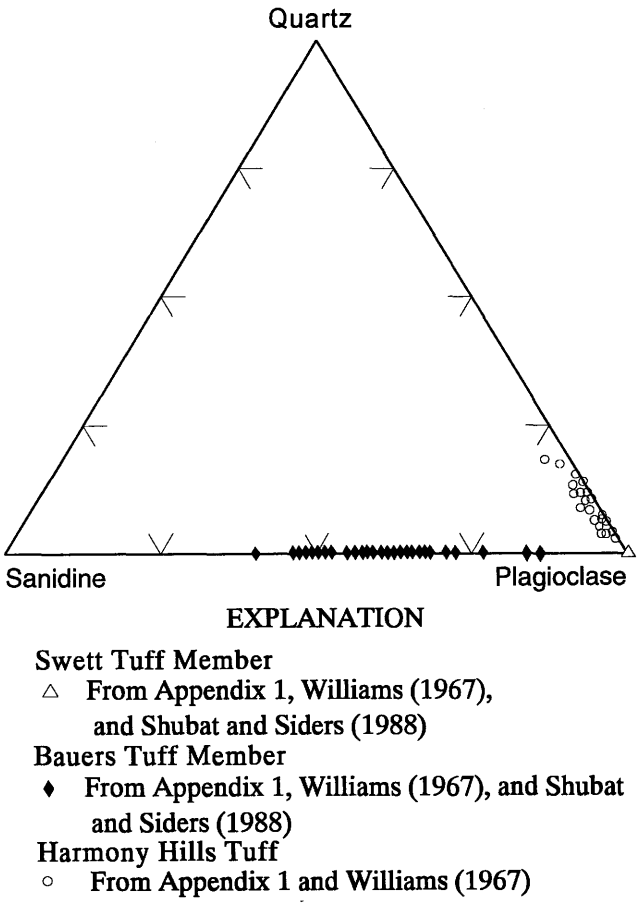

Figure 10. Ternary quartz-sanidine-plagioclase diagram of the Swett and Bauers Tuff Members of the Condor Canyon Formation and of the Harmony Hills Tuff.

unit but locally consists of two cooling units. The unit generally is less than 100 m thick but is as much as 150 m thick. It was spread over about 13,000 km^2 (Best, Christiansen, and others, 1989, fig. R40). Noble and others (1968) and Noble and McKee (1972) predicted that the source of the Harmony Hills is within the Caliente caldera complex, and Ekren and others (1977) cited field relations that suggest that the unit was derived from the southern part of the complex. Rowley (unpub. mapping, 1988) mapped deposits of Harmony Hills megabreccia in the southern Delamar caldera that suggest that the unit was unusually thick south of the Delamar caldera at the time this caldera subsided. Isopach and distribution data (Williams, 1967) and detailed geologic mapping (Blank, 1959; Blank and others, 1992; H.R. Blank, oral commun., 1990), however, suggest that the source is almost certain to be in the eastern Bull Valley Mountains of Utah.

The Harmony Hills Tuff is distinguished from most other ash-flow tuffs in and near the Caliente caldera complex by its general andesitic chemical composition and abundant phenocrysts (fig. 5). It lithologically resembles the Rencher Formation (Cook, 1957, 1960; Blank, 1959; Mackin, 1960; Blank and others, 1992), which overlies the Harmony Hills

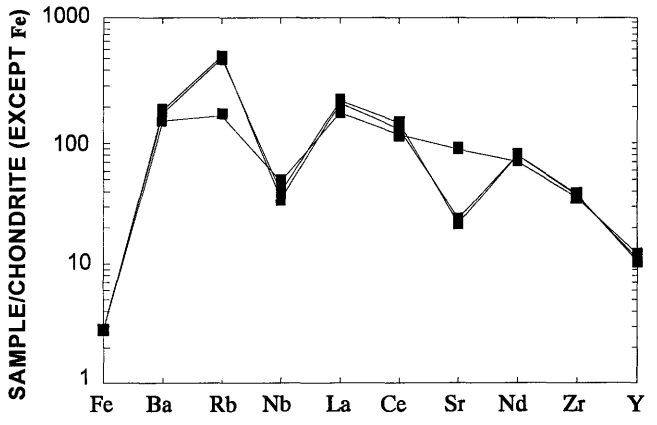

Figure 11. Plot of selected elements determined by energy-dispersive X-ray fluorescence (Kevex) of samples from the Swett Tuff Member of the Condor Canyon Formation. From data in Appendix 2. Iron (in weight percent) values result from dividing the raw data by 0.5; other elements (in parts per million) normalized by dividing the chondrite abundances according to values given by Thompson (1984).

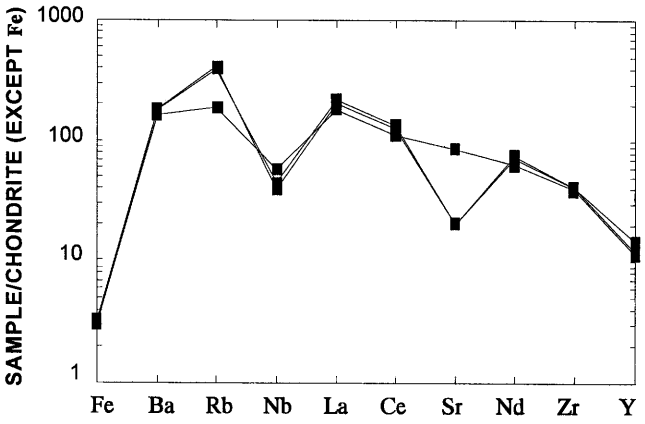

Figure 12. Plot of selected elements determined by energy-dispersive X-ray fluorescence (Kevex) of samples from the Bauers Tuff Member of the Condor Canyon Formation. From data in Appendix 2. Iron (in weight percent) values result from dividing the raw data by 0.5; other elements (in parts per million) normalized by dividing the chondrite abundances according to values given by Thompson (1984).

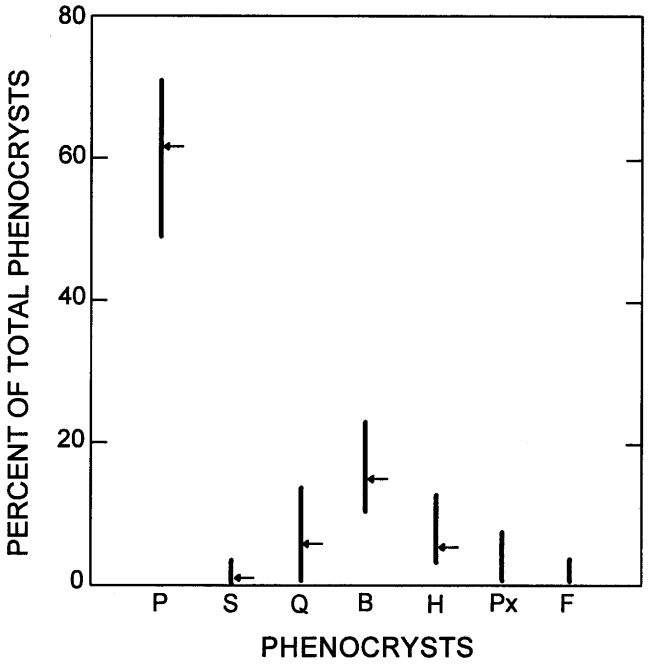

Figure 13. Plot of percentages of major phenocrysts in the Harmony Hills Tuff. From data in Appendix 1 and from Williams (1967). Averages of most abundant minerals shown by arrows. P, plagioclase; S, sanidine; Q, quartz; B, biotite; H, hornblende; Px, pyroxene; F, Fe-Ti oxides.

in the eastern Bull Valley Mountains and vicinity. Quartz and sanidine are absent in the Rencher, providing easy discrimination from the Harmony Hills Tuff. The Harmony Hills Tuff (figs. 10, 13) contains 25–60 percent phenocrysts of quartz (2–15 percent), sanidine (<3 percent), plagioclase (50–70 percent), biotite (10–25 percent), hornblende (5–15 percent), clinopyroxene (1–8 percent), and Fe-Ti oxides (1–4 percent). The formation is chemically distinct from other tuffs in the Caliente area, bearing high iron and strontium (fig. 14). The actual isotopic age of the unit is difficult to establish. A broad range of K-Ar dates average 21.6 Ma (Armstrong, 1970; Noble and McKee, 1972), but the age is considered to be 22.5–22.0 Ma because dates of younger plutonic rocks in the Iron Springs mining district of Utah and of the younger Rencher Formation are in the same range of ages (Rowley and others, 1989).

RACER CANYON TUFF

The Racer Canyon Tuff was first proposed informally, as a member, by Blank (1959). Cook (1960) correlated the unit with the Kane Point Tuff Member of the Page Ranch Formation, but this usage was not adopted by subsequent workers (for example, Noble and others, 1968; Noble and McKee, 1972; Ekren and others, 1977), who used Racer Canyon Tuff at the formation level. Rowley and others (1979) abandoned Kane Point Tuff Member in favor of the formation name Racer Canyon Tuff.

The Racer Canyon Tuff consists of a gray, tan, and pink, crystal-rich, poorly to moderately welded, low-silica rhyolite ash-flow tuff containing from 1 to 12 cooling units. It spread onto rough topography created by active tectonism;

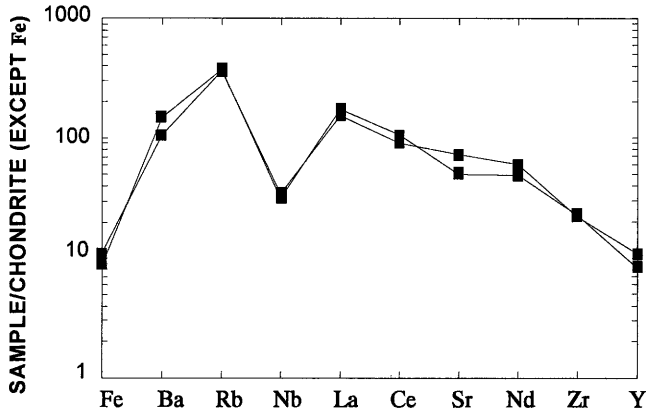

Figure 14. Plot of selected elements determined by energy-dispersive X-ray fluorescence (Kevex) of samples from the Harmony Hills Tuff. From data in Appendix 2. Iron (in weight percent) values result from dividing the raw data by 0.5; other elements (in parts per million) normalized by dividing the chondrite abundances according to values given by Thompson (1984).

outflow cooling units total generally less than 100 m thick but in some places are as much as 450 m thick. The unit is exposed over at least 3,000 km^2. The source of the Racer Canyon is unknown, but it may have been derived from the eastern part of the Caliente caldera complex (Siders and others, 1990; Siders, 1991). The unit (figs. 15, 16) contains about 15–55 percent phenocrysts of quartz (20–50 percent),

sanidine (5–40 percent), plagioclase (15–60 percent), biotite (1–13 percent), hornblende (<5 percent), clinopyroxene (0 to trace amounts), Fe-Ti oxides (1–4 percent), and sphene (<1 percent). Generally quartz exceeds plagioclase, which in turn exceeds sanidine, but Racer Canyon shows considerable variation in modal amounts and ratios. The same high degree of variation upward in stratigraphic sections is also clear in samples of the Racer Canyon Tuff. In some sections, plagioclase increases upward, and more rarely, quartz and sanidine decrease upward. Kevex data (fig. 17) likewise show considerable variation from sample to sample and have no distinctive characteristics.

Three K-Ar dates and one lead-alpha date (summarized by Siders and others, 1990) yield an average age of 19.4 Ma for the Racer Canyon. This average age is somewhat older than the average of two preliminary plateau $^{40}Ar/^{39}Ar$ dates, 18.7±0.1 Ma on sanidine and 19.2±0.8 Ma on biotite, recently determined by L.W. Snee from a sample collected south of Enterprise Reservoir in the eastern Bull Valley Mountains. Biotite ages are less reliable than sanidine ages by this technique, and the biotite age has a greater error bar, so the true age may be closer to 18.7 than 19.2 Ma.

HIKO TUFF

The Hiko Tuff of Dolgoff (1963; see also Noble and McKee, 1972) is a major ash-flow sheet that spread over at least 7,000 km^2 of southeastern Nevada (Best, Christiansen, and others, 1989, fig. R40). The unit is a gray and tan, crystal-rich, poorly to densely welded, low-silica rhyolite. In most places, outflow facies consist of one or two simple cooling

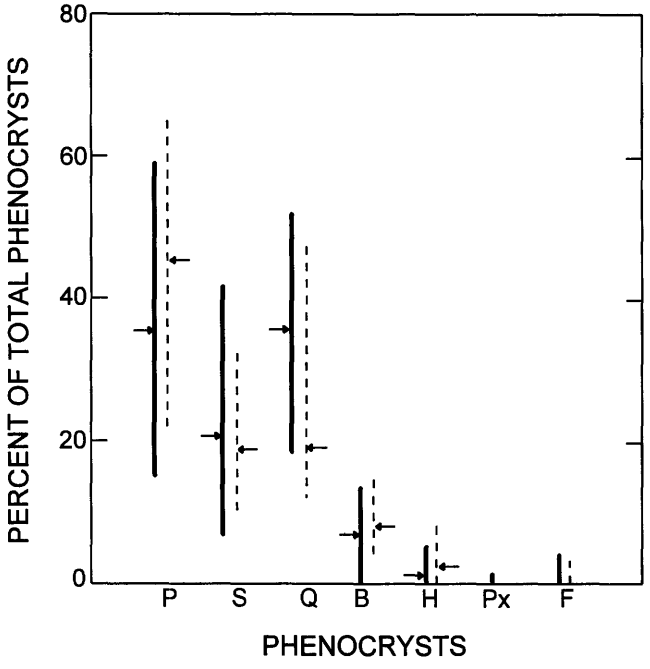

Figure 15. Plot of percentages of major phenocrysts in the Racer Canyon Tuff (solid lines) and Hiko Tuff (dashed lines). From data in Appendix 1, Siders (1985), and Shubat and Siders (1988). P, plagioclase; S, sanidine; Q, quartz; B, biotite; H, hornblende; Px, pyroxene; F, Fe-Ti oxides.

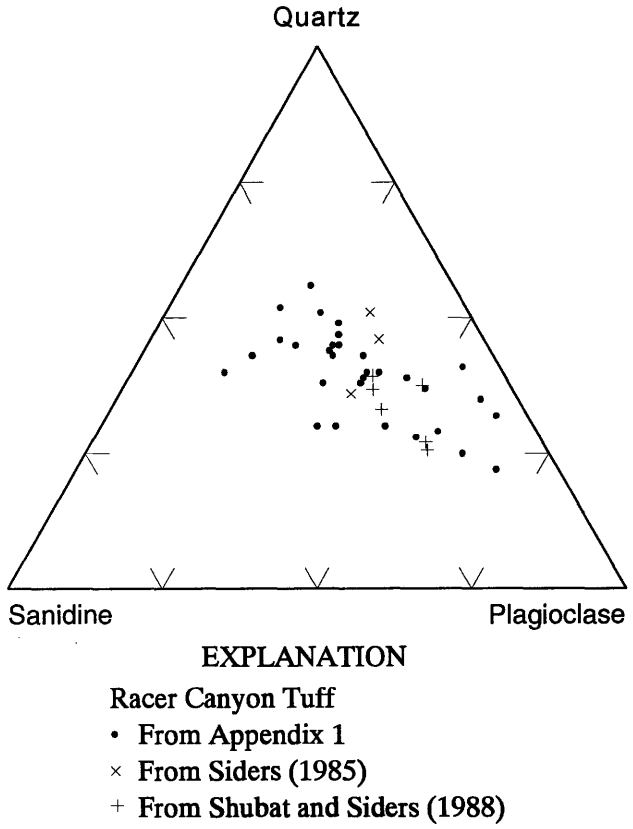

Figure 16. Ternary quartz-sanidine-plagioclase diagram of the Racer Canyon Tuff.

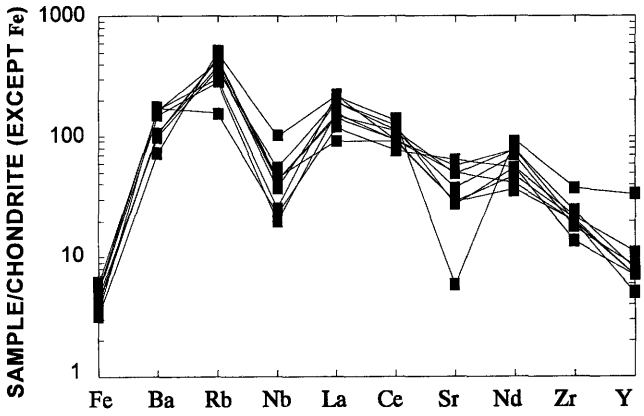

Figure 17. Plot of selected elements determined by energy-dispersive X-ray fluorescence (Kevex) of samples of the Racer Canyon Tuff. From data in Appendix 2. Iron (in weight percent) values result from dividing the raw data by 0.5; other elements (in parts per million) normalized by dividing by chondrite abundances according to values given by Thompson (1984).

units generally less than 50 m thick but locally as much as 250 m thick. Locally, however, at least four cooling units have been identified.

Noble and others (1968) and Noble and McKee (1972) suggested that the source of the Hiko Tuff was the Caliente caldera complex, and this was confirmed by Ekren and others (1977), who further noted that the Hiko came from the "western lobe" of the complex. The western lobe was named the Delamar caldera by Rowley and Siders (1988). In addition, the Hiko Tuff erupted from a vent south of the ghost town of Delamar that herein we name the Cedar Wash vent (fig. 3). This vent is about 2 km in maximum diameter and consists mostly of Hiko Tuff that contains subvertical flow foliation defined by pumice fragments and, at the vent's south edge, of caldera collapse megabreccia (Rowley, unpub. mapping, 1992).

Cook (1965) correlated the Hiko Tuff with the Racer Canyon Tuff, and we also have yet to find firm field and petrographic bases for distinguishing the two units. Our current thinking, however, is that they are separate units erupted nearly synchronously from opposite ends of the Caliente caldera complex (Siders and others, 1990). The similarity in age and composition suggests that the two units erupted from the same magma chamber. This view is supported by preliminary paleomagnetic data by C.S. Grommé (unpub. data, 1991) which suggest that the two units have different paleomagnetic signatures. In addition, other stratigraphic details of the Hiko Tuff are beginning to emerge as a result of recent unpublished mapping by Rowley and R.E. Anderson in the western Caliente caldera complex. For example, intracaldera Hiko Tuff southeast of Caliente differs somewhat in petrography from Hiko that makes up the main mass of the Delamar caldera southwest of Caliente (fig. 3) and from Hiko just east of the area of figure 3 (R.E. Anderson, unpub. data, 1992), and we are now entertaining the possibility of several batches of Hiko-like tuff, including Racer Canyon Tuff, that erupted at different times from separate calderas and vents of the same magma chamber. We have yet to determine the stratigraphic relationship of these batches to one another.

The overall Hiko Tuff (figs. 15, 18) contains 15–45 percent phenocrysts of quartz (10–50 percent), sanidine (10–35 percent), plagioclase (20–65 percent), biotite (5–15 percent), hornblende (<9 percent), clinopyroxene (0 to trace amounts), Fe-Ti oxides (1–4 percent), and sphene (<1 percent). Generally plagioclase exceeds quartz, which in turn exceeds sanidine, but like the Racer Canyon, the Hiko shows considerable variation in modal amounts and ratios. In vertical sections, plagioclase generally increases in abundance and ratio from base to top. Plagioclase is generally more abundant and quartz less abundant in the Hiko Tuff than in the Racer Canyon Tuff, so the plots of the two units are slightly different (figs. 16, 18). Kevex data (fig. 19) are similar to those of Racer Canyon. The wide variability in modes and chemical data within samples of the Hiko and Racer Canyon, which currently prevents us from distinguishing them in the field, probably reflects the preliminary nature of our stratigraphic and petrologic studies.

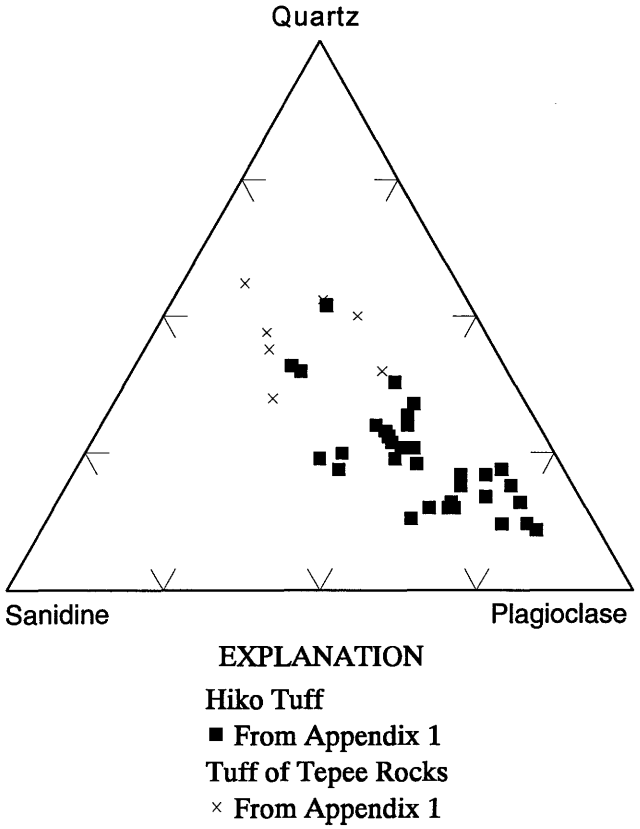

Figure 18. Ternary quartz-sanidine-plagioclase diagram of the Hiko Tuff and the tuff of Tepee Rocks.

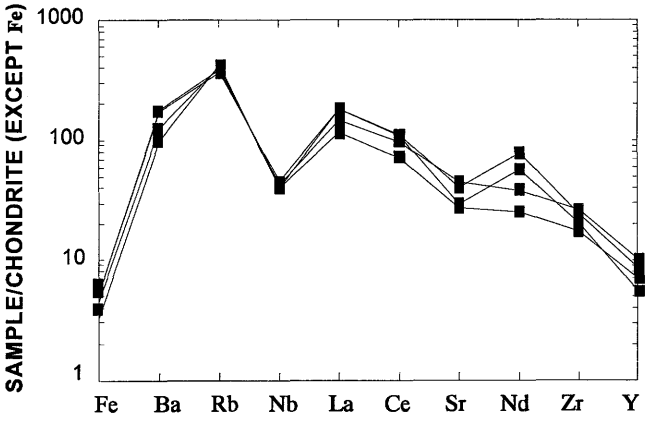

Figure 19. Plot of selected elements determined by energy-dispersive X-ray fluorescence (Kevex) of samples of the Hiko Tuff. From data in Appendix 2. Iron (in weight percent) values result from dividing the raw data by 0.5; other elements (in parts per million) normalized by dividing by chondrite abundances according to values given by Thompson (1984).

Tuffs of the Leach Canyon Formation resemble those of the Racer Canyon and Hiko, and little separates the three modally except that the Leach Canyon contains fewer phenocrysts. Kevex data are more distinctive, however, because the Leach Canyon has lower total iron, barium, strontium, and zirconium. Additional data on the Hiko Tuff and Leach Canyon Formation from du Bray (1995) support this comparison.

Taylor and others (1989) preferred an age of 18.6 Ma for the Hiko, based on an average of several published $^{40}Ar/^{39}Ar$ dates determined in the lab of D.R. Lux (University of Maine, Orono). Recent preliminary plateau $^{40}Ar/^{39}Ar$ dates determined by L.W. Snee of sanidine from Hiko Tuff, from a standard used by Lux and sent to Snee, however, give a Hiko age of 18.2±0.1 Ma (Snee, unpub. data, 1993). Identical dates on the rhyolite volcanic domes of Crows Nest Tank and of Barnes Canyon, both of which are on the rim of the Delamar caldera and probably derived from the same magma chamber as Hiko Tuff, support an age of 18.2 Ma for Hiko Tuff. We are currently continuing geochronologic studies on this standard sample plus other samples of Hiko Tuff.

The relative age of the Hiko Tuff and Racer Canyon Tuff has not been determined because their outflow sheets have not been identified in the same stratigraphic section. The dates on the Racer Canyon Tuff, however, are somewhat older than those on the Hiko. A higher average plagioclase content and lower average quartz content of the Hiko with respect to the Racer Canyon (fig. 15), plus the somewhat lower phenocryst content of the Hiko, supports the hypothesis that the Hiko is younger than the Racer Canyon if one assumes that their magma chambers were connected and compositionally layered during eruption (Lipman and others, 1966).

TUFF OF TEPEE ROCKS

The name tuff of Tepee Rocks is used here for about 100 m of ash-flow tuff exposed at Tepee Rocks, an area of hoodoos about 6 km east-southeast of Caliente. The unit is a gray and tan, crystal-poor, poorly welded, low-silica rhyolite ash-flow tuff that lithologically resembles Hiko Tuff but may be distinguished from it by Kevex data and by a clearly younger isotopic age. Clearly the tuff of Tepee Rocks was derived from the Caliente caldera complex and probably from the same magma chamber as the Hiko, Racer Canyon, and other Hiko-like units. Current field mapping by R.E. Anderson and P.D. Rowley has not located a base to the unit at Tepee Rocks, so it may be an intracaldera sequence. Outflow deposits of the tuff of Tepee Rocks overlie intracaldera Hiko Tuff about 1 km west of Tepee Rocks. Outflow-facies rock of the unit outside the Caliente caldera complex underlies a butte 7 km north of Caliente, where Rowley and Shroba (1991) misidentified the rock as Hiko Tuff.

The tuff of Tepee Rocks (figs. 18, 20) contains 10–25 percent phenocrysts of quartz (35–55 percent), sanidine (20–40 percent), plagioclase (10–35 percent), biotite (1–7 percent), hornblende (generally trace amounts), Fe-Ti oxides (<3 percent), and sphene (trace amounts). Quartz generally exceeds sanidine, which in turn exceeds plagioclase. The low amount of hornblende and biotite helps distinguish the unit from Hiko and Racer Canyon, but the Kevex data (fig. 21) are much more diagnostic because of lower iron, neodymium,

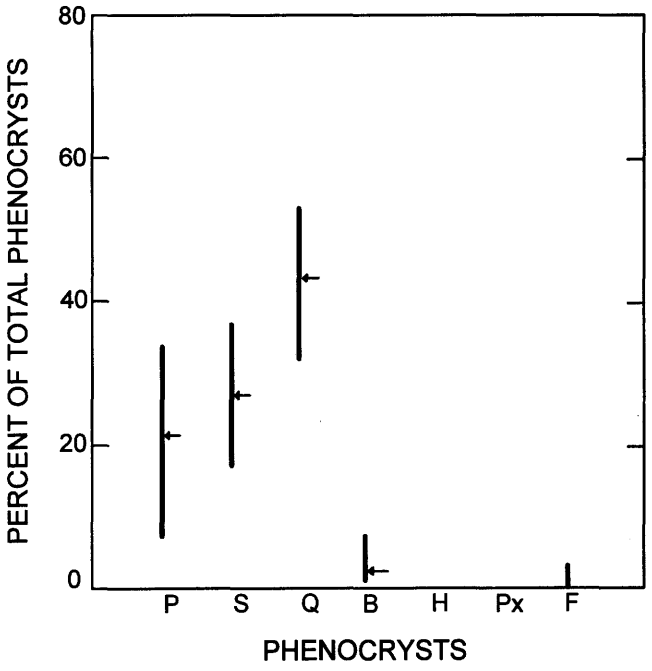

Figure 20. Plot of percentages of major phenocrysts in the tuff of Tepee Rocks. From data in Appendix 1. Averages of most abundant minerals shown by arrows. P, plagioclase; S, sanidine; Q, quartz; B, biotite; H, hornblende; Px, pyroxene; F, Fe-Ti oxides.

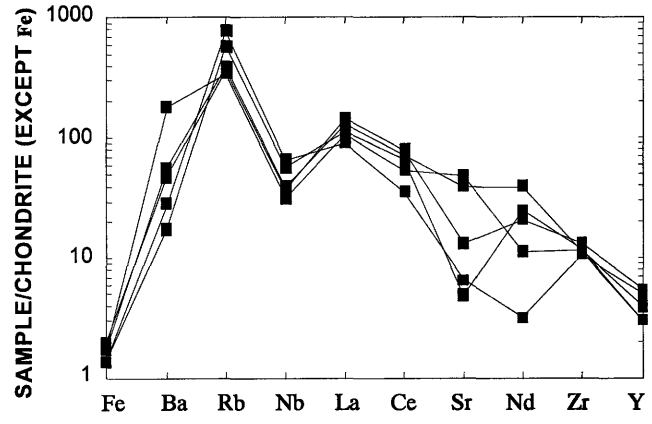

Figure 21. Plot of selected elements determined by energy-dispersive X-ray fluorescence (Kevex) of samples of the tuff of Tepee Rocks. From data in Appendix 2. Iron (in weight percent) values result from dividing the raw data by 0.5; other elements (in parts per million) normalized by dividing by chondrite abundances according to values given by Thompson (1984).

zirconium, and yttrium for the tuff of Tepee Rocks. A preliminary plateau $^{40}Ar/^{39}Ar$ date of 17.8±0.7 Ma was determined by L.W. Snee on a sample of biotite from the unit collected from Tepee Rocks.

DELAMAR LAKE TUFF

The Delamar Lake Tuff, defined by Scott and others (1993), was formerly called member O of the Kane Wash Tuff (Novak, 1984). It is the oldest known unit in the Caliente area that belongs to a basalt and high-silica rhyolite assemblage; this assemblage regionally postdates a calc-alkalic andesite to low-silica rhyolite assemblage that includes the tuff of Tepee Rocks and older volcanic units described previously. In some nearby parts of the Basin and Range province, this petrologic change marked initiation of or an increase in extensional tectonism (for example, Christiansen and Lipman, 1972), but in the area of the Caliente caldera complex no such tectonic change is known to have taken place.

The Delamar Lake Tuff consists of at least four cooling units of crystal-poor, nonwelded to densely welded, high-silica rhyolite ash-flow tuff (Harding, 1991; Harding and others, this volume; Scott and others, 1993; Scott and others, this volume). The thickest part of the outflow facies of the tuff is exposed in the central Delamar Valley near the west edge of the Caliente caldera complex (Swadley and Rowley, 1994), and thus the Delamar Lake Tuff is summarized here to allow comparison with other units described in this report. More details about the unit are provided by Scott and others (this volume). R.B. Scott (written commun., 1992) suggested that the Delamar Lake Tuff came from a source somewhere west of the Delamar Mountains, close to its thickest outflow. Most outflow deposits of the Delamar Lake Tuff occur in an area of about 1,600 km^2 surrounding the Kane Springs Wash caldera (Novak, 1984, fig. 2a; Scott and others, 1993).

Samples of the Delamar Lake Tuff (figs. 22, 23) from Delamar Valley west of the Caliente caldera complex contain 7–20 percent phenocrysts of quartz (30–45 percent), sanidine (55–70 percent), plagioclase (<2 percent, xenocrysts?), biotite (trace amounts, xenocrysts?), amphibole (0 to trace amounts, xenocrysts?), hedenbergite pyroxene (1–5 percent), Fe-Ti oxides (trace amounts), and fayalitic olivine (1–3 percent). Modal analyses of Delamar Lake Tuff from the Kane Springs Wash caldera area (R.B. Scott and A.E. Harding, written commun., 1991) are similar to the samples from near the Caliente caldera complex that we analyzed. Kevex analysis (fig. 24) of only one sample from near the Caliente caldera complex is similar to trace-element data for a single sample given for the unit by Harding (1991, Appendix IIA, unit Tdl; Harding and others, this volume, Appendix 2A). The Delamar Lake Tuff has been dated by K-Ar methods at 15.8–15.5 Ma (Novak, 1984), but its true age is probably slightly older because Novak's dates are consistently

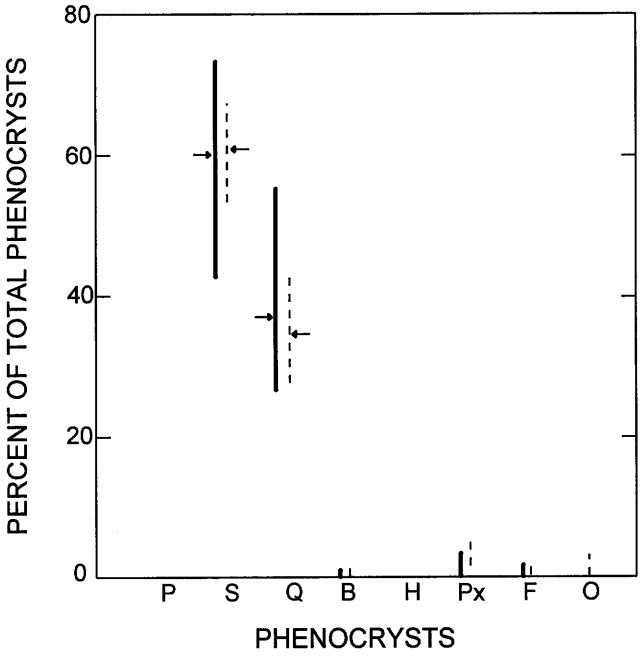

Figure 22. Plot of percentages of major phenocrysts in the tuff of Sawmill Canyon (solid lines) and in the Delamar Lake Tuff (dashed lines). From data in Appendix 1. Averages of most abundant minerals shown by arrows. P, plagioclase; S, sanidine; Q, quartz; B, biotite; H, hornblende; Px, pyroxene; F, Fe-Ti oxides; O, olivine.

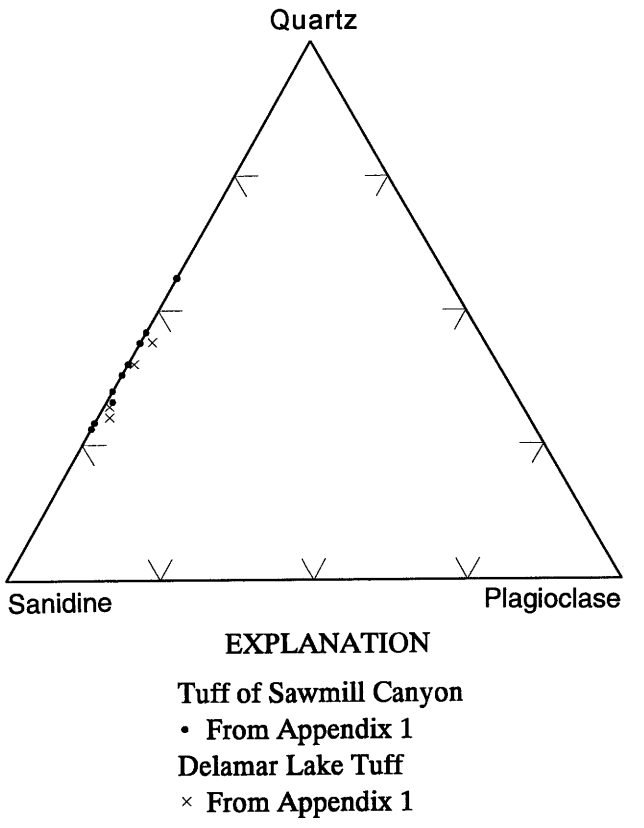

Figure 23. Ternary quartz-sanidine-plagioclase diagram of the tuff of Sawmill Canyon and of the Delamar Lake Tuff.

younger by about 0.4 m.y. than new $^{40}Ar/^{39}Ar$ dates of other tuffs by L.W. Snee (see section on Kane Wash Tuff) (Scott and others, this volume).

Southwest of the Kane Springs Wash caldera, the Delamar Lake Tuff is overlain by a similar ash-flow tuff, formerly called member W of the Kane Wash Tuff by Novak (1984) and recently defined as the Sunflower Mountain Tuff by Scott and others (1993). It is not known to be present in the area of the Caliente caldera complex. Harding (1991), Harding and others (this volume), and Scott and others (this volume) describe the unit, which has been dated by K-Ar methods at 14.7 Ma (Novak, 1984).

TUFF OF RAINBOW CANYON

The name tuff of Rainbow Canyon is used here for nonwelded to poorly welded, crystal-poor, high-silica, rhyolite ash-flow tuff whose intracaldera facies is well exposed in Rainbow Canyon south of Caliente. The unit is lithologically distinct from the Hiko Tuff and tuff of Tepee Rocks. The name was first applied by Bowman (1985), but we restrict the name to the lowermost thick, mostly pink and light-yellow part of the intracaldera sequence. The rock is characterized by conspicuous and locally abundant volcanic rock fragments of dark comagmatic flow rock and abundant, partially collapsed pumice fragments. The exposures define a trapdoor-type caldera inset into the Delamar caldera and named the Buckboard Canyon caldera (fig. 3) by Rowley and Siders (1988). Field relations indicate that the trapdoor nature of the caldera resulted from more subsidence on its north side than on its south side. Outflow ash-flow deposits are not recognized outside the Buckboard Canyon caldera.

Intracaldera deposits of the tuff of Rainbow Canyon (figs. 25, 26) contain 5–25 percent phenocrysts of quartz (35–85 percent), sanidine (15–65 percent), plagioclase (<10 percent), biotite (<3 percent), and Fe-Ti oxides (<2 percent). Kevex data (fig. 27) show that the rock is characterized by low iron and zirconium, and high rubidium, niobium, and barium relative to the other high-silica rhyolite tuffs. Mehnert and others (1989) reported a K-Ar date of 15.2±0.6 Ma from a sample at the top of the unit collected 6 km south-southeast of Caliente, and L.W. Snee recently determined a preliminary

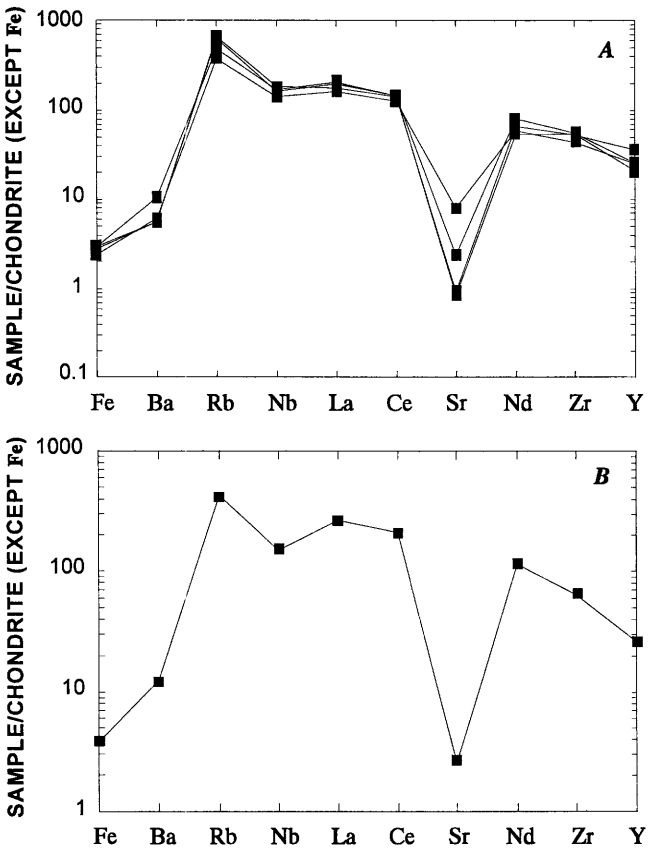

Figure 24. Plot of selected elements determined by energy-dispersive X-ray fluorescence (Kevex) of samples of *A*, the tuff of Sawmill Canyon and *B*, the Delamar Lake Tuff. From data in Appendix 2. Iron (in weight percent) values result from dividing the raw data by 0.5; other elements (in parts per million) normalized by dividing by chondrite abundances according to values given by Thompson (1984).

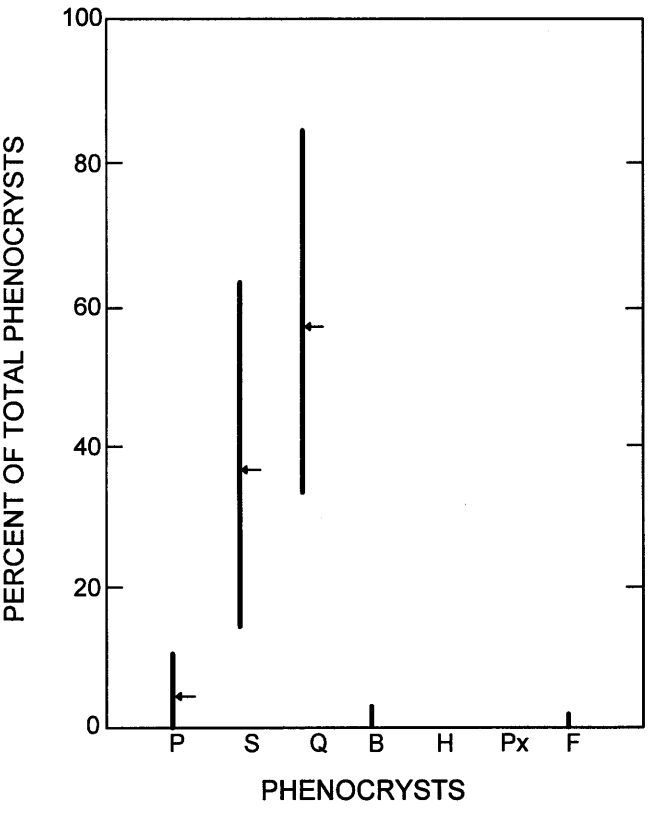

Figure 25. Plot of percentages of major phenocrysts in the tuff of Rainbow Canyon. From data in Appendix 1. Averages of most abundant minerals shown by arrows. P, plagioclase; S, sanidine; Q, quartz; B, biotite; H, hornblende; Px, pyroxene; F, Fe-Ti oxides.

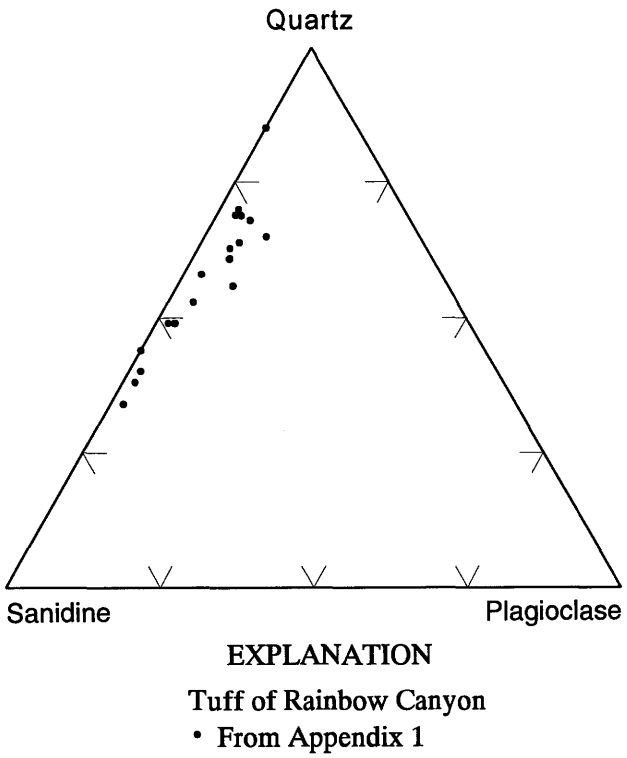

Figure 26. Ternary quartz-sanidine-plagioclase diagram of the tuff of Rainbow Canyon.

plateau $^{40}Ar/^{39}Ar$ date of 15.6±0.2 Ma from sanidine collected from low in the unit 4 km south-southwest of Caliente.

TUFF OF KERSHAW CANYON

The upper part of Bowman's tuff of Rainbow Canyon is herein called the tuff of Kershaw Canyon. The unit is a relatively thin, mostly white and gray sequence of crystal-poor, nonwelded to poorly welded, high-silica rhyolite ash-flow tuff, pyroclastic-fall tuff, and water-laid and mudflow-laid tuff that contains locally abundant volcanic rock fragments and white pumice. Except in general color, hand samples of the unit resemble the tuff of Rainbow Canyon.

The tuff of Kershaw Canyon is thickest and best exposed in Kershaw Canyon, a tributary that enters Rainbow Canyon 2 km south of Caliente. Here the unit is about 150 m thick and its base is not exposed. The tuff here may represent intracaldera deposits, but if so, a caldera wall has not been recognized. Alternatively, a caldera may lie east of Kershaw Canyon, in an area covered by younger fanglomerates informally named the conglomerate of Ash Canyon (Rowley and Shroba, 1991). The unit is thinner just west and south of Kershaw Canyon, where it rests on tuff of Rainbow Canyon and thus presumably represents outflow facies, and it thins and pinches out within about 6 km west and south of Kershaw Canyon. North of Kershaw Canyon, it intertongues with tan and reddish-brown sandstone and conglomerate referred to

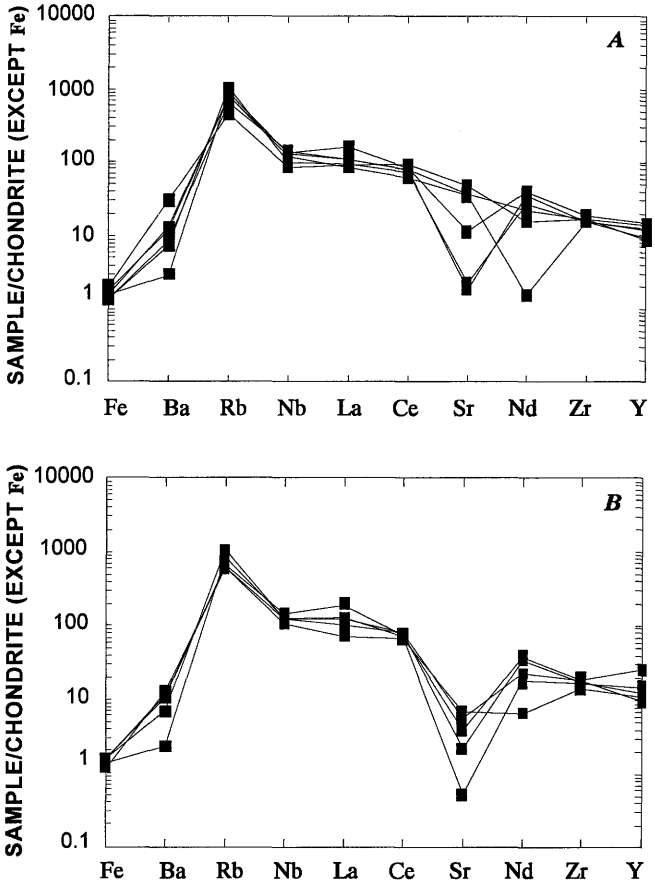

Figure 27. Plot of selected elements determined by energy-dispersive X-ray fluorescence (Kevex) of samples of the tuff of Rainbow Canyon. *A*, samples 87-221, 87-223, 87-1110, 88-115, 88-118, and 88-126d. *B*, samples 88-164, 88-220, 88-224, 88-1158b, and 88-1264. From data in Appendix 2. Iron (in weight percent) values result from dividing the raw data by 0.5; other elements (in parts per million) normalized by dividing by chondrite abundances according to values given by Thompson (1984).

as the sedimentary rocks of Newman Canyon (Rowley, Shroba, and others, 1994). These deposits are well exposed as coarse conglomerate on the east side of Caliente and as sandstone, mudflow, and conglomerate in Newman Canyon west of Caliente, in which are intertongued thin, gray and yellow airfall and ash-flow tuff beds of the tuff of Kershaw Canyon. Clear outflow ash-flow deposits, rarely more than 50 m thick, are exposed west of the Chief Range and about 20 km northwest of the Caliente caldera complex (P.D. Rowley and F.W. Simonds, unpub. mapping, 1991).

The tuff of Kershaw Canyon (figs. 28, 29) contains 5–30 percent phenocrysts of quartz (20–55 percent), sanidine (25–65 percent), plagioclase (10–45 percent), biotite (<6 percent), hornblende (<4 percent), clinopyroxene (<4 percent), Fe-Ti oxides (<7 percent), and olivine (<1 percent, xenocrysts?). These modal data clearly distinguish the unit from the tuff of Rainbow Canyon; the tuff of Kershaw Canyon contains much more abundant plagioclase and more

abundant biotite than the tuff of Rainbow Canyon, and the tuff of Kershaw Canyon contains hornblende and pyroxene that the tuff of Rainbow Canyon does not. Kevex data (fig. 30) are as diagnostic as modal data in distinguishing the unit from the tuff of Rainbow Canyon: the tuff of Kershaw Canyon contains higher iron, strontium, barium, lanthanum, and neodymium, and lower rubidium.

The tuff of Kershaw Canyon is intertongued with outflow sheets of the tuff of Sawmill Canyon and Kane Wash Tuff (sections following) and is overlain by the tuff of Etna (section following). The sedimentary rocks of Newman Canyon, with which the tuff of Etna intertongues, contains a waterlaid pumice bed above the tuff of Etna that received a K-Ar date on sanidine by H.H. Mehnert of 13.8±0.6 Ma (Rowley and others, 1992). A white airfall tuff bed in the McCullough Formation (Axen and others, 1988, fig. 2d) about 45 km north-northwest of Caliente received a plateau $^{40}Ar/^{39}Ar$ date on biotite of 15.3±0.2 Ma (Axen and others, 1988; Taylor and others, 1989). The McCullough is a sequence of landslides deposited syntectonically with movement on the Highland detachment fault. Axen and others (1988) suggested that the tuff correlates with Bowman's (1985) tuff of Rainbow Canyon, and this appears to be confirmed because modal analysis and Kevex data (Appendixes 1, 2; figs. 28, 29, 30) suggest that the McCullough tuff correlates with the tuff of Kershaw Canyon.

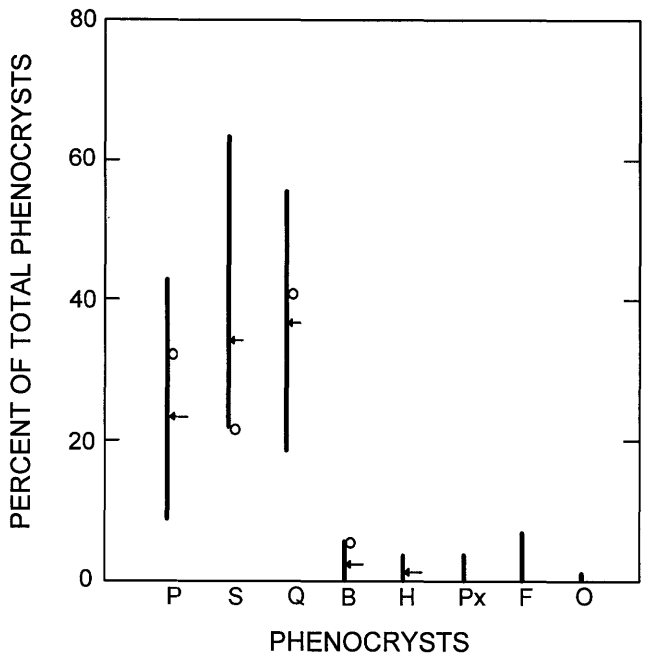

Figure 28. Plot of percentages of major phenocrysts in the tuff of Kershaw Canyon (solid lines) and from a sample of a tuff from the McCullough Formation (open circles) of Axen and others (1988). From data in Appendix 1. Averages of most abundant minerals shown by arrows. P, plagioclase; S, sanidine; Q, quartz; B, biotite; H, hornblende; Px, pyroxene; F, Fe-Ti oxides; O, olivine.

TUFF OF SAWMILL CANYON

The name tuff of Sawmill Canyon is used here for a tan (commonly weathering dark brown), poorly to moderately welded, pumice-rich, crystal-poor, high-silica rhyolite ash-flow tuff that is commonly about 50 m thick. The tuff is well exposed at stream level at the mouth of Sawmill Canyon where it enters Rainbow Canyon 6 km south-southwest of Caliente, and also just northwest of this location, about ½ km east up Buckboard Canyon from where it enters Rainbow Canyon. This single outflow cooling unit underlies only a small area in Rainbow Canyon south of Caliente, where it is interbedded with the lower part of the tuff of Kershaw Canyon; probably both units formerly occupied a valley or basin there. The source of the tuff of Sawmill Canyon is unknown but probably lies near its area of deposition.

The tuff of Sawmill Canyon (figs. 22, 23) contains 3–7 percent phenocrysts of quartz (25–55 percent), sanidine (45–80 percent), plagioclase (trace amounts), biotite (trace amounts), hedenbergite (<3 percent), and Fe-Ti oxides (<2 percent). Quartz phenocrysts tend to be rounded by absorption, and sanidine phenocrysts are commonly adularescent (as this term is used by Mittwede, 1987) and occur as rounded to euhedral crystals; biotite is present but olivine is not, in contrast to the overlying Kane Wash Tuff. Kevex data

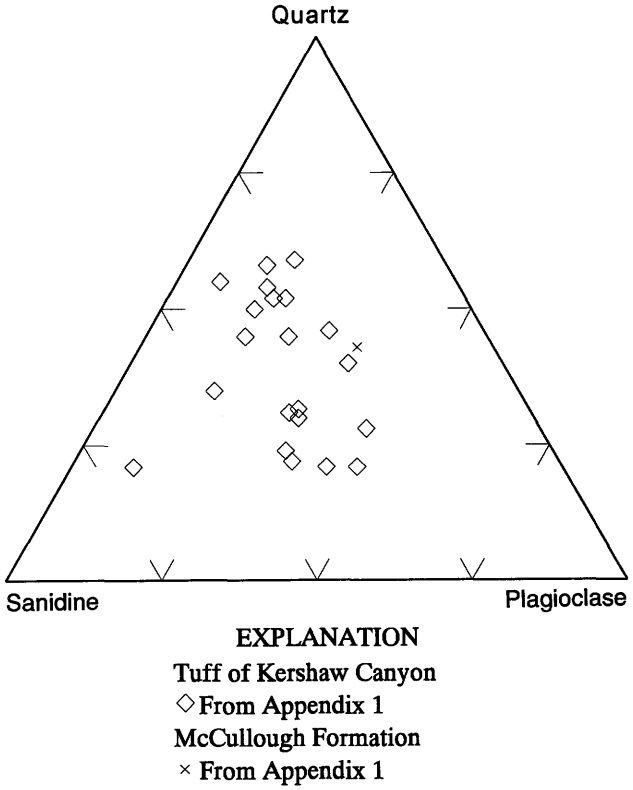

Figure 29. Ternary quartz-sanidine-plagioclase diagram of the tuff of Kershaw Canyon and of a tuff from the McCullough Formation.

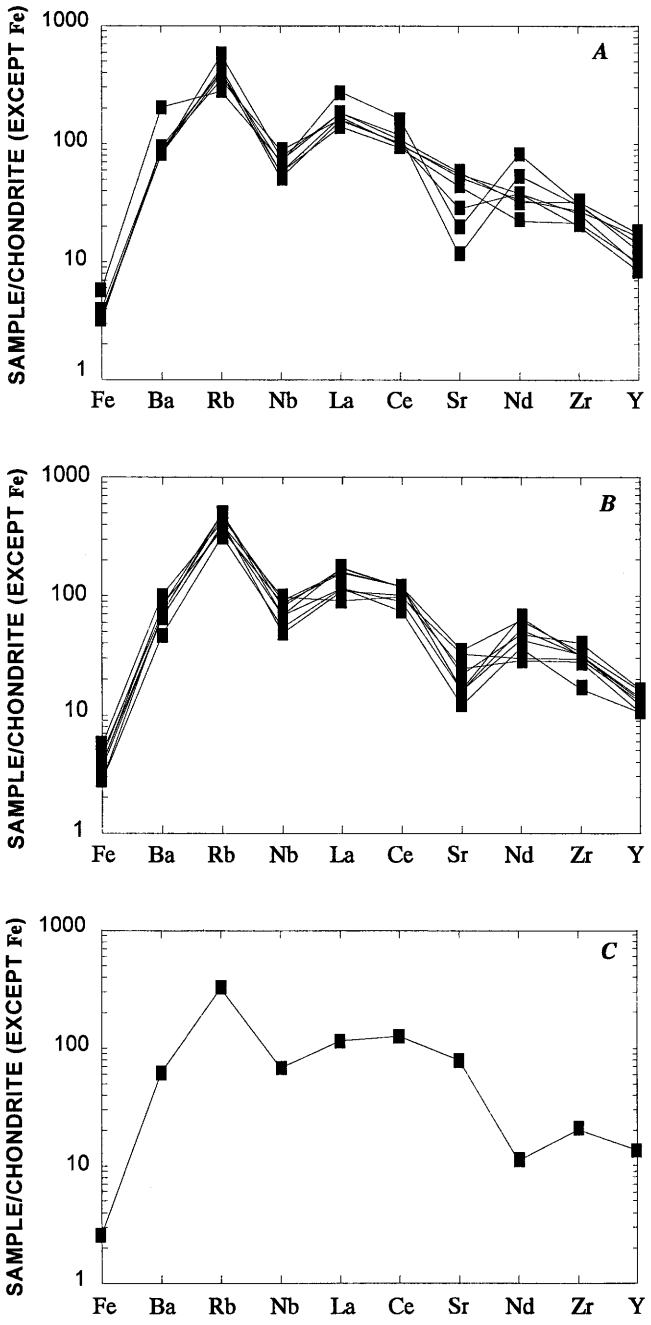

Figure 30. Plot of selected elements determined by energy-dispersive X-ray fluorescence (Kevex) of samples of the tuff of Kershaw Canyon and of a tuff from the McCullough Formation. *A*, samples 88-120c, 88-123, 88-125c, 88-126c, 88-195a, 88-219f, and 88-331. *B*, samples 89-695b, 89-696b, 89-698a, 89-698d, 89-698g, 89-1097a, 89-1097e, and 89-1097f. *C*, McCullough Formation. From data in Appendix 2. Iron (in weight percent) values result from dividing the raw data by 0.5; other elements (in parts per million) normalized by dividing by chondrite abundances according to values given by Thompson (1984).

(fig. 24) somewhat resemble those from the tuff of Rainbow Canyon but represent significantly higher values of cerium, neodymium, and zirconium. The tuff of Sawmill Canyon lithologically and petrographically resembles cooling units of the Delamar Lake, Sunflower Mountain, and Kane Wash Tuffs, but Kevex data and especially paleomagnetic data (C.S. Grommé, unpub. data, 1991) rule out a correlation with those units. The age of the tuff of Sawmill Canyon is constrained by its stratigraphic position above the tuff of Rainbow Canyon and below the Kane Wash Tuff, that is, between 15.6 and 14.6 Ma.

KANE WASH TUFF

The Kane Wash Tuff was originally named by Cook (1965) for quartz- and sanidine-bearing, high-silica rhyolite ash-flow tuffs in Nevada. The unit was redefined several times, most recently by Scott and others (1993), who placed the tuffs of Cook's Kane Wash Tuff into three formations, two of which (Delamar Lake Tuff and Sunflower Mountain Tuff) consist of metaluminous tuff and one of which (the overlying restricted Kane Wash Tuff of Scott and others) consists of a lower member of metaluminous tuff and an upper member of peralkaline tuff. Outflow sheets of these units are generally dark weathering, densely welded cooling units containing adularescent sanidine. The stratigraphic position of the Delamar Lake Tuff relative to the tuff of Rainbow Canyon shown in figure 4 is conjectural inasmuch as these units do not occur in the same area.

As redefined by Scott and others (1993), the Kane Wash Tuff consists of the Grapevine Spring Member and overlying Gregerson Basin Member. Both members were derived from the Kane Springs Wash caldera (Noble, 1968; Scott and others, 1993; Scott and others, this volume). The Grapevine Spring is not found near the Caliente caldera complex but is confined to the area around the Kane Springs Wash caldera, extending especially to the southwest (Novak, 1984, fig. 3a). The member is described by Harding (1991), Harding and others (this volume), and Scott and others (this volume). The Grapevine Spring Member is a crystal-poor, nonwelded to densely welded, metaluminous to nearly peralkaline, high-silica rhyolite ash-flow tuff that was earlier referred to informally as member V_1 by Novak (1984). Trace-element data of two samples by Harding (1991, Appendix IIA, unit Tkg; Harding and others, this volume, Appendix 2A) show higher barium, lanthanum, neodymium, and zirconium, and lower cerium than values for the tuff of Sawmill Canyon; the Grapevine Spring Member has significantly higher cerium, lanthanum, neodymium, and zirconium than the Delamar Lake and Sunflower Mountain Tuffs. The Grapevine Spring Member has been dated by K-Ar methods at 14.2–14.0 Ma (Novak, 1984), but we favor a more precise preliminary $^{40}Ar/^{39}Ar$ date on sanidine of 14.7±0.2 Ma recently determined by L.W. Snee. (See Scott and others, this volume.)

The Gregerson Basin Member consists of two ash-flow units, formerly called members V_2 and V_3 by Novak (1984).

Each is compositionally zoned from a comenditic base to a trachytic top. Outflow deposits of both units are widely exposed near Caliente, where Bowman (1985) informally called them units C2 (lower) and C3 (upper) of the tuff of Rainbow Canyon. Near Caliente, each of the Gregerson Basin units consists of one or two cooling units. Modal analyses of samples from the Caliente area of the lower unit of the Gregerson Basin Member (figs. 31, 32) show that it contains 3–15 percent phenocrysts of quartz (15–50 percent), sanidine (45–80 percent), hedenbergite (1–10 percent), Fe-Ti oxides (<5 percent), fayalitic olivine (<6 percent), and local altered ferromagnesian minerals (as much as 10 percent). Tiny crystals of red acmite(?) occur in nearly all thin sections of the unit. Modal analyses of the Gregerson Basin Member from the Kane Springs Wash caldera (R.B. Scott and A.E. Harding, written commun., 1991) are similar to those from the Caliente area. The abundant crystals of hedenbergite and fayalitic olivine, and the absence of biotite, distinguish tuffs of the Kane Wash Tuff from other tuffs. Kevex data (fig. 33) also clearly identify Kane Wash Tuff, for (as befitting a peralkaline rock) they display especially high zirconium as well as high iron, niobium, lanthanum, cerium, and neodymium. These data are similar to those reported by Novak and Mahood (1986, table 10), Harding (1991, Appendix IIA, unit Tkbi), and Harding and others (this volume, Appendix 2A). Modal analyses of Caliente-area samples of the upper unit of the Gregerson Basin Member (figs. 31, 32) show that it contains 5–15 percent phenocrysts of the same minerals in similar proportions to the lower unit of the Gregerson Basin Member, except that the upper unit seems to have somewhat more quartz relative to sanidine than the lower unit. The same trend, with more quartz relative to sanidine upward, seems to characterize all individual cooling units in the Gregerson Basin Member. The upper unit is identified in the field by the fact that euhedral sanidine phenocrysts are significantly larger than those in the lower unit. Most phenocrysts are euhedral in both units of the member. Kevex data (fig. 33) of the upper unit likewise present a picture nearly identical to that of the lower unit, although the upper unit has trace-element abundances consistent with a more peralkaline composition than the lower unit. These data and comparisons are similar to those reported by Novak and Mahood (1986, table 10) and Harding (1991, Appendix IIA, unit Tkb2). The Gregerson Basin Member has been dated at 14.1 Ma (Novak, 1984) by the K-Ar method, but we favor more precise preliminary $^{40}Ar/^{39}Ar$ dates recently determined by L.W. Snee (Scott and others, this volume) of 14.6±0.1 Ma for the lower unit (member V_2 of Novak, 1984) and 14.4±0.1 for the upper unit (member V_3 of Novak, 1984).

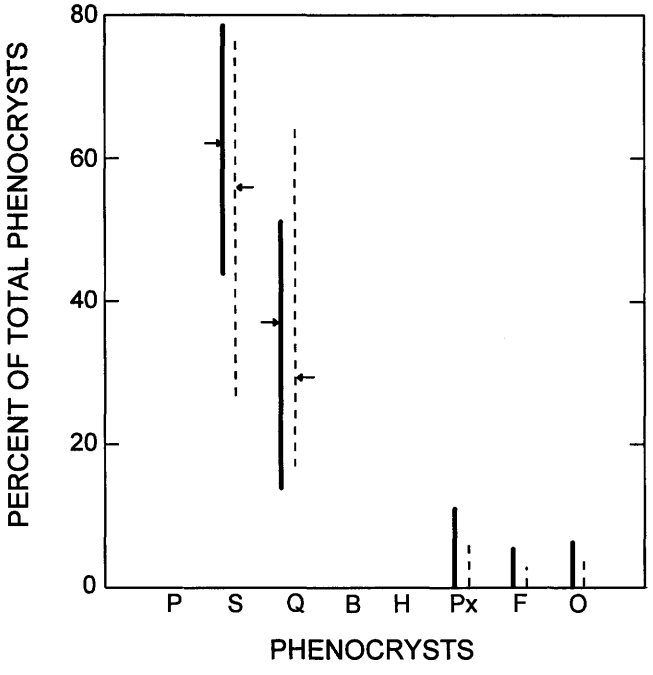

Figure 31. Plot of percentages of major phenocrysts in the lower unit (solid lines) and the upper unit (dashed lines) of the Gregerson Basin Member of the Kane Wash Tuff. From data in Appendix 1. Averages of most abundant minerals shown by arrows. P, plagioclase; S, sanidine; Q, quartz; B, biotite; H, hornblende; Px, pyroxene; F, Fe-Ti oxides; O, olivine.

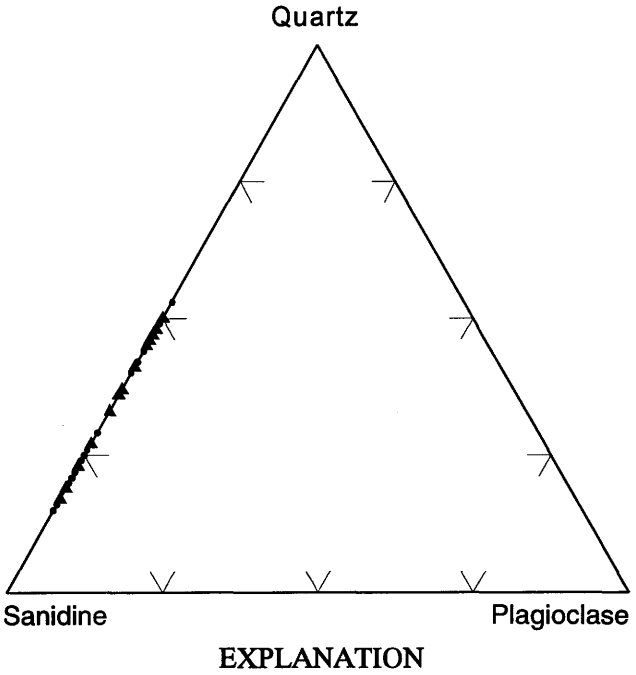

Figure 32. Ternary quartz-sanidine-plagioclase diagram of the lower and upper units of the Gregerson Basin Member of the Kane Wash Tuff.

TUFF OF ETNA

The informal name tuff of Etna was used by Rowley, Shroba, and others (1994) for a light- to medium-gray, outflow ash-flow tuff widely exposed in the Caliente area and named for exposures on the tops of buttes and mesas above the Etna railroad stop in Rainbow Canyon 7 km south-southwest of Caliente. The tuff was mapped by Bowman (1985) as unit C4 of his tuff of Rainbow Canyon, and we later incorrectly correlated it (Snee and others, 1990) with the Ox Valley Tuff, which it closely resembles. The unit consists of one to five crystal-poor to crystal-rich, poorly to highly welded, high-silica rhyolite ash-flow cooling units with a total thickness of about 60 m. The unit is also exposed about 20 km north of the west edge of the Caliente caldera complex in a few scattered areas west of the Chief Range; the southern distal edge is exposed on the northern flank of the Kane Springs Wash caldera (Scott and others, this volume). The source of the tuff of Etna was suggested by Best and others (1993) to be about 9 km south-southwest of Caliente in the east-striking fault zone of the Helene lineament that defines the south side of the Caliente caldera complex, but recent field work and petrologic studies now rule out that hypothesis. We have not found the source but infer that it is somewhere in the central part of the Caliente caldera complex.

The tuff of Etna (figs. 34, 35) contains 5–40 percent phenocrysts of quartz (10–40 percent), sanidine (50–85 percent), plagioclase (<3 percent), biotite (trace amounts), amphibole (<5 percent), pyroxene (<6 percent), Fe-Ti oxides (<4 percent), fayalitic olivine (<9 percent), and altered ferromagnesian minerals (as much as 6 percent). As with the Gregerson Basin Member of the Kane Wash Tuff, there seems to be a trend in stratigraphic sections of the tuff of Etna toward greater quartz in samples collected higher in the section. Distinguishing features of the tuff of Etna include (1) its brown amphibole, which probably replaced pyroxene (apparently hedenbergite, which is sparse and locally occupies cores in the amphibole grains) before tuff eruption; (2) plagioclase phenocrysts that generally occur in the cores of sanidine phenocrysts; (3) deeply embayed quartz; and (4) rounded, rarely euhedral sanidine crystals that are commonly

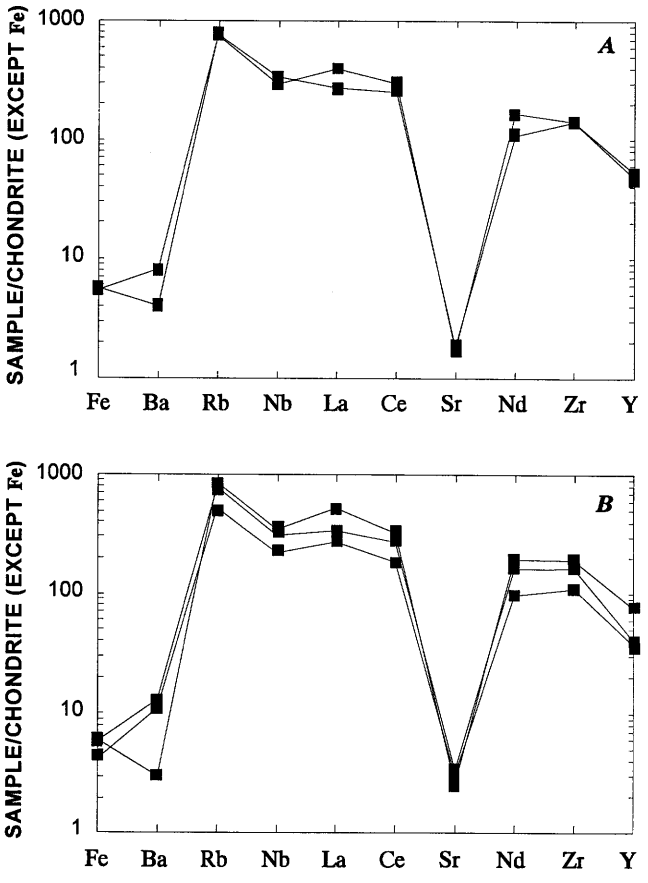

Figure 33. Plot of selected elements determined by energy-dispersive X-ray fluorescence (Kevex) of samples of *A*, lower, and *B*, upper units of the Gregerson Basin Member of the Kane Wash Tuff. From data in Appendix 2. Iron (in weight percent) values result from dividing the raw data by 0.5; other elements (in parts per million) normalized by dividing by chondrite abundances according to values given by Thompson (1984).

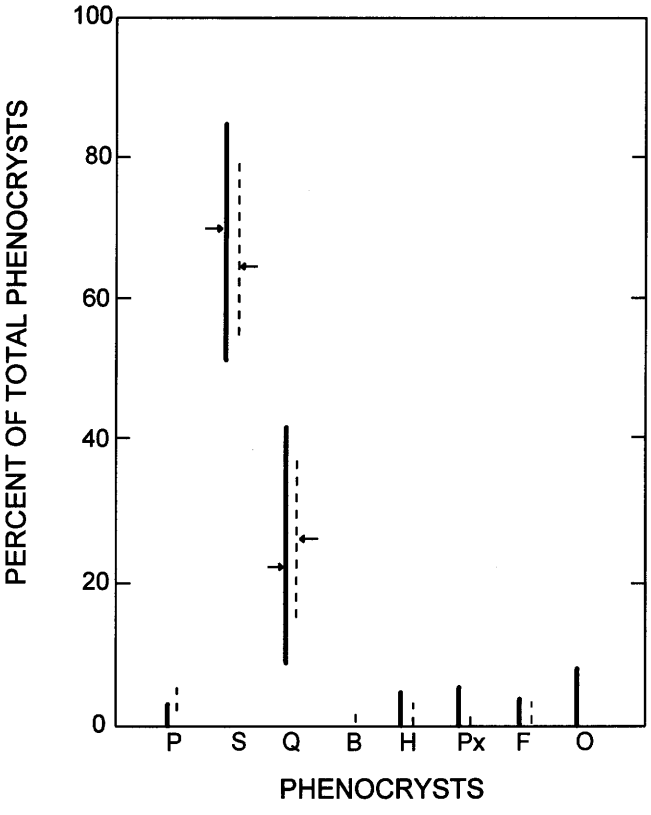

Figure 34. Plot of percentages of major phenocrysts in the tuff of Etna (solid lines) and the Ox Valley Tuff (dashed lines). From data in Appendix 1. Averages of most abundant minerals shown by arrows. P, plagioclase; S, sanidine; Q, quartz; B, biotite; H, hornblende; Px, pyroxene; F, Fe-Ti oxides; O, olivine.

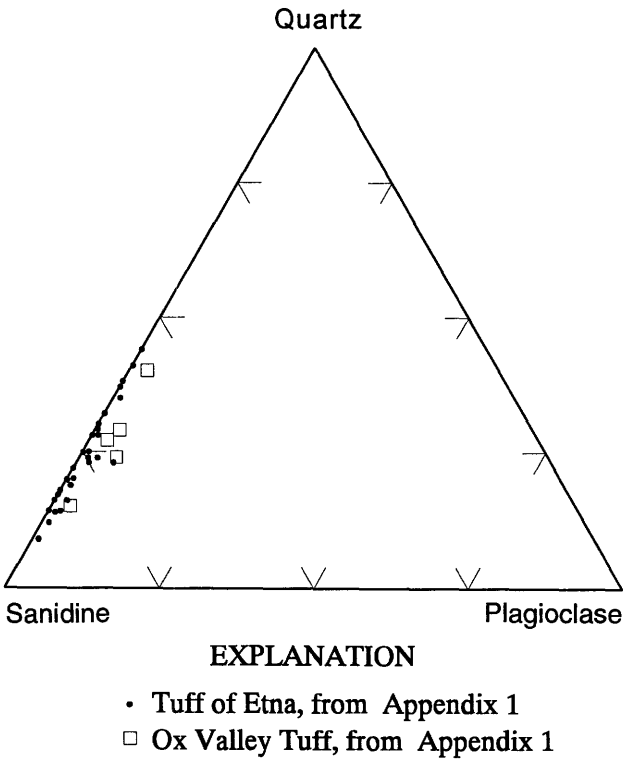

Figure 35. Ternary quartz-sanidine-plagioclase diagram of the tuff of Etna and the Ox Valley Tuff.

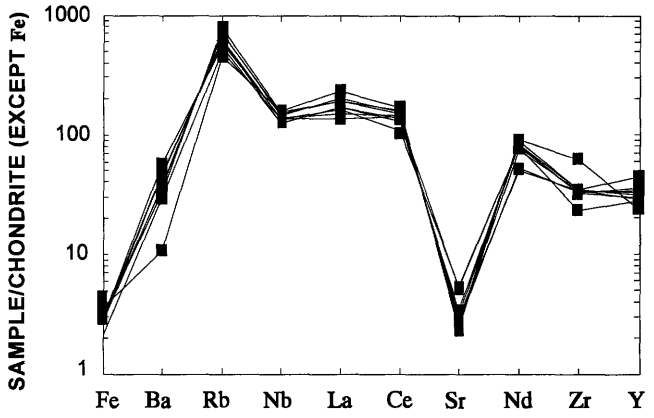

Figure 36. Plot of selected elements determined by energy-dispersive X-ray fluorescence (Kevex) of samples of the tuff of Etna. From data in Appendix 2. Iron (in weight percent) values result from dividing the raw data by 0.5; other elements (in parts per million) normalized by dividing by chondrite abundances according to values given by Thompson (1984).

adularescent. Kevex data (fig. 36) show low zirconium and high barium relative to the Delamar Lake, Sunflower Mountain, and Kane Wash Tuffs. The tuff of Etna was emplaced between 14.4 and 13.8 Ma based on its stratigraphic position between the underlying Gregerson Basin Tuff Member and an overlying airfall tuff in the sedimentary rocks of Newman Canyon. D.R. Lux (University of Maine at Orono) has obtained a compatible $^{40}Ar/^{39}Ar$ date for the tuff of Etna (D.R. Lux, written commun., 1987).

OX VALLEY TUFF

The Ox Valley Tuff of Blank (1959) was formally proposed by Cook (1960) and adopted by Noble and McKee (1972) and Rowley and others (1979). The unit is a light-gray, crystal-poor, poorly to densely welded, high-silica rhyolite ash-flow tuff whose outflow consists in most places of one to four cooling units that generally total less than 40 m thick but may be as thick as 130 m. The Ox Valley Tuff is exposed over an area exceeding 500 km^2 in southwest Utah and adjacent Nevada. The tuff varies greatly in thickness but it is not yet known whether or how those variations are related to volcanotectonic features. Anderson and Hintze (1993) suggested a possible source near the townsite of Motoqua in southwest Utah where the Ox Valley may exceed a kilometer in thickness, but more recent mapping by R.E. Anderson reveals that it is even thicker in the eastern Clover Mountains, west of the Nevada/Utah State line, and this area is more likely as a source.

The Ox Valley Tuff (figs. 34, 35) contains 30–40 percent phenocrysts of quartz (15–40 percent), sanidine (55–80 percent), plagioclase (2–5 percent), biotite (<2 percent), amphibole (1–3 percent), clinopyroxene (1 percent), and Fe-Ti oxides (<3 percent). Sanidine is commonly adularescent. Quartz is more abundant upward in the one stratigraphic section collected. The Ox Valley Tuff is distinguished from the Delamar Lake, Sunflower Mountain, and Kane Wash Tuffs by its conspicuously large rounded quartz phenocrysts that contain embayed edges, by its sanidine crystals that commonly have rounded and ragged edges, and by the presence of plagioclase, brown amphibole, and traces of sphene. It resembles the tuff of Etna in modal amounts and ratios (figs. 34, 35), in the presence of most plagioclase in the cores of sanidine phenocrysts (also noted by Blank, 1959), and in its brown amphibole. It contains somewhat more plagioclase, however, than the tuff of Etna, and it also appears to contain olivine and trace amounts of sphene. Kevex analyses (fig. 37) show higher barium values than occur in the tuff of Etna. The two units have somewhat different paleomagnetic signatures (C.S. Grommé, preliminary data, 1990), but the differences could be explained by vertical-axis structural rotations of the sample sites (M.R. Hudson and J.G. Rosenbaum, oral commun., 1991).

Modal and Kevex data indicate that the Ox Valley Tuff is a similar yet different depositional unit than the tuff of Etna. As with the Hiko and Racer Canyon Tuffs, they appear to have erupted from widely separated sources in the Caliente caldera complex and probably were magmatically related, perhaps from the same magma chamber. Evaluation of such a possibility will require additional geologic mapping and

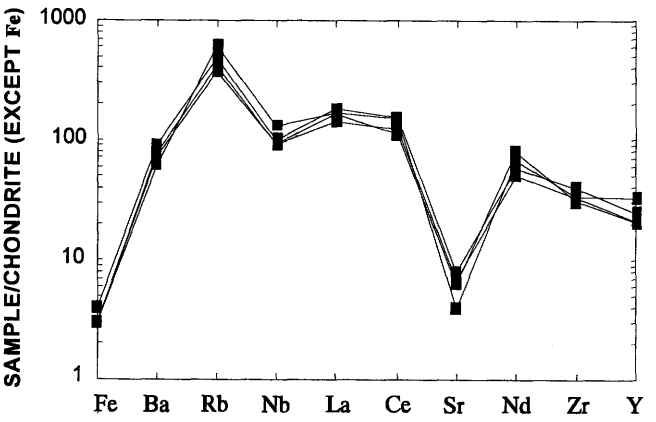

Figure 37. Plot of selected elements determined by energy-dispersive X-ray fluorescence (Kevex) of samples of the Ox Valley Tuff. From data in Appendix 2. Iron (in weight percent) values result from dividing the raw data by 0.5; other elements (in parts per million) normalized by dividing by chondrite abundances according to values given by Thompson (1984).

isotopic analysis of the Ox Valley Tuff, whose actual age remains in doubt. Two discordant K-Ar dates by Noble and McKee (1972), one of 15.5±0.4 Ma from a sample from the Caliente caldera complex in Nevada and one of 12.6±0.3 Ma from a sample from near Ox Valley in southwestern Utah, were attributed by them to Ox Valley Tuff. More likely, however, the date of 15.5 Ma is from a sample of the tuff of Etna and only the 12.6 Ma date is of the Ox Valley Tuff (Rowley, Shroba, and others, 1994). This interpretation is supported by two K-Ar dates determined by H.H. Mehnert and discussed by Anderson and Hintze (1993); one is a published date of a basalt lava flow from Moody Wash, northwest of Gunlock, Utah, that underlies Ox Valley Tuff, of 12.3±0.6 Ma (Best and others, 1980) and the other is an unpublished date of a rhyolite lava flow that overlies it near Enterprise Reservoir, Utah, of 11.4±0.5 Ma (H.H. Mehnert, written commun., 1980). Our best estimate of the age of the Ox Valley Tuff is 12.6–12.3 Ma.

CONCLUSIONS

Eruptions from the Caliente caldera complex began at least by 22.8 Ma, the age of the Bauers Tuff Member of the Condor Canyon Formation, and continued until the apparent age of the Ox Valley Tuff, sometime between 12.6 and 11.4 Ma. If the Swett Tuff Member of the Condor Canyon Formation were derived from the Caliente caldera complex, as seems certain, and if the Leach Canyon Formation also erupted from the complex, as seems possible, then the complex is as old as 24 Ma. The major episode of extension in this part of the Basin and Range province began before 19.4 Ma, the age of the porphyry of Meadow Valley Wash, which was intruded as numerous widely scattered dikes along faults of significant offset. Extension along faults of similar trend and offset continued at least until after 14.0 Ma, the age of the tuff of Etna, and probably after 12.1 Ma, the youngest of two basalt flows (Mehnert and others, 1989). More than likely this deformational episode began earlier, probably as early as 25 Ma, but the evidence is equivocal. The synchroneity of caldera volcanism and extension means that many caldera margins in the Caliente caldera complex are regional faults. In particular, the north and south sides of the complex are bounded by faults of the east-trending Timpahute and Helene lineaments, respectively, and the caldera complex can be viewed as a volcanotectonic trough.

The study of the Caliente caldera complex is just beginning and at the present time has involved mostly stratigraphy of tuff units and locating their source calderas. Mapping has concentrated on areas on the margin of the western part of the caldera complex, where outflow tuffs of the Caliente and other calderas are exposed, and on some parts of the interior of the complex. This report focuses on the stratigraphy and on our effort to correlate tuffs by petrography and chemical analyses.

The oldest tuff discussed here is the poorly welded, widespread, rhyolite Leach Canyon Formation (23.8 Ma), which on the basis of distribution and isopach data has been proposed to be derived from the Caliente caldera complex but whose caldera has not yet been discovered. Densely welded, low-silica rhyolitic tuffs of the Swett (23.7? Ma) and Bauers (22.8 Ma) Tuff Members of the Condor Canyon Formation were widely spread over Nevada and Utah; the Bauers was derived from the poorly exposed Clover Creek caldera of the Caliente complex, and the Swett was derived probably from a nearby caldera—but no trace of it has been found. The source of the moderately welded, widespread, crystal-rich, andesitic Harmony Hills Tuff (22.5–22.0 Ma) has been proposed to be the Caliente caldera complex, but more likely the tuff erupted in or near the eastern Bull Valley Mountains of Utah. The poorly to moderately welded, low-silica rhyolite Racer Canyon Tuff (19.2?–18.7 Ma) is known only from Utah and probably came from the east end of the Caliente caldera complex. The poorly to moderately welded, widespread, low-silica rhyolite Hiko Tuff (18.6–18.2 Ma) was derived from the Delamar caldera, at the west end of the complex. The poorly welded, low-silica rhyolite tuff of Tepee Rocks (17.8 Ma) is a local Hiko-like unit; its source is unknown but probably lies just east of the Delamar caldera. The Racer Canyon, Hiko, and tuff of Tepee Rocks are similar in lithology and age and appear to have erupted from different vents from widely different parts of the Caliente caldera complex that tapped the same magma chamber. What we now map as the Hiko Tuff itself, in fact, probably consists of several more distinct tuff units erupted from isolated vents in and adjacent to the Delamar caldera.

At some time after emplacement of the tuff of Tepee Rocks, about 17.5–16 Ma, the petrologic regime changed in this part of the Basin and Range from one of calc-alkalic

magmatism to one of basalt and high-silica rhyolite magmatism. Although such a change seems in some places in the Basin and Range to have coincided with initiation of or an increase in extensional tectonism, no tectonic change is known in the general area of the Caliente caldera complex. The first of the eruptive products of the new magmatic regime exposed in the Caliente area is the moderately to densely welded, high-silica rhyolite Delamar Lake Tuff (15.8–15.5 Ma), which was derived from an unidentified source well southwest of the Caliente caldera complex. The poorly welded, high-silica rhyolite tuff of Rainbow Canyon (15.6–15.2 Ma) is a local unit derived from the Buckboard Canyon caldera, which is inset into the Delamar caldera. The source of the poorly welded, high-silica rhyolite tuff of Kershaw Canyon (15.3?–14.0 Ma) has not been identified with certainty but probably is just east of the Buckboard Canyon caldera. The moderately welded, high-silica rhyolite tuff of Sawmill Canyon is a local outflow cooling unit interbedded with the lower part of the tuff of Kershaw Canyon; its source is inferred to be in the central Caliente caldera complex. Outflow cooling units of the moderately to densely welded, widespread, peralkaline high-silica rhyolite Gregerson Basin Member (14.6–14.4 Ma) of the Kane Wash Tuff, derived from the Kane Springs Wash caldera 20 km southwest of the Caliente caldera complex, are intertongued with the tuff of Kershaw Canyon in the caldera complex. The moderately to densely welded, widespread, high-silica rhyolite tuff of Etna (14.0 Ma) is derived probably from the central part of the Caliente caldera complex. The youngest known significant tuff in the area of the Caliente caldera complex is the moderately to densely welded, high-silica rhyolite Ox Valley Tuff (12.6?–11.4? Ma). This unit is distributed in the Nevada-Utah border area between the Clover and Bull Valley Mountains and probably was derived from a vent in the southeastern part of the Caliente complex. It is lithologically similar to the tuff of Etna and may have been derived from the same magma chamber. Vents for this lithologic type could be scattered within the southern caldera complex.

REFERENCES CITED

Adair, D.H., 1986, Structural setting of the Goldstrike district, Washington County, Utah, *in* Griffen, D.T., and Phillips, W.R., eds., Thrusting and extensional structures and mineralization in the Beaver Dam Mountains, southwestern Utah: Utah Geological Association Publication 15, p. 129–135.

Anderson, J.J., and Rowley, P.D., 1975, Cenozoic stratigraphy of the southwestern High Plateaus of Utah, *in* Anderson, J.J., Rowley, P.D., Fleck, R.J., and Nairn, A.E.M., eds., Cenozoic geology of southwestern High Plateaus of Utah: Geological Society of America Special Paper 160, p. 1–52.

Anderson, R.E., 1984, Strike-slip faults associated with extension in and adjacent to the Great Basin: Geological Society of America Abstracts with Programs, v. 16, no. 6, p. 429.

———1986, Coeval mixed-mode dip-slip and strike-slip faulting in and adjacent to the Basin and Range, Utah-Nevada: Geological Society of America Abstracts with Programs, v. 18, no. 5, p. 338.

———1987, Neogene geologic history of the Nevada-Utah border area at and near latitude 37°30'N.: Geological Society of America Abstracts with Programs, v. 19, no. 7, p. 572.

———1989, Tectonic evolution of the Intermontane System, Basin and Range, Colorado Plateau, and High Lava Plains, Chapter 10, *in* Pakiser, L.C., and Mooney, W.D., eds., Geophysical framework of the continental United States: Geological Society of America Memoir 172, p. 163–176.

———1990, West-directed tectonic escape between the northern and southern sectors of the Basin and Range province: Geological Society of America Abstracts with Programs, v. 22, no. 3, p. 2.

Anderson, R.E., and Barnhard, T.P., 1993a, Heterogeneous Neogene strain and its bearing on horizontal extension and vertical contraction at the margin of the extensional orogen, Mormon Mountains area, Nevada and Utah: U.S. Geological Survey Bulletin 2011, 43 p.

———1993b, Aspects of three-dimensional strain at the margin of the extensional orogen, Virgin River depression area, Nevada, Utah, and Arizona: Geological Society of America Bulletin, v. 105, p. 1019–1052.

Anderson, R.E., and Bohannon, R.G., 1993, Three-dimensional aspects of the Neogene strain field, Nevada-Utah-Arizona tricorner area, *in* Lahren, M.M., Trexler, J.H., Jr., and Spinosa, Claude, eds., Crustal evolution of the Great Basin and Sierra Nevada: Geological Society of America field trip guidebook, Cordilleran/Rocky Mountain section meeting, Reno, Nev., Mackay School of Mines, p. 167–196.

Anderson, R.E., and Hintze, L.F., 1993, Geologic map of the Dodge Spring quadrangle, Washington County, Utah, and Lincoln County, Nevada: U.S. Geological Survey Quadrangle Map GQ–1721, scale 1:24,000.

Armstrong, R.L., 1970, Geochronology of Tertiary igneous rocks, eastern Basin and Range province, western Utah, eastern Nevada, and vicinity, U.S.A.: Geochimica et Cosmochimica Acta, v. 34, p. 203–232.

Axen, G.J., Lewis, P.R., Burke, K.L., Sleeper, K.G., and Fletcher, J.M., 1988, Tertiary extension in the Pioche area, Lincoln County, Nevada, *in* Bartley, J.M., Axen, G.J., Taylor, W.J., and Fryxell, J.E., Cenozoic tectonics of a transect through eastern Nevada near 38°N. latitude, *in* Weide, D.L., and Faber, M.L., eds., This extended land—Geological journeys in the southern Basin and Range, field trip guidebook, Geological Society of America, Cordilleran section meeting, Las Vegas, Nevada: University of Nevada, Las Vegas, Department of Geoscience, p. 3–5.

Best, M.G., Christiansen, E.H., and Blank, R.H., Jr., 1989, Oligocene caldera complex and calc-alkaline tuffs and lavas of the Indian Peak volcanic field, Nevada and Utah: Geological Society of America Bulletin, v. 101, p. 1076–1090.

Best, M.G., Christiansen, E.H., Deino, A.L., Grommé, C.S., McKee, E.H., and Noble, D.C., 1989, Excursion 3A—Eocene through Miocene volcanism in the Great Basin of the western United States: New Mexico Bureau of Mines and Mineral Resources Memoir 47, p. 91–133.

Best, M.G., McKee, E.H., and Damon, P.E., 1980, Space-time-composition patterns of late Cenozoic mafic volcanism, southwestern Utah and adjoining areas: American Journal of Science, v. 280, p. 1035–1050.

Best, M.G., Miller, D.S., Radke, L.E., and Kowallis, B.J., 1991, Preliminary geologic map of the Panaca Summit and Prohibition Flat quadrangles, Lincoln County, Nevada, and Iron County, Utah: U.S. Geological Survey Open-File Report 91–124, 22 p., scale 1:24,000.

Best, M.G., Scott, R.B., Rowley, P.D., Swadley, W C, Anderson, R.E., Grommé, C.S., Harding, A.E., Deino, A.L., Christiansen, E.H., Tingey, D.G., and Sullivan, K.R., 1993, Oligocene-Miocene caldera complexes, ash-flow sheets, and tectonism in the central and southeastern Great Basin, *in* Lahren, M.M., Trexler, J.H., Jr., and Spinosa, Claude, eds., Crustal evolution of the Great Basin and Sierra Nevada: Geological Society of America field trip guidebook, Cordilleran/Rocky Mountain section meeting, Reno, Nev., Mackay School of Mines, p. 285–311.

Blank, H.R., 1959, Geology of the Bull Valley district, Washington County, Utah: Seattle, Wash., University of Washington Ph. D. dissertation, 177 p.

Blank, H.R., and Kucks, R.P., 1989, Preliminary aeromagnetic, gravity, and generalized geologic maps of the USGS Basin and Range–Colorado Plateau transition zone study area in southwestern Utah, southeastern Nevada, and northwestern Arizona (the "BARCO" project): U.S. Geological Survey Open-File Report 89–432, 16 p., scale 1:250,000.

Blank, H.R., Rowley, P.D., and Hacker, D.B., 1992, Miocene monzonitic intrusions and associated megabreccias of the Iron Axis region, southwestern Utah, *in* Wilson, J.R., ed., Field guide to geologic excursions in Utah and adjacent areas of Nevada, Idaho, and Wyoming, Geological Society of America, Rocky Mountain section meeting: Utah Geological Survey Miscellaneous Publication 92-3, p. 399–420.

Bowman, S.A., 1985, Miocene extension and volcanism in the Caliente caldera complex, Lincoln County, Nevada: Golden, Colo., Colorado School of Mines M.S. thesis, 143 p.

Burke, D.B., and McKee, E.H., 1979, Mid-Cenozoic volcano-tectonic troughs in central Nevada: Geological Society of America Bulletin, v. 90, part I, p. 181–184.

Callaghan, Eugene, 1937, Geology of the Delamar district, Lincoln County, Nevada: University of Nevada Bulletin, v. 31, no. 5 (Nevada Bureau of Mines Bulletin 30A), 69 p.

Christiansen, R.L., and Lipman, P.W., 1972, Cenozoic volcanism and plate tectonic evolution of the western United States, part II—Late Cenozoic: Philosophical Transactions of the Royal Society of London, Series A, v. 271, p. 249–284.

Cook, E.F., 1957, Geology of Pine Valley Mountains, Utah: Utah Geological and Mineralogical Survey Bulletin 58, 111 p.

———1960, Geologic atlas of Utah–Washington County: Utah Geological and Mineralogical Survey Bulletin 70, 119 p.

———1965, Stratigraphy of Tertiary volcanic rocks in eastern Nevada: Nevada Bureau of Mines Report 11, 61 p.

Dolgoff, Abraham, 1963, Volcanic stratigraphy of the Pahranagat area, Lincoln County, southeastern Nevada: Geological Society of America Bulletin, v. 74, p. 875–900.

du Bray, E.A., 1995, Geochemistry and petrology of Oligocene and Miocene ash-flow tuffs of the southeastern Great Basin, Nevada: U.S. Geological Survey Professional Paper 1559, 38 p.

du Bray, E.A., and Hurtubise, D.O., 1994, Geologic map of the Seaman Range, Lincoln and Nye Counties, Nevada: U.S. Geological Survey Miscellaneous Investigations Series Map I–2282, scale 1:50,000.

Ekren, E.B., Bucknam, R.C., Carr, W.J., Dixon, G.L., and Quinlivan, W.D., 1976, East-trending structural lineaments in central Nevada: U.S. Geological Survey Professional Paper 986, 16 p.

Ekren, E.B., Orkild, P.P., Sargent, K.A., and Dixon, G.L., 1977, Geologic map of Tertiary rocks, Lincoln County, Nevada: U.S. Geological Survey Miscellaneous Investigations Series Map I–1041, scale 1:250,000.

Emmons, S.F., 1901, The Delamar and the Horn-Silver mines—Two types of ore-deposits in the deserts of Nevada and Utah: Transactions of American Institute of Mining Engineers, v. 31, p. 658–683.

Ferris, D.E., 1991, The best of times, the worst of times—A biocultural analysis of the Ferguson district, 1892–1909: Las Vegas, Nev., University of Nevada, Las Vegas, M.A. thesis, 296 p.

Harding, A.E., 1991, Evidence of the Kane Springs Wash caldera in the Meadow Valley Mountains, southeastern Nevada: Boulder, Colo., University of Colorado M.S. thesis, 121 p.

Hausel, W.D., and Nash, W.P., 1977, Petrology of Tertiary and Quaternary volcanic rocks, Washington County, southwestern Utah: Geological Society of America Bulletin, v. 88, p. 1831–1842.

Hurtubise, D.O., and du Bray, E.A., 1992, Stratigraphy and structure of the Seaman Range and Fox Mountain, Lincoln and Nye Counties, Nevada: U.S. Geological Survey Bulletin 1988–B, 31 p.

Kowallis, B.J., and Best, M.G., 1990, Fission track ages from volcanic rocks in southwestern Utah and southeastern Nevada: Isochron/West, no. 55, p. 24–27.

Le Bas, M.J., LeMaitre, R.W., Streckeisen, A., and Zanettin, B., 1986, A chemical classification of volcanic rocks based on the total alkali-silica diagram: Journal of Petrology, v. 27, pt. 3, p. 745–750.

Lipman, P.W., Christiansen, R.L., and O'Connor, J.T., 1966, A compositionally zoned ash-flow sheet in southern Nevada: U.S. Geological Survey Professional Paper 524–F, p. 1–47.

Mackin, J.H., 1960, Structural significance of Tertiary volcanic rocks in southwestern Utah: American Journal of Science, v. 258, p. 81–131.

Mammerickx, J., and Klitgord, K.D., 1982, Northern East Pacific Rise—Evolution from 25 m.y. to the present: Journal of Geophysical Research, v. 87, p. 6751–6759.

Mehnert, H.H., Anderson, R.E., and Rowley, P.D., 1989, Constraints on age of faulting and youngest volcanism, western Caliente caldera complex and vicinity, Lincoln County, Nevada [abs.]: Eos, v. 70, no. 43, p. 1414.

Merriam, C.W., 1964, Cambrian rocks of the Pioche mining district, Nevada: U.S. Geological Survey Professional Paper 469, 55 p.

Michel-Noël, G., Anderson, R.E., and Angelier, Jacques, 1990, Fault kinematics and estimates of strain partitioning of a Neogene extensional fault system in southeastern Nevada, *in* Wernicke, B.P., ed., Basin and Range extensional tectonics near the latitude of Las Vegas: Geological Society of America Memoir 176, p. 155–180.

Mittwede, S.K., 1987, Comment and reply on "Correlation of the Peach Springs Tuff, a large-volume Miocene ignimbrite sheet in California and Arizona": Geology, v. 15, no. 4, p. 375.

Noble, D.C., 1968, Kane Springs Wash volcanic center, Lincoln County, Nevada, *in* Eckel, E.B., ed., Nevada Test Site: Geological Society of America Memoir 110, p. 109–116.

Noble, D.C., and McKee, E.H., 1972, Description and K-Ar ages of volcanic units of the Caliente volcanic field, Lincoln County, Nevada, and Washington County, Utah: Isochron/West, no. 5, p. 17–24.

Noble, D.C., McKee, E.H., Hedge, C.E., and Blank, H.R., Jr., 1968, Reconnaissance of the Caliente depression, Lincoln County, Nevada [abs.]: Geological Society of America Special Paper 115, p. 435–436.

Novak, S.W., 1984, Eruptive history of the rhyolitic Kane Springs Wash volcanic center, Nevada: Journal of Geophysical Research, v. 89, p. 8603–8615.

Novak, S.W., and Mahood, G.A., 1986, Rise and fall of a basalt-trachyte-rhyolite magma system at the Kane Springs Wash caldera, Nevada: Contributions to Mineralogy and Petrology, v. 94, p. 352–373.

Rowley, P.D., Anderson, R.E., Snee, L.W., and Mehnert, H.H., 1990, Geology and structural setting of the western Caliente caldera complex, Lincoln County, Nevada: Geological Society of America Abstracts with Programs, v. 22, no. 3, p. 79.

Rowley, P.D., Cunningham, C.G., Steven, T.A., Mehnert, H.H., and Naeser, C.W., in press, Cenozoic igneous and tectonic setting of the Marysvale volcanic field, and its relation to other igneous centers, in Utah and Nevada, *in* Friedman, J.D., and Huffman, A.C., Jr., eds., Laccolith complexes of southeastern Utah—Tectonic control and time of emplacement: U.S. Geological Survey Bulletin.

Rowley, P.D., Lipman, P.W., Mehnert, H.H., Lindsey, D.A., and Anderson, J.J., 1978, Blue Ribbon lineament, an east-trending structural zone within the Pioche mineral belt of southwestern Utah and eastern Nevada: U.S. Geological Survey Journal of Research, v. 6, no. 2, p. 175–192.

Rowley, P.D., McKee, E.H., and Blank, H.R., Jr., 1989, Miocene gravity slides resulting from emplacement of the Iron Mountain pluton, southern Iron Springs mining district, Iron County, Utah [abs.]: Eos, v. 70, no. 43, p. 1309.

Rowley, P.D., Mehnert, H.H., Naeser, C.W., Snee, L.W., Cunningham, C.G., Steven, T.A., Anderson, J.J., Sable, E.G., and Anderson, R.E., 1994, Isotopic ages and stratigraphy of Cenozoic rocks of the Marysvale volcanic field and adjacent areas, west-central Utah: U.S. Geological Survey Bulletin 2071, 35 p.

Rowley, P.D., and Shroba, R.R., 1991, Geologic map of the Indian Cove quadrangle, Lincoln County, Nevada: U.S. Geological Survey Geologic Quadrangle Map GQ–1701, scale 1:24,000.

Rowley, P.D., Shroba, R.R., Simonds, F.W., Burke, K.J., Axen, G.J., and Olmore, S.D., 1994, Geologic map of the Chief Mountain quadrangle, Lincoln County, Nevada: U.S. Geological Survey Geologic Quadrangle Map GQ–1731, scale 1:24,000.

Rowley, P.D., and Siders, M.A., 1988, Miocene calderas of the Caliente caldera complex, Nevada-Utah [abs.]: Eos, v. 69, no. 44, p. 1508.

Rowley, P.D., Snee, L.W., Mehnert, H.H., Anderson, R.E., Axen, G.J., Burke, K.J., Simonds, F.W., Shroba, R.R., and Olmore, S.D., 1992, Structural setting of the Chief Mining District, eastern Chief Range, Lincoln County, Nevada, *in* Thorman, C.H., ed., Application of structural geology to mineral and energy resources of the central and western United States: U.S. Geological Survey Bulletin 2012–H, 17 p.

Rowley, P.D., Steven, T.A., Anderson, J.J., and Cunningham, C.G., 1979, Cenozoic stratigraphic and structural framework of southwestern Utah: U.S. Geological Survey Professional Paper 1149, 22 p.

Samson, S.D., and Alexander, E.C., Jr., 1987, Calibration of the interlaboratory $^{40}Ar/^{39}Ar$ dating standard, MMhb-1: Chemical Geology, v. 66, p. 27–34.

Scott, R.B., Swadley, W C, and Novak, S.W., 1993, Geologic map of the Delamar Lake quadrangle, Lincoln County, Nevada: U.S. Geological Survey Geologic Quadrangle Map GQ–1730, scale 1:24,000.

Shubat, M.A., and Siders, M.A., 1988, Geologic map of the Silver Peak quadrangle, Iron County, Utah: Utah Geological and Mineral Survey Map 108, 13 p., scale 1:24,000.

Siders, M.A., 1985, Geologic map of the Pinon Point quadrangle, Iron County, Utah: Utah Geological and Mineral Survey Map 84, 12 p., scale 1:24,000.

———1991, Geologic map of the Mount Escalante quadrangle, Iron County, Utah: Utah Geological and Mineral Survey Map 131, 9 p., scale 1:24,000.

Siders, M.A., Rowley, P.D., Shubat, M.A., Christenson, G.E., and Galyardt, G.L., 1990, Geologic map of the Newcastle quadrangle, Iron County, Utah: U.S. Geological Survey Geologic Quadrangle Map GQ–1690, scale 1:24,000.

Siders, M.A., and Shubat, M.A., 1986, Stratigraphy and structure of the northern Bull Valley Mountains and Antelope Range, Iron County, Utah, *in* Griffen, D.T., and Phillips, W.R., eds., Thrusting and extensional structures and mineralization in the Beaver Dam Mountains, southwestern Utah: Utah Geological Association Publication 15, p. 87–102.

Snee, L.W., Mehnert, H.H., Rowley, P.D., Anderson, R.E., and Scott, R.B., 1990, New isotopic ages demonstrate extensional faulting of 19–12 Ma in the western Caliente caldera complex and vicinity, Lincoln County, Nevada [abs.]: Eos, v. 71, no. 43, p. 1612.

Steiger, R.H., and Jäger, Emile, 1977, Subcommission on geochronology—Convention on the use of decay constants in geo- and cosmochronology: Earth and Planetary Science Letters, v. 36, p. 359–362.

Steven, T.A., Morris, H.T., and Rowley, P.D., 1990, Geologic map of the Richfield 1°×2° quadrangle, west-central Utah: U.S. Geological Survey Miscellaneous Investigations Series Map I–1901, scale 1:250,000.

Steven, T.A., Rowley, P.D., and Cunningham, C.G., 1984, Calderas of the Marysvale volcanic field, west-central Utah: Journal of Geophysical Research, v. 89, no. B10, p. 8751–8764.

Swadley, W C, and Rowley, P.D., 1994, Geologic map of the Pahroc Spring SE quadrangle, Lincoln County, Nevada: U.S. Geological Survey Geologic Quadrangle Map GQ–1752, scale 1:24,000.

Taylor, W.J., Bartley, J.M., Lux, D.R., and Axen, G.J., 1989, Timing of Tertiary extension in the Railroad Valley-Pioche transect, Nevada–Constraints from $^{40}Ar/^{39}Ar$ ages of volcanic rocks: Journal of Geophysical Research, v. 94, p. 7757–7774.

Thompson, R.N., 1984, Magmatism of the British Tertiary volcanic province: Scottish Journal of Geology, v. 8, pt. 1, p. 49–108.

Tschanz, C.M., and Pampeyan, E.H., 1970, Geology and mineral deposits of Lincoln County, Nevada: Nevada Bureau of Mines and Geology Bulletin 73, 188 p.

Ward, P.L., 1991, On plate tectonics and the geologic evolution of southwestern North America: Journal of Geophysical Research, v. 96, p. 12479–12496.

Wiebe, R.A., 1993, Basaltic injections into floored silicic magma chambers: Eos, v. 74, no. 1, p. 1–3.

Willden, Ronald, and Adair, D.H., 1986, Gold deposits at Goldstrike, Utah, *in* Griffen, D.T., and Phillips, W.R., eds., Thrusting and extensional structures and mineralization in the Beaver Dam Mountains, southwestern Utah: Utah Geological Association Publication 15, p. 137–147.

Williams, P.L., 1967, Stratigraphy and petrography of the Quichapa Group, southwestern Utah and southeastern Nevada: Seattle, Wash., University of Washington Ph. D. dissertation, 182 p.

Zietz, Isidore, Gilbert, F.P., and Kirby, J.R., Jr., 1978, Aeromagnetic map of Nevada—Color coded intensities: U.S. Geological Survey Geophysical Investigations Map GP–922, scale 1:1,000,000.

Zietz, Isidore, Shuey, Ralph, and Kirby, J.R., Jr., 1976, Aeromagnetic map of Utah: U.S. Geological Survey Geophysical Investigations Map GP–907, scale 1:1,000,000.

APPENDIX 1.

Modal analyses of rocks in southeastern Nevada and southwestern Utah. Based on counting about 1,000 points on stained thin sections.

Explanation of headings from left to right: Sample number—asterisk shows Kevex data are available (in Appendix 2); vertical arrows span samples from same stratigraphic section (arrow points toward top of section).
Loc., location of sample (keys to letters given below).
Phenocryst minerals are shown as volume percentages of total rock (percentage of phenocryst minerals to total phenocrysts given in parentheses): quartz, sanidine, plagioclase, biotite, hornblende, pyroxene, Fe-Ti oxides, olivine, altered ferromagnesian minerals, sphene.
Total pheno., total phenocrysts; Q-S-P ratio, relative amounts of quartz, sanidine, and plagioclase; VRFs, volcanic rock fragments; Pum., collapsed pumice, where determined; G'mass, groundmass (for some samples includes pumice). T, trace; blank, not present.

Key to location symbols, which are shown on the Caliente, Nevada-Utah; Cedar City, Utah; and Richfield, Utah 1°×2° quadrangles:
A, Antelope Range, Utah; B, Bald Hills, Utah; BL, Black Mountains, Utah; C, Chief Range and hills to west, Nevada; CA, Caliente area, Nevada; CC, Condor Canyon, Nevada; CN, north of Caliente, Nevada; D, Delamar area, Nevada; E, Enterprise Reservoir area, Utah; EC, Eccles area, Nevada; EL, Elgin area, Nevada; ET, Etna area, Nevada; G, Gunlock-Veyo area, Utah; H, Harmony Mountains, Utah; I, Iron Springs mining district, Utah; IB, south of Islen-Barclay, Nevada; K, Kane Point, Utah; M, Markagunt Plateau, Utah; ME, north of Mount Escalante, Utah; N, Newcastle area, Utah; O, Oak Spring Summit–Grey Dome area, Nevada; OV, Ox Valley, Utah; P, South Pahroc Range, Nevada; PE, east of South Pahroc Range, Nevada; R, Red Hills, Utah; S, Stine area, Nevada; ST, west of Stampede Gap, northern Highland Range, Nevada.

Sample No.	Loc.	Quartz	Sanidine	Plagioclase	Biotite	Hornblende	Pyroxene	Fe-Ti Oxides	Olivine	Alt. Ferr.	Sphene	Total Pheno.	Q-S-P ratio	VRFs	Pum.	G'mass
Leach Canyon Formation, Narrows Tuff Member																
68-8	B	4.4 (34)	2.5 (19)	5.3 (41)	0.4 (3)			0.3 (2)				12.9	36-21-43	0.8		86.3
68-32	B	6.5 (38)	4.9 (28)	4.6 (27)	1.0 (6)	T	T	0.3 (2)				17.3	40-31-29	3.0		79.7
68-33	B	9.4 (36)	7.1 (27)	8.7 (33)	0.6 (2)	T		0.2 (1)				26	37-28-35	1.2		72.8
68-61	B	8.3 (32)	8.7 (33)	8.2 (31)	0.7 (3)	0.1 (T)		0.2 (1)				26.2	33-34-33	0.2		73.6
68-74	BL	3.0 (19)	4.6 (30)	6.7 (43)	0.4 (3)	0.3 (2)	0.2 (1)	0.3 (2)				15.5	21-32-47	0.4		84.1
68-182	I	8.0 (30)	8.8 (33)	8.0 (30)	0.7 (3)	0.7 (3)		0.5 (2)				26.7	32-36-32	1.6		71.7
68-184	M	3.2 (17)	6.4 (34)	8.1 (43)	0.4 (2)	0.4 (2)		0.2 (1)				18.7	18-36-46	1.0		80.3
68-186	M	6.8 (38)	4.7 (26)	4.5 (25)	1.2 (7)	0.2 (1)		0.4 (2)				17.8	43-29-28	0.4		81.8
71-3	I	10.9 (46)	6.2 (26)	6.0 (25)	0.3 (1)			0.2 (1)				23.6	47-27-26	1.3		75.1
71-70	I	1.8 (12)	3.3 (22)	8.7 (57)	0.7 (5)	0.1 (1)		0.6 (4)				15.2	13-24-63	6.1		78.7
71-123	B	5.9 (34)	5.9 (34)	4.3 (25)	1.0 (6)	0.2 (1)		0.2 (1)				17.5	37-37-26	0.9		81.6
71-124	B	4.6 (27)	6.0 (35)	5.4 (32)	0.6 (4)	0.1 (1)		0.4 (2)				17.1	29-37-34	1.4		81.5
71-221	I	7.0 (42)	4.4 (27)	4.2 (25)	0.7 (4)	0.1 (1)		0.2 (1)			T	16.6	45-28-27	2.4		81.0
72-179	BL	2.5 (22)	2.4 (21)	4.4 (39)	1.4 (12)	0.1 (1)	T	0.5 (4)				11.3	27-26-47	4.2		84.5
87-852b*	C	5.2 (28)	8.2 (44)	4.5 (24)	0.4 (2)	0.1 (1)		0.2 (2)			T	18.6	29-46-25	4.3	1.8	75.3
Leach Canyon Formation, Table Butte Tuff Member																
68-56	BL	6.7 (39)	4.4 (25)	5.1 (29)	0.6 (3)	0.2 (1)		0.3 (2)				17.3	41-27-32	10.0		72.7
68-92	BL	6.0 (30)	5.5 (27)	7.4 (37)	0.6 (3)	0.3 (1)	0.1 (T)	0.3 (1)				20.1	32-29-39	3.1		76.7
68-181	I	1.0 (7)	1.8 (12)	9.0 (60)	1.1 (7)	0.9 (6)	0.1 (1)	1.0 (7)				14.9	9-15-76	3.6		81.5
68-196	BL	6.0 (28)	4.9 (23)	9.3 (43)	0.7 (3)	0.3 (1)		0.4 (2)				21.6	30-24-46	3.5		74.9
68-200	R	4.2 (25)	3.3 (19)	8.2 (48)	0.6 (4)	0.2 (1)	T	0.5 (3)				17	27-21-52	4.5		78.5
71-7	I	2.5 (27)	2.6 (28)	2.7 (29)	0.8 (9)	0.3 (3)		0.4 (4)				9.3	32-33-35	3.6		87.1
71-46	I	1.7 (9)	2.7 (15)	12.0 (65)	1.0 (5)	0.4 (2)		0.6 (3)				18.4	10-17-73	4.4		77.2
71-128	B	2.2 (14)	4.4 (29)	6.9 (45)	1.5 (10)	0.2 (1)		0.2 (1)				15.4	16-33-51	3.2		81.4
71-223	I	4.0 (22)	4.1 (23)	7.6 (43)	1.4 (8)	0.5 (3)		0.2 (1)				17.8	26-26-48	3.4		78.8
71-224	I	2.0 (13)	2.8 (18)	8.7 (55)	1.1 (7)	0.6 (4)	T	0.5 (3)				15.7	15-21-64	4.7		79.6
72-37	I	2.2 (15)	0.9 (6)	9.7 (67)	1.1 (8)	0.3 (2)		0.2 (1)				14.4	17-7-76	4.6		81.0
72-182	BL	3.1 (23)	0.9 (7)	7.5 (56)	1.2 (9)	0.5 (4)	T	0.3 (2)				13.5	27-8-65	6.3		80.2
72-199	R	3.8 (25)	3.0 (19)	7.0 (45)	1.1 (7)	0.2 (1)		0.3 (2)				15.4	27-22-51	15.3		69.3
87-851*	C	5.4 (31)	3.8 (22)	7.4 (43)	0.6 (3)			0.2 (1)			T	17.4	33-23-45	3.3	7.3	72.0

Sample No.	Loc.	Quartz	Sanidine	Plagioclase	Biotite	Hornblende	Pyroxene	Fe-Ti Oxides	Olivine	Alt. Ferr.	Sphene	Total Pheno.	Q-S-P ratio	VRFs	Pum.	G'mass
Leach Canyon Formation, undifferentiated as to member																
86-405	H	5.4 (25)	4.6 (21)	7.7 (36)	2.9 (14)			0.5 (2)		0.3 (1)		21.4	31-26-43	1.5		77.1
88-654*	H	6.0 (47)	3.3 (26)	2.9 (23)	0.4 (3)	0.1 (1)		0.1 (1)			T	12.8	49-27-24	5.8	4.9	76.5
91-67b	CC	6.9 (34)	6.7 (33)	4.2 (21)	0.6 (3)	0.5 (2)	0.2 (1)	1.3 (6)				20.4	39-38-23	2.6		77.0
Condor Canyon Formation, Swett Tuff Member																
68-82	B			7.7 (88)	0.8 (9)		T	0.3 (3)				8.8	0-0-100	0.6		90.6
71-47	I			5.2 (81)	0.2 (3)	0.7 (11)		0.3 (5)				6.4	0-0-100	0.7		92.9
71-48	I			7.6 (85)	1.1 (12)			0.2 (2)				8.9	0-0-100	0.7	6.2	84.2
71-71	I			10.7 (82)	1.7 (13)	T		0.6 (5)				13	0-0-100	0.3		86.7
71-72	I			7.5 (82)	1.5 (16)			0.1 (1)				9.1	0-0-100	0.7	2.4	87.8
71-74	I			6.6 (88)	0.9 (12)			Tr				7.5	0-0-100	0.1	2.2	90.2
71-75	I			7.6 (84)	1.0 (11)	T	T	0.4 (4)				9	0-0-100	0.4		90.6
71-132	B	T		5.4 (82)	0.9 (14)			0.3 (5)				6.6	0-0-100	T		93.4
71-133	B			8.0 (88)	0.7 (8)			0.4 (4)				9.1	0-0-100	T		90.9
71-135	B			6.0 (72)	1.7 (20)			0.6 (7)				8.3	0-0-100	0.7		91.0
71-136	B	T		6.8 (88)	0.6 (8)			0.3 (4)				7.7	0-0-100	0.4		91.9
71-153	B			4.5 (79)	1.0 (18)	T		0.2 (4)				5.7	0-0-100	0.5		93.8
71-154	B	T		6.8 (85)	0.9 (11)			0.3 (4)				8	0-0-100	0.2		91.8
71-156	B	T		7.4 (83)	1.1 (12)			0.4 (4)				8.9	0-0-100	0.2		90.9
72-24	I			5.0 (82)	0.9 (15)		T	0.2 (3)				6.1	0-0-100	0.4		93.5
72-27	I	T		5.4 (81)	1.0 (15)			0.3 (5)				6.7	0-0-100	0.3	8.0	85.0
72-180	BL			5.4 (87)	0.7 (11)			0.1 (2)				6.2	0-0-100	1.1		92.7
87-452a*	CC	T		9.5 (88)	1.0 (9)			0.3 (3)				10.8	0-0-100	0.6	1.5	87.1
87-452d*	CC			6.0 (80)	1.1 (15)			0.4 (5)		T		7.5	0-0-100	1.1	11.6	79.8
87-844a	C		T?	9.6 (85)	1.3 (12)			0.4 (4)				11.3	0-0-100	0.4	1.0	87.3
89-1103f*	D		T?	8.1 (84)	1.1 (11)			0.4 (4)				9.6	0-0-100	T		90.3
89-1103h	D			6.6 (86)	0.9 (12)			0.2 (3)				7.7	0-0-100	2.4		89.9
90-339	C		T?	8.3 (86)	1.2 (12)	T		0.2 (2)				9.7	0-0-100	0.9	3.8	85.6
90-400c	C			5.9 (87)	0.8 (12)			0.1 (1)				6.8	0-0-100	0.8	0.4	92.0

Sample No.	Loc.	Quartz	Sanidine	Plagioclase	Biotite	Hornblende	Pyroxene	Fe-Ti Oxides	Olivine	Alt. Ferr.	Sphene	Total Pheno.	Q-S-P ratio	VRFs	Pum.	G'mass
Condor Canyon Formation, Bauers Tuff Member																
68-67	BL		2.7 (27)	5.2 (53)	0.9 (9)		0.3 (3)	0.8 (8)				9.9	0-34-66	0.4		89.7
68-68	BL		4.5 (35)	6.8 (54)	0.8 (6)		0.3 (2)	0.3 (2)				12.7	0-40-60	0.2		87.1
68-69	BL		6.3 (46)	6.2 (46)	0.6 (4)		0.1 (1)	0.4 (3)				13.6	0-50-50	0.5		85.9
68-80	BL		5.1 (30)	9.5 (57)	1.7 (10)		0.2 (1)	0.3 (2)				16.8	0-35-65	0.4		82.8
69-88	BL		2.7 (32)	4.7 (56)	0.6 (7)		0.1 (1)	0.3 (4)				8.4	0-36-64			91.6
69-38	BL		4.1 (26)	9.8 (63)	1.3 (8)			0.3 (2)				15.5	0-29-71	0.2		84.3
71-9	I		7.1 (35)	11.7 (58)	1.0 (5)			0.3 (1)				20.1	0-38-62	2.1		77.8
71-51	I		9.2 (48)	8.7 (45)	0.7 (4)		0.2 (1)	0.4 (2)				19.2	0-51-49	0.2		80.6
71-52	I		6.2 (47)	5.6 (42)	0.9 (7)		0.2 (2)	0.4 (3)				13.3	0-53-47	2.2		84.5
71-54	I		7.3 (33)	12.6 (58)	1.2 (6)		0.3 (1)	0.4 (2)				21.8	0-37-63	0.2		78.0
71-76	I		10.3 (50)	8.7 (42)	1.2 (6)		0.1 (T)	0.3 (1)				20.6	0-54-46	1.1		78.3
71-157	B		7.7 (41)	9.5 (51)	1.1 (6)		0.2 (1)	0.3 (2)				18.8	0-45-55	1.2		80.0
71-158	B		7.5 (35)	12.5 (59)	1.0 (5)			0.3 (1)				21.3	0-38-62	0.2		78.5
71-204	BL		3.8 (37)	5.1 (50)	0.9 (9)		0.1 (1)	0.3 (3)				10.2	0-43-57	0.8		89.0
73-115	I		7.7 (37)	12.3 (59)	0.4 (2)		0.1 (T)	0.3 (1)				20.8	0-39-61			79.2
73-118	I		6.6 (48)	6.2 (45)	0.6 (4)		0.1 (1)	0.2 (1)				13.7	0-52-48	0.2		86.1
87-172a	N		6.0 (31)	11.9 (61)	0.8 (4)		0.3 (2)	0.5 (3)				19.5	0-34-66	0.3		80.2
87-452e*	CC		5.6 (36)	8.4 (54)	1.2 (8)		0.1 (1)	0.3 (2)				15.6	0-40-60	2.5	5.6	76.3
87-452h*	CC		5.2 (36)	8.0 (56)	0.8 (6)	T	0.1 (1)	0.2 (1)				14.3	0-39-61	0.5	4.9	80.3
89-1103L*	D		5.3 (29)	12.3 (68)	0.3 (2)		0.1 (1)	0.2 (1)				18.2	0-30-70	T		81.8
Harmony Hills Tuff																
71-65	I	1.6 (3)		34.4 (67)	6.2 (12)	6.2 (12)	2.6 (5)	0.4 (1)				51.4	4-0-96	0.8		47.8
71-68	I	1.9 (4)		35.1 (71)	6.2 (13)	3.4 (7)	1.4 (3)	1.4 (3)				49.4	5-0-94			50.6
71-69	I	2.5 (5)		35.5 (70)	6.0 (12)	3.2 (6)	2.2 (4)	1.2 (2)				50.6	7-0-93			49.4
72-39	I	0.8 (2)	0.2 (T)	30.6 (67)	7.6 (17)	4.2 (9)	1.4 (3)	1.2 (3)				46	3-1-96			54.0
72-40	I	1.4 (3)		28.8 (60)	9.2 (19)	4.8 (10)	3.2 (7)	0.8 (2)				48.2	5-0-95			51.8
72-41	I	4.3 (8)	0.2 (T)	34.9 (65)	8.2 (15)	3.6 (7)	1.8 (3)	0.6 (1)				53.6	11-1-89			46.4
72-43	I	3.1 (7)	0.6 (1)	30.5 (67)	7.0 (15)	1.8 (4)	1.4 (3)	0.8 (2)				45.2	9-2-89			54.8
72-198	R	1.2 (3)	T	26.2 (63)	6.0 (14)	5.2 (13)	2.0 (5)	1.0 (2)				41.6	4-0-96			58.4
73-105	A	1.6 (3)		35.6 (62)	10.6 (18)	4.6 (8)	3.4 (6)	2.0 (3)				57.8	4-0-96			42.2
73-107	A	2.5 (4)		36.7 (65)	8.2 (14)	5.4 (10)	2.0 (4)	1.8 (3)				56.6	6-0-94			43.4
73-109	A	2.8 (5)	0.2 (T)	34.6 (66)	7.4 (14)	3.8 (7)	2.2 (4)	1.8 (3)				52.8	7-1-92			47.2
73-111	A	4.5 (10)	0.2 (T)	31.7 (69)	5.2 (11)	2.8 (6)	1.0 (2)	0.6 (1)				46	12-1-87			54.0
73-112	A	6.1 (11)		35.7 (62)	8.2 (14)	4.6 (8)	2.0 (3)	0.6 (1)				57.2	15-0-85			42.8
73-113	A	3.8 (8)	0.2 (T)	33.4 (67)	5.2 (10)	3.0 (6)	2.8 (6)	1.6 (3)				50	10-1-89			50.0
87-142	N	1.2 (5)	T	12.8 (55)	2.2 (9)	5.6 (24)	1.0 (4)	0.6 (3)				23.4	9-0-91			76.6
87-500	S	2.1 (5)	0.1 (T)	27.9 (66)	8.3 (20)	2.2 (5)	0.9 (2)	0.8 (2)				42.3	7-0-93	0.4	6.7	50.6
87-501c	S	5.1 (13)	0.5 (1)	23.9 (62)	6.2 (16)	1.7 (4)	0.4 (1)	1.0 (3)				38.8	17-2-81	0.8	12.9	47.5
87-1182h*	CA	2.5 (5)	0.1 (T)	29.0 (64)	6.4 (14)	3.0 (7)	3.1 (7)	1.5 (3)				45.6	8-0-92	2.3	5.1	47.0
88-691	H	0.6 (3)	0.3 (1)	16.2 (70)	2.5 (11)	2.3 (10)	0.8 (3)	0.5 (2)				23.1	11-3-86	0.6	3.5	72.8
88-1143	C	2.6 (11)	0.6 (3)	11.3 (48)	5.3 (23)	1.6 (7)	1.0 (4)	1.1 (4)				49.1	6-1-93	0.9	0.9	49.1
89-558*	CA	1.6 (7)	0.4 (2)	12.8 (55)	4.1 (18)	1.9 (8)	1.8 (8)	0.5 (2)				23.2	3-2-95	9.8	19.1	47.9
89-560	CA	2.1 (4)	0.2 (T)	32.6 (66)	6.7 (14)	3.5 (7)	3.6 (7)	0.4 (1)				23.5	18-4-78	2.1	0.5	73.9

Sample No.	Loc.	Quartz	Sanidine	Plagioclase	Biotite	Hornblende	Pyroxene	Fe-Ti Oxides	Olivine	Alt. Ferr.	Sphene	Total Pheno.	Q-S-P ratio	VRFs	Pum.	G'mass
						Racer Canyon Tuff										
73-89	A	12.6 (37)	7.3 (21)	12.0 (35)	1.9 (6)	T?		0.4 (1)			T	34.2	39-23-38	0.1		65.7
73-90	A	12.4 (39)	7.5 (24)	8.5 (27)	1.8 (6)	0.4 (1)		0.8 (3)			T	31.4	44-26-30	0.4		68.2
73-92	A	13.9 (41)	9.7 (29)	7.2 (21)	2.3 (7)	T?		0.7 (2)				33.8	45-31-24	1.5		64.7
73-94	A	13.4 (35)	8.1 (21)	13.1 (34)	2.8 (7)	T?		0.6 (2)				38	39-23-38	0.7		61.3
73-95	A	16.0 (44)	7.9 (22)	10.1 (28)	2.1 (6)	T		0.3 (1)				36.4	47-23-30	0.8		62.8
73-96	A	16.3 (48)	7.9 (23)	8.1 (24)	1.0 (3)	T?		0.4 (1)			T	33.7	51-24-25	4.6		61.7
86-258d	K	9.0 (41)	4.3 (19)	7.4 (33)	1.0 (5)	0.5 (2)		T			T	22.2	43-21-36	4.3	18.9	54.6
86-258f	K	6.0 (40)	3.1 (21)	4.1 (28)	1.3 (9)	0.2 (1)	T	0.2 (1)			T	14.9	45-24-31	2.4	22.1	60.6
86-258h	K	11.7 (52)	4.9 (22)	4.3 (19)	0.9 (5)	0.4 (2)		0.4 (2)			T	22.6	56-23-21	2.1	23.8	51.5
86-258j	K	15.8 (46)	7.4 (22)	8.3 (24)	1.7 (5)	0.6 (2)		0.5 (2)			T	34.3	50-24-26	0.5	17.7	47.5
86-258m	K	11.6 (45)	5.3 (20)	6.8 (26)	1.2 (5)	0.7 (3)		0.4 (2)			T	26	49-22-29	3.0	12.0	59.0
87-26-17	N	10.1 (33)	6.3 (21)	10.3 (34)	3.1 (10)	0.4 (1)		0.2 (1)			T	30.4	38-24-38	1.0	2.0	66.6
87-26-18	N	12.5 (32)	4.8 (12)	16.5 (43)	3.1 (8)	T		1.6 (4)			T	38.5	37-14-49	2.0	1.5	58.0
87-26-19	N	6.4 (25)	4.5 (18)	11.7 (46)	2.0 (8)	0.3 (1)		0.5 (2)		T	T?	25.4	28-20-52	1.0	3.0	70.6
87-1e*	N	9.8 (36)	6.0 (22)	9.6 (36)	1.0 (4)	0.2 (1)	T	0.4 (1)			T	27	38-24-38	1.5	9.2	62.3
87-1f	N	10.5 (35)	4.3 (14)	12.3 (41)	1.3 (4)	0.4 (1)	0.2 (1)	0.5 (2)			0.2 (1)	29.7	39-16-45	1.7	14.0	54.6
87-1g*	N	13.3 (37)	6.8 (19)	13.3 (37)	1.5 (4)	0.6 (2)	T	0.3 (1)			T	35.8	40-20-40	1.3	T	62.9
87-21b	N	10.1 (43)	7.3 (31)	4.7 (20)	0.6 (3)	0.1 (T)	T	0.5 (2)			T?	23.3	46-33-21	3.0	5.0	68.7
87-697a*	E	10.6 (40)	11.8 (44)	3.9 (15)	0.2 (1)			0.2 (1)				26.7	40-45-15	3.0	15.9	54.4
87-697d	E	10.4 (41)	9.4 (37)	4.5 (18)	0.7 (3)			0.4 (2)			T	25.4	43-39-19	2.7	7.3	64.6
87-697f	E	14.4 (49)	8.2 (28)	5.1 (17)	0.9 (3)			0.6 (2)				29.2	52-30-18	4.4	26.0	40.4
87-697k	E	12.9 (41)	7.3 (23)	8.7 (27)	1.9 (5)	0.2 (1)		0.7 (2)			T	31.7	45-25-30	1.0	7.7	59.6
87-697p*	E	12.1 (35)	9.3 (27)	10.0 (29)	2.6 (7)	0.2 (1)		0.5 (1)			T	34.7	38-30-32	1.9	18.1	45.3
87-697s	E	9.0 (36)	5.0 (20)	8.4 (33)	1.6 (6)	0.7 (3)		0.3 (1)			0.1 (T)	25.1	40-22-38	6.1	18.7	50.1
87-697u*	E	10.4 (38)	6.4 (23)	7.6 (28)	1.9 (7)	0.8 (3)		0.4 (1)			T	27.5	43-26-31	1.7	26.1	44.7
87-697w*	E	8.1 (30)	1.3 (5)	14.0 (51)	2.9 (11)	0.3 (1)		0.6 (2)			T	27.2	35-6-59	2.4	14.8	55.6
88-659a*	H	5.2 (27)	6.0 (31)	6.0 (31)	1.6 (8)	0.1 (1)		0.3 (2)			0.1 (T)	19.3	30-35-35	4.7	20.4	55.6
88-819*	U	10.0 (28)	10.4 (29)	12.3 (34)	1.3 (4)	1.4 (4)		0.4 (1)			0.1 (T)	35.9	30-32-38	0.3	17.7	46.1
90-457*	E	7.3 (29)	1.1 (4)	14.4 (58)	2.0 (8)	T		0.2 (1)			T	25	32-5-63	1.3	16.6	57.1
ME3-21	ME	11.3 (24)	6.4 (13)	21.8 (45)	6.2 (13)	1.6 (3)		0.7 (1)			T	48	29-16-55	T		52.0
ME3-22	ME	18.8 (34)	2.8 (5)	24.2 (44)	4.9 (9)	2.8 (5)		0.9 (2)			0.2 (T)	54.6	41-6-53	0.7		44.7
ME3-23	ME	11.2 (22)	6.1 (12)	27.2 (52)	4.9 (9)	1.9 (4)		0.6 (1)			0.1 (T)	52	25-14-61	T		48.0
ME3-24	ME	9.4 (19)	4.5 (9)	29.2 (59)	4.1 (8)	1.4 (3)		0.3 (1)			0.3 (1)	49.2	22-10-68	2.5		48.3

Sample No.	Loc.	Quartz	Sanidine	Plagioclase	Biotite	Hornblende	Pyroxene	Fe-Ti Oxides	Olivine	Alt. Ferr.	Sphene	Total Pheno.	Q-S-P ratio	VRFs	Pum.	G'mass
							Hiko Tuff									
86-666a	P	7.1 (48)	3.1 (21)	3.5 (24)	0.6 (4)	T		0.4 (4)			T	14.7	52-23-25	3.6	23.0	58.7
86-666c*	P	6.9 (21)	11.2 (34)	11.0 (34)	3.0 (9)	0.2 (1)		0.4 (1)			T	32.7	24-38-38	2.6	0.1	64.6
86-666f	P	14.0 (35)	11.8 (29)	9.6 (24)	3.0 (7)	1.1 (3)		0.8 (2)			0.1	40.3	40-33-37	1.2		58.4
86-666h*	P	9.3 (25)	8.3 (22)	15.3 (41)	2.6 (7)	1.1 (3)	T	0.9 (2)			0.1	37.5	28-25-47	T		62.4
86-666i	P	5.6 (13)	9.4 (22)	22.1 (51)	3.8 (9)	1.5 (3)		0.7 (2)			0.1	43.1	15-25-60	0.4		56.4
86-666j	P	4.5 (11)	9.6 (24)	9.3 (48)	4.5 (11)	1.0 (3)		1.0 (3)			0.1	39.9	13-29-58	T	5.5	44.5
87-452m	CC	3.5 (29)	1.9 (16)	5.0 (42)	1.2 (10)	0.2 (2)		0.2 (2)			T	12.0	34-18-48	0.3	10.6	77.2
87-452n	CC	4.5 (21)	5.2 (25)	8.2 (39)	2.5 (12)	0.3 (1)		0.5 (2)			T	21.2	25-29-46	0.5	10.2	68.2
87-452o	CC	5.5 (25)	3.9 (18)	9.1 (41)	2.1 (10)	1.2 (5)		0.3 (1)			T	22.1	30-21-49	0.6	8.3	69.1
87-452p	CC	5.4 (19)	3.3 (12)	16.5 (59)	2.0 (7)	0.7 (2)		0.3 (1)			0.1	28.2	21-13-66	0.2	7.1	64.4
87-452q	CC	5.4 (19)	4.4 (15)	15.7 (55)	1.9 (7)	0.7 (2)		0.7 (2)			0.2	28.8	21-17-62	T	3.4	67.6
87-846*	C	6.2 (22)	5.3 (19)	12.7 (45)	2.6 (9)	0.6 (2)	T	0.7 (2)			T	28.1	26-22-52	T	8.9	63.0
87-847*	C	8.6 (39)	7.1 (32)	5.2 (23)	0.9 (4)	0.3 (1)	T	0.2 (1)			T	22.3	41-34-25	2.4	17.8	57.5
87-858b	C	8.1 (26)	7.2 (23)	12.1 (39)	2.1 (7)	0.7 (2)	T	0.4 (1)			0.1 (T)	30.7	30-26-44	0.8	0.9	67.6
87-858c	C	7.7 (35)	3.7 (17)	8.6 (39)	1.3 (6)	0.2 (1)		0.5 (2)			T	22	38-19-43	1.7	8.7	67.6
90-186	C	4.8 (21)	3.0 (13)	7.3 (32)	2.0 (9)	0.1 (T)	T?	0.5 (2)		0.2 (1)		22.7	32-20-48	0.6	0.6	80.9
91-208	C	4.4 (22)	4.7 (24)	9.1 (46)	0.9 (5)	0.4 (2)		0.2 (1)			0.2 (1)	19.9	24-26-50	5.2	10.1	64.8
91-463	C	7.3 (27)	6.3 (23)	12.0 (44)	1.0 (4)	0.5 (2)		0.4 (1)			T	27.5	28-25-47	1.4	13.0	58.1
91-470c	C	6.9 (26)	6.0 (22)	10.8 (40)	2.0 (7)	0.5 (2)		0.6 (2)			0.2 (1)	27	29-25-46	2.3	9.9	60.8
Hk-1	PE	4.9 (12)	6.6 (16)	19.9 (49)	7.3 (18)	0.8 (2)		0.8 (2)			0.6 (1)	40.9	16-21-63	T		59.1
Hk-2	PE	7.3 (18)	7.2 (17)	17.1 (42)	5.9 (14)	2.3 (6)		1.3 (3)			0.1 (T)	41.2	23-23-54	0.1		58.7
Hk-3	PE	7.4 (18)	3.5 (8)	22.8 (55)	6.0 (14)	1.0 (2)		0.4 (1)			0.3 (1)	41.4	22-10-68	2.0		56.6
Hk-4a	PE	4.3 (10)	3.7 (9)	26.5 (62)	4.5 (10)	2.5 (6)		1.3 (3)			0.1 (T)	42.9	12-11-77			57.1
Hk-4b	PE	4.0 (9)	3.8 (8)	29.8 (66)	4.2 (9)	2.2 (5)		0.7 (2)			0.3 (1)	45	11-10-79	0.4		54.6
Hk-5	PE	5.5 (13)	3.6 (8)	25.3 (58)	6.0 (14)	2.1 (5)		0.7 (2)			0.5 (1)	43.7	16-10-74	T		56.3
Hk-6	PE	6.9 (16)	3.8 (9)	26.5 (60)	5.3 (12)	0.9 (2)		0.5 (1)			0.3 (1)	44.2	19-10-71	T		55.8
15-7-7	G	4.3 (10)	5.6 (13)	26.6 (64)	2.3 (6)	2.0 (5)		0.9 (2)			0.1 (T)	41.8	12-15-73	0.3		57.9
1-1-48-10	G	6.1 (16)	5.8 (15)	20.2 (53)	3.1 (8)			1.1 (3)		1.5 (4)	0.2 (1)	38	19-18-63	1.4		60.6
c-216g-14	G	5.1 (14)	4.6 (13)	20.3 (57)	3.8 (11)	1.1 (3)		1.0 (3)				35.9	17-15-68			64.1
1-45-11	G	4.0 (21)	6.4 (34)	7.4 (39)	0.9 (5)	T		0.2 (1)			0.2 (1)	19.1	22-36-42	1.5		79.4
1-45-12	G	6.8 (24)	6.3 (22)	12.2 (43)	1.8 (6)	0.7 (2)		0.7 (2)			0.2 (1)	28.7	27-25-48	0.3		71.0
1-45-13	G	7.2 (23)	6.8 (22)	14.2 (45)	2.0 (6)	0.5 (2)		0.5 (2)		0.1 (T)	0.1 (T)	31.4	26-24-50	0.2		68.4
1-45-14	G	4.4 (13)	6.2 (18)	17.9 (51)	3.7 (11)	1.6 (5)		0.8 (2)			0.2 (1)	34.8	15-22-63	3.6		61.6
1-45-15	G	5.6 (12)	8.2 (18)	24.7 (54)	2.2 (5)	4.3 (9)	0.1 (T)	0.7 (2)			0.2 (T)	46	15-21-64	0.2		53.8

Sample No.	Loc.	Quartz	Sanidine	Plagioclase	Biotite	Hornblende	Pyroxene	Fe-Ti Oxides	Olivine	Alt. Ferr.	Sphene	Total Pheno.	Q-S-P ratio	VRFs	Pum.	G'mass
Tuff of Tepee Rocks																
88-30b*	EC	11.2 (48)	4.2 (18)	7.2 (31)	0.5 (2)	T		T			T	23.1	50-19-31	1.7	17.3	57.9
88-311*	EC	8.2 (42)	6.7 (34)	3.9 (20)	0.8 (4)	T					T	19.7	44-36-20	1.0	21.5	56.7
88-910*	EC	10.0 (45)	7.5 (34)	3.9 (17)	0.6 (3)	T		0.2 (1)			0.1	22.3	47-35-18	3.6	40.0	34.1
88-1268*	EC	5.3 (55)	3.2 (33)	0.9 (9)	0.1 (1)			0.1 (1)				9.8	56-34-10			90.4
89-495b*	CN	5.3 (34)	6.0 (38)	3.7 (24)	0.4 (3)			0.2 (1)			T	15.6	35-40-25	0.4	7.4	76.6
89-495c	CN	10.2 (53)	4.4 (23)	4.5 (23)	0.2 (1)	T?	T	T				19.3	53-23-24	3.8	7.9	69.0
91-599a	C	3.7 (35)	1.9 (18)	3.7 (35)	0.8 (7)	0.2 (2)	0.1 (1)	0.3 (3)				10.7	40-20-40	1.6	16.6	71.1
Tuff of Rainbow Canyon																
87-221*	ET	6.8 (67)	2.6 (25)	0.6 (6)	0.1 (1)			0.1 (1)				10.2	68-26-6	1.4	15.0	73.4
87-223*	ET	5.3 (69)	2.1 (27)	0.3 (4)	T			T				7.7	69-27-4	1.2	25.5	65.6
87-241	ET	4.9 (60)	2.6 (32)	0.5 (6)	0.1 (1)		T	0.1 (1)				8.2	61-33-6	10.9	29.4	51.5
87-1110	ET	4.6 (70)	1.8 (27)	0.2 (3)	T			T				6.6	70-27-3	5.4	29.6	58.4
87-1111	ET	2.0 (40)	2.9 (58)	0.1 (2)	T						T	5	40-58-2	0.5	19.3	75.2
87-1113*	ET	5.0 (34)	9.3 (63)	0.2 (1)	0.1 (1)			0.2 (1)				14.8	34-64-2	3.0	7.7	74.5
88-115*	EC	3.5 (38)	5.6 (60)	0.2 (2)	T			T			T	9.3	38-60-2	3.1	24.0	63.6
88-118*	EC	4.0 (64)	1.9 (30)	0.4 (6)	T			T			T	6.3	64-30-6	1.9	24.1	67.7
88-126d*	EC	3.8 (60)	1.9 (30)	0.3 (5)	0.2 (3)			0.1 (2)				6.3	63-32-5	1.9	10.5	81.4
88-164*	EC	4.5 (85)	0.8 (15)	T	T			T				5.3	85-15-0	4.4	19.6	70.7
88-220*	CA	3.1 (53)	1.9 (33)	0.5 (9)	0.1 (2)	0.1 (2)		0.1 (2)			T	5.8	56-35-9	1.8	33.3	59.1
88-224*	CA	3.9 (63)	1.5 (24)	0.6 (10)	0.1 (2)			0.1 (2)		T		6.2	65-25-10	3.6	25.1	65.1
88-225c	CA	6.5 (67)	2.6 (27)	0.3 (3)	0.1 (1)			0.2 (2)		T		9.7	69-28-3	6.3	24.7	59.3
88-226a	CA	3.9 (51)	3.1 (41)	0.3 (4)	0.2 (3)			0.1 (1)				7.6	53-43-4	8.5	18.0	65.9
88-1158b*	EC	4.4 (56)	3.0 (38)	0.2 (3)	0.2 (3)			T				7.8	58-39-3	1.3	25.0	65.9
88-1264*	CA	6.0 (48)	5.9 (48)	0.3 (2)	0.1 (1)			0.1 (1)				12.4	49-48-3	1.1	16.3	70.2
89-696c	CA	10.2 (44)	13.0 (56)	0.1 (T)			0.1 (T)	T				23.4	44-56-0	0.2	10.6	65.8
91-206	C	4.0 (49)	4.0 (49)	0.2 (2)				T				8.2	49-49-2	1.8	22.8	67.2

Sample No.	Loc.	Quartz	Sanidine	Plagioclase	Biotite	Hornblende	Pyroxene	Fe-Ti Oxides	Olivine	Alt. Ferr.	Sphene	Total Pheno.	Q-S-P ratio	VRFs	Pum.	G'mass
Tuff of Kershaw Canyon																
87-177f	CA	1.7 (53)	0.9 (28)	0.3 (9)	T	T	0.1 (4)	0.2 (7)	T?			3.2	58-29-13	0.3	3.0	93.5
87-720a	CA	3.7 (19)	12.2 (64)	1.7 (9)	0.4 (2)	0.8 (4)	0.1 (1)	0.2 (1)				19.1	21-69-10	0.3	1.8	78.8
88-70b	EC	5.3 (43)	3.7 (31)	2.7 (22)	0.1 (1)	0.1 (1)		0.2 (2)				12.1	45-32-23	1.7	17.9	68.3
88-120c*	EC	8.5 (30)	10.8 (38)	8.3 (29)	T	0.3 (1)	0.3 (1)	0.4 (1)	0.2 (1)			28.8	31-39-30	1.3	13.0	56.9
88-123*	EC	13.3 (53)	7.8 (31)	3.7 (15)	0.1 (T)	T	T	T	T			24.9	34-31-15	12.0	17.5	45.6
88-125c*	EC	5.8 (45)	3.1 (24)	3.6 (28)	0.3 (2)	T	T	0.2 (2)			T	13.0	46-25-29	4.5	21.4	61.1
88-126c*	EC	7.3 (48)	5.2 (34)	2.2 (14)	0.3 (2)	T		0.2 (1)				15.2	50-35-15	10.2	11.6	63.0
88-195a*	CA	6.0 (49)	3.6 (30)	1.9 (16)	0.1 (1)	0.2 (2)	0.1 (1)	0.2 (2)	0.1 (1)			12.2	52-31-17	0.4	16.3	71.1
88-219a	CA	3.2 (50)	1.9 (30)	0.7 (11)	0.2 (3)	T	0.1 (2)	0.3 (5)				6.4	55-38-12	2.9	1.9	88.8
88-219c	CA	13.2 (56)	5.4 (23)	3.8 (16)	0.4 (2)	0.2 (1)	T	0.4 (2)				23.4	59-24-17	6.9	3.0	66.7
88-219f*	CA	4.9 (47)	2.8 (27)	1.8 (17)	0.4 (4)	0.1 (1)	0.1 (1)	0.4 (4)				10.5	52-29-19	3.1	9.9	76.5
88-331*	EC	6.3 (44)	5.5 (38)	2.2 (15)	0.3 (2)	T		0.1 (1)				14.4	45-39-16	17.0	16.3	52.4
89-695a*	CA	5.3 (34)	7.5 (48)	2.5 (16)	0.2 (1)	T	T	0.1 (1)			T	15.6	35-49-16	2.7	11.7	70.0
89-696b*	CA	2.5 (27)	3.2 (35)	2.7 (30)	0.3 (3)	T	T	0.4 (4)			T	9.1	30-38-32	1.5	26.0	63.4
89-698a*	CA	3.9 (37)	2.4 (23)	3.4 (32)	0.1 (1)	0.1 (1)	0.1 (1)	0.5 (5)				10.5	40-25-35	7.5	5.0	77.0
89-698d*	CA	1.6 (20)	2.5 (31)	3.4 (43)	0.2 (3)	T	0.1 (1)	0.2 (3)				8	21-33-46	6.3	13.3	72.4
89-698g*	CA	1.3 (24)	2.3 (42)	1.8 (33)	0.1 (2)	T	T	T				5.5	24-43-33	1.2	20.5	72.8
89-1097a*	CA	1.1 (28)	1.4 (35)	1.1 (28)	0.1 (3)	0.1 (3)	T	0.2 (5)				4	31-39-30	0.4	32.3	63.3
89-1097d	CA	0.9 (19)	1.6 (34)	1.7 (36)	0.3 (6)	T	0.1 (2)	0.1 (2)				4.7	21-38-41	1.1	22.2	72.0
89-1097e*	CA	1.3 (20)	2.6 (39)	2.1 (32)	0.3 (5)	0.1 (2)	0.1 (2)	0.1 (2)				6.6	22-43-35	1.3	27.5	64.6
89-1097f*	CA	3.2 (25)	3.3 (26)	5.1 (40)	0.2 (2)	0.1 (1)	0.2 (2)	0.5 (4)				12.6	28-28-44	8.2	17.0	62.2
McCullough Formation																
88-1*	ST	1.6 (41)	0.8 (21)	1.3 (33)	0.2 (5)	T		T				3.9	43-22-25	0.1	1.6	94.4

Sample No.	Loc.	Quartz	Sanidine	Plagioclase	Biotite	Hornblende	Pyroxene	Fe-Ti Oxides	Olivine	Alt. Ferr.	Sphene	Total Pheno.	Q-S-P ratio	VRFs	Pum.	G'mass
Tuff of Sawmill Canyon																
87-476a	EC	1.6 (35)	3.0 (65)	T	T		T	T				4.6	35-65-0	0.7	10.7	84.0
87-479	EC	2.2 (46)	2.6 (54)	T	T		T?	T		T		4.8	46-54-0	0.1	6.3	88.8
87-547a	ET	2.2 (33)	4.1 (62)	T	T		T	0.1 (2)		0.2 (3)		6.6	35-65-0	0.2	21.6	71.6
87-553a	CA	1.9 (56)	1.5 (44)		T			T		T		3.4	56-44-0	T	15.8	80.8
87-573b	ET	1.1 (38)	1.8 (62)		T			T		T		2.9	38-62-0	0.3	16.8	80.0
87-577b	ET	1.4 (35)	2.6 (65)	T	T	T	T	T				4	35-65-0	0.3	8.1	87.6
87-578a*	EC	2.5 (39)	3.8 (59)			T	0.1 (2)	T				6.4	40-60-0	0.5	19.8	73.3
87-578d	EC	0.9 (28)	2.3 (72)		T		T	T				3.2	28-72-0	4.1	9.3	83.4
87-1104a	ET	1.8 (27)	4.5 (68)	T	T		0.1 (2)	0.1 (2)		0.1 (2)		6.6	29-71-0	1.7	13.3	78.4
87-1104b	ET	1.0 (32)	2.0 (65)	T	T		0.1 (3)	T				3.1	33-66-0	0.1	5.8	91.0
88-283a*	CA	2.1 (44)	2.7 (56)		T		T	T				4.8	44-56-0	0.8	6.3	88.1
88-283b	CA	2.6 (46)	3.1 (54)		T		T	T				5.7	46-54-0	0.5	14.6	79.2
88-283c*	CA	0.9 (33)	1.7 (63)		0.1 (4)	T	T	T				2.7	35-65-0	0.3	3.8	93.2
88-1265*	CA	2.2 (32)	4.4 (65)				0.1 (1)	0.1 (1)		T		6.8	33-66-0	0.8	10.8	81.6
Delamar Lake Tuff																
90-801a*	PE	2.9 (28)	6.6 (68)	0.2 (2)	T		0.5 (5)	0.1 (1)	0.2 (2)	T		10.5	30-68-2		3.8	85.7
90-801b	PE	2.3 (30)	4.9 (64)	0.1 (1)	T	T	0.1 (1)	T	0.2 (3)			7.6	32-67-1	0.8	4.1	87.5
90-881a	PE	4.8 (43)	6.0 (54)	0.2 (2)	T	T	0.1 (1)	T	0.1 (1)			11.2	44-54-2	2.1	5.5	81.2
90-885	PE	7.7 (39)	11.4 (58)	0.2 (1)	T		0.1 (1)	T	0.1 (1)	T		19.5	40-59-1	4.8	0.5	75.2
Kane Wash Tuff, Gregerson Basin Member, lower unit																
87-177a	CA	2.1 (40)	2.9 (56)		T		0.2 (4)	T	T			5.2	42-58-0	0.4	1.0	93.4
87-331	CA	1.5 (38)	1.9 (48)	T			0.3 (8)	0.1 (3)	0.2 (5)			4	44-56-0	1.0	22.4	72.6
87-332	CA	1.0 (20)	3.8 (75)				0.2 (4)	0.1 (2)	T			5.1	21-79-0	0.3	1.5	93.1
87-437K	EC	0.5 (13)	2.8 (72)				0.4 (10)	T	0.2 (5)			3.9	15-85-0	0.7	1.0	94.4
87-437L	EC	2.3 (43)	2.4 (45)				0.5 (9)	0.1 (2)	T			5.3	49-51-0	0.2	5.1	89.4
87-456a	CA	2.2 (24)	6.6 (73)				0.2 (2)	T	0.1 (1)			9.1	25-75-0	0.5	3.2	87.3
87-456c	CA	1.3 (20)	4.4 (68)				0.6 (9)	0.1 (2)	0.1 (2)			6.5	23-77-0	0.4	2.6	90.5
87-467a	CA	1.2 (26)	3.0 (65)	T			0.2 (4)	0.1 (2)	T	0.1 (2)		4.6	29-71-0	1.1	3.4	90.9
87-547b	ET	1.3 (19)	5.1 (76)	T			0.2 (3)	T	0.1 (1)			6.7	20-80-0	2.2	3.5	87.6
87-556a	CA	1.6 (52)	1.4 (45)				0.1 (3)	T	T			3.1	53-47-0	0.2	14.1	82.6
87-556b	CA	0.5 (15)	2.7 (79)				0.2 (6)	T	T			3.4	16-84-0	0.9	4.0	91.7
87-557a	CA	1.1 (20)	3.8 (70)				0.5 (9)	T	T			5.4	22-78-0	0.3	2.5	91.8
88-1157b*	EC	3.2 (34)	5.7 (60)				0.4 (4)	T	0.2 (2)			9.5	36-64-0	0.3	2.9	87.3
87-578f	EC	3.2 (23)	10.1 (71)			T	0.5 (4)	T	0.4 (3)			14.2	24-76-0	0.1	2.2	83.5
87-669a	CA	3.2 (35)	5.7 (62)				0.1 (1)	0.1 (1)	0.1 (1)			9.2	36-64-0	0.1	4.5	86.2
87-1104c	ET	1.5 (38)	1.8 (46)					0.2 (5)		0.4 (10)		3.9	45-55-0	0.1	9.7	89.3
87-1104d	ET	1.2 (41)	1.5 (52)					T	T	0.2 (7)		2.9	44-56-0	0.3	7.6	89.2
88-85b	EC	1.6 (21)	5.1 (65)	T		T	0.5 (6)	0.1 (1)	0.5 (6)			7.8	24-76-0	0.1	1.6	90.5
88-125a*	EC	1.9 (37)	2.9 (56)				0.1 (2)	0.1 (2)	0.2 (4)			5.2	40-60-0	0.2	2.4	92.2
88-218a	CA	2.7 (25)	7.7 (72)				0.1 (1)	0.1 (1)	0.1 (1)			10.7	26-74-0	1.4	2.1	85.8
88-341c	EC	1.8 (20)	6.9 (78)				T	0.1 (1)	0.1 (1)			9.9	21-79-0	0.2	2.2	93.7

Sample No.	Loc.	Quartz	Sanidine	Plagioclase	Biotite	Hornblende	Pyroxene	Fe-Ti Oxides	Olivine	Alt. Ferr.	Sphene	Total Pheno.	Q-S-P ratio	VRFs	Pum.	G'mass
Kane Wash Tuff, Gregerson Basin Member, upper unit																
87-177c	EC	2.2 (44)	2.7 (54)			T	0.1 (2)	T	T			5	45-55-0	0.2	3.3	91.5
87-177d	EC	1.9 (35)	3.3 (61)	T	T	T	0.1 (2)	T	0.1 (2)		T?	5.4	37-63-0	0.4	2.0	92.2
87-437m	EC	2.0 (26)	5.5 (71)	T		T	0.2 (3)	T	T			7.7	27-73-0	T	0.5	91.8
87-437o	EC	1.3 (38)	1.3 (38)			T	0.2 (6)	T	T	0.6 (18)		3.4	50-50-0	1.9	13.9	80.8
87-458a	CA	3.6 (36)	6.4 (63)				0.1 (1)	T	T			10.1	36-64-0	0.3	0.7	88.9
87-553c	CA	0.8 (16)	3.8 (78)				T	0.1 (2)	T	0.2 (4)		4.9	17-83-0	1.7	3.6	89.8
88-1157a*	EC	5.9 (47)	6.3 (50)	T		T	0.3 (2)	T	0.1 (1)			12.6	48-52-0	0.4	5.5	81.5
87-578h	EC	3.9 (65)	1.6 (28)	T			0.2 (3)	T	0.3 (5)			6.0	71-29-0	0.7	9.5	83.8
87-669c	CA	3.3 (39)	4.8 (56)		T		0.3 (4)	T	0.1 (1)			8.5	41-59-0	0.5	3.0	88.0
87-1105a	ET	1.4 (21)	4.7 (70)				0.3 (4)	0.1 (1)	0.2 (3)			6.7	23-77-0	0.3	1.2	91.8
87-1105b	ET	1.4 (16)	5.9 (69)		T		0.5 (6)	0.1 (1)		0.6 (7)		8.5	19-81-0	0.7	2.2	88.6
87-1105c*	ET	2.7 (38)	3.9 (54)				0.4 (6)	T	0.2 (3)			7.2	41-59-0	3.4	1.5	87.9
87-1105d	ET	2.6 (43)	3.0 (50)				0.1 (2)	T	T	0.3 (5)		6	46-54-0	0.6	1.6	91.8
88-124*	EC	2.0 (32)	4.1 (65)				0.2 (3)	T	T			6.3	33-67-0	0.6	4.9	88.2
88-197	CA	1.8 (41)	2.0 (45)		T		0.2 (5)	0.1 (2)	0.1 (2)	0.2 (5)		4.4	47-53-0	1.4	5.9	88.3

Sample No.	Loc.	Quartz	Sanidine	Plagioclase	Biotite	Hornblende	Pyroxene	Fe-Ti Oxides	Olivine	Alt. Ferr.	Sphene	Total Pheno.	Q-S-P ratio	VRFs	Pum.	G'mass
							Tuff of Etna									
88-667	IB	11.8 (28)	29.2 (69)	0.2 (T)		T	T	0.3 (1)		1.1 (3)		42.6	29-71-0	T	4.0	53.4
87-177b*	CA	0.7 (13)	4.2 (76)	0.1 (2)		0.1 (2)	0.2 (4)	0.1 (2)	T	0.1 (2)		5.5	14-84-2	4.1	3.1	87.3
87-177d	CA	3.0 (14)	17.0 (81)	0.1 (T)		0.1 (T)	0.1 (T)	0.3 (1)		0.5 (2)		21.1	15-85-0	1.1	7.9	69.9
87-177f*	CA	6.3 (30)	13.6 (65)	T			0.1 (T)	0.2 (1)	T	0.8 (4)		21	32-68-0	0.3	3.3	75.4
87-177h*	CA	3.2 (21)	11.5 (75)	0.1 (1)				0.2 (1)	T	0.3 (2)		15.3	22-78-1	0.2	2.0	82.5
87-177i	CA	3.2 (18)	13.4 (77)	0.2 (1)			0.1 (1)	0.1 (1)		0.3 (2)		17.3	19-80-1	0.2	1.8	80.7
87-177j*	CA	1.1 (9)	10.5 (86)	0.1 (1)				0.1 (1)	T	0.4 (3)		12.2	9-90-1	0.2	3.1	84.5
87-177k	CA	1.3 (15)	6.8 (81)	T				0.1 (1)	T	0.2 (2)		8.4	16-84-0	T	2.8	88.8
87-178a	CA	0.9 (18)	3.5 (70)	T	T	0.1 (2)	T	0.2 (4)		0.3 (6)		5	20-80-0	0.8	2.9	91.3
87-178e	CA	2.3 (19)	9.2 (76)	T			0.1 (1)	0.1 (1)		0.4 (3)		12.1	20-80-0	T	1.6	86.3
87-184	CA	2.5 (16)	12.5 (81)	T			T	0.1 (1)	T	0.3 (2)		15.4	17-83-0	T	2.0	82.6
87-267	EL	5.6 (24)	16.9 (71)	0.6 (3)	T			0.1 (T)		0.6 (3)		23.8	24-73-3	T	23.4	52.8
87-304a	CA	1.8 (20)	6.4 (70)	T		0.4 (4)	T	0.2 (2)	T	0.3 (3)		9.1	22-78-0	0.6	6.0	84.3
87-304b	CA	3.2 (18)	12.7 (73)	0.1 (1)		0.7 (4)	0.2 (1)	0.5 (3)	0.1 (1)			17.5	20-79-1	0.9	6.8	74.8
87-329a	CA	4.7 (39)	6.9 (58)	T	T	0.1 (1)	T	0.1 (1)		0.1 (1)		11.9	41-59-0	1.3	6.2	80.6
87-329b	CA	1.2 (41)	1.5 (52)	T		T	0.1 (3)	T	0.1 (3)			2.9	44-56-0	1.0	1.3	94.8
87-425	ET	1.7 (37)	2.9 (63)	T	T			T				4.6	37-63-0	0.2	5.5	89.7
87-467d	CA	3.8 (18)	16.4 (80)	0.2 (1)	T	0.2 (1)	T	T	T			20.6	19-80-1	2.7	17.3	59.4
87-467e	CA	5.3 (34)	9.8 (62)	0.2 (1)		0.1 (1)	T	0.3 (2)	T			15.7	35-64-1	0.9	16.8	66.6
87-527	S	1.7 (29)	3.9 (67)	T			0.2 (3)	T	T	T		5.8	30-70-0	1.7	4.1	88.4
87-545a	ET	2.3 (12)	16.7 (84)	0.2 (1)			T	0.3 (2)		0.3 (2)		19.8	12-87-1	0.1	33.9	46.2
87-545b	ET	2.2 (14)	13.2 (85)	T		T	T?	T	T?	0.1 (1)		15.5	14-86-0	1.5	3.8	79.2
87-557b	CA	7.2 (24)	22.0 (72)	0.3 (1)		0.3 (1)	0.1 (T)	0.2 (1)		0.4 (1)		30.5	24-75-1	3.0	8.5	58.0
87-570a	ET	6.3 (27)	15.3 (66)	0.3 (1)	T	0.4 (2)	0.1 (T)	0.2 (1)	0.1 (T)	0.4 (2)		23.1	29-70-1	0.1	11.5	65.3
87-570b	ET	7.4 (27)	18.6 (68)	0.1 (T)		0.3 (1)	0.2 (1)	0.2 (1)	0.2 (1)	0.3 (1)		27.3	28-71-1	0.8	5.8	66.1
87-570d	ET	4.2 (29)	9.8 (67)	T				0.2 (1)		0.4 (3)		14.6	30-70-0	0.3	6.2	78.9
87-580b	EC	2.7 (30)	5.7 (63)			T	0.3 (3)	T	0.3 (3)			9	32-68-0	T	3.3	87.7
87-580c	EC	1.5 (26)	3.3 (57)	T		0.3 (5)	0.2 (3)	T	0.5 (9)			5.8	31-69-0	0.6	1.6	92.0
87-581a	EC	1.9 (27)	5.0 (68)	T	0.1 (1)	0.1 (1)	T	T	0.1 (1)	0.2 (3)		7.4	28-72-0	0.3	3.8	88.5
87-581c	EC	1.9 (24)	5.8 (73)	T	T	0.1 (1)		T	T	0.2 (3)		8	25-75-0			92.0
87-720b	CA	1.5 (15)	7.6 (76)	0.2 (2)	0.1 (1)	0.1 (1)	0.1 (1)	0.1 (1)		0.3 (3)		10	16-82-2	1.4	4.2	84.4
87-856c*	C	2.5 (21)	8.0 (68)	0.2 (2)		0.3 (3)	0.1 (1)	0.2 (2)	T	0.5 (4)		11.8	23-75-2	T	1.5	86.7
87-1268	EC	8.1 (27)	20.8 (69)	0.2 (1)		0.5 (2)	T	0.4 (1)		0.3 (1)		30.3	28-71-1	0.3	1.2	68.2
88-121b	EC	1.9 (18)	7.6 (72)	0.1 (1)	T	0.3 (3)		0.2 (2)	0.1 (1)	0.4 (4)		10.6	20-79-1	1.1	1.8	86.5
88-121d	EC	13.0 (36)	21.6 (60)	T	T	T		0.3 (1)	0.1 (T)	1.2 (3)		36.2	38-62-0	0.1	1.3	62.4
88-1209*	O	4.2 (43)	5.3 (55)	T	T		0.1 (1)	T	0.1 (1)			9.7	44-56-0	1.8	5.9	82.6
89-1099*	CA	3.9 (14)	23.4 (81)	0.1 (T)		0.4 (1)	T	0.2 (1)	T	0.8 (3)		28.8	14-85-1	0.1	1.2	69.9
90-31a*	S	6.8 (23)	21.2 (73)	0.2 (1)		0.1 (T)		0.1 (T)	0.1 (T)	0.7 (2)		29.2	24-75-1	1.9	2.8	66.1
90-41a*	S	5.2 (24)	15.1 (71)	0.2 (1)		0.6 (3)		0.1 (T)	T	0.1 (T)		21.3	25-74-1	0.3	1.4	77.0

Sample No.	Loc.	Quartz	Sanidine	Plagioclase	Biotite	Hornblende	Pyroxene	Fe-Ti Oxides	Olivine	Alt. Ferr.	Sphene	Total Pheno.	Q-S-P ratio	VRFs	Pum.	G'mass
							Ox Valley Tuff									
87-697y*	E	9.4 (27)	21.6 (62)	1.3 (4)	0.3 (1)	0.8 (2)	0.4 (1)	1.0 (3)	T?		T?	34.8	29-67-4	0.6	6.1	58.5
87-697z*	E	8.2 (22)	23.8 (64)	2.0 (5)	0.9 (2)	1.0 (3)	0.5 (1)	0.4 (1)	T?	0.3 (1)	T	37.1	24-70-6	3.0	3.4	56.5
87-697aa	E	10.0 (25)	26.3 (67)	1.4 (4)	0.3 (1)	0.5 (1)	0.5 (1)	0.3 (1)	T?	0.1 (T)	T	39.4	27-70-4	1.0	2.2	57.4
87-697bb*	E	14.0 (38)	19.7 (53)	1.1 (3)	0.3 (1)	0.6 (2)	0.3 (1)	1.0 (3)	T?	0.3 (1)	T	37.3	40-57-3	1.1	3.6	58.0
89-672*	OV	4.3 (15)	22.9 (81)	0.6 (2)	T	0.4 (1)		T		0.1 (T)	T	28.3	15-82-2	0.5	2.6	68.6

APPENDIX 2.

Chemical analyses in parts per million (except for Fe, which is in weight percent) of selected elements, from powdered samples whose modal analyses are given in Appendix 1. Determined by energy-dispersive X-ray fluorescence techniques using a Kevex 7000 instrument.

Sample No.	Fe	Rb	Sr	Y	Zr	Nb	Ba	La	Ce	Nd
Leach Canyon Formation, Narrows Tuff Member										
87-852b	1.23	122	436	13	84	13	440	35	72	7
Leach Canyon Formation, Table Butte Tuff Member										
87-851	1.62	158	227	15	135	14	901	38	91	43
Leach Canyon Formation, undifferentiated										
88-654	1.14	163	167	17	103	12	507	44	77	13
Condor Canyon Formation, Swett Tuff Member										
87-452a	1.52	141	242	30	287	16	1,302	74	121	49
87-452d	1.60	149	243	24	287	14	1,306	69	114	46
89-1103f	1.50	69	1,030	23	269	21	1,158	62	100	41
Condor Canyon Formation, Bauers Tuff Member										
87-452e	1.39	176	258	21	260	14	1,240	74	128	50
87-452h	1.40	181	276	22	254	12	1,320	70	114	50
89-1103L	1.40	60	1,054	24	241	17	1,056	59	101	45
Harmony Hills Tuff										
87-1182h	5.53	127	849	22	152	12	727	51	79	38
89-558	4.36	132	588	17	158	11	1,028	58	92	31
Racer Canyon Tuff										
87-1e	2.04	157	343	14	136	16	726	30	79	23
87-1g	2.07	151	345	14	142	15	722	47	82	30
87-697a	1.68	179	68	66	253	35	500	72	118	58
87-697p	1.98	135	437	17	121	15	739	50	96	43
87-697u	1.73	55	756	14	95	8	1,196	39	66	35
87-697w	2.50	100	600	14	135	7	1,039	51	81	26
88-659a	2.27	126	326	22	149	19	683	64	108	35
88-819	3.02	144	570	16	164	13	1,140	64	98	50
90-457	2.74	107	671	10	135	9	1,168	73	81	50

Sample No.	Fe	Rb	Sr	Y	Zr	Nb	Ba	La	Ce	Nd
					Hiko Tuff					
86-666c	2.20	144	347	11	141	14	854	59	96	36
86-666h	2.58	127	467	17	166	16	1,197	59	97	49
87-846	2.55	137	532	20	180	15	1,216	48	84	24
87-847a	1.55	150	317	14	118	14	675	38	62	16
					tuff of Tepee Rocks					
88-30b	0.93	120	572	8	79	11	1,268	35	47	7
88-311	0.89	138	472	6	76	14	389	43	64	25
88-910	0.98	131	156	11	90	13	330	47	69	13
88-1268	0.66	205	57	6	81	20	120	37	58	16
89-495b	0.66	270	79	10	73	23	194	30	31	2
					tuff of Rainbow Canyon					
87-221	0.73	371	27	25	106	34	50	31	62	17
87-223	0.73	229	22	19.3	108	48	60	35	67	22
87-110	0.89	276	136	30	129	46	83	53	71	25
88-115	0.78	287	410	24	107	41	93	27	54	0
88-118	0.76	311	424	28	115	45	20	35	69	14
88-126d	1.02	159	542	18	117	29	206	29	79	10
88-164	0.81	371	65	19	123	43	49	40	70	14
88-220	0.81	238	46	50	128	50	73	63	64	24
88-224	0.72	297	6	29	116	44	16	42	63	11
88-1158b	0.63	214	80	22	96	37	88	24	58	4
88-1264	0.80	215	26	25	118	43	77	33	70	22
					tuff of Kershaw Canyon					
88-120c	2.86	97	681	35	223	25	1,412	61	95	20
88-123	1.74	122	618	33	186	31	619	53	87	21
88-125c	1.72	153	653	17	140	20	573	56	85	24
88-126c	1.98	145	333	19	177	18	612	52	89	24
88-195a	1.63	139	229	25	216	24	653	91	140	52
88-219f	1.70	199	135	29	206	27	570	60	103	34
88-331	1.77	136	522	20	146	20	568	46	81	14
89-695b	1.98	134	189	28	219	24	459	38	78	33
89-696b	1.93	126	190	24	221	30	575	51	104	27
89-698a	2.83	147	289	21	190	17	701	36	88	18
89-698d	2.23	173	408	32	230	24	568	57	103	39
89-698g	1.41	174	193	27	214	28	489	56	103	42
89-1097a	1.41	111	142	21	114	19	324	38	64	23
89-1097e	1.83	140	382	26	203	34	455	30	85	19
89-1097f	2.41	163	260	33	273	32	496	52	104	30

Sample No.	Fe	Rb	Sr	Y	Zr	Nb	Ba	La	Ce	Nd
					McCullough Formation					
88-1	1.29	113	941	27	140	24	427	38	109	7
					tuff of Sawmill Canyon					
87-578a	1.50	170	28	51	378	59	72	68	127	51
88-283a	1.44	220	10	42	373	57	39	65	127	34
88-283c	1.45	232	11	71	359	64	39	59	123	42
88-1265	1.24	132	94	50	304	49	43	53	110	37
					Delamar Lake Tuff					
90-801a	1.94	149	30	52	437	52	86	87	182	72
					Kane Wash Tuff, Gregerson Basin Member, lower unit					
88-1157b	2.68	263	20	94	955	102	56	131	259	104
88-125a	2.77	271	22	104	958	116	28	90	221	70
					Kane Wash Tuff, Gregerson Basin Member, upper unit					
88-1157a	2.96	272	41	81	1,109	107	90	112	236	101
87-1105c	2.07	183	37	75	771	77	77	90	161	61
88-124	3.14	300	31	148	1,299	121	21	173	281	123
					tuff of Etna					
87-177b	1.06	179	64	55	158	48	205	54	92	51
87-177f	1.47	216	40	64	239	44	310	57	114	53
87-177h	1.47	245	32	68	227	52	249	65	129	33
87-177j	1.41	246	31	67	231	51	257	67	136	48
87-856c	1.48	274	32	89	239	54	225	64	141	57
88-1209	1.79	159	28	48	430	56	74	79	149	58
89-1099	1.40	222	37	60	222	48	318	45	126	52
90-31a	1.52	196	62	71	224	44	396	57	121	51
90-41a	1.46	207	35	58	230	49	325	49	129	32
					Ox Valley Tuff					
87-697y	1.48	132	74	42	209	33	497	55	97	51
87-697z	1.52	147	80	43	223	32	542	47	108	32
87-697bb	1.95	172	94	50	274	35	623	59	134	36
89-672	1.47	215	47	66	233	46	418	56	133	42

Preliminary Geochemistry of Miocene Ash-Flow Tuffs in and near the Caliente Caldera Complex, Southeastern Nevada and Southwestern Utah

By L. David Nealey, Peter D. Rowley, Daniel M. Unruh, James R. Budahn, Lawrence W. Snee, Harald H. Mehnert, *and* R. Ernest Anderson

GEOLOGIC STUDIES IN THE BASIN AND RANGE–COLORADO PLATEAU TRANSITION IN SOUTHEASTERN NEVADA, SOUTHWESTERN UTAH, AND NORTHWESTERN ARIZONA, 1992

U.S. GEOLOGICAL SURVEY BULLETIN 2056–C

UNITED STATES GOVERNMENT PRINTING OFFICE, WASHINGTON : 1995

CONTENTS

FIGURES

TABLES

Preliminary Geochemistry of Miocene Ash-Flow Tuffs in and near the Caliente Caldera Complex, Southeastern Nevada and Southwestern Utah

By L. David Nealey, Peter D. Rowley, Daniel M. Unruh, James R. Budahn, Lawrence W. Snee, Harald H. Mehnert, *and* R. Ernest Anderson

ABSTRACT

Chemical compositions of ash-flow tuffs in and near the Caliente caldera complex, Nevada-Utah, are distinctive. Selected samples of ash-flow tuffs were analyzed by X-ray fluorescence, instrumental neutron activation, and inductively coupled plasma. The units under discussion are the Swett Tuff (23.7 Ma) and Bauers Tuff (22.8 Ma) Members of the Condor Canyon Formation, Harmony Hills Tuff (22.5–22.0 Ma), Hiko Tuff (18.6–18.2 Ma), tuff of Tepee Rocks (17.8 Ma), tuff of Rainbow Canyon (15.6–15.2 Ma), tuff of Kershaw Canyon (15.3?–14.2 Ma), Gregerson Basin Member (14.6–14.4 Ma) of the Kane Wash Tuff, tuff of Etna (14.0 Ma), and Ox Valley Tuff (12.6?–11.4? Ma). Most of these units erupted from calderas or vents within the Caliente caldera complex, but probably the Harmony Hills and certainly the Kane Wash Tuff were derived from sources outside the complex.

Ash-flow tuffs erupted from the Caliente caldera complex and other calderas in the area range in composition from high-potassium andesite to very high silica rhyolite. Most of the tuffs are calc-alkaline, with metaluminous and peraluminous affinities. In contrast, the Gregerson Basin Member of the Kane Wash Tuff is tholeiitic, with mildly peralkaline affinities. Very high silica rhyolite tuffs show evidence of alkali loss and silica and calcium gain during postemplacement alteration processes. Calc-alkaline rocks have low concentrations of Zr (<500 ppm), Nb (<60 ppm), and Y (<50 ppm) compared with the tholeiitic Gregerson Basin Member (Zr >800 ppm; Nb >80 ppm; Y >70 ppm). The Gregerson Basin Member, tuff of Etna, Ox Valley Tuff, and tuff of Tepee Rocks have low Sr contents (<100 ppm) compared with the other units, which contain more than 250 ppm Sr. The Gregerson Basin Member, tuff of Etna, tuff of Rainbow Canyon, and tuff of Tepee Rocks show low Ba contents (<200 ppm) that distinguish them from other units that contain at a minimum about 400 ppm Ba. The Gregerson Basin, tuff of Tepee Rocks, Ox Valley Tuff, and tuff of Kershaw Canyon also have low Ba/La values (≤10).

Chemical differences between the various units show up clearly in spider diagrams. In these diagrams the Harmony Hills Tuff is characterized by small negative Ba and Ti anomalies compared with large Ba and Ti anomalies in the Hiko Tuff, tuff of Etna, and the Gregerson Basin Member. Small negative Sr anomalies distinguish the Harmony Hills Tuff and tuff of Rainbow Canyon from the tuff of Etna and Gregerson Basin Member, units with strong negative Sr anomalies. Small negative Nb and Ta anomalies characterize the tuff of Etna and Gregerson Basin Member, whereas large negative Nb and Ta anomalies typify the Swett Tuff and Bauers Tuff Members, Harmony Hills Tuff, Hiko Tuff, and tuff of Tepee Rocks.

INTRODUCTION

The Caliente caldera complex is one of the largest Cenozoic caldera complexes in the western United States, with estimated dimensions of 35×80 km (fig. 1). The complex is centered southeast of the town of Caliente, Nev. (fig. 1), in the eastern part of the Basin and Range province. Like many other middle and upper Cenozoic volcanic fields, the complex is dominated by silicic lava flows and ash-flow tuffs, but it also contains minor amounts of mafic and intermediate volcanic rocks. (See Rowley and others, this volume.) Intracaldera deposits and outflow sheets from the Caliente caldera complex are intercalated with outflow sheets from other late Cenozoic calderas. The best known of these calderas is the Kane Springs Wash caldera, which is located about 30 km south of the Caliente caldera complex (Novak, 1984; Scott and others, this volume; Harding and others, this volume). The Caliente caldera complex is south of the much larger Oligocene Indian Peak caldera complex (Best and others, 1989a), which is 80×120 km. The Caliente caldera complex lies southwest and west of Oligocene and early Miocene

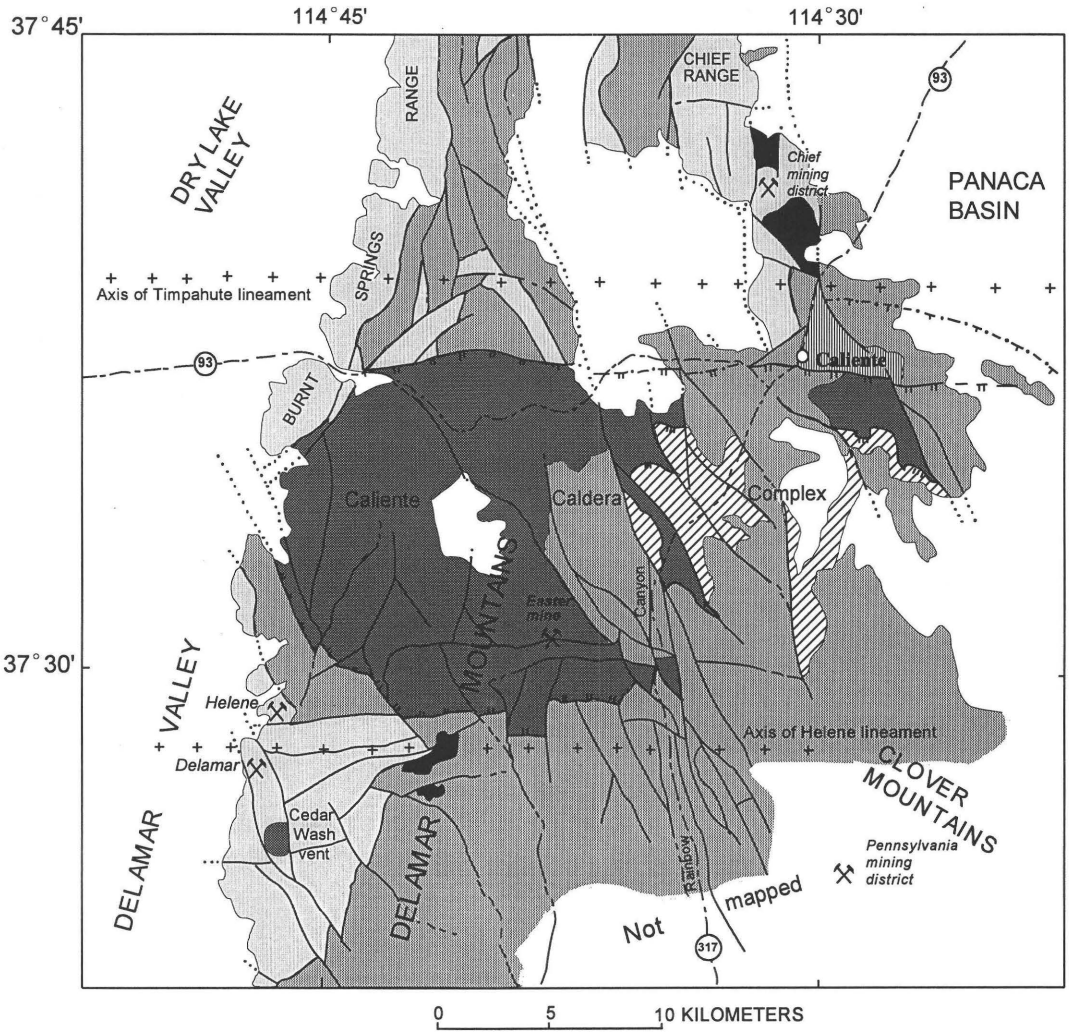

Figure 1 (above and facing page). Generalized geology and location of western part of Caliente caldera complex, Nevada.

volcanic centers that extend from eastern Nevada to the Marysvale volcanic field in southern Utah. Like the source of many other ash-flow tuffs in the western United States, the Caliente caldera complex is a nested caldera complex that resulted from multiple eruptions from closely spaced calderas, lava domes, and satellitic stratovolcanoes.

This report is a product of the USGS Basin and Range–Colorado Plateau (BARCO) Study Unit (see Introduction, this volume) and an earlier project that began in 1986. Both efforts consisted of 7.5-minute quadrangle mapping of a large area that includes the Caliente caldera complex, and related topical studies. We give a preliminary geochemical analysis of ash-flow tuffs in and around the caldera complex. We focus on that part of the ash-flow tuff section that spans the interval from 24 to 12 Ma, when the caldera complex is known or suspected to have been active.

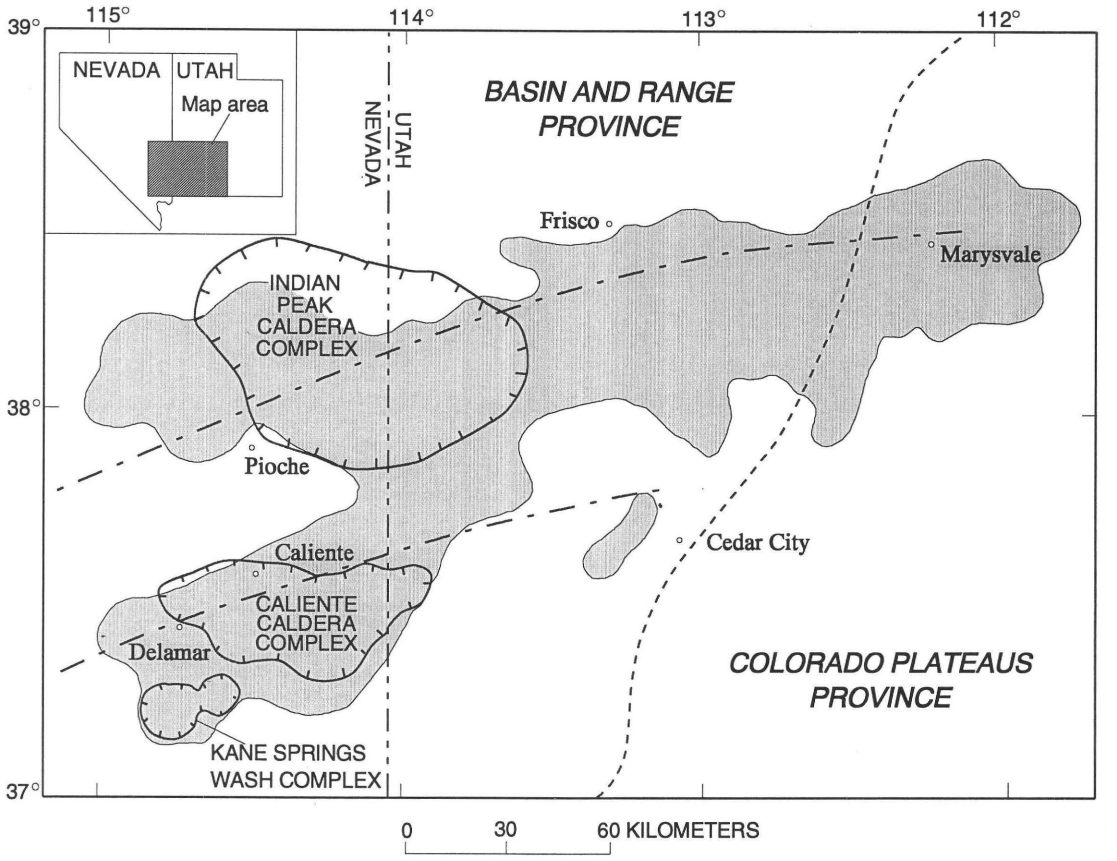

EXPLANATION

Boundary of aeromagnetic ridge (from Zietz and others, 1976, 1978)

Caldera

Colorado Plateau-Basin and Range boundary

Axes of Pioche-Marysvale and Delamar-Iron Springs igneous belts

Additional details on these tuffs are provided by the companion report by Rowley and others (this volume). We include here data for the Gregerson Basin Member of the Kane Wash Tuff (Scott and others, this volume) and the Harmony Hills Tuff. The Gregerson Basin Member erupted from the Kane Springs Wash caldera, which is not a part of the Caliente caldera complex. The Harmony Hills Tuff was probably derived from a source east of the Caliente caldera complex. Data for these rocks are included for comparative purposes and because they are intercalated with ash-flow tuffs known to have erupted from the Caliente caldera complex. The ultimate goal of this study is to use geochemical data to shed light on the tectonic and magmatic evolution of the Caliente caldera complex. And toward this same end, isotopic data for many of the same rock units are given in the companion paper by Unruh and others (this volume).

We present here whole-rock major- and trace-element analyses of the ash-flow tuffs. The data suffer from a variety of unquantifiable uncertainties. First, that an unknown amount of vitric ash was lost during the eruption of the caldera results in phenocryst enrichment compared to the parent magma (Cameron and Hanson, 1982). Second, alteration of tuffaceous material probably began as soon as it was deposited. Although we selected samples that showed no obvious evidence of hydrothermal alteration, our analyses show small to moderate amounts of postemplacement vapor-phase crystallization, devitrification, weathering, and ground-water interaction. We use the terms "alteration" and "altered" in a generic way for all these processes. Lastly, analyzed material contains small but variable amounts of xenolithic material derived from the wallrock material and older volcanic units. Future analyses of vitric lavas, tuffs,

and pumices should more closely represent magmatic compositions than the analyses discussed here. Ideally, pumice and nonhydrated obsidian should be used to characterize the composition of silicic volcanic rocks, but that would mean that some of the most voluminous volcanic units in the Caliente area would never be described chemically. We emphasize that our purpose here is to characterize the units in the vicinity of the Caliente caldera complex, without regard to eruptive differentiation, postemplacement alteration, or xenolith concentration.

ACKNOWLEDGMENTS

We thank R.B Scott and A.E. Harding for sharing data from their mapping south of the Caliente caldera complex. Scott and Harding also helped in the correlation of tuffs and provided conclusions about their sources. Mel Kuntz, Dave Sawyer, Lorna Carter, and Bob Scott provided excellent reviews of early drafts of this report. We also thank all of the analysts who have done their best to provide us with superior results.

GEOLOGIC SETTING

Geologic mapping and geochronologic studies indicate that the Caliente caldera complex was episodically active for at least 10 m.y., beginning about 23 Ma. Volcanism during the interval consisted of caldera- and stratovolcano-forming events, and ended with basalt- and basaltic andesite-dominated volcanism. This progression is typical of late Cenozoic volcanism of western North and Central America and it characterizes volcanic activity that extends from the Sierra Madre Occidental to the Mogollon-Datil field in New Mexico and Arizona and from there to the northern Great Basin (Elston and Bornhorst, 1979; Best, Christiansen, and others, 1989; Wark and others, 1990).

Previous research in the Caliente area predicted that numerous ash-flow tuffs in and near the complex were derived from the Caliente caldera complex: Leach Canyon and Condor Canyon Formations according to Williams (1967), and Harmony Hills, Racer Canyon, Hiko, and Ox Valley Tuffs according to Noble and others (1968) and Noble and McKee (1972). Later mapping by Ekren and others (1977) confirmed that the Hiko Tuff erupted from the western lobe of the Caliente caldera complex, which is now called the Delamar caldera. Four nested calderas are known to compose the Caliente caldera complex: Clover Creek, Delamar, Pine Park, and Buckboard Canyon (Rowley and Siders, 1988). The oldest of these is the Clover Creek caldera, which formed in the northern part of the complex as the result of the eruption of the Bauers Tuff Member (22.8 Ma) of the Condor Canyon Formation (fig. 2). The underlying Swett Tuff Member of the Condor Canyon Formation may have also erupted from the Clover Creek caldera.

About 4 m.y. after the Clover Creek caldera formed, the Hiko Tuff (18.6–18.2 Ma) erupted from the Delamar caldera in the western part of the complex. At about 16 Ma, the eastern part of the complex erupted to form the Pine Park caldera

AGE	UNIT	SOURCE
Miocene	Ox Valley Tuff (12.6?-11.4? Ma)	Caliente
	tuff of Etna (14.0 Ma)	Caliente
	Kane Wash Tuff: Gregerson Basin Member — upper unit (14.4 Ma); lower unit (14.6 Ma)	Kane Springs Wash
	tuff of Kershaw Canyon (15.3?-14.2 Ma)	
	tuff of Sawmill Canyon	Caliente
	tuff of Rainbow Canyon (15.6-15.2 Ma)	Buckboard Canyon
	Delamar Lake Tuff (15.8-15.5 Ma)	?
	tuff of Tepee Rocks (17.8 Ma)	Caliente
	lava flows of Buckboard Spring (18.0 Ma)	Delamar
	volcanic dome of Crows Nest Tank (18.2 Ma)	Delamar
	Hiko Tuff (18.6-18.2 Ma)	Delamar
	Racer Canyon Tuff (19.2?-18.7 Ma)	Caliente
	lava flows of Indian Cove (21.9 Ma)	Clover Creek
	Quichapa Group: Harmony Hills Tuff (22.5-22.0 Ma)	?
	Quichapa Group: Condor Canyon Formation: Bauers Tuff Member (22.8 Ma)	Clover Creek
	Quichapa Group: Condor Canyon Formation: Swett Tuff Member (23.7? Ma)	Caliente
	Quichapa Group: *Leach Canyon Formation (23.8 Ma)*	?
Oligocene	*Cobalt Canyon stock (24.8 Ma)*	

* porphyry of Meadow Valley Wash (19.4-<18.2 Ma)

* dikes

Figure 2. Stratigraphy of ash-flow tuffs and related rocks in and near Caliente caldera complex and vicinity, Nevada-Utah. Note that Kane Springs Wash caldera is not part of Caliente caldera complex. K-Ar, $^{40}Ar/^{39}Ar$ ages and interpreted ages in parentheses; see text and Rowley and others (this volume) for details. Use of "Caliente" for the source indicates that source is considered to be within Caliente caldera complex, but exact caldera has not been named or in some cases has not been mapped. Query, source unknown; blank, not applicable.

(Rowley and Siders, 1988; Siders, 1991), but deposits from this caldera have not been included here because they have not been studied in detail. At about 15.6–15.2 Ma, another major eruption produced the tuff of Rainbow Canyon from an area in the western part of the complex, referred to as the Buckboard Canyon caldera. The Kane Springs Wash caldera, 30 km south of the Caliente caldera complex, produced the Kane Wash Tuff at about 14.7–14.4 Ma (Scott and others, this volume; Harding and others, this volume).

In addition to the four named calderas noted, other calderas and vent areas formed in the complex; but their locations and geometry are poorly known (Rowley and others, this volume). These were the sources of the tuff of Tepee Rocks, tuff of Kershaw Canyon, tuff of Etna, and Ox Valley Tuff. Intermediate to silicic lavas and volcanic mudflow breccia erupted from lava domes and stratovolcanoes at various times during the evolution of the Caliente caldera complex. Intracaldera megabreccias in the caldera complex were derived from collapsing walls of the complex.

Volcanism in the area occurred during the main episode of regional late Cenozoic extension. Faulting comprised high-angle strike-slip, normal-slip, oblique-slip, and low-angle normal types. Some of the calderas that form the Caliente caldera complex are trapdoor calderas or have complex margins that are locally faults, suggestive of concurrent faulting during caldera subsidence (Rowley and others, 1990; Rowley and others, 1992). The inception of this volcanic and tectonic event correlates with a major reorganization of plates in western North America at about 25 Ma (Mammerickx and Klitgord, 1982; Ward, 1991).

Mafic and intermediate magmas erupted from local volcanic centers, probably throughout the history of the complex. Rocks produced by this activity predate and locally intertongue with the upper Miocene and Pliocene Panaca Formation, a sequence of basin-fill sedimentary rocks. The volcanism occurred near the end of the main episode of extension as basin-range faulting took over as the dominant form of crustal deformation. After about 2–4 m.y., volcanism ceased in the area. The cessation of volcanic activity correlates with another reorganization of tectonic plates in western North America between 12 and 10 Ma (Ward, 1991).

GEOCHEMISTRY

ANALYTICAL METHODS

Analyzed whole-rock samples of ash-flow tuffs from the Caliente caldera complex range in composition from andesite to high-silica rhyolite, but most are rhyolite. Due to the inhomogeneity within individual ash-flow tuffs, as many as eight samples from a single unit were analyzed. Before analysis, all samples were crushed in an aluminum shatterbox and ground with an agate mortar and pestle. Major elements are given in table 1 and are plotted in figures 3–8 on a volatile-free basis. Table 2 describes sample localities.

Chemical analyses of the samples were determined in Lakewood, Colo., and Menlo Park, Calif., laboratories of the USGS using standard procedures. Major-element compositions were determined by X-ray fluorescence spectroscopy using methods described in Taggart and others (1987). Minor elements (Nb, Rb, Sr, Zr, Y, Ba, La, Cu) were determined using X-ray fluorescence methods described by Johnson and King (1987). Trace elements (Ba, Co, Cr, Th, Zn, Sc, La, Ce, Nd, Sm, Eu, Gd, Tb, Tm, Yb, Lu) were determined by inductively coupled plasma–atomic absorption spectroscopy (ICPAAS) and instrumental neutron activation analysis (INAA). Methods for ICPAAS and INAA followed those described by Lichte and others (1987) and Baedecker and McKown (1987), respectively. Samples analyzed by INAA provided more complete rare-earth element analyses, whereas samples analyzed by ICPAAS lack data for the middle and heavy rare-earth elements (table 1).

MAJOR-ELEMENT GEOCHEMISTRY

CLASSIFICATION

In this report, we classify ash-flow tuffs in the Caliente area by the potassium versus silica scheme of Peccerillo and Taylor (1976) and the FeO^*/MgO versus silica scheme of Miyashiro (1974). These two schemes allow for the application of common, yet meaningful rock names and are also used commonly to classify subduction-related magmas. In all diagrams, major elements are plotted recalculated volatile-free. Using the potassium versus silica scheme, the majority of Caliente rocks are high-potassium rhyolite (fig. 3). A few samples plot slightly into the high-potassium dacite field. Samples with greater than 76 weight percent silica are definitely altered. A single sample of the Harmony Hills Tuff is classified as high-potassium andesite. On the basis of FeO^*/MgO and SiO_2, the majority of Caliente samples are calc-alkaline (fig. 4). The Gregerson Basin Member of the Kane Wash Tuff and a sample of the tuff of Etna show strong tholeiitic affinities, using Miyashiro's classification scheme.

SILICA VARIATION DIAGRAMS

A variety of techniques exist for showing chemical variations in igneous rocks. The most common method is the Harker diagram, a type of binary diagram in which the abundance of a major or trace element is plotted against another element. Harker diagrams are used herein to show chemical variations within and between the ash-flow tuffs in the vicinity of Caliente (fig. 5).

On a volatile-free basis, our suite of samples contains between 62 and 84 weight percent SiO_2, forming a rock

Table 1. Chemical analyses for ash-flow tuffs in and near Caliente caldera complex.

[Major elements in weight percent, trace elements in parts per million. ICPAAS and INAA indicated by *; nd, not determined; LOI, loss on ignition. Analysts: J.E. Taggart, A. Bartel, D.F. Siems, T.L. Fries, J.R. Evans, J.R. Budahn, R.J. Knight, D.M. McKown, Hezekiah Smith, J.W. Marinenko, W.B. Crandell, D.L. Fey, C.S.E. Papp, G.O. Riddle, K.C. Curry, and F.W. Tippitt. Petrographic data for all samples given in Rowley and others (this volume)]

Unit	Bauers Member					Swett Member		Harmony Hills Tuff
Sample No	87-1181C	87-452E	87-452H	88-1065A	88-1035A	87-452A	87-452D	87-452K
Major-element composition								
SiO_2	68.4	70.0	72.8	70.7	67.3	69.6	71.8	60.9
Al_2O_3	14.7	14.0	13.8	14.8	14.8	14.0	14.1	15.6
$FeTO_3$	1.91	1.62	1.66	1.88	2.06	1.73	1.78	5.67
MgO	0.62	0.42	0.32	0.32	0.62	0.56	0.53	2.93
CaO	1.84	1.21	1.17	1.26	2.11	1.29	1.39	5.12
Na_2O	3.97	3.52	3.51	3.79	3.31	3.52	3.78	3.16
K_2O	4.28	5.63	5.40	5.39	5.02	5.22	5.06	3.46
TiO_2	0.35	0.31	0.30	0.33	0.35	0.35	0.36	0.73
P_2O_5	0.08	<0.05	0.06	0.06	0.08	<0.05	0.06	0.28
MnO	0.05	0.05	0.04	0.04	0.05	0.04	0.03	0.08
LOI	3.46	2.66	0.47	0.71	3.55	3.08	0.62	1.5
Trace-element composition								
Nb	16	18	17	15	16	14	21	8
Rb	224	198	199	190	241	157	168	102
Sr	422	272	306	356	584	267	268	771
Zr	325	292	289	280	301	309	315	185
Y	25	26	24	21	19	25	24	17
Ba	1,110	1,180	1,220	1,390	1,430	1,280	1,270	941
La	66	69	61	58	47	66	58	nd
Cu	9	8	5	8	14	7	4	nd
*Ba	1,100	1,100	1,200	1,200	1,430	1,200	1,200	974
*Co	4	2	3	nd	5	2	4	nd
*Cr	3	2	1	nd	5	1	3	nd
*Hf	nd	nd	nd	nd	nd	nd	nd	5.24
*Ta	nd	nd	nd	nd	nd	nd	nd	0.70
*Th	31	33	30	29	29	21	21	16
*U	nd	nd	nd	nd	nd	nd	nd	3.52
*Zn	46	39	33	39	44	42	38	nd
*Sc	5	4	4	5	5	5	4	nd
*La	66	67	63	63	63	66	62	45.9
*Ce	110	110	110	110	110	110	110	90.8
*Nd	42	41	39	40	41	44	43	36.9
*Sm	nd	nd	nd	nd	6.0	nd	nd	6.74
*Eu	nd	nd	nd	nd	1.3	nd	nd	1.57
*Gd	nd	nd	nd	nd	3.8	nd	nd	nd
*Tb	nd	nd	nd	nd	0.62	nd	nd	0.65
*Tm	nd	nd	nd	nd	0.28	nd	nd	nd
*Yb	2	2	2	2	1.9	3	2	1.82
*Lu	nd	nd	nd	nd	nd	nd	nd	0.27

Table 1. Chemical analyses for ash-flow tuffs in and near Caliente caldera complex—Continued.

Unit	Hiko Tuff							
Sample No.	86-666C	86-666H	87-206G	87-452N	87-4520	87-506	87-1231	88-1267
Major-element composition								
SiO_2	69.4	69.4	71.1	67.5	67	67.6	70.2	67.7
Al_2O_3	13.9	14.6	13.2	14.9	15.2	15.1	14.0	14.6
$FeTO_3$	2.39	2.83	1.79	2.01	2.08	2.88	2.65	2.93
MgO	0.98	0.77	0.98	1.16	1.30	0.94	0.80	1.05
CaO	2.12	2.43	1.79	2.20	2.49	2.37	2.04	3.25
Na_2O	3.16	3.56	2.89	2.99	3.27	3.09	3.26	3.19
K_2O	4.46	4.36	4.07	4.76	3.97	4.41	4.32	4.31
TiO_2	0.37	0.46	0.28	0.33	0.33	0.52	0.43	0.46
P_2O_5	0.14	0.16	0.08	0.11	0.11	0.18	0.15	0.16
MnO	0.05	0.05	0.04	0.04	0.06	0.04	0.03	0.05
LOI	2.29	0.81	3.33	3.27	3.55	2.13	1.31	1.76
Trace-element composition								
Nb	16	14	19	16	17	15	17	13
Rb	148	124	164	164	125	123	150	136
Sr	374	494	318	420	447	531	404	628
Zr	151	194	129	158	151	222	180	196
Y	17	18	15	18	17	17	16	16
Ba	782	1,120	704	852	935	1,230	952	1,120
La	nd	nd	nd	nd	nd	nd	nd	49
Cu	nd	nd	nd	nd	nd	nd	nd	9
*Ba	826	1,240	762	861	981	1,260	944	1,000
*Cr	5.13	5.52	3.97	nd	nd	nd	nd	nd
*Cs	6.53	4.18	14.6	nd	nd	nd	nd	nd
*Hf	4.6	5.84	4.27	4.45	4.98	5.38	4.91	nd
*Ta	1.3	1.37	1.63	1.35	1.44	1.27	1.47	nd
*Th	21.1	17.9	22.5	21.9	23.4	17.1	19.9	17
*U	5.29	4.25	6.3	5.02	4.82	4.23	5.39	nd
*Zr	156	210	137	150	171	197	nd	nd
*La	48.6	51.8	48.9	51.7	52.4	57.8	51.6	65
*Ce	84.6	101	87.2	89.2	96	109	93.7	100
*Nd	29.3	36.4	28	29.2	31	38.6	33.2	37
*Sm	4.7	6.36	4.65	4.76	5.12	6.61	5.77	nd
*Eu	0.94	1.3	0.89	0.92	1.03	1.33	1.11	nd
*Tb	0.44	0.60	0.42	0.40	0.45	0.56	0.52	nd
*Yb	1.5	1.65	1.59	1.44	1.54	1.62	1.68	2
*Lu	0.24	0.26	0.25	0.22	0.24	0.24	0.26	nd

Table 1. Chemical analyses for ash-flow tuffs in and near Caliente caldera complex—Continued.

Unit	Tuff of Tepee Rocks	Tuff of Rainbow Canyon				Tuff of Kershaw Canyon	
Sample No.	88-1268	87-221	87-1111	87-1113	88-226A	88-195A	89-698D
Major-element composition							
SiO_2	73.1	67.5	76.2	76.2	73.5	65.1	67.6
Al_2O_3	12.6	10.7	8.1	8.1	10.2	13.3	12.6
$FeTO_3$	0.77	0.8	0.57	0.59	0.86	2.08	2.46
MgO	0.67	0.90	0.49	0.43	0.60	0.69	1.05
CaO	0.94	2.76	1.74	1.52	1.21	2.32	2.45
Na_2O	2.43	1.38	0.65	1.28	2.33	2.69	1.79
K_2O	5.18	3.30	2.66	2.26	2.58	3.65	4.15
TiO_2	0.11	0.1	0.07	0.07	0.1	0.27	0.31
P_2O_5	<0.05	0.05	0.05	0.05	0.05	0.05	0.08
MnO	0.03	0.07	0.05	0.06	0.06	0.08	0.06
LOI	3.89	12.0	9.01	8.85	8.01	9.44	6.94
Trace-element composition							
Nb	26	43	38	36	45	31	26
Rb	235	398	224	230	154	145	211
Sr	73	32	321	540	590	262	468
Zr	107	114	102	102	124	261	250
Y	16	29	18	26	25	29	29
Ba	97	62	43	65	96	598	546
La	39	nd	nd	nd	nd	nd	54
Cu	4	nd	nd	nd	nd	nd	9
*Ba	96	75	66	35	123	610	520
*Co	nd	0.5	0.2	0.2nd	0.4	1.3	nd
*Cr	nd	1.3	0.7	<.4	0.6d	3.1	nd
*Cs	nd	17.4	9.9	9.3	9.4	5.1	nd
*Hf	nd	5.69	4.18	4.08	5.26	7.76	nd
*Ta	nd	3.62	2.79	2.73	3.37	2.03	nd
*Th	31	39.4	29.9	27.7	37.6	18.6	17
*U	nd	6.15	8.1	15.6	8.85	4.75	nd
*Zr	nd	114	<70	<71	<98	250	nd
*La	37	33.4	23	37.7	33.7	78.7	56
*Ce	53	59.0	44.4	50.5	58.8	152	100
*Nd	12	14.8	11.0	16.9	15.2	47.5	40
*Sm	nd	2.78	2.13	3.05	2.63	8.03	6.3
*Eu	nd	0.12	0.05	0.07	0.11	0.70	0.65
*Gd	nd	nd	nd	nd	nd	nd	5.1
*Tb	nd	0.37	0.30	0.42	0.36	0.83	0.81
*Tm	nd	nd	nd	nd	nd	nd	0.55
*Yb	1	3.42	2.14	2.81	3.01	3.09	2.9
*Lu	nd	0.58	0.34	0.43	0.48	0.47	nd

Table 1. Chemical analyses for ash-flow tuffs in and near Caliente caldera complex—Continued.

Unit	Gregerson Basin Mbr., upper unit	Gregerson Basin Mbr., upper unit	Gregerson Basin Mbr., lower unit	Tuff of Etna	Tuff of Etna	Ox Valley Tuff
Sample No.	87-1105C	88-1157A	88-1157B	88-177B	88-1209	87-697Y
Major-element composition						
SiO_2	80.8	75.1	75.3	80.1	76.3	75.6
Al_2O_3	7.96	11.3	11.4	9.02	11.7	11.7
$FeTO_3$	2.15	2.98	2.78	1.19	1.96	1.70
MgO	0.21	0.17	0.15	0.20	0.21	0.26
CaO	0.42	0.25	0.19	0.58	0.22	0.72
Na_2O	2.81	4.34	4.27	2.36	3.99	3.19
K_2O	3.35	4.62	4.77	4.07	4.62	4.58
TiO_2	0.13	0.19	0.19	0.09	0.13	0.18
P_2O_5	0.05	<0.05	<0.05	0.05	0.05	0.05
MnO	0.05	0.07	0.06	0.03	0.04	0.03
LOI	1.41	0.27	0.31	1.76	0.67	1.35
Trace-element composition						
Nb	84	104	108	52	61	35
Rb	194	261	249	171	164	137
Sr	25	13	7	67	18	86
Zr	825	1110	928	189	462	212
Y	80	77	80	49	44	43
Ba	65	75	26	191	57	457
La	102	127	128	59	78	nd
Cu	12	9	13	3	4	nd
*Ba	67	77	39	170	57	451
*Co	nd	nd	nd	1	nd	nd
*Cr	2	nd	nd	3	nd	nd
*Hf	nd	nd	nd	nd	nd	7.24
*Ta	nd	nd	nd	nd	nd	2.51
*Th	23	30	27	21	17	16.9
*U	nd	nd	nd	nd	nd	3.28
*Zr	nd	nd	nd	nd	nd	237
*Zn	140	200	180	71	98	nd
*La	85	120	130	56	77	43.8
*Ce	170	240	250	92	140	94.1
*Nd	68	93	96	44	58	39.3
*Sm	nd	nd	nd	nd	nd	8.52
*Eu	nd	nd	nd	nd	nd	0.60
*Gd	nd	nd	nd	nd	nd	nd
*Tb	nd	nd	nd	nd	nd	1.14
*Tm	nd	nd	nd	nd	nd	nd
*Yb	9	11	9	5	5	4.26
*Lu	nd	nd	nd	nd	nd	0.62

Table 2. Sample localities for ash-flow tuffs in and near Caliente caldera complex.

Sample No.	Unit	County, State	Latitude N.	Longitude W.	Description
87-1181C	Bauers Member	Lincoln, Nev.	37° 38' 05"	114° 29' 50"	Glass, intracaldera.
87-452E	Bauers Member	Lincoln, Nev.	37°51' 29"	114° 19' 28"	Glass, outflow.
87-452H	Bauers Member	Lincoln, Nev.	37°51' 29"	114° 19' 30"	Outflow.
88-1065A	Bauers Member	Lincoln, Nev.	37° 37' 05"	114° 29' 08"	Intracaldera.
88-1035A	Bauers Member	Lincoln, Nev.	37° 37' 37"	114° 29' 28"	Glass, intracaldera.
87-452A	Swett Member	Lincoln, Nev.	37°51' 29"	114° 19' 22"	Glass, outflow.
87-452D	Swett Member	Lincoln, Nev.	37°51' 29"	114° 19' 24"	Outflow.
86-666C	Hiko Tuff	Lincoln, Nev.	37° 32' 15"	115° 01' 15"	Glass, outflow, type section.
86-666H	Hiko Tuff	Lincoln, Nev.	37° 32' 15"	115° 01' 40"	Outflow, type section.
87-206G	Hiko Tuff	Lincoln, Nev.	37° 35' 32"	114° 36' 04"	Glass, intracaldera.
87-452N	Hiko Tuff	Lincoln, Nev.	37° 51' 34"	114° 19' 25"	Lower outflow unit.
87-452O	Hiko Tuff	Lincoln, Nev.	37° 51 36"	114° 19' 22"	Upper outflow unit.
87-506	Hiko Tuff	Lincoln, Nev.	37° 30' 33"	114° 37' 16"	Glass, intracaldera.
87-1231	Hiko Tuff	Lincoln, Nev.	37° 31 27"	114° 43' 03"	Intracaldera.
88-1267	Hiko Tuff	Lincoln, Nev.	37° 35' 03"	114° 38' 10"	Top, intracaldera.
88-1268	tuff of Tepee Rocks	Lincoln, Nev.	37° 35' 47"	114° 26' 17"	Outflow?, type area.
87-452K	Harmony Hills Tuff	Iron, Utah	37° 51' 31"	114° 19' 31"	Glass, Condor Canyon.
87-697Y	Ox Valley Tuff	Iron, Utah	37° 30' 04"	113° 51' 38"	Outflow, near type section.
87-221	tuff of Rainbow Canyon	Lincoln, Nev.	37° 30' 47"	114° 30' 07"	Intracaldera.
87-1111	tuff of Rainbow Canyon	Lincoln, Nev.	37° 34' 04"	114° 34' 13"	Glass, intracaldera.
87-1113	tuff of Rainbow Canyon	Lincoln, Nev.	37° 34' 27"	114° 34' 40"	Glass, intracaldera.
88-226A	tuff of Rainbow Canyon	Lincoln, Nev.	37° 34' 53"	114° 32' 52"	Intracaldera.
88-195A	tuff of Kershaw Canyon	Lincoln, Nev.	37° 35' 37"	114° 32' 50"	Upper (post-C3) tuff, Little Kershaw Canyon.
89-698D	tuff of Kershaw Canyon	Lincoln, Nev.	37° 34' 21"	114° 33' 02"	Post-C2 tuff.
87-1105C	Gregerson Basin Member	Lincoln, Nev.	37° 34' 02"	114° 33' 46"	Upper unit (C3).
88-1157A	Gregerson Basin Member	Lincoln, Nev.	37° 33' 34"	114° 29' 56"	Upper unit (C3).
88-1157b	Gregerson Basin Member	Lincoln, Nev.	37° 33' 34"	114° 29' 55"	Lower unit (C2).
88-177B	tuff of Etna	Lincoln, Nev.	37° 36' 08"	114° 32' 03"	Outflow.
88-1209	tuff of Etna	Lincoln, Nev.	37° 34' 20"	114° 40' 14"	Outflow.

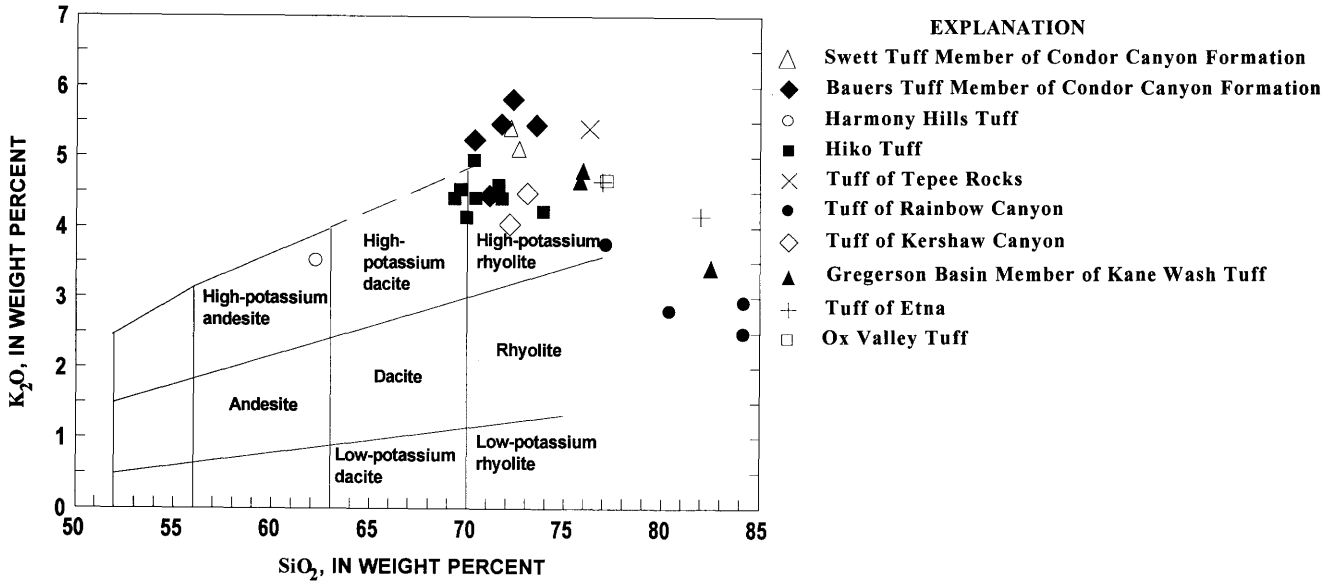

Figure 3. Potassium variation diagram for ash-flow tuffs in and near Caliente caldera complex and vicinity, Nevada-Utah. Rock nomenclature from Peccerillo and Taylor (1976).

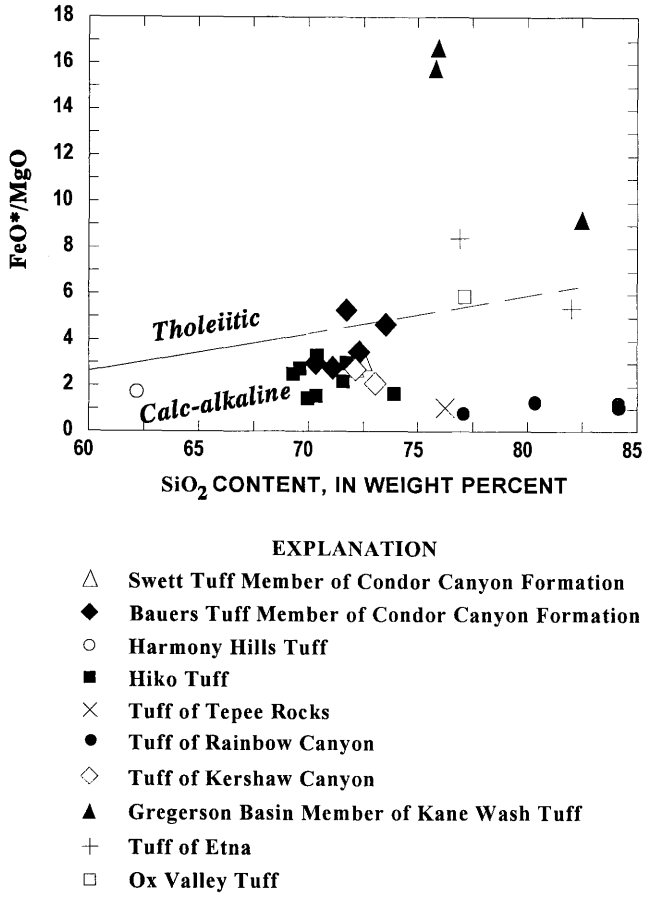

Figure 4. Silica versus FeO^*/MgO variation diagram for ash-flow tuffs in and near Caliente caldera complex and vicinity, Nevada-Utah. Fields modified from Miyashiro (1974). FeO^* is total iron, reported as $FeTO_3$, multiplied by 0.8993.

series from andesite to high-silica rhyolite (greater than 75 weight percent silica). Many samples cluster between about 69 and 74 weight percent SiO_2. Some samples of the tuff of Rainbow Canyon, Ox Valley Tuff, Gregerson Basin Member of the Kane Wash Tuff, and tuff of Etna have unrealistically high silica contents (silica greater than 76 wt. percent SiO_2), probably due to silica gain during alteration. In general, the suite shows an initial increase in potassium with increasing silica content to about 72 wt. percent silica, and a decrease in potassium in yet more silicic samples.

Calcium variability suggests low-temperature alteration of low-potassium, high-silica rocks. Such rocks have high calcium contents compared to the rest of our suite (fig. 5*A*). Unaltered rocks show an almost monotonic decrease in calcium with increasing silica content. Sodium contents give support to the hypothesis that high-silica rhyolite is the product of postemplacement alteration (fig. 5*B*) because all high-silica rhyolites have low and highly variable sodium contents when compared to the other tuffs in the Caliente area. The diagrams suggest that unaltered ash-flow tuffs in the Caliente area originally contained between about 3 and 4.5 weight percent Na_2O. Total alkali contents confirm the disparity between unaltered and altered rocks (fig. 5*C*). Altered rocks apparently lost both sodium and potassium, and gained calcium and silica during alteration. The chemical patterns of altered rocks are consistent with the alteration of glass during advanced stages of hydration. Alumina and titania contents decrease with increasing silica content (fig. 5*D* and 5*E*).

Caliente samples straddle the boundary between peraluminous and metaluminous rocks on plots of the molar $Al_2O_3/(CaO+Na_2O+K_2O)$ (A/CNK) versus silica (fig. 6). The Gregerson Basin Member of the Kane Wash Tuff has

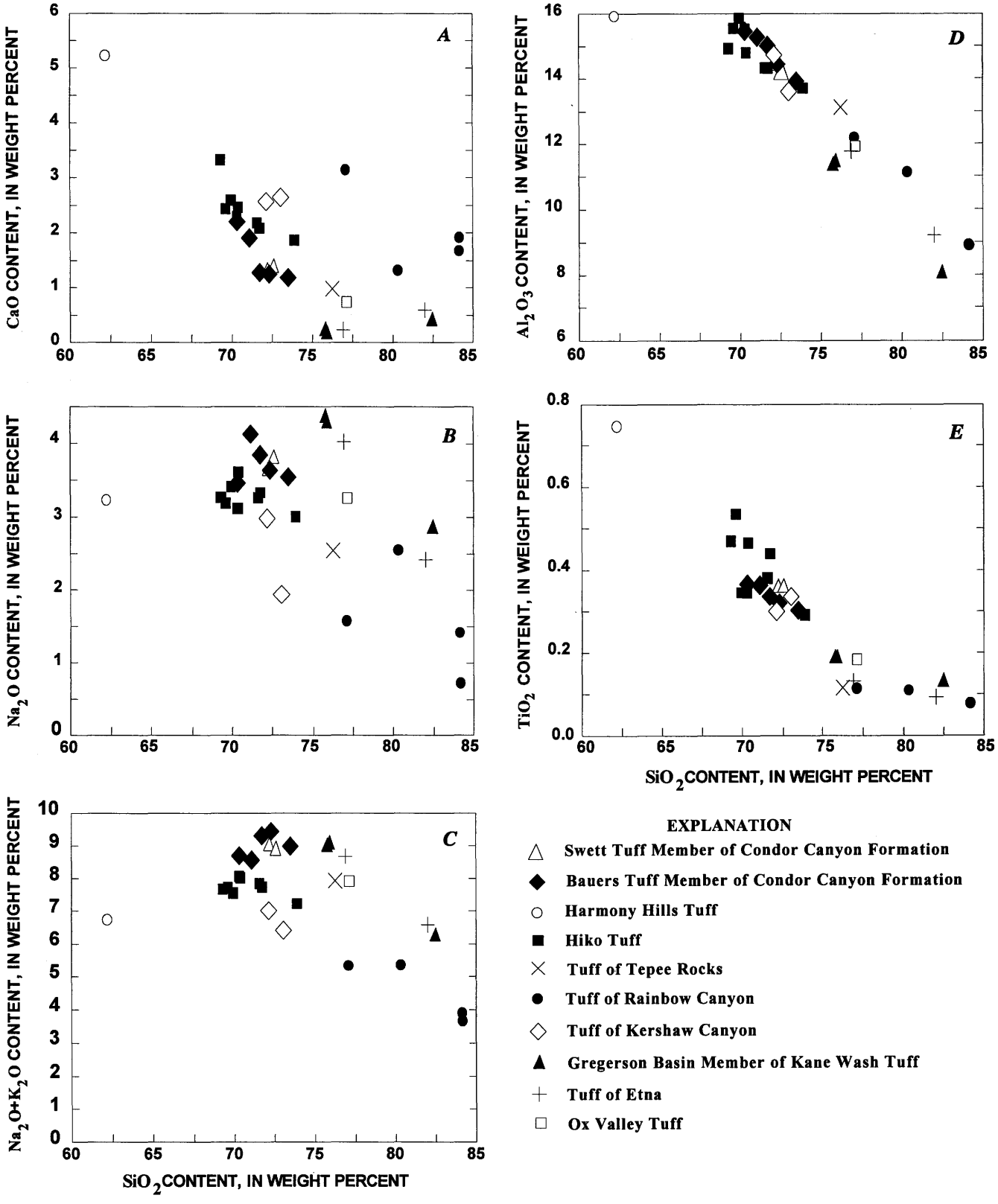

Figure 5. Silica variation diagrams for ash-flow tuffs in and near Caliente caldera complex. *A*, CaO; *B*, Na_2O; *C*, Na_2O+K_2O; *D*, Al_2O_3; *E*, TiO_2.

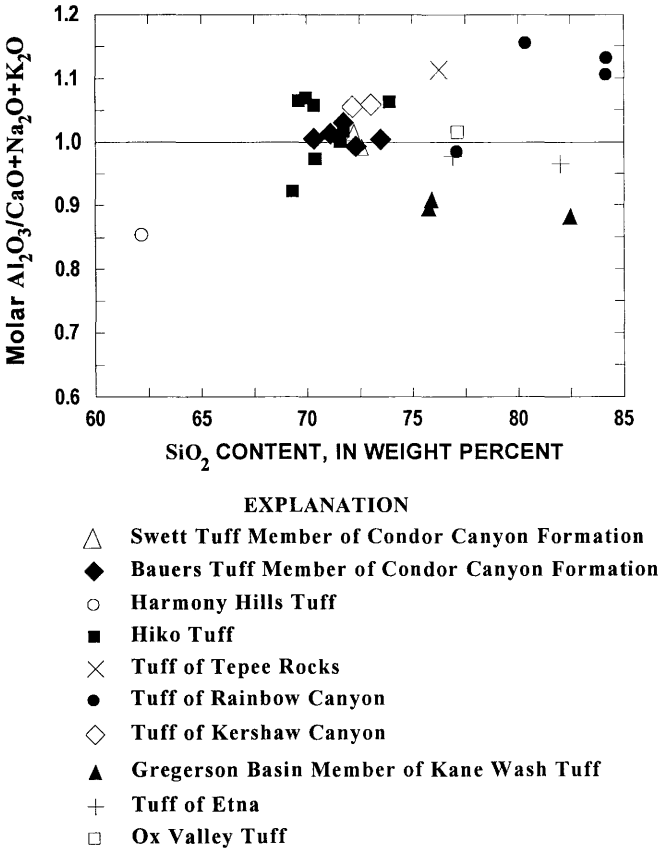

Figure 6. Molar $Al_2O_3/CaO+Na_2O+K_2O$ versus silica variation diagram for ash-flow tuffs in and near Caliente caldera complex.

A/CNK<1, and is technically peralkaline, having molar Na_2O+K_2O in excess of molar Al_2O_3. Altered (>76 weight percent SiO_2) samples show considerable scatter both above and below the A/CNK=1 line.

TRACE-ELEMENT GEOCHEMISTRY

Despite the demonstrable fact that several of our samples are altered, we are compelled to discuss their trace-element abundances because these data are essential to characterize ash-flow tuffs in the Caliente area. Moreover we are not sure that we can unequivocally distinguish altered from unaltered samples. Obviously samples with more than 76 weight percent SiO_2 are altered, but some less silicic rocks may also be altered. So, in this section, we describe the trace-element patterns of all the samples discussed previously. The composition of the Gregerson Basin Member is commonly discussed for the sake of comparison and because this unit occurs within the Caliente caldera complex. Because the Gregerson Basin Member is peralkaline, concentrations of high-field-strength elements (such as Zr, Y, Nb) are higher in it than in the peraluminous and metaluminous rocks.

Peraluminous and metaluminous samples show moderate Zr levels that tend to decrease along convergent trends with increasing silica content (fig. 7*A*). Among the low-silica rhyolites, the Hiko Tuff and tuff of Tepee Rocks have lower Zr contents than the Bauers Tuff Member, Swett Tuff Member, and tuff of Kershaw Canyon. The Gregerson Basin Member has high Zr contents (800–1,100 ppm Zr), consistent with its peralkaline chemistry.

The abundance of Nb in rocks in the Caliente area shows an overall increase with increasing silica content (fig. 7*B*). Post-Hiko units have higher Nb contents than the older units (Swett and Bauers Tuff Members, Harmony Hills Tuff, Hiko Tuff). The Gregerson Basin Member has the highest Nb levels (>80 ppm Nb). The Gregerson Basin also has the highest concentration of Y (fig. 7*C*). Hiko Tuff is distinguished from other peraluminous and metaluminous rhyolites by lower Y concentrations. Thus, as noted by previous workers (Novak, 1984; Novak and Mahood, 1986; Harding and others, this volume; Scott and others, this volume) the Gregerson Basin Member has high concentrations of high-field-strength elements, a chemical characteristic of peralkaline magmas.

The abundance of Sr in most of our samples decreases with increasing silica content, consistent with plagioclase-controlled fractionation (fig. 7*D*). But interestingly, none of the samples have Sr contents between 100 and 250 ppm, allowing the samples to be separated into high-Sr and low-Sr groups. High Sr abundances characterize the Swett Tuff Member, Hiko Tuff, Bauers Tuff Member, and the tuff of Kershaw Canyon. Low Sr abundances characterize the tuff of Tepee Rocks, Gregerson Basin Member, tuff of Etna, and one sample of the tuff of Rainbow Canyon. Altered samples of the tuff of Rainbow Canyon are displaced away from the remainder of the samples toward the high-silica side of figure 7*D*, but they have Sr contents that overlap values of unaltered(?) rocks.

Rubidium shows a four-fold range in ash-flow tuffs of the Caliente area (fig. 7*E*), but Rb is expected to be readily mobilized by postemplacement alteration. The amount of scatter in figure 7*E* is probably evidence of this alteration. The tuff of Rainbow Canyon, for example, shows more variability in Rb content than exists for all other units. The pattern in figure 7*E* may indicate that Rb content for peraluminous and metaluminous rhyolites was the same as it was in peralkaline rhyolite.

Barium shows an overall decrease with increasing silica content (fig. 7*F*). This element ranges in concentration from about 1,400 ppm Ba in the Bauers Tuff Member to less than 100 ppm Ba in the Gregerson Basin Member and some high-silica rhyolite samples. A small gap at about 300 ppm Ba separates high-Ba and low-Ba rocks.

Trace-element ratios are commonly used as petrologic indicators. At similar silica contents, Zr/Nb values of the Bauers and Swett Tuff Members of the Condor Canyon Formation are higher than those of the Hiko Tuff (fig. 8). Low-silica rhyolite samples of the Hiko Tuff have Zr/Nb greater than 8, whereas samples of high-silica rhyolite Hiko Tuff

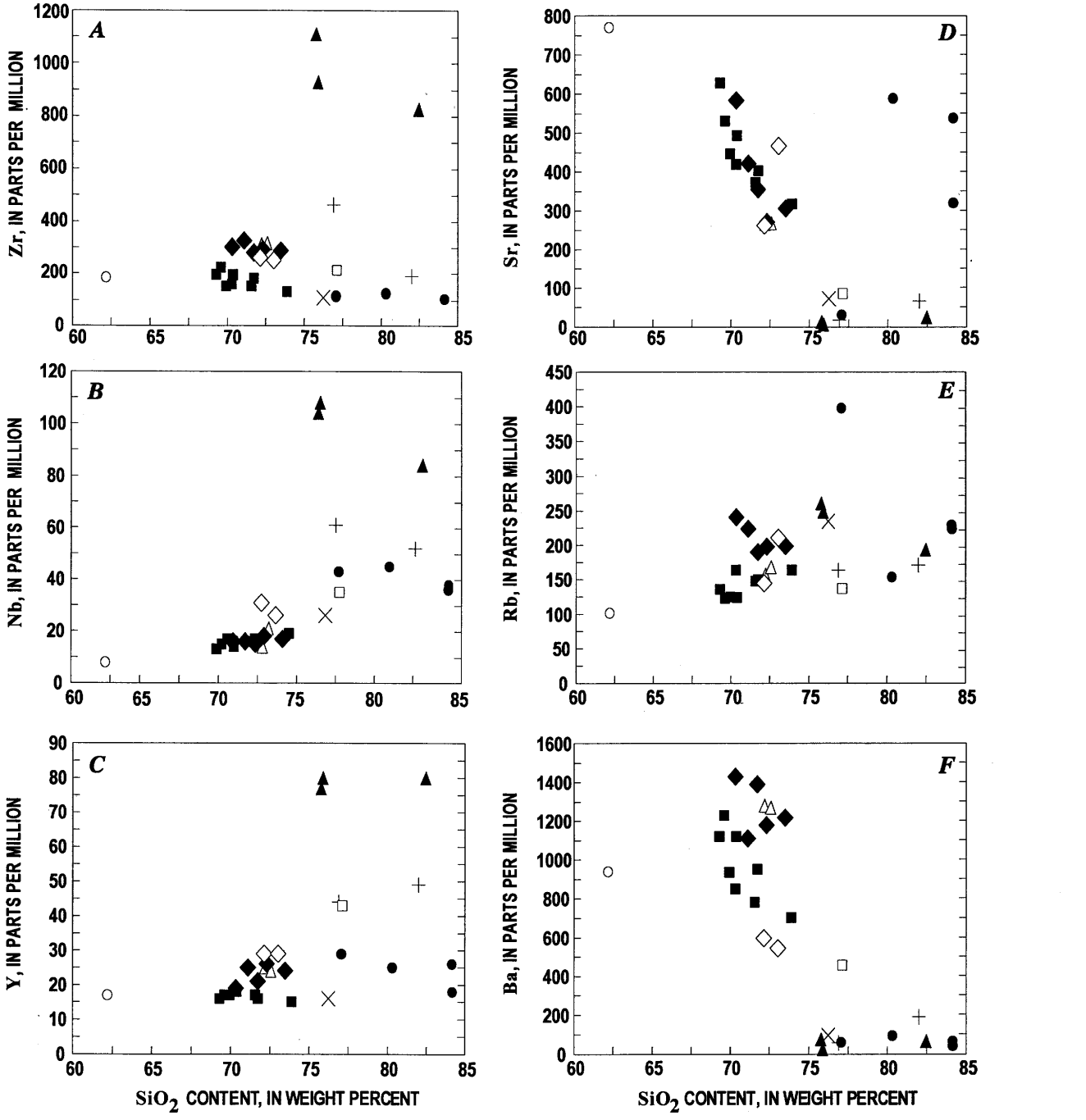

Figure 7. Trace element variation diagrams for ash-flow tuffs in and near Caliente caldera complex. *A*, zirconium; *B*, niobium; *C*, yttrium; *D*, strontium; *E*, rubidium; *F*, barium.

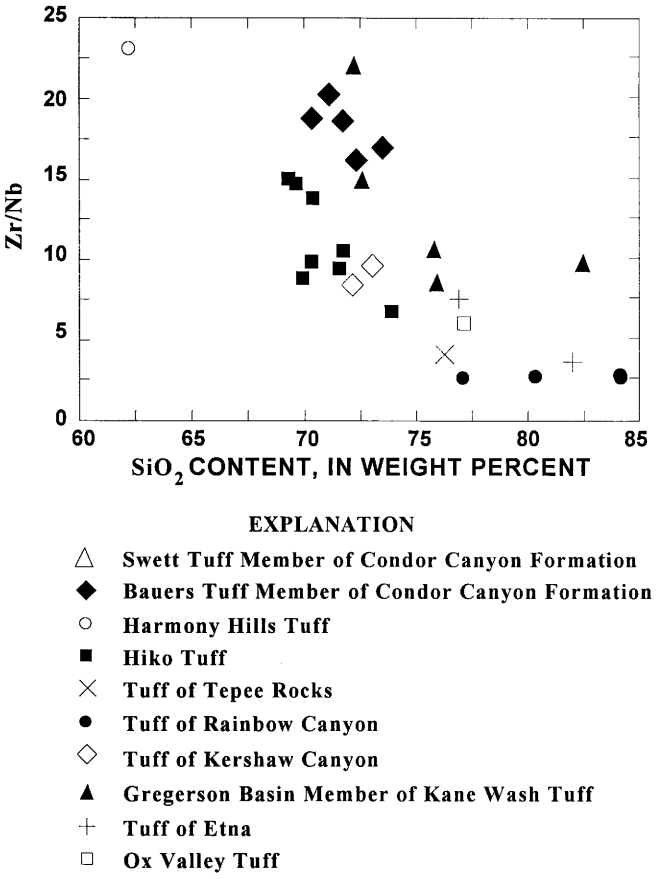

Figure 8. Zr/Nb versus SiO_2 variation diagram for ash-flow tuffs in and near Caliente caldera complex.

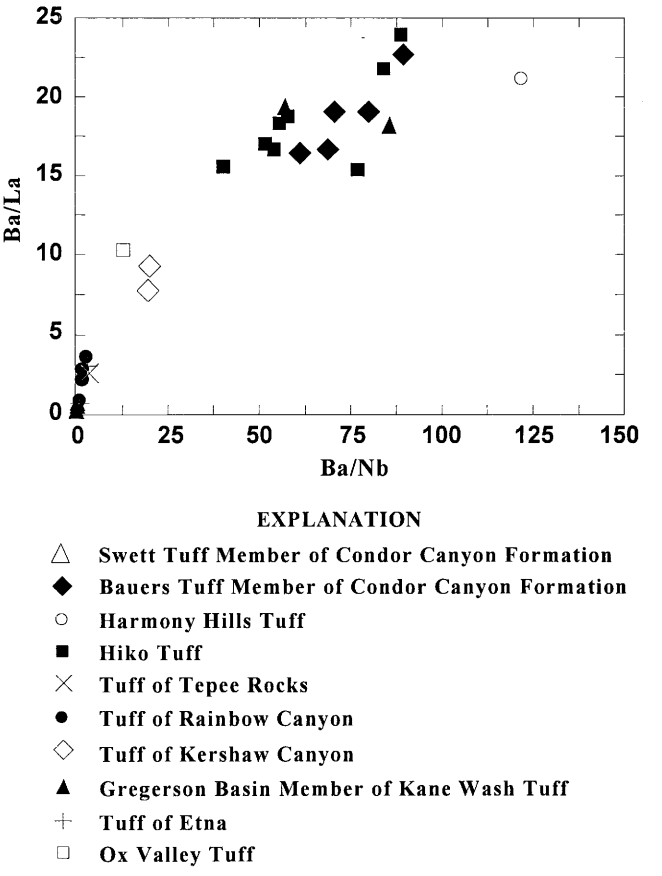

Figure 9. Ba/La versus Ba/Nb diagram for ash-flow tuffs in and near Caliente caldera complex.

have Zr/Nb less than 8. More silicic and locally altered samples of the tuffs of Rainbow Canyon and Kershaw Canyon have low Zr/Nb values (≈3), suggesting that Zr/Nb values did not change during alteration. The decrease in Zr enrichment relative to that of Nb in tuff of the Bauers, Swett, and Hiko also characterizes calc-alkaline rocks from the Chinati Mountains area, West Texas (Cameron and Cameron, 1986). Metaluminous granites, to which the majority of the ash-flow tuffs of the Caliente area are analogous, have similar Zr/Nb values (5–20). Davies and Macdonald (1987) attributed high Zr/Nb and high Rb/Zr (>3) in metaluminous granitic melts to the involvement of significant amounts of crustal material. Cameron and Cameron (1986) suggested that the decrease in Zr/Nb in Chinati Mountains rocks resulted from the fractionation of zircon, an accessory phase in those rocks.

The variability of Ba/La and Ba/Nb serves to distinguish Gregerson Basin Member, tuff of Rainbow Canyon, tuff of Kershaw Canyon, and Ox Valley Tuff from the remainder of the ash-flow tuffs (fig. 9). The tuff of Rainbow Canyon, Gregerson Basin Member, and tuff of Etna have low Ba/Nb and Ba/La values. The tuff of Kershaw Canyon and the Ox Valley Tuff have slightly higher values for both ratios. The remainder of our suite has high Ba/La (>15) and Ba/Nb (>39).

SPIDER DIAGRAMS

In this section we show spider diagrams (fig. 10) for ash-flow tuffs from the Caliente area. These diagrams provide a convenient way of comparing elemental abundances in volcanic rocks. Raw data are normalized to values of Thompson and others (1984), most of which are average chondritic abundances; normalization values for K, Rb, and P are not chondritic. In the spider diagrams, elements are arranged to produce a downward slope from left to right in the patterns of most igneous rocks. Gaps in the patterns appear where no elemental data exist, but allow for easy comparison between all the units.

In general, ash-flow tuffs from the Caliente area show elemental patterns similar to those of many silicic volcanic rocks in western North America. The patterns allow the samples to be separated into four distinct geochemical types: (1) Condor Canyon Formation, Harmony Hills Tuff, Hiko Tuff, tuff of Tepee Rocks, and tuff of Kershaw Canyon; (2) Ox Valley Tuff; (3) tuff of Rainbow Canyon; and (4) Gregerson Basin Member of the Kane Wash Tuff. Type 1 units are characterized by moderate negative Ba, Nb, Ta, Sr, P, and Ti anomalies. Our single sample of the Harmony Hills Tuff is distinguished from the other Type 1 units by the absence of

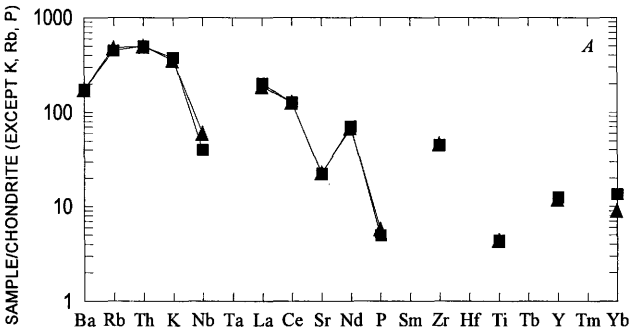
A
SAMPLE/CHONDRITE (EXCEPT K, Rb, P)
1000
100
10
1
Ba Rb Th K Nb Ta La Ce Sr Nd P Sm Zr Hf Ti Tb Y Tm Yb

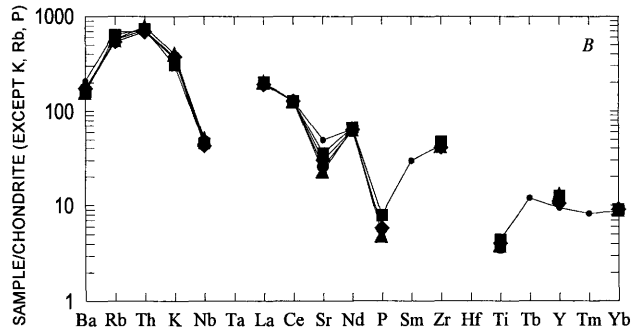
B
SAMPLE/CHONDRITE (EXCEPT K, Rb, P)
1000
100
10
1
Ba Rb Th K Nb Ta La Ce Sr Nd P Sm Zr Hf Ti Tb Y Tm Yb

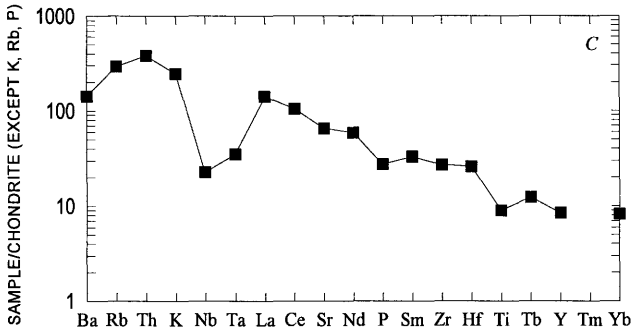
C
SAMPLE/CHONDRITE (EXCEPT K, Rb, P)
1000
100
10
1
Ba Rb Th K Nb Ta La Ce Sr Nd P Sm Zr Hf Ti Tb Y Tm Yb

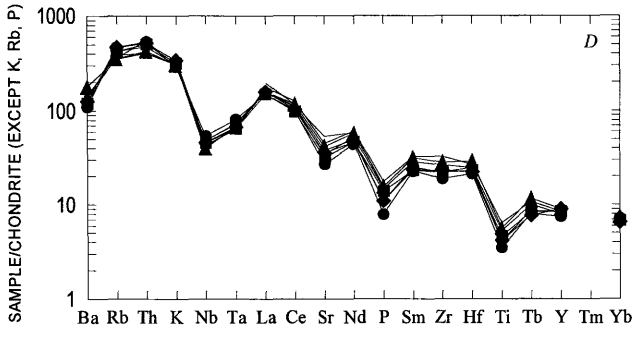
D
SAMPLE/CHONDRITE (EXCEPT K, Rb, P)
1000
100
10
1
Ba Rb Th K Nb Ta La Ce Sr Nd P Sm Zr Hf Ti Tb Y Tm Yb

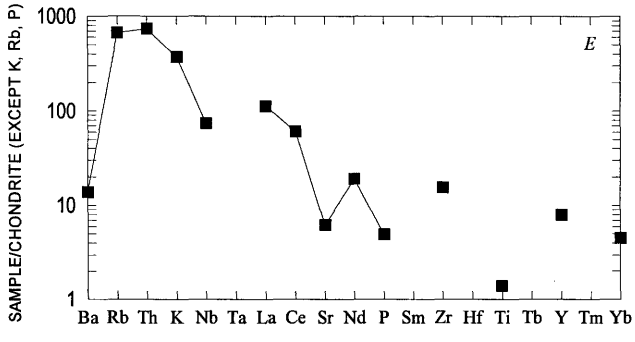
E
SAMPLE/CHONDRITE (EXCEPT K, Rb, P)
1000
100
10
1
Ba Rb Th K Nb Ta La Ce Sr Nd P Sm Zr Hf Ti Tb Y Tm Yb

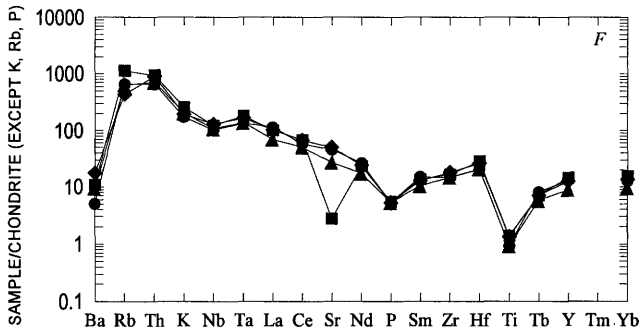
F
SAMPLE/CHONDRITE (EXCEPT K, Rb, P)
10000
1000
100
10
1
0.1
Ba Rb Th K Nb Ta La Ce Sr Nd P Sm Zr Hf Ti Tb Y Tm Yb

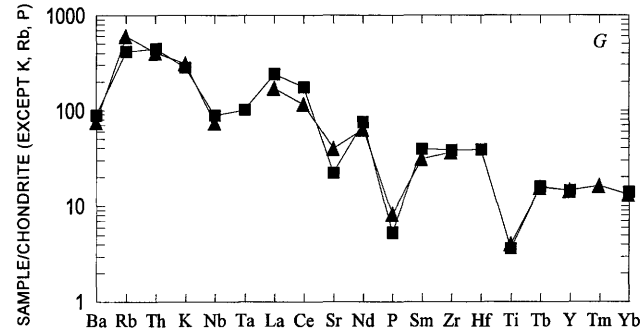
G
SAMPLE/CHONDRITE (EXCEPT K, Rb, P)
1000
100
10
1
Ba Rb Th K Nb Ta La Ce Sr Nd P Sm Zr Hf Ti Tb Y Tm Yb

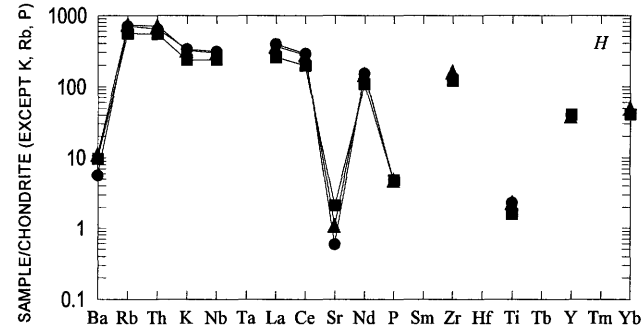
H
SAMPLE/CHONDRITE (EXCEPT K, Rb, P)
1000
100
10
1
0.1
Ba Rb Th K Nb Ta La Ce Sr Nd P Sm Zr Hf Ti Tb Y Tm Yb

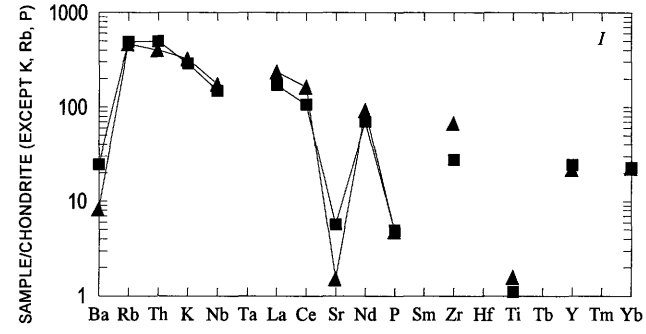
I
SAMPLE/CHONDRITE (EXCEPT K, Rb, P)
1000
100
10
1
Ba Rb Th K Nb Ta La Ce Sr Nd P Sm Zr Hf Ti Tb Y Tm Yb

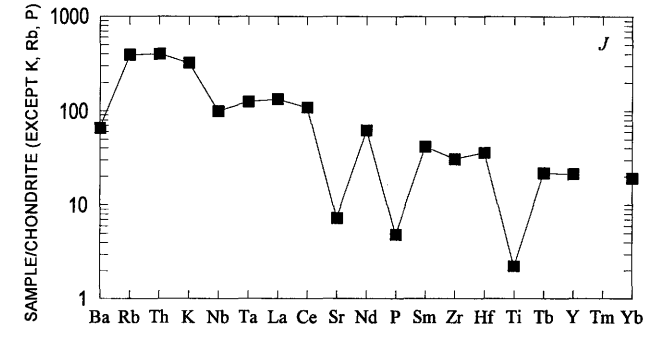
J
SAMPLE/CHONDRITE (EXCEPT K, Rb, P)
1000
100
10
1
Ba Rb Th K Nb Ta La Ce Sr Nd P Sm Zr Hf Ti Tb Y Tm Yb

a Sr anomaly. The single sample of the tuff of Tepee Rocks shows a much larger Ba anomaly than the other Type 1 units. The Ox Valley Tuff (Type 2) is distinctive in that Ba, Sr, and Ti anomalies tend to be larger, and Nb and Ta anomalies are slightly smaller than they are for Type 1 units. The tuff of Rainbow Canyon (Type 3) lacks many of the negative anomalies exhibited by Types 1 and 2. This unit shows a strong Ba and a moderate negative Ti anomaly but small or no anomalies at Nb, Ta, Sr, and only a small one at P. One sample of the tuff of Rainbow Canyon does show a moderate negative Sr anomaly. The Gregerson Basin Member and tuff of Etna have similar elemental patterns. They show large negative Ba and Sr anomalies, and slightly smaller negative P and Ti anomalies. These units lack the negative Nb anomalies of Type 1 units and have Ba and Sr anomalies that are significantly larger than the Ox Valley Tuff (Type 2). Type 4 units are distinguished from the tuff of Rainbow Canyon (Type 3) by large Sr and P anomalies.

The majority of the older units (Condor Canyon Formation to Hiko Tuff) show Type 1 chemical signatures. Post-Hiko Tuff units derived from the Caliente caldera complex tend to have larger negative Ba anomalies than the Hiko Tuff and pre-Hiko Tuff units. Although not derived from the Caliente caldera complex, the Gregerson Basin Member also shows a large negative Ba anomaly. The tuff of Kershaw Canyon and the Ox Valley Tuff show moderate negative Ba anomalies.

COMPARATIVE GEOCHEMISTRY

In this section we compare trace-element abundances of rocks from the Caliente area to those of silicic volcanic rocks from other volcanic fields, mostly those in the western Cordillera. We assume here that the compositions of tuffs from the Caliente area are similar to those of the magma systems from which they erupted. However, we realize that many of the analytical results are not strictly magmatic. Deviations from magmatic compositions, as we have already indicated, probably resulted from physical mixing of juvenile and xenolithic material and from postemplacement alteration.

A variety of chemical diagrams are available for discriminating volcanic rocks erupted in different tectonic environments. Although each type of diagram has been tested over a relatively large range of compositions and tectonic environments, none of the diagrams has been shown to work in all cases. Here we use diagrams proposed by Pearce and others (1984) for discriminating between collisional granite, volcanic-arc granite, within-plate granite, and ocean-ridge granite.

Ash-flow tuffs in the Caliente area show mostly volcanic-arc and within-plate granite signatures (fig. 11). The calc-alkaline (metaluminous to peraluminous) rocks have low total Y+Nb contents compared with the tholeiitic (peralkaline) Gregerson Basin Member. Data for the calc-alkaline units overlap with those for pumices and whole-rock samples of ash-flow tuffs from several volcanic terranes in the Cordillera of North and Central America, including samples of the 19–Ma metaluminous Peach Springs Tuff in northwest Arizona (L.D. Nealey, unpub. data, 1988), the 26.5–Ma peralkaline Amalia Tuff of the Latir volcanic field, New Mexico (Johnson and Lipman, 1988), tuffs in the Sierra Madre Occidental (Cameron and Hanson, 1982), Miocene Thirsty Canyon Tuff of the Black Mountain caldera, Nevada (Vogel and others, 1989), and the 11.6–Ma Rainier Mesa and 11.4–Ma Ammonia Tanks Members of the Timber Mountain Tuff, Nevada (Mills, 1991). Although the Gregerson Basin Member is demonstrably peralkaline, it is transitional between strongly peralkaline rhyolite like that of the Naivasha volcanic center in the Kenya rift (Macdonald and others, 1987) and the peralkaline Amalia Tuff in New Mexico (Johnson and Lipman, 1988; this report, fig. 11).

Although all the ash-flow tuffs erupted in a within-plate environment, their Y+Nb contents in the Pearce plot (fig. 11) suggest that the older units (Swett and Bauers Tuff Members, Harmony Hills Tuff, Hiko Tuff, and tuff of Tepee Rocks) erupted in a volcanic-arc setting. Younger units (tuff of Rainbow Canyon, tuff of Kershaw Canyon, Gregerson Basin Member, tuff of Etna, and Ox Valley Tuff), in contrast, tend to show signatures of within-plate granites. Similar trends have been identified in late Cenozoic ash-flow tuffs of the Mogollon-Datil volcanic field in New Mexico (W.E. Elston, oral commun., 1987).

SUMMARY AND CONCLUSIONS

Major compositional differences exist among ash-flow tuffs in the Caliente area. Rowley and others (this volume) have shown that the ash-flow tuffs can be distinguished *petrographically* into groups using relative proportions of phenocrysts and accessory minerals and *chemically* using minor element concentrations. We have further shown here that these groups can be distinguished into *petrochemical* assemblages using other geochemical data. The majority of the units derived from the Caliente caldera complex are calc-alkaline and metaluminous to peraluminous. The Gregerson Basin Member, which erupted from the nearby Kane Springs Wash caldera, shows tholeiitic affinities and is mildly peralkaline.

Figure 10 (facing page). Spider diagrams for ash-flow tuffs in and near Caliente caldera complex. Normalization values from Thompson and others (1984). *A*, Swett Tuff Member of Condor Canyon Formation; *B*, Bauers Tuff Member of Condor Canyon Formation; *C*, Harmony Hills Tuff; *D*, Hiko Tuff; *E*, tuff of Tepee Rocks; *F*, tuff of Rainbow Canyon; *G*, tuff of Kershaw Canyon; *H*, Gregerson Basin Member of Kane Wash Tuff; *I*, tuff of Etna; *J*, Ox Valley Tuff.

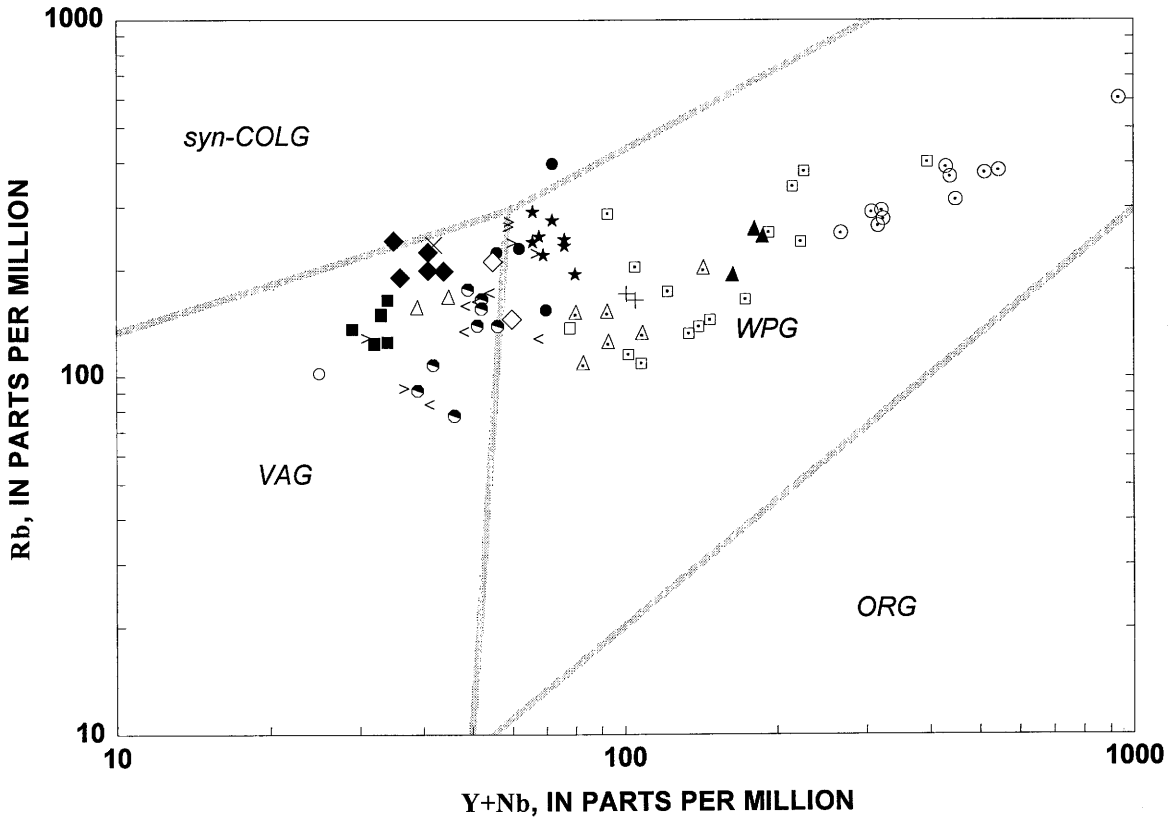

EXPLANATION

- △ Swett Tuff Member of Condor Canyon Formation
- ◆ Bauers Tuff Member of Condor Canyon Formation
- ○ Harmony Hills Tuff
- ■ Hiko Tuff
- × Tuff of Tepee Rocks
- ● Tuff of Rainbow Canyon
- ◇ Tuff of Kershaw Canyon
- ▲ Gregerson Basin Member of Kane Wash Tuff
- + Tuff of Etna
- □ Ox Valley Tuff
- ◬ Amalia Tuff
- ⊙ Naivasha Rhyolite
- ◓ Superstition Mountains Tuff
- > Timber Mountain Tuff
- < Sierra Madre Occidental tuff
- ★ Peach Springs Tuff
- ⊡ Thirsty Canyon Tuff

Figure 11. Rb versus Y+Nb variation for ash-flow tuffs in and near Caliente caldera complex, and selected rhyolites. Data for the Amalia Tuff from Johnson and Lipman (1988); Naivasha Rhyolite from Macdonald and others (1987); silicic rocks from the Superstition Mountains from L.D. Nealey (unpub. data, 1987); tuffs from Timber Mountain caldera from Mills (1991); tuff from the Sierra Madre Occidental from Cameron and Hanson (1982); Peach Springs Tuff from L.D. Nealey (unpub. data, 1988); and Thirsty Canyon Tuff of the Black Mountain caldera from Vogel and others (1989) shown for comparison. Tectonic fields from Pearce and others (1984): VAG, volcanic arc granite; syn-COLG, syncollisional granite; WPG, within-plate granite; ORG, oceanic island granite.

These two groups are easily distinguished using high-field-strength elements (Zr, Y, Nb) which show high concentrations in the Gregerson Basin Member.

Harmony Hill Tuff is the only andesite ash-flow tuff and probably was erupted from a source other than the Caliente caldera complex. It has high Ti and Sr that distinguish it from other units. The Hiko Tuff is distinguished from the Condor Canyon Formation by its lower total alkalies, Y, and Zr. The tuff of Rainbow Canyon is consistently the most altered unit in the Caliente area. It characteristically has high silica and low alkali contents compared with other ash-flow tuffs. The tuff of Kershaw Canyon is distinguished from the underlying tuff of Rainbow Canyon by lower silica and Al, and higher Ba contents. The tuff of Etna and Ox Valley Tuff are characterized by relatively low Ba and Sr compared with other calc-alkaline units.

Original composition of source magmas of ash-flow tuffs in the Caliente area was probably related to a combination of magmatic processes. Melting of intermediate-composition crustal material is likely to have been the ultimate origin of the older (23–17.8 Ma) calc-alkaline magmas. Different degrees of melting, different proportions of crustal materials, and crystal fractionation probably contributed to variations in the composition of these melts. Younger (16–12 Ma) high-silica magmas appear to have originated by variable amounts of crystal fractionation, probably combined with different amounts of crustal assimilation. The ultimate source of the younger magmas may have also been the crust.

Anomalous elemental concentrations in many of the younger high silica rhyolites are due to postemplacement weathering, vapor-phase crystallization, devitrification, and removal and deposition of ions by ground water. These processes are manifested in low K_2O and Na_2O, high SiO_2 and CaO contents, and anomalous trace-element abundances. Probably most of the secondary depletions and enrichments occurred in the glass component of tuffaceous materials.

Although our data are presently insufficient to confirm it, the wide variations in the composition of some units may be due in part to the tapping of compositionally zoned magma chambers, and to differences in the relative proportions of juvenile magma and xenolithic material. Our whole-rock compositions are likely to be intermediate in composition between the extremes of a dominant volume of preeruptive dacitic magma and a less voluminous rhyolitic component (Smith, 1979). Magmatic compositions are better represented by individual pumices, which we have not yet analyzed.

REFERENCES CITED

Baedecker, P.A., and McKown, D.M., 1987, Instrumental neutron activation analysis of geochemical samples, Chapter H, *in* Baedecker, P.A., ed., Methods for geochemical analysis: U.S. Geological Survey Bulletin 1770, p. H1–H14.

Best, M.G., Christiansen, E.H., and Blank, R.H., Jr., 1989, Oligocene caldera complex and calc-alkaline tuffs and lavas of the Indian Peak volcanic field, Nevada and Utah: Geological Society of America Bulletin, v. 101, p. 1076–1090.

Best, M.G., Christiansen, E.H., Deino, A.L., Grommé, C.S., McKee, E.H., and Noble, D.C., 1989, Excursion 3A—Eocene through Miocene volcanism in the Great Basin of the western United States: New Mexico Bureau of Mines and Mineral Resources Memoir 47, p. 91–133.

Cameron, K.L., and Cameron, Maryellen, 1986, Geochemistry of quartz-normative igneous rocks from the Chinati Mountains and Teringua areas, West Texas, a comparison with Cenozoic volcanic rocks from Chihuahua and Baja California Sur, Mexico: University of Texas Guidebook, Bureau of Economic Geology, v. 23, p. 143–163.

Cameron, K.L., and Hanson, G.N., 1982, Rare earth element evidence concerning the origin of voluminous mid-Tertiary rhyolitic ignimbrites and related rocks, Sierre Madre Occidental, Chihuahua, Mexico: Geochimica et Cosmochimica Acta, v. 46, p. 1489–1503.

Davies, G.R., and Macdonald, Ray, 1987, Crustal influences in the petrogenesis of the Naivasha basalt-comendite complex—Combined trace element and Sr-Nd-Pb isotope constraints: Journal of Petrology, v. 28, p. 1009–1031.

Ekren, E.B., Orkild, P.P., Sargent, K.A., and Dixon, G.L., 1977, Geologic map of Tertiary rocks, Lincoln County, Nevada: U.S. Geological Survey Miscellaneous Investigations Series Map I–1041, scale 1:250,000.

Elston, W.E., and Bornhorst, T.J., 1979, The Rio Grande rift in context of regional post–40 m.y. volcanism and tectonic events, *in* Riecker, R.E., ed., Rio Grande Rift—Tectonics and magmatism: American Geophysical Union, p. 416–438.

Johnson, C.M., and Lipman, P.W., 1988, Origin of metaluminous and alkaline volcanic rocks of the Latir volcanic field, northern Rio Grande rift, New Mexico: Contributions to Mineralogy and Petrology, v. 100, p. 107–128.

Johnson, R.G., and King, B.-S., 1987, Energy-dispersive X-ray fluorescence spectrometry, Chapter F *in* Baedecker, P.A., ed., Methods for geochemical analysis: U.S. Geological Survey Bulletin 1770, p. F1–F5.

Lichte, F.E., Golightly, D.W., and Lamothe, P.J., 1987, Inductively coupled plasma atomic emission spectroscopy, Chapter B *in* Baedecker, P.A., ed., Methods for geochemical analysis: U.S. Geological Survey Bulletin 1770, p. B1–B10.

Macdonald, Ray, Davies, G.R., Bliss, C.M., Leat, P.T., Bailey, D.K., and Smith, R.L., 1987, Geochemistry of high-silica peralkaline rhyolites, Naivasha, Kenya Rift Valley: Journal of Petrology, v. 28, p. 979–1008.

Mammerickx, Jacqueline, and Klitgord, K.D., 1982, Northern East Pacific Rise—Evolution from 25 m.y. to the present: Journal of Geophysical Research, v. 87, p. 6751–6759.

Mills, J.G., Jr., 1991, The Timber Mountain Tuff, southwestern Nevada volcanic field; Geochemistry, mineralogy and petrogenesis: East Lansing, Mich., Michigan State University Ph. D. dissertation, 332 p.

Miyashiro, Akiho, 1974, Volcanic rock series in island arcs and active continental margins: American Journal of Science, v. 274, p. 321–355.

Noble, D.C., and McKee, E.H., 1972, Description and K-Ar ages of volcanic units of the Caliente volcanic field, Lincoln County, Nevada, and Washington County, Utah: Isochron/West, no. 5, p. 17–24.

Noble, D.C., McKee, E.H., Hedge, C.E., and Blank, H.R., 1968, Reconnaissance of the Caliente depression, Lincoln County, Nevada [abs.]: Geological Society of America Special Paper 115, p. 435–436.

Novak, S.W., 1984, Eruptive history of the rhyolitic Kane Wash volcanic center, Nevada: Journal of Geophysical Research, v. 89, p. 8603–8615.

Novak, S.W., and Mahood, G.A., 1986, Rise and fall of a basalt-trachyte-rhyolite magma system at the Kane Springs Wash caldera, Nevada: Contributions to Mineralogy and Petrology, v. 94, p. 352–373.

Pearce, J.A., Harris, N.B.W., and Tindle, A.G., 1984, Trace element discrimination diagrams for the tectonic interpretation of granitic rocks: Journal of Petrology, v. 25, p. 956–983.

Peccerillo, A., and Taylor, S.R., 1976, Geochemistry of Eocene calc-alkaline volcanic rocks from the Kastamonu area, Northern Turkey: Contributions to Mineralogy and Petrology, v. 58, p. 63–81.

Rowley, P.D., Anderson, R.E., Snee, L.W., and Mehnert, H.H., 1990, Geology and structural setting of the western Caliente caldera complex, Lincoln County, Nevada: Geological Society of America Abstracts with Programs, v. 22, no. 3, p. 79.

Rowley, P.D., and Siders, M.A., 1988, Miocene calderas of the Caliente caldera complex, Nevada-Utah: Eos, v. 69, no. 44, p. 1508.

Rowley, P.D., Snee, L.W., Mehnert, H.H., Anderson, R.E., Axen, G.J., Burke, K.J., Simonds, F.W., Shroba, R.R., and Olmore, S.D., 1992, Structural setting of the Chief Mining District, eastern Chief Range, Lincoln County, Nevada, Chapter H *in* Thorman, C.W., ed., Application of structural geology to mineral and energy resources of the central region: U.S. Geological Survey Bulletin 2012, p. H1–H17.

Siders, M.A., 1991, Geologic map of the Mount Escalante quadrangle, Iron County, Utah: Utah Geological and Mineral Survey Map 131, 9 p., scale 1:24,000.

Smith, R.L., 1979, Ash flow magmatism, *in* Chapin, C.E., and Elston, W.E., eds., Ash flow tuffs: Geological Society of America Special Paper 180, p. 5–27.

Taggart, J.E., Lindsay, J.R., Scott, B.A., Vivit, D.V., Bartel, A.J., and Stewart, K.C., 1987, Analysis of geologic materials by wavelength-dispersive X-ray fluorescence spectrometry, Chapter E *in* Baedecker, P.A., ed., Methods for geochemical analysis: U.S. Geological Survey Bulletin 1770, p. E1–E19.

Thompson, R.N., Morrison, M.A., Henry, G.L., and Parry, S.J., 1984, An assessment of the relative roles of crust and mantle in magma genesis—An elemental approach: Philosophical Transactions of the Royal Society of London, v. A310, p. 549–590.

Vogel, T.A., Noble, D.C., and Younker, L.W., 1989, Evolution of chemically zoned magma body; Black Mountain volcanic center, southwestern Nevada: Journal of Geophysical Research, v. 94, p. 6041–6058.

Ward, P.L., 1991, On plate tectonics and the geologic evolution of southwestern North America: Journal of Geophysical Research, v. 96, p. 12479–12496.

Wark, D.A., Kempter, K.A., and McDowell, F.W., 1990, Evolution of waning, subduction-related magmatism, northern Sierra Madre Occidental: Geological Society of America Bulletin, v. 102, p. 1555–1564.

Williams, P.L., 1967, Stratigraphy and petrography of the Quichapa Group, southwestern Utah and southeastern Nevada: Seattle, Wash., University of Washington Ph. D. dissertation, 182 p.

Strontium and Neodymium Isotopic Survey of Ash-Flow Tuffs and Related Rocks from the Caliente Caldera Complex, Southeastern Nevada and Southwestern Utah

By Daniel M. Unruh, L. David Nealey, Peter D. Rowley, Lawrence W. Snee, Harald H. Mehnert, *and* R. Ernest Anderson

GEOLOGIC STUDIES IN THE BASIN AND RANGE–COLORADO PLATEAU TRANSITION IN SOUTHEASTERN NEVADA, SOUTHWESTERN UTAH, AND NORTHWESTERN ARIZONA, 1992

U.S. GEOLOGICAL SURVEY BULLETIN 2056–D

UNITED STATES GOVERNMENT PRINTING OFFICE, WASHINGTON : 1995

CONTENTS

FIGURES

TABLES

Strontium and Neodymium Isotopic Survey of Ash-Flow Tuffs and Related Rocks from the Caliente Caldera Complex, Southeastern Nevada and Southwestern Utah

By Daniel M. Unruh, L. David Nealey, Peter D. Rowley, Lawrence W. Snee, Harald H. Mehnert, *and* R. Ernest Anderson

ABSTRACT

Intermediate to silicic intrusive rocks, lava flows, and tuffs of the Caliente caldera complex exhibit isotopic features common among Cenozoic caldera complexes in the western United States. Correlated chemical and isotopic trends are observed among the samples as a group, but are more easily recognized among samples related to a single caldera-forming event. As silica contents increase, strontium and neodymium contents decrease, $^{87}Sr/^{86}Sr$ increases, and $^{143}Nd/^{144}Nd$ decreases. These trends suggest that the silicic magmas were generated by fractionation of mafic (andesitic or perhaps basaltic) parental magmas open to modification by crustal contamination or assimilation. However, crustal interaction appears to be subordinate to fractional crystallization in the generation of the silicic magmas.

Similar correlated variations exist among samples of Hiko Tuff (Delamar caldera) and a related volcanic dome, which suggests that the subvolcanic magma chamber was chemically and isotopically zoned as a result of open system modification of the magma by crustal interaction. Calculations based on neodymium contents and isotopic ratios suggest that high-silica rhyolite (75 percent SiO_2) could be generated from low-silica rhyolite (70 percent SiO_2) by fractional crystallization and assimilation of 5–15 percent wall rock. The low-silica rhyolite can be related to an andesitic parent magma (represented by the lava flows of Buckboard Spring) by fractional crystallization and assimilation of 10–30 percent crustal material, depending upon the particular model chosen. The calculations also suggest that crustal interaction became less important as magmas evolved to more silicic compositions.

Initial $^{143}Nd/^{144}Nd$ values for the parental magmas of the Caliente complex increased from $\varepsilon Nd \approx -10$ at 21–23 Ma, to –8 at 17–19 Ma, to –8 to –5 at 14–15 Ma. Similar temporally related increases in εNd have been observed in the Timber Mountain–Oasis Valley caldera complex in southern Nevada and the central caldera complex of the San Juan volcanic field in Colorado. The apparent temporal evolution of the parental magmas may reflect progressive intrusion of mantle-derived magmas into the lower crust, resulting in a progressive increase in εNd at site of melt-generation near the crust/mantle boundary. Alternatively, the increase in εNd may reflect variations within mantle-derived magmas caused by progressive erosion of lithospheric mantle by upwelling asthenospheric magma.

INTRODUCTION

The Cenozoic Caliente caldera complex, one of the largest caldera complexes in the western United States, is centered in southeastern Nevada southeast of the town of Caliente, Nev. (fig. 1). The complex is intermediate in size and age between the larger Indian Peak caldera complex (27–32 Ma; Best, Christiansen, and Blank, 1989) to the north and the Kane Springs Wash caldera (13–16 Ma; Novak, 1984) to the southwest. The southward progression of Cenozoic nonbasaltic volcanism observed in this area is common throughout the Great Basin. (See, for example, Farmer and others, 1989.)

The Caliente complex includes at least four recently named clustered calderas (Rowley and Siders, 1988) that range in age from about 23 to 15 Ma. The oldest recognized caldera, Clover Creek, formed at about 22.8 Ma (Best, Christiansen, and others, 1989) with the eruption of the Bauers Tuff Member of the Condor Canyon Formation in the northern part of the complex (fig. 2). The Delamar caldera in the western part of the complex formed during eruption of Hiko Tuff at 18.6–18.2 Ma (Taylor and others, 1989; L.W. Snee, unpub. data, 1993). At 16 Ma the Pine Creek caldera formed in the eastern part of the complex (Siders, 1991), and at 15.6 Ma (L.W. Snee, unpub. data, 1991) the Buckboard Canyon caldera formed in the western part of the complex, producing the tuff of Rainbow Canyon.

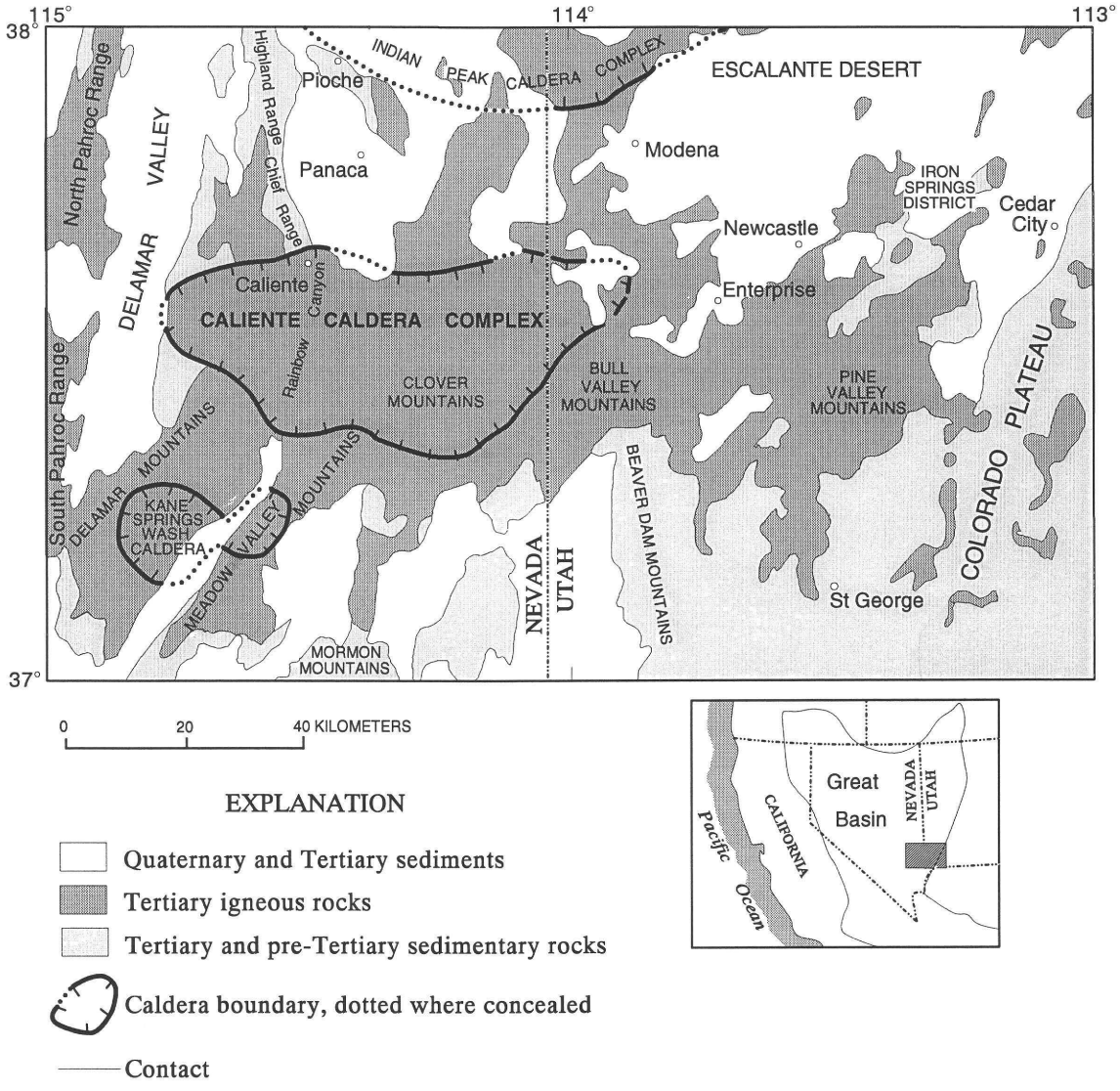

Figure 1. Location map and general geologic and geographic features for western portion of Caliente caldera complex and vicinity, Nevada and Utah (from Rowley and others, this volume).

The Kane Springs Wash caldera formed at 14.7–14.4 Ma (L.W. Snee, unpub. data, 1991), producing the Grapevine Spring and Gregerson Basin Members of the Kane Wash Tuff (Novak, 1984; Scott and others, 1993). In the central part of the Caliente complex, these two members of the Kane Wash Tuff form thin, densely welded, peralkaline beds that are interlayered within upper parts of the tuff of Kershaw Canyon. The tuff of Kershaw Canyon is overlain by the tuff of Etna, which was emplaced between 14.4 Ma and 13.8 Ma, based on its stratigraphic position between the underlying upper unit of the Gregerson Basin Member and an ash-flow tuff bed in overlying sedimentary rocks (H.H. Mehnert, unpub. data, 1990). The tuffs of Kershaw Canyon and Etna are thought to have originated from the Caliente complex (Rowley and others, 1991; Rowley and others, this volume). The locations of their sources have not as yet been identified with certainty, although recent mapping by P.D. Rowley suggests that the tuff of Etna originated from just south of the Delamar caldera. The last major ash-flow eruption in the Caliente area produced the Ox Valley Tuff at between 12.6 and 11.4 Ma (H.H. Mehnert, unpub. data, 1990).

Volcanic rocks of the Caliente complex are predominantly rhyolite ash-flow tuffs. However, temporally associated, intermediate to silicic lava flows, dikes, and plutonic rocks are also present. Postcaldera volcanic rocks are predominantly basalt and basaltic andesite, as is common among Cenozoic caldera complexes in the western United States. (See, for example, Best, Christiansen, and others, 1989.) For a more detailed discussion of the geologic setting of the Caliente complex, the reader is referred to companion reports in this volume by Nealey and others and Rowley and others, as well as to Rowley and others (1991), Rowley and

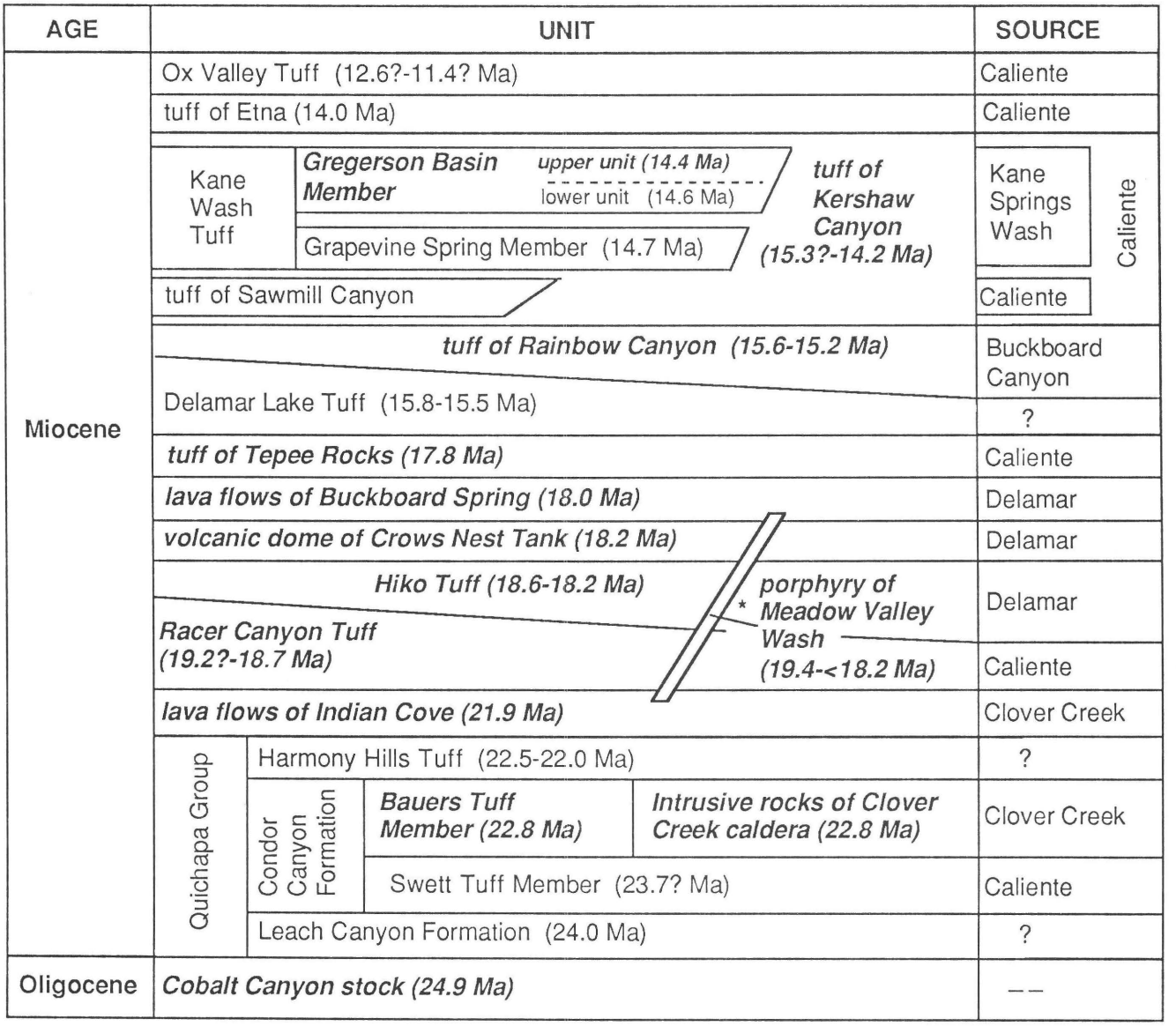

Figure 2. Partial stratigraphic column of ash-flow tuffs and related rocks in and near Caliente caldera complex. Rock units analyzed in this study are shown in bold type. Those units whose source is simply listed as "Caliente" were derived from within Caliente caldera complex, but their relationship to specific calderas within the complex is presently unknown. Sources with unknown locations are indicated by queries. A dash indicates a local source.

others (1992), Rowley and Shroba (1991), and Swadley and Rowley (1992).

In this report we present results from a preliminary Nd and Sr isotopic survey of the Caliente caldera complex. The objectives of this study are to determine the isotopic signatures of the various units and the relationships of these signatures to compositional, spatial, and temporal variations within the complex. This study represents one aspect of an integrated mapping, geochronologic, and geochemical investigation of the Caliente caldera complex done under the auspices of the USGS Basin and Range–Colorado Plateau Transition (BARCO) Study Unit (see the introduction to this volume).

DESCRIPTION OF LITHOLOGIC UNITS

Whole-rock tuff samples from three of the four named calderas in the Caliente complex (the Pine Creek caldera was not included) as well as samples from other major tuffs of the

complex were selected for analyses. These units are described elsewhere in this volume by Rowley and others and by Nealey and others. In addition, our study included samples from three intrusive units—the Cobalt Canyon stock, intracaldera intrusive rocks of the Clover Creek caldera, and the porphyry of Meadow Valley Wash; two andesitic flows—lava flows of Indian Cove and the lava flows of Buckboard Spring; and a rhyolite dome—the volcanic dome of Crows Nest Tank. A brief description of these units follows, because these units were not treated in detail by Nealey and others and by Rowley and others. Major-element chemistry (recalculated to 100 percent) of the samples analyzed is given in table 1.

COBALT CANYON STOCK

The Cobalt Canyon stock consists of discordant dikes and plugs exposed on the southeast side of the Chief Range, Nev. (fig. 1) that are thought to be related to a large stock at depth (Rowley and others, 1991). The rocks are primarily porphyritic quartz monzonite, although compositions as mafic as monzogabbro are found locally. Phenocrysts compose 35–80 percent of the rock and consist of plagioclase (65 percent of the total phenocrysts), biotite (0–10 percent), clinopyroxene (1–25 percent), orthopyroxene (1–10 percent), Fe-Ti oxides (5 percent), and occasional trace amounts of hornblende. The groundmass is holocrystalline and consists of sanidine, quartz, plagioclase, and minor clinopyroxene, biotite, and Fe-Ti oxides. The unit has been dated at 24.9 Ma (Rowley and others, 1992).

INTRUSIVE ROCKS OF CLOVER CREEK CALDERA

A dikelike mass, interpreted to be the upper part of a shallow intracaldera intrusive body of the Clover Creek caldera, is exposed on the east side of the canyon of Meadow Valley Wash about 1 km north of Caliente. The rock is a rhyolite porphyry that resembles the Bauers Tuff Member of the Condor Canyon Formation, except that phenocrysts are larger and generally unbroken. Phenocrysts make up 15–35 percent of the rock and consist of sanidine (3–40 percent), plagioclase (50–90 percent), biotite (5 percent), and Fe-Ti oxides (1 percent). A preliminary $^{40}Ar/^{39}Ar$ age of 22.8 Ma (L.W. Snee, unpub. data, 1991) has been obtained from this unit.

LAVA FLOWS OF INDIAN COVE

Andesitic and dacitic lava flows are found in the vicinity of Indian Cove, near the northern margin of the Caliente caldera complex, and about 4 km north of the town of Caliente (Rowley and Shroba, 1991). These flows are probably the remnants of volcanic domes and may represent the last stages of volcanic activity related to the Clover Creek caldera. A sample of one of the flows has been dated by the $^{40}Ar/^{39}Ar$ method at 21.9 Ma (Snee and others, 1990; Rowley and others, 1992).

Lava flows of Indian Cove show a wide compositional range. They contain 5–45 percent phenocrysts consisting of plagioclase (40–80 percent), clinopyroxene (5–60 percent),

Table 1. Major-element chemistry for selected samples from Caliente caldera complex.

[In weight percent, recalculated to 100 percent on a volatile-free basis. Analyses performed by XRF at the U.S. Geological Survey, Denver, CO 80225]

SAMPLE[1]	89-854	89-530	87-1194	88-382	88-486B	88-1271	87-786	87-997
SiO_2	68.24	73.37	59.51	66.87	70.38	67.05	74.65	55.86
Al_2O_3	13.79	14.33	15.58	13.33	14.22	15.68	13.42	15.48
Fe_2O_3	1.97	1.43	2.51	1.99	1.94	2.23	1.38	2.48
FeO	3.10	0.13	5.82	1.33	1.75	2.54	0.41	6.62
MgO	1.70	0.34	3.08	1.31	1.28	1.92	0.48	5.29
CaO	2.97	0.96	5.36	6.82	2.35	2.49	1.34	6.68
Na_2O	3.12	3.19	3.09	2.76	3.32	3.37	3.23	3.33
K_2O	4.43	6.15	3.58	4.97	4.12	4.23	4.76	2.67
TiO_2	0.49	0.03	1.01	0.43	0.42	0.7	0.22	0.99
P_2O_5	0.15	0.05	0.39	0.15	0.15	0.32	0.07	0.49
MnO	0.05	0.02	0.08	0.04	0.06	0.07	0.04	0.11

[1] 89-854, Cobalt Canyon Stock
89-530, intrusive rocks of Clover Creek caldera.
87-1194, lava flows of Indian Cove.
88-382, 88-486B, 88-1271, porphyry of Meadow Valley Wash.
87-786, volcanic dome of Crows Nest Tank.
87-997, lava flows of Buckboard Spring.

orthopyroxene (0–40 percent), biotite (0–10 percent), sanidine (0–7 percent), hornblende (0–5 percent), and Fe-Ti oxides (2–10 percent) in a glassy groundmass. Some flows contain black basal vitrophyres.

PORPHYRY OF MEADOW VALLEY WASH

Several exposures of coarse-grained, hypabyssal plugs and dikes occur along the traces of major fault zones in and near the Caliente caldera complex, from north of Delamar southwest of the Caliente complex to Panaca Summit about 40 km northeast of the town of Caliente. The rocks are characterized by large (>1.5 cm) abundant phenocrysts of feldspar. These scattered exposures have been correlated by Rowley and Shroba (1991) and Rowley and others (1991) and informally named the porphyry of Meadow Valley Wash for exposures in the canyon of the same name.

The rocks range in composition from dacite to rhyolite. Phenocrysts constitute 35–50 percent of the rock and consist of plagioclase (60–90 percent), quartz (0–10 percent), sanidine (0–10 percent), biotite (7 percent), hornblende (1–10 percent), clinopyroxene (1–10 percent), Fe-Ti oxides (3 percent), and local trace amounts of orthopyroxene in a glassy groundmass.

Analyses of sanidine and hornblende from a sample collected from within the Clover Creek caldera gave an average $^{40}Ar/^{39}Ar$ age of 19.4 Ma (Snee and others, 1990; Rowley and others, 1992). However, dikes also intrude Hiko Tuff in some areas, and therefore some of these dikes must be younger than 18.6–18.2 Ma. A tentative age of 18.5 Ma has been assigned to those samples that postdate Hiko Tuff. The porphyry of Meadow Valley Wash is a key unit because its emplacement coincides with the major episode of extension in the Caliente area (Rowley and others, 1992).

LAVA FLOWS OF BUCKBOARD SPRING

A distinctive fine-grained basaltic andesite lava flow is found near Buckboard Spring in Buckboard Canyon, about 11 km west of the town of Caliente. The rock contains a disequilibrium assemblage of 10–15 percent megacrysts of quartz (5–25 percent), sanidine (5–10 percent), plagioclase (40 percent), hornblende (2 percent), orthopyroxene (10–15 percent), Fe-Ti oxides (1–3 percent), and olivine (20 percent). Large megacrysts of quartz, sanidine, plagioclase, and hornblende are altered or have reaction rims that indicate that they were not in equilibrium with the melt which crystallized to form the rest of the rock.

The flow rests on intracaldera Hiko Tuff, so it probably marks the cessation of volcanism and consolidation of the magma chamber of the Delamar caldera. One sample from the flow has been dated by the $^{40}Ar/^{39}Ar$ method at 18.0 Ma (L.W. Snee, unpub. data, 1991).

VOLCANIC DOME OF CROWS NEST TANK

A rhyolite dome, herein called the volcanic dome of Crows Nest Tank for exposures at the north edge of the Delamar caldera, occurs 9 km west of Caliente. Phenocrysts make up about 35 percent of the rock and consist of quartz (25 percent), sanidine (30 percent), plagioclase (40 percent), biotite (5 percent), hornblende (1 percent), and Fe-Ti oxides (1 percent).

The rock is lithologically similar to Hiko Tuff, although slightly more silicic, and may have tapped the same magma chamber from which Hiko Tuff erupted. The dome has received two preliminary concordant $^{40}Ar/^{39}Ar$ ages that average 18.2 Ma (L.W. Snee, unpub. data, 1991).

ANALYTICAL PROCEDURES

Concentrations of Rb, Sr, Sm, and Nd and isotopic compositions of Sr and Nd were determined by isotope dilution–mass spectrometry using the techniques described by Stille and others (1986). Samples analyzed were powdered splits of the same samples used for major- and trace-element analyses (table 1, and Nealey and others, this volume; Rowley and others, this volume). For a detailed discussion of sample selection and preparation procedures, the reader is referred to the companion report by Nealey and others in this volume. Isotopic measurements of Sr and Nd were obtained on a VG 54R single-collector mass spectrometer. $^{87}Sr/^{86}Sr$ values were normalized to $^{88}Sr/^{86}Sr=0.1194$, and $^{143}Nd/^{144}Nd$ values were normalized to $^{146}Nd/^{144}Nd=0.7219$. Replicate analyses of the NBS Sr standard SRM–987 gave a mean $^{87}Sr/^{86}Sr=0.710273\pm0.000012$ (95 percent C.I.), and replicate analyses of the La Jolla Nd standard produced a mean $^{143}Nd/^{144}Nd=0.511858\pm0.000008$.

MAJOR-ELEMENT CHEMISTRY

Samples chosen for this study represent a suite of intrusive, extrusive, and pyroclastic units that range in composition from andesite to high-silica rhyolite. Caliente complex samples analyzed in this study are all metaluminous to weakly peraluminous. The sample from the upper unit of the Gregerson Basin Member of the Kane Wash Tuff is mildly peralkaline as are samples from other units of the Grapevine Spring and Gregerson Basin Members (units V2 and V3 of Novak, 1985; and see Harding and others, this volume; Rowley and others, this volume). This sample also shows the distinctive trace-element characteristics exhibited by other samples of Kane Wash Tuff (low Sr, Ba; high Zr; Novak and Mahood, 1986; Nealey and others, this volume).

Major-element data for Caliente complex samples analyzed in this study are given in table 1 (recalculated to 100

percent) and are shown on potassium vs. silica and total alkalies vs. silica variation diagrams in figure 3. (For a more complete data set, see Nealey and others, and Rowley and others; this volume.) In the notation of Peccerillo and Taylor (1976), samples range from high-K andesite to high-K rhyolite with K_2O contents that range from about 3 percent to more than 5 percent as SiO_2 ranges from 56 to 76 percent. The two mafic flows analyzed, Indian Cove and Buckboard Spring, are both andesites with 56 percent and 59 percent silica, respectively. The sample of the Cobalt Canyon stock has a quartz monzonite composition, and those of the porphyry of Meadow Valley Wash have dacitic compositions. The intrusive rocks of Clover Creek caldera, the volcanic dome of Crows Nest Tank, and all tuffs analyzed in this study are rhyolites.

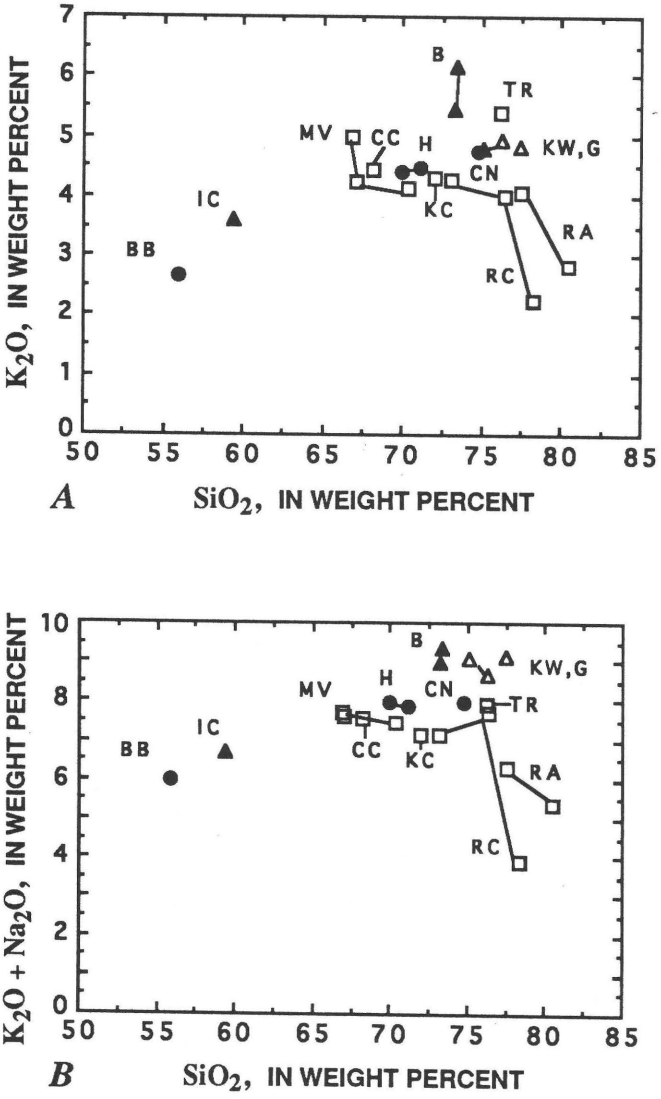

Figure 3. Variation diagrams for *A*, potassium and *B*, total alkalies vs. silica for Caliente samples analyzed in this study. For a more complete data set see Nealey and others and Rowley and others, this volume. CC, Cobalt Canyon stock; B, Bauers Tuff Member, Condor Canyon Formation (includes the intrusive rocks of the Clover Creek caldera); IC, lava flows of Indian Cove; MV, porphyry of Meadow Valley Wash; H, Hiko Tuff; CN, volcanic dome of Crows Nest Tank; RA, tuff of Rainbow Canyon; RC, Racer Canyon Tuff; BB, lava flows of Buckboard Spring; TR, tuff of Tepee Rocks; KC, tuff of Kershaw Canyon; G, Gregerson Basin Member of Kane Wash Tuff; KW, Kane Wash Tuff (from Novak, 1985). Open triangle, sample related to the Kane Springs Wash caldera. Solid circle, solid triangle, samples related to the Delamar caldera and Clover Creek caldera (Caliente caldera complex), respectively. Remaining samples from the Caliente caldera complex are shown by open squares. Samples from the same unit are connected by tie lines.

Some samples of the tuff of Rainbow Canyon and the Racer Canyon Tuff show anomalously high silica and low alkali contents. Nealey and others (this volume) attributed the high recalculated silica and low alkali contents to postemplacement alteration of matrix glass. Samples from the tuff of Rainbow Canyon are commonly altered. The effects of alteration of samples from these two tuffs are also observed in the Sr contents and Sr isotopic data discussed in the next section.

ANALYTICAL RESULTS

Concentrations of Rb, Sr, Sm, and Nd and $^{87}Sr/^{86}Sr$ and $^{143}Nd/^{144}Nd$ for selected Caliente complex samples are shown in table 2. Both measured and age-corrected (initial) Sr and Nd isotopic values are given in table 2, but only the age-corrected values are shown in the subsequent illustrations. However, the age corrections to the Nd data seldom exceed the analytical uncertainties. Initial Nd isotopic data are presented as both the actual ratios and using the conventional εNd notation (DePaolo and Wasserburg, 1976).

STRONTIUM AND NEODYMIUM CONCENTRATIONS

Concentrations of Sr and Nd are summarized as a function of silica content in figure 4 (data from table 2 and from Nealey and others, this volume). Strontium concentrations, in general, exhibit a strong negative correlation with silica content, and vary by more than an order of magnitude (820 ppm in the lava flows of Buckboard Spring to 64 ppm in the tuff of Tepee Rocks, fig. 4*A*) as silica varies from about 56 to 76 percent. This type of correlation is common among differentiation series and probably reflects the fractionation of feldspar (plagioclase or sanidine) into which Sr is strongly partitioned (D_{Sr}=4.5–7.3 and 7–33 for sanidine and plagioclase, respectively, in silicic rocks; for example, Nash and Crecraft, 1985).

Exceptions to the overall trend of the Sr data are found among samples from the tuff of Rainbow Canyon and the Racer Canyon Tuff. These samples show anomalously high Sr contents and are all apparently altered, as shown by the

Table 2. Rb/Sr and Sm/Nd data for selected samples from Caliente caldera complex and Kane Springs Wash caldera.

Sample No.	Rock unit	Age[1] in Ma	SiO_2	Rb ppm	Sr ppm	Sm ppm	Nd ppm	$^{87}Rb/^{86}Sr$	$^{87}Sr/^{86}Sr$	$^{87}Sr/^{86}Sr_I$ [2]	$^{147}Sm/^{144}Nd$	$^{143}Nd/^{144}Nd$	$^{143}Nd/^{144}Nd_I$ [2]	εNd_I
KANE SPRINGS WASH CALDERA:														
87-580A	Gregerson Basin Mbr.	14.4	77.5	228.6	15.44	17.15	95.96	42.86 ± 0.50	0.717654 ± 21	0.709133 ± 102	0.1079 ± 1	0.512350 ± 14	0.512340 ± 14	-5.4
Do	do			232.5	15.50	17.29	97.30	43.42 ± 0.50	0.717687 ± 44	0.709054 ± 109	0.1073 ± 1	0.512364 ± 14	0.512354 ± 14	-5.2
CALIENTE CALDERA COMPLEX:														
89-1097F	Tuff of Kershaw Canyon	(14.2)	72.0	169.3	273.00	12.23	59.34	1.794 ± 0.021	0.708626 ± 20	0.708264 ± 21	0.1244 ± 1	0.512219 ± 15	0.512207 ± 15	-8.0
Do	do			166.7	286.60	--	--	1.682 ± 0.028	0.708588 ± 20	0.708249 ± 21	--	0.512207 ± 12	--	
88-1264	Tuff of Rainbow Canyon, sanidine	15.6	77.5	52.5	64.50	--	--	2.354 ± 0.040	0.708027 ± 21	0.707505 ± 23	--	--	--	
88-226A	Tuff of Rainbow Canyon	15.6	80.5	138.5	514.20	2.40	14.19	0.780 ± 0.009	0.711752 ± 30	0.711579 ± 30	0.1020 ± 1	0.512163 ± 11	0.512153 ± 11	-9.0
88-1268	Tuff of Tepee Rocks	17.8	76.2	223.9	63.75	1.58	12.04	10.160 ± 0.120	0.710036 ± 19	0.707648 ± 36	0.0796 ± 1	0.512090 ± 15	0.512081 ± 15	-10.4
88-1271	porphyry of Meadow Valley W.	(18.5)	67.1	137.3	582.40	9.40	48.56	0.682 ± 0.016	0.707218 ± 20	0.707039 ± 20	0.1168 ± 5	0.512183 ± 14	0.512169 ± 14	-8.6
Do	do			137.3	587.70	--	--	0.686 ± 0.008	0.707301 ± 27	0.707121 ± 27	--	--	--	
88-486B	porphyry of Meadow Valley W.	(18.5)	70.4	164.6	352.30	6.93	36.47	1.351 ± 0.049	0.707209 ± 20	0.706854 ± 24	0.1147 ± 3	0.512106 ± 15	0.512092 ± 15	-10.2
88-382	porphyry of Meadow Valley W.	19.4	66.9	206.5	346.80	6.64	34.00	1.722 ± 0.059	0.707207 ± 21	0.706735 ± 27	0.1179 ± 1	0.512055 ± 14	0.512040 ± 14	-11.1
87-697 A	Racer Canyon Tuff	18.8	76.4	129.8	117.10	3.86	20.52	3.208 ± 0.035	0.708750 ± 20	0.707893 ± 22	0.1137 ± 1	0.512156 ± 14	0.512142 ± 14	-9.2
87-697 P	Racer Canyon Tuff	18.8	73.1	129.9	443.50	5.06	29.67	0.847 ± 0.009	0.707741 ± 34	0.707515 ± 34	0.1030 ± 1	0.512095 ± 14	0.512082 ± 14	-10.3
Do	do			131.4	440.40	5.18	30.35	0.862 ± 0.009	0.707735 ± 20	0.707505 ± 20	0.1031 ± 1	0.512080 ± 12	0.512067 ± 12	-10.6
87-697U	Racer Canyon Tuff	18.8	78.3	56.6	827.60	3.59	22.58	0.198 ± 0.002	0.708947 ± 29	0.708894 ± 29	0.0960 ± 1	0.512104 ± 14	0.512092 ± 14	-10.1
89-854	Cobalt Canyon Stock	24.9	68.2	205.0	294.70	6.73	38.08	2.013 ± 0.037	0.710128 ± 21	0.709419 ± 25	0.1067 ± 1	0.512001 ± 18	0.511984 ± 18	-12.1
Delamar caldera:														
88-997	lava flows of Buckboard Spring	18.0	55.9	54.0	819.80	8.09	46.09	0.190 ± 0.003	0.706494 ± 20	0.706445 ± 20	0.1060 ± 1	0.512220 ± 18	0.512208 ± 18	-7.9
87-786	Volcanic dome of Crows Nest Tank	18.2	74.7	203.9	219.00	3.66	23.00	2.693 ± 0.031	0.708276 ± 14	0.707580 ± 16	0.0962 ± 22	0.512093 ± 13	0.512082 ± 13	-10.4
Do	do			201.9	215.20	--	--	2.714 ± 0.103	0.708274 ± 21	0.707573 ± 34	--	--	--	
88-1185	Hiko Tuff (intracaldera)	(18.6)	71.1	132.6	413.70	5.24	35.0	0.927 ± 0.034	0.707435 ± 21	0.707190 ± 23	0.0904 ± 5	0.512138 ± 12	0.512127 ± 12	-9.5
Do	do			139.4	415.00	--	--	0.972 ± 0.011	0.707479 ± 20	0.707222 ± 20	--	--	--	
88-666H	Hiko Tuff (outflow)	18.6-18.2	70.0	124.1	494.30	6.56	40.03	0.727 ± 0.019	0.707420 ± 17	0.707228 ± 18	0.0990 ± 1	0.512150 ± 11	0.512138 ± 11	-9.3
Clover Creek caldera:														
87-1194	Indian Cove	21.9	59.5	123.1	739.40	8.21	45.74	0.481 ± 0.015	0.706597 ± 24	0.706447 ± 25	0.1084 ± 1	0.512122 ± 15	0.512106 ± 15	-9.8
89-530	Intrusive rocks of Clover Creek caldera	22.8	73.4	218.5	209.80	6.42	42.81	3.012 ± 0.107	0.707700 ± 21	0.706725 ± 41	0.0906 ± 1	0.512089 ± 15	0.512075 ± 15	-10.4
87-452H	Bauers Tuff Mbr. (outflow)	22.8	73.3	181.1	290.20	6.18	41.10	1.805 ± 0.040	0.707226 ± 21	0.706642 ± 25	0.0908 ± 1	0.512107 ± 15	0.512093 ± 15	-10.0

[1]Ages in parentheses are assumed. Age data from Snee and Mehnert (unpub. data, 1990, 1991), Snee and others (1990), Best, Christiansen, and Blank (1989), Taylor and others (1989), and Rowley and others (1992).

[2]Calculated initial ratios. Uncertainties reflect those of the parent-daughter ratios, but not the age uncertainties.

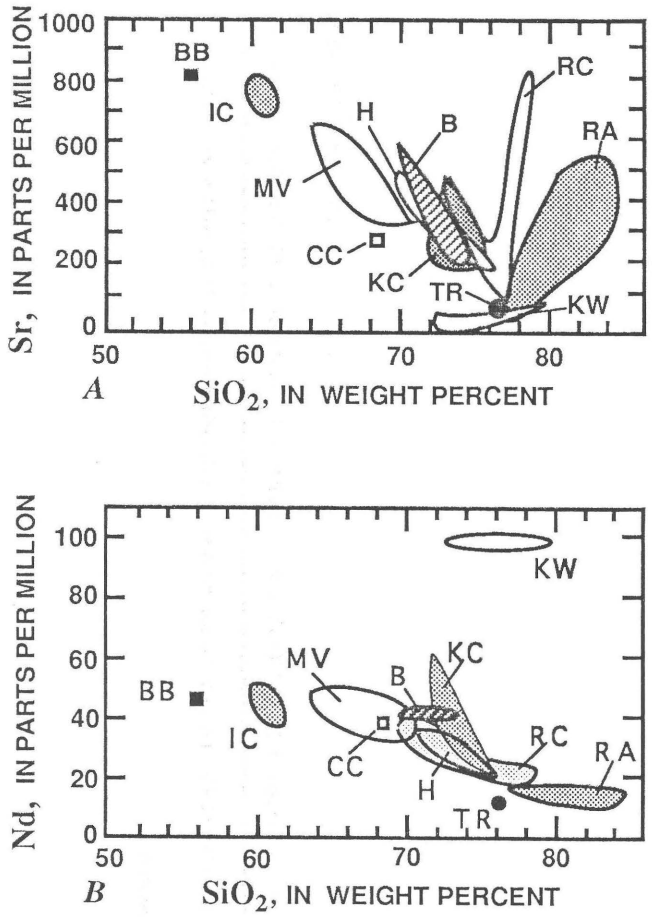

Figure 4. Variation diagrams for *A*, Sr and *B*, Nd vs. silica content for samples from Caliente caldera complex. Data from this study and from Nealey and others, this volume. Silica contents recalculated to 100 percent on a volatile-free basis. CC, Cobalt Canyon stock; B, Bauers Tuff Member, Condor Canyon Formation (includes the intrusive rocks of the Clover Creek caldera); IC, lava flows of Indian Cove; MV, porphyry of Meadow Valley Wash; H, Hiko Tuff (includes volcanic dome of Crows Nest Tank); RA, tuff of Rainbow Canyon; RC, Racer Canyon Tuff; BB, lava flows of Buckboard Spring; TR, tuff of Tepee Rocks; KC, tuff of Kershaw Canyon; KW, Kane Wash Tuff (from this work and Novak, 1985).

low alkali and high recalculated silica contents (fig. 3, and Nealey and others, this volume). The altered Rainbow Canyon sample (88–226A) shows an apparent initial $^{87}Sr/^{86}Sr$ of 0.7116 (table 2), a value much higher than found in any other Caliente complex sample thus far analyzed. A sanidine separate from another sample (88–1264), collected from near 88–226A, shows a much lower initial $^{87}Sr/^{86}Sr$ of 0.7075. Extremely high and anomalous Sr contents and anomalous $^{87}Sr/^{86}Sr$ were also observed in altered (zeolitized) samples of the Paintbrush Tuff in southern Nevada by Peterman and others (1991). Consequently, we suggest that the lower ratio from sample 88–1264 is more representative of unaltered tuff of Rainbow Canyon, and this value will be used in the ensuing discussion. The altered sample of the Racer Canyon Tuff (87–679U) also exhibits a somewhat elevated initial $^{87}Sr/^{86}Sr$ and will be deleted from the following discussion.

Neodymium concentrations for most of the samples also exhibit a negative correlation with silica contents (fig. 4*B*). However, the overall relative variation in Nd concentrations (50–12 ppm) is much less than for Sr, and Nd abundances show only a weak negative covariance with silica contents of about 56–70 percent.

The trend exhibited by the Nd data is also consistent with trends predicted by Nd mineral/liquid distribution coefficients and reflects the strong dependency of D_{Nd} for mafic mineral phases on bulk composition. D_{Nd} values for clinopyroxene and orthopyroxene range from less than 0.2 and 0.5, respectively, in basaltic systems (Grutzeck and others, 1974; Weil and McKay, 1975) to values of 0.6–1.3 and 2.3–5.8, respectively, in silicic systems (for example, Henderson, 1984; Nash and Crecraft, 1985). Nd is also strongly partitioned into biotite (D_{Nd}=0.9–5.8), hornblende (D_{Nd}=3–4; Henderson, 1984; Nash and Crecraft, 1985), and sphene (D_{Nd}=88; Simmons and Hedge, 1978). However, Nd is not strongly partitioned into feldspar at any bulk composition (D_{Nd}<0.2; Nash and Crecraft, 1985). Based upon the phenocryst assemblages and the aforementioned distribution coefficients, we estimate bulk D_{Nd} values of about 1.5 to 2.2 for most Caliente tuffs.

The altered samples from the tuff of Rainbow Canyon and the Racer Canyon Tuff do not show anomalous Nd concentrations. In their study of the Paintbrush Tuff, Peterman and others (1991) found that REE were not significantly affected by alteration, and that the Nd isotopic data were similarly unaffected (Z.E. Peterman, oral commun., 1992). We therefore will use the Nd data for the altered Rainbow Canyon sample in the ensuing discussion, but we recognize that these data need further evaluation and confirmation.

Kane Wash Tuff (table 2; Novak, 1985; Nealey and others, this volume) exhibits considerably lower Sr contents (5–15 ppm) and higher Nd contents (95–110 ppm) than tuffs from the Caliente complex. These differences may reflect primary differences in parental magmas and (or) differences in the crystallizing mineral phases among the parental magmas.

STRONTIUM ISOTOPIC VARIATIONS

Initial $^{87}Sr/^{86}Sr$ values for Caliente samples from table 2 are shown as functions of silica content, age, and Sr content in figure 5. Shown for comparison are data from two analyses of Kane Wash Tuff by Novak (1985). The $^{87}Sr/^{86}Sr$ initial ratios show a rather restricted range of 0.7064 to 0.7094. The Cobalt Canyon stock has the highest initial ratio, whereas the two mafic flows (Buckboard Spring and Indian Cove) have the lowest initial ratios (fig. 5*A*). These latter two samples also have the highest Sr contents.

With the exception of the Cobalt Canyon stock, the data define fairly well correlated trends on all three

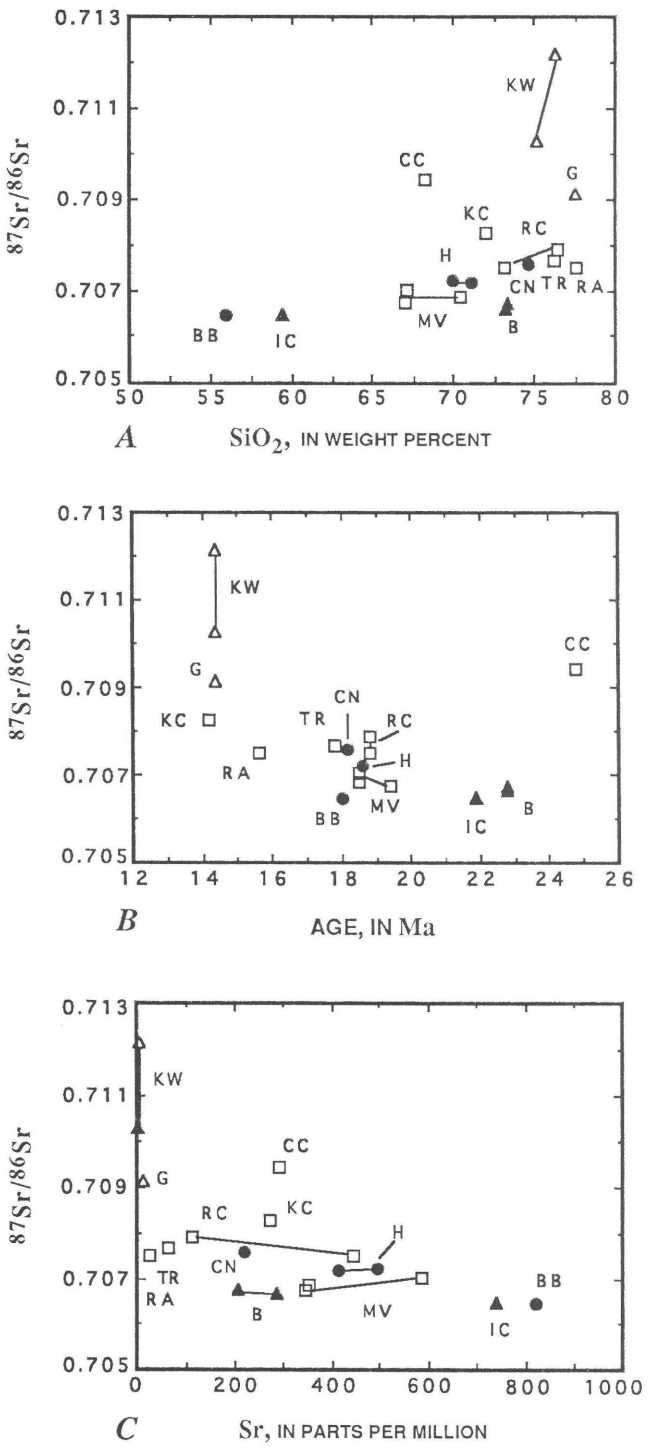

Figure 5. Initial $^{87}Sr/^{86}Sr$ for samples from Caliente caldera complex shown as functions of *A*, silica content; *B*, age; and *C*, Sr content. CC, Cobalt Canyon stock; B, Bauers Tuff Member, Condor Canyon Formation (includes the intrusive rocks of the Clover Creek caldera); IC, lava flows of Indian Cove; MV, porphyry of Meadow Valley Wash; H, Hiko Tuff; CN, volcanic dome of Crows Nest Tank; RA, tuff of Rainbow Canyon; RC, Racer Canyon Tuff; BB, lava flows of Buckboard Spring; TR, tuff of Tepee Rocks; KC, tuff of Kershaw Canyon; G, Gregerson Basin Member of Kane Wash Tuff; KW, Kane Wash Tuff (from Novak, 1985). Open triangle, sample related to the Kane Springs Wash caldera. Solid circle, solid triangle, samples related to the Delamar caldera and Clover Creek caldera (Caliente caldera complex), respectively. Remaining samples from the Caliente caldera complex are shown by open squares. Samples from the same unit are connected by tie lines.

diagrams. Initial $^{87}Sr/^{86}Sr$ increases with increasing silica and decreasing age and Sr contents. The trends are somewhat fan-shaped in fig. 5*A* and 5*C* and show increasing variability in initial $^{87}Sr/^{86}Sr$ with increasing silica and decreasing Sr contents.

The apparent correlation between initial $^{87}Sr/^{86}Sr$ and age could, in part, reflect the fact that no rocks with intermediate compositions are included among samples dated at less than about 18 Ma. However, when compared at approximately constant silica (fig. 5*A*), and constant Sr contents (fig. 5*C*), initial $^{87}Sr/^{86}Sr$ increases from 0.7067 in the Bauers Tuff Member (22.8 Ma), to 0.7075 in Hiko Tuff (18.6–18.2 Ma), to 0.7083 in the tuff of Kershaw Canyon (14.2 Ma).

Radioactive decay of ^{87}Rb in the source region of these magmas could account for apparent relationship between age and initial $^{87}Sr/^{86}Sr$. However, an $^{87}Rb/^{86}Sr$ of about 12–13 is required to account for the observed variations. This ratio is much higher than is observed among any of the units ($^{87}Rb/^{86}Sr$=0.7–3.0; table 2) except the Gregerson Basin Member of the Kane Wash Tuff and tuff of Tepee Rocks. Consequently, such an explanation seems quite unlikely.

The "fan-shaped" trends between initial $^{87}Sr/^{86}Sr$ and both silica and Sr contents (fig. 5*A*, *C*) suggest that the individual units could be related to a common, or at least similar, source represented by the data for the two mafic flows. Given such a model, the open end of the "fans" (high SiO_2 and low Sr contents) would reflect variations in fractional crystallization and crustal-interaction processes that have modified the parental magmas and produced the individual units.

The Cobalt Canyon stock predates known caldera-related magmatism in the area, and the stock is not exposed within the caldera complex. Furthermore, the Sr data for the Cobalt Canyon stock do not plot on the trends defined by the other data in figure 5. Consequently, we suggest that this stock is not directly related to any of the other units under present consideration (Rowley and others, 1992).

NEODYMIUM ISOTOPIC VARIATIONS

Initial $^{143}Nd/^{144}Nd$ for most samples shows a restricted range of 0.5120 to 0.5122 (εNd_I= –7.9 to –11.1; table 2; fig. 6). The single exception, the sample from the Cobalt Canyon

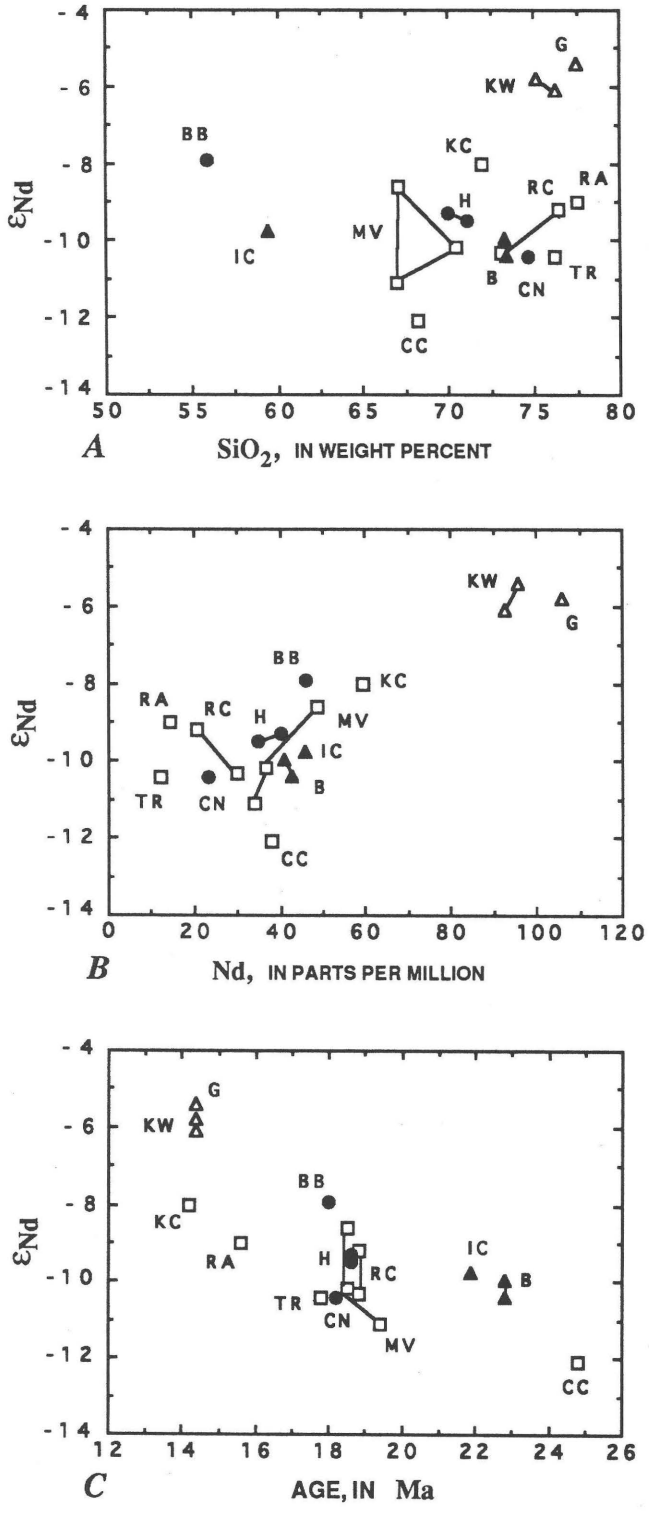

Figure 6. Initial εNd values for Caliente samples plotted as functions of *A*, silica content; *B*, Nd content; and *C*, age. CC, Cobalt Canyon stock; B, Bauers Tuff Member, Condor Canyon Formation (includes the intrusive rocks of the Clover Creek caldera); IC, lava flows of Indian Cove; MV, porphyry of Meadow Valley Wash; H, Hiko Tuff; CN, volcanic dome of Crows Nest Tank; RA, tuff of Rainbow Canyon; RC, Racer Canyon Tuff; BB, lava flows of Buckboard Spring; TR, tuff of Tepee Rocks; KC, tuff of Kershaw Canyon; G, Gregerson Basin Member of Kane Wash Tuff; KW, Kane Wash Tuff (from Novak, 1985). Open triangle, sample related to the Kane Springs Wash caldera. Solid circle, solid triangle, samples related to the Delamar caldera and Clover Creek caldera (Caliente caldera complex), respectively. Remaining samples from the Caliente caldera complex are shown by open squares. Samples from the same unit are connected by tie lines.

stock, shows the lowest initial $^{143}Nd/^{144}Nd$=0.51198 (εNd_I= –12.1). The sample of the Gregerson Basin Member exhibits a higher initial $^{143}Nd/^{144}Nd$ of 0.51235 (εNd_I= –5.3) which is similar to those previously reported for Kane Wash Tuff by Novak (1985). Neodymium concentrations range from 10–15 ppm in the tuffs of Rainbow Canyon and Tepee Rocks, to 59 ppm in the tuff of Kershaw Canyon.

Initial Nd ratios (expressed as εNd in fig. 6) do not show a correlation with silica content (fig. 6*A*). Virtually the entire range of Nd ratios is found among the rhyolite tuffs, and the two andesites have intermediate initial Nd values that differ from one another by about 2 εNd units (1 εNd unit=0.01 percent). However, among those units related to the Delamar caldera (Hiko Tuff, volcanic dome of Crows Nest Tank, lava flows of Buckboard Spring), the data exhibit a trend of decreasing εNd with increasing silica. A similar trend may exist for the units related to the Clover Creek caldera (lava flows of Indian Cove, Bauers Tuff Member, and intrusive rocks of the Clover Creek caldera,) but additional analyses will be required because this apparent trend consists of essentially only two points. The Cobalt Canyon stock shows an anomalously low εNd, which reinforces the suggestion made in the previous section, that this stock is not related to the other units.

A similar lack of correlation exists among εNd and Nd concentrations (fig. 6*B*). Although a weak positively correlated trend exists among the Delamar caldera-related samples, the majority of the samples are clustered between εNd= –8 to –11 and 15–50 ppm Nd, with no correlation within this group as a whole. Samples related to the Clover Creek caldera tend to have slightly higher Nd concentrations at similar εNd than samples related to the Delamar caldera; and the two youngest tuffs (Rainbow Canyon and Kershaw Canyon) have the highest εNd values among Caliente caldera tuffs, although their Nd concentrations differ greatly.

In contrast to figure 6*A* and *B*, the initial Nd ratios yield a good correlation with age (fig. 6*C*), although there is considerable overlap among three general recognizable age groups. Although the data base is limited, average εNd values for the tuffs appear to increase from –10 in Bauers Tuff Member (22.8 Ma) to –9.4 in Hiko Tuff (18.6 Ma) to –8.0 in the tuff of Kershaw Canyon (14.2 Ma). A more pronounced apparent trend is observed between the two mafic flows. The εNd value of the lava flows of Buckboard Spring (18.0 Ma) is 2 units higher than that of the lava flows of Indian Cove, although both units have similar silica and Nd contents.

Unfortunately, no younger (14–16 Ma) mafic flows were included in the present study and the confirmation of the apparent correlation between εNd and age must await further sampling. Similar positive correlations between εNd and age have been observed in the San Juan volcanic field in Colorado (Riciputi and Johnson, 1990) and the Timber Mountain–Oasis Valley caldera complex in southwestern Nevada (Farmer and others, 1991).

In summary, Nd isotopic variations appear to be related primarily to age differences, with a secondary, more subtle compositional dependence within at least the Delamar caldera samples. This general relationship is in marked contrast to that indicated by the Sr isotopic data presented previously. The Sr data show pronounced correlations between $^{87}Sr/^{86}Sr$ and silica and Sr contents, as well as age.

DISCUSSION

Initial $^{87}Sr/^{86}Sr$ and $^{143}Nd/^{144}Nd$ values for Caliente caldera complex samples are summarized in figure 7. Shown for comparison are data from the Kane Springs Wash caldera (Novak, 1985) and the Timber Mountain–Oasis Valley caldera complex (TMOV; Tegtmeyer and Farmer, 1990; Farmer and others, 1991). Also shown are basalt data from Kane Springs Wash (Novak, 1985), and from various locations in the northern Colorado Plateaus and Basin and Range provinces (Menzies and others, 1983; Farmer and others, 1989; Kempton and others, 1991).

Data for the Caliente caldera complex as a whole exhibit a somewhat smaller range in $^{87}Sr/^{86}Sr$ than do those for the TMOV, and only about one-half the range shown by Kane Springs Wash data. In contrast, Nd isotopic data show a range (0.03 percent=3 εNd units) similar to those observed among intermediate and silicic rocks of the Kane Springs Wash caldera and the TMOV. In the latter two caldera complexes, the highest $^{143}Nd/^{144}Nd$ values are found among trachytes and the lowest $^{143}Nd/^{144}Nd$ are found among rhyolites. However, in the Caliente complex the entire range of $^{143}Nd/^{144}Nd$ values is found among rhyolite tuffs (table 2).

The most striking features of the isotopic data in figure 7 are the nearly horizontal trends exhibited by the data for intermediate to silicic rocks from caldera complexes, in contrast to the steep negatively correlated trends exhibited by

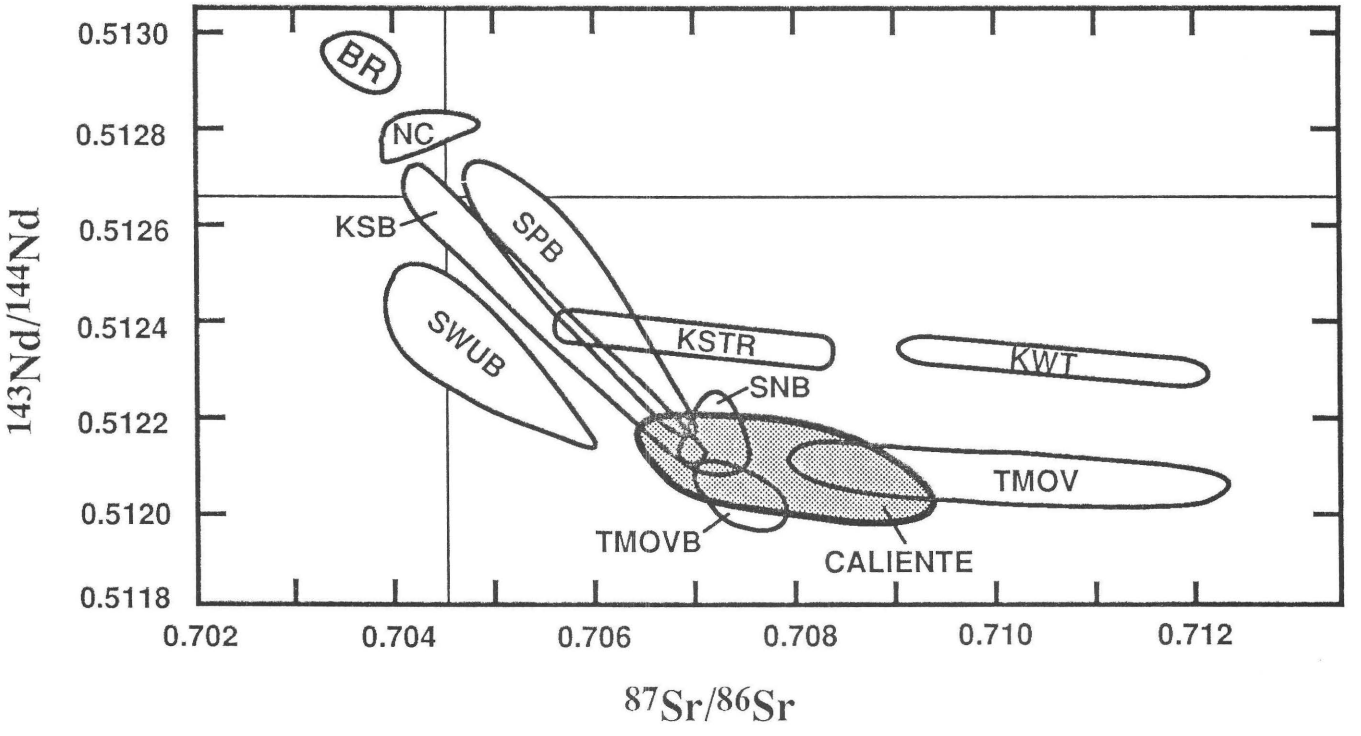

Figure 7. $^{143}Nd/^{144}Nd$ vs. $^{87}Sr/^{86}Sr$ diagram for data from Caliente caldera complex and other selected areas in the western United States. BR, Basin and Range basalts; NC, Nye Canyon, Nev., basalts; SPB, Sierran Province basalts, southern Nevada, and southeastern California; SWUB, southwestern Utah basalts; SNB, southwestern Nevada basalts; KSB, basalts from Kane Springs Wash caldera; KSTR, trachytes from Kane Springs Wash caldera; KWT, Kane Wash Tuff; TMOVB, basalts from Timber Mountain–Oasis Valley caldera complex; TMOV, trachytes and rhyolites from Timber Mountain–Oasis Valley caldera complex. Fields compiled from data taken from Menzies and others (1983; SPB); Novak (1985; KSB, KSTR, KWT); Farmer and others (1989; NC, SNB); Farmer and others (1991; TMOVB, TMOV); and Kempton and others (1991; BR, SWUB). Estimated "bulk-earth" values are shown by the horizontal and vertical lines at $^{143}Nd/^{144}Nd=0.512636$, and $^{87}Sr/^{86}Sr=0.7045$, respectively.

much of the basalt data. The different trends are related to the different sources and processes involved in the generation of the two general types of volcanism. Basalts are thought to derive their isotopic characteristics from two principal sources: "depleted" asthenospheric mantle (as exemplified by the "Basin and Range" field in fig. 7), and remnant Proterozoic(?) lithospheric mantle (for example, Menzies and others, 1983; Perry and others, 1987; Farmer and others, 1989; Kempton and others, 1991) that may range from slightly depleted to moderately enriched (isotopically). The isotopic characteristics of the basaltic magmas may be further modified by interaction with the crust, either near the crust-mantle boundary (Johnson and others, 1990; Riciputi and Johnson, 1990, among others) or during ascent of the magmas to the surface.

Correlated isotopic and geochemical trends observed in a number of studies of silicic volcanic centers (see fig. 7 for example) have been interpreted to reflect open-system modification of crystallizing parental magmas by assimilation of crustal material (Noble and Hedge, 1969; Novak and Mahood, 1986; Leeman and Hawkesworth, 1986; Musselwhite and others, 1989; Johnson and others, 1990; Tegtmeyer and Farmer, 1990; Farmer and others, 1991). In most of these studies, assimilation of crustal material was interpreted to be subordinate to fractional crystallization (see also Halliday and others, 1984; Cameron and Cameron, 1985), particularly as the magma systems evolve to more silicic compositions (Novak and Mahood, 1986; Musselwhite and others, 1989, among others). Because Sr is more effectively partitioned into the fractionating phases than Nd, Sr contents decrease more rapidly than Nd (fig. 4). This decrease coupled with exceptionally high $^{87}Sr/^{86}Sr$ in crustal material causes $^{87}Sr/^{86}Sr$ in the magma to be much more affected than $^{143}Nd/^{144}Nd$ by crustal assimilation. Consequently, a large range in $^{87}Sr/^{86}Sr$ may be observed where only limited variation in $^{143}Nd/^{144}Nd$ is present.

Kane Wash Tuff has the lowest Sr contents (<10 ppm; Novak, 1985) among the tuffs represented in figure 7, and the Kane Springs Wash data (KWT, KSTR) exhibit the largest variation in Sr isotopic ratios. Novak and Mahood (1986) suggested that Kane Wash Tuff could have been derived by fractionation of parental trachytic magmas (KSTR field in fig. 7) and that the elevated $^{87}Sr/^{86}Sr$ in Kane Wash Tuff samples may represent as little as 1 percent crustal contamination/assimilation. They also suggested that the trachytic magmas may have been derived by fractionation of alkali basalt magma with 10–20 percent assimilation of crustal material.

The samples with the highest $^{87}Sr/^{86}Sr$ among the TMOV volcanics also exhibit the lowest Sr contents (25–28 ppm Sr in sanidine; Farmer and others, 1991). Tegtmeyer and Farmer (1990) and Farmer and others (1991) suggested that the high-silica rhyolite of the Topopah Spring Member of the Paintbrush Tuff could have been derived by fractionation of parental trachytic magma accompanied by 10–40 percent assimilation of crustal material, depending upon the type of model invoked. The smaller variation in $^{87}Sr/^{86}Sr$ among Caliente complex silicic samples relative to those of Kane Springs Wash and the TMOV may reflect the more restricted range of Sr contents among Caliente samples.

EVOLUTION OF THE SILICIC MAGMAS

The $^{87}Sr/^{86}Sr$ and $^{143}Nd/^{144}Nd$ of the silicic tuffs from the Caliente complex analyzed in this study are in the range of 0.7067–0.7082, and 0.5121–0.5122 ($\varepsilon Nd = -8$ to -10), respectively (figs. 5, 6). These $^{143}Nd/^{144}Nd$ values are considerably higher, and the $^{87}Sr/^{86}Sr$ are considerably lower than one would expect if these tuffs represented crustal anatexis of Proterozoic felsic basement ($\varepsilon Nd = -15$ to -20, $^{87}Sr/^{86}Sr \approx 0.713$ to >0.72; Bennett and DePaolo, 1987; Kistler and Lee, 1989; Farmer and others, 1991). However, the isotopic variations exhibited by the tuffs and their elevated $^{87}Sr/^{86}Sr$ relative to basalts with similar εNd values (fig. 7) suggest that some crustal interaction is involved.

The trends exhibited by the Sr data in figure 5, and to a lesser extent by the Nd data in figure 6 (at least among samples related to the Delamar caldera), suggest that the magmas related to a single caldera-forming "event" may also be related to a single parental magma, or at least similar parental magmas. In following discussion we assume this to be the case, and we use the Nd data from samples related to the Delamar caldera to outline conditions under which the more silicic samples could have been derived from these parental magmas. Due to the limited data base and the lack of tight constraints on D_{Nd} values and the composition of the crustal component involved, the calculations presented herein are somewhat speculative and subject to revision.

The sample of the lava flows of Buckboard Spring is the least silicic among this group and has the highest εNd (–7.9) and lowest $^{87}Sr/^{86}Sr$ (0.7064) among these samples. The Sr and Nd isotopic ratios of this sample are similar to those of isotopically "enriched" basalts from southern Nevada and southwest Utah (fig. 7). Although we recognize that this unit contains a disequilibrium assemblage of phenocrysts which may be isotopically heterogeneous, we suggest that this sample may still approximate the parental magma to the Delamar "system," and may represent either a fractionated mantle-derived melt or a hybrid melt produced within the lower crust or at its base (Johnson and others, 1990). The crustal contaminant is assumed to contain 30–40 ppm Nd, with $\varepsilon Nd = -15$ to -18 (for example, Bennett and DePaolo, 1987; Farmer and others, 1991).

Results of an assimilation/fractional crystallization model (DePaolo, 1981) are summarized in figure 8. In this model, fractional crystallization is presumed to occur concomitantly with assimilation of wall-rock material. This process may occur as magmas "stope" their way through the crust or as magmas differentiate within a chamber. In the

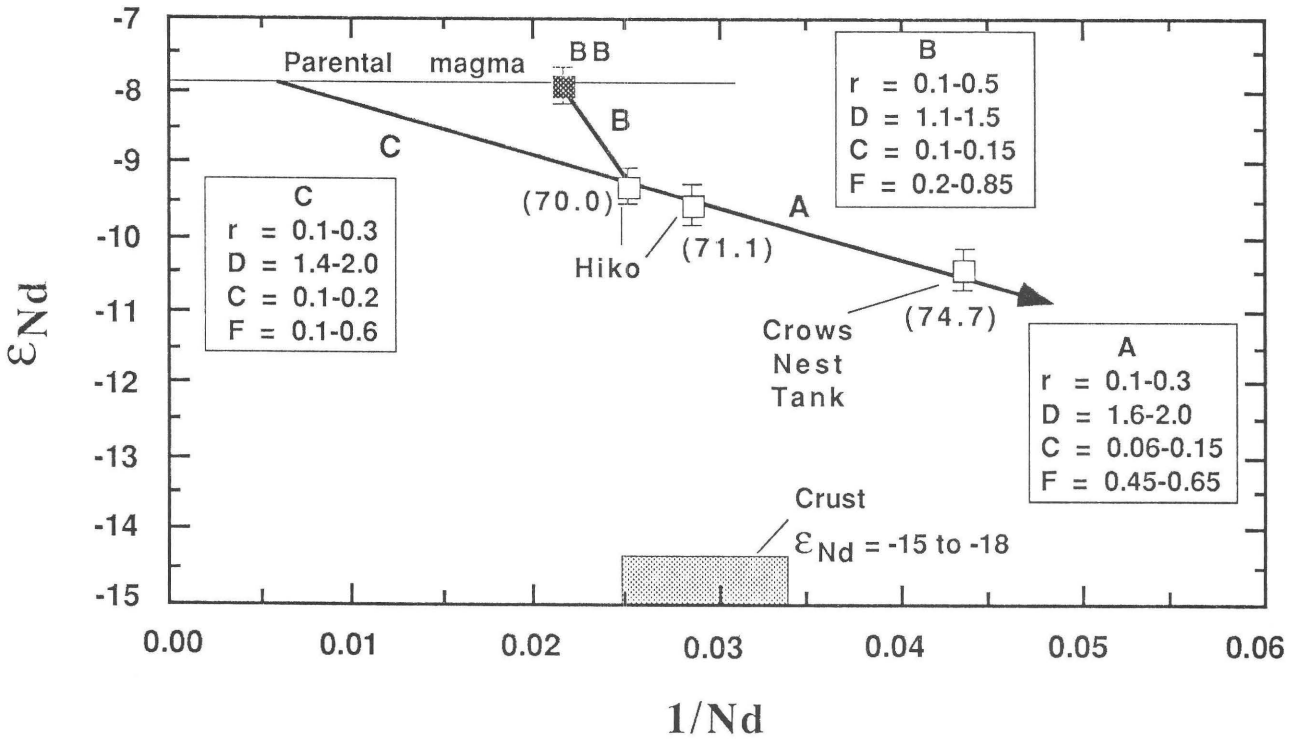

Figure 8. Assimilation/fractional crystallization models for Delamar caldera–related samples based on Nd concentration and εNd (DePaolo, 1981). The parental magma to the system is assumed to have εNd equal to that of BB, the lava flows of Buckboard Spring (εNd= –7.9), and the crustal contaminant an εNd of –15 to –18 and 30–40 ppm Nd (Bennett and DePaolo, 1987). Line segment A reflects the evolution from low-silica (Hiko Tuff) to high-silica (volcanic dome of Crows Nest Tank) rhyolite, and segments B and C reflect possible evolution paths from the lava flows of Buckboard Spring (with variable initial Nd concentrations) to Hiko low-silica rhyolite. Numerical values for each of the variables used in the calculations of the evolution paths are given in the respective boxes: r represents the assumed mass ratio of assimilation to fractional crystallization per unit time, D represents bulk Nd mineral/melt partition coefficients, F represents the mass fraction of original magma remaining at the end point of each trend, and C represents the mass ratio of total material assimilated to original magma ($\equiv M_a/M_{m0}$ of Farmer and DePaolo, 1983) at the end point. Silica contents for individual samples are shown in parentheses.

latter case, a chemically and isotopically zoned magma chamber may be produced, and the chemical and isotopic zoning may be preserved within the erupted products (Tegtmeyer and Farmer, 1990). In the former case, only the end-product may be erupted to the surface.

Limited chemical and isotopic zoning is observed within the three rhyolite samples (fig. 8), although we note that the two low-silica rhyolites are of Hiko Tuff whereas the high-silica rhyolite is from the volcanic dome of Crows Nest Tank and may be 0.4 m.y. younger than Hiko Tuff. The calculations suggest that the high-silica rhyolite could have been derived from the low-silica rhyolite by extensive fractional crystallization and about 5–15 percent assimilation of wall-rock material (line segment A in fig. 8), if reasonably low values for r are assumed (r equals the mass ratio of assimilation to fractional crystallization per unit time; DePaolo, 1981).

Possible conditions under which the low-silica rhyolites could be related to the lava flows of Buckboard Spring are shown by line segments B and C in figure 8. Segment B suggests a scenario in which a magma initially equivalent to the lava flow of Buckboard Spring stopes its way to a level at which the subvolcanic magma chamber forms. At this level the magma has trace element and isotopic characteristics of the low-silica rhyolites. Segment C represents extrapolation of the Hiko trend to the εNd= –7.9 line (parental magma), and represents an "initial" magma that is a fractionated, but uncontaminated derivative of the lava flows of Buckboard Spring with 110 ppm Nd and εNd= –7.9. The actual evolution path (if it exists) probably lies between these two extremes. Although the amount of fractionation required is strongly dependent upon the assumed value for r, and is therefore not well constrained, the amount of assimilant appears to be restricted to about 10–20 percent (C=0.1–0.2) of the original magma mass, regardless of the path chosen. Thus, the high-silica rhyolite could be related to the lava flows of Buckboard Spring by rather extensive fractional crystallization accompanied by about 15–30 percent assimilation of crustal material.

Similar calculations have been performed for samples from the porphyry of Meadow Valley Wash (not shown in fig. 8). These results suggest that Meadow Valley Wash samples could have been derived from a magma with trace

element and isotopic characteristics of the lava flows of Buckboard Spring with assimilation of 20–30 percent crustal material. However, these calculations are not entirely justified, because the three samples of porphyry of Meadow Valley Wash are from different locations within the complex and are not related to a single parent magma, and because the variations in Nd data are not correlated with silica content (fig. 6). Interestingly, the sample with lowest εNd and low silica is also at least 1 m.y. older than the other two (19.4 Ma as opposed to post-18.6–18.2 Ma). Furthermore, this sample was collected from a location near the Clover Creek caldera; thus it may have been derived from a low-εNd parental magma related to Clover Creek caldera activity rather than to Delamar caldera activity.

The data for Hiko Tuff and the volcanic dome of Crows Nest Tank have also been evaluated in terms of a bulk-assimilation model wherein compositional gradients develop in an isotopically homogeneous magma chamber prior to assimilation of crustal material (Johnson, 1989; see fig. 6 of Farmer and others, 1991). If this magma originally had the εNd of the lava flows of Buckboard Spring, then the Hiko and Crows Nest Tank data may reflect approximately 30 percent addition of crustal material to this magma at all levels.

Although the calculations just presented are rather speculative and model dependent, one important conclusion can be obtained from them: fractional crystallization was much more important than crustal anatexis or contamination in the generation of even the high-silica rhyolites (Musselwhite and others, 1989; Tegtmeyer and Farmer, 1990; Farmer and others, 1991; Johnson, 1991). In fact, comparison of the calculations for line segments B and C in figure 8 with those for segment A suggests that crustal interaction becomes less significant as magmas become more silicic (Novak and Mahood, 1986; Johnson, 1989; Musselwhite and others, 1989).

EVOLUTION OF THE PARENTAL MAGMAS

The Nd data presented in figure 6 suggest a good correlation between the initial $^{143}Nd/^{144}Nd$ values and the ages of the samples. A similar trend is observed among the Sr data in figure 5. However, apparent age-correlated variations in $^{87}Sr/^{86}Sr$, particularly among tuffs, may simply result from variations in Sr contents and crustal assimilation processes outlined previously. On the other hand, variations in initial $^{143}Nd/^{144}Nd$, particularly when compared at similar silica contents and initial $^{87}Sr/^{86}Sr$, are more likely related to $^{143}Nd/^{144}Nd$ variations inherited from the mantle (± lower crust) source regions. Consequently, the 2 εNd-unit variation observed among the lava flows of Indian Cove (εNd= –9.8) and Buckboard Spring (εNd= –7.9) should represent primary features of all magmas derived from these presumed parental magmas.

This hypothesis is at least partially supported by the $^{87}Sr/^{86}Sr$ and $^{143}Nd/^{144}Nd$ values for the two groups of Caliente complex samples representing the Clover Creek and Delamar calderas as shown in figure 9. The trend of the data for the Delamar samples appears to be displaced from that for the Clover Creek caldera toward higher εNd, although additional data will be required in order to confirm the existence of these two apparent trends. We note that data for the other two tuffs of approximate Delamar caldera age (Racer Canyon Tuff and the tuff of Tepee Rocks) also plot on or near the trend defined by the data for Delamar caldera samples.

Kane Wash Tuff, on the other hand, was clearly derived from a source with εNd≥ –5.3, the measured value within this tuff (table 2 and Novak and Mahood, 1986). The parental magma to the Kane Wash Tuff probably had $^{87}Sr/^{86}Sr$ and $^{143}Nd/^{144}Nd$ values similar to those of Kane Springs Wash trachytes or intracaldera basalts (εNd≈ –5; Novak, 1985; Novak and Mahood, 1986).

The tuff of Kershaw Canyon may have been derived from a parental magma with isotopic characteristics similar to that parental to Kane Wash Tuff. The tuff of Kershaw Canyon has a much higher Sr/Nd value (4.6) than does Kane Wash Tuff (0.16). Consequently, its evolution path in figure 9 would have been steeper than that for Kane Wash Tuff, and more similar to those of the other Caliente complex samples. Alternatively, the tuff of Kershaw Canyon could have been derived from a parental magma with isotopic characteristics intermediate between those of Kane Wash Tuff and the Delamar samples (εNd= –7 to –5).

The suggestion presented in the previous section, that the sample of porphyry of Meadow Valley Wash with the lowest εNd may be related to Clover Creek rather than Delamar activity, is supported by the combined Sr and Nd data in figure 9. The Sr-Nd isotopic trend for the three Meadow Valley Wash samples cuts across both Delamar and Clover Creek trends, and we speculate that isotopic analyses of samples from this unit could be used to monitor the isotopic evolution in the parental magmas throughout the complex.

The combined data suggest that εNd in the magmas parental to Caliente caldera tuffs increased from –9.8 at 22–23 Ma to –7.9 at 18 Ma to –8 to –5 at about 14.2 Ma. In their study of the Timber Mountain–Oasis Valley caldera complex, Farmer and others (1991) observed an increase of about 1 εNd unit between the Rainier Mesa (εNd= –10.5) and Ammonia Tanks Members (εNd = –9.5) of the Timber Mountain Tuff, which have an age difference of only about 0.2 m.y. (11.6–11.4 Ma). Riciputi and Johnson (1990) have suggested that εNd in the parental magmas in the San Juan volcanic field, Colorado, increased by about 2 εNd units during a 2 m.y. interval, from –8 at 28 Ma to –6 at 26 Ma. Therefore, the larger range in εNd values exhibited by the Caliente complex data probably reflects the prolonged period of non-basaltic volcanism relative to these other areas, rather than unusual Nd isotopic evolution of the source region of the Caliente complex magmas.

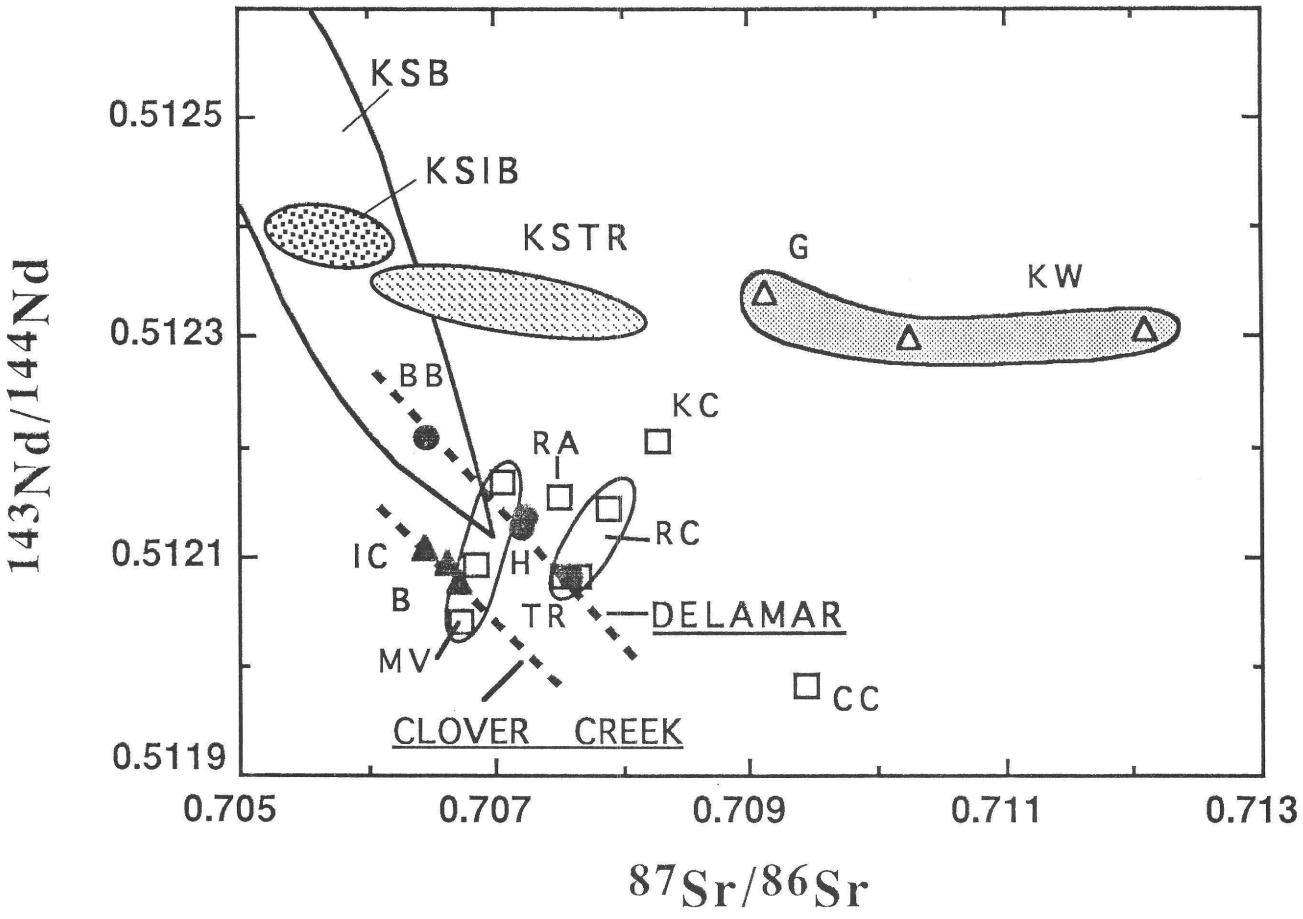

Figure 9. $^{143}Nd/^{144}Nd$ vs. $^{87}Sr/^{86}Sr$ diagram for Caliente samples. Possible assimilation-fractional crystallization evolution paths (heavy dashed lines) for silicic tuffs from mafic parental magmas are shown for the Clover Creek caldera and Delamar caldera groups of samples. Data from the Kane Springs Wash caldera are also shown (Novak, 1985; KSB, KSIB, KSTR, KW=basalts, intracaldera basalts, trachytes, and Kane Wash Tuff, respectively). CC, Cobalt Canyon stock; B, Bauers Tuff Member, Condor Canyon Formation (includes the intrusive rocks of the Clover Creek caldera); IC, lava flows of Indian Cove; MV, porphyry of Meadow Valley Wash; H, Hiko Tuff (includes volcanic dome of Crows Nest Tank); RA, tuff of Rainbow Canyon; RC, Racer Canyon Tuff; BB, lava flows of Buckboard Spring; TR, tuff of Tepee Rocks; KC, tuff of Kershaw Canyon; G, Gregerson Basin Member of Kane Wash Tuff. Open triangle, sample related to the Kane Springs Wash caldera. Solid circle, solid triangle, samples related to the Delamar caldera and Clover Creek caldera (Caliente caldera complex), respectively. Remaining samples from the Caliente caldera complex are shown by open squares.

The variations in εNd observed among Caliente complex parental magmas, as well as in the other areas just mentioned, require that at least two isotopically distinct sources exist at depth within each area. Although, in the present study, we cannot rule out the possibility that these two sources are being randomly sampled, the apparent time-dependence of these variations suggests that the higher-εNd source is, in effect, progressively replacing the lower-εNd source. The data are consistent with two general models as outlined in the following discussion (see Farmer and others, 1991).

The variations in εNd may reflect progressive erosion of lithospheric mantle by upwelling asthenospheric mantle (Perry and others, 1987). If so, then the isotopic characteristics of the asthenospheric mantle in this area may be approximated by the basalt from the Kane Springs Wash caldera which exhibits the highest $^{143}Nd/^{144}Nd$ (εNd≥ 0) and lowest $^{87}Sr/^{86}Sr$ (≤ 0.7043; Novak, 1985). The isotopic ratios of the lava flows of Indian Cove are similar to those of enriched (isotopically) basalts in southern Nevada and southwestern Utah (fig. 7). These isotopic characteristics (εNd≤ –9.8, $^{87}Sr/^{86}Sr$≥0.7064) may approximate those of Proterozoic lithospheric mantle in this area (Menzies and others, 1983; Farmer and others, 1989; Menzies, 1989; Kempton and others; 1991).

Alternatively, the variations may reflect progressive intrusion of mantle-derived magmas into the crust (Johnson and others, 1990). In this model, magmas parental to the caldera-related magmas are derived from near the crust-mantle boundary, and repeated injections of magma into the lower crust cause the lower crust to progressively adopt a more mantle-like isotopic signature. In the Caliente area, the lithospheric mantle might have isotopic characteristics similar to those of Kane Springs Wash intracaldera basalts (εNd≥ –5) or the more depleted (εNd≥0) extracaldera basalts. The

isotopic characteristics of the lower crust are not well constrained. The εNd of the lower crust in this area might resemble that of Proterozoic felsic rocks (–15 to –19; Bennett and DePaolo, 1987) or it may resemble that of the lava flows of Indian Cove (εNd≤ –10). We are presently unable to choose between these two alternatives, but Pb isotopic analyses currently in progress may help to clarify the role of the lower crust in the generation of these parental magmas (Johnson, 1989; 1991; Johnson and others, 1990).

SUMMARY AND CONCLUSIONS

The Sr and Nd isotopic data for samples from the Caliente caldera complex provide significant constraints on the sources and processes involved in the generation of these magmas. Although contamination or assimilation of crustal material is required to account for the isotopic characteristics of the silicic tuffs, fractional crystallization of more mafic magmas appears to be the primary process responsible for the generation of the caldera-forming magmas (Musselwhite and others, 1989; Farmer and others, 1991; Johnson, 1991).

Analyses of two samples of Hiko Tuff and one of a late caldera-related rhyolite dome suggest that the subvolcanic magma chamber that produced the Delamar caldera was chemically and isotopically zoned as a result of fractionation and assimilation of crustal material. Calculations, based on Nd data using several different models, suggest that the high-silica rhyolite of the volcanic dome of Crows Nest Tank could have been derived from low-silica (Hiko) rhyolite by fractional crystallization and addition of about 5–15 percent crustal material. The low-silica rhyolite could have been derived from andesitic or perhaps even basaltic parental magmas with the addition of about 10–20 percent crustal material. Thus the entire evolution from mafic parental magma to high-silica rhyolite may have involved no more than a 20–30 percent contribution from the crustal wall rocks.

Volcanic and intrusive rocks from the Clover Creek caldera (lava flows of Indian Cove, Bauers Tuff Member, intrusive rocks of the Clover Creek caldera) were derived from parental magmas with $^{87}Sr/^{86}Sr \leq 0.7064$ and εNd≥ –10. The parental magmas of volcanic rocks related to the Delamar caldera (lava flows of Buckboard Spring, Hiko Tuff, volcanic dome of Crows Nest Tank) appear to have had a similar $^{87}Sr/^{86}Sr$ to those related to the Clover Creek caldera, but a somewhat higher $^{143}Nd/^{144}Nd$ (εNd≥ –8). The isotopic character of the parental magmas to the post-16 Ma tuffs (tuffs of Rainbow Canyon and Kershaw Canyon) is not well constrained and may have been similar to that for the Delamar caldera (εNd≥ –8) or as high as that for Kane Wash Tuff (εNd≥ –5). The apparent temporal evolution of the parental magmas may reflect repeated injection of mantle-derived melts into the lower crust (Johnson and others, 1990), or lithospheric thinning as a result of erosion by upwelling asthenosphere (Perry and others, 1987). The period of major extensional faulting in this area roughly corresponds to the formation of the Caliente caldera complex (for example, Rowley and others, 1992). Therefore, isotopic data for each of the individual calderas may also reflect local changes in the tectonic setting.

REFERENCES CITED

Bennett, V.C., and DePaolo, D.J., 1987, Proterozoic crustal history of the western United States as determined by neodymium isotopic mapping: Geological Society of America Bulletin, v. 99, p. 674–685.

Best, M.G., Christiansen, E.H., and Blank, R.B., Jr., 1989, Oligocene calc-alkaline rocks of the Indian Peak volcanic field, Nevada and Utah: Geological Society of America Bulletin, v. 101, p. 1076–1090.

Best, M.G., Christiansen, E.H., Deino, A.L., Grommé, C.S., McKee, E.H., and Noble, D.C., 1989, Excursion 3A—Eocene through Miocene volcanism in the Great Basin of the western United States: New Mexico Bureau of Mines and Mineral Resources Memoir 47, p. 91–133.

Cameron, K.L., and Cameron, M., 1985, Rare earth element, $^{87}Sr/^{86}Sr$, and $^{143}Nd/^{144}Nd$ compositions of Cenozoic orogenic dacites from Baja California, northwestern Mexico, and adjacent west Texas—Evidence for the predominance of a subcrustal component: Contributions to Mineralogy and Petrology, v. 91, p. 1–11.

DePaolo, D.J., 1981, Trace element and isotopic effects of combined wallrock assimilation and fractional crystallization: Earth and Planetary Science Letters, v. 53, p. 189–202.

DePaolo, D.J., and Wasserburg, G.J., 1976, Nd isotopic variations and petrogenetic models: Geophysical Research Letters, v. 3, p. 249–252.

Farmer, G.L., Broxton, D.E., Warren, R.G., and Pickthorn, W., 1991, Nd, Sr, and O isotopic variations in metaluminous ash-flow tuffs and related volcanic rocks at the Timber Mountain/Oasis Valley caldera complex, SW Nevada—Implications for the origin and evolution of large-volume silicic magma bodies: Contributions to Mineralogy and Petrology, v. 109, p. 53–68.

Farmer, G.L., and DePaolo, D.J., 1983, Origin of Mesozoic and Tertiary granite in the western United States and implications for pre-Mesozoic crustal structure, I—Nd and Sr isotopic studies in the geocline of the northern Great Basin: Journal of Geophysical Research, v. 88, p. 3379–3401.

Farmer, G.L., Perry, F.V., Semken, S., Crowe, B., Curtis, D., and DePaolo, D.J., 1989, Isotopic evidence on the structure and origin of subcontinental lithospheric mantle in southern Nevada: Journal of Geophysical Research, v. 94, p. 7885–7898.

Grutzeck, M., Kridelbaugh, S., and Weil, D., 1974, The distribution of Sr and REE between diopside and silicate liquid: Geophysical Research Letters, v. 1, p. 273–275.

Halliday, A.N., Fallick, A.E., Hutchinson, J., and Hildreth, W., 1984, A Nd, Sr, and O isotopic investigation into the causes of chemical and isotopic zonation in the Bishop Tuff, California: Earth and Planetary Science Letters, v. 68, p. 379–391.

Henderson, P., ed., 1984, Rare earth element geochemistry, Volume 2 of Developments in geochemistry: New York, Elsevier, 510 p.

Johnson, C.M., 1989, Isotopic zonation in silicic magma chambers: Geology, v. 17, p. 1136–1139.

———1991, Large-scale crust formation and lithosphere modification beneath middle to late Cenozoic calderas and volcanic fields, western North America: Journal of Geophysical Research, v. 96, p. 13485–13507.

Johnson, C.M., Lipman, P.W., and Czamanske, G.K., 1990, H, O, Sr, Nd, and Pb isotope geochemistry of the Latir volcanic field and cogenetic intrusions, New Mexico, and relations between evolution of a continental magmatic center and modifications of the lithosphere: Contributions to Mineralogy and Petrology, v. 104, p. 99–124.

Kempton, P.D., Fitton, J.G., Hawkesworth, C.J., and Omerod, D.S., 1991, Isotopic and trace element constraints on the composition and evolution of the lithosphere beneath the southwestern United States: Journal of Geophysical Research, v. 96, p. 13713–13735.

Kistler, R.W., and Lee, D.E., 1989, Rubidium, strontium, and strontium isotopic data for a suite of granitoid rocks from the basin and range province, Arizona, California, Nevada, and Utah: U.S. Geological Survey Open-File Report 89–199, 13 p.

Leeman, W.P., and Hawkesworth, C.J., 1986, Open magma systems—Trace element and isotopic constraints: Journal of Geophysical Research, v. 91, p. 5901–5912.

Menzies, M.A., 1989, Cratonic, circumcratonic and oceanic mantle domains beneath the western United States: Journal of Geophysical Research, v. 94, p. 7899–7915.

Menzies, M.A., Leeman, W.P., and Hawkesworth, C.J., 1983, Isotope geochemistry of Cenozoic volcanic rocks reveals heterogeneity below western USA: Nature, v. 303, p. 205–209.

Musselwhite, D.S., DePaolo, D.J., and McCurry, M., 1989, The evolution of a silicic magma system—Isotopic and chemical evidence from the Woods Mountains Volcanic Center, eastern California: Contributions to Mineralogy and Petrology, v. 101, p. 19–29.

Nash, W.P., and Crecraft, H.R., 1985, Partition coefficients for trace elements in silicic magmas: Geochimica et Cosmochimica Acta, v. 49, p. 2309–2322.

Noble, D.C., and Hedge, C.E., 1969, $^{87}Sr/^{86}Sr$ variations within individual ash-flow sheets, *in* Geological Survey research: U.S. Geological Survey Professional Paper 650–C, p. C133–C139.

Novak, S.W., 1984, Eruptive history of the Kane Springs Wash volcanic center, Nevada: Journal of Geophysical Research, v. 89, p. 8603–8615.

———1985, Geology and geochemical evolution of the Kane Springs Wash volcanic center, Lincoln County, Nevada: Stanford, Calif., Stanford University Ph. D. dissertation.

Novak, S.W., and Mahood, G.A., 1986, Rise and fall of a basalt-trachyte-rhyolite magma system at the Kane Springs Wash Caldera, Nevada: Contributions to Mineralogy and Petrology, v. 94, p. 352–373.

Perry, F.V., Baldridge, W.S., and DePaolo, D.J., 1987, Role of asthenosphere and lithosphere in the genesis of late Cenozoic basaltic rocks from the Rio Grande Rift and adjacent regions of the southwestern United States: Journal of Geophysical Research, v. 92, p. 9193–9213.

Peterman, Z.E., Spengler, R.W., Futa, K., Marshall, B.D., and Mahan, S.A., 1991, Assessing the natural performance of felsic tuffs using the Rb-Sr and Sm-Nd systems—A study of the altered zone in the Topopah Springs Member, Paintbrush Tuff, Yucca Mountain, Nevada: Materials Research Society Symposium Proceedings, v. 212, p. 687–694.

Riciputi, L.R., and Johnson, C.M., 1990, Nd- and Pb-isotope variations in the multicyclic central caldera cluster of the San Juan volcanic field, Colorado, and implications for crustal hybridization: Geology, v. 18, p. 975–978.

Rowley, P.D., and Shroba, R.R., 1991, Geologic map of the Indian Cove quadrangle, Lincoln County, Nevada: U.S. Geological Survey Geologic Quadrangle Map GQ–1701, scale 1:24,000.

Rowley, P.D., Shroba, R.R., Simonds, F.W., Burke, K.J., Axen, G.J., and Olmore, S.D., 1991, Geologic map of the Chief Mountain quadrangle, Lincoln County, Nevada: U.S. Geological Survey Open-File Report 91–135, scale 1:24,000.

Rowley, P.D., and Siders, M.A., 1988, Miocene calderas of the Caliente caldera complex, Nevada-Utah [abs.]: Eos, v. 69, no. 44, p. 1508.

Rowley, P.D., Snee, L.W., Mehnert, H.H., Anderson, R.E., Axen, G.J., Burke, K.J., Simonds, F.W., Shroba, R.R., and Olmore, S.D., 1992, Structural setting of the Chief Mining District, eastern Chief Range, Lincoln County, Nevada, *in* Thorman, C.H., ed., Application of structural geology to mineral and energy resources of the central and western United States: U.S. Geological Survey Bulletin 2012, p. H1–H17.

Scott, R.B., Swadley, WC, and Novak, S.W., 1993, Geologic map of the Delamar Lake quadrangle, Lincoln County, Nevada: U.S. Geological Survey Geologic Quadrangle Map GQ–1730, scale 1:24,000.

Siders, M.A., 1991, Geologic map of the Mount Escalante quadrangle, Iron County, Utah: Utah Geological and Mineral Survey Map 131, 9 p., scale 1:24,000.

Simmons, E.C., and Hedge, C.E., 1978, Minor-element and Sr-isotope geochemistry of Tertiary stocks, Colorado mineral belt: Contributions to Mineralogy and Petrology, v. 67, p. 379–396.

Snee, L.W., Mehnert, H.H., Rowley, P.D., Anderson, R.E., and Scott, R.B., 1990, New isotopic ages demonstrate extensional faulting of 19–12 Ma in the western Caliente caldera complex and vicinity, Lincoln County, Nevada [abs.]: Eos, v. 71, no. 43, p. 1612.

Stille, P., Unruh, D.M., and Tatsumoto, M., 1986, Pb, Sr, Nd, and Hf isotopic constraints on the origin of Hawaiian basalts and evidence for a unique mantle source: Geochimica et Cosmochimica Acta, v. 50, p. 2303–2319.

Swadley, WC, and Rowley, P.D., 1992, Geologic map of the Pahroc Springs SE quadrangle, Lincoln County, Nevada: U.S. Geological Survey Open-File Report 92–7.

Taylor, W.J., Bartley, J.M., Lux, D.R., and Axen, G.J., 1989, Timing of Tertiary extension in the Railroad Valley–Pioche transect, Nevada—Constraints from $^{40}Ar/^{39}Ar$ ages of volcanic rocks: Journal of Geophysical Research, v. 94, p. 7757–7774.

Tegtmeyer, K.J., and Farmer, G.L., 1990, Nd isotopic gradients in upper crustal magma chambers: Evidence for in situ magma–wall rock interaction: Geology, v. 18, p. 5–9.

Weil, D.F., and McKay, G.A., 1975, The partitioning of Mg, Fe, Sr, Ce, Sm, Eu, and Yb in lunar igneous systems and a possible origin of KREEP by equilibrium partial melting: Proceedings of the 6th Lunar Science Conference, p. 1143–1158.

Evidence of the Kane Springs Wash Caldera in the Meadow Valley Mountains, Southeastern Nevada

By Anne E. Harding, Robert B. Scott, Harald H. Mehnert, *and* Lawrence W. Snee

GEOLOGIC STUDIES IN THE BASIN AND RANGE–COLORADO PLATEAU TRANSITION IN SOUTHEASTERN NEVADA, SOUTHWESTERN UTAH, AND NORTHWESTERN ARIZONA, 1992

U.S. GEOLOGICAL SURVEY BULLETIN 2056–E

UNITED STATES GOVERNMENT PRINTING OFFICE, WASHINGTON : 1995

CONTENTS

FIGURES

TABLES

Evidence of the Kane Springs Wash Caldera in the Meadow Valley Mountains, Southeastern Nevada

By Anne E. Harding,[1] Robert B. Scott, Harald H. Mehnert, *and* Lawrence W. Snee

ABSTRACT

New stratigraphic, structural, chemical, petrographic, and age data suggest that the 14.5–Ma Kane Springs Wash caldera extends into the Meadow Valley Mountains, more than 10 kilometers east of its established boundary in the Delamar Mountains. The newly recognized eastern part of the caldera in the Meadow Valley Mountains has been offset left-laterally between 4 and 7 kilometers from the established western part of the caldera in the Delamar Mountains by the northeast-striking Kane Springs Wash fault located along the western side of the Meadow Valley Mountains.

In the Meadow Valley Mountains, the Grapevine Spring and Gregerson Basin Members of the Kane Wash Tuff, eruptive products of the Kane Springs Wash caldera, cap a southern stratigraphic sequence that terminates abruptly against the southern wall of this newly recognized eastern part of the caldera. Caldera-wall breccia contains clasts of the oldest outflow unit, the Grapevine Spring Member; the youngest intracaldera unit, equivalent to the upper cooling unit of the Gregerson Basin Member, encases a 200-meter-long megaclast of the Grapevine Spring Member. A northern stratigraphic sequence that accumulated within the caldera abuts the caldera wall breccia. After major eruption and collapse, caldera-filling tuff and lava flows covered intracaldera units in the eastern part of the caldera and overflowed southward onto outflow units in the Meadow Valley Mountains. The two youngest intracaldera units are mildly peralkaline and are chemically indistinguishable from the equivalent lower and upper cooling units of the Gregerson Basin Member; no intracaldera equivalent to the metaluminous Grapevine Spring Member is exposed. Comenditic lower parts and trachytic upper parts of each of the two youngest intracaldera units are exposed along the footwall block of the Kane Springs Wash fault and correlate with equivalent parts of respective outflow units. Phenocryst assemblages of quartz, sanidine, hedenbergite, and fayalitic olivine of the Gregerson Basin Member are indistinguishable from the phenocryst mineralogy of equivalent intracaldera units; also, post-collapse lava flows and tuff filling the eastern part of the caldera are similar petrographically to those of the western part. New K-Ar sanidine dates for the two youngest intracaldera units (lower unit, 14.6±0.5; upper unit, 14.6±0.4 and 14.9±0.5 Ma) and a $^{40}Ar/^{39}Ar$ sanidine date for the upper intracaldera unit (14.43±0.14 Ma) are within analytical uncertainty for dates of equivalent outflow units. A new K-Ar biotite date of 13.1±0.5 Ma from a dike intruding eastern caldera fill is comparable to dates from western caldera fill.

In contrast to the nearly undeformed western part of the caldera, the eastern part is moderately faulted, tilted, and injected by dikes; as much as 30° of eastward tilt occurred between major caldera-forming eruptions and emplacement of capping basalts 3 million years later. Apparently, the eastern part of the caldera actively extended during caldera-filling events while the western part passively rode out extension.

INTRODUCTION

This study defines and describes the volcanic stratigraphy of a complex suite of Tertiary volcanic rocks that are well exposed on the rugged northwest flank of the northern Meadow Valley Mountains, Lincoln County, southeastern Nevada, in the Basin and Range province (figs. 1, 2). A major feature recognized during mapping in this part of the Meadow Valley Mountains is an abrupt boundary that separates a southern area largely containing regionally correlated ash-flow tuffs from a northern area containing an unknown stratigraphy. The principal objective of this study became the investigation of this boundary and the rocks north of it.

As discussed following, several relatively small scale field studies of the northern Meadow Valley Mountains east and northeast of the recognized Kane Springs Wash caldera in the Delamar Mountains (fig. 2) did not find that caldera in the Meadow Valley Mountains. In fact, we also had difficulty recognizing, and then becoming confident of, the presence of the Kane Springs Wash caldera in the Meadow Valley Mountains until we had amassed nearly all the stratigraphic, structural, petrographic, chemical, and age

[1]Anne E. Harding, University of Colorado, Boulder, CO 80302.

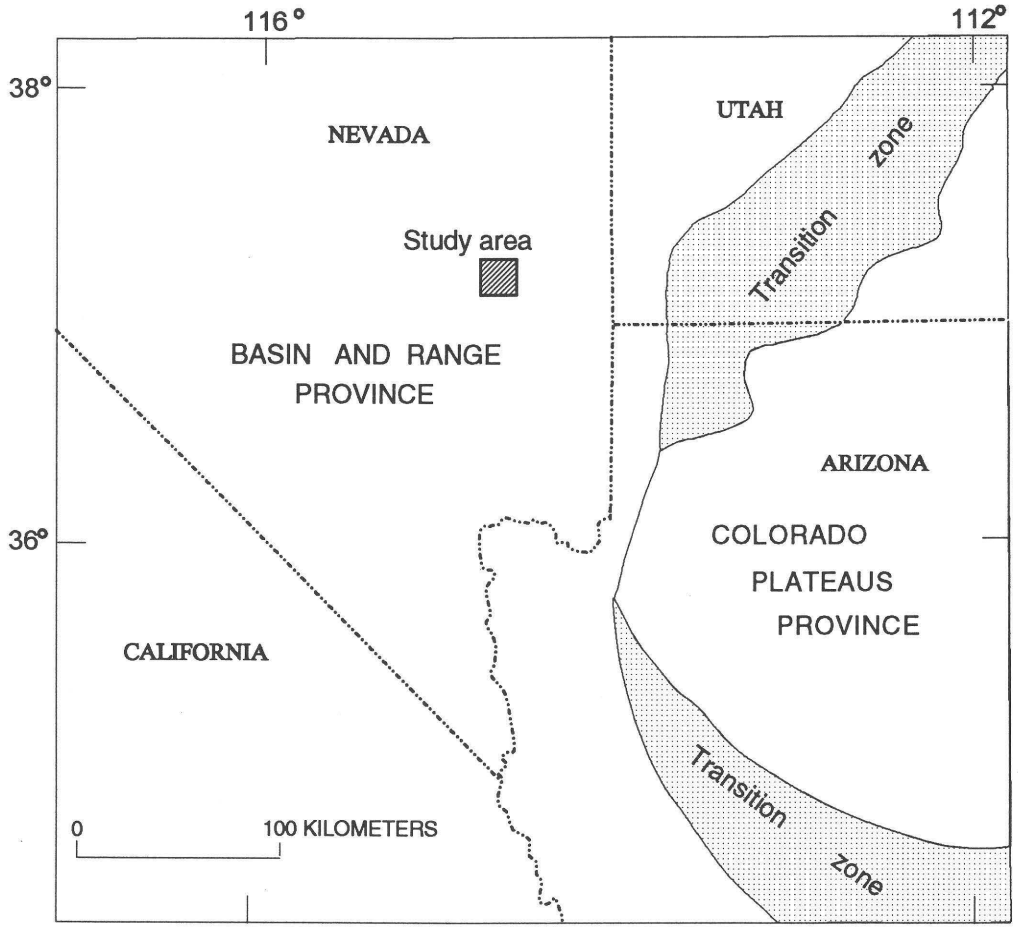

Figure 1. Location of study area, Basin and Range province, southeastern Nevada. Areas of transition zone between stable Colorado Plateau and Basin and Range province are also indicated.

data we present here. Because of this long history of investigation, we have presented our data first, free from conclusions, so that the reader is able to parallel our process of recognizing that the Kane Springs Wash caldera is also in the Meadow Valley Mountains.

REGIONAL GEOLOGY

The major volcano-stratigraphic framework in the northern Meadow Valley Mountains and surrounding areas was first established from Cook's (1965) correlation of widespread ash-flow tuffs in the eastern Basin and Range province in conjunction with Armstrong's (1970) isotopic dating of these tuffs.

Two major volcanic centers were the sources of most of the ash-flow tuffs present in the northern Meadow Valley Mountains (fig. 2). The Caliente caldera complex, located about 30 km north of the study area, produced major regional outflow sheets of ash-flow tuff from about 24 to at least 18 Ma (Rowley and others, 1990; Rowley and others, this volume); its eruptive products include the 18.6–Ma Hiko Tuff, the oldest unit exposed in the study area. In the Meadow Valley Mountains, the Hiko Tuff represents the last of the voluminous eruptions of calc-alkalic quartz-latitic and rhyolitic ash-flow tuffs that typified eruptions in Nevada between about 34 and 17 Ma (Stewart, 1980). In the Delamar Mountains west of the study area, the 14–Ma Kane Springs Wash caldera erupted the Kane Wash Tuff (Noble, 1968; Novak, 1984; Scott and others, 1993; Scott and others, this volume; Best and others, 1993). Both Noble and Novak reported the Kane Springs Wash caldera to be elongate in the east-west direction (about 19 by 13 km), with its eastern boundary buried beneath alluvial deposits in Kane Springs Valley just west of the study area. In the Meadow Valley Mountains, the Kane Wash Tuff and a capping basalt are representative of the bimodal assemblage of rhyolite and basalt, including high-silica subalkaline and peralkaline rhyolite, that followed calc-alkalic activity in Nevada.

Prevolcanic Tertiary extension (Axen and others, 1988; Taylor and Bartley, 1992) and middle-Miocene low-angle normal faulting (Axen and others, 1988; Rowley and others, 1991) north of the Caliente caldera complex apparently did not affect the Meadow Valley Mountains and adjacent areas south of the Caliente caldera complex. In central Lincoln

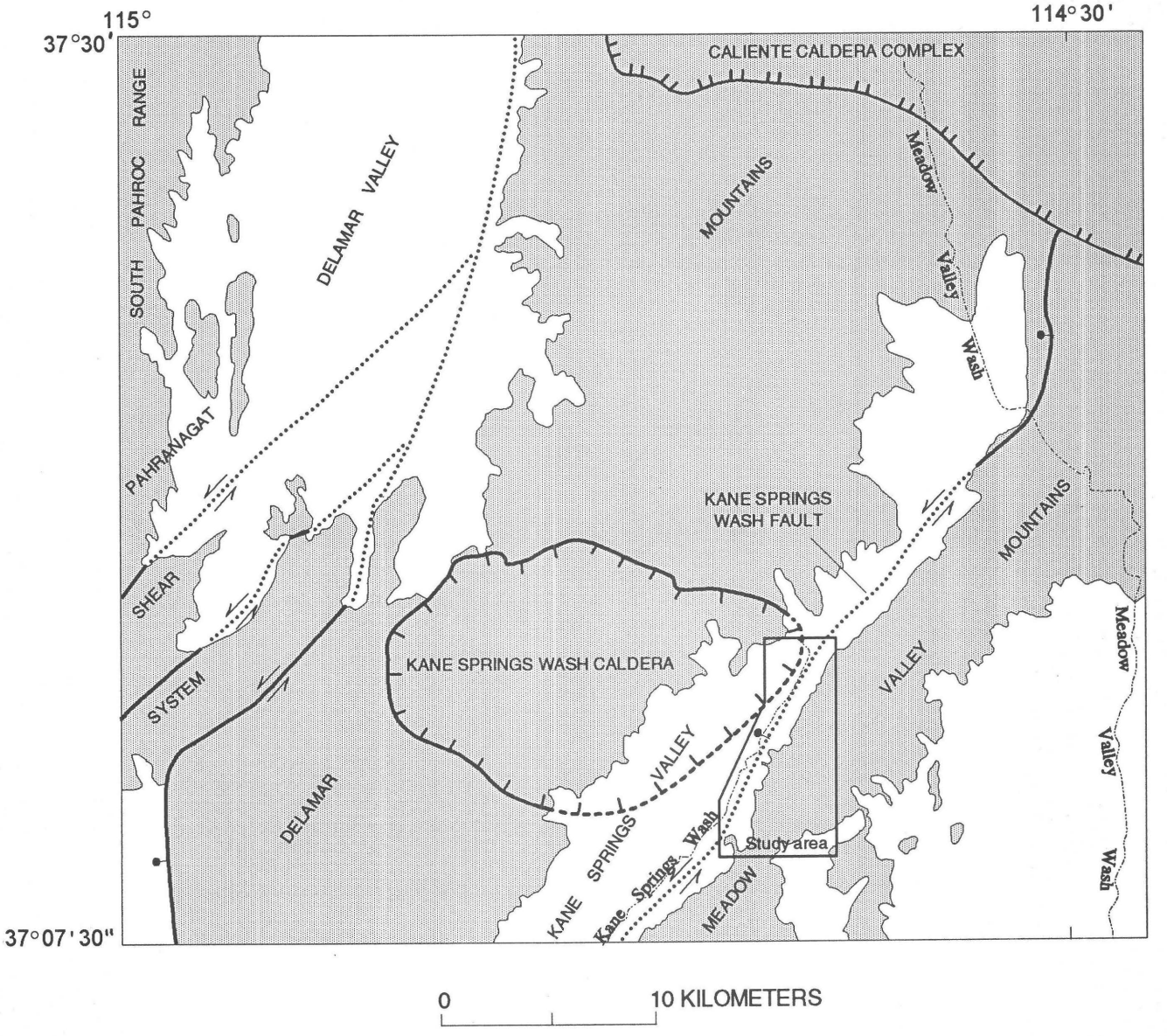

Figure 2. Location of study area in Meadow Valley Mountains and vicinity. Geology generalized from Ekren and others (1977). Bedrock is shaded; surficial deposits unshaded. Heavy lines, faults; dotted where concealed; bar and ball on downthrown side; barbs show relative motion on strike-slip and oblique-slip faults. Single-hachured line marks boundary of Kane Springs Wash caldera; double-hachured line marks boundary of Caliente caldera complex.

County south and west of the Caliente caldera complex, Scott and others (this volume) have recognized progressive tilting of strata associated with normal fault activity between about 23 and 14 Ma, although large areas within the region remained essentially unaffected by extension (Scott, 1990). Between about 15 and 10 Ma, major west-southwest-directed extension affected areas southeast of the Meadow Valley Mountains in southeastern Nevada and southwestern Utah (Wernicke and others, 1988). After about 10 Ma, the direction of extension for this part of the Basin and Range province changed to west-northwest (Zoback and others, 1981), the rate of extension decreased (Wernicke and others, 1988), and the dominant style of extension in the upper crust appeared to have been high-angle, basin-range block faulting (Anderson, 1989).

PREVIOUS INVESTIGATIONS IN THE STUDY AREA

Previous work in the study area falls into two categories: mapping in the Meadow Valley Mountains and investigations of the Kane Wash Tuff. Previous mapping in the Meadow Valley Mountains has been mainly reconnaissance in scope. Tschanz and Pampeyan (1970) mapped (1:250,000 scale) and described the geology and mineral deposits of

Lincoln County, concentrating on pre-Tertiary sedimentary rocks. They showed the northern Meadow Valley Mountains as consisting of undivided Cretaceous or Tertiary volcanic rocks, and younger Tertiary volcanic rocks. They named the western range-front fault the Kane Springs Wash fault and described it as a normal fault that cuts valley fill as young as Pliocene and early Quaternary.

Ekren and others (1977) mapped the distribution of the Tertiary rocks in Lincoln County, also at a scale of 1:250,000, and correlated some of the widespread ash-flow tuffs. In the study area, they reported three rhyolitic units and a younger basalt, most of which could not be correlated with recognized stratigraphic units. Ekren and others (1977) also recognized several ash-flow tuffs that are conspicuously flow laminated and layered and that apparently flowed during the welding process. They cautioned that these rocks are extremely difficult to distinguish from true lavas.

They interpreted the Kane Springs Wash fault as a strike-slip or oblique-slip fault having a minimum of 8 km of left-lateral displacement, based on (1) horizontal slickenlines in and adjacent to the fault zone near the head of Kane Springs Valley, (2) correlation of thick rhyolitic lavas in the northern Meadow Valley Mountains with lavas in the Delamar Mountains to the southwest, and (3) apparent offset of Paleozoic strata in the southern part of Kane Springs Wash.

During reconnaissance mapping for a wilderness study, Pampeyan (1989) mapped the geology of the Meadow Valley Mountains at a scale of 1:50,000. In all but the northern part of his map area, Pampeyan correlated units in the northern Meadow Valley Mountains with the Kane Wash Tuff as subdivided by Novak (1984), but in the northern part, he grouped units as "rhyolite lavas" or "rhyolite lavas and Kane Wash Tuff, undivided."

In written communication (1988), Pampeyan stated that "the complex lithologic, structural, and stratigraphic relations in the volcanic terrane at the northern end of the range may signify that this area is an eastward continuation of the Kane Springs Wash caldera." Although he proposed no caldera boundaries, Pampeyan suggested left-lateral offset of about 8 km across the Kane Springs Wash fault based on his interpretation that two trachyte dikes in the northernmost part of the range may mark the northern edge of the Kane Springs Wash caldera. Alternatively, he interpreted other trachyte lavas as evidence for both right-lateral and no lateral offset. In addition, Pampeyan gave several reasons why the apparent offset of Paleozoic strata proposed by Ekren and others (1977) cannot be used with certainty to indicate left-lateral offset.

Members of the Kane Wash Tuff, eruptive products of the Kane Springs Wash caldera, are among the youngest rocks previously mapped in the study area. Cook (1965) originally applied the name "Kane Wash Formation" to exposures in the Delamar and Meadow Valley Mountains. His type section for the unit in the southern Delamar Mountains contains a basalt flow in addition to eight rhyolitic ash-flow tuffs.

After reconnaissance mapping, Noble (1968) revised the definition of the Kane Wash Formation to exclude basalt, other lavas, and unrelated sedimentary rocks, and renamed it the Kane Wash Tuff. He proposed the presence of as many as 12 cooling units in the Kane Wash Tuff, but did not describe or map them individually. Noble delineated the boundaries of the source caldera (fig. 2) and produced a generalized geologic map of the distribution of the Kane Wash Tuff, showing rocks in the northern Meadow Valley Mountains as outflow units derived from that caldera. Noble recognized the peralkaline chemistry of the rocks and reported a K-Ar date of 14.0±0.5 Ma for the tuff.

Novak (1984) and Novak and Mahood (1986) described the eruptive history and the chemical evolution of the Kane Springs Wash volcanic center based on geochemistry, K-Ar dates, and field mapping (published at a scale of about 1:130,000). Novak (1984) divided the Kane Wash Tuff into five mappable units, members V_3, V_2, V_1, W, and O (in order of decreasing age), and described them along with younger caldera-filling lava flows and tuffs. Based on the distribution of the tuffs and on dating, Novak recognized that members V_1, V_2, and V_3 (14.1±0.4 Ma) were erupted from the Kane Springs Wash volcanic center, but that the older members W and O (14.7±0.4 and 15.6±0.4 Ma, respectively) came from sources south and west of the Kane Springs Wash volcanic center. (Novak reported his dates with one standard deviation; here his results are reported with two standard deviations to be consistent with other literature.) East of the caldera in the Meadow Valley Mountains, in the southern part of the study area, Novak mapped Kane Wash Tuff and basalt, and in the northern part he mapped pre-Kane Wash volcanic rocks.

ACKNOWLEDGMENTS

This study was done in partial fulfillment of Anne Harding's M.S. degree at the University of Colorado, Boulder. During the study she was a volunteer with a U.S. Geological Survey mapping project that is studying the transition between the Basin and Range province and the Colorado Plateau (Basin and Range–Colorado Plateau Transition in southeastern Nevada, southwestern Utah, and northwestern Arizona Study Unit of the National Geologic Mapping Program). See Introduction, this volume, for more information on the project. The U.S. Geological Survey provided her with maps, aerial photographs, field trailer, and laboratory equipment. USGS analytical laboratories performed most of the chemical analyses.

Steve Novak suggested the study area and provided a copy of the geologic map from his Ph. D. dissertation (Novak, 1985). Support from a large number of USGS scientists and technicians is deeply appreciated. Dave Nealey helped us present our chemical data by making REE and spider diagrams. We especially thank reviewers Mark Hudson and Scott Minor for their constructive advice and encouragement.

METHODS OF STUDY

A variety of techniques was used to define and describe the volcanic stratigraphy in the study area and to correlate these strata with regional volcanic units.

About 60 days of detailed field mapping between 1988 and 1990 delineated the stratigraphic and structural relationships in the study area. Most contacts and faults were walked out, as little contrast in color or features is apparent between many of the units both on the photos and in the field. Field data were recorded on color aerial photographs (scale of about 1:30,000) and were compiled on a 1:12,000-scale, stable mylar topographic base map by means of a Kern PG–2 photogrammetric plotter.

About 75 samples were selected and cut for thin-section analysis. The thin sections were stained for identification of potassium-bearing phases. Modes were obtained from about 50 thin sections (Appendix 1). For most of the modal analyses, a minimum of 200 phenocryst points and a minimum of 2,000 total points were counted.

Twenty-three samples were analyzed by energy-dispersive X-ray fluorescence (EDXRF) spectrometry (Appendix 2A) by means of the U.S. Geological Survey Kevex 7000 spectrometer, using methods outlined by Johnson and King (1987). A ^{109}Cd source was used to analyze for Rb, Sr, Y, Zr, and Nb. A ^{241}Am source was used to analyze for Ba, La, Ce, and Nd. The U.S. Geological Survey standard rock GSP–1 was used as a calibration standard. In the illustrations and tables, only the Zr data from the EDXRF analyses were used; more precise data were obtained for other elements by other methods.

Major-element oxides were determined in 21 samples by wavelength-dispersive X-ray fluorescence (WDXRF) spectrometry (Appendix 2B) using the methods of Taggart and others (1987). All major-element data in the diagrams and tables come from WDXRF analyses.

Instrumental neutron activation analysis (INAA) of 15 samples provided data for many major, minor, and trace elements (Appendix 2C), particularly the rare earth elements (Baedecker and McKown, 1987). All minor- and trace-element data except for the elements Zn, Ga, Sr, Y, Nb, and Pb that appear in the diagrams and tables were determined by INAA.

The same 15 samples were also analyzed (Appendix 2D) by inductively coupled plasma–atomic emission spectrometry (ICP-AES) by means of the methods described by Lichte and others (1987). This method provided semiquantitative analyses for some elements not analyzed by another method. The ICP-AES values for the elements Zn, Ga, Sr, Y, Nb, and Pb were used in the diagrams and tables.

To refine the stratigraphic framework, five samples were collected for isotopic dating using potassium-argon dating methods (Appendix 3). Conventional K-Ar dates were obtained from five samples (for methods see Dalrymple and Lanphere, 1969; for constants see Steiger and Jäger, 1977). One sample was redated using the more precise ^{40}Ar/^{39}Ar method (Shubat and Snee, 1992).

STRATIGRAPHY

The two stratigraphic sequences separated by the abrupt boundary mentioned in the Introduction are described separately, beginning with the southern sequence. Units overlying both sequences and the boundary between them are described with the northern sequence. Informal field names are used for new stratigraphic units. Fresh rock colors are given in all descriptions, and color names are from the Rock-Color Chart (Goddard, 1948). A generalized geologic map of the study area is shown in figure 3; detailed field relationships are not shown on this map but are documented elsewhere at scales of 1:12,000 (Harding, 1991) and 1:24,000 (Scott, Harding, and others, 1991).

The nomenclature for the Kane Wash Tuff used in this study follows the usage of Scott and others (1993). After mapping this tuff in nine 7.5-minute quadrangles, Scott and others removed the units of its lower part, members W and O of the Kane Wash Tuff of Novak (1984), from the Kane Wash Tuff because they are now regarded to have separate sources. They reassigned Novak's members W and O to two newly named formations. The name Kane Wash Tuff is now restricted to the three petrologically related ash-flow tuff cooling units that were derived from the Kane Springs Wash caldera. Novak (1984) defined these cooling units as members V_3, V_2, and V_1. Locally, members V_3 and V_2 are indistinguishable in the field and, therefore, these have been combined into one consistently mappable member, the Gregerson Basin Member (fig. 4). Rocks of Novak's member V_1 have been reassigned to the Grapevine Spring Member (Scott and others, 1993).

Novak (1984) also described and named two older cooling units, members W and O of his Kane Wash Tuff, and recognized that these members are distinctly different in age, geographic distribution, and genesis from the younger peralkaline tuffs, members V_1, V_2, and V_3. The rocks of these two units have been designated as separate formations (Scott and others, 1993): in descending order, the Sunflower Mountain Tuff (=member W) and the Delamar Lake Tuff (=member O) (fig. 4).

SOUTHERN STRATIGRAPHIC SEQUENCE

The southern stratigraphic sequence consists of units which are correlated with regional ash-flow tuffs. These units can be traced from the southern part of the study area to about the midpoint of the map (fig. 3), where the units end abruptly against the northern stratigraphic sequence.

EXPLANATION

QUATERNARY

Pliocene

QTa	Alluvium and colluvium

TERTIARY

Miocene

Tb	Upper basalt flow
Tfb	Flow-banded rhyolite
Tlr	Lithophysal rhyolite flow
Tbm	Middle basalt flow
Tyt	Yellow tuff
Tgt	Gray ash-flow tuff
Tbl	Lower basalt flow
Tfl	Flow-lineated rhyolite
Tcj	Columnar-jointed rhyolite
Tlt	Lithic-rich tuff

Try	Youngest rhyolite flows
Tpr	Pumice-rich ash-flow tuff
Td	Rhyolite dike
Tvc	Volcanic center
Tbr	Biotite-rhyolite flow
Trlr	Red lithic rhyolite
Twb	Wall breccia
Tkb	Gregerson Basin Member of the Kane Wash Tuff
Tkg	Grapevine Spring Member of the Kane Wash Tuff
Tpt	Precaldera trachyte flows
Tot	Older tuff
Tsm	Sunflower Mountain Tuff
Tdl	Delamar Lake Tuff
Th	Hiko Tuff

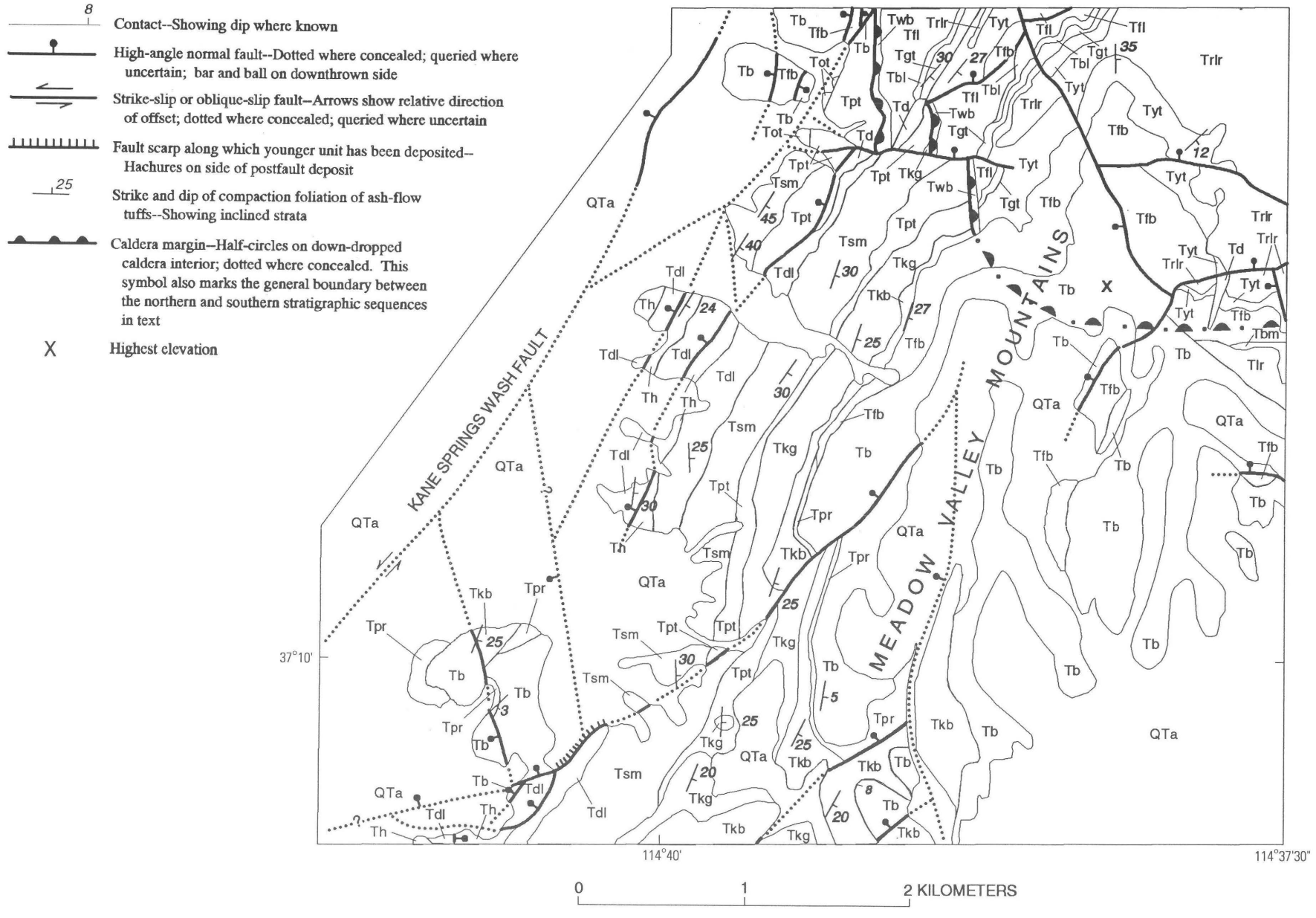

Figure 3. Generalized geologic map of the study area.

HIKO TUFF

The oldest unit exposed in the southern stratigraphic sequence is the Hiko Tuff, a devitrified, moderately welded, rhyolitic ash-flow tuff that forms gentle slopes (fig. 5). The tuff is slightly but pervasively hydrothermally altered throughout the study area and is grayish orange to dark yellowish orange; elsewhere, unaltered rock is light brownish gray. The Hiko Tuff contains 30–40 percent phenocrysts based on two thin-section modal analyses, one from the study area (Appendix 1) and one from a locality north of the study area. The phenocrysts consist of 17–31 percent very pale purple quartz, 14–32 percent sanidine, 28–55 percent plagioclase, 5–12 percent biotite, and 2 percent opaque minerals. The tuff contains 1–16 percent volcanic and distinctive Paleozoic argillitic lithic fragments. Pumice fragments as long as 3 cm form 10–25 percent of the rock. Taylor and others (1989) reported a $^{40}Ar/^{39}Ar$ biotite date of 18.5±0.4 Ma for the Hiko Tuff, but suggested that the best age estimate may be 18.6 Ma based on additional data. The thickness of the Hiko Tuff cannot be determined in the study area because its base is not exposed; however, a thickness of about 75 m for the Hiko Tuff was measured south of the study area in the Vigo NW 7.5-minute quadrangle (Scott, Harding, and others, 1991).

Novak (1984)		Scott and others (1993)	
Kane Wash Tuff	Member V_3	Kane Wash Tuff	Gregerson Basin Member
	Member V_2		
	Member V_1		Grapevine Spring Member
	Member W	Sunflower Mountain Tuff	Upper member
			Lower member
	Member O	Delamar Lake Tuff	Four informal members

Figure 4. Stratigraphic nomenclature changes for the Kane Wash Tuff.

DELAMAR LAKE TUFF

The Delamar Lake Tuff (Scott and others, 1993), which overlies the Hiko Tuff, is a devitrified, moderately welded, rhyolitic ash-flow tuff that forms both gentle slopes and sharp ledges and ranges from about 60 to 120 m thick. The Delamar Lake Tuff is the oldest high-silica rhyolite ash-flow tuff representative of the bimodal basalt-rhyolite volcanism in this part of the Basin and Range province. Like the Hiko Tuff, it is slightly but pervasively hydrothermally altered over an area extending nearly to the southern edge of the study area. Altered rocks are pale pink, pale red purple, pale yellowish orange, and moderate reddish orange; in

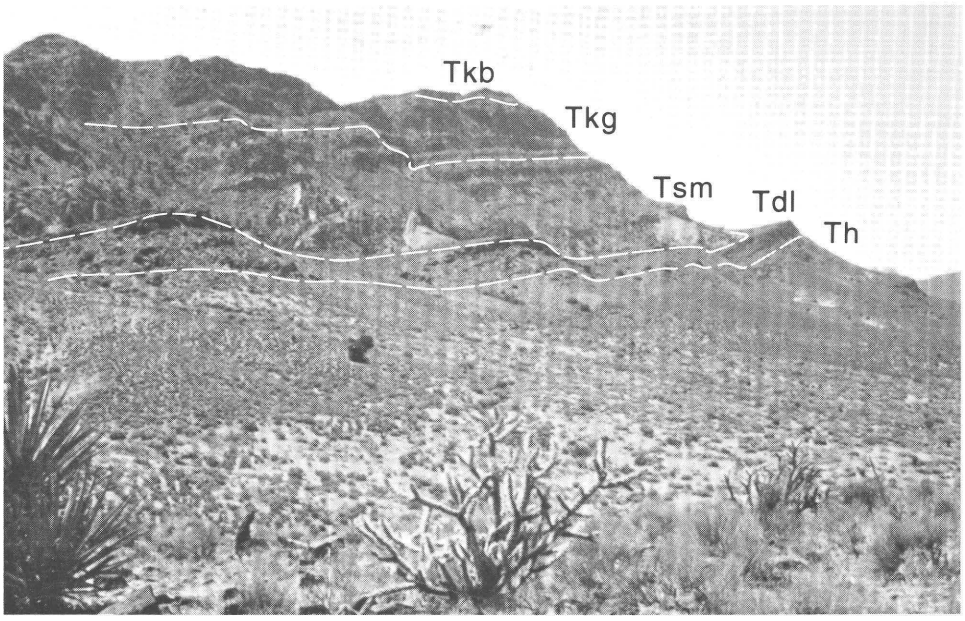

Figure 5. Southern stratigraphic sequence in the Meadow Valley Mountains. In descending order, the Gregerson Basin (Tkb) and Grapevine Spring (Tkg) Members of the Kane Wash Tuff form the bold cliffs on the skyline. The Sunflower Mountain Tuff (Tsm) forms the major bench and the overlying small, bold cliff. The Delamar Lake Tuff (Tdl) forms the lowest sharp ledge above the poorly exposed, slope-forming Hiko Tuff (Th). View to southeast.

some localities, they display Liesegang rings of yellowish-gray to light-red iron oxides. The tuff contains about 20 percent phenocrysts that consist of 25 percent quartz, 70 percent sanidine, and 5 percent altered ferromagnesian and opaque minerals. Less than 2 percent of the rock consists of volcanic lithic fragments. Flattened pumice fragments as long as 4 cm form about 10 percent of the tuff. Sanidine K-Ar dates for the tuff are 15.5±0.4 and 15.8±0.4 Ma (Novak, 1984). The overlying Sunflower Mountain Tuff is not hydrothermally altered, thereby restricting the time of alteration of the Delamar Lake and Hiko Tuffs.

SUNFLOWER MOUNTAIN TUFF

Stratigraphically above the Delamar Lake Tuff, the Sunflower Mountain Tuff (Scott and others, 1993) is a pinkish-gray to grayish-orange, devitrified, rhyolitic ash-flow tuff that typically forms gentle slopes below bold cliffs (fig. 5). The Sunflower Mountain Tuff contains a lower, nonwelded to partially welded zone and an upper, partially to moderately welded zone. A K-Ar date of 14.7±0.4 Ma for the tuff was obtained from sanidine (Novak, 1984).

The lower, nonwelded to partially welded zone of the Sunflower Mountain Tuff is pale orange to grayish orange and forms gentle to moderate slopes (fig. 5). The lower zone ranges in thickness from about 120 to 220 m. The rock contains about 10 percent phenocrysts that consist of subequal amounts of quartz and sanidine and sparse altered ferromagnesian minerals. Pumice fragments, which form about 20 percent of the rock, are 0.5–3 cm long. Rhyolitic volcanic lithic fragments form about 20 percent of the rock.

The upper, partially to moderately welded zone, which is mottled pinkish gray to pale red, forms moderate slopes to bold cliffs. Mottling consists of distinctive moderate-orange-pink to very pale orange altered blotches in a pale-red matrix. In the southern part of the study area, the upper zone of the Sunflower Mountain Tuff is as much as 150 m thick. The rock contains 9–14 percent phenocrysts that consist of 34–37 percent quartz, 60–63 percent sanidine, less than 1 percent plagioclase, and 2–3 percent altered ferromagnesian and opaque minerals (Appendix 1). Pumice fragments form about 20 percent of the rock and are as long as 15 cm. Rhyolitic volcanic lithic fragments form less than 1 percent of the rock.

OLDER TUFF

Three small exposures of a pale-red-purple, devitrified, densely welded, rhyolitic ash-flow tuff form a small bench (2 m high) along the range front, on the footwall of the Kane Springs Wash fault. The tuff contains 4 percent phenocrysts that consist of 20 percent quartz, 70 percent sanidine, and 10 percent altered ferromagnesian and opaque minerals (Appendix 1). The older tuff is considered to be the outflow facies from a peralkaline precursor of the Kane Springs Wash caldera, the Narrow Canyon caldera (Scott, Blank, and Page, 1991); the older tuff lies below the precaldera trachyte flows in the study area. Based on regional correlations made during unpublished mapping, the older tuff is younger than the Hiko Tuff and older than the Kane Wash Tuff. Because the older tuff is mildly peralkaline, like the Kane Wash Tuff, it is probably younger than the less geochemically evolved metaluminous Delamar Lake and Sunflower Mountain Tuffs (based on unpublished geochemical studies by R.B. Scott).

PRECALDERA TRACHYTE FLOWS

Stratigraphically above the older tuff at one locality and above the Sunflower Mountain Tuff elsewhere, pale-red to grayish-red, devitrified, trachytic lava flows form rugged, steep slopes and small cliffs. These trachyte flows were referred to as the precaldera trachyte lavas by Novak (1984) because he found the trachyte flows to be restricted to localities near the Kane Springs Wash caldera margin below the Kane Wash Tuff and to have an age indistinguishable from that of the Kane Wash Tuff. The precaldera trachyte flows are massive and lack megascopic flow banding; however, flow banding can be seen in thin section. A very dusky red to black basal vitrophyre is present locally. Just south of the boundary between the stratigraphic sequences, two cooling breaks indicate the presence of at least three flows. The precaldera trachyte contains 36 percent phenocrysts, 95 percent of which are conspicuous alkali-feldspar phenocrysts that range from 0.25 to 1 cm in diameter. The remainder of the phenocrysts consists of 4 percent pyroxene and 2 percent opaque and altered ferromagnesian minerals (Appendix 1). The precaldera trachyte is about 180 m thick at the northern limit of exposure in the study area, and it pinches out to the south. K-Ar sanidine dates for the precaldera trachyte flows are 13.6±0.4 and 14.2±0.4 Ma (Novak, 1984).

KANE WASH TUFF

The Kane Wash Tuff consists of two newly defined members, the Grapevine Spring Member and the Gregerson Basin Member (Scott and others, 1993), whose rocks were erupted from the Kane Springs Wash caldera. Although Noble (1968) described the rocks of his Kane Wash Tuff as peralkaline, only the upper Gregerson Basin Member (equivalent to members V_2 and V_3 of Novak, 1984) of the Kane Wash Tuff is mildly peralkaline (Novak, 1984). The lower Grapevine Spring Member (equivalent to member V_1 of Novak, 1984) of the Kane Wash Tuff is metaluminous (Novak, 1984), making it chemically distinct from the Gregerson Basin.

The Grapevine Spring Member overlies either the precaldera trachyte or the Sunflower Mountain Tuff and is a

light-brownish-gray to brownish-gray, devitrified, moderately to densely welded, rhyolitic to trachytic ash-flow tuff that forms rugged slopes and cliffs (fig. 5). The tuff is characterized by a moderate abundance of sanidine phenocrysts that are adularescent. (See Mittwede, 1987.) Throughout its regional distribution, phenocryst abundances range from 16 to 35 percent and consist of 8–27 percent quartz, 64–78 percent sanidine, and 4–16 percent hedenbergite, fayalite, and opaque minerals. The basal part of the unit contains 38 percent phenocrysts that consist of less than 1 percent quartz, 94 percent sanidine, less than 1 percent plagioclase, 3 percent hedenbergite, and 2 percent opaque minerals (Appendix 1). The tuff contains few lithic fragments or recognizable pumice fragments. Novak (1984) reported K-Ar dates of 14.0±0.4 and 14.2±0.4 Ma for sanidine from the Grapevine Spring Member (his member V_1). A new $^{40}Ar/^{39}Ar$ date of sanidine from this unit of 14.67±0.22 Ma has been determined (analysis by L.W. Snee) (Appendix 3).

The Gregerson Basin Member of the Kane Wash Tuff consists of a lower and an upper cooling unit equivalent to members V_2 and V_3, respectively, of the Kane Wash Tuff as used by Novak (1984) (fig. 4).

The lower cooling unit is a devitrified, moderately to densely welded ash-flow tuff that forms moderate slopes and cliffs (fig. 5) and is characterized by conspicuous adularescent sanidine phenocrysts. Most of the lower cooling unit is pinkish gray to yellowish gray, but it is pale blue and light bluish gray in some zones. The lower cooling unit is about 100 m thick. Regionally, the tuff contains 24–36 percent phenocrysts that consist of 6–51 percent quartz, 47–78 percent sanidine, and 3–15 percent altered ferromagnesian (some relict hedenbergite and fayalite) and opaque minerals. Distinctive vapor-phase amethyst and blue-green amphibole, probably riebeckite, are present. Samples at and near the base of the lower cooling unit contain 8–11 percent phenocrysts that consist of 30–44 percent quartz, 55–65 percent sanidine, and 1–5 percent altered ferromagnesian (some relict hedenbergite) and opaque minerals (Appendix 1). Highly flattened pumice fragments about 5 cm long that enhance parting parallel to the plane of compaction form about 20 percent of the rock. The lower cooling unit is capped by pale-yellowish-brown, partially to moderately welded ash-flow tuff containing as much as 20 percent cognate trachytic inclusions. These inclusions are from 1 to 30 cm long, scoriaceous, and pale brown to grayish brown; they contain about 50 percent phenocrysts of alkali feldspar. Novak (1984) reported a K-Ar date of 14.1±0.4 Ma for the sanidine from the lower cooling unit (equivalent to his member V_2) of the Gregerson Basin Member. A new $^{40}Ar/^{39}Ar$ date of 14.55±0.14 Ma has been determined for sanidine from the lower cooling unit of the Gregerson Basin Member (analysis by L.W. Snee) (Appendix 3).

The upper cooling unit of the Gregerson Basin Member is a devitrified, moderately to densely welded ash-flow tuff that is nearly indistinguishable lithologically from the lower cooling unit. Modal analysis of a thin section of a sample near the base of the upper cooling unit indicates that the rock contains 10 percent phenocrysts that consist of 33 percent quartz, 64 percent sanidine, and 3 percent altered ferromagnesian (some relict hedenbergite) and opaque minerals (Appendix 1). Some acicular dark-blue-green, vapor-phase crystals, probably riebeckite, are also present. The upper cooling unit is about 20 m thick in the southern part of the study area and pinches out to the north. A new $^{40}Ar/^{39}Ar$ date of 14.39±0.28 Ma has been determined for sanidine from the upper cooling unit (analysis by L.W. Snee) (Appendix 3).

NORTHERN STRATIGRAPHIC SEQUENCE

The northern stratigraphic sequence cannot be correlated directly with regional ash-flow tuff units. Therefore, this sequence must have a local source. The sequence is continuous from the northern part of the map area southward to the midpoint of the map (fig. 3).

LITHIC-RICH TUFF

A lithic-rich tuff forms the oldest rock unit in the northern volcanic sequence. The rock is a quartz-sanidine-bearing, rhyolitic tuff that contains abundant lithic fragments and some pumice fragments. This tuff is poorly exposed, and typically it is brecciated and altered. Only the upper 5 m of this rock unit are exposed over a lateral distance of about 300 m in the footwall block along Kane Springs Wash fault in the northern part of the map area. The lithic-rich tuff has not been dated, and its relative age is uncertain. Welding of pumice fragments and groundmass around lithic fragments and the lack of sorting of the lithic fragments indicate that the lithic-rich tuff was probably emplaced as an ash flow.

The lithic-rich tuff is light brownish gray to grayish red purple and contains as much as 75 percent inclusions. Pumice fragments of the tuff, probably most representative of its magmatic source, contain 10 percent phenocrysts that consist of 42 percent quartz, 54 percent sanidine, and 4 percent altered ferromagnesian minerals (Appendix 1).

Two types of pale-red to grayish-red trachyte, which are probably foreign lithic fragments, are the most conspicuous inclusions in hand samples. Other inclusions, noticeable in thin section, are probably cognate because they were still ductile when incorporated into the lithic-rich tuff (Harding, 1991).

COLUMNAR-JOINTED RHYOLITE

Along the range front in the northern part of the study area, a columnar-jointed rhyolite ash-flow tuff forms steep

slopes and cliffs and weathers into small boulders that form talus cones on the slopes. The columnar-jointed rhyolite contains quartz, sanidine, and ferromagnesian phenocrysts. Most of the quartz phenocrysts are 2 mm or less in diameter. Sanidine phenocrysts are as much as 5 mm long, and some of them are adularescent. Although most of the ferromagnesian phenocrysts were altered to opaque minerals, remnant green-tinged clinopyroxene and olivine can be identified in a few thin sections. The olivine is probably fayalitic, as it coexists with quartz. The columnar-jointed rhyolite also contains accessory phenocrystic zircon, some of which is prismatic. A new K-Ar sanidine date for this unit is 14.6±0.5 Ma (analysis by H.H. Mehnert) (Appendix 3). The columnar-jointed rhyolite, which is about 130 m thick, can be divided into three zones: a basal, layered zone; a middle, densely welded zone; and an upper, partially welded zone. Crude columnar jointing characterizes the densely welded zone in places. The rock has a weak flow foliation along which a parting has developed. Table 1 summarizes the phenocryst mineralogy and thickness for each zone. Complete petrographic modal analyses are in Appendix 1.

The basal, layered zone is exposed only near the Kane Springs Wash fault adjacent to the lithic-rich tuff. Layering is evident from color, contrasting styles of devitrification, degrees of welding, and in one case, a difference in phenocryst abundance. Both a black vitrophyre and the light-bluish-gray layer are densely welded. The pale-red layer is devitrified, moderately welded, and contains abundant microscopic cavities, now partly filled with vapor-phase amphibole and unknown dark acicular crystals. Secondary quartz completely fills the cavities between the vapor-phase minerals.

The layered zone is generally less than 5 m thick and at some exposures is less than 30 cm thick. Where thin, this zone consists of several relatively phenocryst-rich layers (14–17 percent phenocrysts, Appendix 1), separated by several densely welded, phenocryst-poor layers (<2 percent phenocrysts) that are less than 3 cm thick. The basal layered zone is chilled and has preserved its diagnostic ferromagnesian phenocryst mineralogy, particularly in the vitrophyre (fig. 6). Dark-grayish-blue-green amphibole (riebeckite?) can be observed in the bluish-gray layer of the basal zone. In contrast, the middle and upper zones contain only altered ferromagnesian phases.

The middle, densely welded zone consists of devitrified, light-gray to medium-light-gray rhyolite and is about 90 m thick. Both the densely welded and the partially welded zones have less abundant phenocrysts than the layered zone (table 1). The felsic groundmass of the densely welded zone contains aggregates of secondary opaque minerals with irregular crystal boundaries that in some places give the rock a "peppered" appearance in hand sample.

The upper, partially welded zone of the columnar-jointed rhyolite is grayish pink to pale red purple and about 35 m thick. This zone contains abundant unflattened pumice fragments that are as large as 12 cm in diameter, and the zone also contains grayish-red trachytic inclusions tens of centimeters in diameter that consist of as much as 40 percent alkali-feldspar phenocrysts and no quartz. These trachytic inclusions were deformed during compaction of the ash-flow tuff and are considered to be cognate. Flattened pumice fragments and deformed glass shards can be seen in thin sections of the partially welded zone (fig. 7). Abundant small, secondary opaque minerals and aggregates of opaque minerals are present in the groundmass. The partially welded zone is porous and contains abundant microscopic vapor-phase cavities, many of which are lined with dark, acicular, vapor-phase crystals (amphibole?).

Figure 6. Photomicrograph of green-tinged hedenbergite (bottom) and partly altered fayalitic olivine (top) microphenocrysts in vitrophyre in basal, layered zone of columnar-jointed rhyolite. View is 0.64 mm high; plane light.

Although the columnar-jointed rhyolite has flow foliation and lineation, features commonly associated with lava flows, other features indicate that this unit was emplaced as an ash flow. Supportive evidence includes (1) a layered basal zone, (2) the presence of glass shards and pumice fragments, (3) a decrease in the degree of welding toward the top of the

Table 1. Zones in the columnar-jointed rhyolite.

[Percent of phenocrysts refers to percent of rock. Mineral percentages are percent of phenocrysts; nd, not determined]

Zone (thickness)	Phenocrysts (percent)	Quartz (percent)	Sanidine (percent)	Ferromagnesian and opaque (percent)
Partially welded zone (35 m)	3–7	24–30	62–71	5–10
Densely welded zone (90 m)	6	30	66	4
Layered zone (<5 m)				
Light-bluish-gray	16	20	75	5
Pale-red	9	28	71	1
Black vitrophyre	13	30	67	3
Greenish-gray vitrophyre	nd	nd	nd	nd

Figure 7. Photomicrograph of relict glass shard morphology preserved in upper, partially welded zone of columnar-jointed rhyolite. View is 1.26 mm high; plane light.

unit (Smith, 1960), (4) an increase in ferromagnesian phenocryst content toward the top of the unit, and (5) the presence of trachytic inclusions in the uppermost part of the unit. Ash-fall deposits commonly underlie ash-flow tuffs, and the layered basal zone of this unit with its variation in phenocryst abundance may have resulted from several bedded ash deposits that were subsequently welded by the heat of the overlying tuff (Smith, 1960). The layered basal zone lacks textures indicative of pyroclastic surge deposits (Wohletz and Sheridan, 1979). The increase in mafic phases and cognate trachytic inclusions toward the top of the columnar-jointed rhyolite is similar to zonation reported for other ash-flow tuffs that were erupted from chemically zoned magma chambers (Lipman and others, 1966). The weak flow foliation and lineation probably formed during post-emplacement flow.

BRECCIA

A coarse, angular boulder breccia is discontinuously exposed along the boundary between the northern and southern stratigraphic sequences (fig. 3). The breccia is included with the northern stratigraphic sequence because in some places the breccia interfingers with the northern sequence. This unit may be as thick as 40 m locally. The breccia consists mostly of clasts of precaldera trachyte and Grapevine Spring Member of the Kane Wash Tuff, rock units exposed in the abutting southern stratigraphic sequence. These clasts are in a pale-reddish-brown, partially welded, devitrified, tuffaceous matrix that contains phenocrysts of quartz and sanidine. Locally the matrix of the breccia is similar to partially welded flow-lineated rhyolite, a unit described below. At the southern end of the westernmost segment of wall breccia (fig. 3), a 200-m-long megabreccia clast composed of the Grapevine Spring Member is partly enveloped in a vitrophyre of the flow-lineated rhyolite.

The breccia displays a massive to crude bedding that dips away from the southern stratigraphic sequence into the northern sequence at attitudes close to the angle of repose. There is a lack of planar shear in the breccia. The lateral margin of the flow-lineated rhyolite has chilled against the breccia; in some localities the breccia is interbedded with chilled layers of the flow-lineated rhyolite above the westernmost segment of the breccia (fig. 3).

FLOW-LINEATED RHYOLITE

A flow-lineated, rhyolite ash-flow tuff that forms prominent cliffs below gentle, rounded slopes is widely exposed

along the mountain front in the northern part of the area. This unit contains quartz, sanidine, and ferromagnesian phenocrysts. Most of the quartz phenocrysts are 2 mm or less in diameter. Sanidine phenocrysts are as much as 5 mm long and some are adularescent. Although most ferromagnesian phenocrysts were altered to opaque minerals, a few remnant green-tinged clinopyroxene phenocrysts can be identified in thin section. The flow-lineated rhyolite also contains accessory phenocrystic zircon, only some of which is prismatic. Two new K-Ar sanidine dates obtained for this unit are 14.6±0.4 and 14.9±0.5 Ma (analyses by H.H. Mehnert), and a more precise $^{40}Ar/^{39}Ar$ sanidine date is 14.43±0.14 Ma (analysis by L.W. Snee) (Appendix 3). Although within a few meters of its base the rhyolite has layering that is parallel to the base, higher in the unit it is strongly flow foliated and flow lineated (figs. 8, 9). This unit is about 110 m thick and can be divided into three zones: a basal, layered zone; a middle, densely welded zone; and an upper, partially welded zone. Table 2 summarizes the phenocryst mineralogy and thickness of each zone; complete petrographic modal analyses are given in Appendix 1.

The basal, layered zone, which is less than 3 m thick, is commonly covered with colluvium; however, this zone can usually be identified in the field by the presence of distinctively colored float. A black vitrophyre occurs locally at the base of the zone. Layering in the basal, layered zone results from differences in the abundance of phenocrysts as well as from color differences (fig. 10).

Several layers within the basal, layered zone are distinctive. The pale-red, phenocryst-rich layer, ranging from 3 to 5 cm thick, contains vapor-phase amphibole and dark, acicular crystals in cavities. Deformed glass shards and a eutaxitic texture are evident in thin section in the grayish-red, phenocryst-poor layer, which ranges from 1 to 5 cm thick (fig. 11). The pale-red and light-greenish-gray layer is conspicuous in float. Some sanidine phenocrysts in this layer are altered, appearing white in hand sample. In some places this layer is dark yellowish brown.

The 70-m-thick middle, densely welded zone is composed of devitrified, light-gray rhyolite with very light gray stringers aligned parallel to foliation. A strong flow lineation in the plane of the foliation is characteristic of this zone. The groundmass contains granular clumps and sheaf like aggregates of an unknown, pale-green, secondary mineral.

The upper, partially welded zone of the flow-lineated rhyolite is pale red and about 40 m thick. It weathers to form

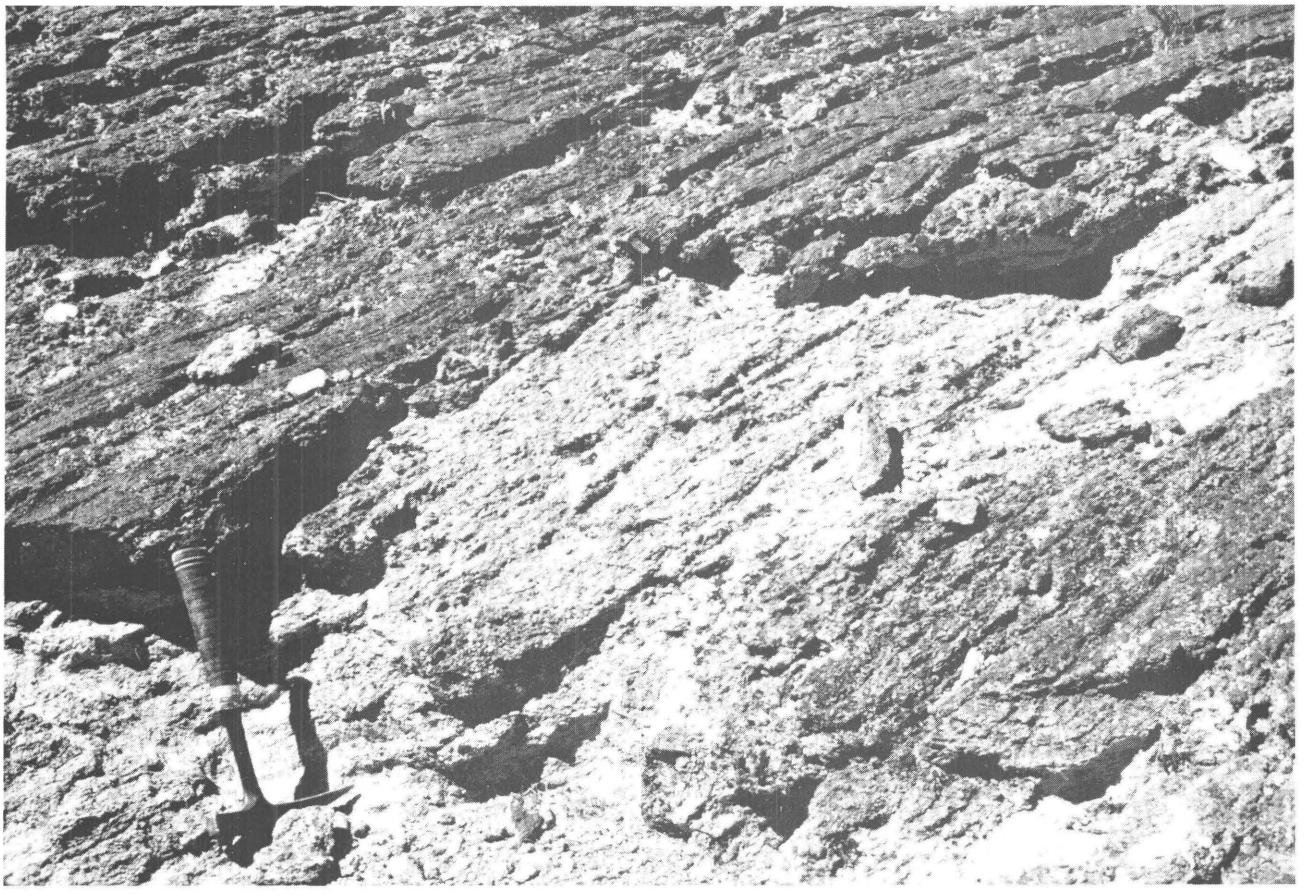

Figure 8. Flow lineation of the flow-lineated rhyolite. Hammer for scale.

Table 2. Zones in the flow-lineated rhyolite.

[Percent of phenocrysts refers to percent of rock. Mineral percentages are percent of phenocrysts; nd, not determined; *, estimated]

Zone (thickness)	Phenocrysts (percent)	Quartz (percent)	Sanidine (percent)	Ferromagnesian and opaque (percent)
Partially welded zone (40 m)	18–39	23–29	57–73	12–14
Densely welded zone (70 m)	13–21	29–37	59–71	3–4
Layered zone (<3 m)				
Pale-red, hackly fractured	*20	nd	nd	nd
Pale-red and light-greenish-gray	*10	*30	*65	*5
Grayish- red, phenocryst-poor	4	54	40	6
Pale-red, phenocryst-rich	45	39	60	1
Black vitrophyre	nd	nd	nd	nd

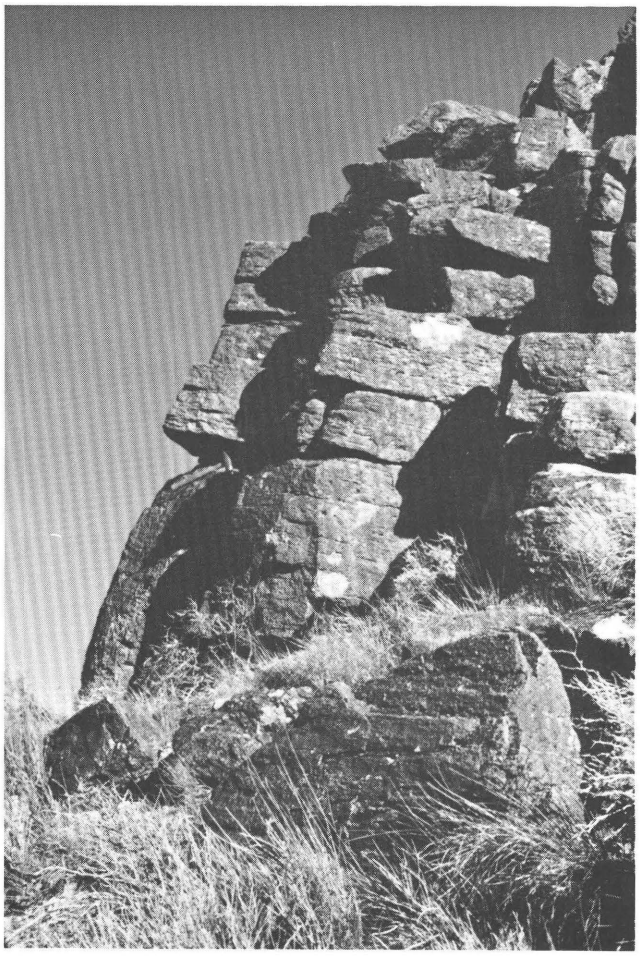

Figure 9. Layering observed a few meters above base of flow-lineated rhyolite in its middle, densely welded zone. Here layering is subparallel with base of flow-lineated rhyolite, but higher in its densely welded zone, flow foliation can be at attitudes significantly different from those at stratigraphic base and top. Boulder in foreground shows flow lineation. Sledge hammer for scale.

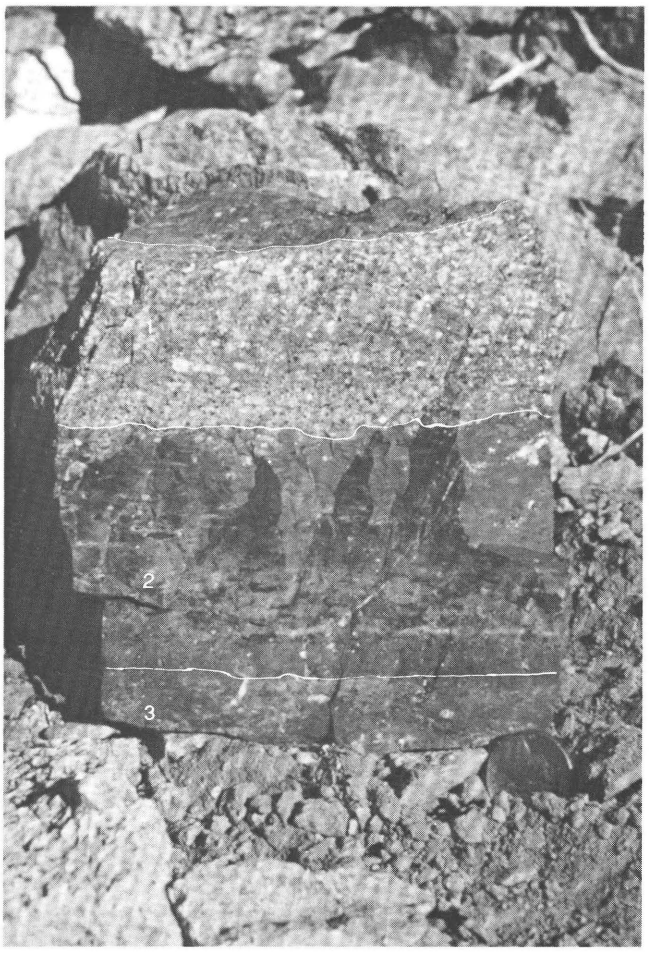

Figure 10. Distinctive layering in basal, layered zone of flow-lineated rhyolite. The grayish-red (2) and light-greenish-gray (3) layers are crystal poor relative to the pale-red layer (1) near the top of this sample. Nickel for scale.

rounded slopes and cavities as large as 6 by 3 m. The upper, partially welded zone contains 1–15 percent grayish-red trachytic inclusions as much as 2 m long; many of these are deformed with their long axes parallel to the foliation of the rock, suggestive of a cognate origin (fig. 12). This zone contains abundant microscopic cavities partially filled with

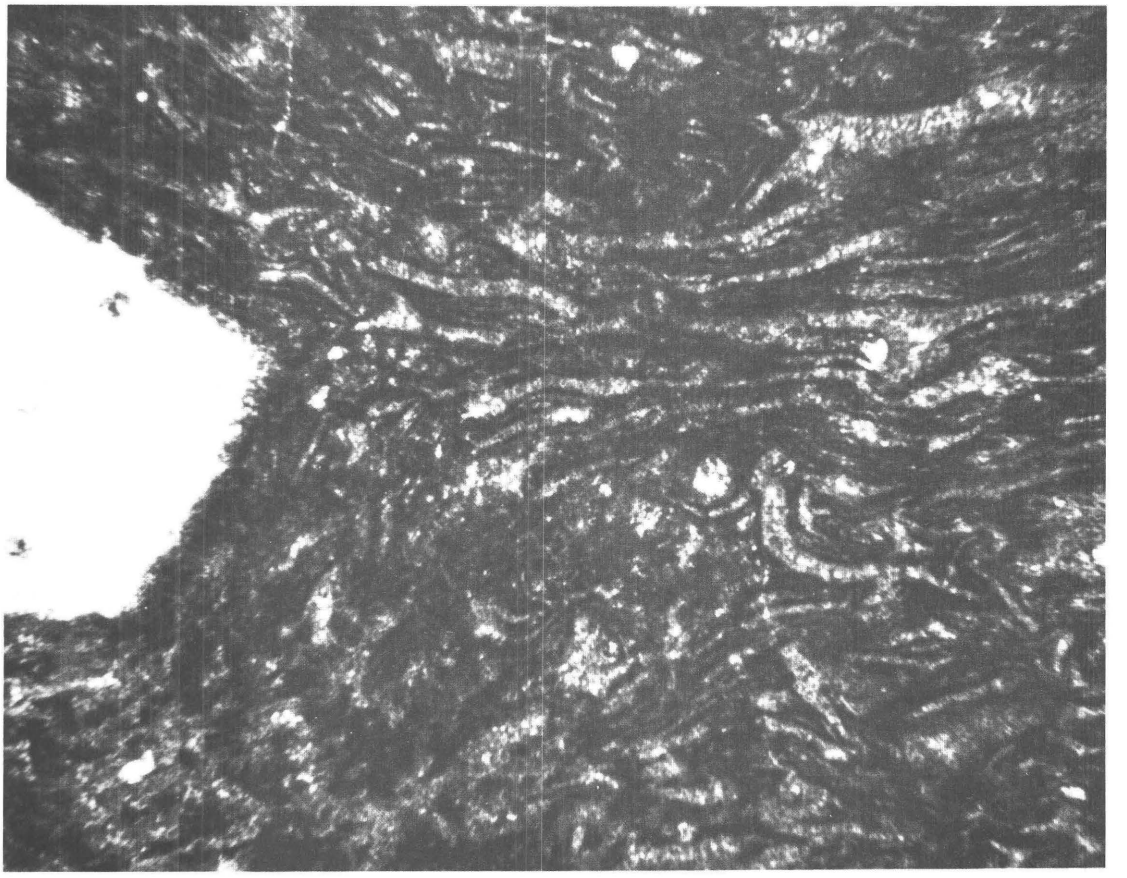

Figure 11. Photomicrograph of eutaxitic glass shard texture in basal, layered zone of flow-lineated rhyolite. Quartz phenocryst at left of photo. Plane light; view is 1.26 mm wide.

vapor-phase amphibole and dark acicular amphibole-like crystals. Secondary quartz completely fills the cavities between vapor-phase growths. One thin section contains lustrous, euhedral, green vapor-phase amphiboles that line cavities. Also, sheaflike aggregates of an unknown, pale-green, secondary mineral occur in the groundmass.

The flow-lineated and columnar-jointed rhyolites are nearly indistinguishable in hand sample and in the field. In faulted areas, discriminating between the two units can be especially difficult. Both have similar types, sizes, and relative proportions of phenocrysts; however, the flow-lineated rhyolite has a higher percentage of phenocrysts (compare tables 1 and 2). Although near their tops both units have trachytic inclusions, they appear to be more abundant in the flow-lineated rhyolite. The flow-lineated rhyolite is interpreted to be an ash-flow tuff for the same reasons given for the columnar-jointed rhyolite.

Several discontinuous, thin tuffaceous layers are present above the flow-lineated rhyolite, each less than 5 m thick; these layers were mapped as part of the flow-lineated rhyolite. They include a yellowish-gray tuffaceous sandstone, a light-greenish-gray nonwelded tuff, and a light-brownish-gray nonwelded tuff.

LOWER BASALT FLOW

A thin, olivine-bearing basalt flow lies above the flow-lineated rhyolite nearly everywhere in the northern area. The best exposures of the lower basalt flow are in gullies, where the unit is grayish black and generally massive. Elsewhere, the lower basalt flow is discontinuously exposed under colluvium. The flow is typically less than a few meters thick, but toward the north it reaches a thickness of 25 m. The lower basalt flow contains fewer than 2 percent plagioclase and altered olivine phenocrysts in a groundmass of a subophitic intergrowth of microcrystalline plagioclase and clinopyroxene.

GRAY ASH-FLOW TUFF

Next in the stratigraphic sequence is a gray devitrified rhyolitic ash-flow tuff that forms a ledge and an overlying gentle slope. This welded tuff contains phenocrysts of quartz, sanidine, plagioclase, biotite, altered ferromagnesian and opaque minerals, and accessory zircon. Basaltic lithic fragments from tenths of millimeters to 5 cm long give the rock a characteristic spotted appearance, although they form less

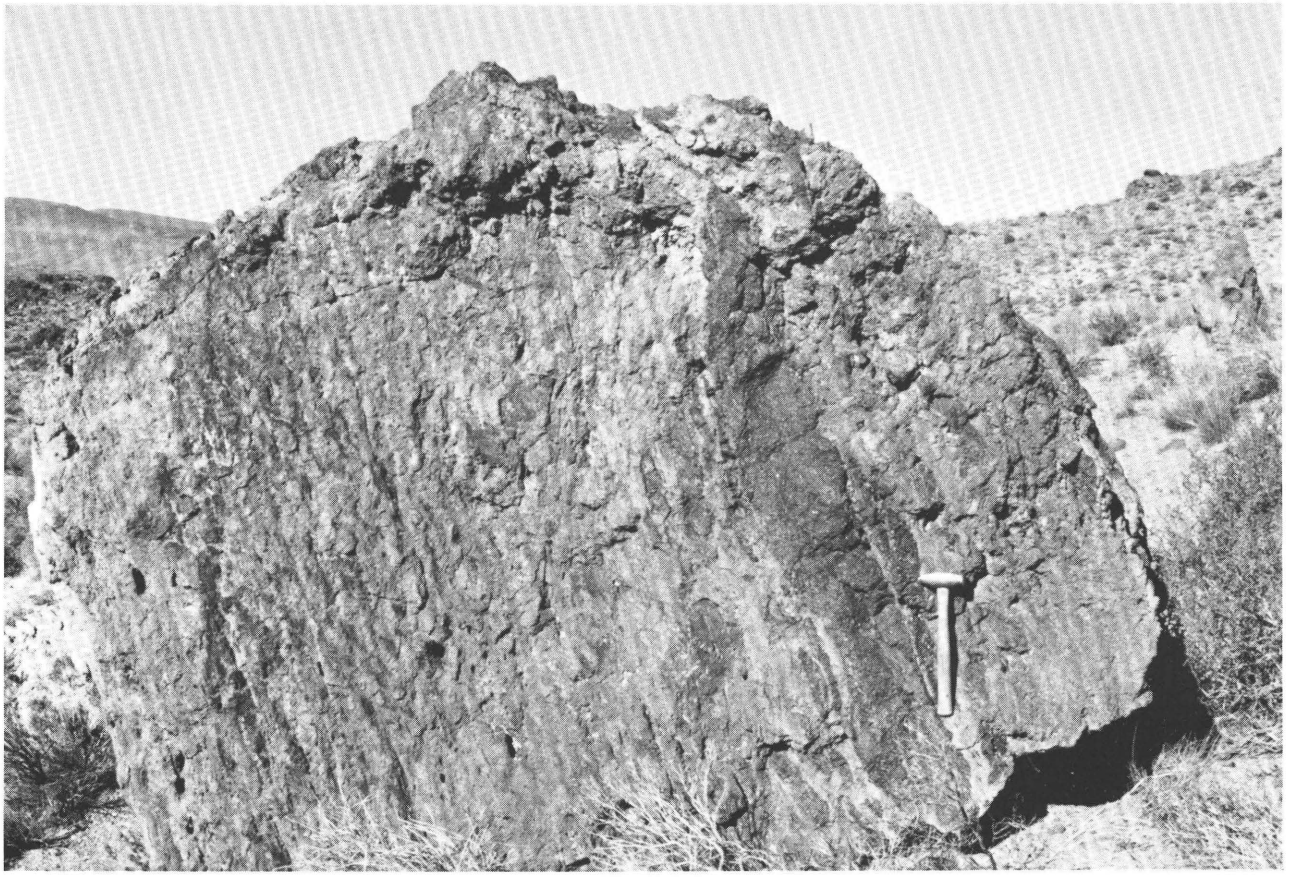

Figure 12. Trachytic inclusions in upper, partially welded zone of flow-lineated rhyolite. This boulder has rolled out of place. Note that inclusions are deformed with their long axes parallel to the foliation of rock. Sledge hammer for scale.

than 1 percent of the tuff. The gray ash-flow tuff forms a distinctive topographic break between the underlying basalt and the overlying tuff. The gray ash-flow tuff is thin, ranging from 5 to 25 m thick, and it consists of two zones: a lower, moderately welded zone and an upper, partially welded zone.

The lower, moderately welded zone of the gray ash-flow tuff is grayish orange pink with moderate-brown basaltic lithic fragments; it forms a ledge as much as 15 m thick. The tuff contains 14 percent phenocrysts that consist of 10 percent quartz, 71 percent sanidine, less than 1 percent plagioclase, a trace of biotite, and 19 percent altered ferromagnesian and opaque minerals (Appendix 1). Some of the sanidine phenocrysts are adularescent. Deformed glass shards and a eutaxitic texture can be observed in thin section.

The upper, partially welded zone is very light gray and forms gentle slopes. Typically, the upper zone is characterized by elongate, rounded exposures just above the lower, moderately welded zone (fig. 13). The maximum thickness of the upper, partially welded zone is about 10 m. The tuff in this zone contains 19 percent phenocrysts that consist of 22 percent quartz, 72 percent sanidine, 3 percent plagioclase, a trace of biotite, and 3 percent altered ferromagnesian and opaque minerals (Appendix 1). Some of the altered ferromagnesian and opaque minerals can be identified as biotite on the basis of phenocryst shape and relict centers.

YELLOW TUFF

Above the gray ash-flow tuff, a thick, crudely bedded, nonwelded to partially welded yellow tuff forms distinctive steep, grayish-yellow, rounded slopes. Deposition of the yellow tuff spanned the eruption of two rhyolite lava flows—a red lithic rhyolite and a biotite rhyolite—and minor sedimentary tuffs and welded ash-flow tuffs (fig. 14). At least three discontinuous, minor tuffaceous layers are present in the basal part of the yellow tuff; these are a tuffaceous sandstone and two densely welded ash-flow tuffs (Harding, 1991).

The yellow tuff is devitrified and is very pale orange, grayish orange pink, and grayish yellow. It contains phenocrysts of quartz, sanidine, plagioclase, biotite, and altered ferromagnesian and opaque minerals. The tuff contains abundant pumice and lithic fragments, many of which are devitrified rhyolite. Numerous crudely bedded ash-fall layers, 0.5–2 m thick, are present in several places. At the southern limit of its exposure, the yellow tuff is undivided and ranges from 0

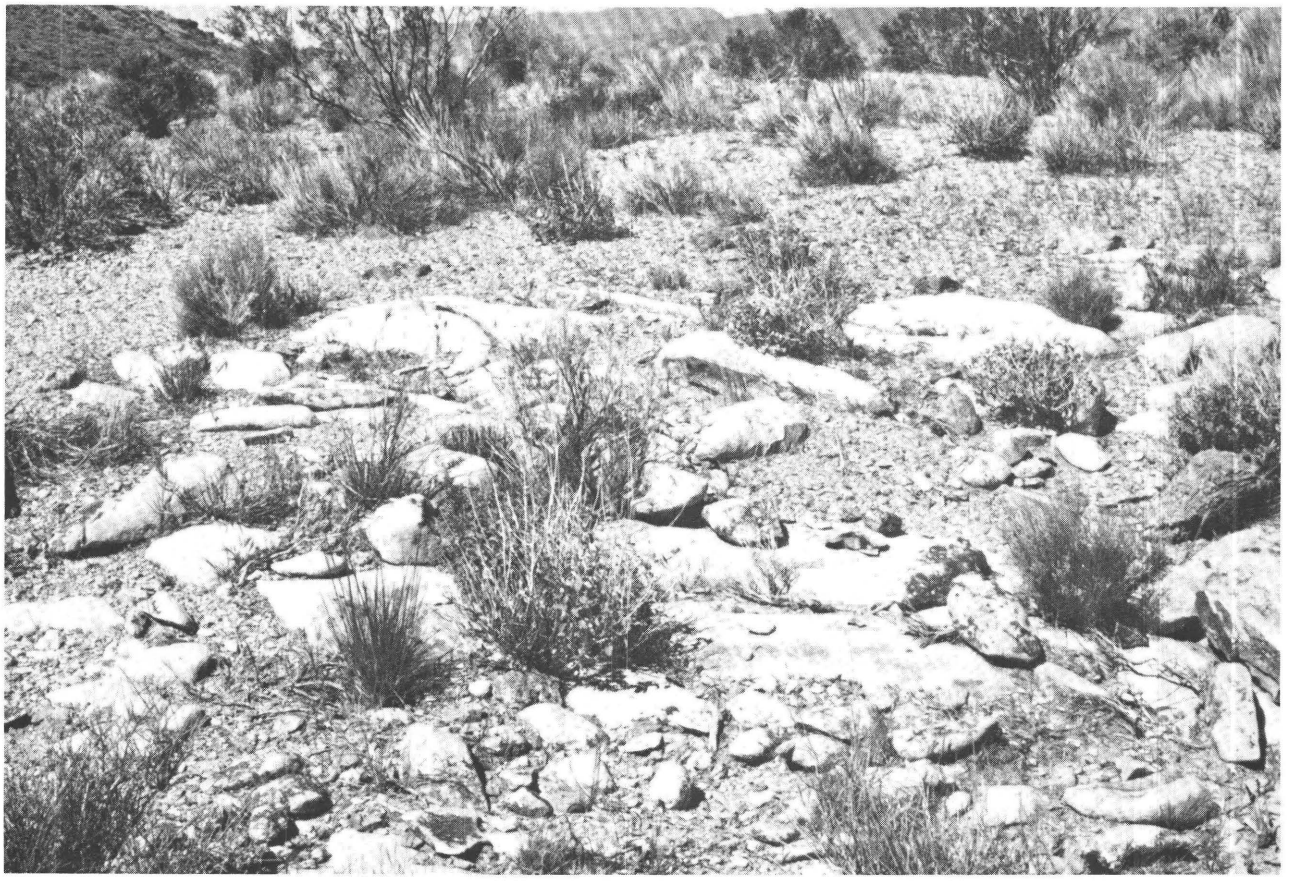

Figure 13. Typical exposure of upper, partially welded zone of gray ash-flow tuff.

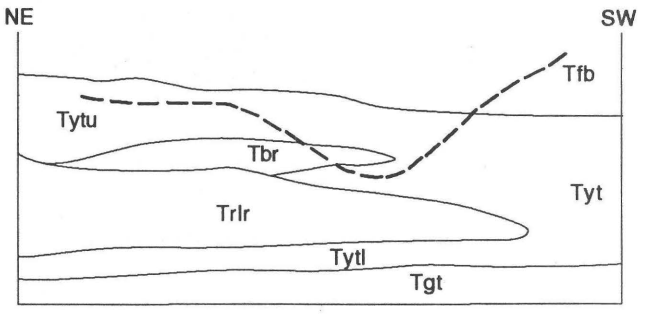

Figure 14. Diagrammatic sketch of probable stratigraphic relationships between the yellow tuff and rhyolite lava flows that erupted during accumulation of the yellow tuff. Dashed line approximates present erosion surface. Not to scale. Tgt, gray ash-flow tuff; Tytl, lower part of the yellow tuff; Trlr, red lithic rhyolite; Tbr, biotite-rhyolite flow; Tytu, upper part of the yellow tuff; Tyt, yellow tuff, undivided; Tfb, flow-banded rhyolite.

to 180 m thick. To the north, it is physically separated into an upper and a lower part by rhyolite lava flows. The lower part of the yellow tuff ranges from 0 to 15 m thick, whereas the upper part of the yellow tuff reaches a maximum thickness of 100 m. The upper and lower parts are indistinguishable except where intervening rhyolite flows are present.

The phenocryst content of the yellow tuff ranges from 2 to 6 percent and consists of 31–60 percent quartz, 21–57 percent sanidine, 2–11 percent plagioclase, a trace of biotite, and 1–10 percent altered ferromagnesian and opaque minerals (Appendix 1). The tuff contains 5–10 percent lithic fragments and abundant pumice fragments.

RED LITHIC RHYOLITE

The red lithic rhyolite occurs within the yellow tuff and separates it into lower and upper parts throughout much of the northern study area. The red lithic rhyolite ranges in thickness from 0 to about 85 m. Where this unit is thin, it forms a ledge; where it is thick, it forms gentle slopes to steep cliffs. The red lithic rhyolite is pale red to dusky red and contains grayish-red basaltic lithic fragments as much as 15 cm long. The size and abundance of lithic fragments change greatly among localities. Flow-banding in the rhyolite is thin, ranging from 1 to 10 mm. The red lithic rhyolite is massive but autobrecciated on a fine scale, so that fragments of flow-banded material are contained in a rhyolite matrix.

The red lithic rhyolite contains only 2–3 percent phenocrysts, but abundant devitrification centers give the

appearance of a greater phenocryst content. The phenocrysts consist of 22–43 percent quartz, 38–69 percent sanidine, 1–19 percent plagioclase, and less than 1 percent opaque minerals (Appendix 1).

Several features indicate that the red lithic rhyolite is a lava flow rather than a welded tuff that flowed after emplacement. (See Bonnichsen and Kauffman, 1987.) These features are (1) an abrupt lateral termination of the rhyolite, (2) the presence of flow layering that was brecciated after cooling, (3) chaotic, tightly folded flow layering, (4) an absence of pumice fragments and glass shards, (5) a lack of internal subhorizontal layering indicative of multiple ash emplacements, and (6) an absence of vertical zonation in phenocryst type or abundance.

BIOTITE-RHYOLITE FLOW

A biotite-rhyolite lava flow was emplaced above the lower part of the yellow tuff in some places and above the red lithic rhyolite in others. This unit is a pinkish-gray to pale-red-purple, devitrified, massive lava flow that displays columnar jointing in vertical cliffs. Locally, it has a vitrophyric base about 20 cm thick. The biotite-rhyolite flow is exposed along the eastern edge of the study area, where it is as much as 55 m thick; it pinches out to the north.

The biotite-rhyolite flow contains 17 percent phenocrysts that consist of 31 percent quartz, 46 percent sanidine, 18 percent plagioclase, 5 percent biotite, a trace of amphibole, and less than 1 percent opaque minerals (Appendix 1; fig. 15). The biotite-rhyolite flow contains accessory phenocrystic zircon.

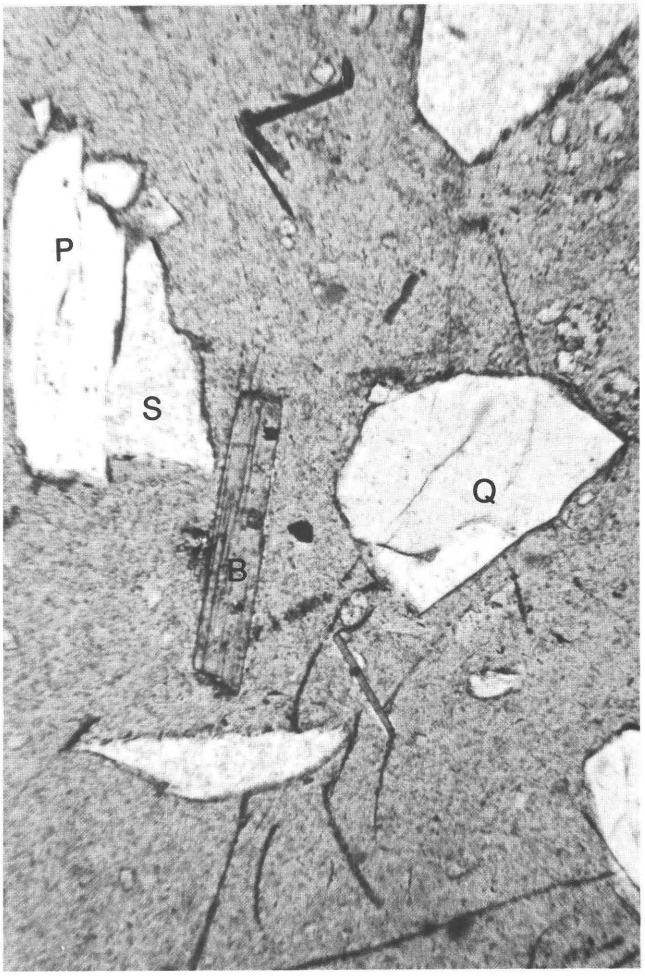

Figure 15. Photomicrograph of some of the phenocryst minerals characteristic of biotite-rhyolite flow. Q, quartz; S, sanidine; P, plagioclase; B, biotite. Plane light; view is 1.26 mm high.

PUMICE-RICH ASH-FLOW TUFF

A nonwelded to moderately welded, vitric, rhyolitic ash-flow tuff that contains conspicuous blackish-red to dark-gray pumice fiamme lies above the Kane Wash Tuff in the southern part of the study area. The pumice-rich ash-flow tuff, which is pale red, grayish orange pink, and pale reddish brown, forms gentle to moderate slopes and is as much as 35 m thick. The nonwelded part of this tuff contains lithic fragments of devitrified rhyolite and white pumice fragments that range from 0.1 to 15 cm long. The tuff forms wedge-shaped layers between the underlying, more steeply dipping Kane Wash Tuff and the overlying, less steeply dipping upper basalt. Locally, a thin, biotite-bearing tuffaceous sandstone is present between the pumice-rich ash-flow tuff and the overlying basalt and is included within this map unit.

The pumice-rich ash-flow tuff contains 7 percent phenocrysts that consist of 12 percent quartz, 25 percent sanidine, 42 percent plagioclase, 5 percent biotite, 3 percent hornblende, 4 percent clinopyroxene, 9 percent opaque minerals, and 0.5 percent zircon. The phenocrysts are unusually small, from less than 0.1 to 0.5 mm. Eighty-five percent of the groundmass consists of pumice fragments that range from 0.25 to 0.8 mm across.

Although this tuff is observed only in the southern part of the study area, it is included with the northern stratigraphic sequence because the tuff cannot be correlated with regional ash-flow tuffs; the large size of pumice fragments in the tuff suggests it had a local source; and the tuff underlies a series of rhyolitic lava flows and basalt flows, some of which overlie the boundary between the northern and southern stratigraphic sequences.

FLOW-BANDED RHYOLITE

Two aphyric rhyolite lava flows form steep slopes above the yellow tuff in the northern part of the study area and continue unbroken southward over the boundary between the two stratigraphic sequences to overlie the Kane Wash Tuff (fig. 3). The lower flow is thinly flow banded in

layers 1–2 mm thick and is more widespread than the upper massive flow. Both flows of the unit locally have 5-m-thick glassy bases; distinctive Apache tears erode from the basal part of the lower flow. The devitrified part of this flow is very light gray, light brownish gray, and pale red. The flow-banded rhyolite is as thick as 110 m and pinches out to the south.

New whole-rock K-Ar dates are 13.7±0.5 and 12.9±0.7 Ma for devitrified and vitric parts of the flow-banded rhyolite, respectively; the vitric material has probably lost argon, resulting in a date that is too young, and therefore the older age is considered to be more representative (analyses by H.H. Mehnert) (Appendix 3).

MIDDLE BASALT FLOW

A 15-m-thick, dark-gray basalt flow that contains about 5 percent olivine phenocrysts occurs at one locality above the flow-banded rhyolite in the central eastern part of the study area. The flow has scoriaceous upper and lower zones and a massive middle zone, all of which form moderate to steep slopes. Although the basalt lies south of the projected boundary between the northern and southern stratigraphic sequences, it is between units of the northern stratigraphic sequence that overlie the boundary; therefore, it is included as part of the northern sequence.

LITHOPHYSAL RHYOLITE FLOW

A light-brownish-gray, devitrified, massive rhyolite flow forms moderate to steep slopes above the middle basalt flow at one locality in the central eastern part of the study area. The lithophysal rhyolite flow contains about 10 percent lithophysal cavities 1–2 cm in diameter. The lithophysae are coated with concentric layers of fine-grained vapor-phase crystals. This rhyolite is nearly aphyric, containing less than 1 percent phenocrysts that consist of hornblende and opaque minerals. The lithophysal flow is considered to be part of the northern stratigraphic sequence for the same reasons given for the middle basalt flow.

YOUNGEST RHYOLITE FLOWS

One exposure of rhyolite lava flow occurs on each side of Kane Springs Valley in the northern part of the study area; based on stratigraphic relationships found elsewhere, this is the youngest unit filling the Kane Springs Wash caldera in the Delamar Mountains (Scott, Harding, and others, 1991). Most of this unit is vitric; some zones contain devitrification spherulites that are from 0.5 to 2 cm in diameter. The youngest rhyolite flows are medium light gray to light gray, are massive to flow banded, and contain 2–5 percent phenocrysts of quartz, sanidine, biotite, and amphibole. The rhyolite flows have a K-Ar sanidine date of 13.3±0.4 Ma (Novak, 1984).

UPPER BASALT FLOW

Capping both the northern and southern stratigraphic sequences are dark-gray to medium-dark-gray basalt and light-brownish-gray basaltic andesite(?) flows that form gentle to steep slopes and cliffs. The upper basalt flow contains sparse plagioclase phenocrysts in a groundmass of flow-oriented plagioclase laths and equant olivine. K-Ar whole-rock dates for the basalt are 11.4±0.4 and 11.6±0.4 Ma (Novak, 1984).

In the eastern part of the study area, this unit forms a basaltic volcano approximately centered over the highest topographic point in the map area (shown by x in fig. 3). The flanks of the volcano consist exclusively of massive and vesicular dark-gray basalt flows. Northwest of the topographic high, deep erosion has exposed light-brownish-gray basaltic andesite(?) and blackish-red, dusky-red, and moderate-red, highly scoriaceous mounds of basaltic ejecta intercalated with dark-gray basalt flows. This heterogeneous sequence of eruptive products is probably close to the volcanic vent for this unit.

INTRUSIVE ROCKS IN THE NORTHERN AREA

RHYOLITE DIKES

Several rhyolite dikes have intruded rocks in the northern part of the study area; one rhyolite dike extends about 550 m southwest of the boundary between the northern and southern stratigraphic sequences (fig. 3). Three types of rhyolite dikes are present: (1) aphyric rhyolite dikes, (2) biotite-absent rhyolite dikes containing quartz and (or) feldspar phenocrysts, and (3) biotite-bearing rhyolite dikes (complete descriptions in Harding, 1991).

Several biotite-bearing rhyolite dikes, which are present within and just to the east of the study area, form sharp ridges and are typically 2–5 m thick. The dikes are massive, devitrified, and very light gray to pale red purple. The new K-Ar biotite date of one of these dikes is 13.1±0.5 Ma, and the sanidine date is 12.8±0.5 Ma (analyses by H.H. Mehnert) (Appendix 3).

The biotite-bearing rhyolite dikes and the biotite-rhyolite flow were initially assumed to have originated from the same source because they contain similar types and abundances of phenocrysts. However, in the eastern part of the study area, a biotite-bearing rhyolite dike intrudes the flow-banded rhyolite, which is younger than the biotite-rhyolite flow (fig. 14). Two (or more) similar sources or, more likely, a single long-lived magmatic source may have

produced both the biotite-rhyolite flow and the biotite-bearing rhyolite dikes.

VOLCANIC CENTER

In the northern part of the study area, a rhyolitic volcanic center consisting of a capping rhyolite lava flow, a lithic-rich tuff, a vitrophyric lava flow, and cross-cutting dikes, truncates older shallowly dipping volcanic rocks along steeply dipping contacts. The volcanic center, which is exposed in steep slopes, is about 100 m thick and 250 m wide. Rocks in the volcanic center cannot be correlated with other map units; they probably represent a local eruptive center.

The capping rhyolite lava flow is devitrified, and contains quartz, sanidine, plagioclase, and ferromagnesian and opaque phenocrysts. This flow is very light gray and has pale-red-purple streaks. A vitrophyre of a petrographically similar rhyolite is present along the northwestern edge of the unit. The rhyolite contains 6–8 percent phenocrysts that consist of 39–48 percent quartz, 43–55 percent sanidine, 4–7 percent plagioclase, and 2–5 percent mafic and opaque minerals (Appendix 1). Amphibole and clinopyroxene phenocrysts are observed in thin section, as well as shattered quartz and sanidine phenocrysts.

Between the devitrified lava flow and the vitrophyre, a nonbedded and nonwelded, very light gray to pinkish-gray tuff contains rhyolitic lithic fragments as large as 1.5 m in diameter, some of which resemble volcanic bombs. In some places the tuff contains as much as 80 percent lithic fragments. The tuff is cut by a 1.5-m-wide, grayish-pink, devitrified rhyolite dike containing about 3 percent phenocrysts of 75 percent quartz and 25 percent sanidine. Under the tuff, a complex network of cross-cutting dikes is poorly exposed in talus slopes. These dikes are partly devitrified and partly vitric; they contain quartz, sanidine, and in one case, biotite phenocrysts.

CHEMISTRY

Chemical analyses of representative samples of rocks from the northern stratigraphic sequence provide data to classify these previously uninvestigated rocks that had not been correlated with regional ash-flow tuffs. The chemical classifications of Shand (1951) and Macdonald (1974) are used.

Major-element chemistries (Appendix 2B) separate silicic rocks of the northern stratigraphic sequence into weakly peralkaline and metaluminous groups (table 3). The lower ash-flow tuffs, the columnar-jointed and flow-lineated rhyolites, can be further classified as comenditic (fig. 16), which indicates that the tuffs are transitional between non-peralkaline rhyolites and more strongly peralkaline pantellerites.

Table 3. Classification of rhyolitic rocks in northern stratigraphic sequence.

[PI=peralkalinity index=(molar [Na+K]/Al). PI=1.0 to 1.1=weakly peralkaline]

Unit	Sample No.	PI	Classification
Flow-banded rhyolite	6AH18.4.88	0.9	Metaluminous.
Biotite-rhyolite flow	1AH23.10.88	0.8	Metaluminous.
Yellow tuff	1AH18.11.88	0.5	Metaluminous.
Red lithic rhyolite	2AH16.5.88	0.8	Metaluminous.
Gray ash-flow tuff	3AH20.11.88	0.9	Metaluminous.
Flow-lineated rhyolite	9AH19.5.88	1.0	Peralkaline.
	7AH19.5.88	1.1	Peralkaline.
Columnar-jointed rhyolite	4AH19.5.88	1.0	Peralkaline.
	5AH12.11.88	1.0	Peralkaline.
	2AH12.11.88	1.0	Peralkaline.
	1AH19.5.88	1.0	Peralkaline.

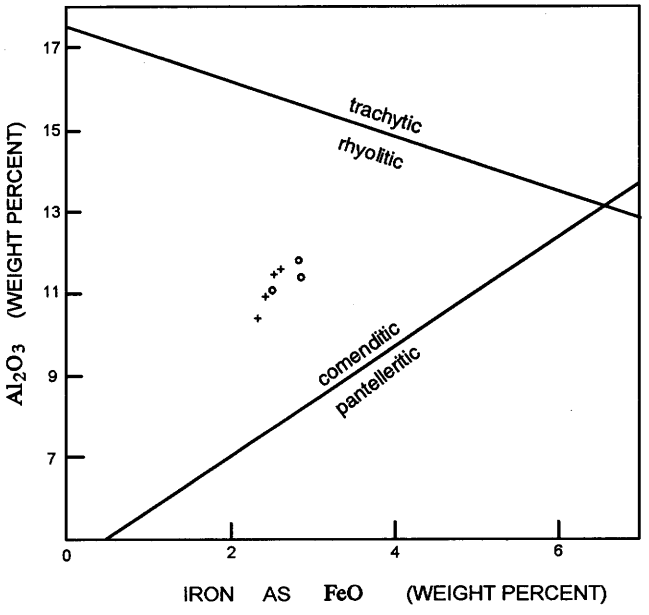

Figure 16. Classification of peralkaline, quartz-normative extrusive rocks (Macdonald, 1974). Oxide data from +, columnar-jointed, and o, flow-lineated ash-flow tuffs are plotted.

The lower ash-flow tuffs have very tightly grouped enriched REE patterns with large negative Eu anomalies (fig. 17) as is typical for peralkaline rocks (Ferrara and Treuil, 1974). In REE diagrams, some of the analyses do not include Gd data (Appendix 2C); a value for Gd was estimated visually in order to express the Eu anomalies uniformly. A trachytic inclusion from the upper part of the flow-lineated rhyolite is less enriched in heavy REE and has a distinctly smaller Eu anomaly.

Incompatible-element patterns (spidergrams) were also determined according to the method of Thompson (1982), who chose elements that are incompatible relative to basalts and arranged them in decreasing degree of incompatibility from left to right. Spider diagrams are used here for comparison only. As in REE patterns, spidergrams for individual

samples from the lower part of the northern stratigraphic sequence cluster tightly with the exception of the trachytic inclusion from the flow-lineated rhyolite (fig. 18). The columnar-jointed and flow-lineated rhyolites are geochemically distinctive for their low relative abundances of Ba, Sr, P, and Ti.

Units in the upper part of the northern stratigraphic sequence show a greater range in REE enrichments than do the lower units, particularly in light rare earths (fig. 19). Degrees of light-REE enrichments do not differ systematically with stratigraphic order. A strong negative Eu anomaly characterizes these units. The spider diagram for the upper units, although similar to that of the lower units, shows more variation in element values (fig. 20). In general, the upper units are less enriched in trace elements than the lower units,

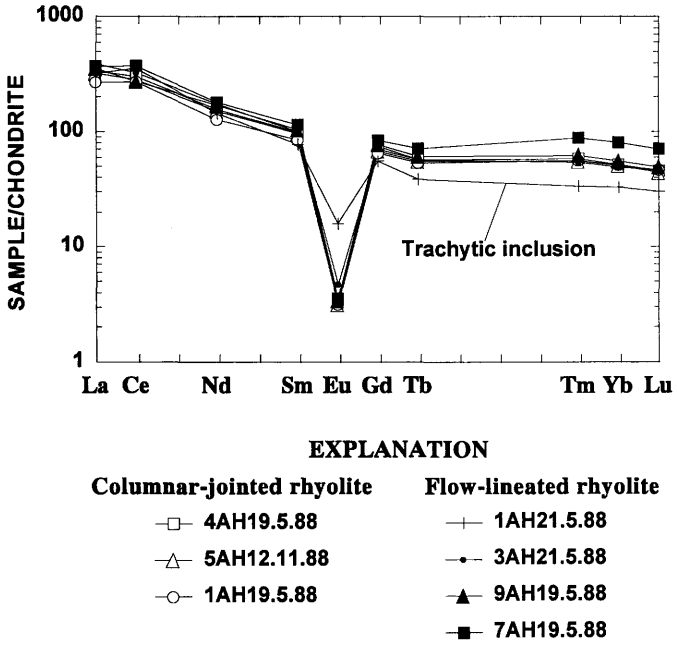

Figure 17. REE patterns for units from lower part of northern stratigraphic sequence. Results shown for columnar-jointed and flow-lineated rhyolites. Elements normalized to chondrite values of Hanson (1980).

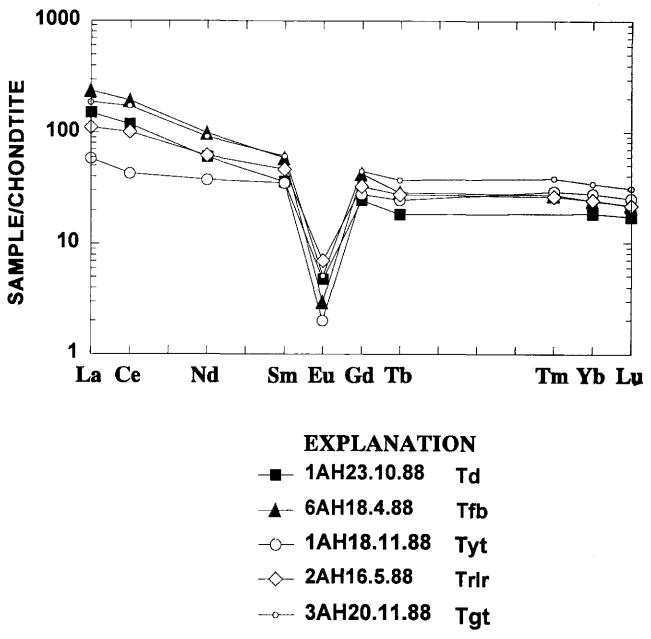

Figure 19. REE patterns for units from upper part of northern stratigraphic sequence. Results are shown for Td, biotite-bearing rhyolite dike; Tfb, flow-banded rhyolite; Tyt, yellow tuff; Trlr, red lithic rhyolite; Tgt, gray ash-flow tuff.

Figure 18. Spider diagram for units from lower part of northern stratigraphic sequence, the columnar-jointed and flow-lineated rhyolites. Elements are normalized to chondritic abundances (except for Rb, K, and P which have been normalized to terrestrial abundances) according to the model of Thompson (1982).

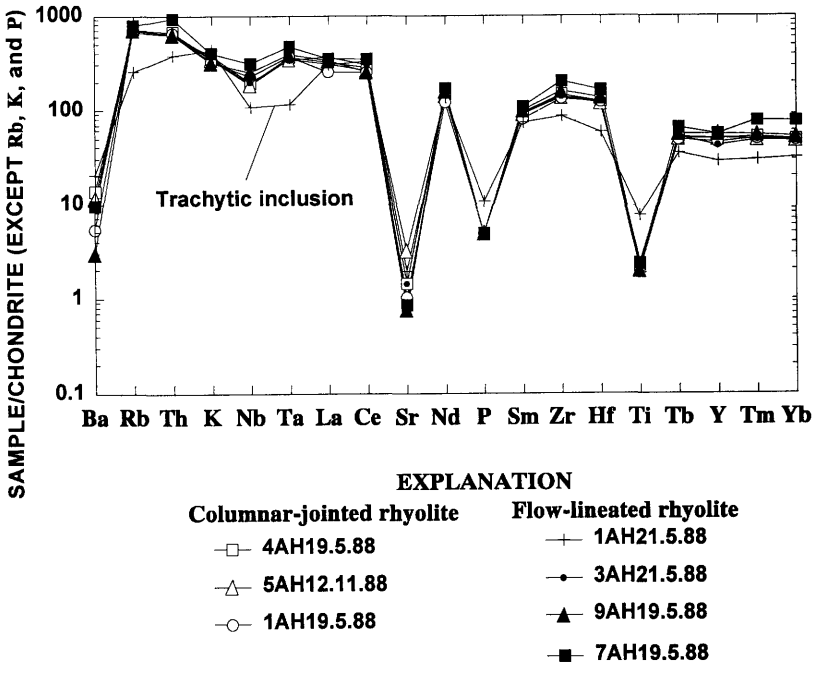

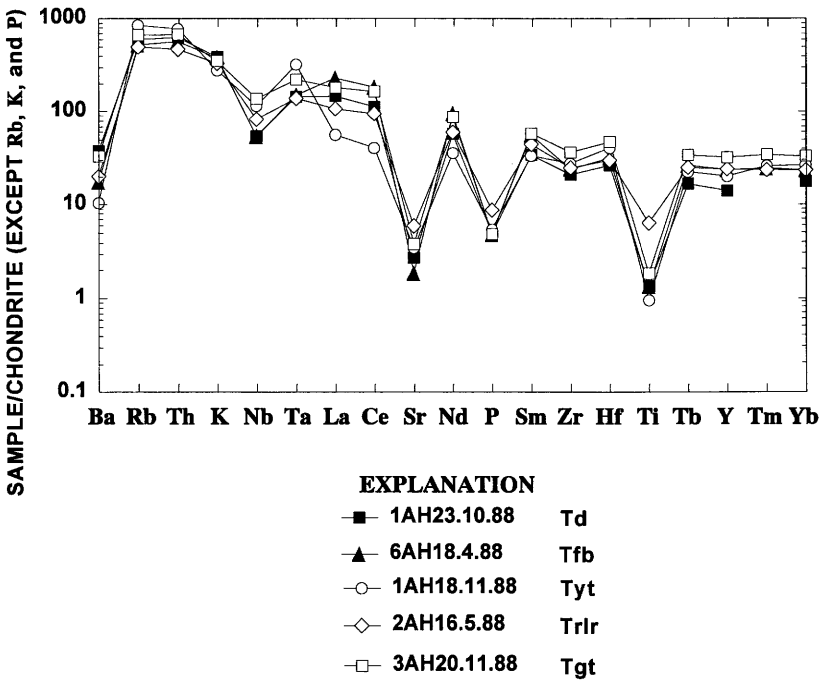

Figure 20. Spider diagram for units from upper part of northern stratigraphic sequence. Results are shown for Td, biotite-bearing rhyolite dike; Tfb, flow-banded rhyolite; Tyt, yellow tuff; Trlr, red lithic rhyolite; Tgt, gray ash-flow tuff.

with the exception of Zr and Hf, which are much less enriched, and of Ba and Sr, which are less depleted. The red lithic rhyolite is distinctive from the other upper units by being significantly higher in Sr and Ti. This difference may reflect contributions from small (< 2 mm) basaltic inclusions that could not be completely removed from the sample.

STRUCTURE

Deformation in the study area was accommodated by normal and strike-slip faulting and tilting of strata. In addition, numerous dikes cut the rocks of the northern part of the study area.

Most faults strike north to northeast and dip steeply west and northwest; the greatest population of these faults strikes about N. 25° E., essentially parallel to the range-front fault (fig. 21). A secondary group strikes slightly west of north and dips west; only a few north-striking faults dip steeply east. A few faults strike nearly east-west and dip steeply south.

Twenty of the observed fault surfaces have slickenlines that constrain the directions of fault slip (fig. 22). Most of the faults have stratigraphic offsets that require a component of normal dip slip; those faults without stratigraphic constraints are assumed to also have normal fault components. Five faults have slickenlines that indicate pure dip-slip movement, but movement on the remaining 15 faults also includes a component of strike slip. Of those oblique-slip faults, eight strike more than 22° east of north and exhibit left-lateral slip; two strike more than 3° west of north and exhibit right-lateral

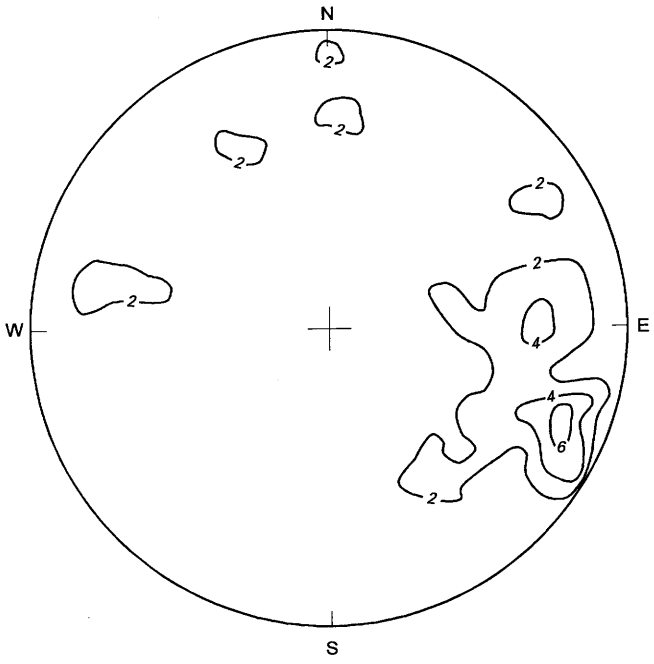

Figure 21. Equal-area lower hemisphere projection. Contours express the relative density of poles to 55 measurements of fault-plane attitudes within the area.

slip; and the intervening 25° segment contains an overlap of both left-lateral and right-lateral slip (figs. 22, 23). Strands of the northeast-striking Kane Springs Wash fault also display left-lateral oblique slip (fig. 3). (See plate I, Harding, 1991.)

Most dikes strike northeast, similar to the strike of most of the measured faults, whereas a smaller group strikes about

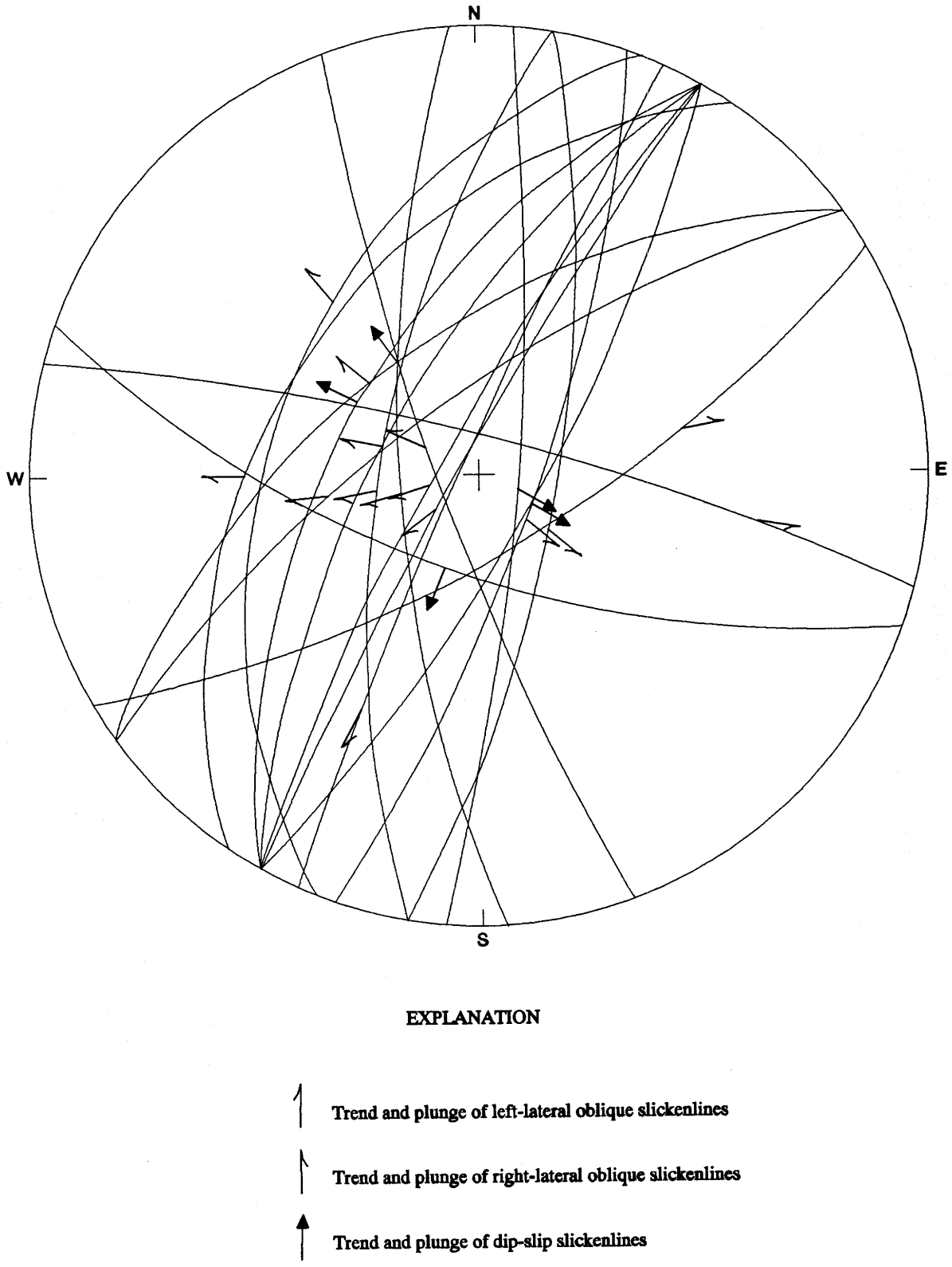

Figure 22. Equal-angle lower hemisphere projection of 20 fault planes showing direction and sense of slip, as determined from slickenlines.

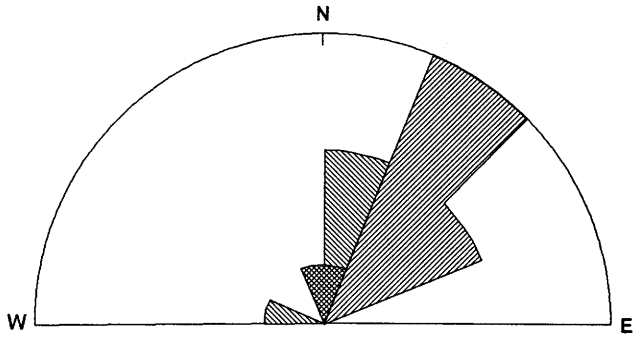

Figure 23. Rose diagram showing strikes of faults with left-lateral oblique-slip movement (northeast diagonals) and right-lateral oblique-slip movement (northwest diagonals). Overlap is cross-hatched. Full radius=five faults. Dip-slip faults are omitted here.

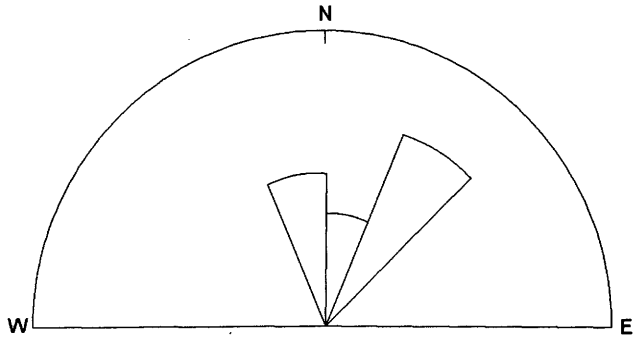

Figure 24. Rose diagram showing trends of 25 dikes. Largest cluster represents 11 dikes. Full radius=15 dikes.

N. 10° W. (fig. 24). Vertical offset of strata across some dikes and a similarity between dike and fault trends suggest that other dikes also intruded along faults (fig. 3). Brecciation of one dike on fault surfaces parallel to the dike suggests that fault movement renewed after dike emplacement.

Throughout the study area, strata dip southeastward, presumably as a result of tilting during extensional deformation. In the southern part of the study area, older strata (Hiko and Delamar Lake Tuffs) dip about 25°–30° whereas the youngest capping basalts dip about 5° (fig. 3). In the northern area a similar relationship is found, although it is less obvious in the field because contrasts in dip are difficult to observe there.

DISCUSSION

CALDERA WALL

The breccia that locally marks the boundary between the northern and southern stratigraphic sections (fig. 3) has characteristics that are commonly associated with caldera collapse (Lipman, 1976). These features, described previously in the stratigraphy section, include a massive to crude bedding that dips approximately at the angle of repose away from the regional ash-flow tuffs of the southern sequence, an absence of shear in the breccia parallel to the boundary between the northern and southern sequences, and the buttress unconformity geometry of the lateral margin of the flow-lineated rhyolite chilled against the breccia. Based on these features, the breccia unit (Twb, fig. 3) is interpreted to be caldera-wall breccia.

This part of the inferred caldera cannot be older than the 14.7–Ma Grapevine Spring Member of the Kane Wash Tuff because clasts derived from the Grapevine Spring are included in the breccia. The upper part of the breccia was being deposited coevally with the 14.4–Ma flow-lineated rhyolite. Also, the caldera cannot be younger than the 13.7–Ma flow-banded rhyolite that stratigraphically overlies the caldera wall (fig. 3). Thus, field relations and dating indicate that the breccia is between 14.7 and 14.4 Ma and that it marks the topographic wall of either the Kane Springs Wash caldera or another caldera that formed between 14.7 and 13.7 Ma. Because no outflow sheets younger than the Kane Wash Tuff have been mapped in the study area, the Kane Springs Wash caldera is the most likely candidate.

CORRELATION OF THE NORTHERN STRATIGRAPHIC SEQUENCE

Results of petrographic, chemical, and geochronologic studies of the northern stratigraphic sequence were compared with results of studies of Kane Wash Tuff outflow sheets and rocks from the Kane Springs Wash caldera in the Delamar Mountains to test whether this caldera extends into the Meadow Valley Mountains.

The lower ash-flow tuffs of the northern stratigraphic sequence, the columnar-jointed and flow-lineated rhyolites (Tcj and Tfl, respectively, in fig. 3) are mineralogically similar to the Kane Wash Tuff. Quartz and sanidine are the dominant phenocrysts in both cases, and these minerals are present in similar ranges of abundances; plagioclase and biotite are absent. Novak (1984) reported hedenbergite, fayalitic olivine, and opaque minerals as ferromagnesian phenocrysts, and amethyst and riebeckite as vapor-phase minerals in the Gregerson Basin Member (equivalent to members V_2 and V_3 of Novak's Kane Wash Tuff). Although most ferromagnesian minerals in the columnar-jointed and flow-lineated rhyolites have been altered beyond recognition in the devitrified tuff, olivine (probably fayalitic) and clinopyroxene were observed in a few thin sections from the chilled margins (fig. 6). The clinopyroxene is green and resembles what Novak (1984) identified as hedenbergite in his Kane Wash Tuff. Dark-blue, vapor-phase riebeckite(?) occurs in a few thin sections of the columnar-jointed rhyolite.

The mineralogical similarity between the Kane Wash Tuff and the lower tuffs of the northern stratigraphic sequence can be attributed to their chemical similarity. Both the Gregerson Basin Member of the Kane Wash Tuff and the lower tuffs of the northern stratigraphic sequence are mildly peralkaline comendites. Trace-element abundances for the two groups of rocks are indistinguishable in the REE (fig. 25) and spider diagrams (fig. 26). The chemical equivalence of these two groups of rocks indicates that the lower ash-flow tuffs of the northern stratigraphic sequence could be equivalent to the intracaldera facies of the Gregerson Basin Member of the Kane Wash Tuff.

Conventional K-Ar dates for the columnar-jointed and flow-lineated rhyolites overlap those for the Kane Wash Tuff within analytical uncertainty (table 4). This overlap is increased if an interlaboratory difference of about 0.4 m.y. is added to Novak's dates (Scott and others, this volume). Moreover, the $^{40}Ar/^{39}Ar$ date for the flow-lineated rhyolite (14.43±0.14 Ma) is comparable to the $^{40}Ar/^{39}Ar$ dates for the lower and upper cooling units of the Gregerson Basin Member (14.55±0.14 and 14.39±0.28 Ma, respectively). These dates further confirm the proposed correlation.

Thus, it is likely that the uppermost intracaldera-facies unit, the flow-lineated rhyolite (Tfl in fig. 3), is equivalent to the uppermost outflow-facies unit, the upper cooling unit of the Gregerson Basin Member (upper cooling unit of Tkb in fig. 3). The next lower intracaldera-facies unit, the columnar-jointed rhyolite (Tcj in fig. 3), is then equivalent to the

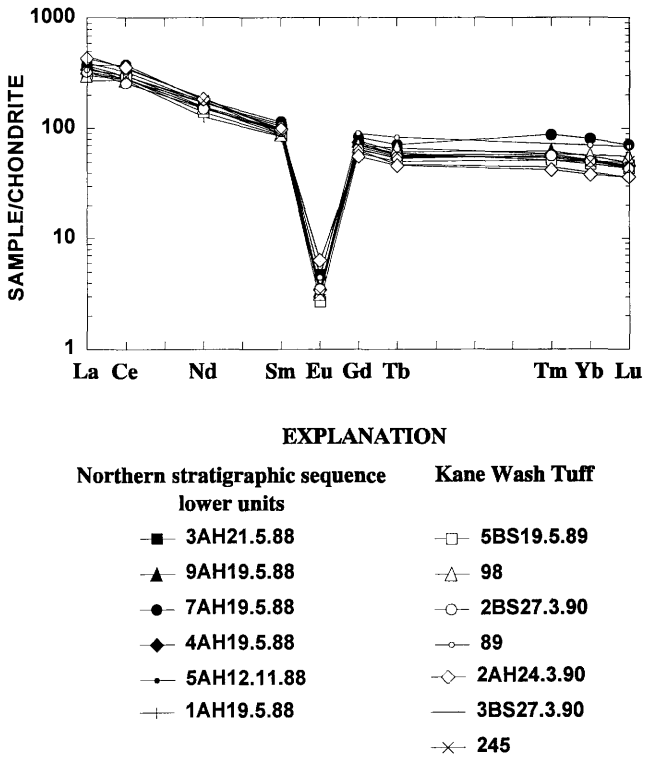

Figure 25. REE patterns for lower units of northern stratigraphic sequence (flow-lineated and columnar-jointed rhyolites) and members of the Kane Wash Tuff. Data for samples 245, 98, and 89 from Novak and Mahood (1986).

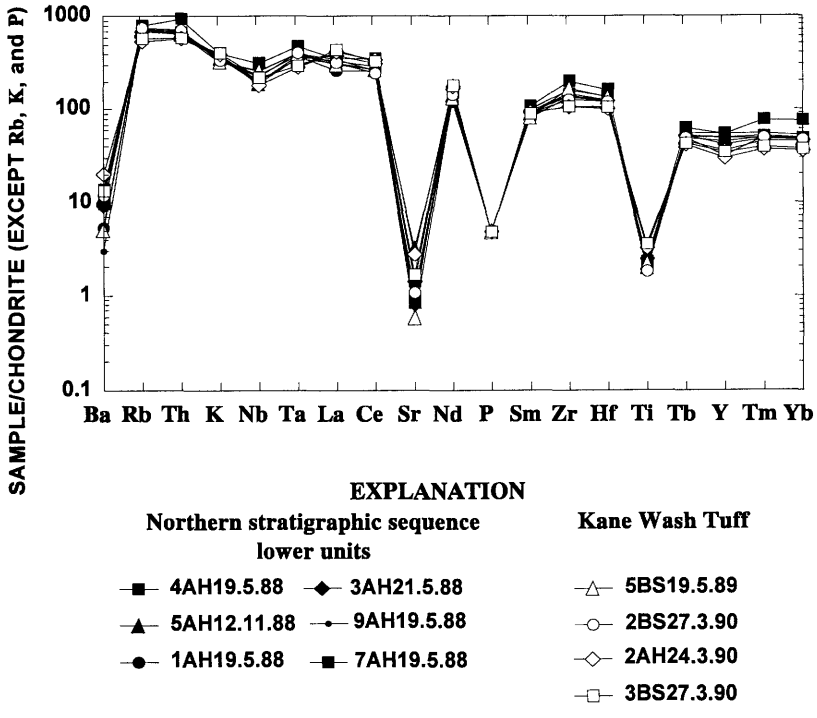

Figure 26. Spider diagram for lower units of northern stratigraphic sequence (flow-lineated and columnar-jointed rhyolites) and members of the Kane Wash Tuff.

Table 4. Comparison of dates (in Ma) for lower units of northern stratigraphic sequence with dates for the Kane Wash Tuff.

[Data analyst heads each column. Tfl, flow-lineated rhyolite; Tcj, columnar-jointed rhyolite; Tkbu, upper cooling unit of the Gregerson Basin Member of the Kane Wash Tuff; Tkbl, lower cooling unit of the Gregerson Basin Member of the Kane Wash Tuff; Tkg, Grapevine Spring Member of the Kane Wash Tuff]

Northern stratigraphic sequence			Kane Wash Tuff		
	K-Ar Mehnert	$^{40}Ar/^{39}Ar$ Snee		K-Ar Novak	$^{40}Ar/^{39}Ar$ Snee
Tfl	14.6±0.4[+]	14.43±0.14[+]	Tkbu		14.39±0.28[*]
	14.9±0.5[+]				
Tcj	14.6±0.5[+]		Tkbl	14.1±0.4[#]	14.55±0.14[*]
			Tkg	14.0±0.4[#]	14.67±0.22[*]
				14.2±0.4[#]	

[+]See Appendix 3 for analytical data.
[#]From Novak (1984).
[*]See Scott and others (this volume) for analytical data.

lower cooling unit of the Gregerson Basin Member. This correlation is further strengthened by the chemical zonation from comenditic lower parts to trachytic upper parts of both the cooling units of the Kane Wash Tuff and the intracaldera equivalents. Sample 1AH21.5.88 (marked trachytic inclusion) in figures 17 and 18 is representative of this upper part in the flow-lineated rhyolite (Appendix 2).

If the lower ash-flow tuffs of the northern sequence are intracaldera facies, then the upper units of the northern sequence are probably caldera fill. Based on conventional K-Ar dates and their analytical uncertainties, the upper units of the northern stratigraphic sequence (13.7±0.5 to 12.8±0.5 Ma, Appendix 3) are coeval with Kane Springs Wash caldera fill (14.4±0.6 to 12.5±0.4 Ma) (Novak, 1984). This correlation is further strengthened by the metaluminous character of both the upper part of the northern sequence (table 3) and the caldera fill in the Delamar Mountains (Novak, 1984). Novak divided the caldera-fill sequence in the Delamar Mountains into edenite-bearing early fill and biotite-bearing late fill. Caldera fill in the Meadow Valley Mountains contains biotite and plagioclase in addition to sanidine and quartz phenocrysts, as does late caldera fill of the Delamar Mountains. However, caldera fill in the Meadow Valley Mountains is slightly chemically distinct from late fill and more similar to early fill in the Delamar Mountains, based on spider diagrams (figs. 27, 28). Mineralogical evidence of correlation between late Delamar Mountains fill and Meadow Valley Mountains fill is probably strong enough to outweigh the small differences in incompatible-element compositions.

The correlation of the lithic-rich tuff remains unresolved. This lowest ash-flow tuff of the intracaldera facies in the Meadow Valley Mountains has a high Zr content (946 ppm; Appendix 2A). This composition is most similar to the mildly peralkaline composition of the Gregerson Basin Member, rather than to that of the Grapevine Spring Member of the Kane Wash Tuff, which has Zr values that range from 497 to 733 ppm (Appendix 2A and Novak and Mahood, 1986). No correlative lithic-rich uppermost part of an outflow cooling unit has been observed (Scott and others, this volume), but the upper parts of intracaldera equivalents may have been restricted to the caldera.

In the Meadow Valley Mountains part of the caldera, post-collapse volcanic units filled and overflowed the caldera wall, with many of the latest units pouring onto the outflow facies, including the pumice-rich tuff (Tpr), the flow-banded rhyolite (Tfb), possibly the middle basalt (Tmb) and lithophysal rhyolite (Tlr), and the upper basalt flow (Tb) (fig. 3). The flow-banded rhyolite directly overlies the yellow tuff in the north and the Kane Wash Tuff in the south. Basalt flows (Tb) capping the stratigraphic sequence also overlie caldera fill and caldera outflow facies (fig. 3). The thickest accumulation of basalt and the probable volcanic vent for the flows are located just inboard from the projected topographic caldera wall (fig. 3); the basaltic magmas may have used concealed caldera ring fractures as conduits to the surface.

STRUCTURAL IMPLICATIONS

Several important structural implications follow from the interpretation that the intracaldera facies and caldera fill in the Meadow Valley Mountains are interpreted to represent the eastern extension of the Kane Springs Wash caldera. The eastern projection of the southern wall of the caldera from the Delamar Mountains into Kane Wash Valley is sinistrally offset at least 4 km and probably closer to 7 km from its continuation in the Meadow Valley Mountains (fig. 29). This confirms the earlier prediction of 8 km of sinistral offset on the Kane Springs Wash fault by Ekren and others (1977) and the generalized hypothesis of E.H. Pampeyan (written commun., 1989).

Location of the fault strands on which this left-lateral movement occurred is constrained by two exposures of the

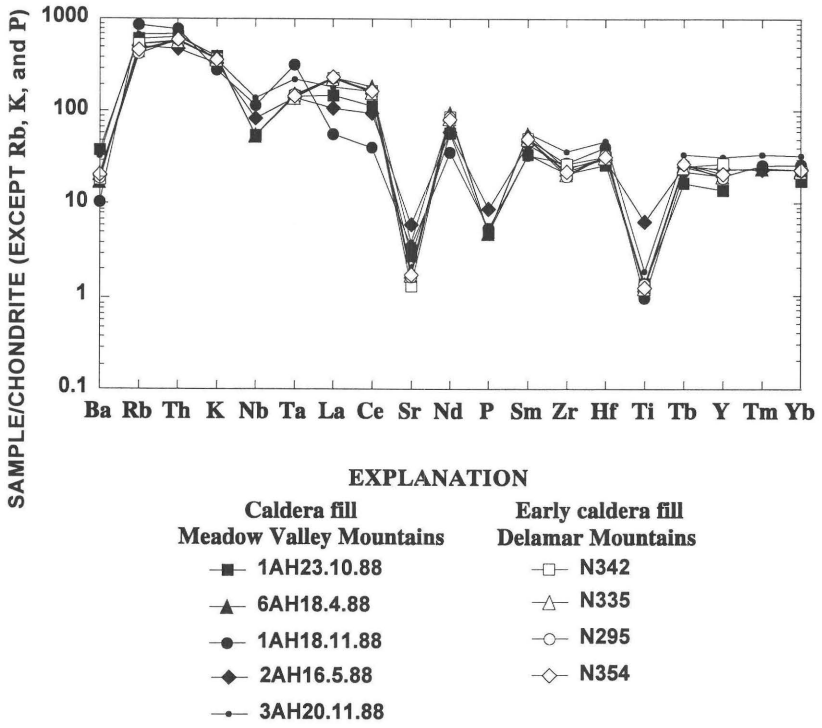

Figure 27. Spider diagram for caldera-fill units in Meadow Valley Mountains and early caldera-fill units in Delamar Mountains. Data for samples N342, N335, N295, and N354 from Novak and Mahood (1986).

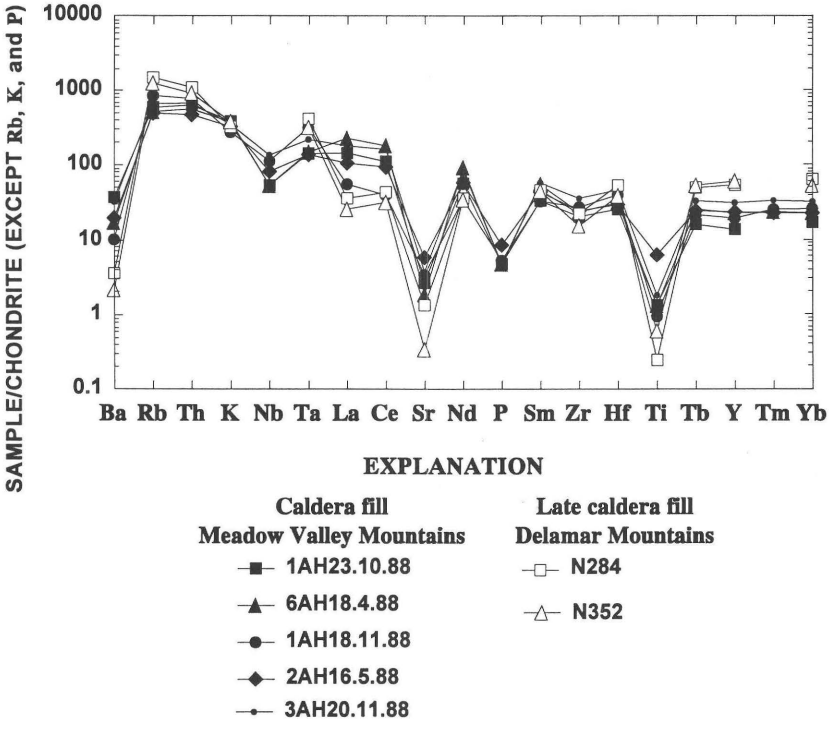

Figure 28. Spider diagram for caldera-fill units in Meadow Valley Mountains and late caldera-fill units in Delamar Mountains. Data for samples N284 and N352 from Novak and Mahood (1986).

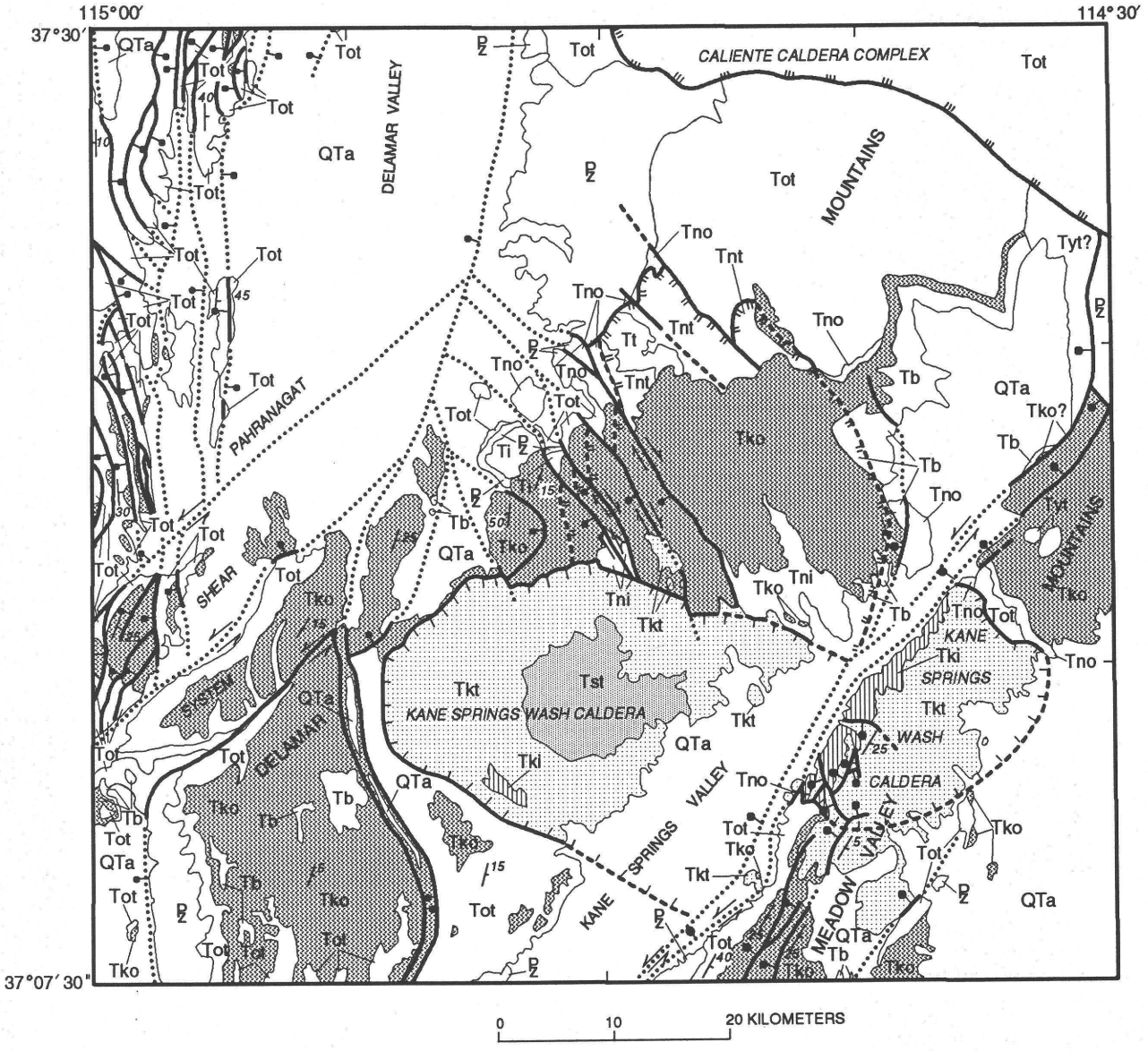

Figure 29 (above and facing page). Generalized geology of northern Meadow Valley and Delamar Mountains and vicinity. Geology outside of study area from R.B. Scott (unpub. mapping, 1991) and Ekren and others (1977).

youngest rhyolite flows along the northern edge of the study area (unit Try, fig. 3). This unit, which is the youngest Kane Springs Wash caldera fill in the Delamar Mountains, does not appear to have been offset along the Kane Springs Wash fault. Therefore, most of the left-lateral movement occurred on fault strands east of these exposures. The method of regional accommodation of the 4–7 km of left-lateral slip on the northern projection of the Kane Springs Wash fault is limited by the apparent lack of offset on the margin of the older Caliente caldera complex (fig. 29). Probably the segment of the Kane Springs Wash fault that has a more northerly strike north of Meadow Valley Wash has a more significant component of dip-slip, making that segment a minor breakaway zone (mapping in progress by R.B. Scott).

Although the role of strike-slip faulting in Cenozoic extension of the Basin and Range province is debated (Shawe, 1965; Anderson, 1973, 1984; Bohannon, 1979; Ron and others, 1986), the observation by Shawe (1965) of numerous northeast-striking left-lateral and northwest-striking right-lateral faults in western Nevada also applies elsewhere in the Basin and Range. Examples of this fault pattern in southern Nevada are the northwest-striking, right-lateral Walker Lane belt, the northeast-striking, left-lateral Lake Mead fault zone, the local northwest-striking, right-lateral faults in the area of the Caliente caldera complex (Best and others, 1993), and the local left-lateral Pahranagat shear system (fig. 2; Stewart and Carlson, 1978). Oblique slip on major and minor faults in the northern Meadow Valley Mountains also fits this pattern (figs. 22, 23).

EXPLANATION

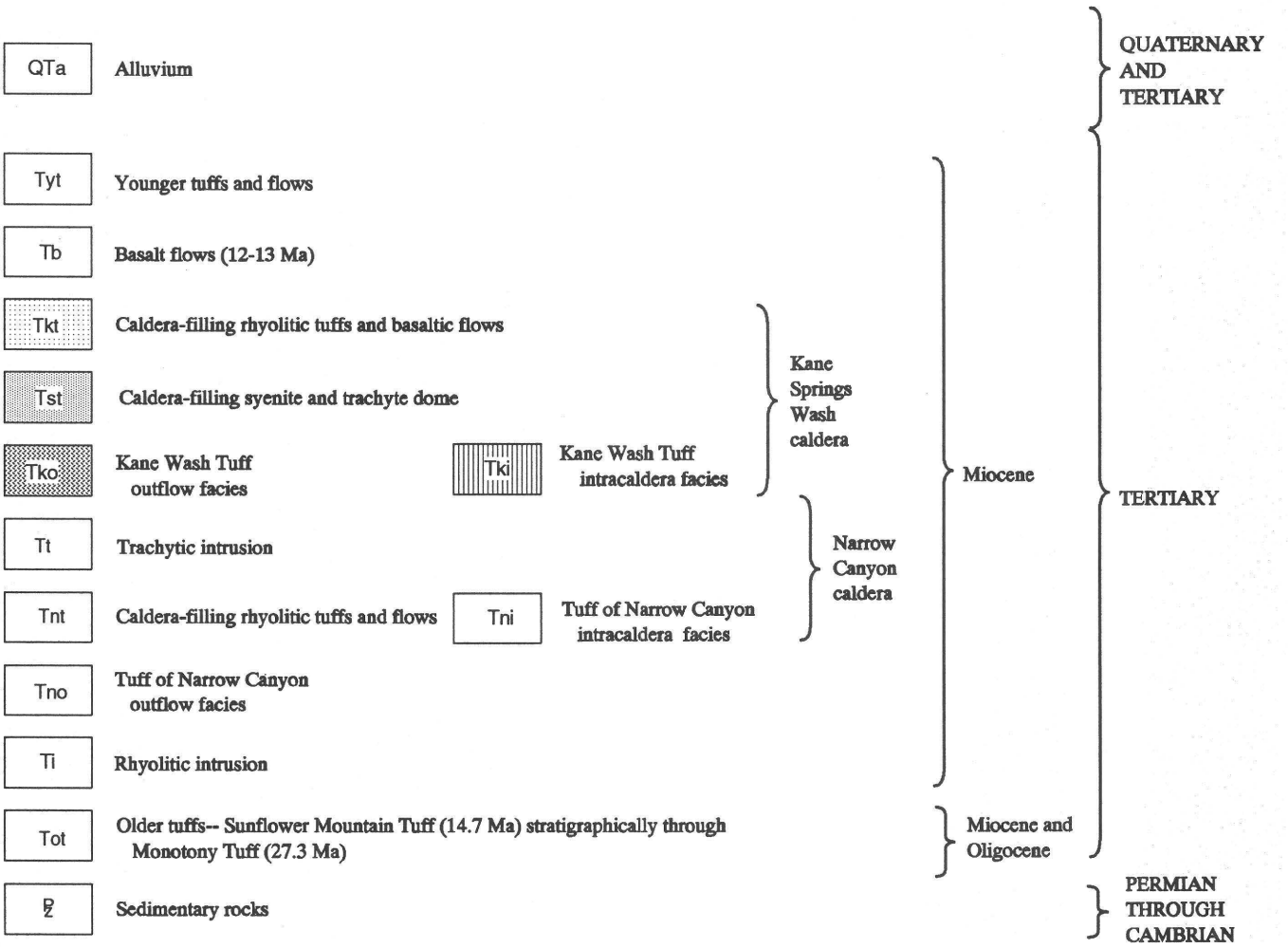

Contact

High-angle normal fault-- Dotted where concealed; bar and ball on downthrown side

Strike-slip fault--May be combined with normal fault symbol where oblique slip; dotted where concealed; barbs show direction of relative movement

25 Strike and dip of bedding

Caldera outlines--Dashed where inferred

Kane Springs Wash caldera

Narrow Canyon caldera

Caliente caldera complex

As discussed earlier, the eastern part of the caldera in the Meadow Valley Mountains shows evidence of faulting, dike injection, and progressive tilting after major collapse and during filling of the caldera between 14.4 and 11.5 Ma. Thus, late-stage volcanism and extension were contemporaneous in the eastern part of the caldera. This relationship stands in contrast to the relatively undeformed and slightly tilted western part of the caldera in the Delamar Mountains, indicating that extensional and strike-slip processes operated primarily east of the Kane Springs Wash fault while the western area in the Delamar Mountains passively rode out extension (Harding and others, 1991). Because the eastern part of the Kane Springs Wash caldera is on the footwall of the Kane Springs Wash fault, stratal tilts and synthetic oblique-slip faults should be expected to be concentrated adjacent to such a half-graben range-bounding fault zone.

During our reconnaissance mapping outside the study area, we searched for the remainder of the caldera wall in the Meadow Valley Mountains. The eastern margin of the caldera is covered both by overflow of caldera fill and by basin deposits in Meadow Valley Wash. Another caldera-wall segment was recognized about 11 km north of the caldera-wall breccia described previously (Best and others, 1993); this distance is consistent with the width of the Kane Springs Wash caldera in the Delamar Mountains. The caldera-wall segment is continuously exposed for 5 km across the northern part of the Meadow Valley Mountains. Along those exposures, the wall breccia dips 10°–40° southwestward, perpendicular to the trend of the wall, as would be expected for the northeastern wall of the caldera. The northern segment of the caldera wall does not contain clasts derived from the Kane Wash Tuff, but rather contains clasts of outflow units of the Narrow Canyon caldera, peralkaline precursor to the Kane Springs Wash caldera, and clasts of older precaldera volcanic units (Scott, Blank, and Page, 1991).

Although the northern and southwestern caldera walls of the Kane Springs Wash caldera trend generally west-northwest along the easternmost exposures in the Delamar Mountains, the trends of the eastern continuation of the caldera in the Meadow Valley Mountains are more diverse, from almost east-west to north. The caldera wall in the Delamar Mountains generally follows a smooth "cookie cutter" curvature, whereas the caldera wall in the Meadow Valley Mountains is highly irregular (fig. 29). We attribute the variability of the trend of the caldera wall in the Meadow Valley Mountains to the influence of preexisting north- to northwest-striking faults on caldera collapse; this contrasts with the absence of such faults in the Delamar Mountains. Such heterogeneity of fault patterns is common in central Lincoln County, as is emphasized by Scott and others (this volume); Rowley and others (this volume) and Best and others (1993) noted a profound influence of preexisting fault attitudes on caldera margin attitudes in the Caliente caldera complex.

The general offset geometry of the Kane Springs Wash caldera is mirrored in gravity and aeromagnetic data (Blank and Kucks, 1991). The contrast in magnetic signature between the areas underlain by the caldera and areas underlain by outflow sheets to the south and east ranges from about 250 to 300 nanoteslas. The magnetic anomaly patterns to the north are obscured by the presence of the Narrow Canyon caldera (Scott, Blank, and Page, 1991). Although the caldera underlies a steep regional gravity gradient that coincides with a regional thinning of the ash-flow tuffs southward, a distinct left-lateral offset of the gradient occurs along the Kane Springs Wash fault. The projected eastern boundary of the caldera under caldera-filling units that overflow the caldera in the Meadow Valley Mountains and under alluvium in Meadow Valley Wash is based upon these geophysical signatures.

We doubt that a convincing case can be made for two calderas, one in the Delamar Mountains with its southeastern wall hidden beneath alluvium in Kane Springs Valley, and a second caldera in the Meadow Valley Mountains with its northwestern wall also hidden beneath alluvium in Kane Springs Valley. Although such a hypothesis would remove the need for about 4–7 km of left-lateral offset of the caldera along the Kane Springs Wash fault, objections to a "two fixed calderas" hypothesis include: (1) The age constraints of the intracaldera units require that the caldera segment in the Meadow Valley Mountains be the source of the Gregerson Basin Member of the Kane Wash Tuff. (2) The distributions of the outflow facies of the Kane Wash Tuff are incompatible with the two segments being separate sources for specific members of the Kane Wash Tuff. (3) By using abrupt, and fortuitously hidden, curvatures to the caldera wall, it is possible, but in our opinion contrived, to terminate the Delamar Mountains caldera segment beneath the alluvium in Kane Springs Valley as proposed by Noble (1968) and Novak (1984). The Kane Springs Valley narrows at its northern end, allowing less than 1 km for the northern wall to curve from a N. 40° W. trend to a S. 60° W. trend, a change of about 80°; this makes a termination of the Meadow Valley Mountain caldera segment buried beneath alluvium of Kane Springs Valley highly unlikely (fig. 29). Also, recent unpublished mapping by R.B. Scott in the northeastern Delamar Mountains indicates that the northwest-trending segment of the northeastern caldera wall in the Meadow Valley Mountains does not continue into the eastern part of the Delamar Mountains. (4) A hypothesis that assumes "two fixed calderas" must accept the coincidences that not only are both abrupt changes of caldera wall attitudes hidden by alluvium in Kane Springs Valley, but also the trace of the Kane Springs Wash fault coincidentally separates the two calderas. We conclude that the simplest interpretation is that the once-continuous caldera walls were offset by left-lateral oblique motion along strands of the Kane Springs Wash fault.

CONCLUSIONS

1. The Kane Springs Wash caldera extends into the Meadow Valley Mountains (Harding and others, 1991) (figs. 29, 30).

2. The lower ash-flow tuffs of the northern stratigraphic sequence are intracaldera facies of the Kane Wash Tuff; the columnar-jointed rhyolite is equivalent to the lower cooling unit of the Gregerson Basin Member of the Kane Wash Tuff, and the flow-lineated rhyolite is equivalent to the upper cooling unit of the Gregerson Basin Member of the Kane Wash Tuff.

3. The upper units of the northern sequence represent post-collapse caldera-fill rocks that are mineralogically similar to the late caldera-fill rocks of the Delamar Mountains.

4. The southern caldera wall in the Delamar Mountains is offset left-laterally across the Kane Springs Wash fault about 4–7 km from its continuation in the Meadow Valley Mountains (fig. 29).

5. Extensional deformation significantly affected the eastern part of the caldera in the Meadow Valley Mountains, whereas the western part in the Delamar Mountains was generally unaffected.

REFERENCES CITED

Anderson, R.E., 1989, Tectonic evolution of the Intermontane System, Basin and Range, Colorado Plateau, and High Lava Plains, *in* Pakiser, L.C., and Mooney, W.D., eds., Geophysical framework of the continental United States: Geological Society of America Memoir 172, p. 165–176.

———1973, Large-magnitude late Tertiary strike-slip faulting north of Lake Mead, Nevada: U.S. Geological Survey Professional Paper 794, 18 p.

———1984, Strike-slip faults associated with extension in and adjacent to the Great Basin: Geological Society of America Abstracts with Programs, v. 16, no. 6, p. 429.

Armstrong, R.L., 1970, Geochronology of Tertiary igneous rocks, eastern Basin and Range province, western Utah, eastern Nevada, and vicinity, U.S.A.: Geochimica et Cosmochimica Acta, v. 34, p. 203–232.

Axen, G.J., Lewis, P.R., Burke, K.J., Sleeper, K.G., and Fletcher, J.M., 1988, Tertiary extension in the Pioche Area, Lincoln County, Nevada, *in* Bartley, J.M., Axen, G.J., Taylor, W.J., and Fryxell, J.E., Cenozoic tectonics of a transect through eastern Nevada near 38° N. latitude, *in* Weide, D.L., and Faber, M.L., eds., This extended land, geological journeys in the southern Basin and Range: Geological Society of America, Cordilleran Section, Field Trip Guidebook, p. 3–5.

Baedecker, P.A., and McKown, D.M., 1987, Instrumental neutron activation analysis of geochemical samples, *in* Baedecker, P.A., ed., Methods for geochemical analysis: U.S. Geological Survey Bulletin 1770, p. H1–H14.

Best, M.G., Scott, R.B., Rowley, P.D., Swadley, W C, Anderson, R.E., Grommé, C.S., Harding, A.E., Deino, A.L., Christiansen, E.H., Tingey, D.G., and Sullivan, K.R., 1993, Oligocene-Miocene caldera complexes, ash-flow sheets, and tectonism in the central and southeastern Great Basin, *in* Lahren, M.M., Trexler, J.H., Jr., and Spinosa, C., eds., Crustal evolution of the Great Basin and Sierra Nevada: Cordilleran/Rocky Mountain Section, Geological Society of America Guidebook, Department of Geological Sciences, University of Nevada, Reno, p. 285–311.

Blank, H.R., and Kucks, R.P., 1989, Preliminary aeromagnetic, gravity, and generalized geologic maps of the USGS Basin and Range–Colorado Plateau transition zone study area in

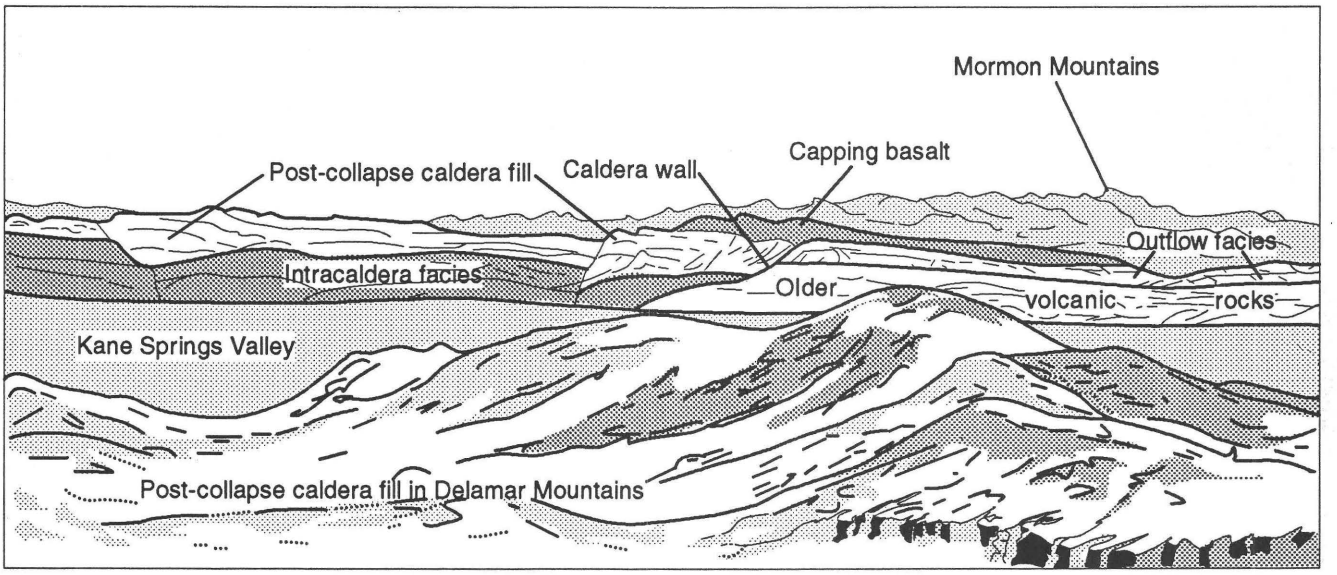

Figure 30. Sketch of major features north and south of the caldera wall in northern Meadow Valley Mountains. View from within Kane Springs Wash caldera in Delamar Mountains to east across Kane Springs Valley.

southwestern Utah, southeastern Nevada, and northeastern Arizona (the "BARCO" project): U.S. Geological Survey Open-File Report 89–432, scale 1:250,000.

Bohannon, R.G., 1979, Strike-slip faults of the Lake Mead region of southern Nevada, *in* Armentrout, J.M., and others, eds., Cenozoic paleogeography of the western United States: Society of Economic Paleontologists and Mineralogists, Pacific Section, Pacific Coast Paleogeography Symposium 3, p. 129–139.

Bonnichsen, Bill, and Kauffman, D.F., 1987, Physical features of rhyolite lava flows in the Snake River Plain volcanic province, southwestern Idaho, *in* Fink, J.H., ed., The emplacement of silicic domes and lava flows: Geological Society of America Special Paper 212, p. 119–145.

Cook, E.F., 1965, Stratigraphy of Tertiary volcanic rocks in eastern Nevada: Nevada Bureau of Mines Report 11, 61 p.

Dalrymple, G.B., and Lanphere, M.A., 1969, Potassium-argon dating: San Francisco, W.H. Freeman, 258 p.

Ekren, E.B., Orkild, P.P., Sargent, K.A., and Dixon, G.L., 1977, Geologic map of Tertiary rocks, Lincoln County, Nevada: U.S. Geological Survey Miscellaneous Investigations Series Map I–1041, scale 1:250,000.

Ferrara, G., and Treuil, M., 1974, Petrological implications of trace element and Sr isotope distributions in basalt-pantellerite series: Bulletin Volcanologique, v. 38, no. 3, p. 548–574.

Goddard, E.N., Chairman, Rock-Color Chart Committee, 1948, Rock-color chart: Geological Society of America.

Hanson, G.N., 1980, Rare earth elements in petrogenetic studies of igneous systems: Annual Reviews of Earth and Planetary Sciences, v. 8, p. 371–406.

Harding, A.E., 1991, Evidence of the Kane Springs Wash caldera in the Meadow Valley Mountains, southeastern Nevada: Boulder, Colo., University of Colorado M.S. thesis, 121 p.

Harding, A.E., Scott, R.B., Mehnert, H.H., and Pampeyan, E.H., 1991, Kane Springs Wash caldera, southeast Nevada—The other half of the story: Geological Society of America Abstracts with Programs, v. 23, no. 4, p. 30.

Johnson, R.G., and King, B.-S. L., 1987, Energy-dispersive X-ray fluorescence spectrometry, *in* Baedecker, P.A., ed., Methods for geochemical analysis: U.S. Geological Survey Bulletin 1770, p. F1–F5.

Lichte, F.E., Golightly, D.W., and Lamothe, P.J., 1987, Inductively coupled plasma–atomic emission spectrometry, *in* Baedecker, P.A., ed., Methods for geochemical analysis: U.S. Geological Survey Bulletin 1770, p. B1–B10.

Lipman, P.W., 1976, Caldera-collapse breccias in the western San Juan Mountains, Colorado: Geological Society of America Bulletin, v. 87, p. 1397–1410.

Lipman, P.W., Christiansen, R.L., and O'Connor, J.T., 1966, A compositionally zoned ash-flow sheet in southern Nevada: U.S. Geological Survey Professional Paper 524–F, p. F1–F47.

Macdonald, R., 1974, Nomenclature and petrochemistry of the peralkaline oversaturated extrusive rocks: Bulletin Volcanologique, v. 38, no. 3, p. 498–516.

Mittwede, S.K., 1987, Comment and reply on "Correlation of the Peach Springs Tuff, a large-volume Miocene ignimbrite sheet in California and Arizona": Geology, v. 15, no. 4, p. 375.

Noble, D.C., 1968, Kane Springs Wash volcanic center, Lincoln County, Nevada, *in* Eckel, E.B., ed., Nevada Test Site: Geological Society of America Memoir 110, p. 109–116.

Novak, S.W., 1984, Eruptive history of the rhyolitic Kane Springs Wash volcanic center, Nevada: Journal of Geophysical Research, v. 89, p. 8603–8615.

———1985, Geology and geochemical evolution of the Kane Springs Wash volcanic center, Lincoln County, Nevada: Stanford, Calif., Stanford University Ph. D. dissertation, 173 p.

Novak, S.W., and Mahood, G.A., 1986, Rise and fall of a basalt-trachyte-rhyolite magma system at the Kane Springs Wash caldera, Nevada: Contributions to Mineralogy and Petrology, v. 94, p. 352–373.

Pampeyan, E.H., 1989, Preliminary geologic map of the Meadow Valley Mountains, Lincoln and Clark Counties, Nevada: U.S. Geological Survey Open-File Report 89–182, scale 1:50,000.

Ron, Hagai, Aydin, Atilla, and Nur, Amos, 1986, Strike-slip faulting and block rotation in the Lake Mead fault system: Geology, v. 14, no. 12, p. 1020–1023.

Rowley, P.D., Anderson, R.E., Snee, L.W., and Mehnert, H.H., 1990, Geology and structural setting of the western Caliente caldera complex, Lincoln County, Nevada: Geological Society of America Abstracts with Programs, v. 22, no. 3, p. 78–80.

Rowley, P.D., Shroba, R.R., Simonds, F.W., Burke, K.J., Axen, G.J., and Olmore, S.D., 1991, Geologic map of the Chief Mountain quadrangle, Lincoln County, Nevada: U.S. Geological Survey Open-File Report 91–135, scale 1:24,000.

Scott, R.B., 1990, Significance of mild extension of a relatively stable area within highly extended terrane, southeastern Nevada: Geological Society of America Abstracts with Programs, v. 22, no. 3, p. 81.

Scott, R.B., Blank, H.R., Jr., and Page, W.R., 1991, Evidence for a precursor to the Kane Springs Wash caldera, Lincoln County, Nevada: Geological Society of America Abstracts with Programs, v. 23, no. 4, p. 91.

Scott, R.B., Harding, A.E., Swadley, W C, Novak, S.W., and Pampeyan, E.H., 1991, Preliminary geologic map of the Vigo NW quadrangle, Lincoln County, Nevada: U.S. Geological Survey Open-File Report 91–389, scale 1:24,000.

Scott, R.B., Swadley, W C, and Novak, S.W., 1993, Geologic map of the Delamar Lake quadrangle, Lincoln County, Nevada: U.S. Geological Survey Geologic Quadrangle Map GQ–1730, scale 1:24,000.

Shand, S.J., 1951, Eruptive rocks: New York, John Wiley, 488 p.

Shubat, M.A. and Snee, L.W., 1992, High-precision $^{40}Ar/^{39}Ar$ geochronology, volcanic stratigraphy, and mineral deposits of Keg Mountain, west-central Utah, Chapter G *in* Thorman, C.H., ed., Application of structural geology to mineral and energy resources of the central and western United States: U.S. Geological Survey Bulletin 2012, p. G1–G16.

Shawe, D.R., 1965, Strike-slip control of Basin-Range structure indicated by historical faults in western Nevada: Geological Society of America Bulletin, v. 76, p. 1361–1378.

Smith, R.L., 1960, Zones and zonal variations in welded ash flows: U.S. Geological Survey Professional Paper 354–F, p. 149–159.

Steiger, R.H., and Jäger, Emile, 1977, Subcommission on geochronology—Convention on the use of decay constants in geo- and cosmochronology: Earth and Planetary Science Letters, v. 36, p. 359–362.

Stewart, J.H., 1980, Geology of Nevada: Nevada Bureau of Mines and Geology Special Publication 4, 136 p.

Stewart, J.H., and Carlson, J.E., 1978, Geologic map of Nevada: U.S. Geological Survey and Nevada Bureau of Mines and Geology, scale 1:500,000.

Taggart, J.E., Jr., Lindsay, J.R., Scott, B.A., Vivit, D.V., Bartel, A.J., and Stewart, K.C., 1987, Analysis of geologic materials by wavelength-dispersive X-ray fluorescence spectrometry, *in* Baedecker, P.A., ed., Methods for geochemical analysis: U.S. Geological Survey Bulletin 1770, p. E1–E19.

Taylor, W.J., and Bartley, J.M., 1992, Prevolcanic extensional Seaman breakaway fault and its geological implications for eastern Nevada and western Utah: Geological Society of America Bulletin, v. 104, p. 255–266.

Taylor, W.J., Bartley, J.M., Lux, D.R., and Axen, G.J., 1989, Timing of Tertiary extension in the Railroad Valley–Pioche transect, Nevada—Constraints from $^{40}Ar/^{39}Ar$ ages of volcanic rocks: Journal of Geophysical Research, v. 94, no. 66, p. 7757–7774.

Thompson, R.N., 1982, Magmatism of the British Tertiary volcanic province: Scottish Journal of Geology, v. 18, pt. 1, p. 49–108.

Tschanz, C.M., and Pampeyan, E.H., 1970, Geology and mineral deposits of Lincoln County, Nevada: Nevada Bureau of Mines and Geology Bulletin 73, scale 1:250,000, 188 p.

Wernicke, Brian, Axen, G.J., and Snow, J.K., 1988, Basin and Range extensional tectonics at the latitude of Las Vegas, Nevada: Geological Society of America Bulletin, v. 100, p. 1738–1757.

Wohletz, K.H., and Sheridan, M.F., 1979, A model of pyroclastic surge, *in* Chapin, C.E., and Elston, W.E., eds., Ash-flow tuffs: Geological Society of America Special Paper 180, p. 125–136.

Zoback, M.L., Anderson, R.E., and Thompson, G.A., 1981, Cainozoic evolution of the state of stress and style of tectonism of the Basin and Range province of the United States: Philosophical Transactions of the Royal Society of London, v. A300, p. 407–434.

APPENDIX 1. THIN SECTION MODAL ANALYSIS

Northern stratigraphic sequence

Sample No.	3AH15 .11.88	2AH18 .10.88	7AH30 .10.90	5AH19 .11.88	1AH14 .10.88	4AH19 .11.88
Map unit	Td	Td	Td	Tvc	Tvc	Tvc
Qtz	43.4	46.8	31.3	47.8	39.1	39.9
San	53.3	51.1	60.9	43.3	54.9	51.1
Plag	2.9	0	6.9	4.5	4.2	6.7
other	0.2 Op	tr Bt	0.9 Op	4.5 Op	0.1 Op	0.4 Bt
pheno	Al	0.2 Op				0.9 Am
	Zir					tr Cpx
						0.9 Op
						Ap+Zir
% pheno	23.4	5.0	16.6	6.8	7.8	6.4
% lithic	3.5	8.8	2.1	0.2	0	0.4
		granoph		granoph		
pheno pts	486	188	335	201	215	223
total pts	2,073	3,724	2,014	2,967	2,972	3,498
other		gr in		gr in	vit	

Sample No.	3AH15 .10.88	1AH23 .10.88	5AH21 .5.88	8AH27 .10.90	5AH28 .10.90	1AH18 .11.88
Map unit	Tbr	Tbr	Trlr	Trlr	Trlr	Tyt
Qtz	30.6	29.0	40.4	22.1	43.4	30.7
San	46.3	43.5	53.5	68.6	38.0	57.4
Plag	17.6	32.5	0.6	9.3	17.8	10.9
other	4.7 Bt	3.2 Bt			0.8 Op	tr Bt
pheno	tr Am	tr Am				0.9 Am
	0.8 Op	0.9 Op				1.0 Op
	Zir	Zir				
% pheno	17.0	16.2	2.7	2.3	3.4	2.4
% lithic	0	0	7.5	7.4	10.2	10.2
			bsltic	bsltic	bsltic	pumice
pheno pts	363	345	99	86	129	101
total pts	2,139	2,135	3,613	3,764	3,760	4,121

Sample No.	9AH18 .4.88	1AH24 .5.88	4AH21 .5.88	2AH21 .11.88	3AH25 .10.88	2AH18 .5.88
Map unit	Tyt	Tyt	Tyt	Tyt	Tyt	Tyt
Qtz	43.6	59.7	58.8	52.6	49.2	14.4
San	45.3	20.9	34.4	36.7	39.7	80.7
Plag	1.7	9.7	5.7	0	0.8	0
other	1.7 Bt	tr Bt	1.0 Op	10.6 Op	10.3 Op	tr Bt
pheno	7.7 Op	9.7 Op				4.9 Op
% pheno	3.0	5.7	7.3	6.1	3.5	13.7
% lithic	5.0	8.9	5.9	44.2	24.3	0.2
		pumice	pumice	some bsltic		
pheno pts	117	206	209	245	126	223
total pts	3,930	3,616	2,878	4,013	3,598	1,629
other					def gl	

Northern stratigraphic sequence--Continued

Sample No.	4AH16 .5.88	6AH14 .5.88	3AH20 .11.88	5AH14 .5.88	1AH21 .3.90	3AH21 .5.88
Map unit	Tyt	Tyt	Tgt	Tgt	Tfl	Tfl
Qtz	25	25	22.2	11.3	23.1	32.2
San	7	69	72.5	83.1	73.4	62.8
Plag	1	2	2.7	0.4	0	0
other	tr Bt	2 Bt	tr Bt	tr Bt	3.5 Op	5.0 Op
pheno	1 Op Zir	2 Op Zir	2.7p Zir	5.2 Op	vap Am	sec Min
% pheno	40	45	18.7	12.0	18.2	19.9
% lithic	10	5	0.1	0.6	0.3	0
pheno pts	est	est	374	248	398	538
total pts			2,000	2,065	2,184	2,707
other				eutax		

Sample No.	2AH21 .5.88	1AH28 .10.90	4AH26 .5.88	5AH19 .5.88a	5AH19 .5.88b	7BS26 .4.90
Map unit	Tfl	Tfl	Tfl	Tfl	Tfl	Tyt
Qtz	30.6	37.0	29.0	53.7	38.8	30.0
San	68.7	59.4	71.0	40.0	60.1	45.0
Plag	0	0	0	0	0	18.4
other	0.7 Op	3.6 Op		6.3 Op	0.5 Op	1.2 Bt
pheno	sec Min	Zir	sec Min	Zir sec Min		2.5 Am 2.5 Op
% pheno	34.3	20.9	12.9	4.5	44.8	2.6
% lithic	0	0	0.6 trachy	1.6	0.4	12.1 pumice
pheno pts	710	446	269	95	1,015	80
total pts	2,069	2,133	2,092	2,122	2,266	3,041
other		gr in		xl-p b eutax	xl-r b	

Sample No.	5AH12 .11.88	4AH12 .11.88	4AH19 .5.88	5AH26 .5.88	2AH3 .11.90	3AH3 .11.90
Map unit	Tcj	Tcj	Tcj	Tcj	Tcj	Tcj
Qtz	30.0	23.5	27.2	29.7	20.4	27.8
San	61.7	71.1	62.4	66.2	74.9	70.9
Plag	0	0	0	0	0	0
other	8.3 Op	5.4 Op	8.0 Cp?	4.1 Op	4.6 Op	1.3 Op
pheno		Zir		Ol Zir	Zir	
% pheno	3.1	6.1	7.2	5.9	15.6	8.7
% lithic	0.4	0	0	0	0	0
pheno pts	120	204	250	219	323	230
total pts	3,923	3,356	3,483	3,690	2,073	2,643
	gl sh		gr in		bg base	r base

Northern stratigraphic sequence--Continued

Sample No.	1AH5 .11.90b	1AH5 .11.90a	5AH10 .4.89	4AH3 .11.90
Map unit	Tcj	Tcj	Tcj	Tlt
Qtz	31.4	33.4	30.1	41.6
San	66.6	63.6	67.2	54.3
Plag	0	0	0	0
other	2.1 Op	0.6 Ol	2.7 Cp	4.1 Op
pheno	Zir	2.4 Op	Ol	Ol
			Zir	Zir
% pheno	14.2	16.6	12.6	10.0
% lithic	0	0	0	0
pheno pts	287	341	259	221
total pts	2,015	2,059	2,061	2,208
other	ul base	ll base		

Southern stratigraphic sequence

Sample No.	5AH16 .4.89	1AH18 .4.89	6AH20 .4.89	2AH8 .4.88	1AH22 .3.90	3AH20 .4.89	2AH21 .4.89	1AH14 .4.89
Map unit	Tkbu	Tkbl	Tkg	Tpt	Tot	Tsm	Tsm	Th
Qtz	32.6	44.0	0.1	0	19.7	36.7	33.8	16.8
San	63.8	54.6	94.2	94.7	70.1	60.3	63.3	13.7
Plag	0	0	0.1	0	0	0.3	0.5	55.2
other	0.4 Ol	tr Cp	3.0 Cp	3.6 Cp	10.2 Op	2.6 Op	0.5 Bt	11.7 Bt
pheno	2.3 Cp	1.3 Op	2.5 Op	1.7 Op		Zir	1.9 Op	2.5 Op
	0.9 Op	Zir	Zir					
	Zir							
	vap Ri?							
% pheno	10.4	7.9	37.8	36.4	3.6	14.5	9.0	29.5
% lithic	0	0	0	0	0	0.05	0.1	0.6
pheno pts	221	227	800	777	137	305	210	786
total pts	2,118	2,866	2,119	2,137	3,825	2,105	2,333	2,664
Other		base	base					

Abbreviations used:

Op, opaque; Bt, biotite; Cp, clinopyroxene; Am, amphibole; Ri, riebeckite; Ol, olivine; Zir, zircon; Ap, apatite; Al, allanite; Qtz, quartz; San, sanidine; Plag, plagioclase

est, estimate; pts, points; pheno, phenocrysts; tr, trace

trachy, trachytic; sec Min, secondary green, sheaflike minerals; gr in, granophyric intergrowth of quartz and feldspar (lithic fragments); vap, vapor phase; bsltic, basaltic; gl sh, glass shards; def gl, deformed glass shards; eutax, eutaxitic texture

xl-p b, crystal-poor base; xl-r b, crystal-rich base; b g base, blue-gray base; r base, red base; ul, upper layered; ll, lower layered; vit, vitrophyre

Td, rhyolite dike; Tvc, volcanic center; Tbr, biotite rhyolite flow; Trlr, red lithic rhyolite; Tyt, yellow tuff; Tgt, gray ash-flow tuff; Tfl, flow-lineated rhyolite; Tcj, columnar-jointed rhyolite; Tlt, lithic-rich tuff; Tkbu, upper cooling unit of the Gregerson Basin Member of the Kane Wash Tuff; Tkbl, lower cooling unit of the Gregerson Basin Member of the Kane Wash Tuff; Tkg, Grapevine Spring Member of the Kane Wash Tuff; Tpt, precaldera trachyte; Tot, older tuff; Tsm, Sunflower Mountain Tuff; Th, Hiko Tuff

APPENDIX 2. CHEMICAL DATA

2A. EDXRF TRACE-ELEMENT ANALYSIS

Values reported as ppm.

Northern stratigraphic sequence

Map Unit	Sample No.	Rb	Sr	Y	Zr	Nb	Ba	La	Ce	Nd
Tbr	1AH23.10.88	206	36	31	143	26	280	49	85	40
Td	1AH23.4.89	181	56	27	139	16	508	56	87	36
Td	3AH15.11.88	183	37	35	133	38	110	54	116	51
Tb	5AH21.4.89	36	653	24	162	17	593	28	60	38
Tfb	6AH18.4.88	185	30	45	164	36	123	80	138	59
Tyt	1AH18.11.88	313	47	46	189	55	66	20	43	25
Tyt	7BS26.4.90	215	259	39	128	31	24	40	69	37
Tyt	2BS26.4.90	153	170	22	121	30	21	31	50	34
Trlr	2AH16.5.88	178	81	49	169	37	141	40	86	43
Tgt	3AH20.11.88	229	61	62	249	55	233	66	134	56
Tbl	4AH14.5.88	23	552	32	190	18	644	27	54	29
Tfl	1AH21.5.88	100	39	56	589	49	145	113	251	89
Tfl	3AH21.5.88	249	29	88	952	90	74	129	228	88
Tfl	9AH19.5.88	262	27	104	1,097	110	46	120	204	95
Tfl	3AH14.5.88	271	26	99	1,081	115	63	127	227	97
Tfl	7AH19.5.88	299	27	129	1,376	131	49	139	265	106
Tcj	5AH12.11.88	272	50	91	938	103	82	120	207	86
Tcj	4AH19.5.88	279	32	87	999	107	75	120	226	96
Tcj	2AH12.11.88	271	22	104	979	107	56	106	199	90
Tcj	1AH19.5.88	263	28	90	909	103	64	99	207	78
Tcj	2AH3.11.90	246	12	108	1,018	96	27	114	217	90
Tlt	4AH3.11.90	226	37	86	946	100	80	103	195	80

Southern stratigraphic sequence

Tkbu	5BS19.5.89	265	22	66	1,134	119	32	114	225	96
Tkbl	2BS27.3.90	255	29	75	860	112	76	104	201	93
Tkg	2AH24.3.90	182	45	67	725	80	154	142	265	106
Tkg	3BS27.3.90	214	39	71	733	83	109	149	253	121
Tsm	13BS16.11.87	266	156	58	231	62	208	27	66	27
Tdl	2AH11.5.88	194	24	55	467	68	47	43	116	38

2B. WDXRF MAJOR-ELEMENT ANALYSIS

Values reported as weight percent.

Northern stratigraphic sequence

Oxide	Map unit symbol and sample number					
	Tbr AH23. 10.88	Td 1AH23. 4.89	Td 3AH15. 11.88	Tbu 5AH21. 4.89	Tfb 6AH18. 4.88	Tyt 1AH18. 11.88
SiO_2	74.3	74.3	75.0	51.8	75.4	66.3
Al_2O_3	12.4	12.8	11.9	16.3	12.5	11.4
Fe_2O_3T	1.23	1.12	1.42	10.8	1.28	1.17
MgO	0.18	0.24	0.36	5.61	0.16	0.96
CaO	0.46	0.70	0.97	8.09	0.39	3.58
Na_2O	2.67	3.47	3.55	3.54	3.61	0.94
K_2O	5.51	5.64	4.65	1.60	5.40	3.54
TiO_2	0.11	0.13	0.14	2.10	0.11	0.07
P_2O_5	<0.05	<0.05	<0.05	0.61	<0.05	<0.05
MnO	<0.02	<0.02	<0.02	0.14	<0.02	<0.02
LOI	0.89	0.78	0.76	1.85	<0.01	0.52

	Tyt 7BS26. 4.90	Tyt 2BS26. 4.90	Trlr 2AH16. 5.88	Tgt 3AH20. 11.88	Tbm 4AH14. 5.88	Tfl 1AH21. 5.88
SiO_2	73.5	72.2	71.1	72.7	46.8	62.1
Al_2O_3	10.4	9.98	13.2	12.7	16.0	16.9
Fe_2O_3T	0.99	0.95	3.36	1.73	13.8	5.12
MgO	0.65	0.74	0.57	0.31	4.27	0.42
CaO	2.22	2.66	1.26	1.46	8.17	0.66
Na_2O	0.89	0.58	3.69	3.82	3.56	5.59
K_2O	3.06	2.76	4.68	4.97	1.32	6.23
TiO_2	0.07	0.06	0.52	0.15	2.73	0.62
P_2O_5	<0.05	<0.05	0.09	0.05	0.66	0.11
MnO	<0.02	<0.02	0.04	0.05	0.10	0.16
LOI	8.65	9.29	0.56	1.24	2.31	1.14

	Tfl 3AH21 5.88	Tfl 9AH19. 5.88	Tfl 7AH19. 5.88	Tcj 5AH12. 11.88	Tcj 4AH19 5.88	Tcj 2AH12. 11.88	Tcj 1AH19. 5.88
SiO_2	73.5	74.8	73.4	72.9	73.7	74.5	74.5
Al_2O_3	11.8	11.1	11.4	10.4	10.9	11.6	11.4
Fe_2O_3T	3.13	2.77	3.17	2.57	2.68	2.89	2.79
MgO	0.30	<0.10	0.14	0.48	0.12	0.14	0.15
CaO	0.25	0.65	0.28	1.74	1.25	0.12	0.42
Na_2O	2.94	3.90	3.97	3.23	3.22	3.65	3.81
K_2O	5.41	4.56	5.74	4.91	5.10	5.07	4.71
TiO_2	0.20	0.16	0.19	0.16	0.17	0.19	0.17
P_2O_5	<0.05	<0.05	<0.05	<0.05	<0.05	<0.05	<0.05
MnO	0.03	0.05	0.06	0.02	0.03	0.05	0.04
LOI	1.20	0.66	0.49	2.46	1.40	0.58	0.86

Southern stratigraphic sequence

	Tkbu 5BS19. 5.89	Tkbl 2BS27 3.90	Tkg 2AH24. 3.90	Tkg 3BS27. 3.90	Tsm 13BS16. 11.87	Tdl 2AH11. 5.88
SiO_2	74.7	75.5	68.0	70.0	70.6	75.2
Al_2O_3	11.1	11.1	13.5	14.0	11.7	11.8
Fe_2O_3T	3.18	2.46	3.38	3.34	1.66	2.04
MgO	<0.10	0.17	0.26	0.17	0.64	0.15
CaO	0.26	0.33	1.96	0.34	2.13	0.13
Na_2O	4.29	3.73	4.22	4.35	1.70	3.70
K_2O	4.61	4.74	5.41	5.67	3.98	5.29
TiO_2	0.18	0.15	0.26	0.29	0.13	0.12
P_2O_5	<0.05	<0.05	<0.05	<0.05	<0.05	<0.05
MnO	0.07	0.04	0.07	0.06	<0.02	<0.02
LOI	0.57	0.74	1.85	0.74	6.72	0.55

2C. INAA ANALYSIS

Values reported as ppm.

Northern stratigraphic sequence

Element	Map unit symbol and sample number					
	Tbr 1AH23. 10.88	Tbf 6AH18. 4.88	Tyt 1AH18. 11.88	Trlr 2AH16. 5.88	Tgt 3AH20. 11.88	Tfl 1AH21. 5.88
Fe	9,070	9,210	7,830	23,300	12,400	35,200
Na	20,000	27,200	6,430	27,200	28,000	40,100
Rb	209	183	297	174	233	91.4
Sr	17.6	17.6	54.2	54.9	34.0	19.9
Cs	2.34	2.49	7.09	2.01	2.34	4.23
Ba	259	120	71.6	137	226	142
Th	26.5	23.7	32.4	19.7	28.4	16.2
U	6.22	5.16	8.62	4.24	6.03	2.93
La	47.9	75.2	18.5	35.1	59.4	101
Ce	97.1	158	34.9	82.2	141	289
Nd	36.2	59.1	22.4	37.4	54.8	86.3
Sm	6.91	11.3	6.77	8.98	11.8	14.8
Eu	0.345	0.214	0.146	0.509	0.370	1.15
Gd	6.41	11.0	0.00	8.49	0.00	14.3
Tb	0.862	1.36	1.16	1.30	1.76	1.81
Ho	1.24	1.87	1.88	1.87	2.54	2.30
Tm	0.00	0.829	0.883	0.797	1.16	1.01
Yb	3.87	5.11	5.84	5.14	7.24	6.83
Lu	0.567	0.718	0.822	0.715	1.02	0.976
Zr	160	207	218	218	303	593
Hf	5.25	6.34	8.13	5.95	9.43	11.6
Ta	2.87	3.00	6.38	2.77	4.42	2.33
W	0.820	1.75	0.522	2.19	1.24	3.18
Sc	2.01	1.87	2.04	5.45	1.76	7.47
Cr	0.00	1.65	0.00	3.02	2.45	1.79
Co	0.661	0.547	0.518	6.24	1.25	0.553
Ni	0.00	1.39	0.00	0.00	2.39	0.00
Zn	24.3	38.8	64.1	66.2	77.5	148
As	0.911	20.2	2.69	3.66	2.65	4.03
Sb	0.224	0.201	0.494	0.00	0.195	0.841
Au	0.570	0.043	0.492	0.662	0.00	0.894

Northern stratigraphic sequence--Continued

Element	Map unit symbol and sample number					
	Tfl 3AH21. 5.88	Tfl 9AH19. 5.88	Tfl 7AH19. 5.88	Tcj 5AH12. 11.88	Tcj 4AH19. 5.88	Tcj 1AH19. 5.88
Fe	21,700	19,400	22,200	17,700	18,600	18,900
Na	20,700	28,300	29,000	23,000	23,200	26,700
Rb	237	252	278	252	254	244
Sr	18.3	0.00	0.00	35.5	18.4	0.00
Cs	2.04	2.76	1.67	2.26	2.58	5.48
Ba	64.4	20.9	67.1	79.9	95.3	37.5
Th	26.8	26.7	39.5	27.0	28.3	27.6
U	7.85	4.24	7.46	7.20	9.78	9.24
La	123	112	117	102	107	84.5
Ce	265	222	304	230	245	221
Nd	104	101	107	90.7	93.7	75.9
Sm	19.2	20.0	21.9	18.9	18.9	16.2
Eu	0.338	0.246	0.255	0.227	0.247	0.226
Gd	18.3	19.9	21.6	17.5	19.30	16.8
Tb	2.69	2.87	3.33	2.61	2.69	2.53
Ho	3.71	4.09	5.18	3.85	4.00	3.74
Tm	1.62	1.86	2.63	1.66	1.75	1.68
Yb	10.7	11.5	16.7	10.5	10.7	10.6
Lu	1.48	1.58	2.27	1.43	1.47	1.50
Zr	956	1,030	1,270	894	927	915
Hf	24.6	27.2	32.6	23.7	24.8	24.5
Ta	6.96	7.96	9.55	7.02	7.37	7.43
W	1.28	0.651	0.00	1.33	0.00	2.20
Sc	1.18	0.452	0.537	0.478	0.514	0.476
Cr	2.61	0.00	0.00	0.00	3.02	0.00
Co	0.233	0.170	0.174	0.174	0.215	0.148
Ni	0.00	2.04	0.00	2.75	4.42	0.00
Zn	140	164	200	144	171	141
As	4.97	1.09	6.84	6.84	7.01	2.32
Sb	0.773	0.882	1.28	0.660	1.21	0.772
Au	1.57	0.00	0.630	1.32	0.669	0.00

Southern stratigraphic sequence

Element	Map unit symbol and sample number					
	Tkbu 5BS19. 5.89	Tkbl 2BS27. 3.90	Tkg 2AH24. 3.90	Tkg 3BS27. 3.90	Tsm 13BS16. 11.87	Tdl 2AH11. 5.88
Fe	18,800	17,100	23,900	22,600	10,700	14,300
Na	28,500	26,800	31,400	32,200	11,900	27,100
Rb	243	261	186	200	252	201
Sr	0.00	0.00	42.8	12.6	139	0.00
Cs	2.29	3.72	1.75	5.96	8.04	3.10
Ba	35.2	82.2	139	91.6	198	52.6
Th	29.3	29.8	23.8	24.4	24.2	21.7
U	3.43	8.27	5.69	5.23	3.77	7.22
La	98.2	103	135	142	28.4	45.9
Ce	229	209	290	280	68.4	128
Nd	83.6	89.7	110	112	32.5	43.8
Sm	16.5	18.1	18.7	18.2	9.63	10.2
Eu	0.195	0.250	0.456	0.446	0.309	0.089
Gd	15.6	16.6	14.5	16.5	10.10	10.7
Tb	2.37	2.56	2.16	2.22	1.50	1.54
Ho	3.50	3.76	3.02	0.00	2.16	2.16
Tm	1.54	1.69	1.26	1.34	0.957	0.936
Yb	9.87	10.4	7.89	8.25	6.10	5.97
Lu	1.41	1.41	1.17	1.17	0.818	0.838
Zr	985	846	761	823	265	448
Hf	26.9	24.1	20.3	21.0	9.56	12.7
Ta	7.81	8.08	5.64	5.78	5.25	5.27
W	1.87	2.28	2.97	3.57	0.00	1.41
Sc	0.416	0.496	3.13	2.83	1.19	0.953
Cr	2.13	0.00	2.38	0.00	0.642	0.00
Co	0.186	0.206	0.846	0.642	1.14	0.331
Ni	0.00	3.51	0.00	0.00	0.00	0.00
Zn	155	154	99.5	113	80.0	89.7
As	3.36	4.16	3.85	0.00	3.99	3.62
Sb	0.246	0.629	0.388	0.490	0.419	0.430
Au	1.50	0.712	0.616	0.00	0.462	0.00

2D. ICP ANALYSIS

Values reported as ppm except where noted.

	Northern stratigraphic sequence					
Element	Map unit symbol and sample number					
	Tbr 1AH23. 10.88	Tfb 6AH18. 4.88	Tyt 1AH18. 11.88	Trlr 2AH16. 5.88	Tgt 3AH20. 11.88	Tfl 1AH21. 5.88
Al%	6.5	6.6	6.1	7.0	6.7	8.5
Ca%	0.34	0.31	2.6	0.96	1.1	0.48
Fe%	0.93	0.86	0.84	2.5	1.2	3.6
K %	4.5	4.5	3.0	3.9	4.2	5.0
Mg%	0.09	0.08	0.59	0.35	0.17	0.23
Na%	1.9	2.6	0.72	2.7	2.8	3.8
Ti%	0.08	0.06	0.05	0.34	0.09	0.34
Mn	220	180	170	420	380	1,200
Ag	<2	<2	<2	<2	<2	<2
As	<10	20	<10	<10	<10	<10
Au	<8	<8	<8	<8	<8	<8
B	-	-	-	-	-	-
Ba	240	110	65	130	210	120
Be	4	5	12	5	5	4
Bi	<10	<10	<10	<10	<10	<10
Cd	<2	<2	<2	<2	<2	<2
Ce	83	140	41	82	130	260
Co	1	<1	<1	8	2	1
Cr	<1	<1	<1	2	<1	<1
Cu	2	3	4	8	4	3
Eu	<2	<2	<2	<2	>2	>2
Ga	19	23	26	24	23	32
Ge	-	-	-	-	-	-
Ho	<4	<4	<4	<4	<4	<4
La	48	80	21	39	66	110
Li	58	26	38	24	34	29
Mo	<2	<2	<2	<2	<2	5
Nb	19	19	40	29	48	38
Nd	31	53	23	36	51	85
Ni	<2	<2	2	4	<2	<2
Pb	18	20	18	22	17	15
Sc	2	<2	2	6	2	8
Sn	<5	<5	5	<5	<5	<5
Sr	32	22	41	70	45	23
Ta	<40	<40	<40	<40	<40	<40
Th	25	22	33	20	27	17
U	<100	<100	<100	<100	<100	<100
V	3	24	3	58	7	<2
W	-	-	-	-	-	-
Y	28	47	40	48	64	57
Yb	3	5	6	5	6	7
Zn	30	35	75	70	78	160
Zr	-	-	-	-	-	-

Northern stratigraphic sequence--Continued

Element	Map unit symbol and sample number					
	Tfl 3AH21. 5.88	Tfl 9AH19. 5.88	Tfl 7AH19. 5.88	Tcj 5AH12. 11.88	Tcj 4AH19. 5.88	Tcj 1AH19. 5.88
Al%	6.2	5.9	6.0	5.6	5.8	6.0
Ca%	0.18	0.49	0.22	1.3	0.93	0.32
Fe%	2.2	2.1	2.4	1.9	2.0	2.1
K %	4.4	3.8	4.8	4.1	4.3	3.9
Mg%	0.16	0.03	0.06	0.29	0.05	0.07
Na%	2.1	2.9	2.9	2.4	2.4	2.7
P %	0.009	0.006	0.007	0.01	0.02	0.01
Ti%	0.10	0.10	0.13	0.10	0.11	0.11
Mn	280	470	560	260	310	360
Ag	<2	<2	<2	<2	<2	<2
As	<10	<10	<10	<10	<10	<10
Au	<8	<8	<8	<8	<8	<8
B	-	-	-	-	-	-
Ba	59	39	37	68	62	52
Be	7	9	14	9	9	7
Bi	<10	<10	<10	<10	<10	<10
Cd	<2	<2	<2	<2	<2	<2
Ce	230	210	280	220	230	200
Co	<1	<1	<1	<1	<1	<1
Cr	<1	<1	<1	<1	<1	<1
Cu	4	4	3	3	4	4
Eu	<2	<2	<2	<2	<2	<2
Ga	31	32	36	28	30	31
Ge	-	-	-	-	-	-
Ho	<4	<4	<4	<4	<4	<4
La	130	120	130	120	120	91
Li	35	32	82	80	43	33
Mo	<2	<2	<2	<2	<2	<2
Nb	70	89	110	66	68	81
Nd	98	96	100	88	90	73
Ni	<2	<2	<2	<2	<2	<2
Pb	36	38	22	27	36	32
Sc	<2	<2	<2	<2	<2	<2
Sn	<5	<5	<5	<5	<5	<5
Sr	17	9	10	38	17	12
Ta	<40	<40	<40	<40	<40	<40
Th	19	27	37	28	26	23
U	<100	<100	<100	<100	<100	<100
V	2	<2	2	3	<2	<2
W	-	-	-	-	-	-
Y	83	110	110	99	99	90
Yb	9	12	15	11	10	8
Zn	160	180	220	160	190	180
Zr	-	-	-	-	-	-

Southern stratigraphic sequence

Element	Map unit symbol and sample number					
	Tkbu 5BS19. 5.89	Tkbl 2BS27. 3.90	Tkg 2AH24. 3.90	Tkg 3BS27. 3.90	Tsm 13BS16. 11.87	Tdl 2AH11. 5.88
Al%	5.8	5.8	7.1	7.2	6.2	6.3
Ca%	0.20	0.23	1.4	0.26	1.6	1.5
Fe%	2.2	1.7	2.4	2.4	1.2	1.5
K %	3.8	3.9	4.5	4.6	3.3	4.6
Mg%	0.03	0.08	0.14	0.08	0.38	0.07
Na%	3.1	2.7	3.1	3.1	1.3	2.7
P %	0.009	0.01	0.02	0.01	0.01	0.007
Ti%	0.12	0.08	0.13	0.19	0.08	0.09
Mn	560	380	540	560	210	170
Ag	<2	<2	<2	<2	<2	<2
As	<10	<10	<10	<10	<10	<10
Au	<8	<8	<8	<8	<8	<8
B	-	-	-	-	-	-
Ba	29	69	130	93	190	42
Be	8	8	6	7	8	6
Bi	<10	<10	<10	<10	<10	<10
Cd	<2	>2	>2	>2	>2	<2
Ce	230	180	260	260	68	120
Co	<1	<1	1	<1	2	<1
Cr	<1	<1	<1	1	2	2
Cu	3	4	5	4	4	3
Eu	<2	<2	<2	<2	<2	<2
Ga	33	31	29	29	29	29
Ge	-	-	-	-	-	-
Ho	<4	<4	<4	<4	<4	<4
La	120	110	150	160	32	51
Li	63	57	29	28	50	42
Mo	<2	<2	<2	4	<2	<2
Nb	90	78	63	76	48	56
Nd	89	81	100	110	33	43
Ni	<2	<2	<2	<2	<2	<2
Pb	38	34	20	25	20	20
Sc	<2	<2	4	4	<2	<2
Sn	<5	<5	5	<5	<5	<5
Sr	7	13	33	20	160	14
Ta	<40	<40	<40	<40	<40	<40
Th	32	20	23	25	26	23
U	<100	<100	<100	<100	<100	<100
V	4	2	3	3	7	4
W	-	-	-	-	-	-
Y	72	63	60	69	58	54
Yb	11	6	6	8	6	5
Zn	190	170	120	130	97	100
Zr	-	-	-	-	-	-

APPENDIX 3. ISOTOPIC DATES

K-Ar determinations

Sample No.	3AH18 .5.89	3AH18 .5.89	1AH26 .5.88	2AH26 .5.88	4AH26 .5.88	4AH26 .5.88	5AH26 .5.88
Map unit	Td	Td	Tfb vit	Tfb devit	Tfl	Tfl	Tcj
Material	sanidine	biotite	whole rock	whole rock	sanidine	sanidine	sanidine
K_2O%	10.7 10.8	8.36 8.37	4.97 4.95	4.84 4.86	6.71 6.71	6.71 6.71	6.41 6.42
$^*Ar^{40}$ 10^{-10}mol/g	1.9833	1.5812	0.9262	0.9619	1.4188	1.4426	1.3513
%$^*Ar^{40}$	62.3	57.1	38.9	77.7	85.7	69.5	72.5
Age, Ma	12.8	13.1	12.9	13.7	14.6	14.9	14.6
± 2 sigma	±0.5	±0.5	±0.7	±0.5	±0.4	±0.5	±0.5

Constants: $K^{40}\lambda\varepsilon = 0.581 \times 10^{-10}$/yr
$\lambda\rho = 4.962 \times 10^{-10}$/yr
$^{40}K/K = 1.167 \times 10^{-4}$

40Ar/39Ar determinations

Sample No.	4AH26 .5.88.	5BS19 .5.88	2BS27 .3.90	3BS27 .3.90
Map unit	Tfl	Tkbu	Tkbl	Tkg
Material	sanidine	sanidine	sanidine	sanidine
Sample wt.mg	60	59.3	68	50
Ar40/36 meas atm	298.8	298.9	298.9	298.9
J-value	0.007432	0.007412	0.007415	0.007368
error	0.25%	0.25%	0.1%	0.1%
Plateau age, Ma	14.43 ± 0.14	14.39 ± 0.28	14.55 ± 0.14	14.67 ± 0.22

Preliminary Correlation of Quaternary and Late Tertiary Alluvial Deposits in Southeastern Nevada

By W C Swadley, D.L. Schmidt, R.R. Shroba, V.S. Williams, *and* D.L. Hoover

GEOLOGIC STUDIES IN THE BASIN AND RANGE–COLORADO PLATEAU TRANSITION IN SOUTHEASTERN NEVADA, SOUTHWESTERN UTAH, AND NORTHWESTERN ARIZONA, 1992

U.S. GEOLOGICAL SURVEY BULLETIN 2056–F

UNITED STATES GOVERNMENT PRINTING OFFICE, WASHINGTON : 1995

CONTENTS

FIGURES

TABLES

Preliminary Correlation of Quaternary and Late Tertiary Alluvial Deposits in Southeastern Nevada

By W C Swadley, D.L. Schmidt, R.R. Shroba, V.S. Williams, *and* D.L. Hoover

ABSTRACT

Surficial mapping in parts of the Basin and Range–Colorado Plateau Transition (BARCO) Study Unit area in southeastern Nevada has defined the sequence of Quaternary and late Tertiary alluvial deposits in four areas based chiefly on age-dependent geomorphic criteria. Alluvial-fan, pediment, terrace, and flood-plain deposits of these areas are correlated on the basis of similarities in these geomorphic aspects. Using these same criteria, correlations are extended to similar deposits in the Nevada Test Site area for which isotopic ages have been determined. Tentative ages for the deposits of the four study areas are inferred from the correlations to the NTS area. With minor exceptions, the sequence of alluvial deposits in the four areas of this study consists of, in order of increasing age, a late Holocene unit, an early Holocene to late Pleistocene unit, three middle Pleistocene units, and an early Pleistocene to Pliocene(?) unit.

INTRODUCTION

Alluvial deposits are common geologic features in southern Nevada and in much of the southern Great Basin, forming extensive alluvial piedmonts along the flanks of mountain ranges and prominent flood plains and terraces along major streams. Alluvial deposits in four areas in southeastern Nevada (fig. 1) were mapped as part of the Basin and Range–Colorado Plateau Transition (BARCO) Study Unit (see the Introduction to this volume for a discussion of the BARCO Study Unit, its history, activities, and goals). The mapped areas discussed in this report are (1) Chief Mountain, by Shroba; (2) Delamar Mountains, by Swadley; (3) Moapa Valley, by Schmidt; and (4) Mesquite area, by Williams and Hoover.

The sequences of alluvial deposits recognized in each of the four areas are similar; however, variations in drainage-basin characteristics, tectonic settings, bedrock lithologies, and climatic conditions have resulted in minor differences. Deposits in the Chief Mountain and Delamar Mountains areas are mostly alluvial-fan deposits, whereas deposits in the Moapa Valley and Mesquite areas include flood-plain, terrace, pediment, and alluvial-fan deposits.

The numerical ages of alluvial deposits in the four areas are difficult to determine, because the deposits commonly lack fossils or other materials that are suitable for age determination by radiogenic methods. Therefore, in order to make tentative correlations, we have used traditional stratigraphic correlation, based chiefly on age-dependent geomorphic criteria, to show correspondence in character and in stratigraphic sequence among deposits. Criteria used include geomorphic position, preservation and modification of original depositional topography, soil development, rock and mineral weathering, and formation of desert pavements. (See, for example, Colman and others, 1987; Hoover and others, 1981.) These same criteria were used to make tentative correlation with similar surficial deposits at and near the Nevada Test Site (NTS; fig. 1), because many NTS deposits have numerical ages determined by isotopic, radiogenic, and tephrochronologic methods.

A standardized nomenclature is not in place for the four areas. In this report, the alluvial deposits of each area are designated by informal map unit names and symbols that have been used by the authors in their respective areas. Some map units have been given informal place names; others have only been given relative age designations.

CHIEF MOUNTAIN AREA

The Chief Mountain area is near the eastern margin of the Great Basin in southeastern Nevada near Caliente (fig. 1). The area covers primarily the north-trending Chief Range and the Panaca basin, a deep, fault-bounded basin on the east side of the Chief Range. Chief Mountain (2,278 m), in the western part of the area, is the highest peak in the Chief Range. Two gently sloping alluvial piedmonts along the southern and eastern flanks of the Chief Range characterize the area. The piedmonts range in altitude from about 1,425 to 1,885 m, are typically 3–12 km wide, and slope southward toward Antelope Canyon and eastward toward Meadow Valley. Both are drained by southward- and eastward-flowing

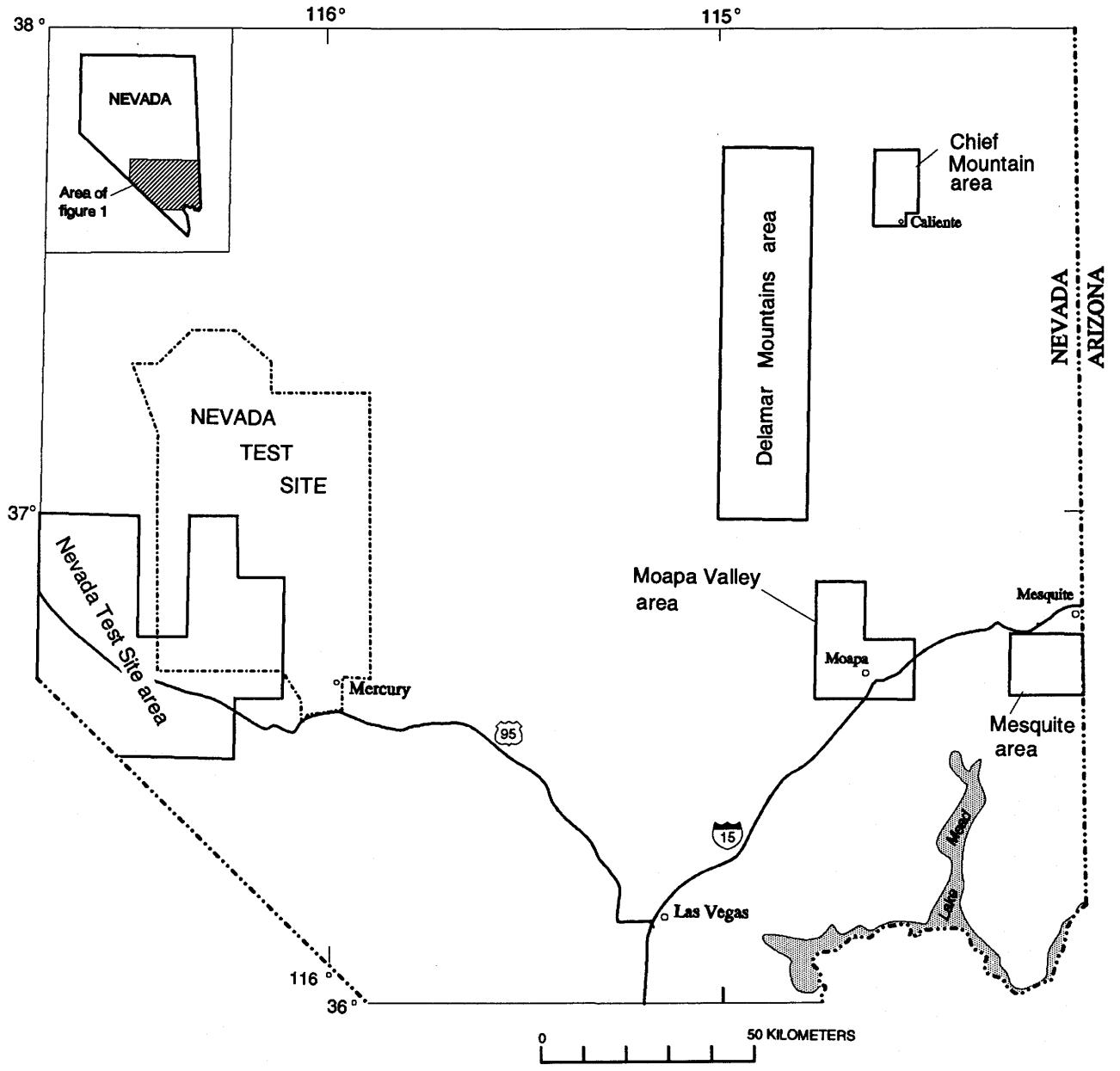

Figure 1. Location of the four study areas of this report, and the Nevada Test Site area.

intermittent streams that are tributary to the unnamed wash in Antelope Canyon and Meadow Valley Wash (fig. 2). Meadow Valley Wash flows south and ultimately joins the Colorado River about 165 km south of Caliente.

Bedrock in the Chief Range is the source of the alluvial-fan deposits on the piedmonts. Composition of the bedrock is mostly Late Proterozoic and Cambrian quartzite, a minor amount of Cambrian limestone and shale, Oligocene and Miocene volcanic rocks, and Miocene intrusive porphyry. The volcanic rocks are mostly rhyolitic ash-flow tuffs and andesitic to basaltic lava flows, flow breccias, and volcanic mudflow breccias (Rowley and Shroba, 1991; Rowley and others, 1992).

The climate of the area is semiarid and is characterized by warm, dry summers and cool, moist winters. Mean annual temperature and mean annual precipitation vary with elevation and are about 11–12 °C and 22–34 cm, respectively (Borup and Bagley, 1976).

The surficial deposits on the piedmonts are mostly alluvial-fan deposits that were deposited by minor intermittent streams about 5–15 km long. The fans are commonly about 0.5–1 km wide, 1–4 km long, and have surfaces that slope 4–5 percent. Some of the older fans coalesced into fan aprons that were dissected by subsequent stream erosion. Some of the older alluvial-fan deposits may grade into pediment deposits near the mountain front.

The alluvial-fan deposits on the piedmonts are typically clast supported pebble and cobble gravel in a sand matrix that is interbedded with matrix-supported sandy pebble gravel and pebbly sand. These deposits locally contain minor beds of clast-supported, cobbly, small-boulder gravel and are typically poorly sorted to moderately sorted and thin to medium bedded. The clasts in most of these deposits are chiefly angular to subangular quartzite and a minor amount of subrounded volcanic rocks. Near the south end of Meadow Valley, the clasts are chiefly subrounded tuffs and lavas. Near the north end of the Chief Range, the clasts are mostly angular to subrounded limestone.

The soils developed in the alluvial-fan deposits are characterized by horizons of secondary calcium carbonate accumulation. The thickness and the morphology of these calcic horizons are useful age indicators for these deposits (table 1). The youngest alluvial-fan deposits have stage I carbonate morphology (Gile and others, 1966), which forms thin coatings on the bottoms of clasts. These coatings are found to depths of greater than 3.5 m. The older alluvial-fan deposits are distinguished from the youngest ones by the presence of soil K horizons that range in thickness from 0.3 m to as much as 2.5 m in the oldest deposits. K horizons less than 1 m thick have stage III carbonate morphology, and those greater than 1 m thick commonly have stage IV carbonate morphology in the upper part and stage III carbonate morphology in the lower part. Thick K horizons with stage IV carbonate morphology in the upper part are resistant to erosion and locally form resistant ledges at the top of the oldest alluvial-fan deposits.

The alluvial-fan deposits on the piedmonts were subdivided into six map units chiefly on the basis of their geomorphic position, topographic expression, and extent of calcic horizon development (table 2). The six units, from oldest to youngest, are: fan alluvium of Antelope Canyon (Tfa), fan alluvium of Chief Mountain (QTfc), fan alluvium of Oxborrow Ranch (Qfo), fan alluvium of Miller Spring Wash (Qfms), fan alluvium of 1001 Ranch (Qfr), and fan alluvium of Meadow Valley (Qfm) (Rowley and Shroba, 1991; Rowley and others, 1991). These alluvial-fan deposits are of Pliocene to Holocene age and underlie five well-expressed geomorphic surfaces that range in elevation from 5 m or less above stream level to as much as 120 m above stream level near the lower part of Antelope Canyon. These deposits are interpreted to postdate the development of a through-flowing drainage in the Panaca basin via Meadow Valley Wash (Rowley and others, 1992). The oldest alluvial-fan deposits (unit Tfa) are of Pliocene age. They are eroded,

Table 1. Stages of calcium carbonate morphology observed in calcic soils developed in noncalcareous surficial deposits under arid and semiarid climates of the southwestern United States

[Modified from Gile and others (1966, table 1) and Machette (1985, table 1)]

Stage	Diagnostic morphologic characteristics	Calcium carbonate distribution
I	Thin, discontinuous coatings on clasts, usually on undersides.	Coatings sparse to common.
II	Continuous, thin to thick coatings on tops and undersides of clasts.	Coatings common, some calcium carbonate in matrix, but matrix still loose.
III	Massive accumulations between clasts, becomes cemented in advanced form.	Essentially continuously dispersed in matrix (K fabric).
IV	Thin (<0.2 cm) to moderately thick (1 cm) laminae in upper part of K horizon. Thin laminae may drape over fractured surfaces.	Cemented platy to weak tabular structure and indurated laminae.
V	Thick laminae (>1 cm) and thin to thick pisolites. Vertical faces and fractures are coated with laminated carbonate (case-hardened surface).	Indurated dense, strong platy to tabular structure.
VI	Multiple generations of laminae, breccia, and pisolites; recemented. Many case-hardened surfaces.	Indurated and dense, thick strong tabular structure.

Table 2. Characteristics used in distinguishing alluvial-fan deposits in Chief Mountain area.

Map unit and symbol	Topographic expression		Calcic horizon development		Pavement development
	Preservation of depositional features	Erosional modification of depositional features	Thickness of conspicuous carbonate[1] (m)	Typical maximum stage of carbonate morphology[2]	
Fan alluvium of Meadow Valley (Qfm).	Depositional surfaces are preserved; little or no modification of bar-and-swale topography.	Commonly incised by narrow, shallow, steep-sided main washes; little or no surface drainage development.	0	I	None.
Fan alluvium of 1001 Ranch (Qfr).	Depositional surfaces are preserved; little or no preservation of bar-and-swale topography.	Commonly incised by narrow, shallow, steep-sided main washes; minor surface drainage development characterized by a few shallow washes.	0.3	III	No data.
Fan alluvium of Miller Spring Wash (Qfms).	Depositional surfaces are mostly preserved in areas between major washes.	Commonly incised by steep-sided major washes that are as much as 20 m deep; moderate surface drainage development characterized by numerous minor washes on broad interfluves.	0.8	III	Smooth, relatively continuous.
Fan alluvium of Oxborrow Ranch (Qfo).	Depositional surfaces are mostly to locally preserved in areas between major washes.	Commonly incised by wide major washes as much as 30 m deep; moderate surface drainage development characterized by numerous minor washes on broad interfluves and a few minor washes on narrow interfluves.	1.7	IV	Smooth, relatively continuous; numerous calcrete fragments on ground surface.

Map unit and symbol	Topographic expression: Preservation of depositional features	Topographic expression: Erosional modification of depositional features	Calcic horizon development: Thickness of conspicuous carbonate[1] (m)	Calcic horizon development: Typical maximum stage of carbonate morphology[2]	Pavement development
Fan alluvium of Chief Mountain (QTfc).	Depositional surfaces are locally preserved on narrow interfluves.	Commonly incised by wide major washes as much as 60 m deep; well-developed surface drainage characterized by numerous deep washes that have rounded side slopes.	2.5	IV	Do.
Fan alluvium of Antelope Canyon (Tfa).	Depositional surfaces are not preserved.	Commonly incised by numerous major washes as much as 70 m deep; well developed surface drainage characterized by numerous deep washes and by sharp to narrow rounded ridges.	([3])	IV	No data.

[1]Thickness values are for soil K horizons that have stage III and IV carbonate morphology. Values for fan alluvium of Oxborrow Ranch and fan alluvium of Chief Mountain are minimum values because the upper part of the K horizon in these units is eroded.

[2]Stages of carbonate morphology are those of Gile and others (1966). See table 1.

[3]The soil that is formed in fan alluvium of Antelope Canyon is poorly exposed and has an eroded K horizon of unknown thickness.

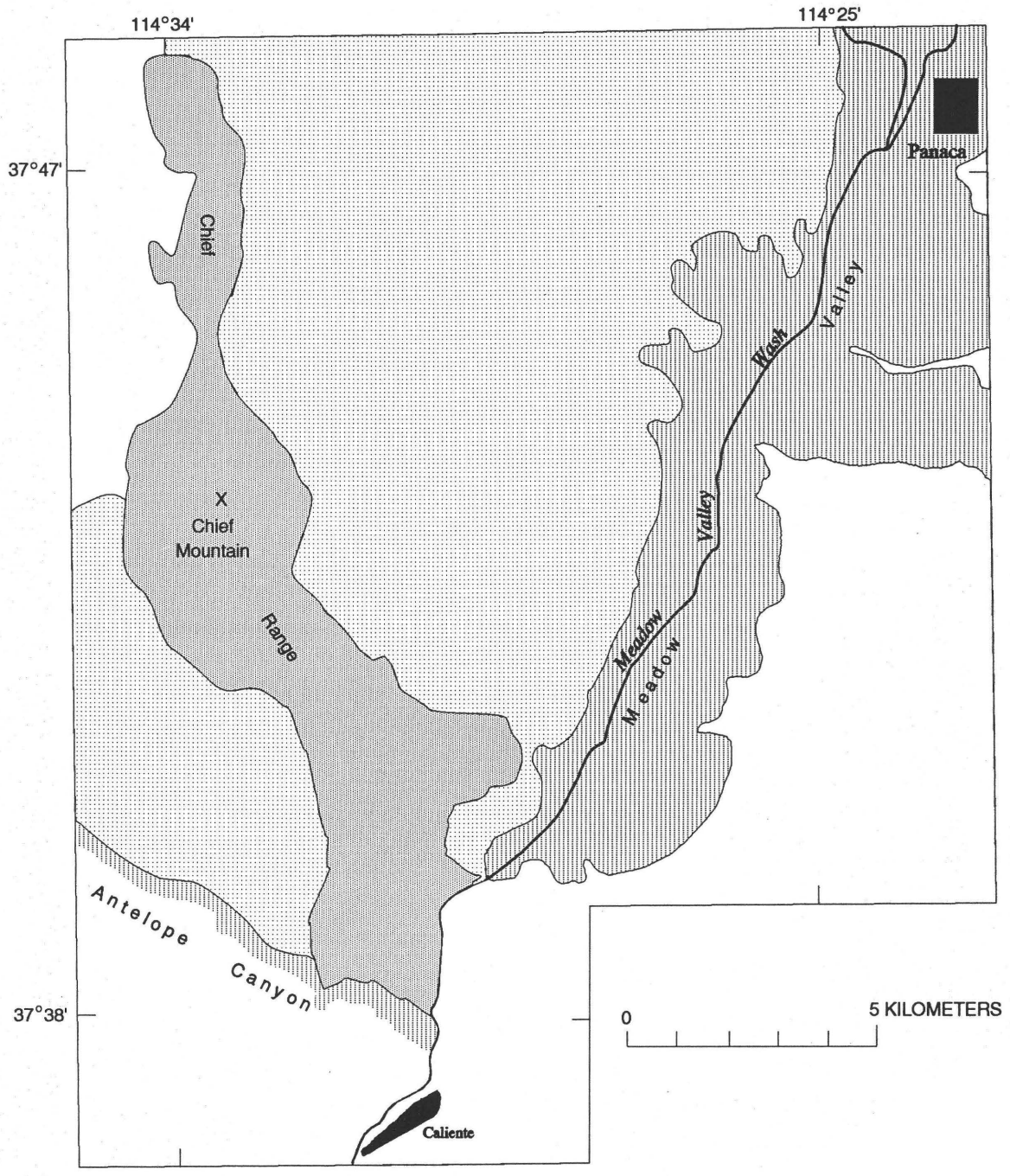

Figure 2. Sketch map of Chief Mountain area. Light dot pattern, distribution of alluvial piedmonts. Shade, distribution of bedrock in the Chief Range and adjacent area. Vertical pattern, distribution of alluvial surficial deposits in Meadow Valley and Antelope Canyon. Unpatterned area, distribution of undifferentiated surficial deposits and bedrock.

lack original depositional topography, and overlie an eroded surface cut on the Panaca Formation of late Miocene and Pliocene age (Rowley and Shroba, 1991; Rowley and others, 1991). They are locally overlain by younger alluvial-fan deposits and are most extensive along the mountain front and in and near Antelope Canyon where they make up the upper part (possibly 300 m or more) of a thick sequence of basin-fill deposits (Rowley and Shroba, 1991; Rowley and others, 1991). The younger alluvial-fan deposits (units QTfc through Qfm) are of Pliocene(?) and Quaternary age (Rowley and Shroba, 1991; Rowley and others, 1991). These deposits retain some or all of their original depositional topography, are commonly 2–20 m thick, and underlie geomorphic surfaces that are inset into geomorphic surfaces that are underlain by older alluvial-fan deposits. The younger alluvial-fan deposits overlie surfaces that are cut on

the oldest alluvial-fan deposits (unit Tfa) or on the Panaca Formation. The youngest alluvial-fan deposits (units Qfr and Qfm) form small fans that are 0.2 km^2 or less in area and commonly are graded to surfaces that are 5 m or less above the modern washes.

Meadow Valley and Antelope Canyon are major valleys that border the piedmonts of the Chief Mountain area. These valleys are underlain by stream alluvium and locally by minor deposits of hillslope colluvium and fan alluvium. Most of the alluvium in Meadow Valley is flood-plain alluvium; a minor amount of fan and low-terrace alluvium occurs near the mouths of intermittent streams tributary to Meadow Valley Wash. On the west side of the valley, a volcanic-rich, high terrace gravel (unit QTam of Rowley and Shroba, 1991) is present at one or more levels above Meadow Valley Wash. The flood-plain alluvium is a silty aggradational sequence composed mostly of fine-grained sediment eroded from the Panaca Formation, which is exposed along washes that flow into Meadow Valley. The alluvium is at least 7 m thick (Rowley and Shroba, 1991), and driller's logs of water wells in Meadow Valley suggest that the silty alluvium may be about 10–40 m thick (Rush, 1964). The alluvium that underlies the flood plain and low terraces in Antelope Canyon is derived mostly from quartzite and volcanic rocks and is much coarser than the flood-plain alluvium in Meadow Valley. The alluvium in Antelope Canyon may be as much as 15 m thick and is composed mostly of thin- to medium-bedded, clast-supported, cobbly pebble gravel, pebble gravel, and matrix-supported pebbly sand (Rowley and others, 1991). Minor terrace deposits in Antelope Canyon are not discussed in this report.

DELAMAR MOUNTAINS AREA

The Delamar Mountains are near the east edge of the Great Basin in southeastern Nevada (fig. 1), an area drained chiefly by tributaries of the Colorado River. This region is characterized by short, northerly trending mountain ranges separated by intermontane valleys, some of which have internal drainage. The mountains are commonly bounded by linear range-front faults.

The bedrock that is the major source of alluvial deposits in the Delamar Mountains area consists chiefly of Paleozoic marine limestone, dolomite, and quartzite overlain unconformably by Tertiary rhyolitic ash-flow tuff, minor rhyolitic lava, basaltic lava, and sparse shallow silicic to intermediate intrusive rocks. The Paleozoic sedimentary rocks weather to coarse gravel; the Tertiary volcanic rocks locally weather to gravel, but many of them commonly weather to sand-sized detritus.

The climate of the area is arid. The average rainfall is less than 20 cm per year. In the valley of Pahranagat Wash the mean annual temperature is 15 °C. At Caliente, Nev., 25 km east of Dry Lake Valley, annual temperature averages 12 °C (Houghton and others, 1975). The altitude of the alluvial deposits ranges from about 850 m at the south end of the Delamar Range to about 1,750 m in the northern part of Dry Lake Valley (fig. 3).

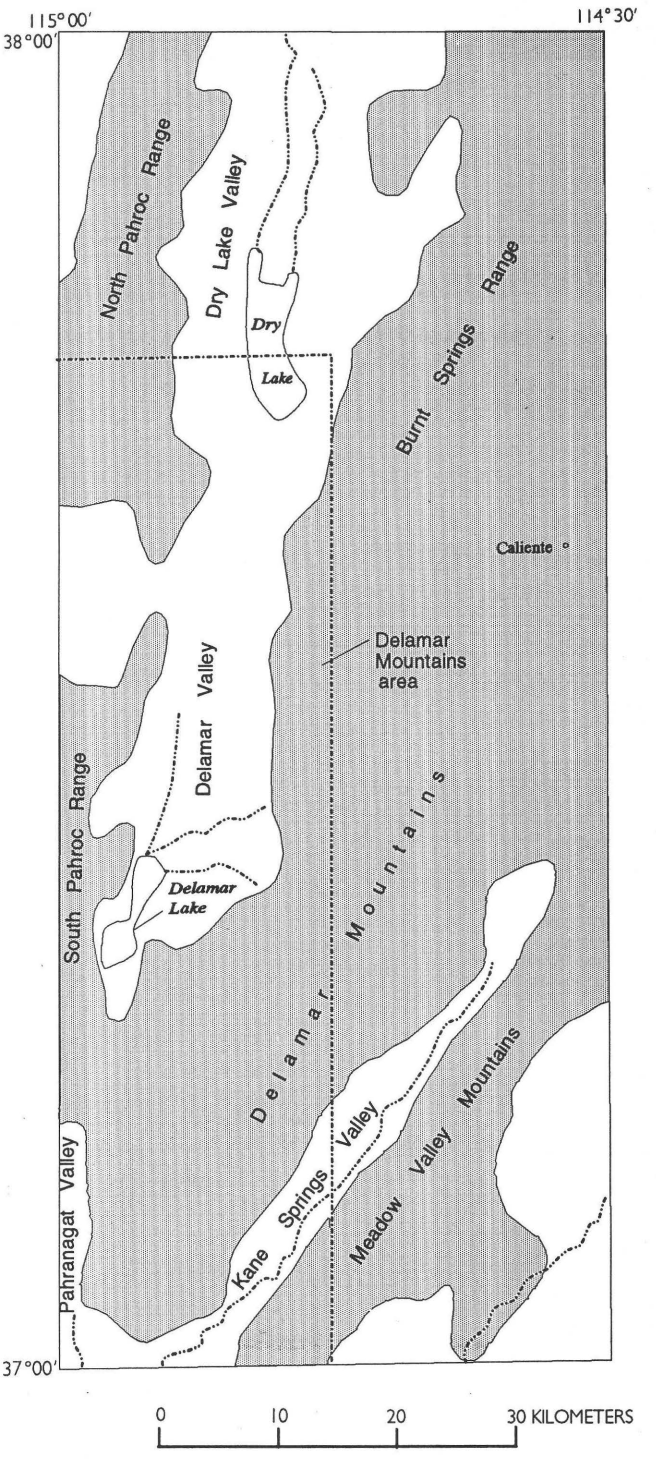

Figure 3. Sketch map of Delamar Mountains area and vicinity. Unpatterned areas within Delamar Mountains area show the major areas of mapped alluvium.

Quaternary alluvial-fan deposits of the Delamar Mountains area have been mapped and described over an area of about 2,100 km^2. The principal mapped areas are along the Pahranagat, Kane Springs, Delamar, and Dry Lake Valleys (fig. 3). Pahranagat Wash is a south-flowing intermittent stream on the southwest flank of the Delamar Mountains. At the south end of the Delamar Mountains, Pahranagat Wash is joined by the southwest-flowing intermittent Kane Springs Wash. Delamar Valley and Dry Lake Valley are contiguous elongate, north-trending closed basins along the northwest side of the Delamar Mountains and along their northward extension, the Burnt Springs Range.

The alluvial fans of the area were deposited by small intermittent streams 5–10 km long that flow into the main valleys approximately perpendicular to the range fronts. In the upper and middle parts of the piedmonts, successively younger fans typically are inset into one or more older fans. Locally, younger fans overlie older fans in the middle parts of the piedmonts. On the lower piedmont slopes in closed basins, older fan deposits are buried by successively younger deposits toward the center of the basins.

The fans are commonly 1–3 km wide and have coalesced into continuous fan aprons. The aprons vary in width from 1 to 3 km along the valleys of Pahranagat and Kane Springs Washes and the aprons on both sides of the valleys have similar topographic expression. The fan aprons in the Delamar and Dry Lake Valleys are typically 2–6 km wide. The aprons on the east side of these valleys commonly are more deeply dissected, and younger fans are more deeply inset into older fans than those on the west side. Minor terrace deposits of limited extent along Kane Springs and Pahranagat Washes are not described in this report.

The alluvial fans consist of interbedded gravel, gravelly sand, and sand. The relative amounts of each of these components and the proportion of the various lithologies of gravel clasts vary from fan to fan and reflect the bedrock composition within the drainage basin of the depositing wash. Deposits are typically poorly sorted and poorly to moderately well bedded. Clasts in the deposits are commonly angular to subrounded.

Soils developed in the alluvial fans are typical of arid-climate soils. The horizon of secondary calcium carbonate enrichment is the most conspicuous feature and is a useful age indicator for all but the youngest soils. The amount of carbonate enrichment varies from no visible carbonate accumulation in the youngest soils to a 2-m-thick carbonate-cemented horizon that locally forms a resistant ledge in exposures of the oldest Quaternary deposits.

Pliocene(?) and Quaternary alluvial-fan deposits of the area have been divided into six map units based largely on topographic sequence, soil development, preservation of depositional features, and amount of surface dissection within each map unit. This sequence of fan deposits is estimated to range in age from late Pliocene(?) to late Holocene. Although age designations are included in the informal names of some of the map units (QTa, Qae, and Qal), these age designations are preliminary and are based chiefly on the amount of carbonate enrichment in the soil developed in each unit. The six map units, in order of decreasing age, are: Quaternary and Tertiary alluvium (QTa); alluvium of Coyote Spring Valley (Qac), of Willow Spring (Qaw), and of Jumbo Wash (Qaj); late Pleistocene and early Holocene alluvium (Qae); and late Holocene alluvium (Qal). The mapping criteria for each of the map units are shown in table 3.

No ages have been determined for these deposits using isotopic dating. Samples of an ash bed exposed at one locality at the base of unit Qaw and of an ash bed in fluvial deposits that are locally overlain by fan units Qaw and Qac have been submitted for possible age determinations by chemical correlation methods. Preliminary results are inconclusive. The age of unit Qae is somewhat constrained in Dry Lake Valley by its field relations with lacustrine deposits of a latest Pleistocene pluvial lake (Mifflin and Wheat, 1979). Here, lacustrine beach deposits locally overlie unit Qae, and wave-cut scarps related to the beach deposits locally cut unit Qae, indicating that Qae is in part as old as latest Pleistocene. Other deposits of unit Qae that extend into the area formerly occupied by the lake seem not to have been eroded, suggesting that the deposition of Qae continued after the lake disappeared and, therefore, that part of the unit may be as young as early Holocene.

MOAPA VALLEY AREA

The verdant Muddy River flood plain of the Moapa Valley (fig. 4) is set in a stark, barren landscape exhibiting spectacular terraces that were produced and preserved in a generally arid climate (Gardner, 1972a). The arid climate has favored the development of thick, resistant carbonate-rich soils that protect the old terrace surfaces from erosion. These surfaces have steep scarps from tens of meters to more than 200 m high (fig. 5; Gardner, 1972b). The high, old terraces, including the Mormon Mesa terrace about 200 m above the Muddy River, are of late Tertiary age and are the products of erosional isolation caused by deep dissection since the Colorado River was integrated through the region about 5 m.y. ago (Longwell, 1928; Damon and others, 1978). Four conspicuous terraces at lower levels are the products of pluvial-arid climatic cycles of Quaternary age and are discussed herein.

The main streams of the Moapa Valley area are Pahranagat Wash and Meadow Valley Wash (fig. 4), which slope from about 750 m altitude in the north and west parts of the area to 335 m in the south at the confluence of the Muddy River with the Virgin River; Pahranagat Wash becomes the Muddy River at Muddy River Springs. Wide piedmont slopes rise above these main streams to an altitude of about 760 m at the surrounding range fronts. The Muddy

Table 3. Characteristics for distinguishing alluvial-fan deposits in Delamar Mountains area.

Map unit and symbol	Topographic expression		Calcic horizon development		Pavement development
	Preservation of depositional features	Erosional modification of depositional features	Thickness of conspicuous carbonate (m)	Typical maximum stage of carbonate[1]	
Late Holocene alluvium (Qal).	Depositional surface intact; bar-and-swale topography commonly preserved.	None	None	None	None.
Early Holocene and late Pleistocene alluvium (Qae).	Depositional surface intact; local preservation of subdued bar-and-swale topography.	Minor local dissection.	0.4-0.7	I	None.
Alluvium of Jumbo Wash (Qaj).	Depositional surface mostly intact; soil commonly preserved on interfluves.	Minor dissection.	1	II	Loosely packed pavement locally developed.
Alluvium of Willow Spring (Qaw).	Depositional surface mostly intact; soil locally to commonly stripped to upper part of K horizon on interfluves.	Moderate dissection by v-shaped washes; flat interfluves.	1-1.5	III	Moderately to tightly packed pavement common; pedogenic carbonate chips common in surface layer.
Alluvium of Coyote Spring Valley (Qac).	Depositional surface moderately preserved; soil on interfluves commonly stripped to upper part of K horizon.	Moderate dissection by washes with rounded edges.	1-2	III	Tightly packed pavement common; pedogenic carbonate chips common in surface layer.
Quaternary and Tertiary alluvium (QTa).	Depositional surface completely eroded.	Extensive dissection; rounded interfluves.	1-2	III	Tightly packed pavement on some rounded interfluves.

[1]Stages follow standards defined by Gile and others (1966). See table 1.

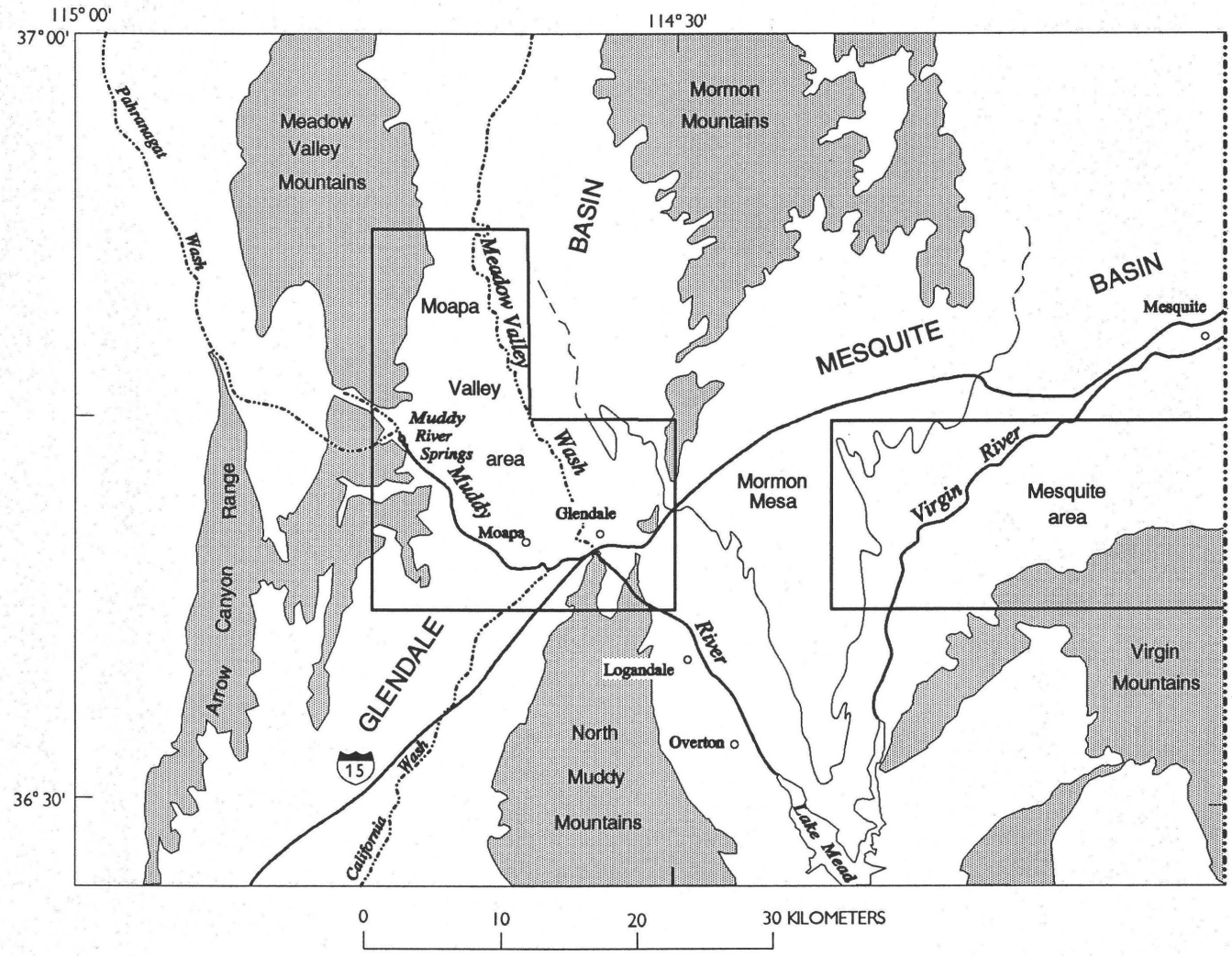

Figure 4. Sketch map of Moapa Valley and Mesquite areas.

River drains to the Colorado River via the Virgin River in the lower Virgin Valley (now the Overton Arm of Lake Mead).

The climate of the area is arid. At Logandale on the lower Muddy River, the average annual rainfall is 10 cm and the average annual temperature is 18 °C; the average summer temperature is 29 °C, the average winter temperature is 8 °C, and the daily winter temperature seldom falls below freezing (Bagley, 1980; records for 1968–75).

The Moapa Valley area is situated in the extensionally deformed Basin and Range province and includes parts of two basins and five ranges. The upper Moapa Valley is centered in the Glendale basin (lower Meadow Valley Wash–California Wash), which is bounded by the Arrow Canyon Range (1,555 m maximum altitude) and Meadow Valley Mountains (1,738 m maximum altitude) on the west and the Mormon Mountains (2,260 m maximum altitude) on the east. The lower Moapa Valley occupies the southwestern part of the large Mesquite basin, which is bounded by the Muddy Mountains (1,006 m maximum altitude) on the west and the Virgin Mountains (2,356 m maximum altitude) on the east. The five ranges consist mostly of Paleozoic carbonate rocks, with the exception that the Virgin Mountains contain about 50 percent Precambrian crystalline rocks and the Muddy Mountains contain abundant Mesozoic clastic and carbonate rocks. The two basins are separated by a narrow ridge composed of Paleozoic and Mesozoic rocks.

The Glendale and Mesquite basins contain thick, synextensionally deformed, basin-fill deposits (equivalent to Horse Spring Formation, less than 20 m.y. to about 11.5 m.y. old; Bohannon, 1984) overlain by a thick fill of postextensional, only slightly deformed sediments of the Muddy Creek Formation (about 11.5 m.y. to 5.5 m.y. old; Bohannon, 1984). Since deposition of the Muddy Creek Formation, the two basins have been open basins with exterior drainage to the Colorado River, in contrast to closed basins of the Great Basin that have interior drainage.

The water table along the Muddy River and Meadow Valley Wash is at channel level and, being so shallow, has

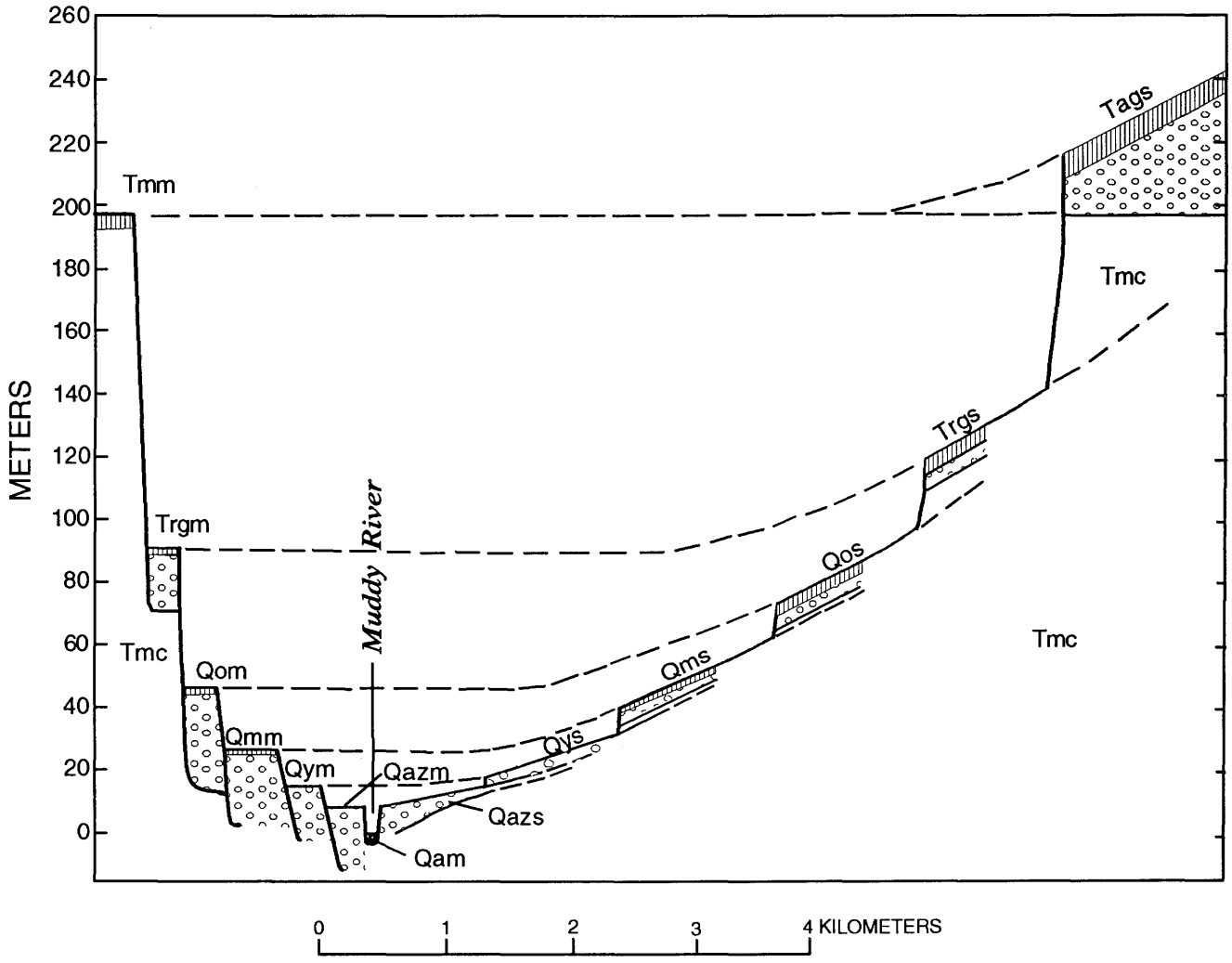

Figure 5. Idealized composite cross section showing Quaternary and late Tertiary terraces of the Moapa Valley area. Vertical scale greatly exaggerated. Dashed lines across valley connect mainstream terraces on left to side-stream terraces on right. Terrace and alluvium symbols as on table 4: Qo, alluvium of old terrace; Qm, alluvium of middle terrace; Qy, alluvium of young terrace; Qaz, silty alluvium of lowest terrace; Qa, modern channel and flood-plain alluvium; added m (as, Qmm), mainstream deposit; added s (as, Qms), side-stream deposit. Tmc, lacustrine deposits of the Muddy Creek Formation; Tmm, Mormon Mesa soil developed on Muddy Creek Formation; Tag, aggradational gravel deposit graded to top of Muddy Creek Formation; and Trg, regraded gravel deposit, representing initial grading to entrenched Colorado River.

strongly influenced mainstream deposition during the Quaternary. The shallow ground water along the Muddy River is largely supplied by discharge of the voluminous, deep, regional ground-water system at Muddy River Springs at the head of the Muddy River (Eakin, 1964). This regional system is recharged in the high, carbonate-rock ranges some 200 km farther north near Ely, Nev.

The regional ground-water system has existed since the beginning of extensional deformation less than 20 m.y. ago, and subsequently a large component of its flow (about 37,000 acre-feet per year) has been through the Paleozoic carbonate rocks of the northern Arrow Canyon Range and southern Meadow Valley Mountains. The ground water is saturated in bicarbonate ions, some of which are precipitated as limestone (travertine) on discharge, a process which over time has greatly added to the carbonate content of the upper Tertiary sediments. Carbonate materials, transported by stream, rain, and wind, have been abundantly available for carbonate soil development. This carbonate availability is a consequence of (1) long-term carbonate discharge from springs, (2) abundant carbonate detrital rocks from the surrounding bedrock ranges, and (3) abundant carbonate reworked from the basin fill.

The Quaternary mainstream alluvial deposits of the Muddy River and lower Meadow Valley Wash are unusual in the arid part of the Basin and Range province because they were deposited under conditions of a shallow ground-water table and exterior drainage. These two factors mean that the

main-stream depositional regime was especially sensitive to climatic fluctuations during the Pleistocene, that is, fluctuations between pluvial (moist) and arid (dry) episodes. In contrast, the adjacent side streams on the long piedmont slopes had deep ground-water tables, making the effects of Pleistocene climatic fluctuations much less dramatic. As a suggested general rule for these integrated basins: pluvial mainstream aggradation equates to side-stream pedimentation whereas arid main-stream entrenchment equates to side-stream entrenchment.

During the pluvial episodes of the Pleistocene, the Muddy River and lower Meadow Valley Wash flowed through perennially wet flood plains and aggraded as fine detritus accumulated on lushly vegetated flood plains (Quade, 1986). Aggradation was probably enhanced by a more uniform annual distribution of rainfall during a pluvial part of the climatic cycle as compared to an uneven seasonal distribution of rainfall and localized flash flooding during an interpluvial (arid) part of the climatic cycle.

On broad piedmonts, the side streams did not aggrade in the absence of a shallow water table during the pluvial episodes. In much of the Moapa Valley area where the shallow suballuvial bedrock is the easily erodible Muddy Creek Formation, the side streams mostly cut laterally (incipient pedimentation) during the pluvial episodes. However, on either side of the narrow axial mainstream valley, the piedmont side-stream alluvium thickens to form a narrow alluvial wedge against the mainstream aggradational deposit with which it intertongues. During the ensuing arid part of the climatic cycle, localized flash flooding strongly affected the piedmont, and the side streams entrenched into their pediments (Lustig, 1965).

Entrenchment of the mainstreams into their aggradational deposits and entrenchment of the side streams into their piedmont deposits during the interpluvial episode resulted in terrace remnants in both deposits that were isolated from vigorous fluvial action. Once isolated, carbonate-rich soils characteristic of the arid environment developed in these deposits. This isolation was particularly enhanced by deep entrenchment, a characteristic of tributary streams near the Colorado River. Deep entrenchment of the main streams, however, was also a function of the thickness of the pluvial aggradational deposit, which in turn was dependent in part on the length of the pluvial episode. Where the deposits were isolated long enough for thick carbonate-rich soils to develop on both the mainstream terraces and the piedmont pediments, the resistant soils greatly slowed the erosion of the underlying deposits.

In the Moapa Valley area, the recent valley floor of the Muddy River is underlain by a wide, aggradational silt deposit (Qaz, fig. 5) that has been sharply entrenched (from 3 to as much as 9 m) by the Muddy River. This silt deposit mostly accumulated during the latest Wisconsin pluvial aggradation and may have been mostly entrenched since about 1880 (Longwell, 1928). If the last pluvial episode ended about 10,000 yr ago, then the deposit has survived entrenchment, at least in many places, for about 10,000 yr during the current arid episode and probably would have survived much longer had man not upset the balance of nature. A narrow, youthful mainstream terrace deposit (unit Qym, fig. 5) is preserved about 7.5 m above the recent silt aggradational terrace (Qaz); it is probably a higher and older Wisconsin aggradational deposit.

Four alluvial terrace deposits of Quaternary age are recognized in the Moapa Valley area. These are designated by relative age as old, middle, young, and recent (Qo, Qm, Qy, and Qaz, respectively). The deposits of the active stream channels and low flood plains (Qa) were deposited during the arid part of the current climatic cycle. The terrace deposits are diagrammatically shown in figure 5, and some of the distinctive characteristics of their surfaces and soils are described in table 4.

MESQUITE AREA

The large, perennial Virgin River flows in a narrow, deeply entrenched valley across the Mesquite basin along the east edge of the Basin and Range province in southeastern Nevada (fig. 1). The Mesquite basin, about 28 km wide, lies between the Mormon Mountains (maximum altitude 2,260 m) to the northwest and the Virgin Mountains (maximum altitude 2,356 m) to the southeast and east (fig. 4). The Mormon Mountains are composed largely of Paleozoic carbonate rocks and minor Precambrian and Mesozoic rocks, whereas the Virgin Mountains are composed chiefly of Precambrian igneous and metamorphic rocks with lesser areas of Paleozoic carbonate rocks and Mesozoic clastic rocks in approximately equal amounts. Along the west side of the basin, Mormon Mesa, altitude about 560 m, is an erosional remnant of lacustrine and fluvial basin-fill deposits, the flattish top of which is underlain by an ancient, thick, resistant carbonate-rich soil (Gardner, 1972a). The Virgin River flows westward and southward from an altitude of about 550 m where it debouches from its gorge through the Virgin Mountains to about 335 m at its confluence with the Muddy River at the south end of Mormon Mesa. The piedmont plains rise steeply from the river to about 1,000 m altitude against the rugged Virgin and Mormon Mountains. Along the Virgin River at Littlefield, Ariz., near the east edge of the Mesquite basin (fig. 4), the mean annual temperature is 18 °C and the mean annual rainfall is 16 cm (U.S. Department of Commerce, 1975).

The Mesquite basin is a large tectonic basin that was extensionally deformed during late Tertiary time and filled with a thick sequence of basin-fill deposits. The exposed part of the basin fill is the postextensional Muddy Creek Formation, which consists of several hundreds to many hundreds of meters of mostly well bedded, moderately consolidated silt and sand that are probably largely fluvial (Kowallis and

Table 4. Characteristics for distinguishing alluvial deposits in Moapa Valley area.

Map unit and symbol	Topographic expression: Preservation of depositional features	Topographic expression: Erosional modification of depositional features	Calcic horizon development: Thickness of conspicuous carbonate (m)	Calcic horizon development: Typical maximum stage of carbonate[1]	Pavement development
Modern channel and flood-plain alluvium (Qa).	Active alluvial channel and flood plain, abandoned channelways conspicuous.	None----------	None	None	No pavement; depositional gravel, sand, and silt exposed.
Silty alluvium of lowest terrace (Qaz).	Depositional surface intact; bar-and-swale topography conspicuous.	Abrupt, narrow entrenchment by parent stream; surface not eroded.	None conspicuous.	None	No pavement; surface is silty; exposed gravel uncommon.
Alluvium of young terrace (Qy).	Depositional surface partly intact, some bar-and-swale relief preserved.	A few short, narrow gullies serrate terrace scarp; surface not eroded.	Thinly disseminated, powdery carbonate.	Stage I	Firm, light-brown-varnished cobble pavement overlying several centimeters loose cobbly silt; less than 1 mm carbonate undercoat on cobbles.
Alluvium of middle terrace (Qm).	Surface well preserved but depositional surface features not preserved.	Surface slightly eroded near shallowly incised washes of local, intraterrace origin; scarp edge in many places exposes a thin soil-calcrete rim.	2 m conspicuous carbonate includes 0.3 m calcrete upper part.	Stage III	Very firm, brown-varnished cobble pavement overlying about 5 cm of silt, as much as 1 cm carbonate undercoat on cobbles; terrace surface shows about 10 percent undercoat carbonate.
Alluvium of old terrace (Qo).	Slightly rolling surface, no depositional surface features preserved.	Surface decidedly eroded by broad, shallow washes of local origin; scarp edge mostly exposed as a thick soil-calcrete rim.	3.1 m conspicuous carbonate, includes 0.8 m calcrete upper part.	Stage IV to IV+	Very firm, darkly varnished, resistant cobble pavement overlying silt as thick as 15 cm; terrace surface is distinctly light colored showing about 40 percent carbonate soil fragments and cobble undercoating.

[1]Stages follow standards defined by Gile and others (1966). See table 1.

Everett, 1986). The Muddy Creek Formation is about 11.5 m.y. to 5.5 m.y. old. To the west and southwest the formation is composed mostly of lacustrine deposits. Muddy Creek lake was abruptly drained when the Colorado River was integrated through the present-day Lake Mead area.

The top of the Muddy Creek Formation and the adjacent piedmont slopes were deeply entrenched by newly established tributary drainages of the Virgin River system after the Muddy Creek lake was drained. The result of the entrenchment was the erosional isolation of large parts of the lake floor and adjacent piedmont slopes. A thick carbonate-rich soil developed during the Pliocene and Quaternary on these flat and gently sloping deposits; the cap rock on Mormon Mesa is a classic example of this ancient carbonate-rich soil.

By the beginning of Quaternary time the Colorado–Virgin River system had entrenched itself to its present depth. All the Quaternary terrace deposits along the perennial Virgin River are the result of cyclical aggradation and degradation caused mostly by climatic fluctuations. The aggradational silt and sand deposits were probably the products of pluvial episodes during the Quaternary (Quade, 1986). The piedmont side streams had base levels controlled by the Virgin River. These side streams deposited inset fan and inset channel gravels in response to climatic fluctuations.

The Quaternary and Tertiary alluvial deposits of the Mesquite area (fig. 4) are divided into four categories according to source of sediment and environment of deposition. For each category two to seven generations of deposits have been distinguished by the geomorphic and pedogenic criteria in table 5.

Mainstream deposits of the Virgin River are predominantly sand and gravel and include little silt or clay. The gravel consists of a mixture of subangular Precambrian, Paleozoic, and Mesozoic detritus from the adjacent ranges as well as distinctive well-rounded cobbles of chert and quartzite from the uplands of southwestern Utah. Flights of terraces indicate at least four prior intervals of deposition at levels about 6, 20, 55, and 85 m above the modern channel. The surface at 55 m tops a fill more than 55 m thick (units Qav, Qgv) and records a major period of aggradation during the early middle Pleistocene or early Pleistocene, probably during a major pluvial episode.

Alluvium from major tributaries on the north side of the river, such as Toquop Wash, is dominated by rocks eroded from the Mormon Mountains, and includes abundant limestone. Toquop Wash terraces record substantial lateral shifting of the channel and at least five prior intervals of deposition at about 6, 20, 35, 55, and 80 m above the modern channel. Toquop Wash terraces are all graded to corresponding Virgin River terraces except that the 35-m terrace is not preserved along the Virgin River.

Minor tributaries on the north side of the river deposited alluvium derived by erosion of the escarpment of Muddy Creek Formation exposed on the side of Mormon Mesa and by reworking of high terrace deposits of the Virgin River. Such tributaries deposited thin layers of sandy pediment alluvium that includes well-cemented angular boulders eroded from the carbonate-enriched soil on the surface of Mormon Mesa. The deposits cover a bench between the Mormon Mesa escarpment and the inset canyon of the Virgin River, and are graded to resistant ledges of cemented Virgin River terrace gravels 50 to 60 m above the modern Virgin River channel. Only two generations of such deposits have been distinguished.

Tributaries on the south and east side of the Virgin River have deposited coarse alluvium dominated by angular clasts of metamorphic and igneous Proterozoic rocks. These deposits form alluvial fans, thin alluvial mantles on pediment surfaces cut on older alluvium, and stream terraces inset into alluvial fans. At least six prior depositional intervals are recorded. The last five correspond approximately to terrace levels along the Virgin River and Toquop Wash, whereas the oldest depositional interval, represented by alluvium of Bunkerville Ridge (Tab), was probably contemporary with the upper part of the Muddy Creek Formation.

The oldest and most widespread piedmont deposit in the Mesquite area is the alluvium of Bunkerville Ridge (Tab) that underlies about two-thirds of the piedmont slope below the Virgin Mountains in the central part of the area (fig. 4). The alluvium consists of coarse poorly sorted bouldery gravel, sandy gravel, and gravelly sand eroded from the Virgin Mountains during late Tertiary time. The deposit is dissected 20–150 m deep by tributary streams of the Virgin River, and its surface, entirely erosional, has rounded bouldery interfluves. Remnants of a stage IV–V carbonate-rich soil 3–6 m thick underlie these eroded interfluves.

On the lower part of the piedmont slope, remnants of five Pleistocene fan deposits are deeply inset below the ridges of the alluvium of Bunkerville Ridge (Tab) and above the modern depositional surface (Qany). They overlie the easily eroded silt and sand of the Muddy Creek Formation. The fan deposits consist mostly of eroded detritus from the alluvium of Bunkerville Ridge. The oldest of the inset fan deposits (Qof) is preserved only as a few scattered ballenas. None of the original depositional surface is preserved. The next youngest (Qmf) has been reduced to ballenas in the western part of the area but retains a greater proportion of its original depositional surface toward the east (upstream). It is entrenched as much as 55 m and locally contains remnants of a stage IV carbonate-rich soil. The third youngest fan deposit, the alluvium of Nevada Highway 170 (Qah), consists mostly of sandy gravel and has a preserved depositional surface that overlies a stage II–III carbonate-rich soil capped by a tightly packed cobble and pebble pavement. Modern washes are entrenched 20–40 m below the depositional surface of this deposit. The second youngest deposit, the alluvial fan deposits of Meadowlands Farm (Qam), consists of sandy gravel and has a well-preserved depositional surface that overlies a stage II–III carbonate-rich soil capped by a firm cobble and

Table 5. Characteristics for distinguishing alluvial deposits in Mesquite area.

Map unit and symbol	Topographic expression		Calcic horizon development		Pavement development
	Preservation of depositional features	Erosional modification of depositional features	Thickness of conspicuous carbonate (m)	Typical maximum stage of carbonate[1]	
Channel sand of Virgin River (Qsv).	Depositional surface intact; bar-and-swale topography common.	None.	None.	None.	None.
Younger alluvium of Nickel Creek (Qany).	do	None.	None.	None.	None.
Floodplain deposits of Virgin River (Qfp).	Depositional surface intact; traces of abandoned channels remain.	Eroded by lateral migration of the river; entrenched 1-2 m.	None.	None.	None.
Older alluvium of Nickel Creek (Qano).	Depositional surface locally preserved in terrace remnants.	Eroded by migration of tributary streams; entrenched 0.3-1 m.	0.5	I	None.
Sandy terrace deposits of the Virgin River (Qtv).	Depositional surface preserved in small remnants commonly covered with thin eolian sand.	Most of deposit removed by river; entrenched 6 m.	0.3	I	None.
Young terrace alluvium of Virgin River (Qyv) and Toquop Wash (Qyt).	Depositional surface extensively preserved in terrace remnants commonly covered with thin eolian sand.	Entrenched about 20 m.	1	II	Moderately packed pavement where not covered by sand.
Alluvium of Meadowlands Farm (Qam).	About 40 % of depositional surface preserved.	Entrenched 30 m by steep-sided washes with sharp edges.	0.8-1.3	II	Moderately packed pavement.
Young sandy pediment and fan alluvium (Qsy).	Depositional surface mostly intact.	Moderately dissected. Generally entrenched 10 m, but 30 m at lower end.	0.5-1	II	None.
Younger middle terrace alluvium of Toquop Wash (Qymt).	Depositional surface preserved in small remnants along a former course of Toquop Wash.	Entrenched about 35 m by steep-sided washes with sharp edges.	1-2	III	Moderately packed pavement.
Alluvium of Nevada Highway 170 (Qah).	Depositional surface extensively preserved.	Moderately dissected by steep-sided washes with rounded edges.	0.5-1	II-III	Moderately to tightly packed pavement.
Older sandy pediment and fan alluvium (Qsh).	Depositional surface mostly eroded.	do	0.5-1.5	III	None.
Middle terrace alluvium of the Virgin River (Qav, Qgv) and Toquop Wash (Qmt).	do	Moderately dissected by steep-sided washes with rounded edges; entrenched 55 m.	1-2	III-IV	Tightly packed pavement locally developed on gravel-rich part.
Middle mountain fan alluvium (Qmf).	Small areas of the depositional surface are locally preserved.	do	1-1.5	III-IV	Moderate to tightly packed pavement.
Old terrace alluvium of Virgin River (Qov).	Depositional surface entirely eroded.	Extensively dissected; entrenched 85 m.	1-2	IV	Tightly packed pavement.
Old terrace alluvium of Toquop Wash (Qot).	Depositional surface extensively preserved as a terrace capping a mesa along a former course of Toquop Wash.	Moderately dissected; entrenched 85 m.	1-2	IV	Tightly packed pavement.
Old mountain fan alluvium (Qof).	Depositional surface entirely eroded.	Most of deposit removed; remnants are isolated ballenas.	1-2	III-IV	None.
Alluvium of Bunkerville Ridge (Tab).	Depositional surface entirely eroded.	Rounded interfluves; entrenched 60 m.	3-6	V	None.

[1]Stages follow standards defined by Gile and others (1966). See table 1.

pebble pavement. Modern washes are entrenched 20–30 m below the depositional surface of this deposit.

Holocene alluvium on the piedmont is restricted to narrow washes entrenched into the alluvium of Bunkerville Ridge (Tab) and Pleistocene alluvial deposits. The older alluvium of Nickel Creek (Qano) of late(?) Pleistocene to early Holocene age forms deposits about 1 m above the younger alluvium of Nickel Creek (Qany). The younger alluvial unit of late Holocene age constitutes the flood plains of the modern piedmont washes.

The narrowness (0.3 to 1 km wide) of the entrenched valley of the Virgin River demonstrates the dominance of alluviation by the high-gradient, piedmont, side-stream washes over valley-widening lateral erosion by the Virgin River. The Virgin River meanders across the full width of its valley floor, giving it the appearance of an overfit stream. Its channel deposit is the channel sand of the Virgin River (Qsv) that consists of fine to medium sand, silt, and gravel. About 2–4 m above the active river channel are flood-plain deposits of the Virgin River (Qfp) that consist of overbank deposits of sand and subordinate amounts of sandy gravel and gravel.

NEVADA TEST SITE AREA

The Nevada Test Site (NTS) is in the southern part of the Great Basin (fig. 1). Surficial deposits in part of the NTS area were mapped in 1978–87 as part of a study of a proposed repository for radioactive waste at Yucca Mountain in the western part of NTS. Recognition of surficial map units and their correlation within and among valleys in the area was based on correlation characteristics similar to those described in this report. These characteristics, which include topography, drainage, topographic relations, soils, desert pavement, and depositional environment, are described in detail by Hoover and others (1981). The relative ages, which were based on geomorphic data, were quantified by isotopic ages for some of the surficial units as discussed following.

The physiography and the stratigraphy of the surficial deposits in the NTS area are described by Hoover (1989). This information and the bedrock geology of the NTS area are briefly summarized as follows. Bedrock of the NTS area consists of Proterozoic and Paleozoic sedimentary rocks, chiefly marine limestone, dolomite, quartzite, and argillite, and Miocene and Pliocene volcanic rocks, chiefly rhyolitic ash-flow tuff and lava. These rocks are exposed in northward-trending, fault-block mountain ranges separated by alluvial valleys (Frizzell and Shulters, 1990).

Surficial deposits, chiefly alluvial fan deposits, were mapped in an area of approximately 2,400 km^2, principally in Crater Flat and Jackass Flats, west and east of Yucca Mountain, respectively, and in the northern part of the Amargosa Desert, south of Yucca Mountain (fig. 6). These areas are drained by southward-flowing intermittent washes that are tributary to the Amargosa River. The climate of the region is arid. Average annual precipitation is less than 18 cm and mean annual temperature is about 17 °C (Houghton

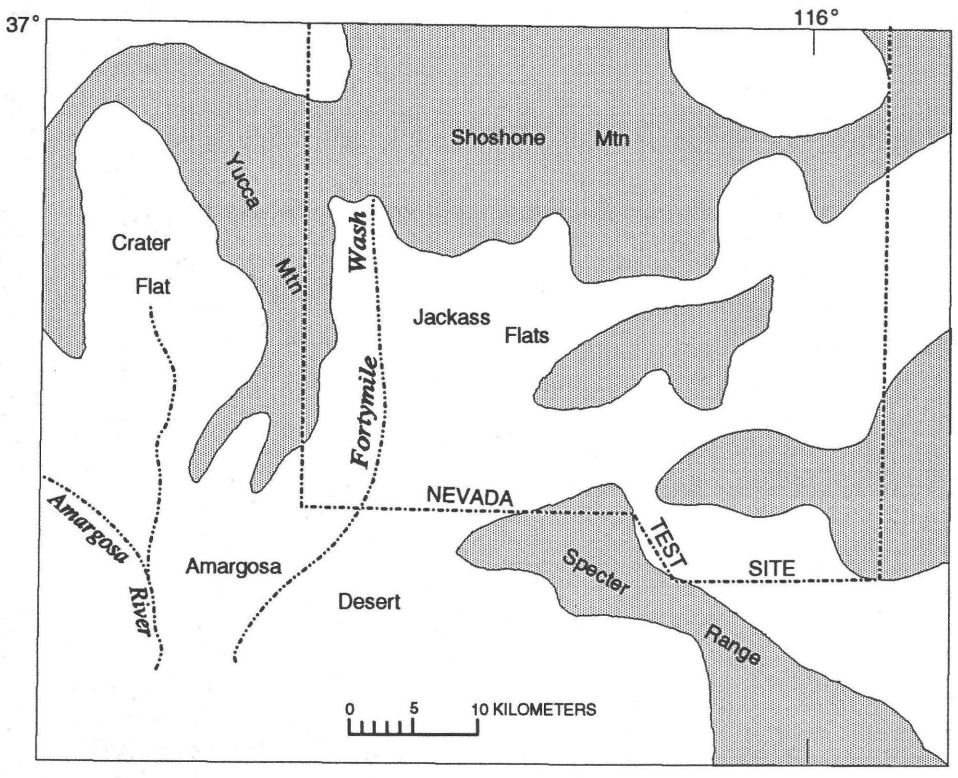

Figure 6. Sketch map of part of Nevada Test Site area showing major areas where surficial deposits were mapped. Pattern indicates bedrock areas.

and others, 1975). The altitude of the alluvial deposits ranges from about 1,200 m at the north end of Crater Flat to about 730 m along the Amargosa River near the south border of the area (fig. 6).

Alluvial deposits of the NTS area form almost continuous piedmont aprons along the mountain fronts. These aprons consist of coalescing fan and pediment remnants along with numerous inset fans and minor terrace and stream-channel deposits. Washes that head in bedrock are typically incised into the piedmont aprons, and successively younger deposits form inset fans or terraces at successively lower levels in these washes. Interfluves are generally smooth but commonly exhibit greater dissection of successively older fans by small washes that head within the piedmont. The fans consist of interbedded gravel and gravelly sand. The relative amounts of gravel and sand vary greatly among fans as does the composition of the gravel; both depend largely on the bedrock exposed in the drainage basin of the depositing wash.

These alluvial deposits have been divided into seven map units of Pliocene(?) and Quaternary age. Table 6 lists these units by map symbol in order of increasing age and shows the characteristics used to distinguish these units in the field.

Numerical ages have been determined for some of the surficial deposits of the NTS area. These ages were obtained using radiocarbon dating, fission-track dating, tephrochronologic identification, and the experimental uranium-trend method (Rosholt, 1980, 1985). The ages of the deposits range from about 8 to <2,100 ka as shown in table 7. The methods of age determination and the sample localities for each unit are discussed by Hoover (1989).

DISCUSSION

Similarities in some of the physical characteristics used to identify and map the alluvial deposits in the four study areas permit tentative correlation of these deposits (table 7). These correlations are also extended to similar deposits of known and inferred ages in the NTS area.

Several differences among the sequences of alluvial deposits of the four study areas are apparent. Unit Qfm in the Chief Mountain area probably includes deposits equivalent to the two youngest units that are identified and mapped in the other three areas. More detailed studies in the Chief Mountain area may identify criteria that will permit the subdivision of unit Qfm into two separate units. Late Pleistocene deposits that correlate with those mapped in the Moapa and Mesquite areas were not observed in the Chief Mountain and Delamar Mountains areas. In the areas where late Pleistocene deposits were mapped, they occur along permanent streams that have large drainage basins. Streams of this type do not occur in the Chief Mountain and Delamar Mountains areas.

The largest difference between the sequences of deposits in the four areas is the absence of deposits of early Quaternary age in the Moapa Valley area (table 7). In that area all the terrace deposits higher and older than the old Quaternary deposit (unit Qo) are of late Tertiary age, according to D.L. Schmidt. These late Tertiary alluvial deposits (estimated 3.5 to 5 m.y. old) have terrace surfaces that are well preserved by resistant stage V and VI carbonate soils. These thick soils developed because of long development time, low rainfall, and a large aerial carbonate flux in the Moapa Valley area.

Comparison of the alluvial deposits of the study area with those of the NTS area indicates two significant differences. The age of unit Qlc of the NTS area is reported as early Holocene. However, data from the Delamar Mountains area indicate the deposits here correlated with unit Qlc are late Pleistocene and early Holocene age. Unit Q2c (middle Pleistocene) of the NTS area includes two soils that yielded uranium-trend ages of about 270 and 440 ka (table 7). These ages suggest that unit Q2c includes deposits of at least two depositional episodes that could not be mapped separately because of similar topographic expression. The deposits of these two depositional episodes at NTS may correlate with the two oldest units of middle Pleistocene age in the Chief Mountain, Delamar Mountains, Moapa Valley, and Mesquite areas. In part of the Delamar area, the two units that probably correlate with unit Q2c (units Qaw and Qac) may locally be mapped as a single unit (Qaw) where the topographic separation between the two units is slight.

REFERENCES CITED

Bagley, D.G., 1980, Soil survey of Virgin River area, Nevada-Arizona—Parts of Clark and Lincoln Counties, Nevada and part of Mohave County, Arizona: U.S. Department of Agriculture, Soil Conservation Service, 149 p.

Bohannon, R.G., 1984, Nonmarine sedimentary rocks of Tertiary age in the Lake Mead region, southwestern Nevada and northwestern Arizona: U.S. Geological Survey Professional Paper 1259, 72 p.

Borup, H.J., and Bagley, D.G., 1976, Soil survey of Meadow Valley area, Nevada-Utah—Parts of Lincoln County, Nevada and Iron County, Utah: U.S. Department of Agriculture, Soil Conservation Service, 167 p.

Colman, S.M., Pierce, K.L., and Birkeland, P.W., 1987, Suggested terminology for Quaternary dating methods: Quaternary Research, v. 28, p. 314–319.

Damon, P.E., Shafiqullah, Muhammed, and Scarborough, R.B., 1978, Revised chronology for critical stages in the evolution of the lower Colorado River: Geological Society America Abstracts with Programs, v. 10, no. 3, p. 101.

Eakin, T.E., 1964, Ground-water appraisal of Coyote Spring and Kane Springs Valleys and Muddy River Springs area, Lincoln

Table 6. Characteristics for distinguishing alluvial-fan deposits in Nevada Test Site area.

[Modified from Hoover and others, 1981]

Map unit	Topographic expression		Calcic horizon development		Pavement development
	Preservation of depositional features	Erosional modification of depositional features	Thickness of conspicuous carbonate (m)	Typical maximum stage of carbonate[1]	
Q1a	Depositional surface intact; local bar-and-swale topography.	None----------	None	None	None.
Q1b	Depositional surface intact; bar-and-swale topography common.	None----------	0-<0.2	I	Do.
Q1c	Depositional surface intact.	Bar-and-swale topography largely obliterated by postdepositional smoothing.	<0.2	I	Weak pavement locally developed.
Q2a	Depositional surface intact.	Minor local dissection.	0.3	I	Loosely packed pavement.
Q2b	Depositional surface largely intact.	None to local minor dissection by steep-sided washes with sharp edges.	0.3	I-II	Loosely to moderately packed pavement.
Q2c	Depositional surface largely intact.	Moderate dissection by steep-sided washes with sharp edges.	1-1.5	III-IV	Moderately to tightly packed pavement common.
QTa	Depositional surface completely eroded.	Extensive dissection; rounded interfluves.	2-3	IV	Tightly packed pavement locally preserved on rounded interfluves.

[1]Stages follow standards defined by Gile and others (1966). See table 1.

Table 7. Correlation of alluvial deposits in five areas in southeastern Nevada and age control for deposits in NTS area.

[Refer to tables 2–5 for names of map units. Time subdivisions of the Pleistocene correspond to those of Richmond and Fullerton (1986). Time subdivisions of the Quaternary are informal. FR, field relations with radiocarbon dated deposits; FT, fission-track age of volcanic ash underlying QTa; no, not observed; RC, radiocarbon age of charcoal; T, tephrochronologic identification of Bishop ash in deposits that intertongue with Q2c; UT, uranium-trend age. Query indicates age boundary uncertain]

Age			Chief Mountain area[1]	Delamar Mountains area	Moapa Valley area	Mesquite area	NTS area	Age control for deposits in NTS area: Age (ka)	Dating method	Source of data
QUATERNARY	Holocene	late	Qfm	Qal	Qa	Qany Qsv	Q1a	<1	FR	Hoover, 1989.
						Qfp	Q1b	>1	FR	Do.
		early		Qae	? Qaz	Qano	Q1c	>5	FR	Do.
								8	RC	Do.
		late	no	no	Qy	Qtv	Q2a	40±15	UT	Rosholt and others, 1985.
	Pleistocene	middle	Qfr	Qaj		Qyv Qyt Qam Qsy	Q2b	170±40	UT	Do.
			Qfms	Qaw	Qm	Qymt Qah Qsh	Q2c	270±50	UT	Do.
								440±60	UT	Do.
			Qfo	Qac	Qo	Qav Qgv Qmt Qmf		738	T	Hoover, 1989.
TERTIARY	Pliocene	early	QTfc	QTa	no	Qov Qot Qof	QTa	<2100	FT	Do.
			--?--	--?--	Trg	Tab	--?--			
			Tfa	Ta	Tag					

[1]Age assignments for units Qfr, Qfo, and QTfc reflect current interpretation and differ from those in Rowley and Shroba (1991).

and Clark counties, Nevada: Nevada Department of Conservation and Natural Resources, Ground-Water Resources—Reconnaissance Report 25, 40 p.

Frizzell, V.A., Jr., and Shulters, Jacqueline, 1990, Geologic map of the Nevada Test Site, southern Nevada: U.S. Geological Survey Miscellaneous Investigations Series Map I–2046, scale 1:100,000.

Gardner, L.R., 1972a, Pediments and terraces along the Moapa Valley, Clark County, Nevada: Geological Society of America Bulletin, v. 83, p. 3479–3486.

———1972b, Origin of the Mormon Mesa caliche, Clark County, Nevada: Geological Society of America Bulletin, v. 83, p. 142–156.

Gile, L.H., Peterson, F.F., and Grossman, R.B., 1966, Morphological and genetic sequences of carbonate accumulation in desert soils: Soil Science, v. 101, p. 347–360.

Hoover, D.L., 1989, Preliminary description of Quaternary and late Pleistocene surficial deposits at Yucca Mountain and vicinity, Nye County, Nevada: U.S. Geological Survey Open-File Report 89–359, 45 p.

Hoover, D.L., Swadley, W C, and Gordon, A.J., 1981, Correlation characteristics of surficial deposits with a description of surficial stratigraphy in the Nevada Test Site region: U.S. Geological Survey Open-File Report 81–512, 27 p.

Houghton, J.C., Sakamoto, C.M., and Gifford, R.O., 1975, Nevada's weather and climate: Nevada Bureau of Mines and Geology Special Publication 2, 78 p.

Kowallis, B.J., and Everett, B.H., 1986, Sedimentary environments of the Muddy Creek Formation near Mesquite, Nevada, *in* Griffen, D.T., and Phillips, W.R., eds., Thrusting and extensional structures and mineralization in the Beaver Dam Mountains, southwestern Utah: Utah Geological Association Publication 15, p. 69–75.

Longwell, C.R., 1928, Geology of the Muddy Mountains, Nevada: U.S. Geological Survey Bulletin 798, 152 p.

Lustig, L.K., 1965, Clastic sedimentation in Deep Springs Valley, California: U.S. Geological Survey Professional Paper 352–F, p. F131–F192.

Machette, M.N., 1985, Calcic soils of the southwestern United States, *in* Weide, D.L., ed., Soils and Quaternary geomorphology of the southwestern United States: Geological Society of American Special Paper 203, p. 1–21.

Mifflin, M.D., and Wheat, M.M., 1979, Pluvial lakes and estimated pluvial climates of Nevada: Nevada Bureau of Mines and Geology Bulletin 94, 57 p.

Quade, Jay, 1986, Late Quaternary environmental changes in the upper Las Vegas Valley, Nevada: Quaternary Research, v. 26, p. 340–357.

Richmond, G.M., and Fullerton, D.S., 1986, Introduction to Quaternary glaciations in the United States of America, *in* Sibrava, V., Bowen, D.Q., and Richmond, G.M., eds., Quaternary glaciations in the northern hemisphere: Quaternary Science Reviews, v. 5, p. 3–10.

Rosholt, J.N., 1980, Uranium-trend dating of Quaternary sediments: U.S. Geological Survey Open-File Report 80–1087, 65 p.

———1985, Uranium-trend systematics for dating Quaternary sediments: U.S. Geological Survey Open-File Report 85–298, 34 p.

Rowley, P.D., and Shroba, R.R., 1991, Geologic map of the Indian Cove quadrangle, Lincoln County, Nevada: U.S. Geological Survey Geologic Quadrangle Map GQ–1701, scale 1:24,000.

Rowley, P.D., Shroba, R.R., Simonds, F.W., Burke, K.J., Axen, G.J., and Olmore, S.D., 1991, Geologic map of the Chief Mountain quadrangle, Lincoln County, Nevada: U.S. Geological Survey Open-File Report 91–135, scale 1:24,000.

Rowley, P.D., Snee, L.W., Mehnert, H.H., Anderson, R.E., Axen, G.J., Burke, K.J., Simonds, F.W., Shroba, R.R., and Olmore, S.D., 1992, Structural setting of the Chief mining district, eastern Chief Range, Lincoln County, Nevada, chapter H *in* Thorman, C.H., ed., Application of structural geology to mineral and energy resources of the central and western United States: U.S. Geological Survey Bulletin 2012, p. H1–H17.

Rush, F.E., 1964, Ground-water appraisal of the Meadow Valley area, Lincoln and Clark Counties, Nevada: State of Nevada Department of Conservation and Natural Resources, Ground-Water Resources–Reconnaissance Series Report 27, 43 p.

U.S. Department of Commerce, 1975, Climatological data annual summary, Nevada.

Low-Angle Normal Faults in Devonian Rocks of the Southern Delamar Mountains, Lincoln County, Nevada

By William R. Page

GEOLOGIC STUDIES IN THE BASIN AND RANGE–COLORADO PLATEAU TRANSITION IN SOUTHEASTERN NEVADA, SOUTHWESTERN UTAH, AND NORTHWESTERN ARIZONA, 1992

U.S. GEOLOGICAL SURVEY BULLETIN 2056–G

UNITED STATES GOVERNMENT PRINTING OFFICE, WASHINGTON : 1995

CONTENTS

FIGURES

Low-Angle Normal Faults in Devonian Rocks of the Southern Delamar Mountains, Lincoln County, Nevada

By William R. Page

ABSTRACT

A system of low-angle normal faults occurs in the Paleozoic rocks of a major west-dipping ramp above the Sevier-age Delamar thrust fault on the west flank of the southern Delamar Mountains, southeastern Nevada. The most prominent fault in the system is a west-dipping low-angle fault that places Middle and Upper Devonian Guilmette Formation and the uppermost member of the Middle Devonian Simonson Dolomite in the hanging wall above Lower Devonian Sevy Dolomite in the footwall, omitting parts of the Simonson and the Sevy Dolomites. The hanging wall of this fault contains west-vergent folds, high-angle normal faults, and bedding-plane faults.

The normal fault system also includes networks of ramping low-angle faults within the Guilmette Formation. These faults dip westward, occur at multiple stratigraphic levels, and are distinguished by local bedding discordances as great as 35°. The faults generally follow bedding planes, but locally ramp down section to the west.

The age of the normal faults is poorly constrained; however, map relations suggest that these normal faults predate Oligocene volcanic rocks (27 Ma). The faults are interpreted to have formed in Late Cretaceous or early Tertiary time by gravitational collapse off the west flank of the Delamar allochthon following ramping of the Sevier-age Delamar thrust fault. Restoration of the prominent low-angle fault in the system to postfault, pre-erosion geometry indicates that a minimum of about 1.7 kilometers of Paleozoic and Mesozoic rocks was eroded off the upthrown block of the fault prior to the emplacement of the volcanic rocks, which strongly suggests that faulting occurred either during or shortly following Sevier compression, rather than during regional, middle Tertiary prevolcanic extension.

INTRODUCTION

This report examines the geometry, timing, and tectonic implications of low-angle normal faults in Paleozoic rocks in the southern part of the Delamar Mountains, southeastern Nevada. The southern Delamar Mountains are located about 110 km north of Las Vegas, Nev. (fig. 1), in the eastern part of the Basin and Range province. The mountains are bounded by Coyote Spring Valley on the west, Kane Springs Valley on the southeast, and the Pahranagat shear system on the northwest. Topographic relief from the base of Coyote Spring Valley to the top of adjacent mountains in the range is approximately 1 km. Steeply dipping, folded Paleozoic rocks underlie a gentle irregular erosional surface below a veneer of gently dipping Tertiary volcanic rocks. The study area, shown in figure 2, has been mapped in detail as part of the Basin and Range to Colorado Plateau Transition (BARCO) Study Unit (see Introduction to this volume) (Page and others, 1990; Scott and others, 1990; and Swadley and others, 1990). The low-angle normal fault system is located on the west flank of the mountain range, near the southwest terminus of the Delamar Mountains.

The southern Delamar Mountains are within the Sevier orogenic belt that trends northeast from southeastern California, through southern Nevada, and into southwestern and central Utah (Armstrong, 1968; Fleck, 1970) (fig. 1). The belt consists of east- to southeast-directed decollement-style thrust faults that formed during the Cretaceous in southern Nevada. The Delamar thrust fault, the major structure in the southern Delamar Mountains, is one of these thrusts.

Numerous low-angle normal faults attenuate strata in the Sevier orogenic belt. Some of these low-angle normal faults are interpreted as middle Tertiary structures formed as a result of regional crustal extension. Examples near the study area include the Mormon Peak and Tule Springs detachments in the Mormon Mountains of southern Nevada (Axen and others, 1990; Wernicke and others, 1985), and the Stampede and Highland Peak detachments in east-central Nevada (Axen, 1986; Axen and others, 1988; Axen and others, 1993).

In contrast, some low-angle normal faults in the hinterland of the Sevier orogenic belt attenuate strata and were described as Cretaceous to early Tertiary extensional structures. Examples include faults in the Drum Mountains in

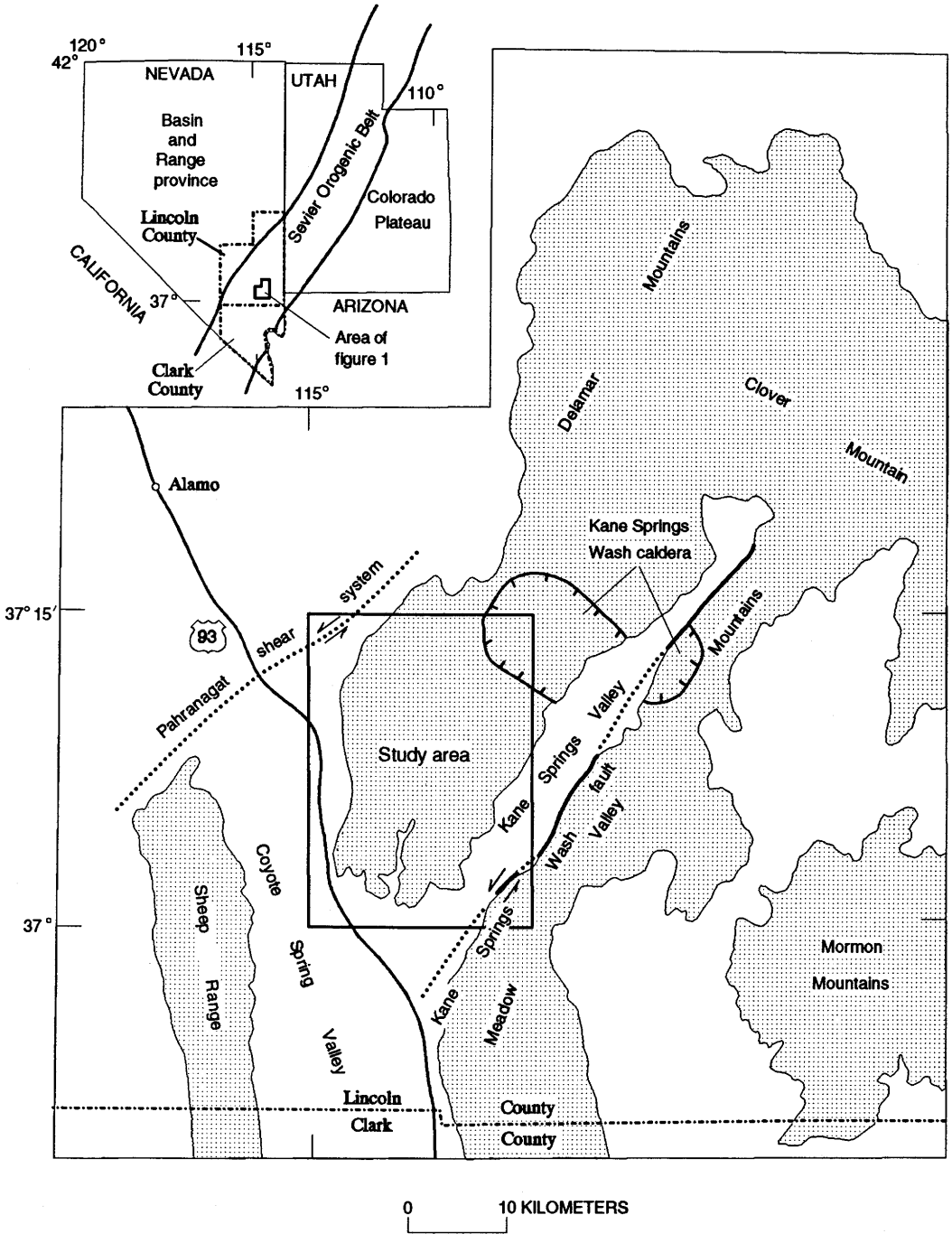

Figure 1. Index map showing location of study area, southeastern Nevada.

west-central Utah and the southwestern Deep Creek Range, western Utah and eastern Nevada (Nutt and Thorman, 1992; Nutt and others, 1992), and in the Raft River and Black Pine Mountains in northeastern Utah and southern Idaho (Wells and others, 1990).

Many questions arise concerning the age, origin, and tectonic implications of the low-angle normal faults in the southern Delamar Mountains. A prevolcanic age of these normal faults is inconsistent with Miocene and younger regional extensional structures observed in the Delamar Mountains. In this report, I address the possibility that these normal faults represent localized gravitational collapse of probable Late Cretaceous or early Tertiary age, either synchronous with or following regional compression and crustal thickening related to ramping of the Delamar allochthon.

GEOLOGIC SETTING

About 4.3 km of Cambrian through Lower Permian rocks are exposed in the southern Delamar Mountains (figs. 2, 3). These rocks comprise predominantly dolomite and limestone and subordinate sandstone and shale, deposited near the eastern margin of the Cordilleran miogeocline.

The Paleozoic rocks are overlain unconformably by as much as 450 m of gently dipping Tertiary volcanic rocks (figs. 2, 3) that are subdivided into two groups. The older group consists of late Oligocene to early Miocene ash-flow tuffs deposited from regional ash flows erupted from the Central Nevada caldera complex (Best and others, 1993), and the Caliente caldera complex (Rowley and others, this volume). These rocks range in age from about 27 Ma to 18.6 Ma. The younger group of rocks include the Kane Wash Tuff, erupted from the Kane Springs Wash caldera in the central Delamar Mountains (fig. 2) about 14.5 Ma (Scott and others, this volume), and two other units, the Delamar Lake and Sunflower Mountain Tuffs that erupted from undetermined sources and were dated at 15.6 Ma and 14.7 Ma, respectively, by Novak (1984).

The structural history of the southern Delamar Mountains records compression of the northeast-trending Sevier orogenic belt followed by middle Cenozoic to modern extension. During the Sevier orogeny in Cretaceous time, the Paleozoic rocks in the study area formed an allochthon that ramped eastward on the Delamar thrust fault. The hanging-wall block consists of lower Paleozoic rocks that form a ramp anticline, and the footwall block consists of upper Paleozoic rocks that form a tightly folded overturned syncline (fig. 2).

Following the Sevier orogeny and an erosional period of about 35–50 million years, extensional tectonics dominated southern Nevada. The onset of extension in this area remains poorly understood, but early phases of extension in the southern Basin and Range province are believed to have begun in latest Eocene or Oligocene time (Wernicke and others, 1987). Major regional extensional episodes occurred mostly during the Miocene in the Delamar Mountains (Scott, 1990) and to the south, in northern Clark County (Bohannon, 1984; Guth, 1981; Guth and others, 1988; Wernicke and others, 1985, 1988). However, examples of regional Oligocene, prevolcanic extensional faulting have been reported from areas north of the Delamar Mountains in Lincoln and northeastern Nye Counties (Axen, 1986; Axen and others, 1988; Axen and others, 1993; Jayko, 1990; Lewis, 1987; Taylor and others, 1989).

The major extensional structures in the southern Delamar Mountains are Miocene and younger and include the Kane Springs Wash fault, and Coyote Spring fault, the southernmost strand of the Pahranagat shear system (fig. 2). The Pahranagat shear system is a zone of northeast-trending, steeply northwest dipping faults that show both dip-slip and left-lateral strike-slip displacement (Tschanz and Pampeyan, 1970; Ekren and others, 1977). Liggett and Ehrenspeck (1974) interpreted the system as a fault zone that accommodates differentially extending domains, a model also used to explain the Las Vegas Valley shear zone, which separates highly extended blocks in the Sheep Range north of the shear from less extended blocks in the Spring Mountains south of the shear (Guth, 1981). Tschanz and Pampeyan (1970) estimated approximately 9–16 km of left-lateral displacement on the shear zone. The maximum age of major deformation of the Pahranagat shear system is unknown; however, Tschanz and Pampeyan (1970) postulated that the shear system might have originally been active as a right-lateral tear fault during Sevier orogenic thrusting. Fault scarps and fissures in alluvial deposits within the shear system suggest a modern age for the minimum age of deformation in the shear system (Swadley and Scott, 1988; Jayko, in press). Current seismicity on faults within the shear system suggests that it is presently active (Rogers and others, 1987).

The Coyote Spring fault consists of two segments: a western segment strikes north and dips west, and a northern segment strikes northeast and dips northwest, and is parallel to other strands of the Pahranagat shear system (fig. 2). The northern segment is interpreted as a sinistral oblique fault; however, where the fault strike bends about 60°, the fault becomes the western segment interpreted as a minor breakaway with predominantly dip-slip displacement on the west side of the southern Delamar Mountains block (Scott and others, 1990). Stratigraphic offset on the western segment is estimated to be about 300 m by Tschanz and Pampeyan (1970), and I estimate at least 650 m based on exposure of Tertiary volcanic rocks (Kane Wash Tuff) on the downthrown block of the Coyote Spring fault in Coyote Spring Valley. The age of the Coyote Spring fault is not well established. The youngest units cut by the fault are Tertiary alluvial sediments of probable Pliocene to Miocene age, but the earliest time of movement cannot be determined.

The Kane Springs Wash fault is a northeast-striking, northwest-dipping sinistral oblique-slip fault that bounds the west flank of the Meadow Valley Mountains. Progressive tilting of volcanic strata in the Meadow Valley Mountains both south of and within the Kane Springs Wash caldera indicates that this area was being affected by extension at least as early as about 16 Ma (Scott and others, this volume; Harding and others, this volume). Yet no progressive tilting has been observed west of the Kane Springs Wash fault in the Delamar Mountains. This suggests that the Kane Springs Wash fault formed the western limit of that tilting and therefore was active at least as early as 16 Ma.

The Kane Springs Wash caldera is a 12×25 km oval-shaped caldera located in the northwestern part of the study area (fig. 1). Outflow sheets of the Kane Wash Tuff erupted from the caldera 14.5 Ma (Scott and others, this volume). Rocks in the western part of the caldera in the Delamar Mountains have been undisturbed structurally for the most

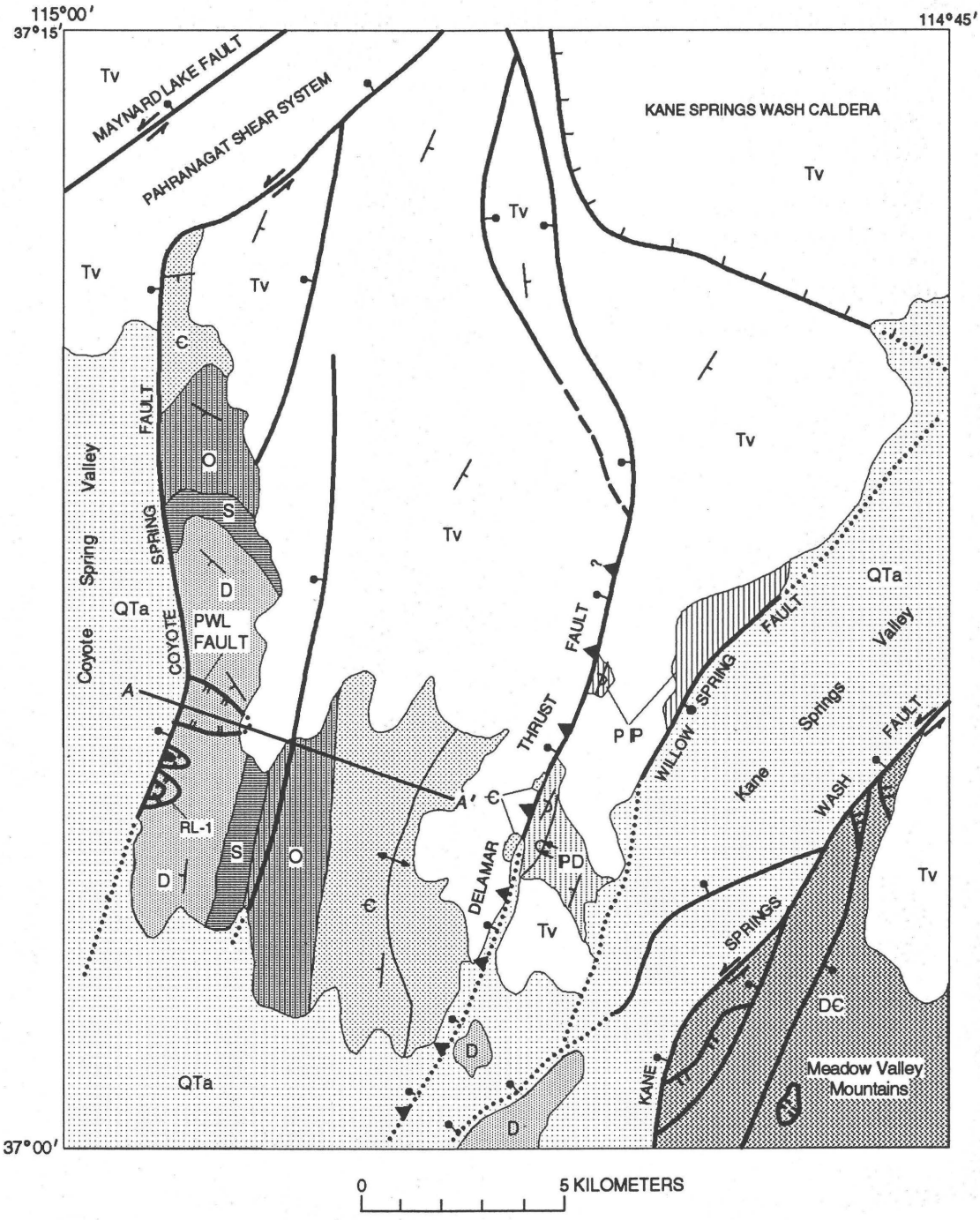

Figure 2 (above and facing page). Generalized geology of study area. Geology modified from Page and others (1990), Scott and others (1990), and Swadley and others (1990). Cross section *A–A′* in figure 5.

part, except for a slight 5°–10° dip to the east. In contrast, rocks in the eastern part of the caldera in the Meadow Valley Mountains were tilted eastward about 15°–20° on normal faults between 14.5 and 11.5 Ma (Harding and others, this volume) and were subsequently offset 4–7 km by the sinistral Kane Springs Wash fault (fig. 1).

Rocks in the southern Delamar Mountains appear to be only mildly extended by high-angle normal faults, but are surrounded by highly extended regions to the north across the Pahranagat shear system (Hudson and others, 1991; Scott and others, 1993), to the southeast in the Mormon Mountains (Wernicke and others, 1985), and to the southwest in the Sheep Range (Guth, 1981; Guth and others, 1988). The southern Delamar Mountains are considered as "stable terrane" in the context of regional extensional tectonics (Wernicke and others, 1985). Although exposed regional

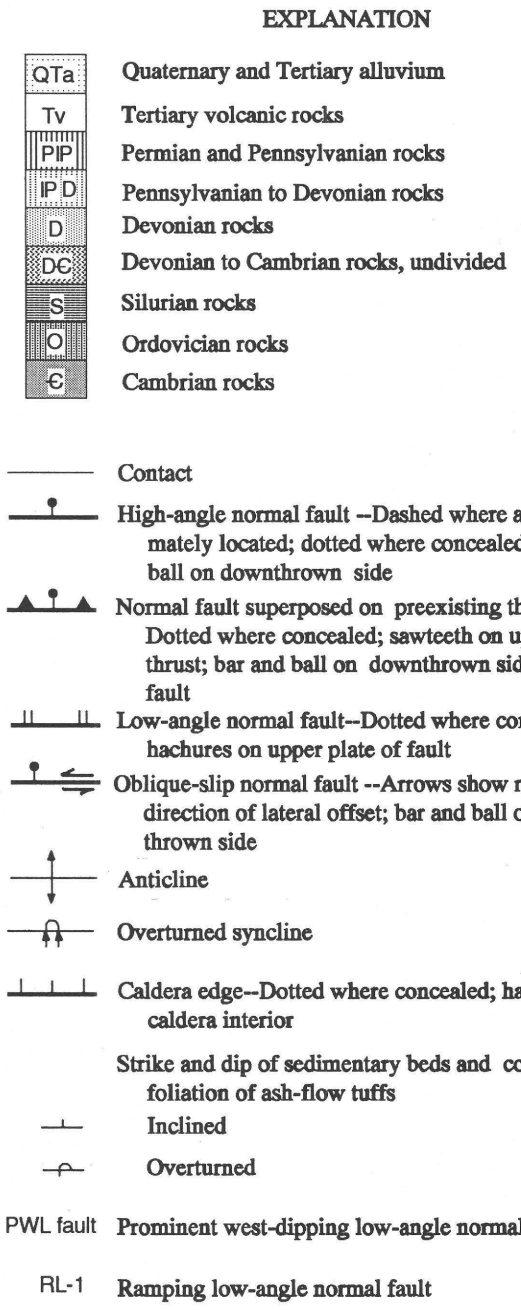

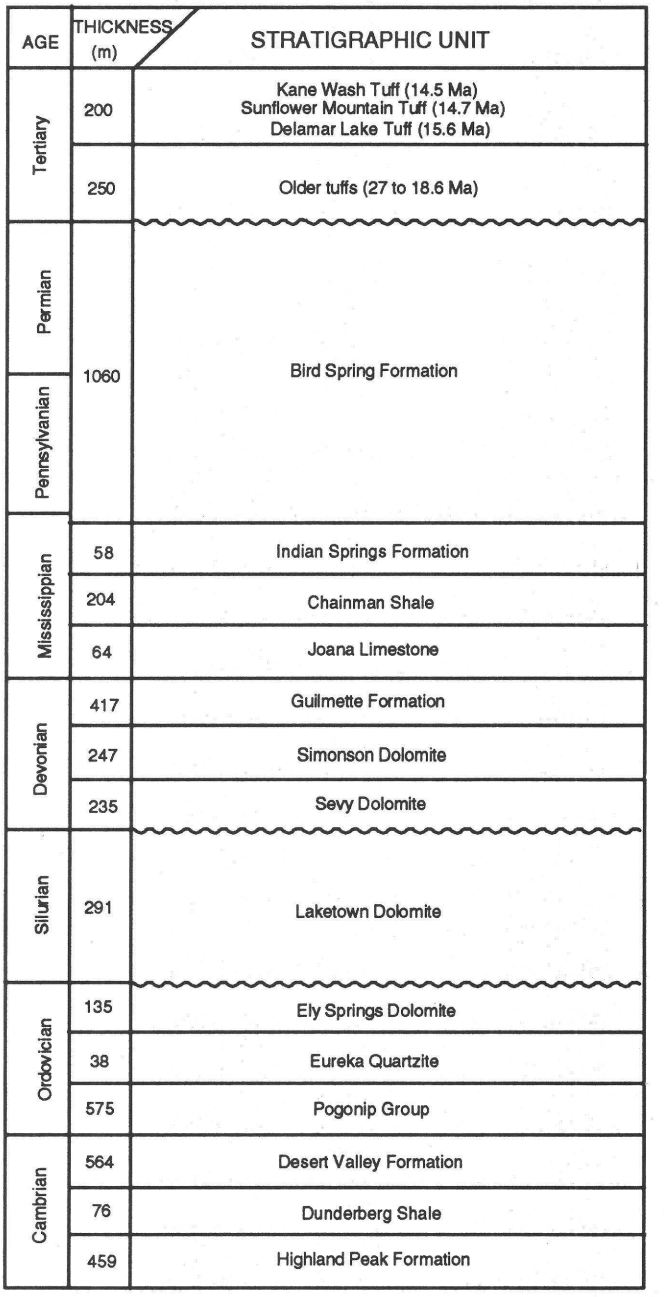

Figure 3. Generalized stratigraphic column of Tertiary volcanic and Paleozoic rocks exposed in the southern Delamar Mountains.

detachment faults are absent, these structures are proposed to underlie the southern Delamar Mountains at depth (Scott, 1990). In Scott's interpretation, large stable island-like blocks, such as the southern Delamar Mountains, are envisioned to be adrift, riding passively above detachment systems at depth that connect adjacent extended areas. The presence within the block of Miocene and younger structures such as gravity-slides, high-angle normal faults bounding strike-slip faults, and grabens floored by steeply dipping middle Miocene strata demonstrates local denudation and internal breakup of the stable block, reflecting differential movement of the block on the underlying detachment system.

DESCRIPTION OF LOW-ANGLE FAULT SYSTEM

The low-angle, ramping properties of the fault system in the southern Delamar Mountains are geometrically similar to those of minor thrust faults, except that one of the fundamental rules of thrust geometry is violated (Dahlstrom, 1970). Detailed stratigraphic and structural studies have shown that the low-angle faults attenuate rather than thicken the stratigraphic section; in most cases these faults place

younger rocks over older rocks in contrast to older over younger as generally shown by thrust faults. Therefore, these faults are proposed to be low-angle normal faults rather than compressional thrust faults.

The prominent west-dipping low-angle (PWL) normal fault and ramping low-angle faults are viewed as one integrated fault system. Although the PWL and ramping faults occur at different scales, observed similarities among them suggest that these low-angle normal faults are contemporaneous, and have a common genesis. These similarities include (1) restriction of these structures to one specific geographic area within the mountain range, (2) restriction to Devonian rocks, (3) consistent low-angle, westward dip, and (4) offset by the Coyote Spring fault.

PWL FAULT

The PWL fault is exposed along the west flank of the southern Delamar Mountains. Here the Guilmette Formation and uppermost member of the Simonson Dolomite in the hanging wall overlie the lower member of the Sevy Dolomite in the footwall, eliminating about 270 m of the stratigraphic section.

Canyons that dissect the western range front expose the scoop-shaped PWL fault plane along 1.5 km from its north to its south boundary (fig. 2). The fault plane steepens at its boundaries, and flattens between boundaries, making a scoop or shovel-shaped fault. Along the southern fault boundary, the fault plane dips approximately 55° NNW. Although exposures are limited along the northern boundary, the fault plane appears to dip south at about 50°–60°. In the deepest canyon on the southern interior of the fault block, the fault plane dips southwest at approximately 15° (fig. 4*A*, 4*B*), and slickenlines on the fault plane trend N. 67° W. and plunge 12° SW. (Page and others, 1990). The fault is also exposed at several other places within the interior of the fault block and dips gently to the west. About 1 m of fault gouge is exposed along the fault plane, and abundant small-scale, high-angle west-dipping normal faults sole into the master fault plane (fig. 4*A*).

I interpret the eastern projection of the PWL fault to be covered by tuff of the Leach Canyon Formation (dated at 23.8 Ma; Best and others, 1993). The projection of the PWL fault is probably covered by the Shingle Pass Tuff (26.7 Ma; Best and others, 1989) and the Monotony Tuff (27.3 Ma; Best and others, 1989) as well, because these units are exposed north and south of the PWL fault and conformably underlie the Leach Canyon Formation (fig. 5*A*) (Page and others, 1990). This interpretation requires that the fault formed prior to deposition of these late Oligocene and early Miocene volcanic rocks and can be assigned a minimum date of about 27 Ma (late Oligocene); however, field evidence is somewhat equivocal because landslide deposits largely conceal a poorly exposed Paleozoic-Tertiary contact at this locality. Discontinuous, high-angle, small-offset normal faults are present in the volcanic rocks near the east edge of the PWL fault (Page and others, 1990), but these high-angle normal faults do not appear to be associated with the PWL fault. Restoration of the PWL fault to postfault, pre-erosion geometry (fig. 5*B*) indicates that minimum offset on the PWL fault must have been at least 1.7 km; no faults of this magnitude cut the volcanic strata, which are nearly undeformed. For further discussion on the age of faulting, see the section, "Discussion."

The PWL fault cuts up stratigraphic section in the direction of transport because the strata dip about 30° W. whereas the fault only dips at 15° W. Although this geometry seems atypical for normal faults, it can be explained by normal faulting of the west-dipping panel of rocks previously deformed in the Mesozoic during the Sevier orogeny. The volcanic rocks which overlie both the Paleozoic rocks and the eastern extension of the PWL fault dip about 10° E., indicating that the west side of the mountain range has been slightly tilted at least since late Oligocene time. Therefore, the original tilt of the Paleozoic rocks probably was about 10° greater during faulting, or about 40° W., making the original dip of the PWL fault about 25° W.

Several west-vergent folds are present in the upper plate of the PWL fault, some with amplitudes as great as 20 m and wavelengths of about 30 m (fig. 6). These folds are interpreted as local ductile shear structures that probably formed in response to drag as upper layers in hanging-wall rocks were transported westward over lower plate rocks. Local contractional structures associated with attenuated regimes have been found in other areas of the Basin and Range (Bartley and Wernicke, 1984; Campagna and Aydin, 1991; Hodges and others, 1984; Lund and others, 1991; Wernicke and others, 1985).

RAMPING LOW-ANGLE FAULTS

Exposed directly south of the PWL fault are complex fault networks described as ramping low-angle faults (Page and Scott, 1991). These fault networks were examined on outcrop scale (fig. 2) to better define their structural geometry. An example of these structures (RL–1) is shown in figure 7.

Exposures of RL–1 (fig. 7) show two major discordances—both of which are faults. The two faults occur at different stratigraphic levels and separate the rocks into lower, middle, and upper panels. Rocks in the lower panel dip about 30° W. whereas beds in the middle panel dip about 15° W. and SW. The fault that separates lower from upper panels dips about 30° W. and is bedding-plane parallel to the lower panel. A discordance of about 15° is recorded between lower and middle panels. I do not know whether or not the lower panel rocks are bounded by a buried fault; however, as regional dips from this part of the mountain range average about 30° W., a buried fault is not required. Rocks in the fault

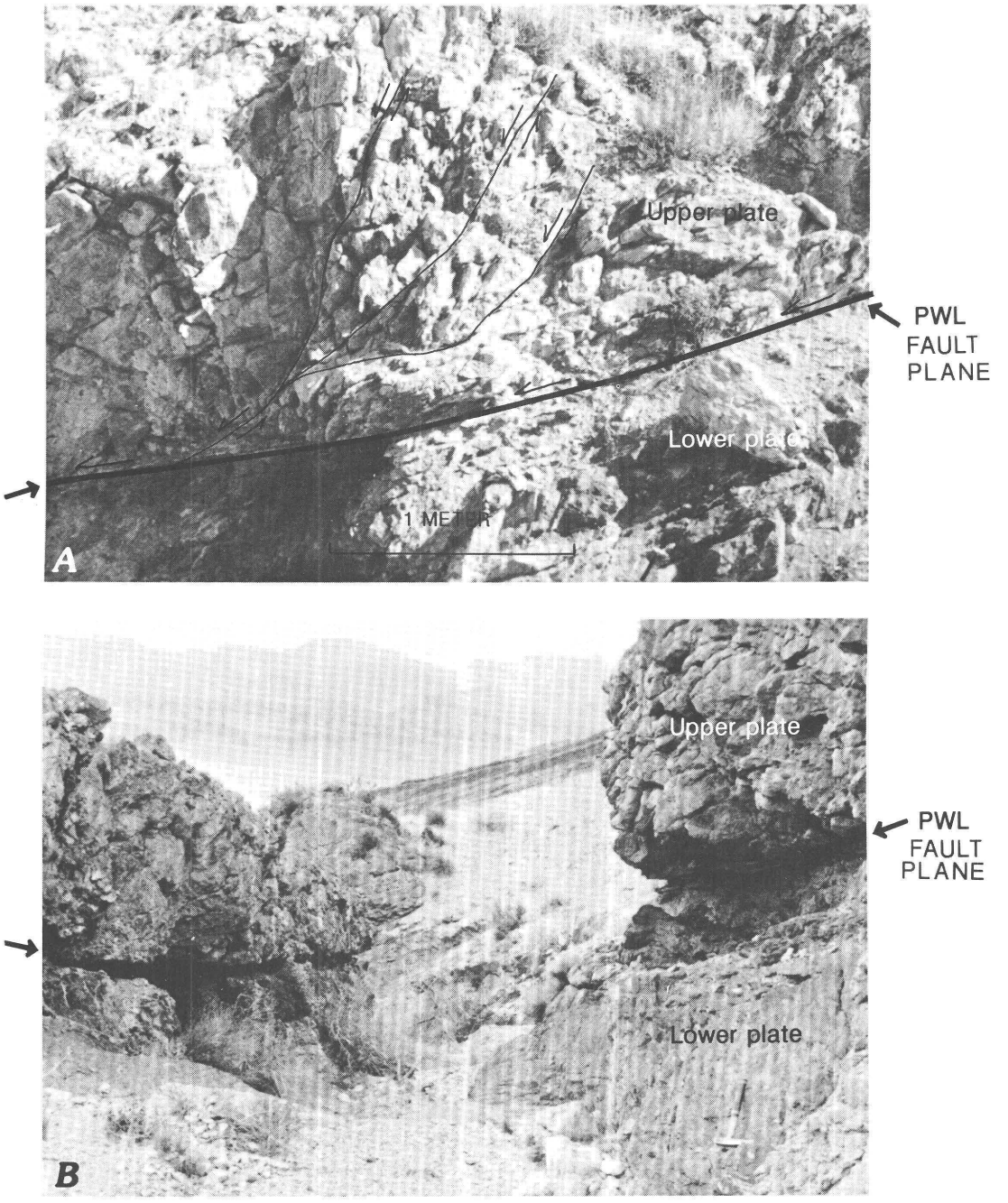

Figure 4. Views of PWL fault plane. *A*, View toward north, of fault plane dipping about 15° W. (left); Guilmette Formation in upper plate, Sevy Dolomite in lower plate; note small-scale high-angle normal faults that sole into PWL fault. Barbs show direction of relative movement. *B*, Same location as *A*, except view is to west, looking down fault plane. Coyote Spring Valley is in background. Hammer on lower right for scale.

zone of the lower fault are highly brecciated, altered, and preferentially dolomitized. The upper fault at RL–1 occurs at a higher stratigraphic level and separates the middle and upper panels. The upper fault shows a typical footwall ramp that dips approximately 50° W. The ramp truncates bedding sharply in the footwall and abruptly flattens to the west, becoming a west-dipping bedding-plane fault. Along the ramp, strata in the upper panel dip approximately 50° W., whereas in the middle panel they dip about 15° W., a discordance of about 35°.

DISCUSSION

The minimum age of the low-angle normal fault system in the southern Delamar Mountains is believed to be

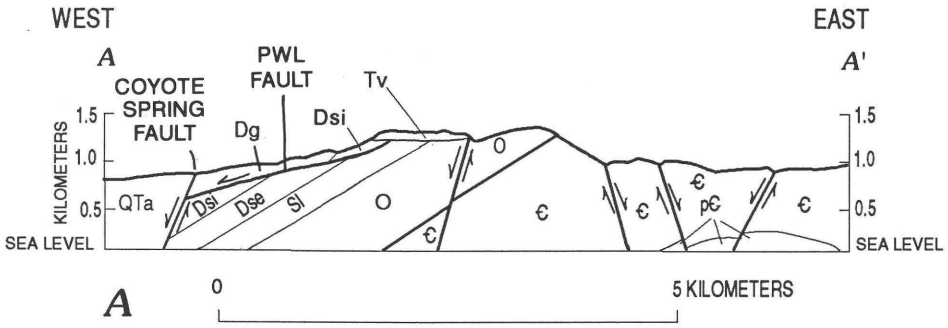

EXPLANATION

QTa	Quaternary and Tertiary alluvium
Tv	Tertiary volcanic rocks
Dg	Guilmette Formation (Devonian)
Dsi	Simonson Dolomite (Devonian)
Dse	Sevy Dolomite (Devonian)
Sl	Laketown Dolomite (Silurian)
O	Ordovician rocks
€	Cambrian rocks
pC	Precambrian rocks
	Contact
	Prominent west-dipping low-angle normal fault (PWL)—Barb shows direction of relative movement
	High-angle normal fault

Figure 5 (above and facing page). Views of cross section *A–A′* from figure 2. *A*, Present-day cross section *A–A′*. PWL fault is restricted to tilted Paleozoic rocks below overlying volcanic rocks. *B*, Restored cross section of PWL fault along *A–A′* to postfault, pre-erosion geometry.

pre–27 Ma (late Oligocene) based on the age of the oldest volcanic strata that overlie the PWL fault. Although the maximum age is poorly constrained, faulting is proposed to be either Late Cretaceous or early Tertiary based on restoration of the PWL fault to postfault, pre-erosion geometry (fig. 5*B*); that geometry shows vertical offset of about 1.7 km. This offset represents the minimum amount of erosion of Paleozoic and Mesozoic rocks off the upthrown block of the fault necessary to form the topography onto which the volcanic rocks were deposited. The volcanic rocks above the PWL fault show no thickness variation across the fault indicating that no relief was left across the fault at the time of ash flow emplacement. The length of time required for this erosion is probably on the order of tens of millions of years, suggesting that faulting is more likely to have occurred either during or shortly following Sevier thrusting rather than during middle Tertiary prevolcanic extension reported north of the southern Delamar Mountains, in Lincoln and Nye Counties.

These extensional structures in the southern Delamar Mountains are interpreted to have formed as a result of gravitational collapse in response to relief produced by overthickening of the crust during Sevier thrusting. The concept of gravitational collapse along orogenic belts has been reviewed by many workers. Coney (1987) and Wernicke and others (1987) proposed that thickening of the crust in the Sevier orogenic belt was the ultimate driving force of regional Tertiary crustal extension in the Basin and Range province. Dewey (1988) reported that orogenic belts with topographic relief of 3 km or greater have the gravitational potential to collapse and spread laterally due to a decrease in boundary forces controlled by inhomogeneities

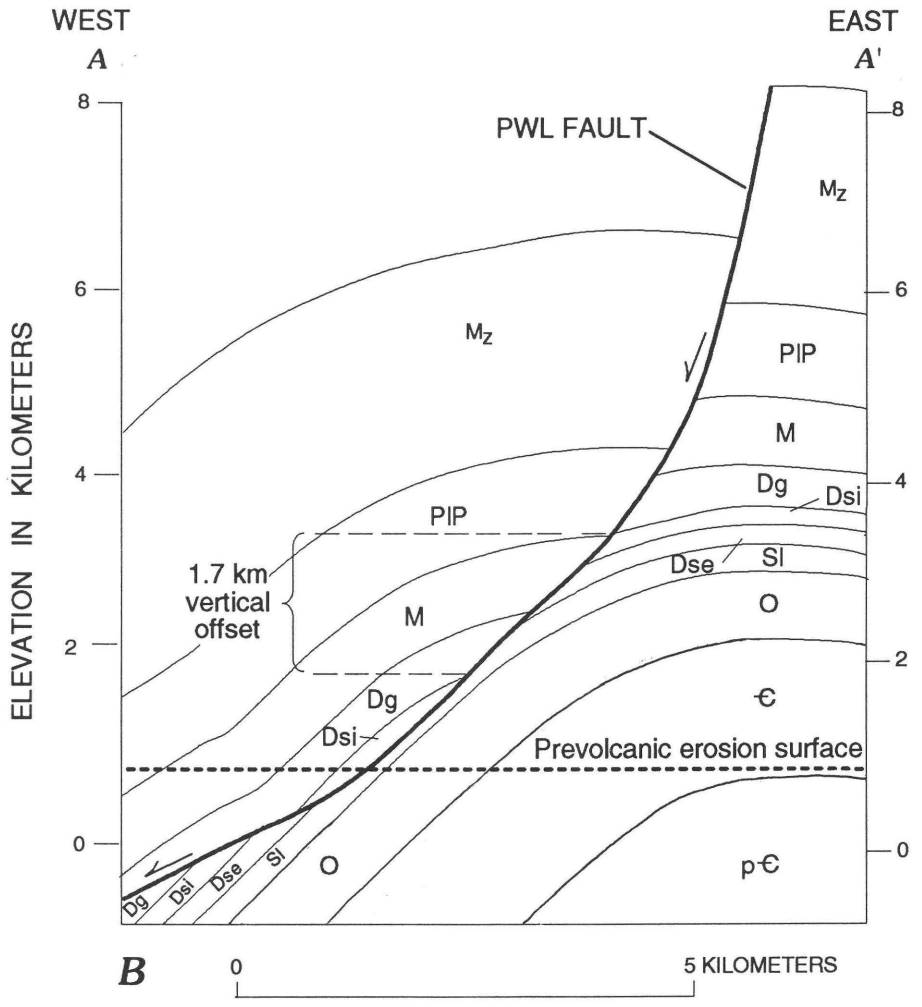

EXPLANATION

M_z	Mesozoic rocks
PIP	Permian and Pennsylvanian rocks
M	Mississippian rocks
Dg	Guilmette Formation (Devonian)
Dsi	Simonson Dolomite (Devonian)
Dse	Sevy Dolomite (Devonian)
Sl	Laketown Dolomite (Silurian)
O	Ordovician rocks
€	Cambrian rocks
p-€	Precambrian rocks

Contact

Prominent west-dipping low-angle normal fault (PWL)—Barb shows direction of relative movement

within thickened continental crust. The decrease in boundary forces is also dependent on thermal constraints within the continental lithosphere. Sonder and others (1987) also discussed the concept of thickened crust as being gravitationally unstable, leading to spreading under its own weight. They concluded that the time interval between compression and the onset of extension depends on rates of thermal relaxation in the crust; the higher the thermal regime, the shorter time interval between compression and the response of gravitational spreading or collapse. Burchfiel

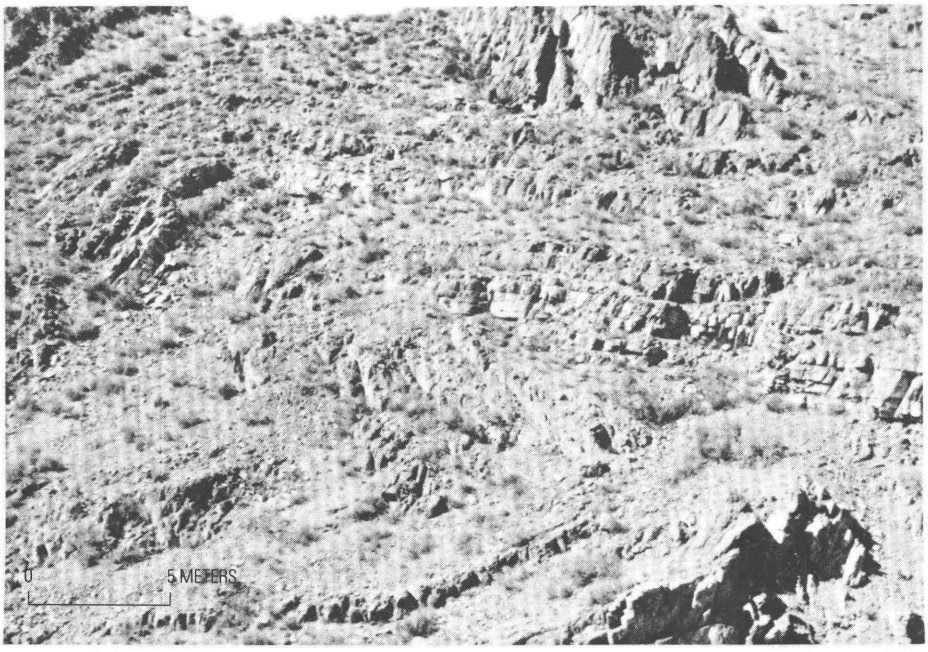

Figure 6. West-vergent fold, amplitude about 20 m, exposed in upper plate of PWL fault. View toward northwest.

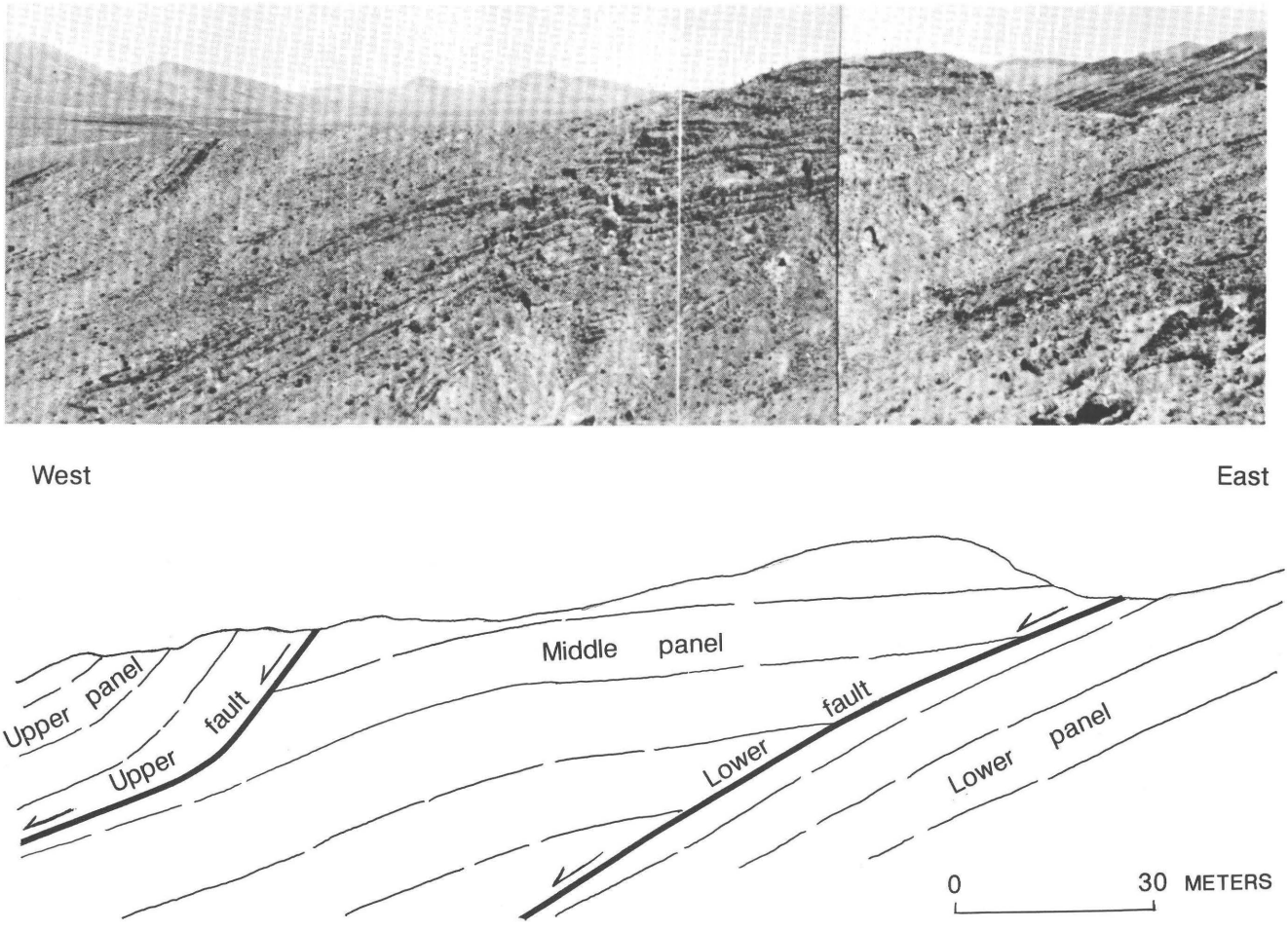

Figure 7. Photograph and sketch of ramping low-angle fault network at RL–1. View toward north.

and others (1992), Burchfiel and Royden (1985), Chen and others (1990), and Hodges and others (1992) have documented gravitational collapse in the Himalayan orogenic belt that is believed to be contemporaneous with compression. In these examples, basic requirements for gravitational collapse were met: crustal thickening, topographic relief (represented by the elevated Tibetan plateau), and a high thermal regime. Other examples of gravitational collapse in collisional plate-tectonic settings occur in the Caledonides in northern Norway (Cashman, 1990), and the eastern Alps (Ratschbacher and others, 1989). The Raft River and Black Pine Mountains in northwestern Utah and southern Idaho provide an example of gravitational collapse in the hinterland of the Sevier orogenic belt (Wells and others, 1990).

These examples support the conclusion that gravitational collapse related to regional crustal extension is contemporaneous with or follows crustal thickening. However, no evidence exists to suggest that the low-angle normal faults in the southern Delamar Mountains are related to regional crustal extension. Although the mechanics of both regional and localized gravitational collapse are probably similar, an alternative explanation, independent of a regional extensional process, must be postulated for these upper crustal faults. Height of the Delamar ramp anticline above areas to the west prior to erosion and at the time of thrust emplacement is estimated to have been about 5 km, based on restoration of the ramp anticline to the time of thrust emplacement (fig. 8). This estimate includes about 2.5 km of Mesozoic rocks assumed to have been deposited in the southern Delamar Mountains, but subsequently eroded. The thickness of the Mesozoic rocks is based on exposures of these rocks just 15 km east of the study area on the west flank of the Meadow Valley Mountains (Pampeyan, 1989). I propose that gravitational instabilities occurring along incompetent bedding planes on a 40°-dipping thrust ramp elevated by Sevier thrusting induced local gravity-sliding westward off that ramp.

In the southeast part of the study area in the Meadow Valley Mountains, Swadley and others (1990) mapped two stratigraphic levels of low-angle faults (fig. 2). The upper fault placed rocks of the brown cliff member of the Simonson Dolomite in the hanging wall above the middle to upper part of the Sevy Dolomite (Swadley and others, 1990). The fault followed the the stratigraphic level of the 13-m-thick quartzite at the base of the Simonson Dolomite (Swadley and others, 1990), converted the quartzite to fault gouge, and removed about 130 m of strata including middle and lower parts of the Simonson, and upper parts of the Sevy. The lower fault generally followed the stratigraphic level of

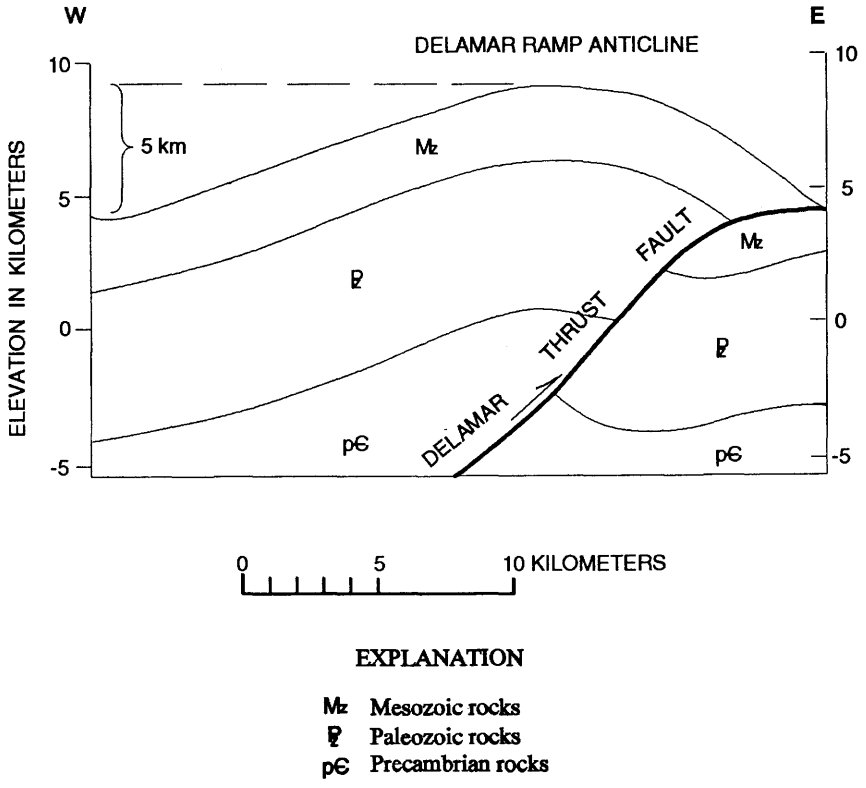

Figure 8. Restored cross section of the Delamar ramp anticline to the time of thrust emplacement (Cretaceous), and prior to low-angle normal faulting. Restoration shows sufficient relief of ramp anticline to induce gravity-sliding off the west flank.

the Eureka Quartzite, converted the quartzite to fault gouge, and truncated strata of the underlying Pogonip Group, and overlying Ely Springs Dolomite. At many locations in the Meadow Valley Mountains, the Eureka Quartzite is absent, or is only several meters thick where it has been tectonically omitted or thinned by low-angle faulting. Although upper plate Ordovician strata are locally altered to jasperoid and are highly faulted, overlying Tertiary volcanic rocks are neither altered nor highly faulted. This suggests that these low-angle faults predate Tertiary volcanism and major regional extension in the Meadow Valley Mountains. Perhaps these faults formed as gravity-slides similar to the low-angle normal faults in the southern Delamar Mountains during Late Cretaceous or early Tertiary time, or they may be related to some other regional prevolcanic episode of extension such as the prevolcanic Oligocene regional extension noted in northern Lincoln and northeastern Nye Counties (Axen and others, 1988; Axen and others, 1993; Taylor and others, 1989).

Kellogg (1992) reported evidence for Late Cretaceous or early Tertiary gravity-sliding in the Deep Creek Mountains of southeastern Idaho. He interpreted the Deep Creek fault as a west-dipping, west-directed, low-angle fault formed by localized gravity-sliding off topographic relief developed by ramping of a Sevier-age thrust, much like the case in the Delamar Mountains. Vandervoort and Schmitt (1990) suggested that the presence of Upper Cretaceous scarp-front alluvial facies in the Sevier hinterland was evidence of normal-faulting-related localized gravitational collapse of Late Cretaceous to early Tertiary age; this high-level crustal deformation may also be similar to that of the southern Delamar Mountains.

CONCLUSIONS

A system of low-angle normal faults occurs in Devonian rocks along the west flank of the southern Delamar Mountains. Faults of that system dip westward, attenuate the stratigraphic section, and place younger rocks over older rocks. The age of the fault system is poorly constrained; however, evidence from geologic mapping suggests that the minimum age is greater than 27 Ma. Although the maximum age of faulting cannot be determined, the fault system is interpreted as Late Cretaceous or early Tertiary, based on restoration of the most prominent low-angle fault (PWL) of the fault system to postfault, pre-erosion geometry. The low-angle fault system is interpreted to have formed by processes of brittle, gravitational collapse off the steeply west dipping, west flank of the Delamar allochthon, following ramping of the Sevier-age Delamar thrust fault. This deformation is viewed as localized gravity-sliding in contrast to regional crustal extension.

REFERENCES CITED

Armstrong, R.L., 1968, Sevier orogenic belt in Nevada and Utah: Geological Society of America Bulletin, v. 79, p. 429–458.

Axen, G.J., 1986, Superposed normal faults in the Ely Springs Range, Nevada—Estimates of extension: Journal of Structural Geology, v. 8, p. 711–713.

Axen, G.J., Lewis, P.R., Burke, K.J., Sleeper, K.G., and Fletcher, J.M., 1988, Tertiary extension in the Pioche area, Lincoln County, Nevada, *in* Weide, D.L., and Faber, M.L., eds., This extended land; geological journeys in the southern Basin and Range: Geological Society of America Cordilleran Section Field Trip Guidebook, p. 3–5.

Axen, G.J., Taylor, W.J., and Bartley, J.M., 1993, Space-time patterns and tectonic controls of Tertiary extension and magmatism in the Great Basin of the western United States: Geological Society of America Bulletin, v. 105, p. 56–76.

Axen, G.J., Wernicke, B.P., Skelly, M.F., and Taylor, W.J., 1990, Mesozoic and Cenozoic tectonics of the Sevier thrust belt in the Virgin River valley area, southern Nevada, *in* Wernicke, B.P., ed., Basin and Range extensional tectonics near the latitude of Las Vegas, Nevada: Geological Society of America Memoir 176, p. 123–153.

Bartley, J.M., and Wernicke, B.P., 1984, The Snake Range decollement interpreted as a major extensional shear zone: Tectonics, v. 3, p. 647–657.

Best, M.G., Christiansen, E.H., Deino, A.L., Grommé, C.S., McKee, E.H., and Noble, D.C., 1989, Eocene through Miocene volcanism in the Great Basin of the western United States: New Mexico Bureau of Mines and Mineral Resources Memoir 47, p. 91–143.

Best, M.G., Scott, R.B., Rowley, P.D., Swadley, W C, Grommé, C.S., Harding, A.E., Deino, A.L., Christiansen, E.H., Tingey, D.G., and Sullivan, K.R., 1993, Oligocene-Miocene caldera complexes, ash-flow sheets, and tectonism in the central and southeastern Great Basin, *in* Lahren, M.M., Trexler, J.H., Jr., and Spinosa, C., eds., Crustal evolution of the Great Basin and Sierra Nevada: Cordilleran/Rocky Mountain Section, Geological Society of America Guidebook, Department of Geological Sciences, University of Nevada, Reno, p. 285–311.

Bohannon, R.G., 1984, Nonmarine sedimentary rocks of Tertiary age in the Lake Mead region, southeastern Nevada and northwestern Arizona: U.S. Geological Survey Professional Paper 1259, 72 p.

Burchfiel, B.C., Chen, Zhiliang, Hodges, K.V., Liu, Yuping, Royden, L.H., Deng, Changrong, and Xu, Jiene, 1992, The south Tibetan detachment, Himalayan orogen—Extension contemporaneous with and parallel to shortening in a collisional mountain belt: Geological Society of America Special Paper 269, 41 p.

Burchfiel, B.C., and Royden, L.H., 1985, North-south extension within the convergent Himalayan region: Geology, v. 13, p. 679–682.

Campagna, D.J., and Aydin, Atilla, 1991, Tertiary uplift and shortening in the Basin and Range; the Echo Hills, southeastern Nevada: Geology, v. 19, p. 485–488.

Cashman, P.H., 1990, Evidence for extensional deformation during a collisional orogeny, Rombak Window, north Norway: Tectonics, v. 9, p. 859–886.

Chen, Z., Liu, Y., Hodges, K.V., Burchfiel, B.C., Royden, L.H., and Deng, C., 1990, The Kangmar dome—A metamorphic complex in southern Xizang (Tibet): Science, v. 250, p. 1552–1556.

Coney, P.J., 1987, The regional tectonic setting and possible causes of Cenozoic extension in the North America cordillera, *in* Coward, M.P., Dewey, J.F., and Hancock, P.L., eds., Continental extensional tectonics: Geological Society of London Special Publication 28, p. 177–186.

Dahlstrom, C.D.A., 1970, Structural geology in the eastern margin of the Canadian Rocky Mountains: Bulletin of Canadian Petroleum Geology, v. 18, no. 3, p. 332–406.

Dewey, J.F., 1988, Extensional collapse of orogens: Tectonics, v. 7, no. 6, p. 1123–1139.

Ekren, E.B., Orkild, P.P., Sargent, K.A., and Dixon, G.L., 1977, Geologic map of Tertiary rocks, Lincoln County, Nevada: U.S. Geological Survey Miscellaneous Investigations Series Map I–1041, scale 1:250,000.

Fleck, R.J., 1970, Tectonic style, magnitude, and age of deformation in the Sevier orogenic belt in southern Nevada and eastern California: Geological Society of America Bulletin, v. 81, p. 1705–1720.

Guth, P.L., 1981, Tertiary extension north of the Las Vegas Valley shear zone, Sheep and Desert Ranges, Clark County, Nevada: Geological Society of America Bulletin, v. 92, p. 763–771.

Guth, P.L., Schmidt, D.L., Deibert, J., and Yount, J., 1988, Tertiary extensional basins of northwestern Clark County, *in* Weide, D.L., and Faber, M.L., eds., This extended land; geological journeys in the southern Basin and Range: Geological Society of America Cordilleran Section Field Trip Guidebook, p. 239–253.

Hodges, K.V., Parrish, R.R., Housh, T.B., Lux, D.R., Burchfiel, B.C., Royden, L.H., and Chen, Z., 1992, Simultaneous Miocene extension and shortening in the Himalayan orogen: Science, v. 258, p. 1466–1470.

Hodges, K.V, Walker, J.D., and Wernicke, B.P., 1984, Tertiary folding and extension, Tucki Mountain area, Death Valley region: Geological Society of America Abstracts with Programs, v. 16, no. 6, p. 540.

Hudson, M.R., Rosenbaum, J.G., and Scott, R.B., 1991, Counterclockwise rotation in a broad extensional transfer zone, southeastern Nevada—Paleomagnetic evidence from the lower Miocene Hiko Tuff: Geological Society of America Abstracts with Programs, v. 23, no. 4, p. 34.

Jayko, A.S., 1990, Shallow crustal deformation in the Pahranagat area, southern Nevada, *in* Wernicke, B.P., ed., Basin and Range extensional tectonics near the latitude of Las Vegas, Nevada: Geological Society of America Memoir 176, p. 213–235.

———in press, Pahranagat Range 30×60 minute quadrangle, Lincoln and Nye Counties, Nevada: Nevada Bureau of Mines and Geology, scale 1:100,000.

Kellogg, K.S., 1992, Low-angle detachment faulting in the Deep Creek Mountains, southeastern Idaho: Geological Society of America Abstracts with Programs, v. 24, no. 6, p. 21.

Lewis, P.R., 1987, Structural geology of the Northern Burnt Springs Range and Robber Roost Hills, Lincoln County, Nevada: Flagstaff, Ariz., Northern Arizona University M.S. thesis, 90 p.

Liggett, M.A., and Ehrenspeck, H.E., 1974, Pahranagat shear system, Lincoln County, Nevada: U.S. National Aeronautics and Space Administration Report CR–136388, 9 p.

Lund, Karen, Beard, L.S., and Perry, W.J., Jr., 1991, Structures of the northern Grant Range and Railroad Valley, Nye County, Nevada—Implications for oil occurrences, *in* Flanigan, D.M.H., Hansen, Mike, and Flanigan, T.E., eds., Geology of the White River Valley, the Grant Range, Eastern Railroad Valley and Western Egan Range, Nevada: Nevada Petroleum Society 1991 Guidebook, p. 1–6.

Novak, S.W., 1984, Eruptive history of the rhyolitic Kane Springs Wash volcanic center, Nevada: Journal of Geophysical Research, v. 89, p. 8603–8615.

Nutt, C.J., and Thorman, C.H., 1992, Mesozoic to early Tertiary attenuation and Tertiary uplift on the Goshute Indian Reservation, southwestern Deep Creek Range, Nevada-Utah: Geological Society of America Abstracts with Programs, v. 24, no. 6, p. 55.

Nutt, C.J., Thorman, C.H., Snee, L.W., and Zimmermann, R.A., 1992, Mesozoic to early Tertiary low-angle younger-over-older faults in the Drum Mountains, west-central Utah: Geological Society of America Abstracts with Programs, v. 24, no. 6, p. 56.

Page, W.R., and Scott, R.B., 1991, Ramping extensional faults in the Devonian Guilmette Formation, southern Nevada: Geological Society of America Abstracts with Programs, v. 21, no. 4, p. 55.

Page, W.R., Swadley, W C, and Scott, R.B., 1990, Preliminary geologic map of the Delamar 3 SW quadrangle, Lincoln County, Nevada: U.S. Geological Survey Open-File Report 90–336, scale 1:24,000.

Pampeyan, E.H., 1989, Preliminary geologic map of the Meadow Valley Mountains, Lincoln and Clark Counties, Nevada: U.S. Geological Survey Open-File Report 89–182, scale 1:50,000.

Ratschbacher, L., Frisch, W., Neubauer, F., Schmid, S.M., and Neugebauer, J., 1989, Extension in compressional orogenic belts—The eastern Alps: Geology, v. 17, p. 404–407.

Rogers, A.M., Harmsen, S.C., and Meremonte, M.E., 1987, Evaluation of the seismicity of the Southern Great Basin and its relationship to the tectonic framework of the region: U.S. Geological Survey Open-File Report 87–408, 196 p.

Scott, R.B., 1990, Significance of mild extension of a relatively stable area within highly extended terrane, southeastern Nevada: Geological Society of America Abstracts with Programs, v. 22, no. 3, p. 81.

Scott, R.B., Page, W.R., and Swadley, W C, 1990, Preliminary geologic map of the Delamar 3 NW quadrangle, Lincoln County, Nevada: U.S. Geological Survey Open-File Report 90–405, scale 1:24,000.

Scott, R.B., Swadley, W C, and Novak, S.W., 1993, Geologic map of the Delamar Lake quadrangle, Lincoln County, Nevada: U.S. Geological Survey Geologic Quadrangle Map GQ–1730, scale 1:24,000.

Sonder, L.J., England, P.C., Wernicke, B.P., and Christiansen, R.L., 1987, A physical model for Cenozoic extension of western North America, *in* Coward, M.P., Dewey, J.F., and Hancock, P.L., Continental extensional tectonics: Geological Society of London Special Publication 28, p. 187–201.

Swadley, W C, Page, W.R., Scott, R.B., and Pampeyan, E.H., 1990, Preliminary geologic map of the Delamar 3 SE quadrangle, Lincoln County, Nevada: U.S. Geological Survey Open-File Report 90–221, scale 1:24,000.

Swadley, W C, and Scott, R.B., 1988, Modern fissures in the Pahranagat shear system, southeastern Nevada [abs.]: Eos, v. 69, p. 1459.

Taylor, W.J., Bartley, J.M., Lux, D.R., and Axen, G.J., 1989, Timing of Tertiary extension in the Railroad Valley–Pioche Valley transect, Nevada—Constraints from $^{40}Ar/^{39}Ar$ ages of volcanic rocks: Journal of Geophysical Research, v. 94, p. 7757–7774.

Tschanz, C.M., and Pampeyan, E.H., 1970, Geology and mineral deposits of Lincoln County, Nevada: Nevada Bureau of Mines Bulletin 73, 188 p.

Vandervoot, D.S., and Schmitt, J.G., 1990, Cretaceous to early Tertiary paleogeography in the hinterland of the Sevier thrust belt, east-central Nevada: Geology, v. 18, p. 567–570.

Wells, M.L., Dallmeyer, R.D., and Allmendinger, R.W., 1990, Late Cretaceous extension in the hinterland of the Sevier thrust belt, northwestern Utah and southern Idaho: Geology, v. 18, p. 929–933.

Wernicke, Brian, Axen, G.J., and Snow, J.K., 1988, Basin and Range extensional tectonics at the latitude of Las Vegas, Nevada: Geological Society of America Bulletin, v. 100, p. 1738–1757.

Wernicke, Brian, Walker, J.D., and Beaufait, M.S., 1985, Structural discordance between Neogene detachments and frontal Sevier thrusts, central Mormon Mountains, southern Nevada: Tectonics, v. 4, no. 2, p. 213–246.

Wernicke, B.P., Christiansen, R.L., England, P.C., and Sonder, L.J., 1987, Tectonomagmatic evolution of Cenozoic extension in the North American cordillera, *in* Coward, M.P., Dewey, J.F., and Hancock, P.L., eds., Continental extensional tectonics: Geological Society of London Special Publication 28, p. 203–221.

Paleomagnetic Data from the Miocene Hiko Tuff, Southeastern Nevada, and Their Tectonic Implications

By Mark R. Hudson, Joseph G. Rosenbaum, Robert B. Scott, *and* Peter D. Rowley

GEOLOGIC STUDIES IN THE BASIN AND RANGE–COLORADO PLATEAU TRANSITION IN SOUTHEASTERN NEVADA, SOUTHWESTERN UTAH, AND NORTHWESTERN ARIZONA, 1992

U.S. GEOLOGICAL SURVEY BULLETIN 2056–H

UNITED STATES GOVERNMENT PRINTING OFFICE, WASHINGTON : 1995

CONTENTS

FIGURES

TABLE

Paleomagnetic Data from the Miocene Hiko Tuff, Southeastern Nevada, and Their Tectonic Implications

By Mark R. Hudson, Joseph G. Rosenbaum, Robert B. Scott, *and* Peter D. Rowley

ABSTRACT

Paleomagnetic data from the 18.6–Ma Hiko Tuff constrain the nature of fault-block rotations during Miocene and younger extensional deformation in an area of southeastern Nevada. A mean remanent magnetization direction of five sites from the relatively undeformed southern Delamar Mountains and Meadow Valley Mountains (D=165.6°, I=–44.5°, α_{95}=6.2°) established a reference for comparison to mean directions from sites from fault blocks in nearby deformed areas. After tilt correction, mean directions from three sites from tilted fault blocks above the Highland detachment fault, west of the Chief Range, had little or no significant declination difference from the reference direction, suggesting that rotation of these blocks occurred principally by tilt about their strike axes.

In contrast, mean declinations for 18 sites that lie within or north of the Pahranagat shear system, distributed over a 30-kilometer-long belt from the southern Delamar Mountains to the South Pahroc Range, are moderately but consistently counterclockwise from the reference direction. These data suggest that this area was affected by 15°–20° of counterclockwise vertical-axis rotation. This interpretation is complicated, however, by the identification of a lower cooling unit of the Hiko Tuff locally in the South Pahroc Range whose declination is 13° counterclockwise of that recorded by upper parts of the tuff. Comparison of declinations from these different cooling units of the Hiko Tuff could suggest an apparent counterclockwise rotation of magnitude similar to that inferred for the South Pahroc Range. However, the declination discordance for most sites in the South Pahroc Range is most likely due to tectonic rotation, because five sites that we are confident were from the upper part of the Hiko have declinations that are 13°–26° discordant to the reference direction, whereas declinations from three sites from the lower cooling unit are 27°–40° discordant. These data suggest that sinistral shear in the South Pahroc Range area was accomplished not only by offset along sinistral faults but also by counterclockwise rotation of fault blocks within and north of the presently recognized Pahranagat shear system. Offset on the sinistral faults and the counterclockwise block rotations both may be components of deformation within a broad transfer zone that accommodated differential extension of the area.

INTRODUCTION

Rigid body rotation of fault blocks has been an important mechanism in accommodating strain during Cenozoic deformation within the Basin and Range province of western North America (Emmons and Garrey, 1910; Thompson, 1960; Proffett, 1977). Although components of rotation of fault blocks about horizontal axes can commonly be estimated from dips of stratified rocks within the blocks, components of rotation about vertical axes are in most places difficult to constrain. In appropriate rocks, paleomagnetic information can be used to assess components of vertical-axis rotation (Magill and others, 1982; Hudson and Geissman, 1987, 1991; Wells and Hillhouse, 1989; Rosenbaum and others, 1991). This report describes paleomagnetic data from the Miocene Hiko Tuff obtained to assess the importance of vertical-axis rotation of fault blocks in an area of southeastern Nevada (fig. 1). These data suggest that rocks within an area including and extending at least 15 km north of the sinistral Pahranagat shear system in the South Pahroc Range were affected by 15°–20° of counterclockwise vertical-axis rotation.

ACKNOWLEDGMENTS

Laboratory analyses for this study were conducted by W.C. Rivers and S. Morikawa, whose services are greatly appreciated. Discussions with C.S. Grommé during the course of this study have been particularly helpful. Useful reviews were provided by G.J. Calderone and H.R. Blank, Jr.

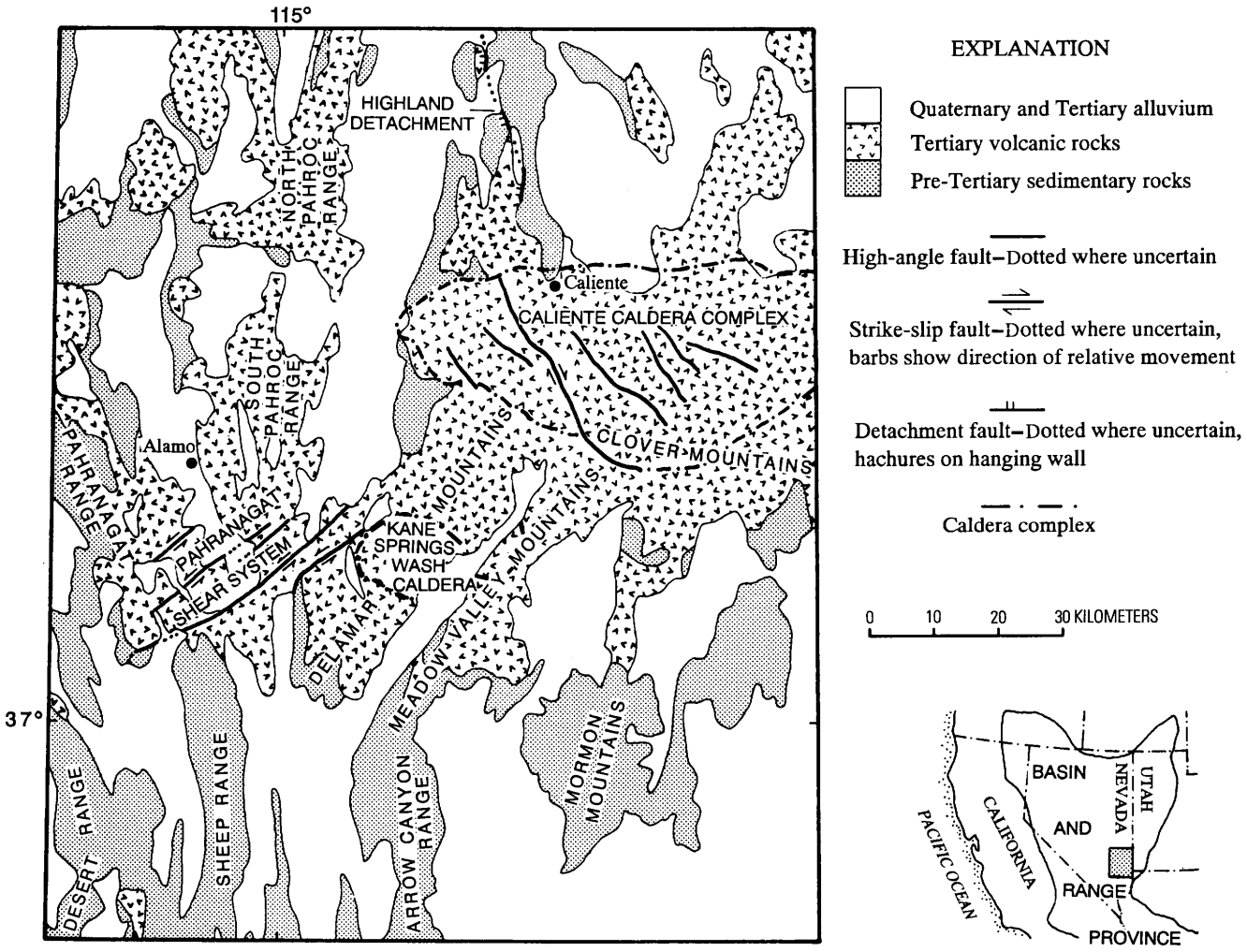

Figure 1. Generalized geology of southeastern Nevada. Only selected faults are shown.

GEOLOGIC SETTING

Within the Basin and Range province in southeastern Nevada (fig. 1), regions that were only mildly tilted and faulted during Cenozoic deformation contrast with more highly extended regions. This study compares paleomagnetic data from relatively undeformed Tertiary strata in the Meadow Valley and southern Delamar Mountains with data from equivalent rocks from more extended regions in the adjacent South Pahroc and Chief Ranges (fig. 1). Tertiary volcanic strata in this region overlie Paleozoic rocks, commonly with angular unconformity (Tschanz and Pampeyan, 1970). Tertiary rocks predominantly are Oligocene to Miocene silicic ash-flow tuffs (Cook, 1960, 1965; Ekren and others, 1977; Best and others, 1989; Scott and others, this volume). Although Oligocene ash-flow tuffs erupted from calderas outside the study area (Best and others, 1989), two Miocene caldera complexes lie within the area. The Caliente caldera complex was the source of several calc-alkaline ash-flow tuffs (Williams, 1967; Noble and McKee, 1972; Ekren and others, 1977; Rowley and Siders, 1988) between about 23 and 17 Ma. The younger Kane Springs Wash volcanic center includes the 14–Ma Kane Springs Wash caldera (Noble and others, 1968; Novak, 1984) and a probable precursor caldera (Scott and others, 1991) that erupted mildly peralkaline ash-flow tuffs between about 15 and 14 Ma.

The Hiko Tuff is a rhyolitic ash-flow tuff erupted from the western Caliente caldera complex (Ekren and others, 1977; Rowley and Siders, 1988). The Miocene Hiko Tuff (Dolgoff, 1963) was selected for paleomagnetic study because it is lithologically distinctive, widely distributed, and sufficiently old to have been involved in much Cenozoic deformation of the area. Taylor and others (1989) concluded that the best estimated $^{40}Ar/^{39}Ar$ age for Hiko Tuff is 18.6 Ma based on unpublished data of D.R. Lux and W.J. Taylor. In many regions the outflow Hiko Tuff appears to be a simple cooling unit lacking evidence of significant internal cooling breaks (Dolgoff, 1963). In the central and northern South Pahroc Range, however, outflow Hiko Tuff is notably thicker than elsewhere, and its basal portions are anomalously lithic

rich. In this area, the Hiko Tuff appears to be a compound cooling unit with cooling breaks indicated by small reversals of degree of welding and by the presence of multiple vitrophyres.

Cenozoic deformation of the study area was heterogeneous in both style and degree. Tertiary volcanic rocks are least deformed in the southern Delamar and Meadow Valley Mountains, where generally west dipping normal faults are widely spaced and volcanic strata are generally east dipping at less than 15°. Only narrow zones within this belt are more highly deformed. In areas due north of the Kane Springs Wash caldera, including the Caliente caldera complex, rocks are broken by numerous northwest-striking faults having both dextral and normal components of slip (Bowman, 1985; Michel-Noel and others, 1990; Scott and others, 1990). Caldera formation was in part coeval with activity of these faults (Rowley and others, 1990; Rowley and others, 1992; Snee and others, 1990). Still farther north, Tertiary volcanic rocks are present in several east-tilted normal-fault blocks that lie in the upper plate of the Highland detachment fault of Axen and others (1988). Several northeast-striking sinistral faults that constitute the Pahranagat shear system (Tschanz and Pampeyan, 1970; Ekren and others, 1977) separate the southern Delamar Mountains from the South Pahroc Range. Tschanz and Pampeyan estimated total sinistral displacement across the shear system to be about 16 km. North of the Pahranagat shear system, along the east side of the South Pahroc Range, Tertiary rocks are broken by numerous closely spaced normal faults and are tilted as much as 30° to the east (Scott and others, 1993). Farther west in the South Pahroc Range, the volcanic rocks dip more gently.

METHODS

We collected all samples for the paleomagnetic study with a portable rock drill, orienting them with a clinometer and both magnetic and solar compasses. Most sites consisted of seven to nine samples collected over several tens of square meters. Forty-three samples at one site spanned 235 m through a thick stratigraphic section of Hiko Tuff to assess possible intraunit dispersion of remanent magnetization directions. Averaging 3 to 10 independent measurements of compaction foliations gave stratal attitudes for the sites. These attitudes were generally concordant with independently derived attitudes obtained from field measurements of contact surfaces or from attitudes calculated from the geometric trace of contacts across topography.

The laboratory procedure subjected samples to progressive alternating field demagnetization. Six or more samples from each site were demagnetized at eight steps to peak inductions of 80 mT (millitesla). We plotted demagnetization results on vector diagrams and determined directions of components by principal component analysis (Kirschvink, 1980) for visually linear segments. For most samples, demagnetization path trajectories visually trended toward the origin of vector diagrams, and we included the zero magnetization value (representing the diagram origin) as an additional data point in principal component analysis. We calculated site mean directions and their dispersion parameters (table 1) using statistics of Fisher (1953) and corrected site mean directions for tectonic tilt by rotation about their strike axes.

PALEOMAGNETIC RESULTS

The Hiko Tuff carries a component of remanent magnetization interpreted to be a thermoremanent magnetization acquired during cooling of the tuff after deposition. For most samples, a single reverse-polarity component of magnetization was isolated at demagnetization levels greater than 15 mT (fig. 2*A*, *B*). These characteristic components have well-grouped directions within a site, as shown by the high values (typically exceeding 100) of the site mean concentration parameter, k (Fisher, 1953, table 1). At some sites the characteristic component was overprinted to a variable extent by a low-coercivity, large-moment component that is interpreted to be a lightning-induced isothermal remanent magnetization (fig. 2*C*). Data for 10 samples for which demagnetization did not convincingly remove lightning-induced magnetization components were omitted from site mean calculations. For samples from a few sites (for example, B90–14), demagnetization path trajectories slightly missed the origin of vector diagrams (fig. 2*D*), indicating that a low-moment, high-coercivity component of magnetization having a direction different than the characteristic component was present in these samples. The maximum offsets of demagnetization trajectories from diagram origins, however, are small relative to the magnitude of the characteristic components, and thus potential contamination of characteristic directions by the high-coercivity component is unlikely to be significant. Principal component analysis for samples with this type of demagnetization behavior did not include the origin. At one site (B90–27) the Hiko was highly altered, and the component of magnetization isolated during demagnetization was more dispersed and of greatly different direction than at other sites. Results from this site were excluded from further analysis because they probably reflect at least partial remagnetization during alteration.

Dispersion of Hiko site mean directions is reduced by tilt correction (fig. 3). For averages of the 30 site mean directions, k increases from 17 to 46 after tilt correction. Declinations of the tilt-corrected site means, however, still vary from 125.6° to 181.8°. The k values based only on inclinations (McFadden and Reid, 1982), which are more appropriate to examine if the Hiko Tuff was affected by vertical-axis rotation, increased from 20 to 85 after tilt correction. The increase of k values after tilt correction is in

Table 1. Paleomagnetic data from the Miocene Hiko Tuff, southeastern Nevada.

[N/No, number of samples accepted/number of samples demagnetized; R, resultant vector length; *k*, concentration parameter (Fisher, 1953); α_{95}, radius of 95 percent confidence cone about mean; Du, Iu, uncorrected declination and inclination of site mean; St/Dp, strike and dip of site (dip direction 90° clockwise from strike); Dc, Ic, tilt-corrected declination and inclination of site mean; VAR, vertical-axis rotation with respect to reference direction with 95 percent confidence limits (Demarest, 1983) (positive and negative values indicate clockwise and counterclockwise rotation, respectively]

Site	Lat °N	Long °W	N/No	R	α_{95}	*k*	Du	Iu	St/Dp	Dc	Ic	VAR
B90-1[RD]	37.0833	114.8680	6/8	5.9900	3.0	501	155.8	-55.5	285/4.5	159.5	-51.9	-6.1 ± 7.7
B90-3[RD]	37.2100	114.8585	8/8	7.9852	2.6	475	178.9	-52.3	235/16	170.8	-38.4	+5.2 ± 7.2
B90-6[RD]	37.2083	114.9563	8/8	7.9837	2.7	430	165.7	-47.2	0/0	165.7	-47.2	+0.1 ± 7.4
B90-7[RD]	37.2098	114.9662	8/8	7.9855	2.5	482	151.7	-65.6	270/30	165.7	-38.4	+0.1 ± 7.1
B90-8[RD]	37.0665	114.7510	7/7	6.9946	1.8	1117	180.8	-47.1	175/15	164.7	-46.5	-0.9 ± 7.0
B90-9	37.2260	114.9823	8/8	7.9116	6.3	79	184.7	-45.0	193/3	181.8	-44.4	+16.2 ± 9.6
B90-10	37.2318	114.9980	8/8	7.9622	4.1	185	138.6	-28.3	13/35	161.5	-53.0	-4.1 ± 8.5
B90-11	37.2587	114.9667	8/8	7.9661	3.9	207	144.6	-23.4	359/17	152.4	-32.1	-13.2 ± 7.6
B90-12	37.2678	114.9685	8/8	7.9828	2.8	407	134.8	-44.8	335/16	151.5	-48.1	-14.1 ± 7.4
B90-13	37.2630	114.9273	7/7	6.9934	2.0	916	160.5	-41.5	32/11	168.1	-49.7	+2.5 ± 7.1
B90-14	37.2958	114.8867	8/8	7.9580	4.3	167	107.4	-31.5	325/26	125.6	-44.2	-40.0 ± 8.2
B90-15	37.2725	114.9933	6/8	5.9837	3.8	307	157.4	-53.3	343/15	177.3	-52.1	+11.7 ± 8.3
B90-16	37.2705	115.0000	6/8	5.9900	3.0	501	100.6	-58.1	276/15	133.0	-48.7	-32.6 ± 7.6
B90-17	37.2840	114.9960	6/8	5.9564	6.1	123	131.2	-34.8	352/26	151.5	-48.4	-14.1 ± 9.8
B90-18	37.3090	114.9882	8/8	7.9636	4.0	192	133.3	-33.9	15/19	142.7	-49.9	-22.9 ± 8.3
B90-19	37.3363	114.9423	8/8	7.9862	2.5	506	140.0	-28.3	15/24	152.3	-46.6	-13.3 ± 7.3
B90-20	37.3422	114.9973	7/7	6.9899	2.5	595	123.2	-38.7	343/29	150.4	-52.1	-15.2 ± 7.4
B90-21	37.3658	114.9977	8/8	7.9655	3.9	203	130.1	-34.1	341/24	148.3	-43.2	-17.3 ± 7.9
B90-22[l]	37.3698	114.9747	8/8	7.9916	1.9	835	130.2	-51.2	287/9	139.4	-47.0	-26.2 ± 7.0
B90-23[l]	37.3632	114.9658	8/8	7.9900	2.1	698	121.8	-16.9	0/17	126.1	-31.0	-39.5 ± 7.0
B90-24[l]	37.4110	114.9978	8/8	7.9760	3.3	291	138.4	-33.0	0/0	138.4	-33.0	-27.2 ± 7.4
B90-25	37.4333	114.9993	8/8	7.9865	2.4	519	151.2	-46.3	0/0	151.2	-46.3	-14.4 ± 7.2
B90-26[*]	37.3533	114.7623	8/8	7.9770	3.2	305	102.1	-61.5	294/36	157.1	-50.2	-8.5 ± 7.7
B90-27[*]	37.3717	114.7725	7/8	6.8535	9.5	41	171.5	68.0	20/82	129.2	-2.7	-36.4 ± 10.0
B90-28	37.4173	114.9385	8/8	7.8959	6.8	67	124.7	-16.7	11/27	131.6	-40.9	-34.0 ± 9.7
B90-29	37.4395	114.9417	8/8	7.9864	2.5	513	130.2	-23.7	14/33	144.7	-51.7	-20.9 ± 7.4
B90-30	37.5033	114.9290	7/8	6.9923	2.2	783	140.9	-34.0	1/25	159.7	-47.1	-5.9 ± 7.2
B90-32	37.6974	114.6655	8/8	7.9619	4.1	184	125.5	-30.0	338/37	152.5	-42.8	-13.1 ± 8.0
B90-33	37.7696	114.5967	6/7	5.9830	3.9	294	127.2	-47.7	340/30	165.5	-55.4	-0.1 ± 8.6
B90-34	37.7939	114.5993	9/9	8.9853	2.2	545	154.9	-39.9	11/14	166.4	-47.0	+0.8 ± 7.2
B91-6 (all)	37.3908	114.9992	43/43	42.5711	2.2	98	138.8	-44.2	196/3	137.3	-41.7	-28.3 ± 7.3
(lower)			20/20	19.8600	2.8	136	131.6	-41.1		130.6	-38.4	-35.0 ± 7.5
(upper)			23/23	22.9195	1.8	273	145.5	-46.5		143.7	-44.1	-21.9 ± 7.2
Reference direction				4.9738	6.2	153				165.6	-44.5	

[RD] Site used to calculate reference direction.
[l] Site that probably sampled the lower cooling unit of the Hiko Tuff in the South Pahroc Range.
[*] Site from altered Hiko whose mean was not used for further analysis.

both cases statistically significant and yields a positive fold test (McElhinny, 1964) at the 99 percent confidence level based on an F-test of *k* ratios (Watson, 1956). Although McElhinny's (1964) fold test makes assumptions that may be invalid in detail (McFadden and Jones, 1981), it generally errs by being too conservative. These results indicate that characteristic magnetizations in the Hiko predated tectonic tilting.

An atypically thick section of outflow Hiko Tuff that was present in parts of the South Pahroc Range was sampled at site B91–6 to assess any stratigraphically controlled change of remanent magnetization direction. In this stratigraphic section, a relatively thick zone of poorly welded, lithic-rich basal tuff grades upward into densely welded vitrophyre, about 15 m thick, which in turn grades upward into a platy-weathering devitrified tuff. Still farther upward, a second thinner (about 2 m thick) densely welded vitrophyre is present which also grades upward into devitrified tuff. Lithic content of the tuff appeared to decrease in the vicinity of this second vitrophyre, although this was not quantified. The upper devitrified tuff contains two topographic ledges separated by a mostly covered interval. The upper

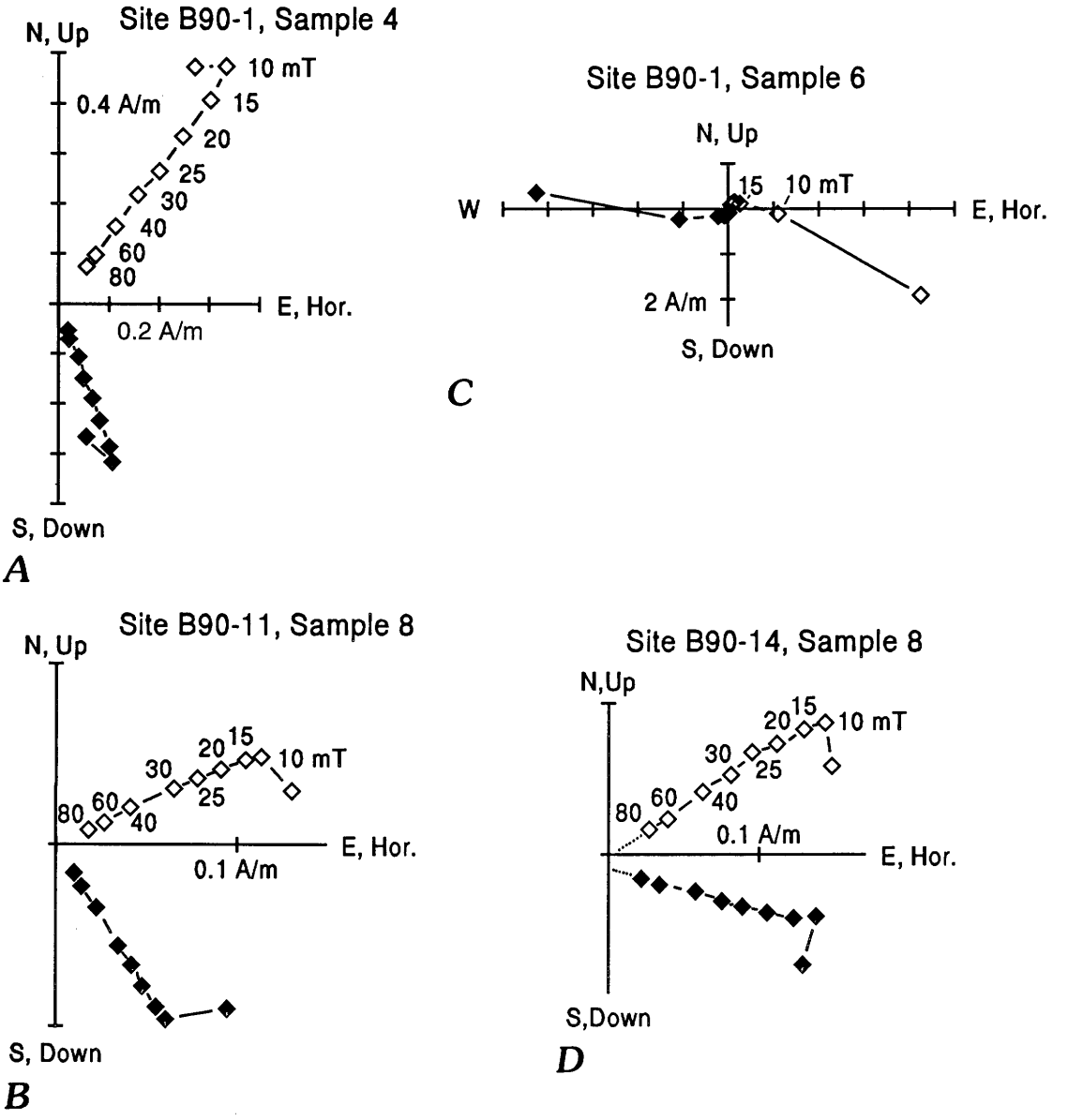

Figure 2. Representative orthogonal demagnetization diagrams, uncorrected for tectonic tilt, from the Miocene Hiko Tuff. Solid diamond, projection on horizontal plane; open diamond, projection on vertical plane. *A*, *B*, Typical demagnetization behavior. *C*, Lightning-induced magnetization overprinting the characteristic magnetization. The trajectory of the horizontal demagnetization path (dashed line) for *D* does not intersect the origin, indicating presence of small-magnitude component of different direction than the characteristic magnetization. Demagnetization levels are given in millitesla (mT). Magnetizations are given in Amperes/meter (A/m). Scales are the same for both axes of each diagram.

ledge forms the ridge crest. Forty-three samples were collected, starting in the basal poorly welded part, spanning about a 235-m thickness of the Hiko Tuff, and stopping about 30 m below the top of the upper topographic ledge to avoid lightning-prone areas.

Declinations and inclinations of remanent magnetizations for the 43 samples show systematic changes when displayed versus height (fig. 4). A shift in declination is present near the level of the second vitrophyre (fig. 4*A*). The average declination of 20 samples below the vitrophyre is 130.6°, whereas the average declination of 23 samples above this horizon is 143.7°. The general concordance of this declination shift with the second vitrophyre and an apparent upward decrease in lithic content suggest that a complete cooling break occurred between deposition of these lower and upper parts of the Hiko. Sufficient time must have elapsed between emplacement of the lower and higher flows to allow a detectable change of the geomagnetic field direction. The exact

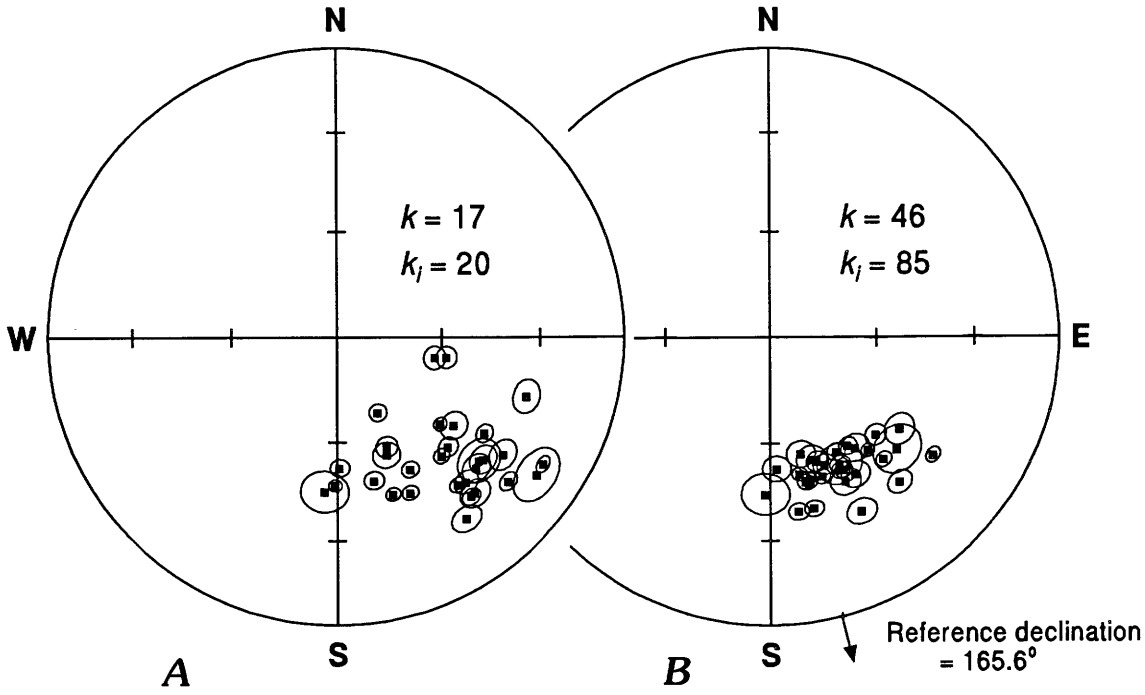

Figure 3. Equal-area projections of *A*, uncorrected, and *B*, tilt-corrected site mean directions for the Hiko Tuff with their associated cones of 95 percent statistical confidence. All projections are on the upper hemisphere. Values for k are concentration parameters (Fisher, 1953) for an average of the site mean directions. Values for k_i are concentration parameters based solely on inclinations (McFadden and Reid, 1982) of the site mean directions. In *B*, arrow labeled 165.6° represents the declination of the reference direction calculated for the Hiko Tuff (table 1).

location of the cooling break is debatable because declinations of three samples beneath the second vitrophyre, down to the 90-m level, are intermediate between mean declinations for the lower and upper units. The cooling break could occur as low as the 90-m level. Alternatively, the cooling break could lie just beneath the second vitrophyre and the intermediate declinations of the underlying samples might be caused by a partial remagnetization of the top of the underlying cooling unit.

Inclinations of remanent magnetizations vary in a more complicated way through the section (fig. 4*B*). The postulated cooling break near the second vitrophyre is less marked as a change in inclination, although the lower part has, on average, shallower inclinations than the upper part (fig. 4*C*). Systematic variations of inclination, however, exist within both the lower and upper parts of the Hiko. We suspect that these variations may reflect inclination shallowing caused by rotation of magnetic grains at temperatures below their magnetic blocking temperatures during welding, as was documented by Rosenbaum (1986) for a silicic welded ash-flow tuff from southwestern Nevada. Post-blocking welding explains particularly well the inclination pattern of the lower lithic-rich unit, in which inclinations in the lowest poorly welded tuff are steepest but shallow upward to a minimum within the vitrophyre and then gradually steepen upwards toward the devitrified top of the flow. Two steepening-upward intervals are seen in inclination data from the upper part of the Hiko, with the maximum of the lower interval present in samples from the top of the first topographic ledge. This inclination pattern, if interpreted in terms of a welding-related shallowing, implies that the upper part of the Hiko at this section contains two flows separated by a short cooling break that presently lies within a mostly covered interval between the two topographic ledges (that is, the upper cooling unit of the Hiko is compound). However, if a hiatus occurred during deposition of the upper part of the Hiko, it was not recorded as a detectable difference of remanence declination.

The recognition that, at least locally, separate cooling units of the Hiko recorded two geomagnetic field directions, and that inclinations of magnetizations within these cooling units may have been shallowed during welding may explain some dispersion that remains among the tilt-corrected site means of figure 3. In particular, although tilt-corrected inclinations of Hiko site mean directions cluster at about –48° (fig. 3), inclinations of several site mean directions are significantly shallower (as low as –28°). These low inclinations may largely be due to welding-related shallowing and (or) to a shallower geomagnetic field inclination recorded by the lower cooling unit. Likewise, an approximately 13° difference between the declinations of magnetizations from the lower and upper parts of the Hiko Tuff in the thick section can explain some, although not all,

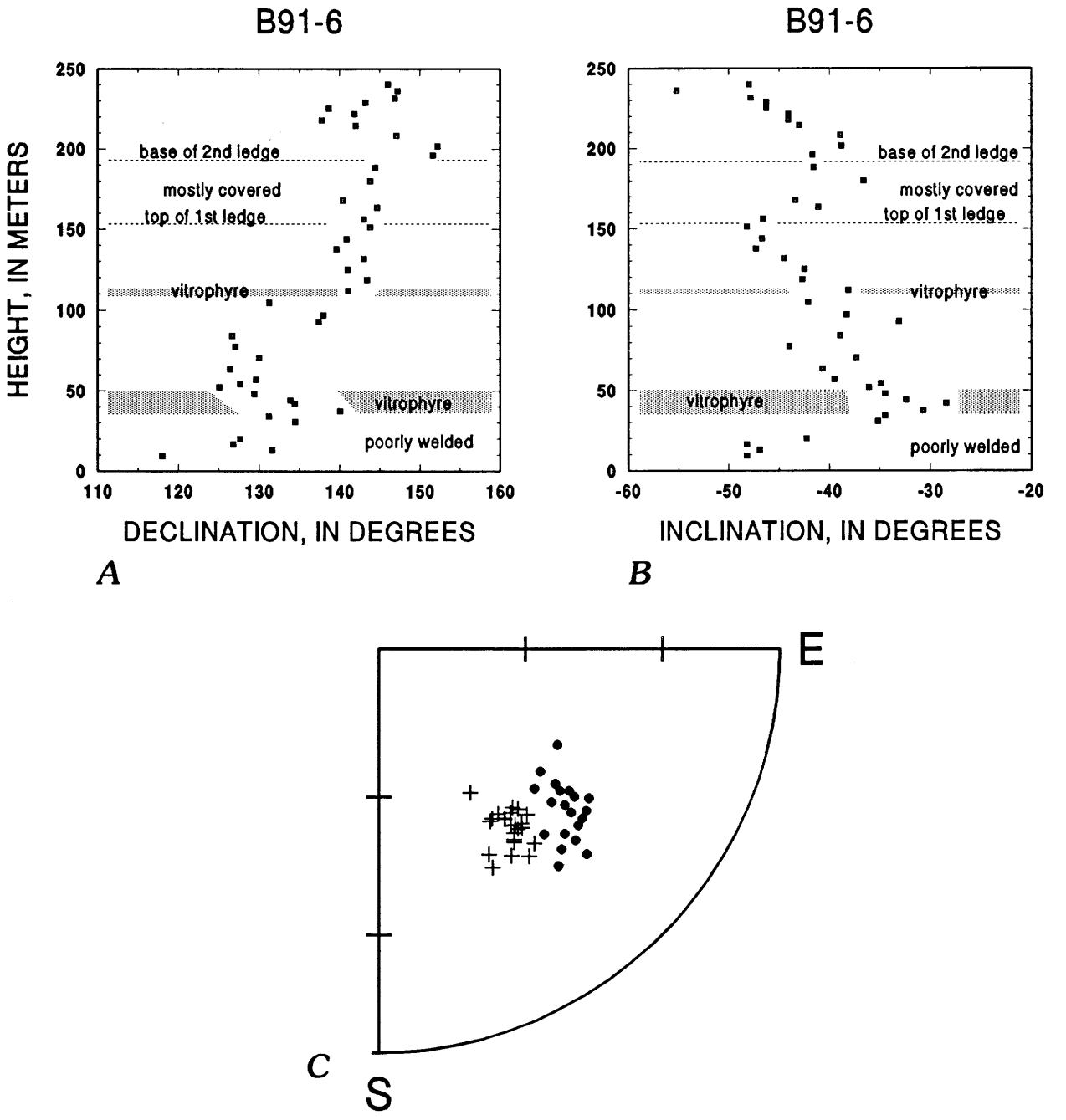

Figure 4. Paleomagnetic data from the stratigraphic section of Hiko Tuff sampled at site B91–6. *A*, Declinations of remanent magnetizations versus sample height. *B*, Inclinations of remanent magnetizations versus sample height. *C*, Directions of remanent magnetizations from lower (solid dot) and upper (plus) parts of the tuff on an equal-area net. Projections are on the upper hemisphere.

of the approximately 56° range of declinations (125.6° to 181.8°) among the tilt-corrected Hiko site means.

DISCUSSION

If vertical-axis rotation has affected some sites where we sampled the Hiko Tuff, this may be apparent from the declinations of their tilt-corrected site means. To determine relative vertical-axis rotation (VAR), we have compared individual site mean directions to a reference direction (D=165.6°, I=–46.0°, α_{95}=6.2°) calculated by averaging five site mean directions from the relatively little deformed southern Delamar and Meadow Valley Mountains (table 1). If samples from all sites initially recorded the same geomagnetic field direction, then the difference between the declination of individual site means and the declination of the reference direction is, within error limits, an estimate of relative vertical-axis rotation of the individual sites. The potential complication raised by comparison of results from

noncontemporaneous cooling units of the Hiko Tuff, such as found at site B91–6, is discussed later in this section. The VAR values for individual sites calculated with respect to the reference direction (fig. 5) range from +11.7° to –40.0°, where positive and negative VAR values suggest clockwise and counterclockwise rotations, respectively. Uncertainties for such rotation estimates (table 1) can be partly quantified as functions of the dispersions and inclinations of the individual site and reference mean directions (Demarest, 1983). This type of analysis, however, does not account for possible errors introduced by tilt corrections for individual sites, which may be significant for some ash-flow tuffs (Hagstrum and Gans, 1989; Rosenbaum and others, 1991). Tilt-correction errors for individual sites in the Hiko Tuff are difficult to quantify, but most are probably less than 10° considering (1) the general concordance of attitudes estimated from compaction foliations and map patterns and (2) the conformable stratigraphic relations of the Hiko Tuff with underlying and overlying ash-flow tuffs throughout the region of study. For the five individual site mean directions averaged to calculate the reference direction, tilt-correction errors, if random and less than about 20° (Calderone and Butler, 1991), should partly cancel and increase dispersion about the reference mean. Therefore, the VAR uncertainties of table 1 may at least partly account for tilt-correction error of the reference direction.

The VAR values obtained from the Hiko Tuff paleomagnetic data suggest several points of tectonic interest. Tilt-corrected mean directions for the five sites from the southern Delamar and Meadow Valley Mountains that were used to derive the reference direction show little dispersion of declinations (table 1; fig. 5). This observation suggests that these sites probably were in the same cooling unit of the Hiko Tuff and that there was little relative vertical-axis rotation between the sites. These points justify the use and combination of data from these five sites to estimate a reference direction. The declination of the reference mean (165.6°) is similar, although slightly clockwise of declinations of site means for the Hiko at Condor Canyon (D=162.5°) and White River Narrows (D=157.9°) sections to the northeast and northwest of our study area, respectively (C.S. Grommé, written commun., 1990).

Small VAR values for three sites (B90–32, B90–33, and B90–34) from tilted fault blocks that lie above the Highland detachment fault west of the Chief Range suggest that these sites experienced little or no significant vertical-axis rotation, assuming the Hiko Tuff here is the same cooling unit as was sampled in the reference sites. This result suggests that rotation of fault blocks above the Highland detachment fault occurred principally as tilt about their strike axes.

In contrast, a band of sites distributed over approximately 30 km from just northwest of the stable southern Delamar Mountains into the South Pahroc Range have moderate but consistently negative VAR values (table 1, fig. 5). For most sites these VAR values range between –15° and –20°. These data imply that much of the South Pahroc Range was affected by moderate counterclockwise vertical-axis rotation. There is no obvious difference between the magnitude or range of estimated rotation for sites within and north of the Pahranagat shear system. A mean direction of all 18 sites (B90–10–12, 15–25, 28–30, B91–6) that lie within or north of the shear system (D=146.4°, I=–45.8°, α_{95}=4.7°) suggests counterclockwise rotation of 19.2°±8.7° of this area with respect to the southern Delamar Mountains. This conclusion must be further qualified, however, because it is likely that not all sites in the South Pahroc Range sampled the same cooling unit. Results from site B91–6 (fig. 4) show that the declination of remanence in the lower cooling unit is 13° counterclockwise of that recorded by the upper cooling unit. A moderately negative VAR value that does not reflect tectonic rotation could be calculated if a site mean direction from the lower cooling unit was compared to a reference direction derived from sites in the upper cooling unit.

Several lines of evidence suggest that the declination discordance of most sites from the South Pahroc Range with respect to the reference direction derived from sites in the southern Delamar and Meadow Valley Mountains is due to tectonic rotation rather than to an inappropriate comparison of data from different cooling units of the Hiko Tuff. For site B91–6, VAR estimates for both the lower and upper cooling units of the Hiko are significant (–35.0°±7.5° and –21.9°±7.2°, respectively), and the value from the upper unit is more typical of those for most sites in the South Pahroc Range. We believe that several other sites with significant negative VAR values (for example, B90–11, B90–17, B90–20–22) were in the upper part of the Hiko because of their position within a few tens of meters of the upper contact of the tuff. Conversely, we are fairly certain that two sites (B90–23 and B90–24) sampled the lower cooling unit of the Hiko Tuff on the basis of their location within basal, lithic-rich vitrophyres of thick sections of Hiko Tuff near the B91–6 section. Both sites B90–23 and B90–24 have VAR values (–39.5° and –27.2°, respectively) that are greater than typical for this area (for example, –17.3° to –26.2° from sites B90–21, B90–22, upper B91–6) and both sites have anomalously shallow

Figure 5 (facing page). Generalized geology for part of southeastern Nevada and estimates of vertical-axis rotation (angle between line and geographic north) for individual sites from the Hiko Tuff. Location of reference sites shown by squares whereas remaining sites are shown by dots. Amount of rotation is the angle between the declination of an individual site mean and the declination for the Hiko reference mean. Numbers by site locations are keyed to individual B90 sites on table 1. Two rotation estimates shown for site B91–6 are calculated from means from the lower and upper parts of the Hiko Tuff.

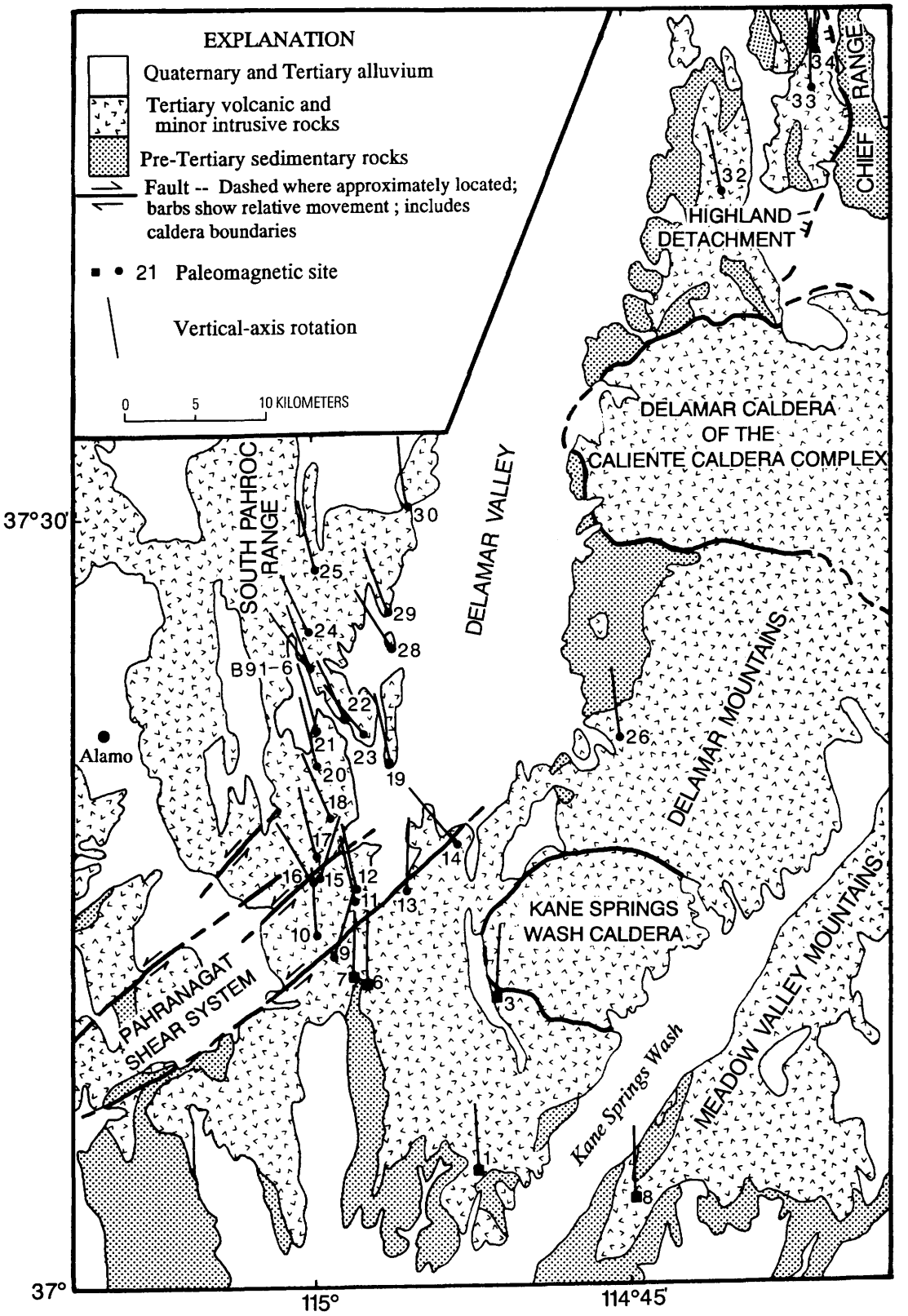
EXPLANATION
Quaternary and Tertiary alluvium
Tertiary volcanic and minor intrusive rocks
Pre-Tertiary sedimentary rocks
Fault -- Dashed where approximately located; barbs show relative movement ; includes caldera boundaries
21 Paleomagnetic site
Vertical-axis rotation
0 5 10 KILOMETERS
CHIEF RANGE
HIGHLAND DETACHMENT
DELAMAR CALDERA OF THE CALIENTE CALDERA COMPLEX
DELAMAR VALLEY
SOUTH PAHROC RANGE
DELAMAR MOUNTAINS
KANE SPRINGS WASH CALDERA
MEADOW VALLEY MOUNTAINS
PAHRANAGAT SHEAR SYSTEM
Kane Springs Wash
Alamo
B91-6
37°30'
37°
115°
114°45'

inclinations (–31° and –33°, respectively). In the B91–6 section, inclinations this shallow were found only in the basal vitrophyre of the lower cooling unit (fig. 4*B*). If mean directions from sites B90–23 and B90–24 are omitted and the mean direction from only the upper part of B91–6 is used, the average of mean directions from the remaining 16 sites that lie within or north of the shear system is D=149.1°, I=–47.4°, α_{95}=4.1°. This mean direction suggests a revised average counterclockwise rotation of –16.5°±8.4° of this area with respect to the southern Delamar Mountains. These VAR calculations assume that the reference sites were in the upper cooling unit of the Hiko Tuff. If, instead, the reference sites were in the lower cooling unit of the Hiko, VAR values calculated for sites from the upper part of the Hiko would underestimate counterclockwise vertical-axis rotation by about 13°.

Paleomagnetic data from the Hiko Tuff suggest that parts of the South Pahroc Range were affected not only by sinistral offset along northeast-striking faults of the Pahranagat shear system but also by counterclockwise rotation of fault blocks within and north of the identified shear system. We interpret this sinistral shear to have accommodated a difference in extension between the mildly extended southern Delamar Mountains and the more extended terrane of the South Pahroc Range to the northwest. If the sinistral shear zone trends roughly east-west, its width must be at least 30 km to encompass the northward extent of sites where counterclockwise rotation has been inferred. Gibbs (1984) used the term "transfer fault" to describe a discrete fault having a substantial strike-slip component of offset that has acted to transmit extensional displacement between spatially offset loci of extension. We suggest that both counterclockwise block rotation and displacement along sinistral faults in the South Pahroc Range are deformation components of a broad "transfer zone" that transmitted extensional strain from areas north and northeast of the relatively stable southern Delamar Mountains to areas to the southwest (perhaps to highly extended areas west of the Sheep Range (Guth, 1981; Guth and others, 1988)).

CONCLUSIONS

Paleomagnetic data from the 18.6 Ma Hiko Tuff allow constraints to be placed on components of vertical-axis rotation of fault blocks in an area of southeastern Nevada. A mean direction of five sites from the relatively little deformed southern Delamar and Meadow Valley Mountains was used as a reference direction for comparison with paleomagnetic data from more deformed adjacent areas. Tilt-corrected directions for three sites from fault blocks above the Highland detachment fault, west of the Chief Range, are little different from the reference direction, indicating that rotation of these blocks principally occurred by tilt about their strike axes. Mean directions of sites distributed over a 30-km-long belt extending into the South Pahroc Range from the southern Delamar Mountains are rotated moderately but consistently counterclockwise from the reference direction. Interpretation of these data is complicated by recognition of a lower cooling unit of the Hiko Tuff in parts of the South Pahroc Range that recorded a declination of remanent magnetization that is about 13° counterclockwise from magnetizations in the overlying Hiko. Comparisons to data from sites that were probably restricted to either upper or lower parts of the Hiko suggests that about 15°–20° of the declination discordance found at sites from the South Pahroc Range was probably caused by counterclockwise vertical-axis rotation of fault blocks. Areas affected by counterclockwise rotation include but also extend north of a system of northeast-striking sinistral faults of the Pahranagat shear system. Sinistral shear accommodated by counterclockwise rotation and displacement on northeast-striking faults is interpreted to have occurred within a broad transfer zone that transmitted extensional strain from areas northeast of the relatively stable southern Delamar Mountains to areas to the southwest.

REFERENCES CITED

Axen, G.J., Lewis, P.R., Burke, K.J., Sleeper, K.G., and Fletcher, J.M., 1988, Tertiary extension in the Pioche area, Lincoln County, Nevada, *in* Bartley, J.M., Axen, G.J., Taylor, W.J., and Fryxell, J.E., Cenozoic tectonics of a transect through eastern Nevada near 38° N latitude, *in* Weide, D.L., and Faber, M.L., eds., This extended land—Geological journeys in the southern Basin and Range: Geological Society of America Cordilleran Section Field Trip Guidebook, p. 3–5.

Best, M.G., Christiansen, E.H., Deino, A.L., Grommé, C.S., McKee, E.H., and Noble, D.C., 1989, Eocene through Miocene volcanism in the Great Basin of the western United States: New Mexico Bureau of Mines and Mineral Resources Memoir 47, Excursion 3A, p. 91–133.

Bowman, S.A., 1985, Miocene extension and volcanism in the Caliente caldera complex, Lincoln County, Nevada: Golden, Colo., Colorado School of Mines M.S. thesis, 143 p.

Calderone, G.J., and Butler, R.F., 1991, The effects of noise due to random undetected tilts and paleosecular variation on regional paleomagnetic directions: Journal of Geophysical Research, v. 96, p. 3973–3977.

Cook, E.F., 1960, Geologic atlas of Utah—Washington County: Utah Geological and Mineralogical Survey Bulletin 70, 119 p.

———1965, Stratigraphy of Tertiary volcanic rocks in eastern Nevada: Nevada Bureau of Mines Report 11, 61 p.

Demarest, H.H., 1983, Error analysis for the determination of tectonic rotation from paleomagnetic data: Journal of Geophysical Research, v. 88, p. 4321–4328.

Dolgoff, Abraham, 1963, Volcanic stratigraphy of the Pahranagat area, Lincoln County, southeastern Nevada: Geological Society of America Bulletin, v. 74, p. 875–900.

Ekren, E.B., Orkild, P.P., Sargent, K.A., and Dixon, G.L., 1977, Geologic map of Tertiary rocks, Lincoln County, Nevada: U.S. Geological Survey Miscellaneous Investigations Series Map I–1041, scale 1:250,000.

Emmons, W.H., and Garrey, G.H., 1910, General geology, *in* Ransome, F.L., ed., Geology and ore deposits of the Bullfrog District: U.S. Geological Survey Bulletin 407, p. 19–89.

Fisher, R.A., 1953, Dispersion on a sphere: Royal Society of London Proceedings, v. A217, p. 295–305.

Gibbs, A.D., 1984, Structural evolution of extensional basin margins: Geological Society of London Quarterly Journal, v. 141, p. 609–620.

Guth, P.L., 1981, Tertiary extension north of the Las Vegas Valley shear zone, Sheep and Desert Ranges, Clark County, Nevada: Geological Society of America Bulletin, v. 92, p. 763–771.

Guth, P.L., Schmidt, D.L., Deibert, Jack, and Yount, J.C., 1988, Tertiary extensional basins of northwestern Clark County, Nevada, *in* Weide, D.L., and Faber, M.L., eds., This extended land—Geological journeys in the southern Basin and Range: Geological Society of America, Cordilleran Section Field Trip Guidebook, p. 239–252.

Hagstrum, J.T., and Gans, P.B., 1989, Paleomagnetism of the Oligocene Kalamazoo Tuff—Implications for middle Tertiary extension in east central Nevada: Journal of Geophysical Research, v. 94, p. 1827–1842.

Hudson, M.R., and Geissman, J.W., 1987, Paleomagnetic and structural evidence for middle Tertiary counterclockwise block rotation in the Dixie Valley region, west-central Nevada: Geology, v. 15, p. 638–642.

———1991, Paleomagnetic evidence for the age and extent of middle Tertiary counterclockwise rotation, Dixie Valley region, west-central Nevada: Journal of Geophysical Research, v. 96, p. 3979–4006.

Kirschvink, J.L., 1980, The least-squares line and plane and analysis of paleomagnetic data: Geophysical Journal of the Royal Astronomical Society, v. 62, p. 699–718.

Magill, J.R., Wells, R.E., Simpson, R.W., and Cox, A.V., 1982, Post 12 m.y. rotation of southwestern Washington: Journal of Geophysical Research, v. 87, p. 3761–3776.

McElhinny, M.W., 1964, Statistical significance of the fold test in palaeomagnetism: Geophysical Journal of the Royal Astronomical Society, v. 89, p. 338–340.

McFadden, P.L., and Jones, D.L., 1981, The fold test in palaeomagnetism: Geophysical Journal of the Royal Astronomical Society, v. 67, p. 53–58.

McFadden, P.L., and Reid, A.B., 1982, Analysis of paleomagnetic inclination data: Geophysical Journal of the Royal Astronomical Society, v. 69, p. 307–319.

Michel-Noel, Gerard, Anderson, R.E., and Angelier, Jacque, 1990, Fault kinematics and estimates of strain partitioning of a Neogene extensional fault system in southeastern Nevada, *in* Wernicke, B.P., ed., Basin and Range extensional tectonics near the latitude of Las Vegas, Nevada: Geological Society of America Memoir 176, p. 155–180.

Noble, D.C., and McKee, E.H., 1972, Description and K-Ar ages of volcanic units of the Caliente volcanic field, Lincoln County, Nevada, and Washington County, Utah: Isochron/West, no. 5, p. 17–24.

Noble, D.C., McKee, E.H., Hedge, C.E., and Blank, H.R., Jr., 1968, Reconnaissance of the Caliente depression, Lincoln County, Nevada: Geological Society of America Special Paper 115, p. 435–436.

Novak, S.W., 1984, Eruptive history of the rhyolitic Kane Springs Wash volcanic center, Nevada: Journal of Geophysical Research, v. 89, p. 8603–8615.

Proffett, J.M., Jr., 1977, Cenozoic geology of the Yerington district, Nevada, and implications for the nature and origin of Basin and Range faulting: Geological Society of America Bulletin, v. 99, p. 247–266.

Rosenbaum, J.G., 1986, Paleomagnetic directional dispersion produced by plastic deformation in a thick Miocene welded tuff, southern Nevada: Journal of Geophysical Research, v. 91, p. 12817–12834.

Rosenbaum, J.G., Hudson, M.R., and Scott, R.B., 1991, Paleomagnetic constraints on the geometry and timing of deformation at Yucca Mountain, Nevada: Journal of Geophysical Research, v. 96, p. 1963–1979.

Rowley, P.D., Anderson, R.E., Snee, L.W., and Mehnert, H.H., 1990, Geology and structural setting of the western Caliente caldera complex, Lincoln County, Nevada: Geological Society of America Abstracts with Programs, v. 22, no. 3, p. 79–80.

Rowley, P.D., and Siders, M.A., 1988, Miocene calderas of the Caliente caldera complex, Nevada-Utah: Eos, v. 69. p. 1508.

Rowley, P.D., Snee, L.W., Mehnert, H.H., Anderson, R.E., Axen, G.J., Burke, K.J., Simonds, F.W., Shroba, R.R., and Olmore, S.D., 1992, Structural setting of the Chief Mining district, eastern Chief Range, Lincoln County, Nevada, Chapter H in Thorman, C.H., ed., Application of structural geology to mineral and energy resources of the Central and Western United States: U.S. Geological Survey Bulletin 2012, p. H1–H17.

Scott, R.B., Blank, H.R., Jr., and Page, W.R., 1991, Evidence for a precursor to the Kane Springs Wash caldera, Lincoln County, Nevada: Geological Society of America Abstracts with Programs, v. 23, no. 4, p. 91.

Scott, R.B., Swadley, W C, and Novak, S.W., 1993, Geologic map of the Delamar Lake quadrangle, Lincoln County, Nevada: U.S. Geological Survey Geologic Quadrangle Map GQ–1730, scale 1:24,000.

Scott, R.B., Swadley, W C, Page, W.R., and Novak, S.W., 1990, Preliminary geologic map of the Gregerson Basin quadrangle, Lincoln County, Nevada: U.S. Geological Survey Open-File Report 90–646, scale 1:24,000.

Snee, L.W., Mehnert, H.H., Rowley, P.D., Anderson, R.E., and Scott, R.B., 1990, New isotopic ages demonstrate extensional faulting of 19–12 Ma in the western Caliente caldera complex and vicinity, Lincoln County, Nevada: Eos, v. 71, p. 1612.

Taylor, W.J., Bartley, J.M., Lux, D.R., and Axen, G.J., 1989, Timing of Tertiary extension in the Railroad Valley–Pioche transect, Nevada—Constraints from $^{40}Ar/^{39}Ar$ ages of the volcanic rocks: Journal of Geophysical Research, v. 94, p. 7757–7774.

Thompson, G.A., 1960, Problem of late Cenozoic structure of the Basin Ranges, *in* Proceedings of the 21st International Geological Congress, Copenhagen: v. 18, p. 62–68.

Tschanz, C.M., and Pampeyan, E.H., 1970, Geology and mineral deposits of Lincoln County, Nevada: Nevada Bureau of Mines and Geology Bulletin 73, 188 p.

Watson, G.S., 1956, Analysis of dispersion on a sphere: Monthly Notices of the Royal Astronomical Society Geophysical Supplement, v. 7, p. 153–159.

Wells, R.E., and Hillhouse, J.W., 1989, Paleomagnetism and tectonic rotation of the lower Miocene Peach Springs Tuff—Colorado Plateau, Arizona, to Barstow, California: Geological Society of America Bulletin, v. 101, p. 846–863.

Williams, P.L., 1967, Stratigraphy and petrography of the Quichapa Group, southwestern Utah and southeastern Nevada: Seattle, Wash., University of Washington Ph. D. dissertation, 182 p.

Decoupling of Mid-Tertiary Rocks, Red Hills–Western Markagunt Plateau, Southwestern Utah

By Florian Maldonado

GEOLOGIC STUDIES IN THE BASIN AND RANGE–COLORADO PLATEAU TRANSITION IN SOUTHEASTERN NEVADA, SOUTHWESTERN UTAH, AND NORTHWESTERN ARIZONA, 1992

U.S. GEOLOGICAL SURVEY BULLETIN 2056–I

UNITED STATES GOVERNMENT PRINTING OFFICE, WASHINGTON : 1995

CONTENTS

FIGURES

TABLE

Decoupling of Mid-Tertiary Rocks, Red Hills–Western Markagunt Plateau, Southwestern Utah

By Florian Maldonado

ABSTRACT

A succession of Oligocene and Miocene volcanic and volcaniclastic rocks about 610 meters thick is inferred to have been decoupled at a shallow crustal level from underlying Tertiary rocks within the Red Hills. Evidence of detachment of the upper plate along a basal low-angle shear zone is (1) a low-angle, dipping pulverized zone, interpreted as fault gouge, that separates an upper (allochthonous) plate from an underlying lower (autochthonous) plate; (2) attitudes of upper plate rocks that are steeper than those of underlying lower plate rocks and that locally dip into lower plate rocks; (3) intense faulting and fragmentation of upper plate rocks; (4) faults that appear to be restricted to the upper plate; and (5) omission of strata along the shear zone. The upper plate is overlain by blocks of megabreccia composed of chaotically mixed, upper plate rock types. These blocks are inferred to be gravity-slide blocks emplaced during decoupling and breakage of the upper plate.

Because the stratigraphy of the Red Hills is almost identical to that in the Markagunt Plateau, about 15 kilometers east of the Red Hills, and the same low-angle shear zone is also present in the Markagunt Plateau, the shear zone documented in the Red Hills may be of regional extent. The age of the shear zone is bracketed between 22.5 Ma (age of the youngest rocks in the upper plate) and 20 Ma (approximate age of dikes cutting the shear zone). The shear zone apparently formed due to decoupling of strata through tilting. Tilting may have resulted from crustal extension and associated block faulting, or from emplacement of magma at shallow depths.

INTRODUCTION

The Red Hills, approximately 20 km north-northeast of Cedar City, in southwestern Utah (fig. 1), lie along the eastern margin of the Basin and Range province, just west of the High Plateaus subprovince of the Colorado Plateaus province. In its structure, the High Plateaus subprovince is a structural transition zone between the two provinces. The Red Hills have been mapped by Thomas and Taylor (1946), Threet (1952), Rowley and Threet (1976), and most recently by Maldonado and Williams (1990, 1993a, b). The results of mapping discussed in this report are part of the Basin and Range to Colorado Plateau Transition (BARCO) Study Unit described in the Introduction to this volume.

Low-angle extensional faults (detachment faults) and associated upper plate faults in the Basin and Range province of the western United States have been described extensively (Anderson, 1971; Wernicke, 1981; Gross and Hillemeyer, 1982; Wernicke and Burchfiel, 1982; Gans and Miller, 1983; Reynolds and Spencer, 1985; Hamilton, 1988; Maldonado, 1990). Some detachment faults may extend to the middle crust and possibly deeper, as suggested by the presence of high-grade metamorphic rocks, mineral assemblages indicative of high temperature-pressure regimes, and mylonitic metamorphic fabrics in their lower (autochthonous) plates presumably acquired at depths greater than 15 km (Davis and Coney, 1979; Davis and others, 1980; Wernicke, 1981; Wernicke and Burchfiel, 1982; Davis, 1983; Hamilton, 1988). This type of faulting has not been identified in the Colorado Plateau. In this report, I present evidence of a low-angle but otherwise dissimilar shear zone and associated upper plate fault complex in the Red Hills. I stress "dissimilar," because I believe that this low-angle shear zone may have formed entirely as a shallow structure, rather than as a deep-seated detachment fault analogous to those suggested for the Basin and Range. The Red Hills shear zone probably developed at less than 2 km depth as indicated by the absence of features that would suggest formation in the middle crust (greater than 15 km). A similar shallow type of structure has been described by Pierce in Wyoming and Montana (1973, 1987).

The author first mapped the low-angle shear zone in the Red Hills (Maldonado and Williams, 1990) (fig. 2), and by inference extended it into the adjacent Markagunt Plateau

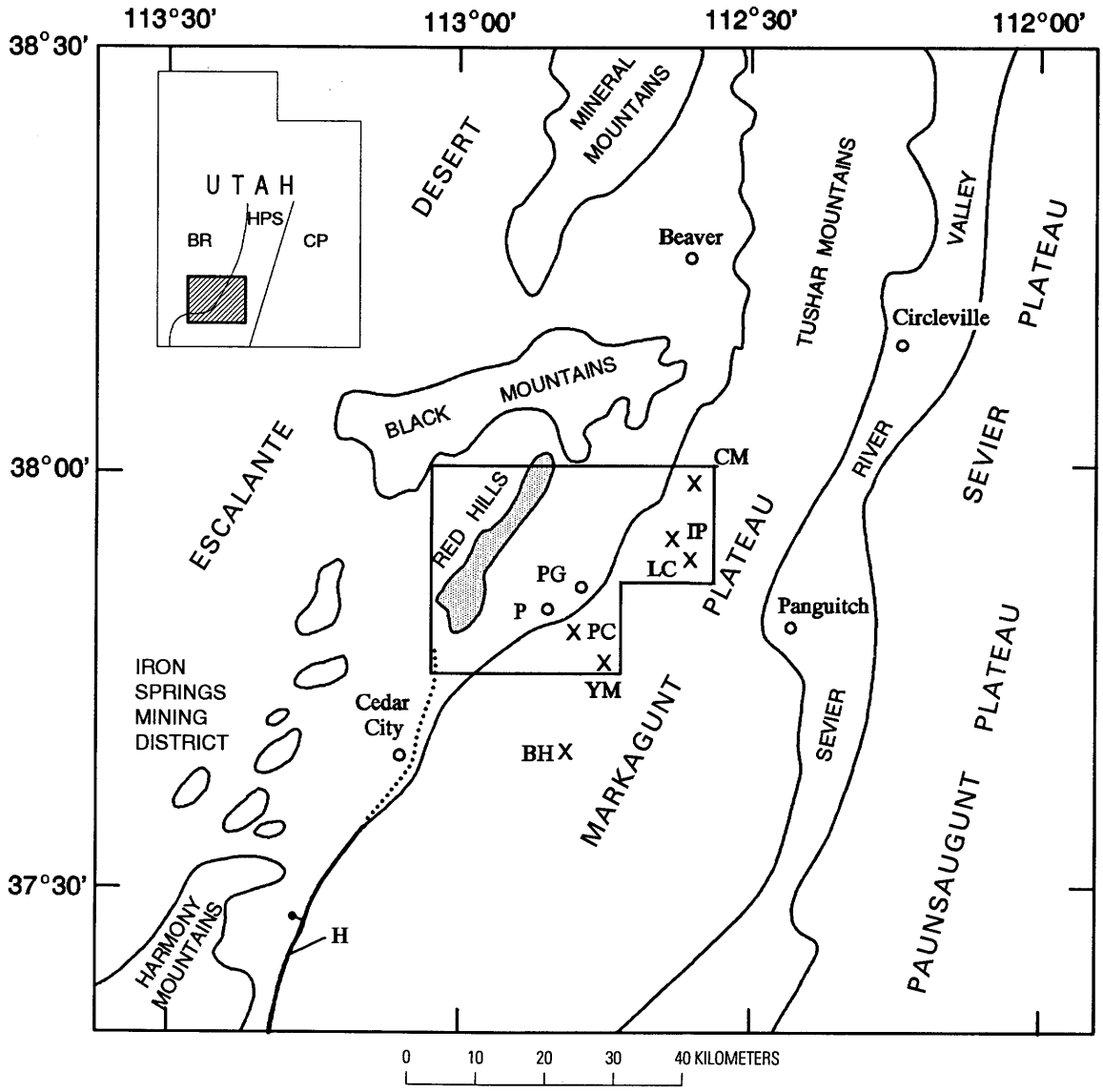

Figure 1. Location map of the Red Hills (shaded area) and surrounding area, southwestern Utah. BH, Brian Head (Peak); H, Hurricane fault (dotted where speculative); PC, Parowan Canyon; YM, Yankee Meadow Reservoir; P, Parowan; PG, Paragonah; LC, Little Creek; IP, Iron Peak; CM, Cottonwood Mountain; BR, Basin and Range province; HPS, High Plateaus subprovince; CP, Colorado Plateaus province. Solid outline, area of figure 2.

east of the Red Hills (Maldonado and others, 1989 and 1992). The fault zone separates an upper plate composed of Oligocene and Miocene volcanic and volcaniclastic rocks from an underlying lower plate composed of Tertiary, Cretaceous, and Jurassic rocks. Rocks in the upper plate are intensely broken and tilted, as expected of a detached plate; the underlying lower plate, in contrast, is structurally less complex. In some areas, the top of the shear zone is at the top of an Eocene and Oligocene sequence of rocks originally called the sedimentary and volcanic rocks of the Red Hills (Trs unit of Maldonado and others, 1992, and Maldonado and Williams, 1993a, b) but now referred to as the Brian Head unit (Tbh unit of fig. 2) for rocks exposed near the Brian Head (Peak) area (fig. 1) that will be formalized (E.G. Sable and Florian Maldonado, work in progress). This unit is described in the next section. In other areas, the shear zone may occur stratigraphically lower in the sequence. Thus, the upper plate in some places includes rocks correlative with the uppermost part of the Brian Head unit (fig. 3). The shear zone is shown as a single fault (fig. 2), arbitrarily placed between the Brian Head unit and the overlying Oligocene and Miocene volcanic rocks.

ACKNOWLEDGMENTS

This study is part of the Basin and Range to Colorado Plateau Transition Study Unit described in the Introduction to this volume. I appreciate discussions with J.J. Anderson, P.D. Rowley, D.L. Schmidt, R.E. Anderson, and H.R. Blank, Jr., that aided in presentation of ideas in this report. I thank K.F. Fox, Jr. and E.G. Sable for their review comments.

GEOLOGY OF THE UPPER PLATE

Upper plate rocks in the Red Hills contain a sequence of ash-flow tuffs and minor volcaniclastic rocks approximately 610 m thick that consists of the following units, in ascending order (ages corrected for new decay constants of Steiger and Jäger, 1977): uppermost part of the Brian Head unit (map unit Tbh) (locally present); Wah Wah Springs Formation (29.5 Ma, Best and Grant, 1987) and Lund Formation (27.9 Ma, Best and Grant, 1987), both of the Needles Range Group; Baldhills Tuff Member of the Isom Formation (27 Ma, Best, Christiansen, and Blank, 1989); Bear Valley Formation (25 Ma, Fleck and others, 1975); Leach Canyon Formation (24 Ma, Rowley and others, 1994) of the Quichapa Group; Bauers Tuff Member (22.8 Ma, Best, Christiansen, and others, 1989) of the Condor Canyon Formation of the Quichapa Group; Harmony Hills Tuff (22–22.5 Ma, Rowley and others, 1989; Siders and others, 1990) of the Quichapa Group; and Mount Dutton Formation (21–26 Ma, Anderson and Rowley, 1975)—map unit Tv (figs. 2, 3) includes these units. The upper plate is discordantly overlain by masses of Tertiary megabreccia (shown as Tm in figs. 2, 3) inferred to be gravity-slide blocks. These blocks contain rock types of the upper plate and are interpreted to have formed as a consequence of action of the Red Hills shear zone (see section, "Origin of megabreccia").

Upper plate rocks dip gently (5°) to very steeply (as much as 75°) and are locally concordant and elsewhere discordant to the underlying rocks. The rocks are intensely faulted and fragmented (fig. 4), in contrast to structures in the lower plate rocks (fig. 5). The faults are mostly high angle, but some low-angle or bedding-plane faults are also present. In general, the high-angle faults strike northwest and northeast. Most of the high-angle faults cutting the upper plate terminate at its base, but some extend below the base. This relationship suggests that most faults are upper plate faults that propagated upward from the Red Hills shear zone (fig. 3). Those faults that extend below the base of the volcanic sequence may represent reactivation and upward growth of lower plate faults or new faults (fig. 3).

The upper plate may also contain faults unrelated to and earlier than the Red Hills shear zone. Anderson (1985, 1988) has presented evidence from the northern Markagunt Plateau that indicates west- and northwest-trending block faulting that began about 26 Ma. These faults are older than the upper plate faults that propagated from the Red Hills shear zone, and may be difficult to separate from those caused by movement of the upper plate. The older faults may have been rotated as well as reactivated by decoupling of the upper plate.

GEOLOGY OF THE LOWER PLATE

Rocks in the lower plate generally dip less than 15°, and are less faulted than rocks in the overlying allochthonous plate. They are composed of sedimentary rocks and minor volcaniclastic rocks and thin ash-flow tuffs (part of Tbh map unit). These rocks as exposed in the Red Hills consist of the Navajo Sandstone (Lower Jurassic), Temple Cap(?) Sandstone (Middle Jurassic), Carmel Formation (Middle Jurassic), Iron Springs Formation (Upper? Cretaceous), Grand Castle unit of Goldstrand (1991) (Paleocene) (equivalent to conglomerate of Parowan Gap, Maldonado and others, 1992 and Maldonado and Williams, 1993b), Claron Formation (Paleocene and Eocene) (Goldstrand, 1994) (all included in TKJ, fig. 3), and part of the Brian Head unit (Eocene and Oligocene).

The Brian Head unit (Tbh map unit) provides one key to understanding the Red Hills shear zone. The unit is approximately 213 m thick (fig. 6) in the northern part of the Red Hills, thin to absent in the southern Red Hills (figs. 2, 7) and as thick as 350 m in the Markagunt Plateau (Anderson and Kurlich, 1989). The upper half of the unit is equivalent to "local volcanic and sedimentary strata," a unit mapped on the Markagunt Plateau by Anderson and others (1987, 1990). The lower half is equivalent to the upper "white" subunit (Doelling and others, 1989) of the Claron Formation. The unit is composed mostly of sandstone, minor limestone and limy shale beds, and tuffaceous sandstone. Pebble- to boulder-size conglomerate (boulder beds), mudflow breccia, thin ash-fall(?) tuff, and ash-flow tuff are present in the uppermost part of the unit. Plagioclase and biotite from the ash-flow tuff have been dated respectively at 34.2±2.1 Ma and 26.3±1.3 Ma using the K-Ar method (H.H. Mehnert, written commun., 1992), and 33.00±0.13 Ma and 33.70±0.14 Ma using the Ar^{40-39} method (L.W. Snee, written commun., 1994). The younger age appears to be discordant in contrast to the older ages. The boulder beds contain well-rounded clasts as large as 0.6 m in diameter in the Red Hills and about 1.5 m in diameter along the western margin of the Markagunt Plateau (fig. 8). Rocks composing some clasts closely resemble rock types of the upper plate units, principally those of the Needles Range Group and Isom Formation. If the boulder beds do indeed contain clasts of these upper plate rocks, then the boulder beds are much younger than the underlying uppermost part of the Brian Head unit. One possible interpretation is that the upper plate

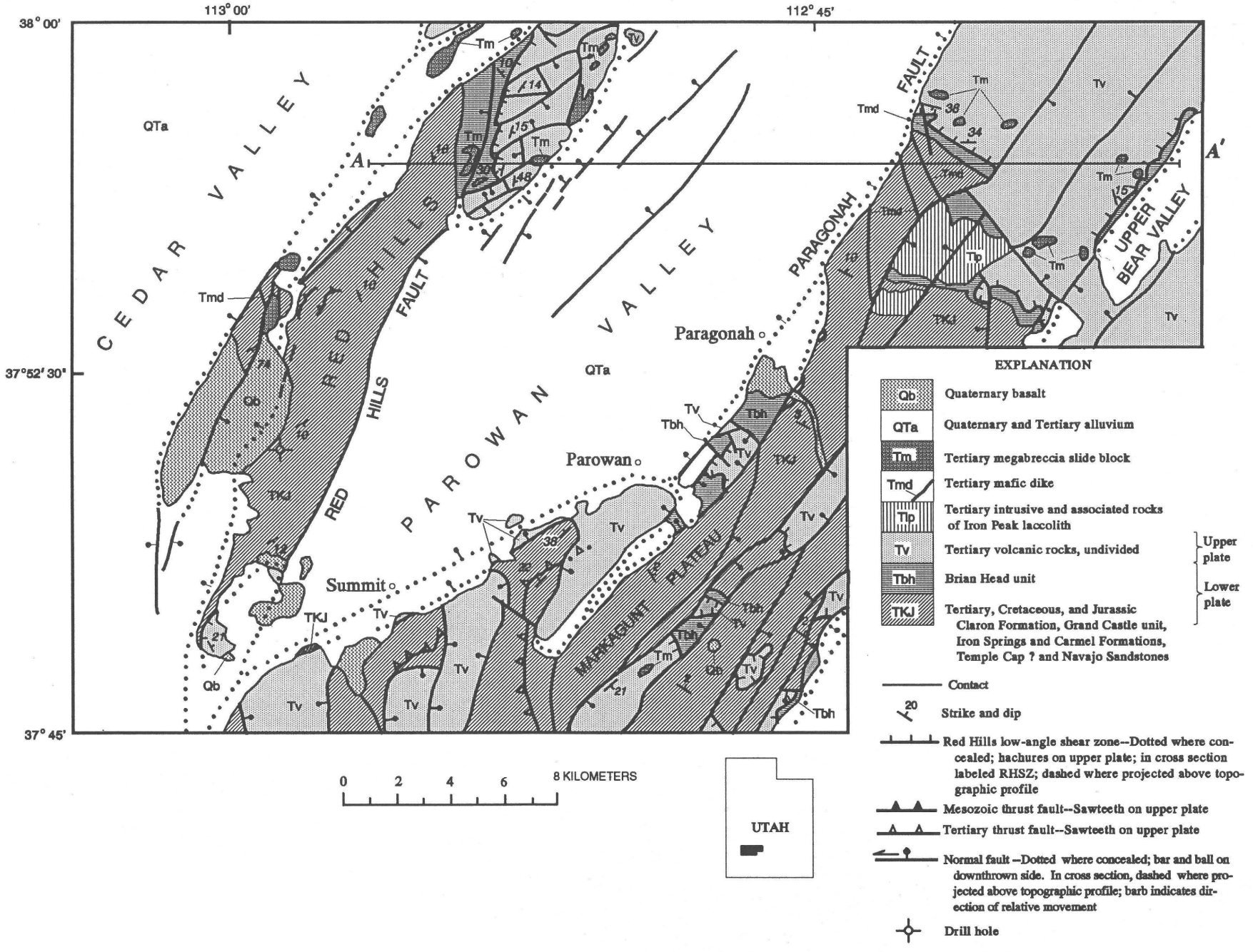
113° 00'
112° 45'
38° 00'
37°52' 30"
37° 45'
CEDAR VALLEY
RED HILLS
RED HILLS FAULT
PAROWAN VALLEY
PARAGONAH FAULT
UPPER BEAR VALLEY
MARKAGUNT PLATEAU
Paragonah
Parowan
Summit
A
A'
QTa
Tm
Tmd
Tv
Tbh
TKJ
Qb
Tlp
0 2 4 6 8 KILOMETERS
UTAH
EXPLANATION
Quaternary basalt
Quaternary and Tertiary alluvium
Tertiary megabreccia slide block
Tertiary mafic dike
Tertiary intrusive and associated rocks of Iron Peak laccolith
Tertiary volcanic rocks, undivided
Brian Head unit
Tertiary, Cretaceous, and Jurassic Claron Formation, Grand Castle unit, Iron Springs and Carmel Formations, Temple Cap ? and Navajo Sandstones
Upper plate
Lower plate
Contact
Strike and dip
Red Hills low-angle shear zone--Dotted where concealed; hachures on upper plate; in cross section labeled RHSZ; dashed where projected above topographic profile
Mesozoic thrust fault--Sawteeth on upper plate
Tertiary thrust fault--Sawteeth on upper plate
Normal fault --Dotted where concealed; bar and ball on downthrown side. In cross section, dashed where projected above topographic profile; barb indicates direction of relative movement
Drill hole

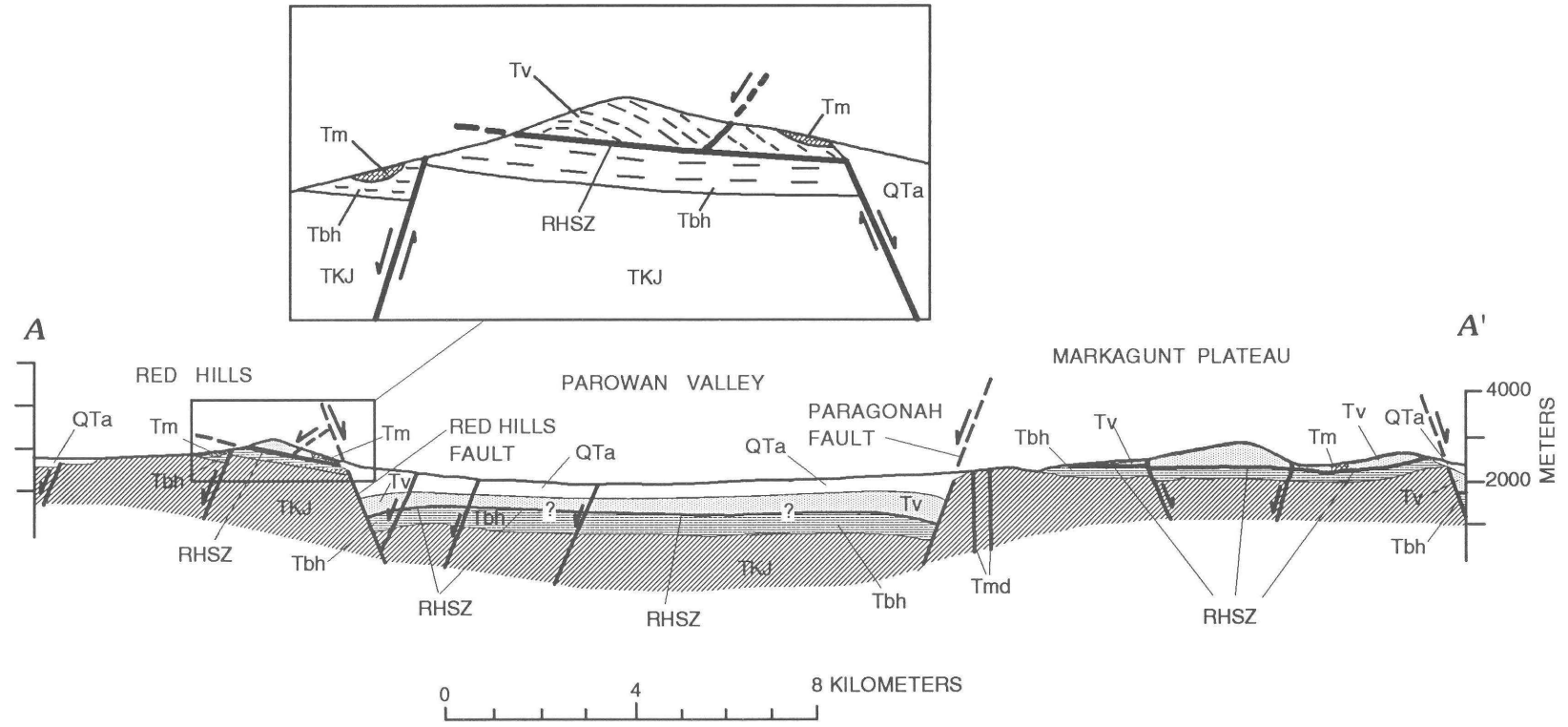

Figure 2. Generalized geology of the Red Hills and Markagunt Plateau, southwestern Utah, and geologic section on line *A–A'*. RHSZ, Red Hills shear zone; queried in cross section where uncertain. Dashed lines within insert indicate dip planes. Geology of Markagunt Plateau modified from Anderson (1965), Judy (1974), Moore (1982), Maldonado and Moore (1993), F. Maldonado (unpub. data, 1991), and F. Maldonado and E.G. Sable (unpub. data, 1992).

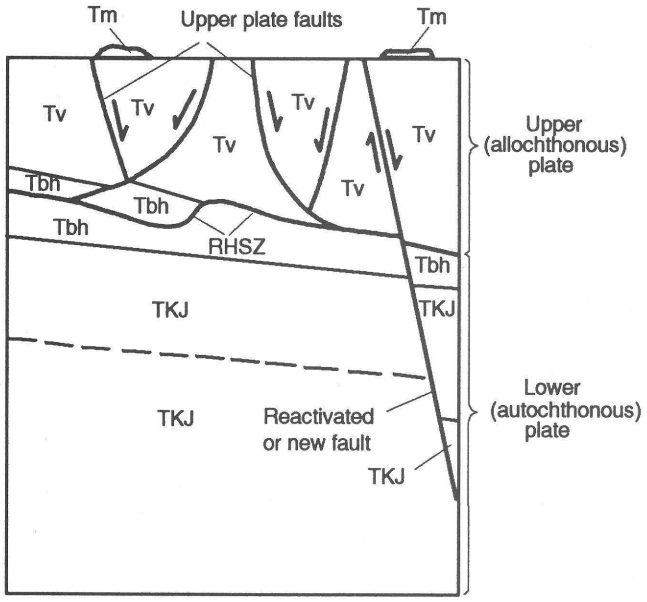

Figure 3. Schematic relationships of gravity-slide blocks (Tm), upper and lower plates, upper plate faults, reactivated upper plate faults or new faults, and the Red Hills shear zone (RHSZ). Tv, Tertiary volcanic rocks undivided; Tbh, Brian Head unit; TKJ, Tertiary, Cretaceous, and Jurassic rocks undivided. Light line, contact; heavy line, fault; barbs show direction of relative movement. Dashed line indicates bed within TKJ.

slid over its own erosional debris. In areas where the shear zone forms the contact between the base of the overlying volcanic rocks and the underlying boulder beds, the clasts may, in fact, have acted as ball bearings, allowing the upper plate to translate on those beds. An alternate interpretation is that the clasts are debris of older units that only resemble units of the upper plate, but additional data are needed to test this hypothesis. In areas where the shear zone is within the uppermost part of the Brian Head unit, the shear zone lies within a tuffaceous sandstone interval. The tuffaceous sandstone is comminuted and pulverized, forming a soft fault gouge of intensely sheared (fig. 9) and folded rock (fig. 10). The structurally incompetent nature of the tuffaceous sandstone perhaps caused slip to be localized within this stratigraphic interval. Other sheared and comminuted lithologies include the thin ash-flow tuff and mudflow breccia units.

EVIDENCE FOR LOW-ANGLE SHEAR ZONE

Evidence for the proposed low-angle shear zone is (1) the comminuted zone within the Brian Head unit that separates upper plate from lower plate; (2) attitudes in upper plate rocks that are steeper than those in lower plate rocks, and upper plate rocks that locally dip into and are cut off by

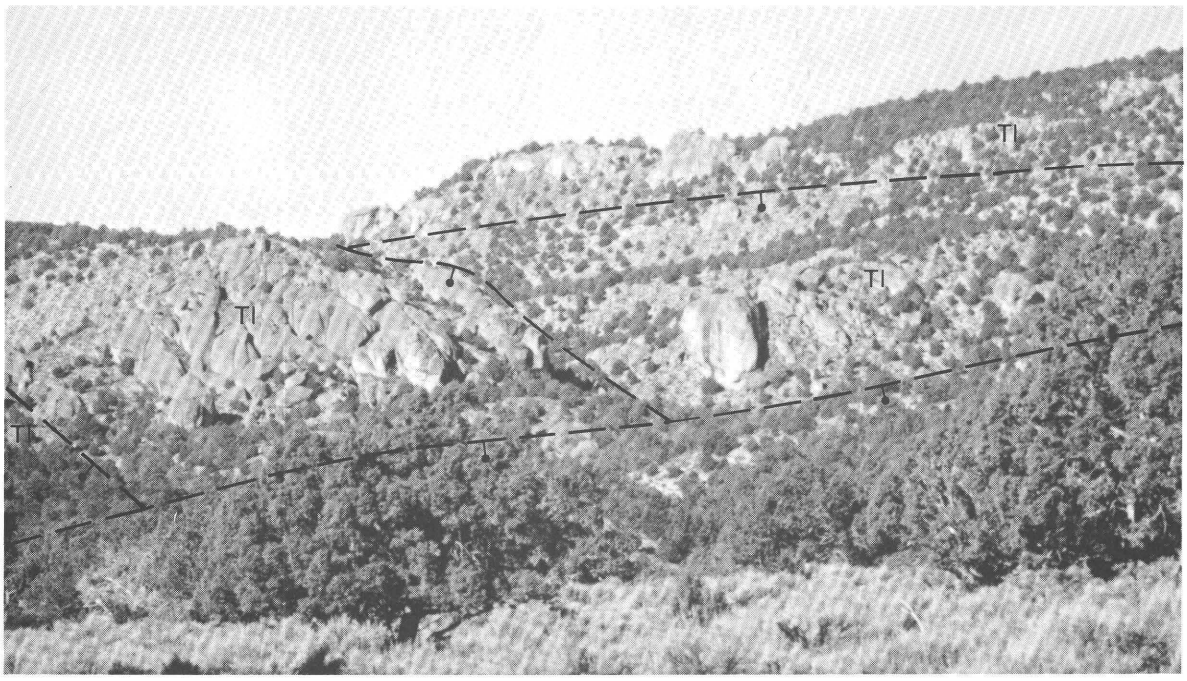

Figure 4. Intense faulting and fragmentation of upper plate (Tl, Leach Canyon Formation), northern part of Red Hills. Pumice foliations of unit dip from 10° to 50°. Dashed line, fault; bar and ball on downthrown side. View looking southwest.

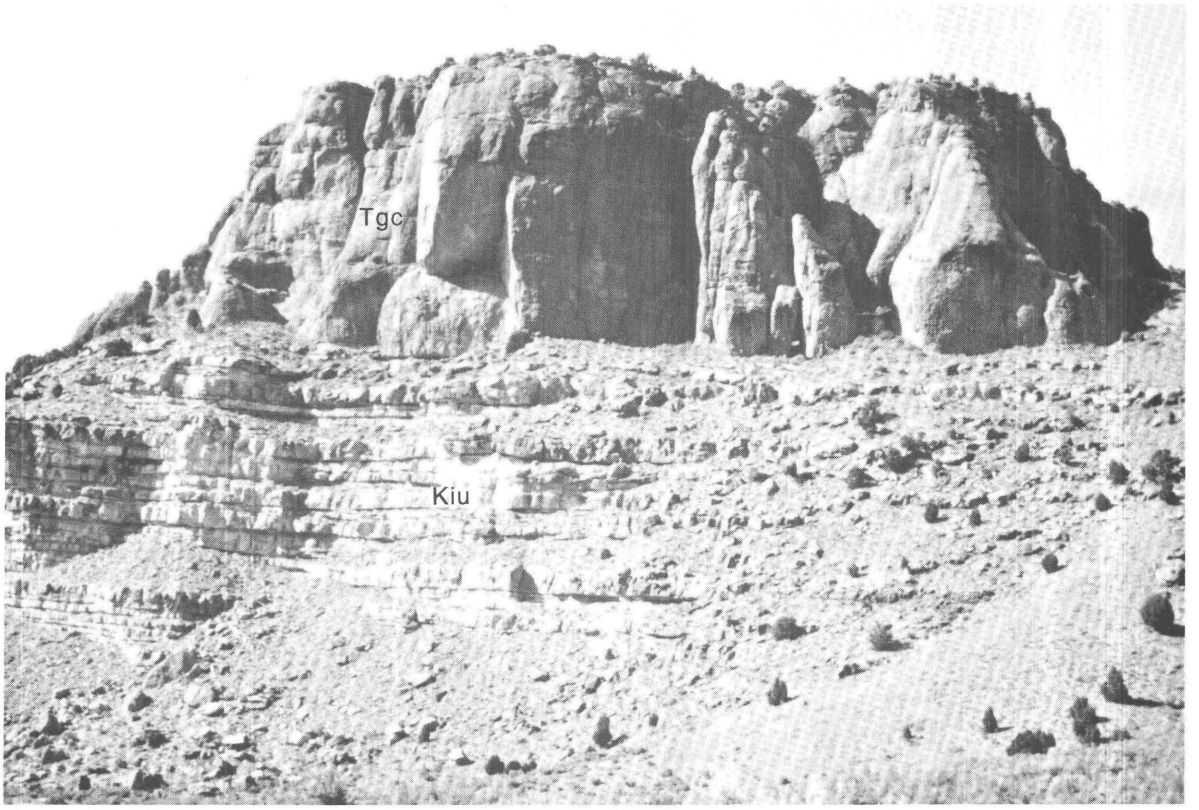

Figure 5. Flat-lying and essentially unfragmented lower plate, Parowan Canyon area (fig. 1). Tgc, Grand Castle unit; Kiu, upper part of Iron Springs Formation. View looking northwest.

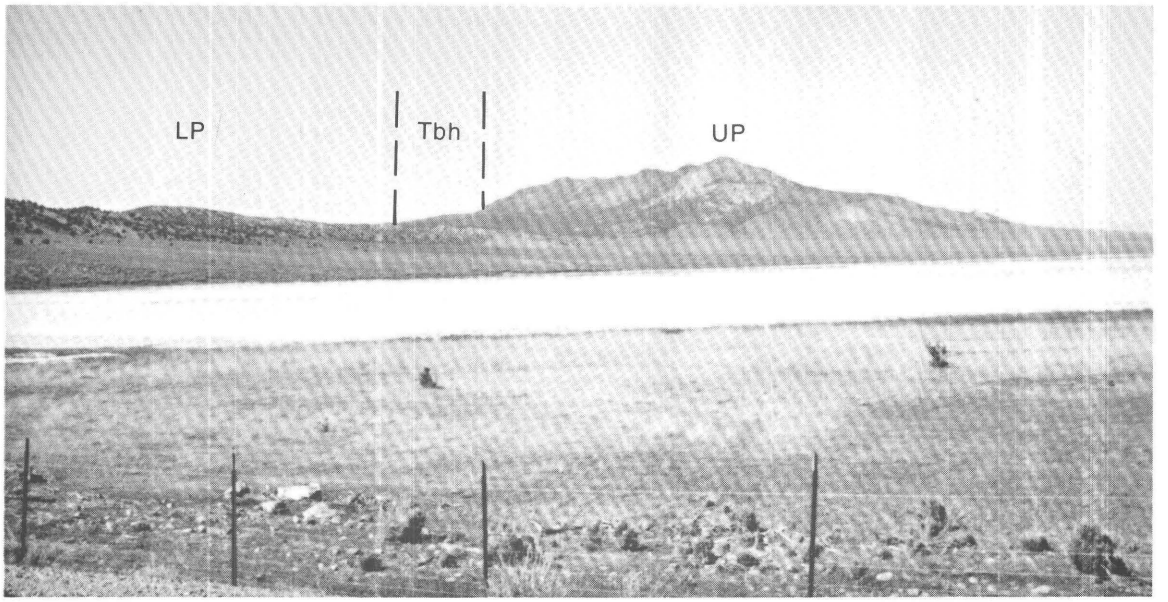

Figure 6. Northern part of Red Hills showing upper plate (UP) and lower plate (LP) (Brian Head unit, Tbh). View looking northwest.

the shear zone (northern Red Hills area, fig. 2); (3) intense faulting and fragmentation of upper plate rocks in contrast to relatively simple structures in lower plate rocks (fig. 2); (4) faults in the upper plate that do not appear to penetrate into the lower plate (fig. 3); and (5) omission of strata along the contact between the plates (fig. 11).

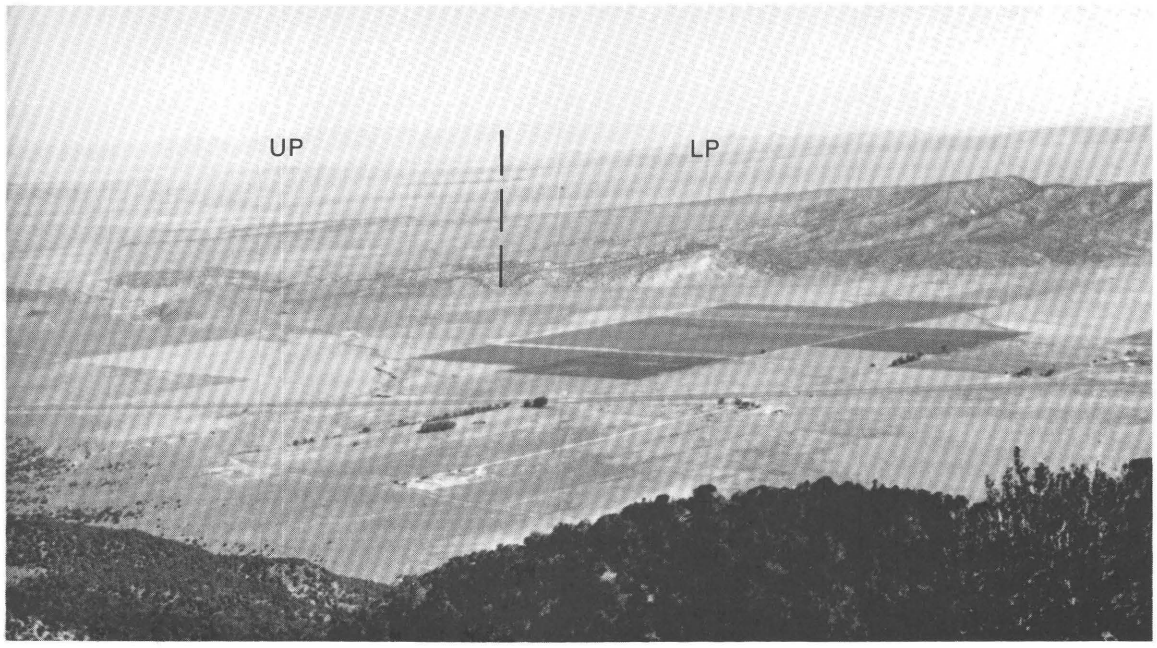

Figure 7. Southern part of Red Hills showing upper plate (UP) and lower plate (LP); upper plate is attenuated, and Brian Head unit is missing. View looking southwest.

Figure 8. Well-rounded clasts in boulder bed of the Brian Head unit, south of Cottonwood Mountain (fig. 1).

Field relationships in the Red Hills and Markagunt Plateau record at least two major episodes of late Tertiary and Quaternary deformation. An early episode formed the low-angle Red Hills shear zone and a later episode fragmented the Markagunt Plateau and offset the Red Hills shear zone, breaking away the Red Hills from the Markagunt Plateau. The date of the earliest episode is probably less than 22–22.5 Ma (age of the Harmony Hills Tuff), the youngest unit in the upper plate. The later episode of faulting in the area was high-angle faulting during the late Tertiary to middle or late Pleistocene (Anderson and Christenson, 1989) that resulted in the present physiography.

Figure 9. Intensely sheared tuffaceous sandstone of the Brian Head unit near Yankee Meadow Reservoir (fig. 1). Hammer for scale.

POSSIBLE MECHANISMS FOR DECOUPLING OF UPPER PLATE

Decoupling was a consequence of regional tilting of the area in which units of the upper plate were deposited. At least two possible mechanisms exist for tilting of this area: (1) local uplift caused by magmatic intrusion (such as in the Iron Springs mining district, fig. 1), and (2) block rotations associated with normal faulting and regional extension.

Numerous exposures of intrusive bodies are scattered within the region. Figure 12 shows the distribution of these intrusive bodies. Most intrusive bodies are laccoliths and stocks; however, only one body of batholithic dimensions is exposed, in the central and northern Mineral Mountains (fig. 12) approximately 40 km north of the Red Hills. Exposed intrusive bodies within the immediate vicinity of the Red Hills include laccoliths at Three Peaks, Granite Mountain, and Iron Mountain at the Iron Springs mining district (fig. 12) and Iron Peak (fig. 12) approximately 20 km east of the Red Hills in the western part of the Markagunt Plateau.

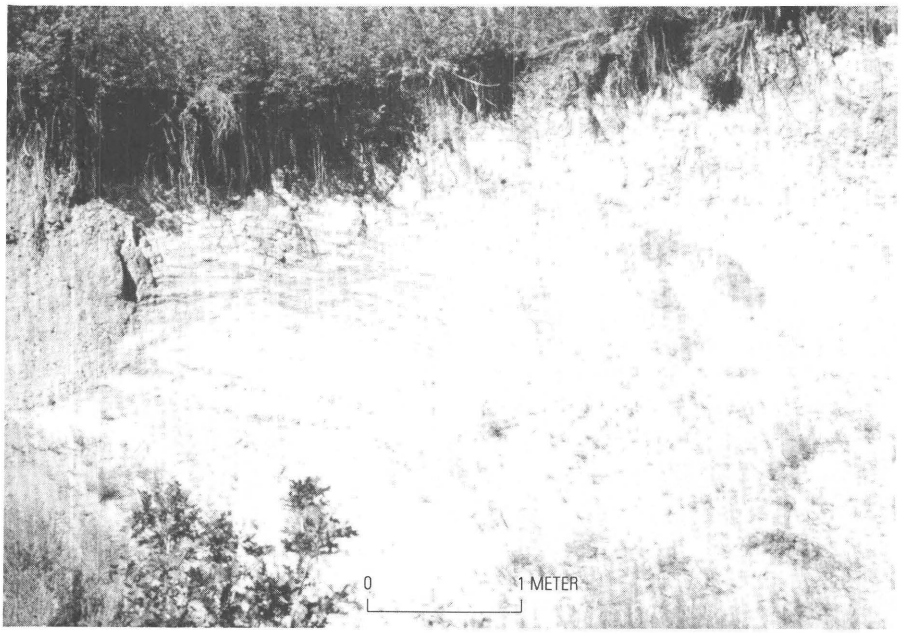

Figure 10. Folded and sheared tuffaceous sandstone of the Brian Head unit, eastern Little Creek (fig. 1). Scale is approximate.

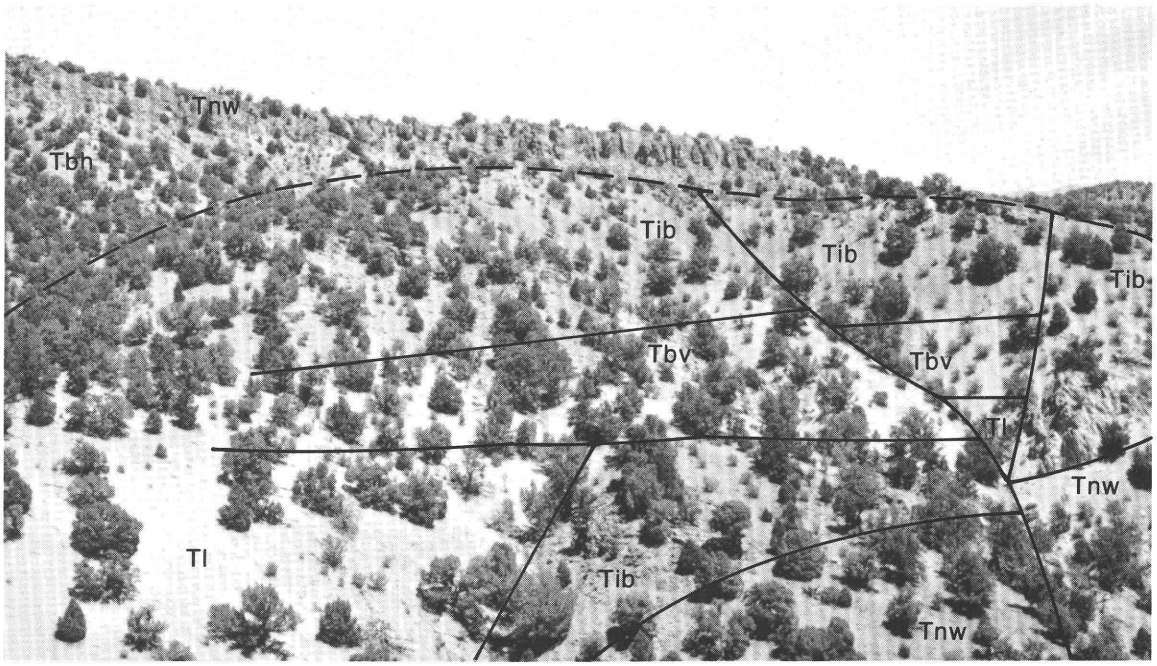

Figure 11. Chaotic mixture of rocks of upper plate interpreted as megabreccia. Heavy lines, faults. Dashed line is extent of outcrop of megabreccia exposure. Tl, Leach Canyon Formation; Tbv, Bear Valley Formation; Tib, Baldhills Member of the Isom Formation; Tnw, Wah Wah Springs Formation. The Wah Wah Springs Formation and the Brian Head unit (Tbh) toward the horizon, not part of megabreccia deposit, separated by a fault in wash not shown.

These intrusive bodies form parts of a belt that has been referred to as the "Iron Axis" (Tobey, 1976) that is part of the larger east-northeast-trending Delamar–Iron Spring igneous belt (Shawe and Stewart, 1976; Rowley and others, in press). Slide blocks forming a zone of structural chaos 30 km^2 in area in the Iron Springs mining district were attributed to tilting associated with emplacement of the Iron Mountain pluton (Blank and Mackin, 1967; Rowley and others, 1989; Blank and others, 1992).

Aeromagnetic and gravity highs appear to be associated with some intrusive bodies in this region, for example, the Three Peaks, Granite Mountain, and Iron Mountain intrusive bodies (Blank and Mackin, 1967; Blank and others, 1992; Blank and Kucks, 1989). Figures 13 and 14 show aeromagnetic and gravity data respectively for the Red Hills–western Markagunt Plateau area. The data indicate a magnetic and gravity high for the southernmost part of the Red Hills. Magnetic and gravity signatures like those at the Iron Springs district suggest the presence of an intrusive body in the subsurface under the southwest part of the Red Hills, which was confirmed by a drill hole (fig. 2) that penetrated a quartz monzonite body at 1,064 m and bottomed in it at 1,340 m (Tompkins and others, 1963). In Parowan Valley, the data indicate a magnetic high but gravity low. The absence of a gravity high does not preclude the presence of an intrusive body under Parowan Valley, however, because low-density basin fill may mask a higher density intrusive body at depth (H.R. Blank, Jr., oral commun., 1990).

The potential role of intrusion in tilting and decoupling of an upper plate is apparent. However, in order to decouple an intact plate the size of the upper plate here postulated in the Red Hills–Markagunt Plateau area, an intrusive body would have to be of batholithic dimensions; no such body is exposed at the surface, but geophysical data suggest a batholith at depth (Blank and Mackin, 1967; Blank and others, 1992) for the Iron Springs mining district that may extend into the Markagunt Plateau area (Rowley and others, in press). The smaller intrusive bodies (laccoliths and stocks) that are exposed may conceivably be apophyses connected to an underlying batholith at great depth. Alternatively, the "upper plate" may in fact have been fragmented as a result of decoupling and independent movement over several bulges, each developed above a small pluton. The distribution of these smaller plutons may be great enough and the separation between them short enough to have the same effect as a batholith. Decoupling would result in movement of upper plate fragments in differing directions.

Block rotations associated with normal faulting may also explain decoupling of the upper plate. Figure 15 shows normal faults at various stages of development. Early, down-to-the-west normal faults or breakaway faults may have resulted in formation of a regional, east-dipping slope on the Markagunt Plateau. This proposed east-dipping slope may have formed during a period of uplift, forming an east-dipping homocline (fig. 15*B*). The combination of the slope

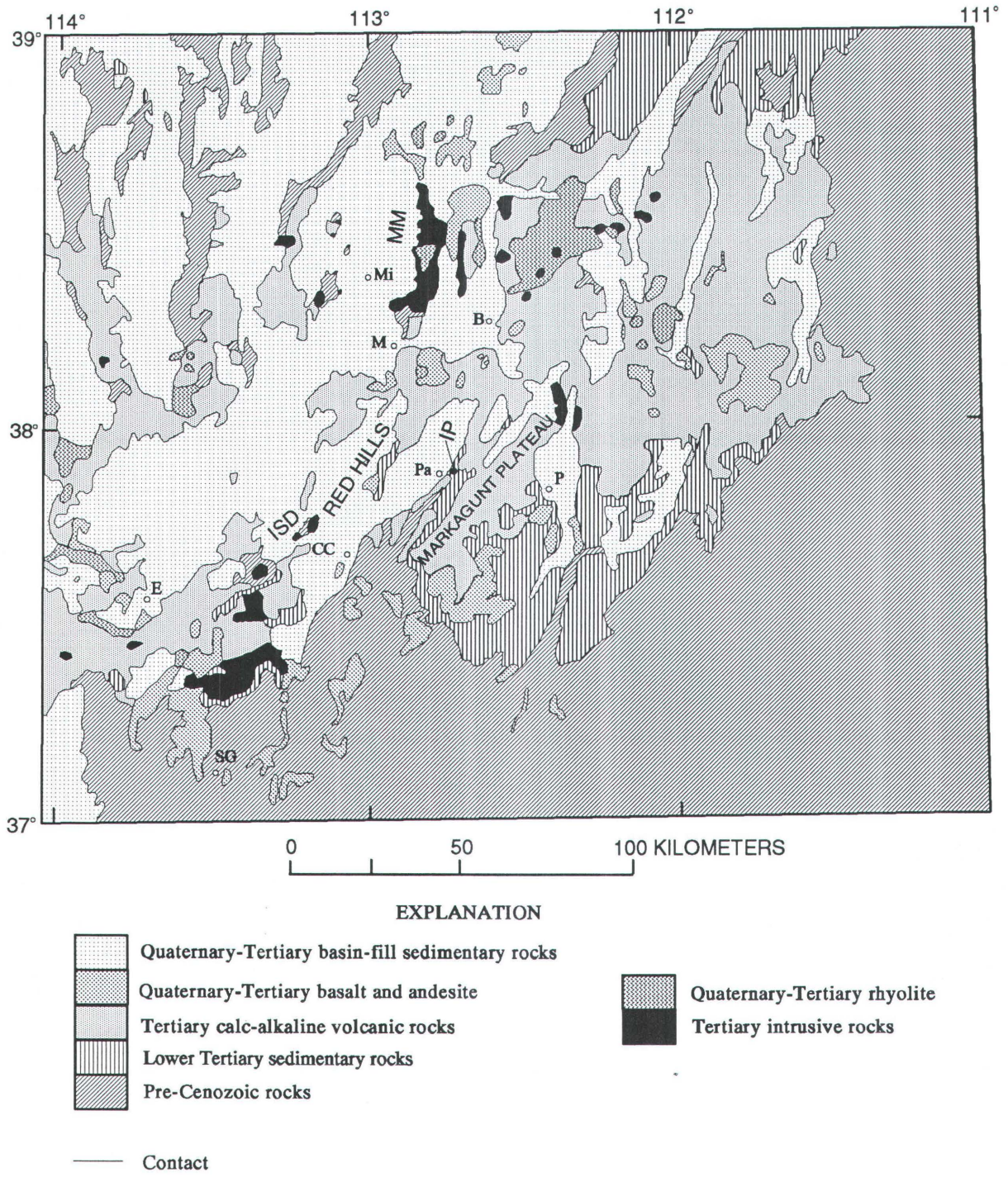

Figure 12. Distribution of intrusive bodies, southwestern Utah (from Rowley and others, 1979). B, Beaver; CC, Cedar City; E, Enterprise; IP, Iron Peak; ISD, Iron Springs mining district; M, Minersville; Mi, Milford; MM, Mineral Mountains; P, Panguitch; Pa, Parowan; SG, Saint George.

and thin succession of upper plate rocks (at least 610 m thick) within the uplifted block allowed the upper plate succession of rocks to decouple along the incompetent Brian Head unit, thus forming the Red Hills low-angle shear zone (fig. 15*C*). The transport direction of the upper plate is not well known and may be difficult to determine. The proposed slope direction (and thus the transport direction of the upper plate) has been tilted in various directions by subsequent faulting. In the Red Hills, the low-angle shear zone surface dips to the northeast, but weak evidence (fault geometry and stratal rotation) suggests a westerly direction of movement. Southwest of Cottonwood Mountain (fig. 1), the shear zone

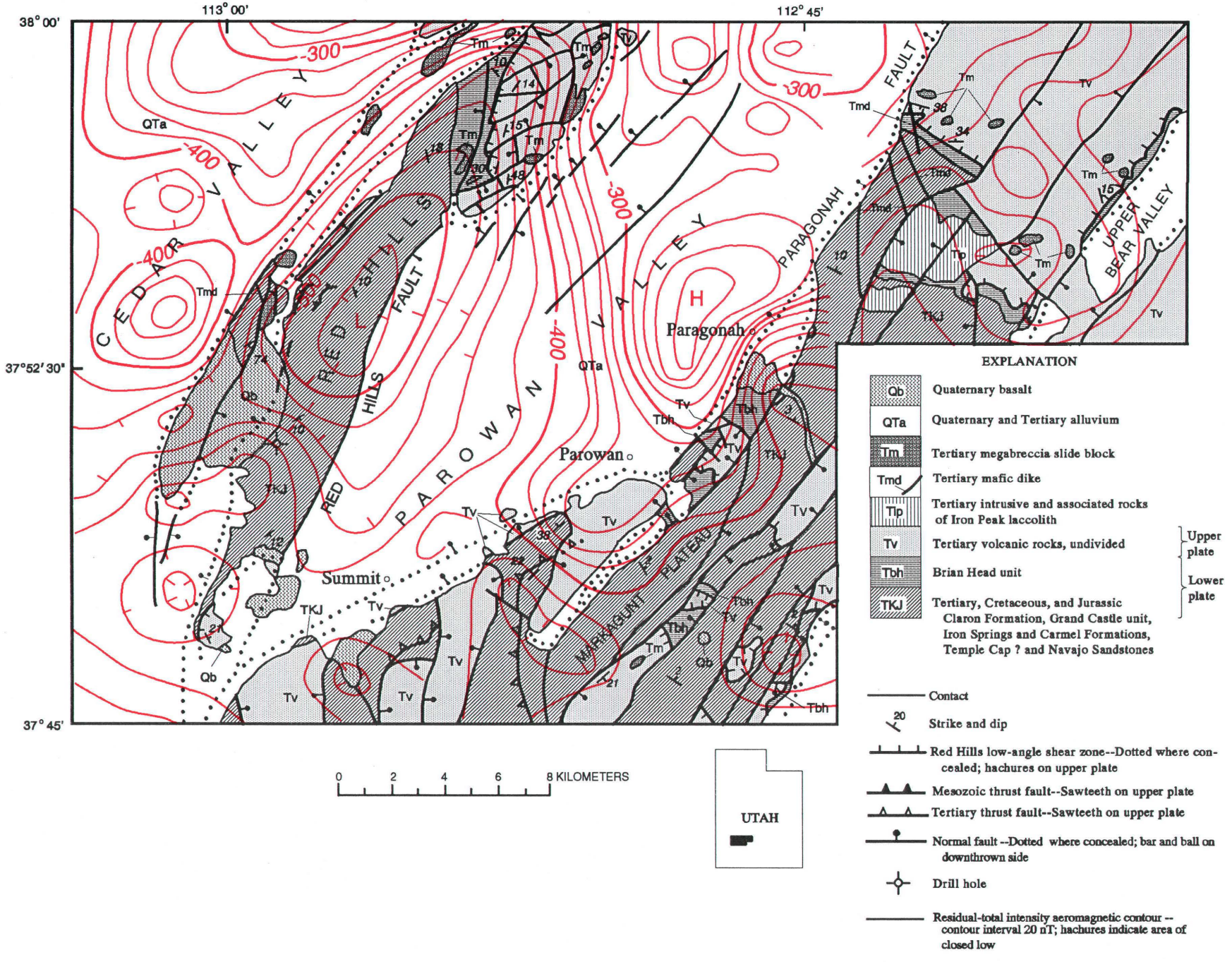

Figure 13. Aeromagnetic data for the Red Hills–western Markagunt Plateau area (Blank and Kucks, 1989).

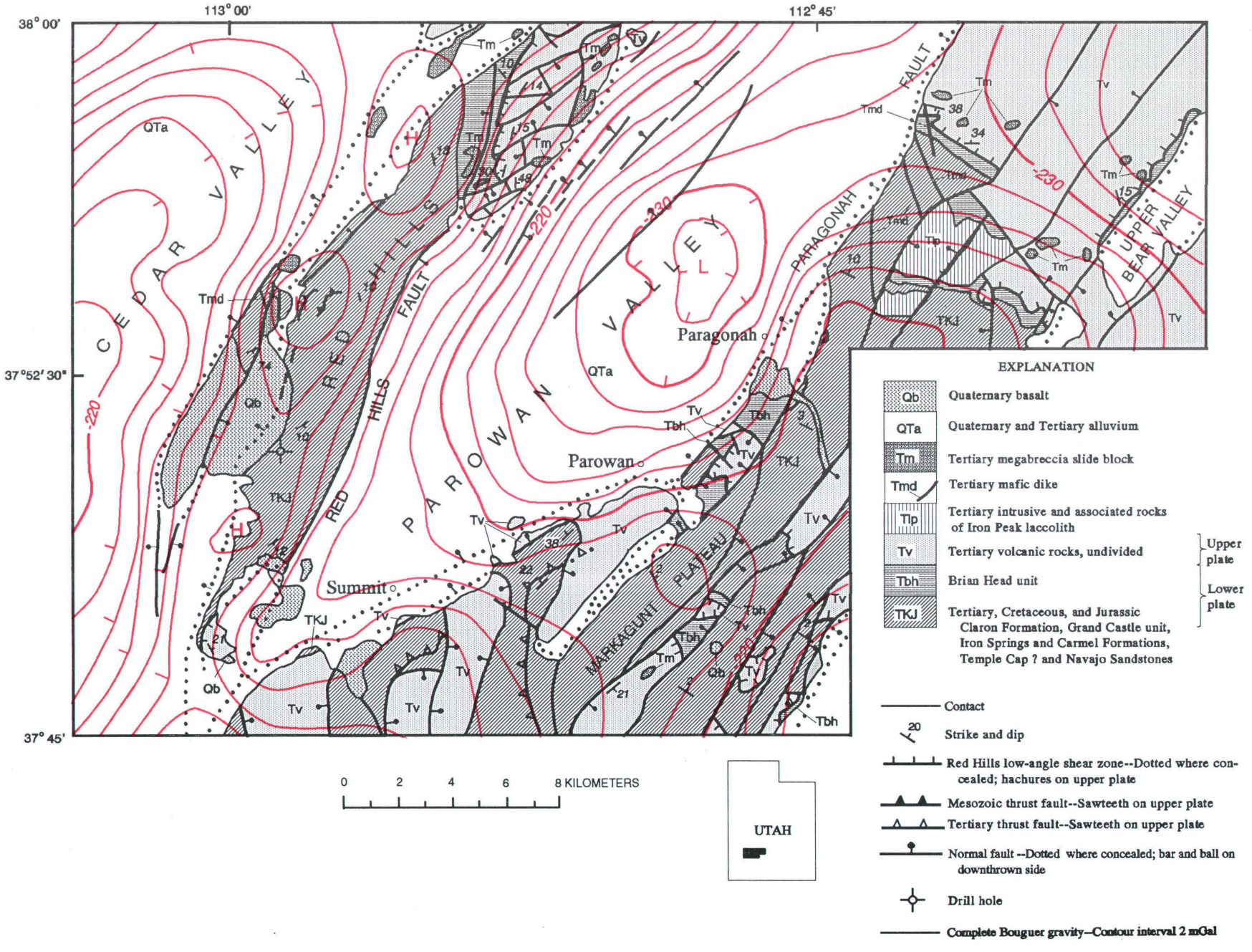

Figure 14. Gravity data for the Red Hills–western Markagunt Plateau area (Blank and Kucks, 1989).

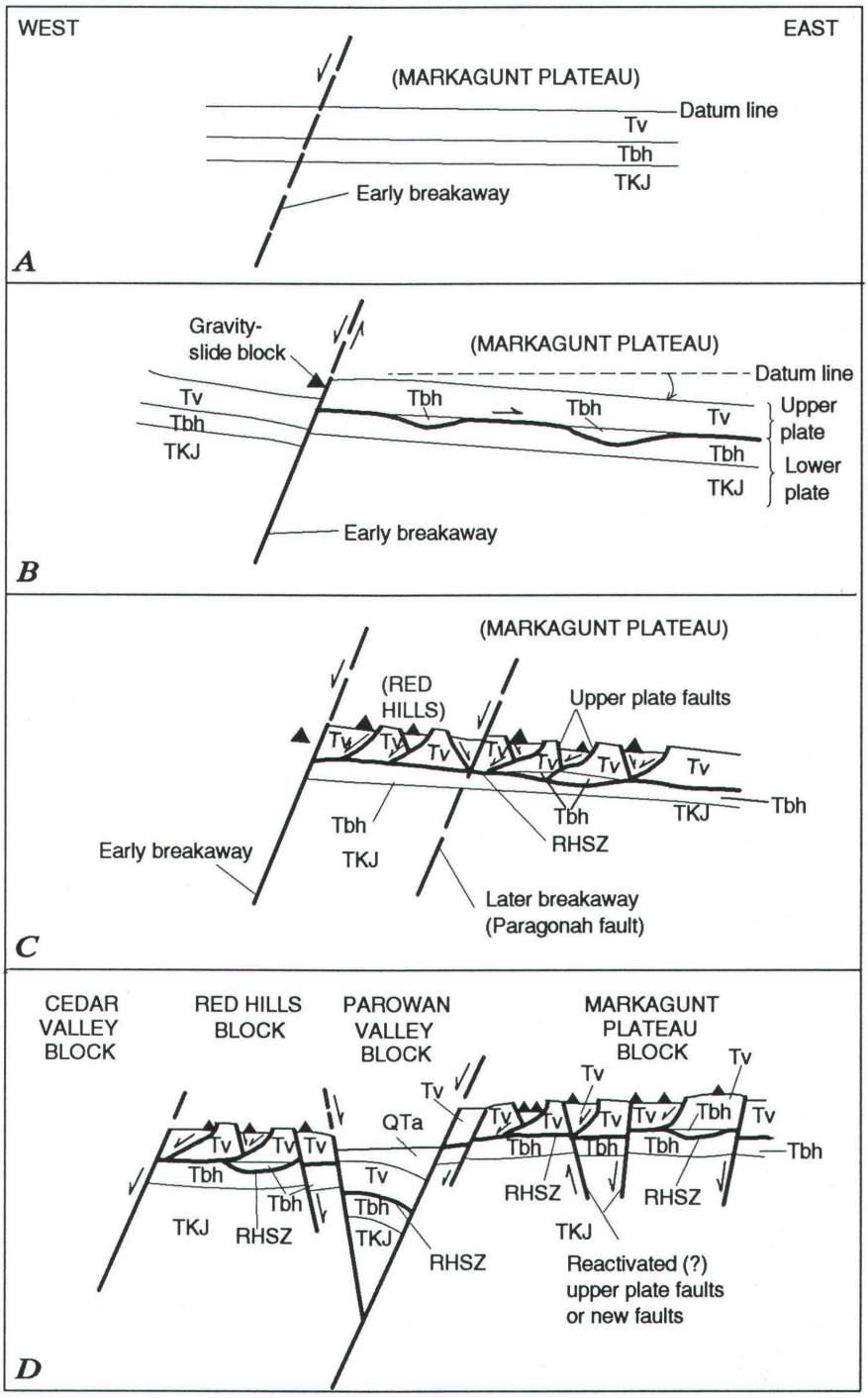

Figure 15. Normal fault model as possible mechanism for decoupling of upper plate at various stages of development (*A–D*). QTa, Quaternary and Tertiary alluvium; Tv, Tertiary volcanic rocks undivided; Tbh, Brian Head unit; TKJ, Tertiary Claron Formation and older rocks (Cretaceous and Jurassic); RHSZ, Red Hills shear zone. Light line, contact; heavy line, fault; dashed where inferred or where projected above topographic profile; barbs show direction of relative movement; triangle, gravity-slide block.

surface dips to the north. Weak evidence here suggests a southerly direction of movement. Thus, transport direction for the upper plate is not conclusive.

Decoupling of the upper plate resulted in fragmentation of upper plate rocks, forming upper plate faults that in part emplaced gravity-slide blocks (fig. 15*C*). Most of the upper

plate faults are high angle, but some are low-angle or bedding plane faults that are difficult to map due to their geometry. Later deformation as represented by the Paragonah fault resulted in separation of the Red Hills from the Markagunt Plateau (fig. 15*D*) offsetting the Red Hills shear zone. This period of deformation also formed grabens that preserved the shear zone (fig. 2) and further fragmented the upper plate; new faults formed that extend from the lower plate into the upper plate and generally strike northeast. These faults may have reactivated previously formed upper plate faults and emplaced additional gravity-slide blocks (fig. 15*D*).

ORIGIN OF MEGABRECCIA

In the Red Hills, numerous megabreccia blocks (map unit Tm, figs. 2, 3), composed of relatively simple monolithologic breccia to chaotically mixed polylithologic breccia, lie atop the upper plate. The megabreccia is composed of brecciated units present within the upper plate. As indicated earlier, these blocks are inferred to be gravity-slide blocks emplaced during formation of upper plate faults. The gravity-slide blocks may have been emplaced as sheets along low-angle faults, forming megabreccia deposits that are presently found as scattered blocks and may represent erosional remnants of those sheets. Other gravity-slide blocks may have been shed from scarps that formed along high-angle faults.

On the Markagunt Plateau numerous blocks of megabreccia, as much as 2.5 km^2 in areal extent and 100 m thick (Sable and Anderson, 1985; J.J. Anderson, 1993) are scattered over an area of as much as 1,000 km^2 (E.G. Sable, oral commun., 1994). Most of these blocks are interpreted here to have been emplaced during breakage of the upper plate by faults propagating from or as a consequence of movement along the Red Hills shear zone. Some blocks, however, may be related to later deformation; others may be due to secondary movements as slide blocks; others may have been emplaced during intrusion of local magmatic bodies of Miocene (21.5–22 Ma) age, as suggested by Mackin (1960, p. 121), Rowley and others (1989), and Blank and others (1992) for the Iron Springs mining district (approximately 15 km southwest of the Red Hills); and still others may be related to late stages of Mount Dutton volcanism. In some areas, extensive erosion of the upper plate has left only erosional remnants that resemble slide blocks. Differentiating remnant blocks of the upper plate from slide blocks may be impossible in some areas.

RELATIONSHIP OF PARAGONAH FAULT TO RED HILLS SHEAR ZONE

The Paragonah fault (fig. 2) is interpreted as a breakaway fault with possible listric geometry at great depth, along which the Red Hills block broke away from the western Markagunt Plateau, carrying with it the Red Hills shear zone. The fault may be manifested by small scallop-shaped blocks of Claron Formation (included with unit TKJ in fig. 2) that have been mapped along the west edge of the Markagunt Plateau in the Parowan Valley area east of Paragonah. These blocks may be relicts of the footwall block on the downdropped side of the Paragonah fault. Measured fault planes that bound these blocks are generally of intermediate angle rather than high angle, suggesting a listric geometry in the subsurface. In some areas also along the west edge of the Markagunt Plateau, similar blocks overlie what appears to be Quaternary colluvium. This suggests that some of the blocks may simply represent landslides or block slides.

The Paragonah fault bounds Parowan Valley on the east side and the Red Hills fault bounds the valley on the west (fig. 2). The Red Hills fault is herein assumed to be antithetic to the Paragonah fault, propagating from it at depth. Development of both the Paragonah and Red Hills faults thus may have formed the Parowan Valley.

The history of the Paragonah fault may be similar to that of the Hurricane fault discussed by previous workers. Anderson and Christenson (1989) stated that the Hurricane fault probably formed after the late Miocene and remained active into the Pleistocene. The Paragonah fault may be the same age as the Hurricane fault. The following data support this interpretation: (1) A regional ash-flow tuff, the Harmony Hills Tuff, whose source area was thought to be the Caliente caldera complex (Noble and others, 1968; Ekren and others, 1977) in eastern Nevada, is now thought to be from the Bull Valley Mountains of southwestern Utah by Rowley and others (this volume), as originally suggested by Blank (1959) and Williams (1967). This unit has been mapped on the Markagunt Plateau (Maldonado and Moore, 1993) in the Parowan Canyon area (fig. 1). The presence of this unit on the Markagunt Plateau suggests that it spread from its source area in southwestern Utah across the present boundary that separates the Markagunt Plateau from the Basin and Range province. This implies that no major barriers blocked the spread of the Harmony Hills Tuff and that the Markagunt Plateau did not exist until after the emplacement of the Harmony Hills Tuff (22–22.5 Ma). (2) In Parowan Valley, along the west edge of the Markagunt Plateau, south of the town of Paragonah, the Paragonah fault offsets a basalt lava flow referred to here as the basalt of Water Canyon. The basalt flowed down a paleovalley in the Markagunt Plateau and over the Paragonah fault scarp, flowing out onto the Parowan Valley where it was subsequently cut by the Paragonah fault. This basalt has been dated at 0.45±0.04 Ma (Fleck and others, 1975, age corrected for new decay constants of Steiger and Jäger, 1977) using the K-Ar method. This relationship indicates recurrent movement along the Paragonah fault in relatively recent geologic time. (3) Along the same fault strand, north of the town of Paragonah, the Paragonah fault truncates a set of N. 10° W.-striking faults filled with mafic

dike material (figs. 2, 16) (Anderson, 1965; J.J. Anderson and F. Maldonado, unpub. data, 1990). These dikes have been dated at 20 Ma using the K-Ar method (H.H. Mehnert and R.E. Anderson, written commun., 1988). The dikes are likely related to the nearby Iron Peak gabbroic laccolith (fig. 2) described by Anderson (1965), Judy (1974), and Spurney (1984) and dated at about 20.2±0.5 Ma (Fleck and others, 1975, age corrected for new decay constants of Steiger and Jäger, 1977). The laccolith is also offset by high-angle faults that are inferred to be of the same age as the Paragonah fault.

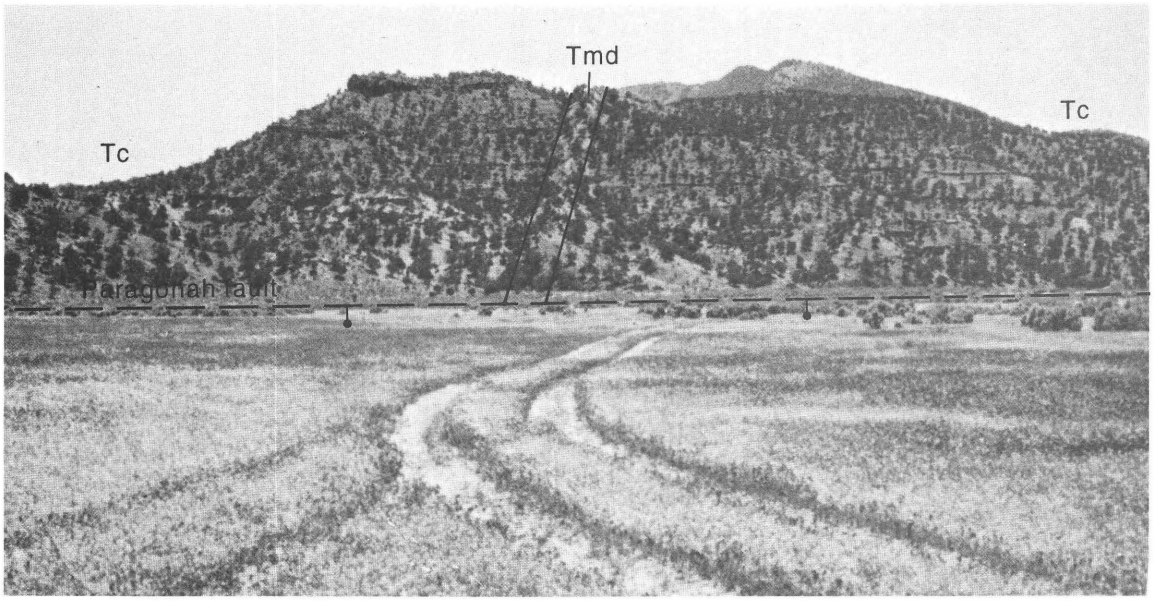

Figure 16. Mafic dike truncated by inferred Paragonah fault along western margin of the Markagunt Plateau north of Paragonah (fig. 1). Tmd, mafic dike; Tc, Claron Formation. Bar and ball on downthrown side of fault. View looking east from Parowan Valley.

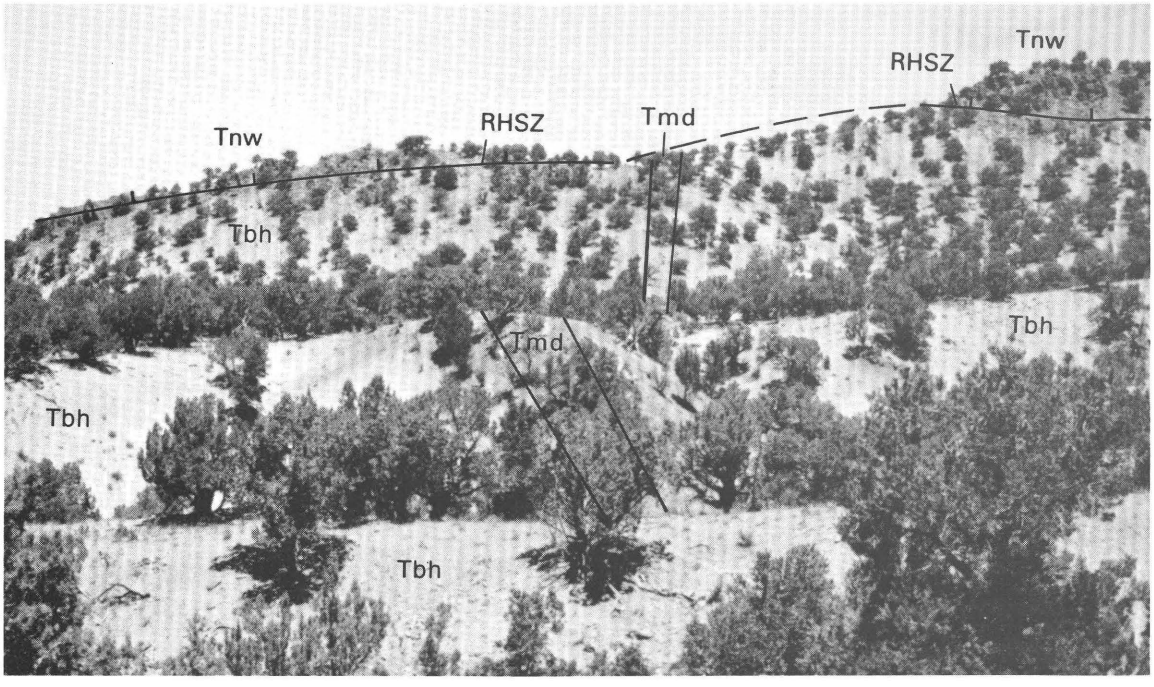

Figure 17. Mafic dike (Tmd) cutting the Brian Head unit (Tbh) west of Cottonwood Mountain. Tnw, Wah Wah Springs Formation; RHSZ, Red Hills shear zone; ticks on upper plate, dashed where projected.

The relations just discussed suggest that the Paragonah fault and related faults have been active in the Quaternary and are not older than approximately 20 Ma. Southwest of Cottonwood Mountain (figs. 1, 2), the aforementioned 20–Ma dikes intruded the Claron Formation, the Brian Head unit (Tbh, fig. 17), and upper plate rocks of the Red Hills low-angle shear zone. The age of the shear zone is thus bracketed between 22.5 Ma (age of Harmony Hills Tuff) and 20 Ma (age of mafic dikes) or very likely 20.2±0.5 Ma (age of the Iron Peak gabbroic laccolith).

FEATURES RELATED TO LOW-ANGLE SHEAR ZONE

Several zones of replacement chalcedony (jasper) are found within the Brian Head unit in the Red Hills and Markagunt Plateau. The relationship between the chalcedony and the Red Hills shear zone is not well understood. The shear zone may have formed low-angle barriers to flow, channeling fluids within the strata of the Brian Head unit. The chalcedony deposits may have formed between the barriers within permeable strata. In the southern Red Hills, the chalcedony locally replaces limestone. In the Markagunt Plateau, the chalcedony zone is well developed in the Brian Head (Peak) area, approximately 8 km south of the area of figure 2 and shown in figure 1, where it was first described by Gregory (1949). Samples of chalcedony from the zone at Brian Head were collected for geochemical analyses to determine possible metal association with the zone. The results of analyses are shown in table 1. Analysis indicates generally low metal values and suggests a hydrothermal source. Metals with some anomalous values are Mn, As, Ba, Co, Mo, and V (Richard Van Loenen, oral commun., 1993). Gold is at limit of detection.

The Iron Peak gabbroic laccolith (fig. 18) intrudes the Brian Head unit. Evidence discussed previously suggests that the age of the shear zone is pre-20 Ma, while the age of the laccolith has been determined to be 20±0.5 Ma (Fleck and others, 1975, age corrected for new decay constants of Steiger and Jäger, 1977). I propose here that magma was

Table 1. Geochemical analyses of chalcedony zone in the Brian Head unit, Brian Head (Peak) area.

[Analyses in parts per million; in percent for Al, Ca, Fe, K, Mg, Na, P, Ti (analysis by D.L. Fey and C.A. Motooka, U.S. Geological Survey). Analysis by 40 element ICP (inductively coupled plasma) method and by flame method for Au. Limit of detection for the following elements in parentheses in ppm for Au (0.05), Cr (1), Cu (1), Sr (2), and V (2). Leaders (--), no detection; *, anomalous value]

Sample No.	RH738A	RH738B	RH738C	RH738D	Sample No.	RH738A	RH738B	RH738C	RH738D
Al	0.1	2.12	0.06	0.05	La	<2.	12.	3.	<2.
Ca	.20	.95	.05	.21	Li	3.	9.	<2.	<2.
Fe	.12	.83	.14	.07	Mo	<2.	<2.	6.*	<2.
K	.06	.48	.13	<.05	Nb	4.	<4.	<4.	<4.
Mg	.01	.27	.01	.01	Nd	<4.	8.	<4.	<4.
Na	.01	.42	.01	.008	Ni	<2.	3.	6.	<2.
P	<.005	.03	<.005	<.005	Pb	19.	12.	<4.	<4.
Ti	<.005	.09	<.005	<.005	Sc	<2.	3.	<2.	<2.
Mn	74.	297.00	17,000.0*	181.	Sn	<10.	<10.	<10.	<10.
Ag	<2.	<2.	<2.0	<2.	Sr	3.	125.	46.	2.
As	10.	<10.	20.0*	<10.	Ta	<40.	<40.	<40.	<40.
Au	.05	.05	.05	.05	Th	<4.	<4.	5.	<4.
B	--	--	--	--	U	<100.	<100.	<100.	<100.
Ba	94.	339.	2,070.0*	54.	V	3.	20.	132.*	5.
Be	<1.	<1.	<1.0	<1.	W	--	--	--	--
Bi	<10.	<10.	<10.	<10.	Y	<2.	4.	<2.	<2.
Cd	<2.	<2.	<2.	<2.	Yb	<1.	<1.	<1.	<1.
Ce	<4.	19.	7.	<4.	Zn	<2.	16.	15.	9.
Co	<1.	5.	13.*	<1.	Zr	--	--	--	--
Cr	2.	10.	3.	2.					
Cu	2.	4.	5.	4.					
Eu	<2.	<2.	<2.	<2.					
Ga	<4.	<4.	8.	<4.					
Ge	--	--	--	--					
Ho	<4.	<4.	<4.	<4.					

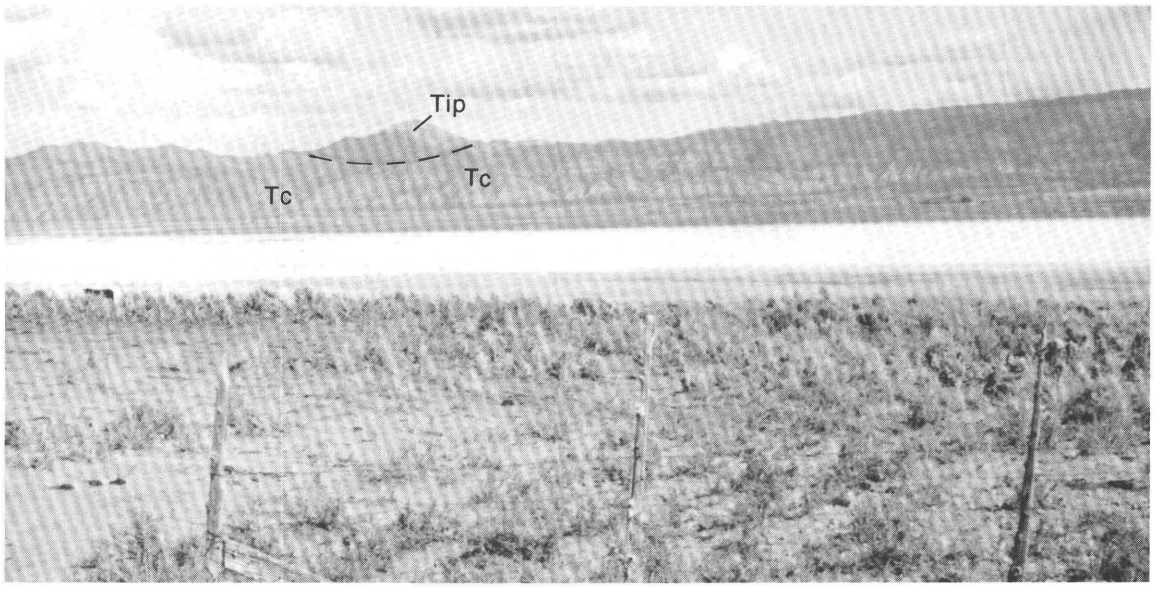

Figure 18. Iron Peak laccolith, Markagunt Plateau. Tip, Iron Peak laccolith; Tc, Claron Formation; dashed line, contact; view looking northeast from Parowan Valley.

intruded along the Red Hills shear zone, forming the laccolithic body.

CONCLUSIONS

Field evidence from the Red Hills and adjacent Markagunt Plateau of Utah records two major episodes of deformation following mid-Tertiary deposition of the Brian Head unit. An early episode between 22.5 and 20 Ma resulted in decoupling of the upper plate, forming the Red Hills low-angle shear zone and the upper plate faults. The upper plate faults are mostly high angle that may become listric to the shear zone, but some low-angle or bedding plane faults are also present. The gravity-slide blocks may have been emplaced as sheets along some of the low-angle faults forming megabreccia deposits, presently found as scattered blocks that may represent erosional remnants of those sheets. Other blocks may have been shed from scarps that formed along high-angle faults. A later episode (post-20 Ma) fragmented the Markagunt Plateau and offset the Red Hills shear zone. This later episode of faulting cut the Red Hills shear zone and created slopes along which blocks on top of the upper plate were mobilized as young gravity slides. The upper plate contains gravity-slide blocks emplaced during formation of the Red Hills shear zone and gravity-slide blocks emplaced during later deformation.

At least two possible mechanisms could have triggered decoupling of the upper plate: (1) uplift caused by intrusion, or (2) normal faulting (extension). The mechanism for decoupling of the upper plate is enigmatic; intrusion, normal faulting, or a combination of the two models appears to be valid.

REFERENCES CITED

Anderson, J.J., 1965, Geology of northern Markagunt Plateau, Utah: Austin, Texas, University of Texas Ph. D. dissertation, 194 p.

———1985, Mid-Tertiary block faulting along west and northwest trends, southern High Plateau, Utah: Geological Society of America Abstracts with Programs, v. 17, no. 7, p. 513.

———1988, Pre-Basin-Range block faulting along west and northwest trends, southeastern Great Basin and southern High Plateaus: Geological Society of America Abstracts with Programs, v. 20, no. 3, p. 139.

———1993, The Markagunt megabreccia—Large Miocene gravity slide mantling the northern Markagunt Plateau, southwestern Utah: Utah Geological Survey Miscellaneous Publication 93–2, 37 p.

Anderson, J.J, Iivari, T.A., and Rowley, P.D., 1987, Geologic map of the Little Creek Peak quadrangle, Garfield and Iron Counties, Utah: Utah Geological and Mineral Survey Map 104, scale 1:24,000.

Anderson, J.J., and Kurlich, R.A., 1989, Post-Claron Formation, pre-regional ash-flow tuff early Tertiary stratigraphy of the southern High Plateaus of Utah: Geological Society of America Abstracts with Programs, v. 21, no. 5, p. 50.

Anderson, J.J, and Rowley, P.D., 1975, Cenozoic stratigraphy of southwestern high plateaus of Utah, *in* Anderson, J.J., Rowley, P.D., Fleck, R.J., and Nairn, A.E.M., eds., Cenozoic geology of southwestern High Plateaus of Utah: Geological Society of America Special Paper 160, p. 1–51.

Anderson, J.J., Rowley, P.D., Machette, M.N., Decatur, S.H., and Mehnert, H.H., 1990, Geologic map of the Nevershine Hollow area, eastern Black Mountains, southern Tushar Mountains, and northern Markagunt Plateau, Beaver and Iron Counties, Utah: U.S. Geological Survey Miscellaneous Investigations Series Map I–1999, scale 1:50,000.

Anderson, R.E., 1971, Thin-skinned distension in Tertiary rocks of southern Nevada: Geological Society of America Bulletin, v. 82, p. 42–58.

Anderson, R.E., and Christenson, G.E., 1989, Quaternary faults, folds, and selected volcanic features in the Cedar City 1°×2° quadrangle, Utah: Utah Geological and Mineral Survey Miscellaneous Publication 89–6, 29 p.

Armstrong, R.L., 1970, Geochronology of Tertiary igneous rocks, eastern Basin and Range province, western Utah, eastern Nevada, and vicinity, U.S.A.: Geochimica et Cosmochimica Acta, v. 34, p. 203–232.

Best, M.G., Christiansen, E.H., and Blank, H.R., Jr., 1989, Oligocene caldera complex and calc-alkaline tuffs and lavas of the Indian Peak volcanic field, Nevada and Utah: Geological Society of America Bulletin, v. 101, p. 1076–1090.

Best, M.G., Christiansen, E.H., Deino, A.L., Grommé, C.S., McKee, E.H., and Noble, D.C., 1989, Excursion 3A—Eocene through Miocene volcanism in the Great Basin of the western United States: New Mexico Bureau of Mines and Mineral Resources Memoir 47, p. 91–133.

Best, M.G., and Grant, S.K., 1987, Stratigraphy of the volcanic Oligocene Needles Range Group in southwestern Utah and eastern Nevada: U.S. Geological Survey Professional Paper 1433–A, p. 1–28.

Blank, H.R., Jr., 1959, Geology of the Bull Valley district, Washington County, Utah: Seattle, Wash., University of Washington Ph. D. dissertation, 177 p.

Blank, H.R., Jr., and Kucks, R.P., 1989, Preliminary aeromagnetic, gravity, and generalized geologic maps of the USGS Basin and Range–Colorado Plateau transition zone study area in southwestern Utah, southeastern Nevada, and northwestern Arizona: U.S. Geological Survey Open-File Report 89–432, 16 p., map scale 1:250,000.

Blank, H.R., Jr., and Mackin, J.H., 1967, Geologic interpretation of an aeromagnetic survey of the Iron Springs district, Utah: U.S. Geological Survey Professional Paper 516–B, 14 p.

Blank, H.R., Jr., Rowley, P.D., and Hacker, D.B., 1992, Miocene monzonitic intrusions and associated megabreccias of the Iron Axis region, southwestern Utah, *in* Wilson, J.R., ed., Field guide to geologic excursions in Utah and adjacent areas of Nevada, Idaho, and Wyoming, Geological Society of America Rocky Mountain Section Meeting: Utah Geological Survey Miscellaneous Publications 92–3, p. 399–420.

Davis, G.H., 1983, Shear-zone model for the origin of metamorphic core complexes: Geology, v. 11, p. 342–347.

Davis, G.H., Anderson, J.L., Frost, E.G., and Shackelford, T.J., 1980, Mylonitization and detachment faulting in the Whipple–Buckskin–Rawhide Mountains terrane, southeastern California and western Arizona, *in* Crittenden, M.D., Jr., Coney, P.J., and Davis, G.H., eds., Cordilleran metamorphic core complexes: Geological Society of America Memoir 153, p. 79–129.

Davis, G.H., and Coney, P.J., 1979, Geologic development of the Cordilleran metamorphic core complexes: Geology, v. 7, p. 120–124.

Doelling, H.H., Fitzhugh, D.D., and Brandt, C.J., 1989, The geology of Kane County, Utah: Utah Geological and Mineral Survey Bulletin 124, 192 p.

Ekren, E.B., Orkild, P.P., Sargent, K.A., and Dixon, G.L., 1977, Geologic map of Tertiary rocks, Lincoln County, Nevada: U.S. Geological Survey Miscellaneous Investigations Series Map I–1041, scale 1:250,000.

Fleck, R.J., Anderson, J.J, and Rowley, P.D., 1975, Chronology of mid-Tertiary volcanism in High Plateaus region of Utah, *in* Anderson, J.J., Rowley, P.D., Fleck, R.J., and Nairn, A.E.M., eds., Cenozoic geology of southwestern High Plateaus of Utah: Geological Society of America Special Paper 160, p. 53–61.

Gans, P.B. and Miller, E.L., 1983, Styles of mid-Tertiary extension in east-central Nevada, *in* Guidebook, Part I, Geological Society of America Rocky Mountain and Cordilleran Sections Meeting: Utah Geological and Mining Survey Special Studies, v. 59, p. 107–160.

Goldstrand, P.M., 1991, Tectonostratigraphy, petrology, and paleogeography of Upper Cretaceous to Eocene rocks of southwest Utah: Reno, Nev., University of Nevada at Reno Ph. D. dissertation, 205 p.

———1994, Tectonic development of Upper Cretaceous–Eocene strata of southwestern Utah: Geological Society of America Bulletin, v. 106, p. 145–154.

Gregory, H.E., 1949, Geologic and geographic reconnaissance of eastern Markagunt Plateau, Utah: Geological Society of America Bulletin, v. 60, p. 969–998.

Gross, W.W., and Hillemeyer, F.L., 1982, Geometric analysis of upper-plate fault patterns in the Whipple-Buckskin detachment terrane, California and Arizona, *in* Frost, E.G., and Martin, D.L., eds., Mesozoic-Cenozoic tectonic evolution of the Colorado River region, California, Arizona and Nevada: San Diego, Calif., Cordilleran Publishers, p. 257–265.

Hamilton, W.B., 1988, Death Valley tectonics—Hingeline between active and inactivated parts of a rising and flattening master normal fault, *in* Gregory, J.L., and Baldwin, E.J., eds., Geology of the Death Valley region: South Coast Geological Society Annual Field Trip Guidebook 16, p. 179–205.

Judy, J.R., 1974, Cenozoic stratigraphic and structural evolution of the west-central Markagunt Plateau, Utah: Kent, Ohio, Kent State University M.S. thesis, 107 p.

Mackin, J.H., 1960, Structural significance of Tertiary volcanic rocks in southwestern Utah: American Journal of Science, v. 258, no. 2, p. 81–131.

Maldonado, Florian, 1990, Structural geology of the upper plate of the Bullfrog Hills detachment fault system, southern Nevada: Geological Society of America Bulletin, v. 102, p. 992–1006.

Maldonado, Florian, and Moore, R.C., 1993, Preliminary geologic map of the Parowan quadrangle, Iron County, Utah: U.S. Geological Survey Open-File Report 93–3, scale 1:24,000.

Maldonado, Florian, Sable, E.G., and Anderson, J.J., 1989, Evidence for shallow detachment faulting of mid-Tertiary rocks, Red Hills (Basin and Range), with implications for a more extensive detachment zone in the adjacent Markagunt Plateau (Colorado Plateau), southwest Utah [abs.]: Eos, v. 70, no. 43, p. 1336.

———1992, Evidence for a Tertiary low-angle shear zone, Red Hills, with implications for a regional shear zone in the adjacent Colorado Plateau, *in* Engineering and environmental geology of southwestern Utah: Utah Geological Association Publication 21, Field Symposium, 1992, p. 315–323.

Maldonado, Florian, and Williams, V.S., 1990, Preliminary geologic map of the Parowan Gap quadrangle, Iron County, Utah: U.S. Geological Survey Open-File Report 90–495, scale 1:24,000.

———1993a, Geologic map of the Paragonah quadrangle, Iron County, Utah: U.S. Geological Survey Geologic Quadrangle Map GQ–1713, scale 1:24,000.

———1993b, Geologic map of the Parowan Gap quadrangle, Iron County, Utah: U.S. Geological Survey Geologic Quadrangle Map GQ–1712, scale 1:24,000.

Moore, R.C., 1982, The geology of a portion of the west-central Markagunt Plateau, southwestern Utah: Kent, Ohio, Kent State University M.S. thesis, 72 p.

Noble, D.C., McKee, E.H., Hedge, C.E., and Blank, H.R., Jr., 1968, Reconnaissance of the Caliente depression, Lincoln County, Nevada [abs.]: Geological Society of America Special Paper 115, p. 435–436.

Pierce, W.G., 1973, Principal features of the Heart Mountain fault and the mechanism problem, *in* De Jong, K.A., and Scholten, Robert, eds., Gravity and tectonics: New York, John Wiley, p. 457–471.

———1987, Heart Mountain detachment fault and clastic dikes of fault breccia, and Heart Mountain break-away fault, Wyoming and Montana: Geological Society of America Centennial Field Guide—Rocky Mountain Section, p. 147–154.

Reynolds, S.J., and Spencer, J.E., 1985, Evidence for large-scale transport on the Bullard detachment fault, west-central Arizona: Geology, v. 13, p. 353–356.

Rowley, P.D., Cunningham, C.G., Steven, T.A., Mehnert, H.H., and Naeser, C.W., in press, Cenozoic igneous and tectonic setting of the Marysvale volcanic field, and its relation to other igneous centers in Utah and Nevada, *in* Friedman, J.D., and Huffman, A.C., Jr., eds., Laccolith complexes of southeastern Utah—Tectonic control and time of emplacement: U.S. Geological Survey Bulletin.

Rowley, P.D., Mckee, E.H., and Blank, H.R., Jr., 1989, Miocene gravity slides resulting from emplacement of the Iron Mountain pluton, southern Iron Springs mining district, Iron County, Utah [abs.]: Eos, v. 70, no. 43, p. 1309.

Rowley, P.D., Mehnert, H.H., Naeser, C.W., Snee, L.W., Cunningham, C.G., Steven, T.A., Anderson, J.J., Sable, E.G., and Anderson, R.E., 1994, Isotopic ages and stratigraphy of Cenozoic rocks of the Marysvale volcanic field and adjacent areas, west-central Utah: U.S. Geological Survey Bulletin 2071, 35 p.

Rowley, P.D., Steven, T.A., Anderson, J.J., and Cunningham, C.G., 1979, Cenozoic stratigraphic and structural framework of southwest Utah: U.S. Geological Survey Professional Paper 1149, 22 p.

Rowley, P.D., and Threet, R.L., 1976, Geologic map of the Enoch quadrangle, Iron County, Utah: U.S. Geological Survey Geologic Quadrangle Map GQ–1296, scale 1:24,000.

Sable, E.G., and Anderson, J.J., 1985, Tertiary tectonic slide megabreccias, Markagunt Plateau, southwestern Utah: Geological Society of America Abstracts with Programs, v. 17, no. 3, p. 263.

Shawe, D.R., and Stewart, J.H., 1976, Ore deposits as related to tectonics and magmatism, Nevada and Utah: Transactions of American Institute of Mining, Metallic, and Petroleum Engineers, v. 260, p. 225–232.

Siders, M.A., Rowley, P.D., Shubat, M.A., Christenson, G.E., and Galyardt, G.L., 1990, Geologic map of the Newcastle quadrangle, Iron County, Utah: U.S. Geological Survey Geologic Quadrangle Map GQ–1690, scale 1:24,000.

Spurney, J.C., 1984, Geology of the Iron Peak intrusion, Iron County, Utah: Kent, Ohio, Kent State University M.S. thesis, 84 p.

Steiger, R.H., and Jäger, Emile, 1977, Subcommission on geochronology—Convention on the use of decay constants in geo- and cosmochronology: Earth and Planetary Science Letters, v. 36, p. 359–362.

Thomas, H.E., and Taylor, G.H., 1946, Geology and ground-water resources of Cedar City and Parowan Valleys, Iron County, Utah: U.S. Geological Survey Water-Supply Paper, 210 p.

Threet, R.L., 1952, Geology of the Red Hills area, Iron County, Utah: Seattle, Wash., University of Washington Ph. D. dissertation, 107 p.

Tobey, E.F., 1976, Geology of the Bull Valley intrusive-extrusive complex and genesis of the associated iron deposits: Eugene, Oregon, University of Oregon Ph. D. dissertation, 244 p.

Tompkins, F.V., Goodwin, J.C., and Malin, W.J., 1963, Cedar City, Utah, to Parowan, Utah, via Iron Springs mining district and Parowan Gap, Road log 3, *in* Heylmun, E.B., ed., Geology of southwestern Utah: Intermountain Association of Geologists Guidebook 12th Annual Field Conference, 1963, p. 222–226.

Wernicke, Brian, 1981, Low-angle faults in the Basin and Range province—Nappe tectonics in an extending orogen: Nature, v. 291, p. 645–648.

Wernicke, Brian, and Burchfiel, B.C., 1982, Modes of extensional tectonics: Journal of Structural Geology, v. 4, p. 105–115.

Williams, P.L., 1967, Stratigraphy and petrography of the Quichapa Group, southwestern Utah and southeastern Nevada: Seattle, Wash., University of Washington Ph. D. dissertation, 182 p.

Quaternary Geology and Tectonics of the Red Hills Area of the Basin and Range–Colorado Plateau Transition Zone, Iron County, Utah

By Van S. Williams *and* Florian Maldonado

GEOLOGIC STUDIES IN THE BASIN AND RANGE–COLORADO PLATEAU TRANSITION IN SOUTHEASTERN NEVADA, SOUTHWESTERN UTAH, AND NORTHWESTERN ARIZONA, 1992

U.S. GEOLOGICAL SURVEY BULLETIN 2056–J

UNITED STATES GOVERNMENT PRINTING OFFICE, WASHINGTON : 1995

CONTENTS

FIGURES

Quaternary Geology and Tectonics of the Red Hills Area of the Basin and Range–Colorado Plateau Transition Zone, Iron County, Utah

By Van S. Williams *and* Florian Maldonado

ABSTRACT

Near the Red Hills in southwestern Utah, upper Tertiary and Quaternary deposits and faults give some indication of the late Cenozoic history of geologic processes active in the transition zone between the relatively undisturbed structure of the Colorado Plateau and the highly faulted and tilted extensional structure of the Basin and Range province. The Red Hills, a north-northeast-trending, fault-bounded range formed of Tertiary volcanic rocks overlying Mesozoic and Tertiary sedimentary rocks, are part of a fault-block system that separated from the Colorado Plateau along west-dipping normal faults, slid westward, and tilted as much as 20° eastward.

Ages of the extensive alluvial deposits around the Red Hills are indicated by their stratigraphic relation to isotopically dated Quaternary basalts, coupled with their relative geomorphic position, modification of original depositional form, and degree of soil development, especially the morphology and thickness of carbonate-enriched horizons. These alluvial deposits consist for the most part of old alluvium (late Tertiary and early Quaternary) containing sparse intercalated tephra beds. The deposits are more than 1 km thick where preserved in down-faulted basins east and west of the Red Hills, but they are discontinuous and thinner on the uplifted Red Hills block. Post-depositional tectonism has tilted, faulted, and uplifted the old deposits in the basins; erosion, dominant over deposition since middle Pleistocene, has also modified original forms. Thus post-middle Pleistocene alluvial deposits are mostly very thin, overlying erosion surfaces cut on old alluvium and soft bedrock.

Besides alluvium, Quaternary deposits include playa silt, as well as basalt flows. The silt beds were deposited in Little Salt Lake during late Pleistocene and Holocene time. Basalt erupted during middle Pleistocene time in the eastern Parowan Valley and in early Pleistocene time in the Enoch graben.

The Little Salt Lake fault, one of a series of normal faults along the east side of the Red Hills, strikes N. 45° E. and dips 75° SE. It exhibits the highest fault scarp in alluvium near the Red Hills: the scarp's maximum height is 18 meters at a point where the maximum slope of the scarp is 19°. We postulate at least three episodes of movement on Little Salt Lake fault beginning before middle Pleistocene and continuing through late Pleistocene and perhaps into the Holocene; offset of middle Pleistocene geomorphic surfaces across the fault exceeds 60 meters, and offset of the late Pleistocene surface exceeds 10 meters. The average rate of vertical motion since middle Pleistocene has been about 0.12 mm/yr±50 percent, whereas the average rate since late Pleistocene has been at least 0.5 mm/yr±50 percent. Vertical offset on the fault bounding the east side of the Hieroglyph horst, in the southwestern Red Hills, has been as much as 70 meters since eruption of basalt flows 1.28±0.4 million years ago; vertical offset on the west-side-bounding fault is as much as 230 meters. Offset on the fault bounding the east side of the Enoch graben during the same period is as much as 50 meters. These relationships indicate vertical slip rates in the range of 0.054 mm/yr±30 percent on the east side and 0.178 mm/yr±30 percent on the west side of the horst, and 0.039 mm/yr±30 percent on the east side of the graben.

INTRODUCTION

Near the Red Hills, in southwestern Utah, geologic terrain evolves across a transition zone from the relatively less disturbed structure of the Colorado Plateau to the highly faulted and tilted extensional structure of the Basin and Range province. Examination of the upper Tertiary and Quaternary deposits and faults indicates the late history of geologic processes active in this transition zone.

The Red Hills are a north-northeast-trending, fault-bounded range of Tertiary volcanic rocks overlying Mesozoic and Tertiary sedimentary rocks. The range is located about 40 km north of Cedar City in the northeast corner of Iron County, southern Utah (fig. 1). Maldonado and others (1990) and Maldonado (this volume) have interpreted the

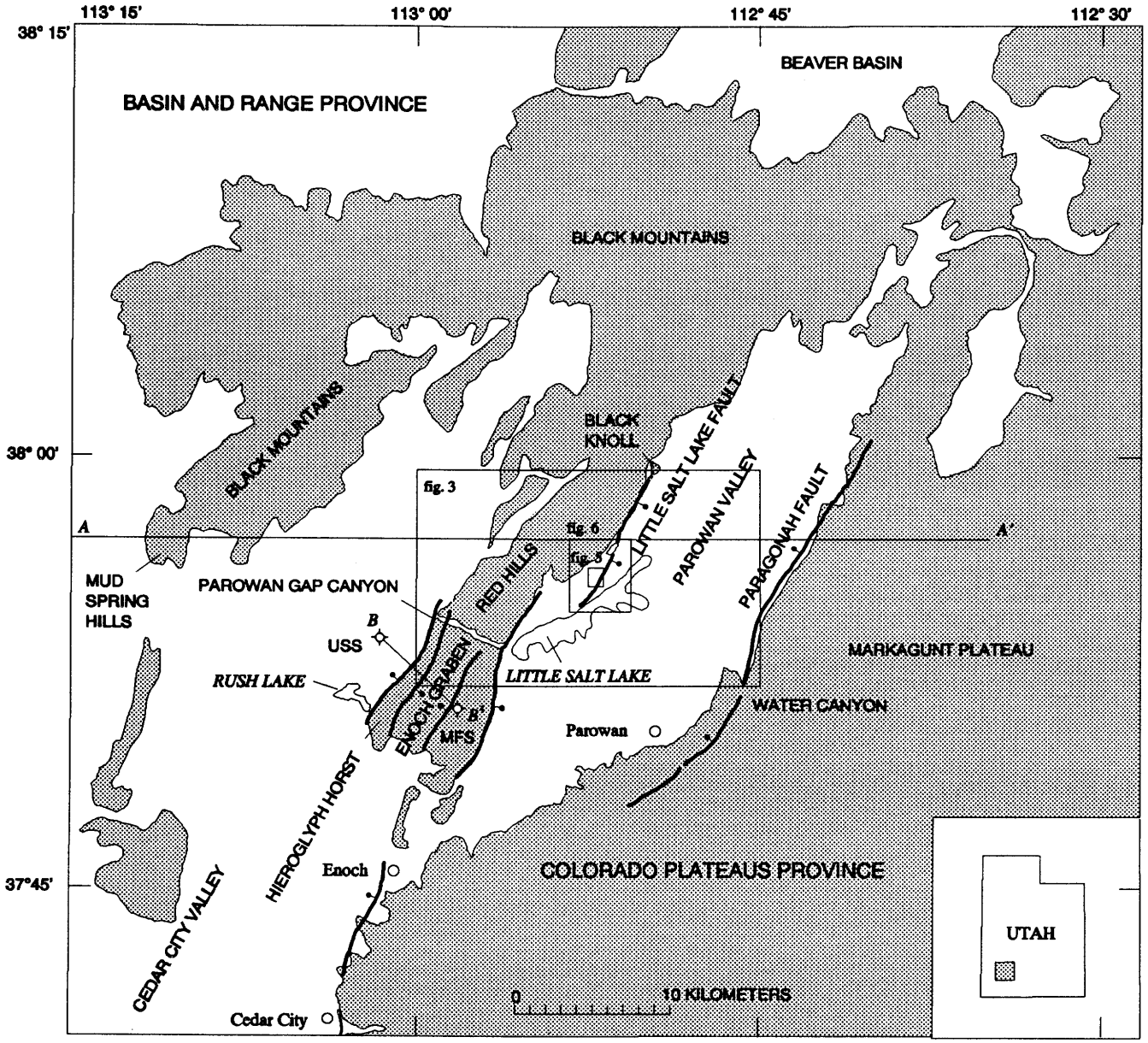

Figure 1. Map showing area surrounding the Red Hills, and location of other maps and cross sections in this report. Heavy line, fault; bar and ball on downthrown side. USS, U.S. Steel drill hole. MFS, Mountain Fuel Supplies drill hole.

Red Hills as part of a structural block that has been transported away from the Colorado Plateau along the Paragonah fault, detached from the basement along listric and low-angle faults, and migrated westward in response to gravitational forces and crustal extension (fig. 2). Normal faulting antithetic to the Paragonah fault has broken the detached block so that the western third of the block now forms a horst relative to the eastern two-thirds, which have dropped down to form a graben. The horst forms the Red Hills, and the graben underlies the alluvium-filled Parowan Valley, between the Red Hills on the west and the Markagunt Plateau on the east (fig. 1).

West of the Red Hills an alluvium-filled graben forms the north end of the Cedar City basin. Subsequent to deposition of a thick alluvial fill in the graben, the block has been uplifted and tilted eastward, and the Tertiary and Quaternary alluvium deeply dissected. Along the west side of that structural block, erosion has completely removed the alluvium to expose Tertiary volcanic rocks that now form part of the Black Mountains. The pattern of deformation that formed the Red Hills continues, as reflected by deformation of the bounding Tertiary and Quaternary alluvial deposits, and offset of Pleistocene and Holocene depositional surfaces by faults.

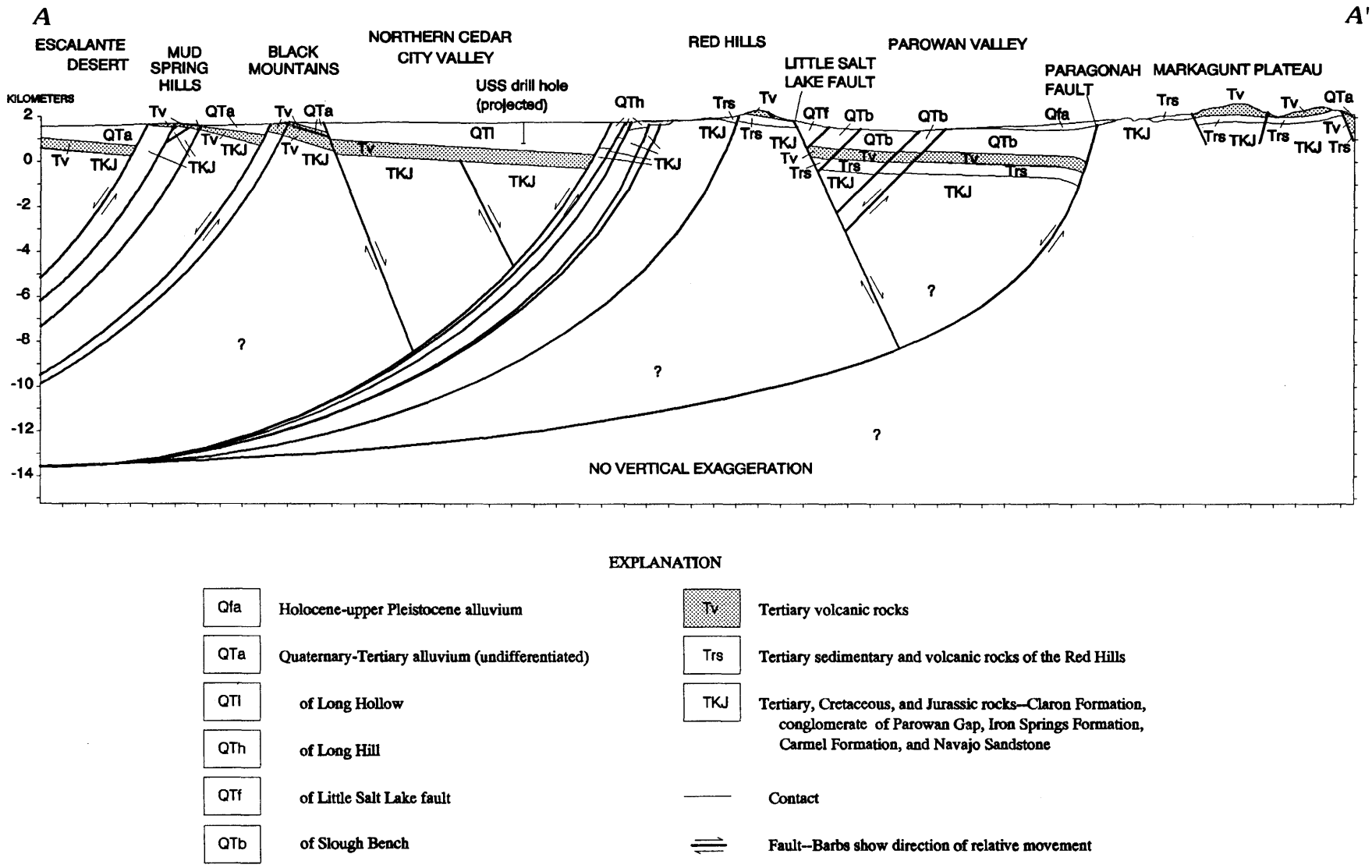

Figure 2. Generalized cross section *A–A′* across the Red Hills, showing westward movement and eastward tilting of structural blocks extending from the Markagunt Plateau west to the Escalante Desert basin. Queried at depth where relations uncertain. East-dipping faults are antithetic.

ACKNOWLEDGMENTS

Several residents of Cedar City assisted this study by sharing their knowledge of the area acquired over many years. These include Dr. Fred Lohrengel, Professor of Geology at Southern Utah University; Gorden Crandell, soil scientist with the U.S. Soil Conservation Service; Woodard Sandberg, hydrologist with the U.S. Geological Survey, and Gerald Staker, Utah State Engineer's Office. Profile surveys of the fault scarps would not have been completed without the much-appreciated assistance of four geology students at Southern Utah University: Dean Child, David Bateman, Dan Barton, and Paula Prichard.

QUATERNARY AND UPPER TERTIARY DEPOSITS

Thick, unconsolidated, alluvial fills are preserved in the deep, down-faulted basins east and west of the Red Hills. These are mostly of late Tertiary and early Quaternary age, except for thick upper Quaternary fan alluvium deposited on the east side of the Parowan Valley (fig. 3) by sediment-laden streams from the Markagunt Plateau. Tectonism within the basins has deformed and uplifted the older deposits so that they crop out in many places. Several generations of extensive but thin deposits of middle Pleistocene, upper Pleistocene, and Holocene alluvium overlie erosion surfaces cut on upper Tertiary and lower Pleistocene alluvium or weakly consolidated bedrock. Little Salt Lake Playa presently covers 21 km^2 on the floor of Parowan Valley, but older playa deposits have not been found at the surface or in drill holes (Thomas and Taylor, 1946). Ages of alluvial deposits are estimated based on their relation to isotopically dated Quaternary basalts, relative geomorphic position, modification of original depositional form, and degree of soil development, especially the morphology and thickness of carbonate-enriched horizons. No isotopic dates are available that directly apply to alluvial materials.

OLD ALLUVIAL DEPOSITS

The upper Tertiary and lower Quaternary basin fills on both sides of the Red Hills are quite thick. A U.S. Steel drill hole (USS) on the west side of the range in sec. 31, T. 33 S., R. 10 W. (fig. 4), only 2 km west of the range-front fault, reached a depth of 918 m without penetrating the base of the alluvium (Rowley, 1975). A gravity low (Cook and Hardman, 1967) centered south of the drill hole suggests a maximum depth to bedrock of about 1,200 m. On the east side of the range the alluvium may also be thick, but no deep holes have been drilled. A gravity profile across the southern Parowan Valley (Pe and Cook, 1980) placed the base of the alluvium at about 1,200 m. The deepest water well penetrated more than 180 m of alluvium without reaching the base (Bjorklund and others, 1977).

Uplift of the Red Hills has deformed old basin fill alluvium and raised it to a level where it is subject to erosion. On the west side, much of the bedrock on the uplifted block is still partially covered by eroded basin fill deposits (alluvium of Long Hill, unit QTh, fig. 3). To the east of the Red Hills, old alluvium on the west side of the Parowan Valley graben has been exposed by eastward tilting of the graben along normal faults, so that low hills of old alluvium protrude above depositional level west of the axis of the Parowan Valley (alluvium of Slough Bench, unit QTb, fig. 3).

PAROWAN VALLEY

Two distinct types of old basin fill alluvium are exposed on the west side of the Parowan Valley. The deposits forming low hills west of the axis of the valley consist of eroded remnants of uplifted distal alluvial fan and basin-center sheet flow deposits (unit QTb, fig. 3). The coarsest beds are sandy, pebbly silt and contain about 35 percent quartzite and volcanic pebbles less than 3 cm in diameter. The finest beds contain as much as 50 percent clay. Original calcium carbonate content of the sediment is variable depending on source rock, but probably is less than the 14 percent average determined for young sediment eroded from the Paleocene and Eocene Claron Formation, the main local source of calcium carbonate. Surface soils formed under surfaces cut on unit QTb are thicker than 1.5 m, and include as much as 46 percent total calcium carbonate, small amounts of gypsum, and some salt (Gorden Crandell, U.S. Soil Conservation Service, Cedar City, written commun., 1989). The deposits are poorly exposed and commonly veneered with windblown sand and silt from the Little Salt Lake playa. They are overlain by younger playa deposits and alluvium (units Ql, Qfa, and Qf, fig. 3). Direct evidence of the numerical age of unit QTb is scant, but its stratigraphic position, thick carbonate-enriched soil, and lack of original depositional form all indicate that it is relatively old.

Calculations based on the measured calcium carbonate of horizons in the top 1.5 m of the soil, an assumed bulk density of 1.6, and assumed original calcium carbonate content of about 14 percent indicate that at least 36 g $CaCO_3$ /cm^2 has been added to the soil profile. This compares approximately to the accumulation in soils developed in alluvium of North Creek in the Beaver Basin (Machette, 1985, p. 32), which is 50 km northeast of the study area. The age of alluvium of North Creek indicated by U-trend dating is 290±80 ky (Steer, 1980), but unit QTb is probably much older, because it was uplifted and eroded prior to the start of soil carbonate accumulation.

Old alluvium (QTf, fig. 5) that is distinct from that in the center of the valley (QTb, fig. 3) is exposed at a few

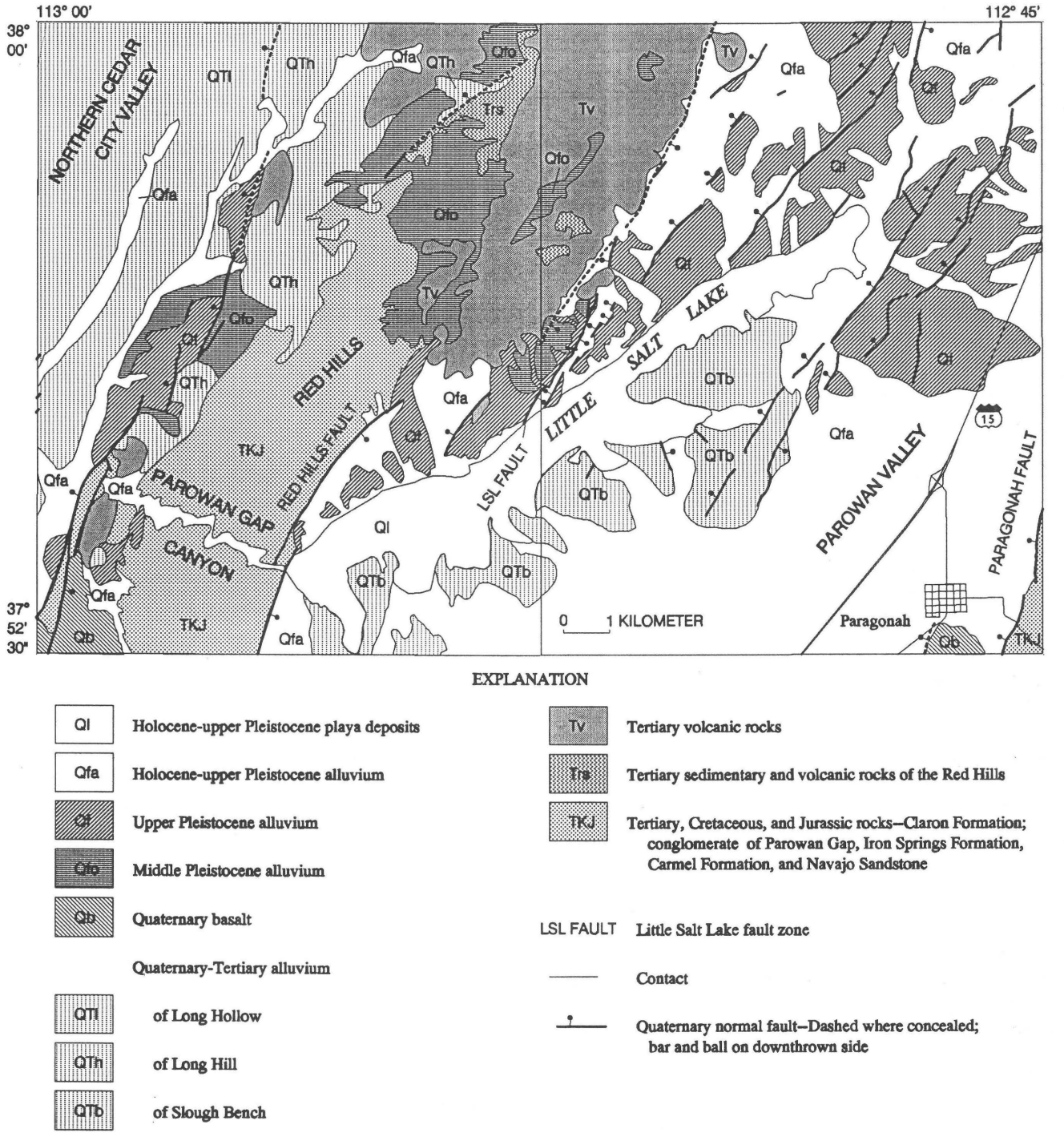

Figure 3. Quaternary deposits and faults, and generalized bedrock geology of the Red Hills and surrounding basins. Parowan Gap (left) and Paragonah (right) 7.5–minute quadrangles.

places along ravines cut into the upthrown block on the west side of the Parowan Valley, west of the Little Salt Lake fault. Unit QTf is coarser, better bedded, more intensely deformed than unit QTb, and includes more mafic volcanic clasts and beds of silicic volcanic ash. It is primarily yellowish brown, medium-grained, subangular, weakly indurated tuffaceous sandstone interbedded with light-brownish-gray, silty, tuffaceous, weakly indurated mudstone, and reddish-black, subangular, coarse-grained, weakly indurated, mafic volcanic sandstone. The mafic volcanic sandstone beds locally contain matrix-supported, subrounded mafic lava clasts as large as 50 cm in diameter, probably derived from mafic lava blocks in the Mount Dutton Formation (20–26 Ma). The Mount Dutton Formation is missing from the Red

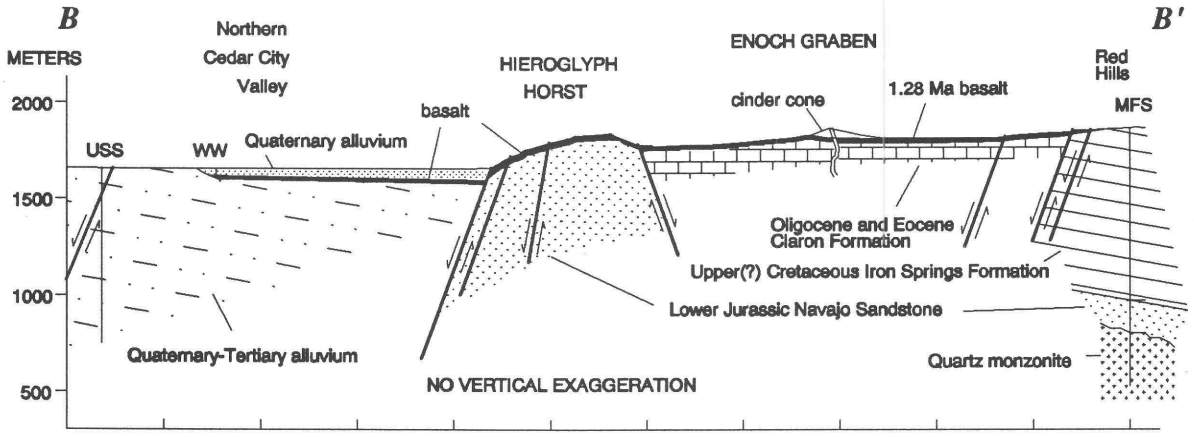

Figure 4. Cross section *B–B′* across the Hieroglyph horst and Enoch graben. Geologic contacts from Maldonado and Williams (1993b), Rowley (1975), and Rowley and Threet (1976). Heavy line, fault; barbs show direction of relative movement. USS, U.S. Steel drill hole; WW, Endrody Ranch water well; MFS, Mountain Fuel Supplies drill hole.

Hills except for three small erosional remnants on the east side of the range (fig. 3, outliers of unit Tv) (Maldonado and Williams, 1993a); however, it is several hundred meters thick 10 km north of the Little Salt Lake fault and probably existed on the Red Hills prior to its removal by erosion. The exposures of unit QTf near the Little Salt Lake fault (fig. 5) are extensively sheared, faulted, folded, and tilted as much as 41°. Some fault planes are coated by calcium carbonate.

The mudstone in unit QTf locally contains at least one bed of reworked gray silicic volcanic ash more than 1 m thick. At the base of the reworked ash bed, a thin layer of white air-fall ash averages about 1 cm thick. This ash is weathered, and it has not yet been possible to identify its source or determine its age. In a structural basin similar to the Parowan Valley but 40 km to the north, lake deposits in the Beaver Basin contain at least five different Tertiary and early Pleistocene ash beds ranging in age from 2.4 to 1.6 Ma, and post-lake Quaternary alluvium contains the 0.55 Ma tephra of Ranch Canyon (Machette, 1985).

No direct evidence of the numerical age of unit QTf has been found, but it seems to be the oldest alluvial unit exposed in the Parowan Valley. It is folded and dips as steeply as 41°, but it is overlain by unfolded Pleistocene alluvium (units Qf and Qfo). Unit Qfo has lost much of its original depositional form but locally retains a thick, well-developed carbonate-enriched soil suggesting that unit Qfo is at least as old as middle Pleistocene. Unit QTf is rich in mafic lava clasts from the Mount Dutton Formation, a thick volcanic deposit that has been completely stripped from the drainage area that formerly contributed sediment to unit QTf. Parts of the unit are well consolidated and highly oxidized. The tephra beds are more altered and appear older than the 0.55 Ma tephra of Ranch Canyon, and they probably correlate to one of the Tertiary tephras found in the Beaver Basin, although the correlation has not been proven.

NORTHERN CEDAR CITY VALLEY

Most of the basin fill in the northern Cedar City Valley (alluvium of Long Hollow, unit QTl, figs. 2, 3) has been raised and tilted southwest as much as 20° as part of the uplift of the Black Mountain structural block (Rowley, 1975). The eastern part of the basin fill (alluvium of Long Hill, unit QTh, figs. 2, 3), however, rests on the Red Hills structural block, and has been further uplifted by the growth of the Red Hills to a level above that of the adjacent east edge of the Black Hills block in the northern Cedar City Valley. This difference in structural settings is the primary basis for distinguishing two old alluvial units on the west side of the Red Hills (Maldonado and Williams, 1993b).

Both unit QTl and unit QTh are poorly sorted, poorly bedded, gravelly fan alluvium, but unit QTh is distinguished from unit QTl by its relative thinness, greater deformation, inclusion of large allochthonous blocks of volcanic rocks, greater proportion of quartzite clasts, and greater dissection. Unit QTh probably correlates to the older, basal part of unit QTl that is buried at great depth west of the range-front fault. An early Pleistocene or older age is indicated for unit QTh because it underlies 1.28±0.4 Ma basalt flows in the Enoch graben (figs. 3, 4).

Unit QTl consists of subangular to angular gravel of mostly volcanic rocks and sparse rounded quartzite cobbles supported by a matrix of light-reddish-brown sand. The deposits are generally uncemented but locally are moderately well cemented by calcium carbonate. Clasts average 6 cm in diameter and are as large as 50 cm in diameter. The original depositional form is not preserved because the deposit has been uplifted and tilted, and the beds truncated by lateral erosion that has cut pediments across the deposits at several levels. Streams are now entrenched as deep as 60 m below the pediment surfaces.

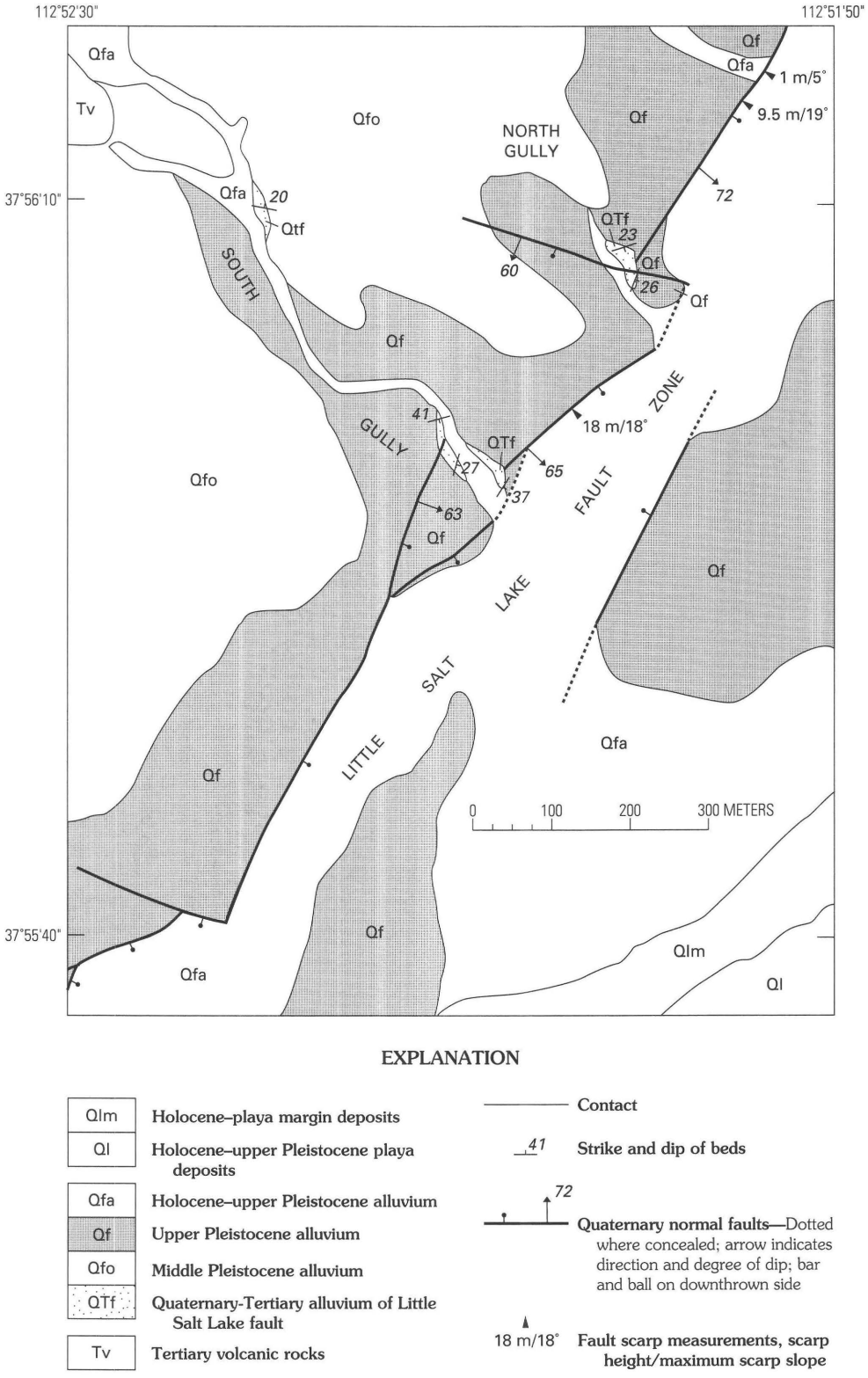

Figure 5. Geologic map along a section of the Little Salt Lake fault zone showing details of faulting.

Despite the small amount of calcium carbonate in the alluvium of unit QTl, thick petrocalcic soils are developed under the relict pediment surfaces, which are much younger than the underlying unit QTl. Upper soil horizons have been stripped leaving stage IV laminar calcium carbonate (of Gile and others, 1966) exposed from the surface down to 25 cm

depth and a strongly cemented stage III carbonate-enriched horizon from 25 to 150 cm depth. These are the most strongly developed soils in the Red Hills area; they are approximately comparable in development to the soils below the Table Grounds Surface in the Beaver Basin, 50 km to the northeast, which are estimated to be 750 ky old (Machette, 1985, p. 32). If the comparison is valid, it indicates a minimum age of latest early Pleistocene for the pediments and a much older age for deposition of unit QTl.

Unit QTh, resting on the Red Hills block, is poorly bedded, poorly sorted, and locally weakly cemented by calcium carbonate. Clasts are angular to subangular and consist primarily of volcanic rocks averaging 6 cm in diameter and as large as 1 m in diameter in the northern part of the range; southward the predominant clast type changes gradually to rounded quartzite cobbles less than 10 cm in diameter. Clasts are supported by a matrix of light-reddish-brown sand that is redder and more calcareous southward. The original depositional form of unit QTh is not preserved.

Within unit QTh are allochthonous blocks of volcanic rock as long as 400 m formed of the same rock units that are exposed in the northern Red Hills. These blocks probably represent the syntectonic deposit that resulted from opening of a depression west of the present Red Hills through down-to-west offset at the western margin of the Red Hills structural block. Although such detached blocks are exposed only along the western margin of the northern Red Hills, they may also be present within the basal alluvial deposits of the northern Cedar City Valley (unit QTl) to the west.

YOUNG ALLUVIAL DEPOSITS

During the middle and late Pleistocene, erosional processes have been more effective than depositional ones in the area surrounding the Red Hills. Consequently, young alluvial deposits are generally quite thin except on the east side of the Parowan Valley, where sediment-laden streams from the Markagunt Plateau have built up alluvial fans thick enough to completely bury the underlying older alluvial sediments (unit Qfa, figs. 2, 3). The extensive low-level surfaces east and west of the Red Hills consist typically of pediments cut on old alluvium (units QTl, QTh, QTf, and QTb) and are veneered with a thin layer of young alluvium (units Qfa, Qf, and Qfo). Similar surfaces have been cut on soft bedrock exposed within the Red Hills; these are now preserved on high benches or in embayments of the mountain front. The young alluvium resembles the old alluvium in its composition, but it is less consolidated and less oxidized, retains depositional form, and is not tilted.

At least four distinct levels of pediment surfaces, estimated on the basis of soil development and geomorphology to range in age from middle Pleistocene to Holocene, record periods when downcutting was minimal and local base level relatively stable. The relation of most late Pleistocene and some Holocene surfaces to fault scarps implies that some of the episodic instability was caused by uplift of these surfaces relative to local base level in the Parowan Valley, uplift that occurred along normal faults on the west side of the Parowan Valley. Late Pleistocene surfaces thinly covered with unit Qf are extensively preserved on the upthrown side of faults (figs. 3, 5), although the surfaces are interrupted by entrenched streams. Late Pleistocene surfaces are preserved as high as 10 m above modern surfaces of planation, and late Pleistocene and Holocene surfaces (unit Qfa, figs. 3, 5) as high as 1 m above those surfaces. Middle Pleistocene surfaces are generally preserved as small remnants near the apical areas of the younger surfaces and cannot be directly related to fault scarps. Two middle Pleistocene surfaces covered with unit Qfo (figs. 3, 5) are preserved at about 60 m and 18 m above modern, active surfaces of planation.

Soils in unit Qfo on the middle Pleistocene surfaces have been truncated by erosion in most places, but locally profiles are preserved that have stage III (Gile and others, 1960) development of carbonate-enriched horizons 55 cm thick that extend from 35 to 90 cm depth; in addition, they have calcium carbonate rinds and pendants as thick as 5 mm beneath clasts (Gorden Crandell, written commun., 1989). Where the soils were observed, units Qfo and Qf contain little or no Claron Formation detritus and have little original calcium carbonate. Soils on unit Qfo depositional surfaces are approximately comparable in development to the middle Pleistocene soils in alluvium of Greenville in the Beaver Basin that are estimated to be 140 ky old (Machette, 1985, p. 32).

Soils on unit Qf have stage II development of carbonate-enriched horizons 40 cm thick that extend from 35 to 75 cm depth, and the bottoms of clasts have thin carbonate coatings (Gorden Crandell, written commun., 1989). These soils are slightly more developed than the late Pleistocene soils in alluvium of Beaver in the Beaver Basin that are estimated to be 12–15 ky old (Machette, 1985, p. 32).

The youngest (late Pleistocene to Holocene) alluvial deposits (unit Qfa) generally thinly cover active pediments cut on units QTb and QTf on the west side of the Parowan Valley and accumulate as thick fan deposits on the east side. Small fans of unit Qfa have also grown along the sides of Parowan Gap Canyon and in the narrow graben east of the Little Salt Lake fault. The base of the deposits is not exposed. Surfaces underlain by unit Qfa are generally not eroded, although they are slightly disrupted by faults at a few places. The material in unit Qfa is similar to that in the older alluvial deposits, although a surface layer of sand and silt exists that has been largely stripped from the older deposits. Virtually no soil has developed beneath the Holocene surfaces. The large fans on the east side of the Parowan Valley must include lower, middle, and upper Pleistocene alluviums, but they are mapped as unit Qfa because this unit is exposed at the surface.

PLAYA DEPOSITS

On the west side of the Parowan Valley are young deposits of Little Salt Lake playa (unit Ql, figs. 3, 5) that are dammed by the combination of late Cenozoic uplift of the Red Hills relative to the Parowan Valley graben (Threet, 1952; Anderson and Christenson, 1989) and deposition of alluvial fans within Parowan Gap Canyon near its east end (fig. 3) (Neilson, 1983). The great depth of Parowan Gap Canyon cutting across the Red Hills indicates that significant stream flow westward from the Parowan Valley has occurred throughout the history of Red Hills uplift, although little flow occurs at present, and even less occurred before local farmers cut a trench 3 m deep through the alluvial fan deposits within the canyon. Whether the present lack of significant flow through the canyon is representative of conditions prior to settlement 150 years ago is uncertain. Since agricultural development, the loss of water from Parowan Valley is much greater due to evapotranspiration by crops, and peak runoff is reduced by impoundment in reservoirs and infiltration to replace ground-water withdrawals.

Under natural conditions, the balance among several competing processes determines the situation in the canyon and the lowest portion of the Parowan Valley floor. Increased precipitation on the Markagunt Plateau, such as occurred during the pluvial periods of the Pliocene and Pleistocene, would tend to increase stream flow and sediment production, and would work to destroy Little Salt Lake, both by filling the basin with sediment and by eroding the threshold that retains the lake. When increased stream flow filled the playa basin to overflowing, flow through Parowan Gap Canyon carried away sediment from the canyon walls and prevented it from building up on the canyon floor, and it may have also eroded the bedrock threshold. Increased deposition of sediment in the lake tended to fill the lake basin above the level of the canyon threshold, so that all runoff tributary to Parowan Valley flowed through the Parowan Gap Canyon, increasing the efficiency of erosion and counteracting the damming effects of both uplift of the bedrock threshold and deposition of sediment from the canyon sides. High evapotranspiration in the Parowan Valley, low sediment influx, and rapid uplift of the Red Hills relative to the Parowan Valley worked in combination to prevent flow through Parowan Gap Canyon and consequently to promote blockage of the canyon by sediment from the canyon walls and expansion of the lake floor.

Unlike many ephemeral lakes in the Basin and Range province, Little Salt Lake was probably not significantly larger during pluvial periods. No shorelines are observed more than a few meters above the present playa floor, and the many water wells drilled in the Parowan Valley have not encountered playa deposits at depth; thus the playa probably was no more extensive during the Pleistocene than it is at present.

Deposits on the playa floor (unit Ql) are calcareous, saline, and gypsiferous gray beds of clay, silt, and sand. Deposits on the playa margin (unit Qlm) up to former high water level are similar but sandier and include pebbles transported by sheet wash. Sand and sand-sized aggregates of silt and clay are eroded from the playa floor by wind and transported to the northeast and east, where they accumulate as low, saline dunes and sheets that support a distinctive sodium-tolerant brushy vegetation, dominated by greasewood.

QUATERNARY BASALTS

Quaternary basalts are found at two different locations around the Red Hills. Volcanism from centers in the Enoch graben in the southwestern Red Hills has produced flows (figs. 1, 3, 4) that extend into the southwest corner of the Parowan Gap quadrangle (fig. 3) and have an isotopically determined age of 1.28±0.4 Ma (Anderson and Mehnert, 1979). Those flows are localized along and offset by a system of normal faults.

Basalt flows that extend into the southeast corner of the Paragonah quadrangle from Water Canyon (figs. 1, 3) have an isotopically determined age of 0.44±0.04 Ma (Fleck and others, 1975). The vent for these flows is about 4.5 km south of the Paragonah quadrangle and 2.5 km southeast of the Paragonah fault, on the upthrown side. The flow surface drops down about 130 m where it crosses the Paragonah fault, and at least 70 m more where it crosses a parallel range-front fault 1.5 km east of the Paragonah fault (Hamblin and others, 1981). The westward extension of the flow is buried at unknown depth beneath alluvium in the Parowan Valley graben.

If the steps in the basalt flow surface are entirely caused by post-flow displacement along the faults rather than cascades over preexisting scarps, combined average rate of vertical displacement across the two mountain-front faults since the middle Pleistocene exceeds 0.46 mm/yr±9 percent. The Paragonah fault alone has averaged 0.30 mm/yr±9 percent. The uncertainty of 9 percent reflects only the analytical uncertainty of the date.

In addition to the Quaternary basalts, another source of basaltic sediment that is probably of Tertiary age is a string of three small, basaltic exposures along the range-front fault on the west side of Parowan Valley in the northwest corner of the Paragonah quadrangle (fig. 3, outliers of unit Tv). This group of exposures is probably a remnant of Mount Dutton Formation, which has otherwise been completely stripped from the Red Hills but is extensively preserved 5 km to the north of Black Knoll (fig. 1) (Maldonado and Williams, 1993a). The range-front fault in this part of the range is the northward extension of the Little Salt Lake fault. The northernmost and largest of these exposures, Black Knoll, includes dikes, large, angular blocks of mafic lava, and beds of scoria

dipping radially outward at about 17°. Flow rocks and dikes within Black Knoll have reversed magnetic polarity.

QUATERNARY FAULTS

GENERAL PATTERN

Figure 3 shows faults around the Red Hills that displace alluvium and volcanic rocks of Quaternary age. Where there is an absence of Quaternary deposits within bedrock areas of the Red Hills, many more faults may also have been active during the Quaternary. All the faults cutting upper Tertiary and Quaternary alluvial deposits have a northeasterly trend, but within the Oligocene volcanic bedrock of the northern Red Hills many older faults have other trends. The randomly oriented faults do not extend downward into the Eocene Claron Formation sediments, and probably reflect only local stresses that developed as the volcanic rocks slid along their contact with the underlying sedimentary rocks.

With a few important exceptions, faults within the alluvium on both sides of the Red Hills are down to the west. The cross section in figure 2 shows most faults in the Parowan Valley to be antithetic to the Little Salt Lake fault, which forms the western boundary of the Parowan Valley graben, but synthetic to the Paragonah fault, the major fault that defines the western margin of the Markagunt Plateau as well as the base of the Red Hills horst and Parowan Valley graben (fig. 2). Displacement of aquifers within the alluvium of the Parowan Valley by faulting has produced abundant springs along the fault traces (Thomas and Taylor, 1946). In some cases, no offset of the ground surface is apparent, yet the trace of the fault is prominent on the aerial photographs because of the aligned springs.

On the east side of the Parowan Valley and on the west side of the Red Hills, faults dip in the same direction as the ground-surface slope, and fault scarps as high as 7.7 m are preserved. On the west side of the Parowan Valley, all faults but the westernmost dip opposite to the direction of ground surface slope, and fault scarps tend to be buried by sediment from upslope. Some buried fault scarps maintain surface expression in the form of a subtle break in slope where the pediment surface slopes opposite to the fault dip slightly less steeply than in other parts of the pediment. Other upslope-facing faults have scarps protruding as high as 3 m above the postfaulting young alluvium burying the downthrown side.

Several west-facing scarps on the east side of the Parowan Valley are estimated to have formed during the Holocene or late Pleistocene (Anderson and Christenson, 1989, p. 15), and one clearly offsets Holocene alluvium about 1 m (Maldonado and Williams, 1993a). Several west-facing scarps west of the Red Hills are estimated to have middle to late Pleistocene ages, and the age of one on the west side of the Red Hills horst was estimated as early to middle Pleistocene (Anderson and Christenson, 1989, p. 14).

At only two localities around the Red Hills are down-to-the-east Quaternary faults prominent. One is the east side of the Red Hills (fig. 3), where mountain-front faults are antithetic to the Paragonah fault. Two right-stepping en-echelon range-front faults on the east side of the Red Hills generally form the boundary between bedrock and alluvium without significantly offsetting the alluvium, except where the northernmost fault extends southward through alluvium as the Little Salt Lake fault. The other major east-dipping faults bound the west side of the Enoch graben (Threet, 1963) (figs. 1, 4) on the west side of the southern part of the range. The faults along the Enoch graben offset Quaternary basalt flows at the north end and Quaternary alluvium at the south end, near Enoch.

LITTLE SALT LAKE FAULT

The east side of the Red Hills is bounded by a series of right-stepping, en-echelon, northeast-trending, down-to-the-east faults, but only the fault near the center of the range front has produced a prominent scarp in Quaternary alluvium (figs. 3, 5). In the southern part of the range, the Red Hills fault (figs. 1, 3) is along the bedrock alluvium contact, and forms few scarps in alluvium (Anderson and Christenson, 1989). In the northern part, the range-front fault is covered, and there are no east-facing scarps in the alluvium.

In the central part of the Red Hills, where the mountain front jogs to the right (fig. 3), a 3.5-km-long fault scarp (fig. 6) that offsets alluvial surfaces down to the east by 10 m projects southward from the northern mountain front. This scarp disappears southward beneath deposits of Little Salt Lake playa, and was named Little Salt Lake fault by Thomas and Taylor (1946). It is the highest Quaternary fault scarp in alluvium in the area surrounding the Red Hills.

STRUCTURE

Strands of the Little Salt Lake fault, small antithetic faults, and a cross fault are exposed in two gullies where streams have eroded 15 m into the upthrown block (figs. 5, 7, 8, 9). The fault planes can be recognized only where they cut the semiconsolidated alluvium of unit QTf. The strands of the main fault are indistinct because they mostly cut uniformly brown, poorly bedded, coarse sand within the small areas of exposure. Measurements were made by carefully brushing the exposure to emphasize weak preferential cementation along the anastomosing fault strands (fig. 7). The strike of the exposed east-dipping fault surfaces averages about N. 45° E., dipping 75° SE. (figs. 5, 8, 9). Beds east of the fault plane could not be matched with those to the west to estimate vertical offset. In most places the fault is covered by the boulder-rich colluvium that mantles the fault scarp.

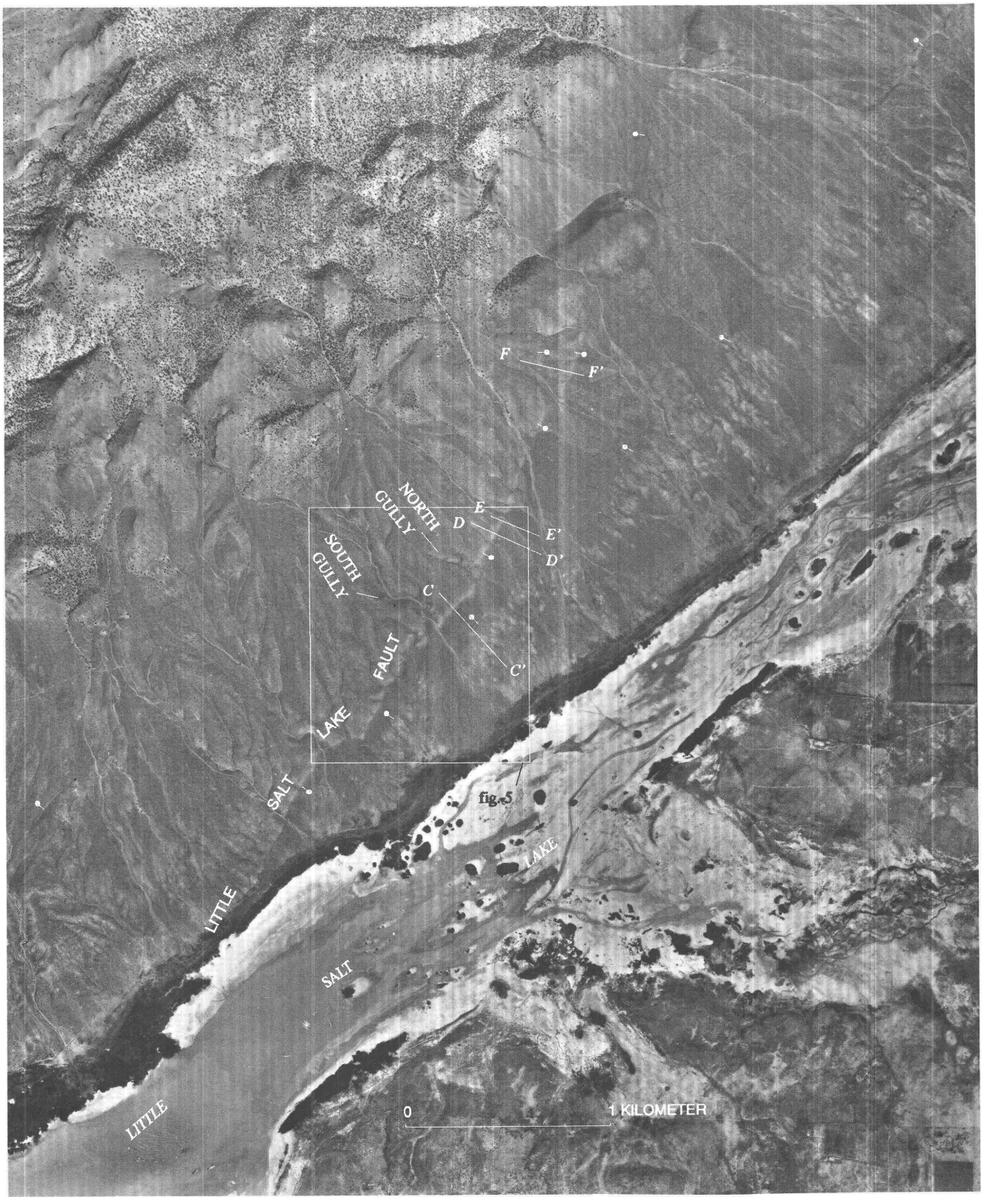

Figure 6. Aerial view of Little Salt Lake fault scarp showing location of profiles *C–C′*, *D–D′*, *E–E′*, and *F–F′*; north and south gullies; and location of figure 5.

Around the area of exposures, the Little Salt Lake fault is not a single plane, but splits into several strands, only some of which are exposed (figs. 5, 8, 9). Between the strands, blocks of downdropped unit QTf are preserved that expose small west-dipping antithetic faults. These antithetic faults are more obvious in exposures than the east-dipping faults,

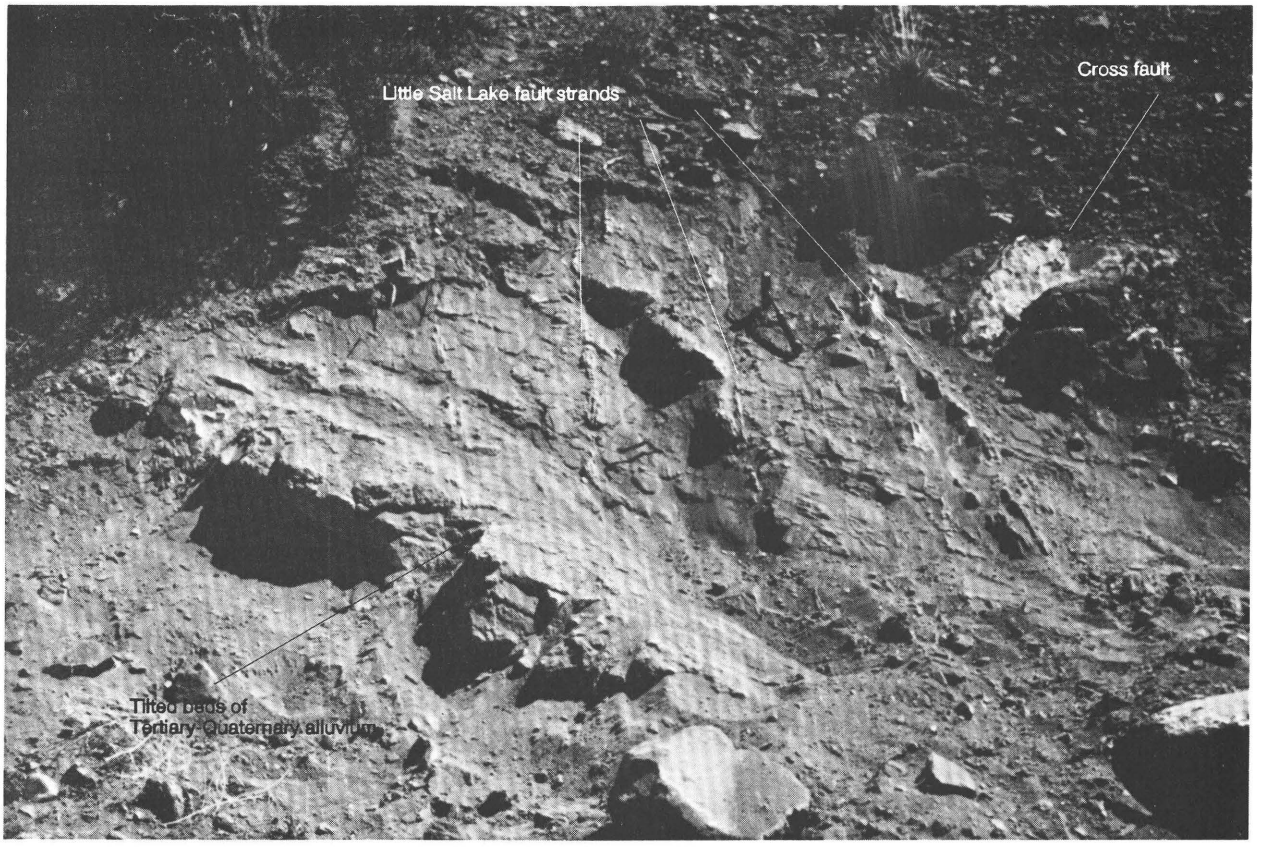

Figure 7. Exposure of the Little Salt Lake fault and small antithetic faults cutting tilted Tertiary and Quaternary alluvium unit associated with the fault (unit Qtf). North wall of north gully at intersection of Little Salt Lake fault with cross fault. Hammer between fault strands indicates scale.

because they offset well-bedded strata of contrasting lithology. The antithetic faults dip northwestward at 37° to 46° and strike about S. 30° W., converging toward the Little Salt Lake fault northward.

The Tertiary and Quaternary alluvium (unit QTf) is tilted on both sides of the fault. Strikes of beds measured in a limited number of exposures in the downthrown block are rotated counterclockwise about 50° relative to those on the upthrown block (fig. 5). On the downthrown side of the Little Salt Lake fault exposure, the beds strike about N. 20° E. and dip from 26° to 37° E. Immediately west of the Little Salt Lake fault exposure, beds in the upthrown block strike about N. 70° E. and dip from 23° to 41° S. About 500 m west of the Little Salt Lake fault, the beds strike west but dip 20° N. (figs. 5, 8, 9), indicating that proximity to the fault is not the sole cause of folding.

In both gullies where the Little Salt Lake fault is exposed, the structure is further complicated by crossfaulting and splaying (figs. 5, 8, 9). At the north gully (fig. 8) the fault scarp is displaced about 75 m to the left along an apparent cross fault exposed along the wall of the gully. The cross-fault surface consists of several parallel calcite-coated surfaces with slickensides and mullions parallel to the direction of dip, indicating normal rather than strike-slip or oblique-slip fault movement. These surfaces strike generally S. 70° E. and dip 60° SW. (figs. 5, 8).

South of the south gully (figs. 5, 9), the Little Salt Lake fault scarp is offset to the right through splaying rather than crossfaulting. The west splay is expressed as a continuation of the scarp south of the south gully that dies out at the gully. The east splay crosses the gully and merges with the scarp north of the south gully. The west splay is well exposed in the south wall of the southern gully but could not be traced north of the gully. The east splay is well exposed in the northern wall of the gully.

MORPHOLOGY

At its south end, the Little Salt Lake fault scarp disappears beneath the Holocene deposits of Little Salt Lake playa. No offset of the playa surface, cracking, or tonal contrast was detected along the surface projection of the fault (fig. 6). Northward, the down-to-the-east scarp increases in height, and splays, cross faults, and en-echelon steps offset the fault scarp slightly to the right (figs. 5, 6). Near the north end, the fault splits into two strands with about equal vertical

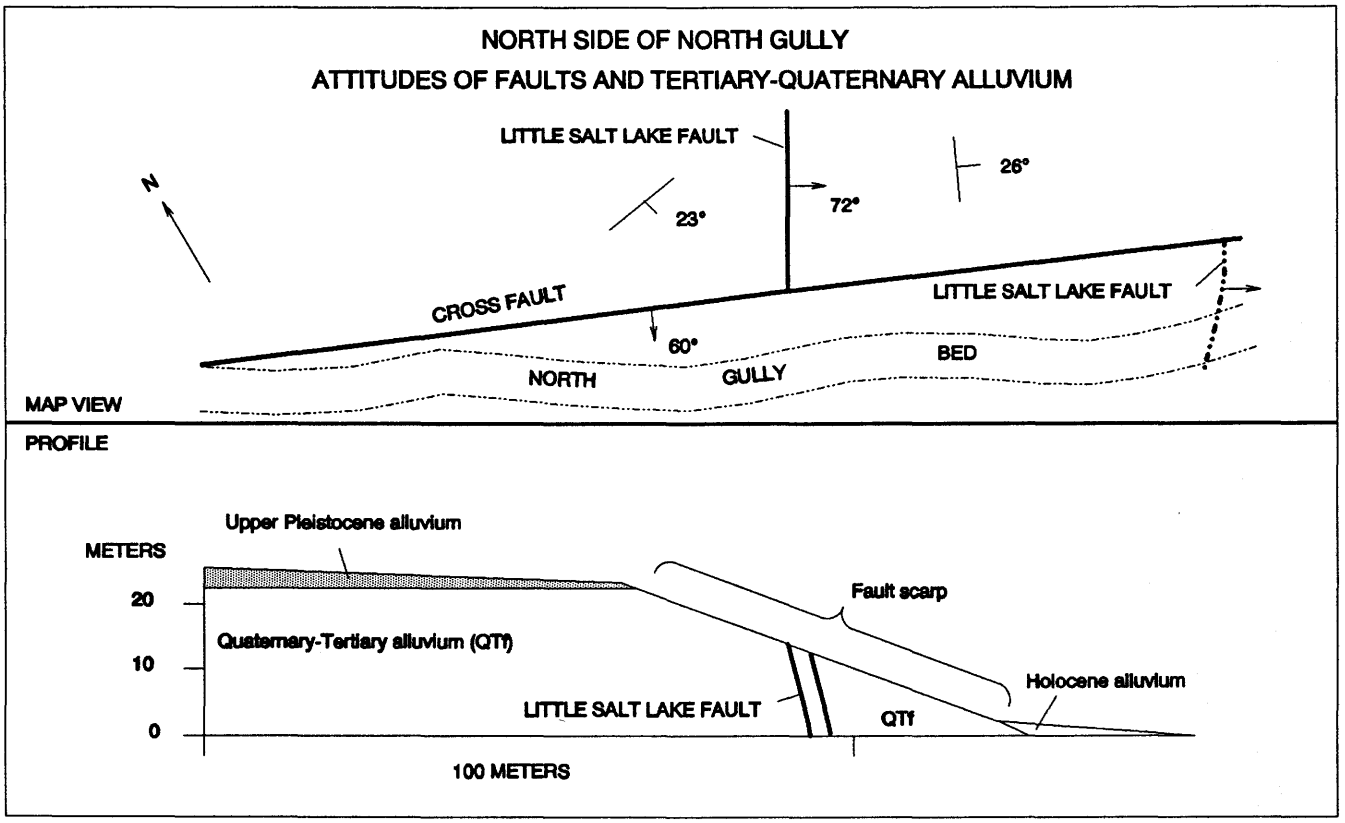

Figure 8. Map and cross section of fault and bedding attitudes in tilted Tertiary and Quaternary alluvium (unit Qtf) near Little Salt Lake fault exposed in walls of north gully. Map at same scale as profile.

scarp height, and a total scarp height about the same as farther south (figs. 3, 6). Both strands appear to end where they butt into basalt exposures of the Miocene Mount Dutton Formation that extend about 700 m east of the main mountain front (fig. 6). The bedrock was evidently strong enough to resist the forces that broke and displaced the alluvium. North of the basalt exposures, another fault on the same trend as the east splay of the Little Salt Lake fault extends from the basalt exposures north to the mountain front, but the scarp is down to the west (figs. 3, 6), opposite to the Little Salt Lake fault.

On the upthrown side of the Little Salt Lake fault, remnants of at least two pediment surfaces are preserved. The lower is relatively planar except where incised by gullies. Four to eight meters higher, rounded ridges of alluvium represent the remnants of at least one older surface. These pediment surfaces are covered by a relatively thin veneer of unfolded alluvium (units Qfo and Qf) and are cut on much older alluvial sediments (unit QTf) deformed by folding and faulting.

East of the Little Salt Lake fault is a graben, filled with upper Pleistocene and Holocene alluvium (unit Qfa), that is bounded on its east side by a down-to-the-west fault antithetic to the Little Salt Lake fault (figs. 3, 5, 6, 10). The graben narrows southward from 1,000 to 100 m in width over a distance of 4 km as the antithetic fault converges with the Little Salt Lake fault. The pediment surface east of the graben appears, on the basis of slope, geomorphic form, and soil development, to be equivalent to the uplifted pediment surface west of the graben, which is underlain by unit Qf.

A measure of the age of the fault scarps can be estimated from their slope morphology. Four profiles across the Little Salt Lake fault scarp (figs. 6, 10) were measured using a surveying level and rod. Profile *C–C′* (fig. 10) extends across the graben and has a maximum slope of 18°, and a scarp height of 17.7 m. The upslope-facing scarp of the antithetic fault is expressed as a flat bench along the slope, because the scarp is mostly buried. A scarp rise of 17.7 m over a horizontal distance of 75 m and a depositional slope of about 5.6° indicates that the late Pleistocene fault offset is about 10.3 m plus the unknown thickness of graben fill. Equivalent surfaces east and west of the graben are offset about 8.5 m down to the east as projected parallel to the depositional slope angle. This geometry implies that displacement on the antithetic fault is about 1.8 m plus the thickness of graben fill. Direct evidence on the antithetic fault is lacking because the antithetic fault scarp has been buried by the graben fill, and there are no exposures of the antithetic fault surface or the graben floor beneath the Holocene fill.

In profile *D–D′* the scarp height is 9.5 m and the maximum slope is 19.2°. The horizontal distance from top to

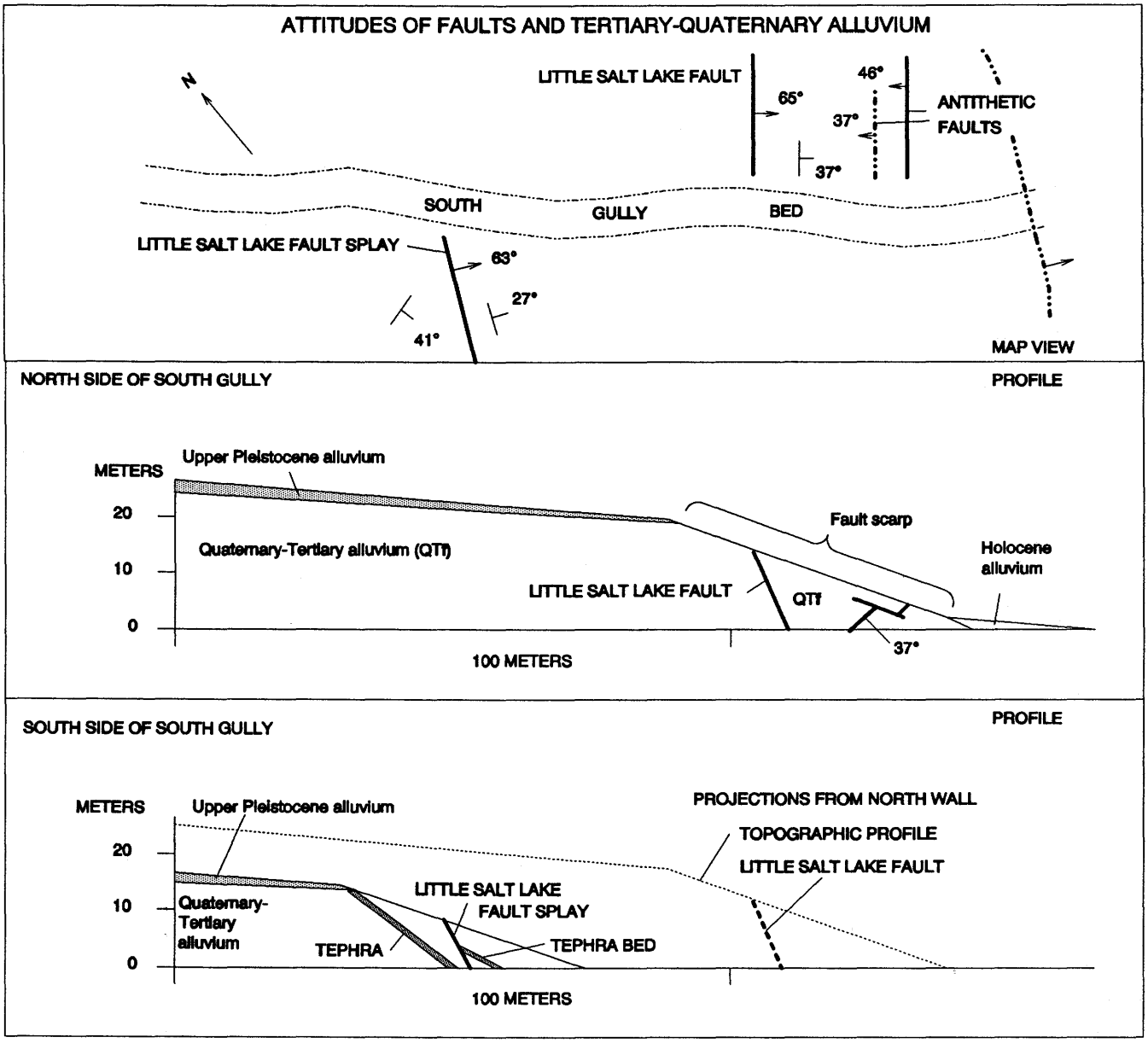

Figure 9. Map and cross section of fault and bedding attitudes in tilted Tertiary and Quaternary alluvium (unit Qtf) near Little Salt Lake fault exposed in walls of south gully. Map at same scale as profile. Dip of faults and strike and dip of bedding shown in map view; broken line, inferred or concealed.

bottom of the scarp is about 30 m and the depositional slope 5.6°. This indicates late Pleistocene fault offset of about 6.9 m plus the thickness of graben fill. The low scarp height at *D–D′* compared to *C–C′* probably reflects an unusually thick graben fill of Holocene fan alluvium from a stream that has entrenched the scarp only 50 m north of *D–D′*.

Profile *E–E′*, just 53 m north of *D–D′*, crosses the Little Salt Lake fault in a ravine cut into the upthrown block and extends down an active Holocene fan within the graben. Profile *E–E′* shows a slight inflection in slope where it crosses the fault scarp that could be interpreted as a very low fault scarp modified by active alluvial fan deposition. On aerial photographs, a tonal difference across this Holocene alluvial fan and across the next one to the north can also be interpreted as representing the trace of the fault. The offset of the Holocene depositional surface across the scarp estimated from the profile is about 1 m, and the slope about 5°. Scarp morphology has little meaning in such an active depositional environment, and the slope inflection may be caused by the transition from confined stream flow in the gully to unconfined flow on the fan. The slope inflection is linear exactly along the fault plane rather than radial about the fan apex. The evidence for Holocene fault movement across profile *E–E′* is thus not conclusive, but is permissive. It is the only

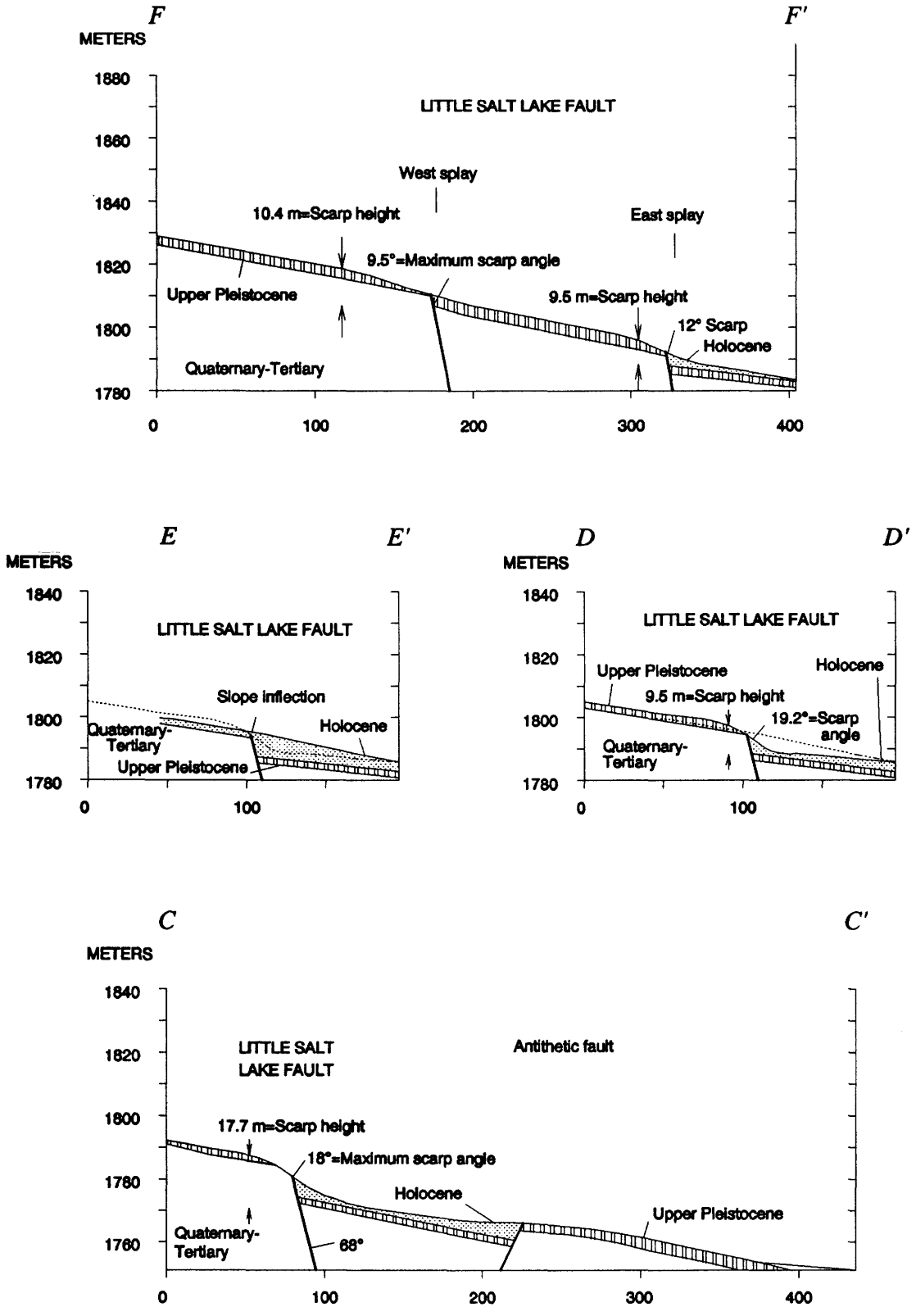

Figure 10. Profiles across Little Salt Lake fault at the four locations shown in figure 6. Vertical exaggeration ×2; altitudes above mean sea level. In *D–D′*, dotted line is profile *E–E′* projected. In *E–E′*, dotted line is profile *D–D′* projected.

indication of Holocene movement on the Little Salt Lake fault. The closest confirmed Holocene movement is a 1 m scarp on a west-dipping fault near the center of the Parowan Valley, about 6.5 km to the east.

Profile *F–F′* was measured north of the point where the Little Salt Lake fault splits into two strands. Each strand has a scarp height of about 10 m, about the same as that measured in profile *D–D′*, but the combined height of the two separate scarps is 19.9 m, about the same as that measured in profile *C–C′*. The slope of the scarp for each of the strands is less than at places where a single high scarp occurs, as at *C–C′* and *D–D′* to the south. Calculated offset of the western strand is about 2.6 m, plus the unknown thickness of post-faulting sediment at the foot of the scarp. No graben occurs at the foot of the western strand, and no sharp break in slope, so the sediment is probably thin. Calculated offset of the eastern strand is about 5.6 m plus the unknown thickness of post-faulting graben fill, which is thicker than usual because of a nearby ravine and alluvial fan. The combined offset of 8.2 m plus unknown thickness of graben fill for both strands may be comparable to 10.3 m at *C–C′* and 6.9 m at *D–D′*.

HISTORY

The various episodes of movement on the Little Salt Lake fault have not been radiometrically dated; however, the morphology of the scarp and the degree of soil development on uplifted surfaces can be used to constrain an estimate. A reasonable inference is that movement on the Little Salt Lake fault began prior to the late Pleistocene (more than 130 ka) and has continued into the Holocene (less than 10 ka). Two middle Pleistocene, one late Pleistocene, and possibly one Holocene geomorphic surfaces have been offset across the fault, implying a minimum of three or four distinct pulses of movement. Each of the pre-Holocene pulses totaled more than 10 m, and probably consisted of several distinct events. Total uplift of the highest surface is about 60 m.

The youngest evidence of displacement is lineations in Holocene graben-filling alluvial fans that correspond to an inflection where the slope steepens slightly down slope. These lineations are limited in extent and are ambiguous. If they do represent fault offset, the amount was small, probably less than 1 m. Late Pleistocene offset exceeds 10 m. Two uplifted pediment surfaces with middle Pleistocene soils are preserved about 8 and 50 m above the late Pleistocene surface, implying one pulse of multiple movement events totaling about 42 m followed by another pulse totaling about 8 m.

The present scarp, which indicates a minimum fault offset of 10 m, was formed mostly during the late Pleistocene and was probably preceded by other scarps that were obliterated by erosion. The thickness of the carbonate-enriched soil horizon on unit Qf implies that start of formation of the present scarp probably was more than 15 ka.

Figure 11 plots log of scarp height against maximum slope angle for four profiles measured along the Little Salt Lake fault. Those points can be compared with lines fit to similar measurements on Lake Bonneville shoreline scarps cut in gravelly alluvium and known to date from about 15 ka and on Drum Mountain fault scarps considered to date from about 10 ka (Bucknam and Anderson, 1979). The Little Salt Lake fault scarps are also developed in gravelly alluvium and are located only about 40 km southeast from the southern Bonneville shoreline, so the geographic proximity and similarities in climate and deposits between the shoreline profiles and the Little Salt Lake fault profiles enhance the validity of the comparison. However, the shoreline scarps have degraded from a particular moment in time and never been rejuvenated, whereas the higher fault scarps are likely to have been produced by multiple events separated by substantial time intervals. The fault scarp height reflects the summation of all events, whereas the maximum scarp slope angle is more likely to be controlled by the most recent event. For the high, composite, fault scarps of the Little Salt Lake fault, the point on figure 11 represents neither the

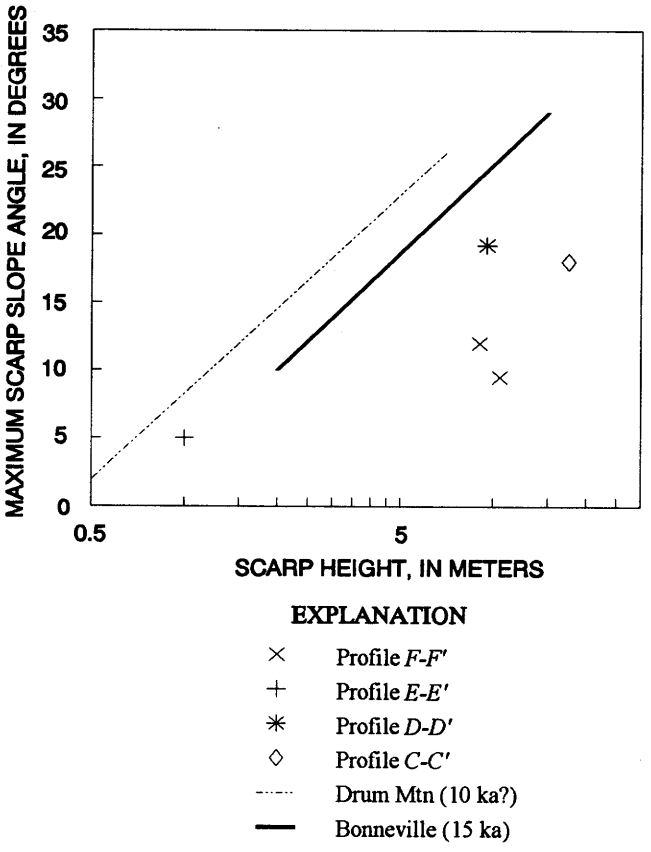

Figure 11. Plot of maximum slope angle in degrees against log of scarp height for the four profiles measured along Little Salt Lake fault and reference lines for similar measurements on the 15 ka Lake Bonneville shoreline scarps and the 10 ka(?) Drum Mountain fault scarps cut in alluvium (modified from Bucknam and Anderson, 1979).

inception of faulting nor the most recent event, but should fall between. Profile *E–E′* lies near the 15 ka line, and all the other profiles plot older than the 15 ka line.

Profile *E–E′* (fig. 10) crosses a very low, indistinct break in slope that can be interpreted as a degraded scarp from faulting that offsets young fan alluvium where it extends across the fault trace into an embayment in the high fault scarp. Soils on both sides of the scarp show virtually no pedogenic calcium carbonate; hence the alluvium is thought to be of Holocene age. That location is subject to direct deposition from a ephemeral stream draining about 1 km^2, so the maximum fault scarp slope and height has probably been reduced faster than in the case of the Bonneville shorelines and the other Little Salt Lake scarp profiles. No valid comparison can be made between profile *E–E′* and any other data in figure 11.

Study of points plotted for the three profiles (fig. 10) that include the full scarp height reveals some differences. The scarp at *D–D′* plots "younger" than scarps on profiles *C–C′* and *F–F′*; it may represent a slightly younger fault offset than those scarps. Profile *D–D′* is only 53 m south of profile *E–E′*, so Holocene faulting at profile *E–E′* is likely to affect the older scarp at profile *D–D′* and tend to rejuvenate it.

The degree of development of soils in unit Qf on the alluvial surface offset by the Little Salt Lake fault scarp suggests a late Pleistocene age for the fault movement that ended alluvial deposition on the surface. On the upthrown side of the fault and about 8 m higher than the late Pleistocene (unit Qf) alluvial surface are remnants of the older depositional surface of unit Qfo that have a more developed carbonate-enriched soil, probably of middle Pleistocene age. The elevation of this surface suggests at least 8 m of mid-Pleistocene uplift along the Little Salt Lake fault prior to the formation of the late Pleistocene scarp.

The absence of numerical dating of the offset pediment surfaces introduces great uncertainty in estimating the average rate of fault slip. The following calculations use age estimates of 20 ka for the late Pleistocene surface (+>10 m), 150 ka for the lower middle Pleistocene surface (+18 m), and 700 ka for the higher middle Pleistocene surface (+60 m), based on their soil development, degree of erosion, and relative elevation. The uncertainty of these age estimates is at least 50 percent. On that basis, the average rate of vertical motion since the middle Pleistocene has been about 0.12 mm/yr±50 percent, whereas the average rate since the late Pleistocene has been at least 0.5 mm/yr±50 percent.

ENOCH GRABEN

Quaternary basalt with a K-Ar age of 1.28±0.4 Ma (Anderson and Mehnert, 1979) is faulted near the southwest corner of the Parowan Gap quadrangle (figs. 3, 4). The vents and central part of the lava flows have been dropped down along two parallel fault zones that define the Enoch graben. The east side of the graben has dropped from 15 to 50 m along a narrow zone or single fault. The Hieroglyph horst (Threet, 1963), which forms the west wall of the graben, apparently has been uplifted about 70 m relative to the graben floor across a fault zone about 200 m wide. Faults along the west side of the horst have dropped flows down about 230 m across a zone about 400 m wide into the low valley north of Rush Lake (fig. 1), where they are buried beneath alluvium. The basalt was intersected in a drill hole for a water well beneath 30 m of alluvium, 2 km west of its last exposure at the surface (Gerald Staker, Utah State Engineers Office, Cedar City, Utah, written commun., 1989).

The average rate of fault movement over about the last 1.28±0.4 m.y. along cross section *B–B′* is about 0.012 mm/yr±35 percent for the fault bounding the east side of the Enoch graben, about 0.054 mm/yr±35 percent for the fault between the Enoch graben and the Hieroglyph horst, and about 0.178 mm/yr±35 percent for the fault on the west side of the Hieroglyph horst. The analytical uncertainty in the date and these rates is at least ±31 percent. The amount of offset of the basalt and thus the rate of offset also vary along the strike of the faults. Throw increases southward to a maximum of about 50 m on the east side of the graben, indicating a slip rate averaging as much as 0.039 mm/yr±35 percent. At their south end, the faults bounding the Enoch graben cut late Pleistocene, and possibly Holocene alluvium (Anderson and Christenson, 1989, p. 14).

The Hieroglyph horst is an anomalous structural block. At the south end the basalt rests on Tertiary and Quaternary alluvium, and at the north it rests on steeply dipping, highly sheared Lower Jurassic Navajo Sandstone cut by narrow siliceous dikes. This horst extends northward to Parowan Gap Canyon, where the rapid uplift across established drainage has produced "the Narrows," a short section of canyon through the Navajo Sandstone that is much narrower than the rest of Parowan Gap Canyon.

The basalt in the Enoch graben overlies primarily Paleocene and Eocene Claron Formation, but also overlies Upper(?) Cretaceous Iron Springs Formation, Tertiary and Quaternary alluvium (unit QTh), and exotic blocks of Tertiary volcanic rocks. Immediately east of the Enoch graben, a hole drilled by Mountain Fuel Supply (fig. 4) in sec. 9, T. 34 S., R. 10 W. penetrated quartz monzonite porphyry at a depth of 1,341 m (Tompkins and others, 1963) (fig. 4), establishing that the southern part of the Red Hills is underlain by an intrusive body. The quartz monzonite porphyry is overlain by 171 m of Lower Jurassic Navajo Sandstone, and 893 m of Upper(?) Cretaceous Iron Springs Formation.

CONCLUSIONS

The Red Hills, and the alluvium-filled basins on either side, formed as a result of down-to-west normal block

faulting, eastward tilting of the faulted blocks, and secondary down-to-east antithetic faulting. Thick alluvial fills are preserved in the deep, down-faulted basins east (>1,000 m) and west (>900 m) of the range. Tectonism within the basins has deformed and locally uplifted the older alluvial deposits so that they crop out in many places. Several generations of widespread but thin deposits of younger alluvium overlie erosion surfaces cut on the older alluvium and areas of soft bedrock. The youngest deposits are lacustrine silts and clays of Little Salt Lake playa that cover 21 km^2 on the west side of Parowan Valley.

Most faults within alluvium on both sides of the Red Hills are down to the west and synthetic to the Paragonah fault (figs. 1, 2), a major west-dipping fault that forms the eastern and lower bound of the detached terrain. Two major east-dipping faults antithetic to the Paragonah fault form the boundary between the Red Hills horst and the Parowan Valley graben. The southern part is bounded by the Red Hills fault (fig. 3), and the northern by the Little Salt Lake fault. The Little Salt Lake fault is best expressed where it extends 3.5 km through alluvium from Little Salt Lake north to the mountain front (figs. 5, 6). A segment without young scarps continues northward at least 8 km parallel to the range front of the northern Red Hills (fig. 3).

The Little Salt Lake fault strikes generally N. 45° E. and dips about 75° SE. It is expressed as an 18-m-high scarp with maximum slope of 19° offsetting upper Pleistocene pediment alluvium. On the upthrown block, remnants of middle Pleistocene pediment surfaces record uplift prior to formation of the late Pleistocene scarp. Parallel strands of the fault can be seen beneath the pediment alluvium in isolated exposures of folded upper Tertiary(?) to lower Pleistocene(?) alluvial sediments that contain silicic volcanic ash. Minor antithetic faults dipping 45° NW. are exposed in the folded sediments a few meters east of the main fault. Larger faults antithetic to the Little Salt Lake fault bound the southeast side of a scarp-front graben, filled with Holocene alluvium, that narrows southward from 1,000 to 100 m width in a distance of 4 km.

Movement on the Little Salt Lake fault probably began prior to middle Pleistocene time and has continued through the late Pleistocene and perhaps into the Holocene. The fault moved during at least three major pulses of activity. A small event may have offset a short segment of the fault about 1 m during the Holocene, but evidence is not conclusive. Total offset of mid-Pleistocene(?) geomorphic surfaces across the fault exceeds 60 m. The present scarp, which was formed by vertical fault movement of at least 10.3 m, was initiated during the late Pleistocene and was preceded by other scarps that have been obliterated by erosion. The average rate of vertical motion since the middle Pleistocene has been about 0.12 mm/yr±50 percent, whereas the average rate since the late Pleistocene has been at least 0.5 mm/yr±50 percent.

The Hieroglyph horst in the southwestern Red Hills has moved up 70 m relative to the Enoch graben on its east side and about 230 m relative to the northern Cedar City Valley on its west side since eruption of basalt flows 1.28±0.4 Ma, indicating fault movement averaging 0.054 mm/yr±35 percent on the east side and 0.178 mm/yr±35 percent on the west. This recent rapid uplift is responsible for the narrowing of the Parowan Gap Canyon where it crosses the horst exposing Navajo Sandstone. The east side of the Enoch graben has moved down 15–50 m relative to the part of the Red Hills to the east, indicating average fault movement between 0.012 and 0.039 mm/yr±35 percent.

REFERENCES CITED

Anderson, R.E., and Christenson, G. E., 1989, Quaternary faults, folds, and selected volcanic features in the Cedar City 1°×2° quadrangle, Utah: Utah Geological and Mineral Survey Miscellaneous Publication 89–6, 29 p.

Anderson, R.E., and Mehnert, H.H., 1979, Reinterpretation of the history of the Hurricane fault in Utah: Rocky Mountain Association of Geologists–Utah Geological Association, 1979 Basin and Range Symposium, p. 145–173.

Bjorklund, L.J., Sumsion, C.T., and Sandberg, G.W., 1977, Selected hydrologic data, Parowan Valley and Cedar City Valley drainage basins, Iron County, Utah: U. S. Geological Survey, Utah Basic Data Release No. 28, 54 p.

Bucknam, R.C., and Anderson, R.E., 1979, Estimation of fault-scarp ages from scarp-height–slope-angle relationship: Geology, v. 7, p. 11–14.

Cook, K.L., and Hardman, Elwood, 1967, Regional gravity survey of the Hurricane fault area and Iron Springs district, Utah: Geological Society of America Bulletin, v. 78, no. 9, p. 1063–1076.

Fleck, R.J., Anderson, J.J., and Rowley, P.D., 1975, Chronology of mid-Tertiary volcanism in High Plateaus region of Utah, *in* Anderson, J.J., Rowley, P.D., Fleck, R.J., and Nairn, A.E.M., eds., Cenozoic geology of southwestern high plateaus of Utah: Geological Society of America Special Paper 160, p. 53–61.

Gile, L.H., Peterson, F.F., and Grossman, R.B., 1966, Morphological and genetic sequences of carbonate accumulation in desert soils: Soil Science, v. 101, p. 247–260.

Hamblin, W.K., Damon, P.E., and Bull, W.B., 1981, Estimates of vertical crustal strain rates along the western margins of the Colorado Plateau: Geology, v. 9, p. 293–298.

Machette, Michael, 1985, Late Cenozoic geology of the Beaver Basin, southwestern Utah: Brigham Young University Geology Studies, v. 32, pt. 1, p. 19–37.

Maldonado, Florian, Sable, E.G., and Anderson, J.J., 1990, Shallow detachment of mid-Tertiary rocks, Red Hills (Basin and Range), with implications for a regional detachment zone in the adjacent Markagunt Plateau (Colorado Plateau), southwest Utah: Geological Society of America Abstracts with Programs, v. 22, no. 3, p. 94.

Maldonado, Florian, and Williams, V.S., 1993a, Geologic map of the Paragonah quadrangle, Iron County, Utah: U.S. Geological Survey Geologic Quadrangle Map GQ–1713, scale 1:24,000.

———1993b, Geologic map of the Parowan Gap quadrangle, Iron County, Utah: U.S. Geological Survey Geologic Quadrangle Map GQ–1712, scale 1:24,000.

Neilson, R.L., 1983, Pleistocene and Holocene evolution of Little Salt Lake Playa (Lake Parowan), southwest Utah: Geological Society of America Abstracts with Programs, v. 15, no. 5, p. 300.

Pe, Win, and Cook, K.L., 1980, Gravity survey of the Escalante Desert and vicinity in Iron and Washington Counties, Utah: Earth Sciences Laboratory / University of Utah Research Institute Paper, DOE ID 12079–14, 169 p.

Rowley P.D., 1975, Geologic map of the Enoch NE quadrangle, Iron County, Utah: U.S. Geological Survey Geologic Quadrangle Map GQ–1301, scale 1:24,000.

Rowley, P.D., and Threet, R.L., 1976, Geologic map of the Enoch quadrangle, Iron County, Utah: U.S. Geological Survey Geologic Quadrangle Map GQ–1296, scale 1:24,000.

Steer, H.M., 1980, The seismo-tectonic history and morphological evolution of fault scarps in southwestern Utah: Boulder, Colo., University of Colorado Ph. D. dissertation, 252 p.

Thomas, H.E., and Taylor, G.H., 1946, Geology and ground-water resources of Cedar City and Parowan valleys, Iron County, Utah: U.S. Geological Survey Water Supply Paper 993, 210 p.

Threet, R.L. 1952, Geology of the Red Hills area, Iron County, Utah: Seattle, Wash., University of Washington Ph. D. dissertation, 107 p.

———1963, Geology of the Parowan Gap area, Iron County, Utah, *in* Heylmun, E.B., ed., Geology of southwestern Utah: Intermountain Association Geologists Guidebook, 12th, Annual Field Conference, 1963, p. 136–145.

Tompkins, F.V., Goodwin, J.C., and Malin, W.J., 1963, Cedar City Utah to Parowan, Utah, via Iron Springs mining district and Parowan Gap, Road log 3, *in* Heylmun, E.B., ed., Geology of southwestern Utah: Intermountain Association Geologists Guidebook, 12th, Annual Field Conference, 1963, p. 222–226.

Manuscript approved for publication February 14, 1994
Published in the Central Region, Denver, Colorado
Photocomposition by Denny Welp
Graphics by Ramon E. Sabala;
final graphics preparation by Denny Welp
Edited by Lorna Carter

☆U.S. GOVERNMENT PRINTING OFFICE: 1995-673-046/86118


U.S. DEPARTMENT OF THE INTERIOR
MARCH 3, 1849